UNIVERSITY OF CALIFORNIA
RIVERSIDE

# Further Understanding the Physical Phenomena of Crowded Protein Osmotic Pressure and Its Application to Medical Devices

A Dissertation submitted in partial satisfaction
of the requirements for the degree of

Doctor of Philosophy

in

Bioengineering

by

Devin William M$^{c}$Bride

June 2013

Dissertation Committee:
Dr. Victor G. J. Rodgers, Chairperson
Dr. Devin K. Binder
Dr. Dimitrios Morikis

The Dissertation of Devin William M$^{c}$Bride is approved:

---

---

---

Committee Chairperson

University of California, Riverside

ACKNOWLEDGEMENTS

I would like to first thank God for all the blessings that He has given to me and for everything that He has allowed me to accomplish.

I would like to give thanks from the bottom of my heart for the love and support I have received from my wife, Corena Valencia-M$^{c}$Bride. If not for Corena, I would not be the man I am today, nor would I have been able to achieve anything in life. With you by my side I feel like I can accomplish anything I set my mind to. Words are not enough to express what you mean to me. Mi amor, te amo con todo mi corazon.

I would like to express my sincerest thanks to Professor Victor G. J. Rodgers, my advisor, for his mentoring and guidance in all aspects of this dissertation. Without Dr. Rodgers' support and faith in me and my abilities, this dissertation would not have come to pass. Dr. Rodgers has taught me how to approach any biotransport, bioreaction kinetic, and reversible and irreversible thermodynamic problems in order to develop mathematical expressions for understanding physical phenomenon or developing technologies. Without Dr. Rodgers' expertise in these areas, and his life-long dedication to membrane transport, I could not have been able to develop a treatment for cerebral edema. One day, we will be able to say that the research in this dissertation is saving numerous lives. Thank you Dr. Rodgers for providing me with the skills to be able to tackle any problems I might face. A final thank you for all your love and support, for your determination to help me become more positive about facing challenges, and for your aid in developing my critical thinking. PMA!

I would also like to thank Professor Devin K. Binder for his mentoring, guidance, and expertise in neurosurgery. Without Dr. Binder, I would not have had the insight into

the major problem of cerebral edema. In your lab I learned invaluable skills and techniques with animal models.

I would like to thank my parents for the life they gave me and for all of the lessons I learned from them. I use these lessons daily, and can only hope to pass them on to my children. They supported all of my decisions and let me tackle life, as well as feel the sting of it. Without your lessons and support I would have not known all the joys and sorrows life has to offer. Thank you for your love and support. To my brother and sister: thank you for your love and support; our childhood memories are ones that I will always cherish and would not change for anything. I would like to thank Tony for his love and always supporting my decisions. I love you all.

I would also like to thank my father in-law, mother in-law, sisters in-law, and brother in-law. To my father in-law and mother in-law: thank you very much for all the love and support you have shown me and treating me as if I were one of your children. Without all of the days of manual labor and things I have learned, I would not have been able to appreciate this moment as much as I do. To my sisters in-law and brother in-law: thank you for your love and support and for treating me like family. To my nephews: thank you for showing me how amazing life is and that I should approach everyday as you both do – determined to learn as much as you can each day. I love you all.

A hearty thanks to the B2K Group; without all the love and support from the B2K Group, I would not have been able to develop my research and mentoring skills, and most importantly, my presentation skills, for which I have won multiple presentation awards. I am honored to have been a part of the B2K Group which has won awards at every conference we have attended.

I would like to thank Dr. Binder's Translational Neuroscience Laboratory for their support with the animal studies in this dissertation. I would like to thank Mr. Mike S. Hsu for his knowledge of neurosurgery and taking the time to teach me the techniques, and many other skills, pertaining to animal studies. The other group members, Ms. Jenny Szu and Ms. Jacqueline Hubbard, were great assets in the day-to-day operations and animal care; thank you very much.

I would like to thank Mr. Chris Hale for his help in designing (and redesigning), machining and building, and data collection. Chris' hand was in many of the research studies in this dissertation including osmotic pressure of single and binary protein solutions and development of a concentrating osmometer. Without Chris, all of the work pertaining to the concentrating osmometer would have been incomplete and the world would not yet have a concentrating osmometer. Thank you very much for all you have done.

I would like to thank the Professor Dimitrios Morikis and the BioMoDeL group, especially Dr. Chris Kieslich, for their help with the computational modeling and its application to the work in this dissertation.

I would like to thank Professor B. Hyle Park and the Park Research Group for allowing me to use their machine shop for the development of many prototypes.

My sincerest thanks to the staff of the Department of Bioengineering. A special thank you to Mrs. Denise Sanders for her love and support, and for always having an open door; I cannot thank Denise enough. Mrs. Hong Xu, thank you very much for your help with maintaining the safety of the B2K Laboratory. Thank you Hong for always helping me decide the appropriate safety protocols when designing a new experiment. Thank you to all of the other staff: Ms. Crissy Reising and Ms. Jennifer Morgan for their hard work.

I would like to thank the Mechanical Engineering Machine Shop for use of the equipment and their help with building the devices designed for this dissertation.

I would like to thank Dr. Andre Obenaus and Dr. Bir Bhanu for their guidance and help in the analysis of magnetic resonance images and the development of algorithms for detecting lesions. I would like to thank Dr. Ehsan T. Esfahani for his expertise with algorithm development of the lesion detection code. I would also like to thank Asong Tambo, Albert Cruz, and Anthony Bianchi for their help with the development of the traumatic brain injury prediction algorithm.

I would like to thank Richard Hausman and Professor Isabel Escobar at the University of Toledo for their valuable discussions and expertise in potting hollow fibers. Without them I would not have learned how to successfully pot hollow fibers.

I would like to thank Dr. Monica Carson for being able to use the Zeiss microscope in her lab for taking the histology images.

I would like to thank the following funding support for me and the research in this dissertation: NSF Integrative Graduate Education and Research Traineeship (IGERT) Program in Video Bioinformatics Fellowship (Grant DGE 0903667), UCR Dissertation Year Program (DYP) Award, UCR Dissertation Research Grant, UCR Graduate Research Mentorship Program (GRMP) Fellowship, U.S. Department of Education Graduate Assistance in Areas of National Need (GAANN) Fellowship, and UCR Chancellor's Distinguished Fellowship. I would also like to thank the following Organizations for travel grants: Biomedical Engineering Society (BMES) for the BMES Student Travel Award (2010 and 2011) and Earle C. Anthony Research Funds for the Earle C. Anthony Academic Senate Graduate Student Travel Award (2012).

I would like to thank John Wiley and Sons for the use of the article titled "Obtaining Protein Solvent Accessible Surface Area When Structural Data is Unavailable Using Osmotic Pressure" printed in the AIChE Journal Vol. 58(4) pages 1012-7 (2012). Parts of the said publication were used in Chapter 2. I would also like to thank the American Association of Neurological Surgeons (AANS) for the use of the article titled "Improved Survival Following Cerebral Edema Using a Novel Hollow Fiber-Hydrogel Device" printed in the Journal of Neurosurgery Vol. 116(6) pages 1389-94 (2012). Parts of this publication were used in Chapters 11 and 13.

DEDICATION

I would like to dedicate this dissertation to the love of my life, Corena Valencia-McBride, who supported me whole-heartedly. I would not have been able to get this far in life without her by my side. She has been by my side through the thick and the thin, the good and the bad, and the rich and the poor. Tu eres mi vida y mi razón de que vivo.

ABSTRACT OF THE DISSERTATION

Further Understanding the Physical Phenomena of
Crowded Protein Osmotic Pressure and Its
Application to Medical Devices

by

Devin William M$^{c}$Bride

Doctor of Philosophy, Graduate Program in Bioengineering
University of California, Riverside, June 2013
Dr. Victor G. J. Rodgers, Chairperson

Extending the understanding of the physical phenomena of crowded and concentrated protein osmotic pressure is the focus of this dissertation. Herein, the free-solvent osmotic pressure model is developed to understand additional physical phenomena such as solvent accessible surface area (SASA), to provide insight into the meaning of the second virial coefficient and the activity coefficient of water in proteinaceous solutions, and to account for effect of protein-protein interactions on crowded protein osmotic pressure.

The free-solvent osmotic pressure model has been extended to allow for the SASA of proteins to the determined. The free-solvent model predicted SASA is in excellent agreement with the SASA computed using the molecular structure for various macromolecules. The physical parameters of the free-solvent model are assessed to determine the sensitivity of these parameters when overlapping osmotic pressure data is observed for two proteins.

The free-solvent model is used to give insight into the fitted parameters of two empirical osmotic pressure models, the activity coefficient and the second virial coefficient;

both of these coefficients are defined in terms of solute-solvent interactions. The negative virial coefficient was also elucidated to understand its physical meaning in terms of solute-solvent parameters for solutions in which protein-protein interactions do not occur. The virial coefficients based on solute-solvent interactions are shown to provide similar values to those obtained by osmotic pressure data curve fitting. Furthermore, the virial coefficients are also correlated to the ionic strength of the solute influenced solvent and the conditions for achieving negative virial coefficients are examined.

In addition, a concentrating osmometer is developed to obtain multiple concentration-osmotic pressure values with a single solution. The concentrating osmometer is tested using bovine serum albumin solutions which have known osmotic pressure profiles for near-saturation concentrations.

In the second part of this dissertation, the use of concentrated protein osmotic pressure for the development of a treatment for cerebral edema is presented. A novel therapy, direct osmotherapy (DOT), is proposed and a device which utilizes this therapy, an osmotic transport device (OTD), is developed. DOT using an OTD is shown to successfully enhance the survival of animals which have received fatal water intoxication and reduce the edema associated with posttraumatic cerebral edema induced by a traumatic brain injury. The OTD components are examined as a preliminary analysis to determine the optimal OTD parameters for the treatment of severe cerebral edema.

TABLE OF CONTENTS

LIST OF FIGURES

LIST OF TABLES

# LIST OF SYMBOLS

| | |
|---|---|
| $A_i, B_i, C_i$ | Fitted parameters for charge dependent virial coefficients for $B_i$ |
| $A, B, C$ | Number of monomers of protein $j$ $(A)$, $a$ $(B)$, $b$ $(C)$ forming a hetero-multimer of proteins $j$, $a$, and $b$ |
| $a_i$ | Relative activity of species $i$ |
| $B_i$ | $i^{th}$ virial coefficient |
| $B_1$ | First virial coefficient |
| $B_2$ | Second virial coefficient |
| $B_3$ | Third virial coefficient |
| $B_i'$ | Virial coefficient which is a function of the potential mean force of species $i$ |
| $B_{ii}'$ | Virial coefficient which is a function of the potential mean force for a two-body interaction for protein $i$ with protein $i$ |
| $B_{22}'$ | Virial coefficient which is a function of the potential mean force for a two-body interaction for protein 2 |
| $c_i$ | Concentration of species $i$ |
| $d_1, d_2$ | Diameter of a tube |
| $G$ | Gibbs free energy |
| $g$ | Gravity |
| i | Place holder for terms |
| $J$ | Flux |
| $k$ | Boltzmann constant |
| $L_p$ | Hydraulic permeability |
| $l_{\text{homo}-\text{multimer}}$ | Number of homo-multimers formed |
| $l_{\text{hetero}-\text{multimer}}$ | Number of hetero-multimers formed |
| $l_{\text{hetero}-\text{multimer},h}$ | Number of hetero-multimers forming the $h$ multimer |
| $M_i$ | Molecular weight of species $i$ |
| $m_i$ | Molal concentration of species $i$ |
| $N_i$ | Number of moles of species $i$ |
| $N^K$ | Initial total number of moles in compartment $K$ |
| $N_*^K$ | Final total number of moles, after interactions, in compartment $K$ |
| $N_i^K$ | Initial number of moles of species $i$ in compartment $K$ |

| | |
|---|---|
| $N^{\mathrm{II}}_{\mathrm{homo-multimers}}$ | Moles of protein forming homo-multimers (intra-protein interactions) in chamber II |
| $N^{\mathrm{II}}_{\mathrm{hetero-multimers}}$ | Moles of protein forming hetero-multimers (inter-protein interactions) in Chamber II |
| $N^{\mathrm{II}}_{\mathrm{monomers}}$ | Moles of protein remaining as unbound monomers in chamber II |
| $P$ | Pressure |
| $P_1$ | Pressure at the inlet of the hollow fibers |
| $P_2$ | Pressure at the outlet of the hollow fibers |
| $P_3$ | Pressure of the permeate |
| $P_{\mathrm{feed}}$ | Pressure of the feed solution |
| $P_L$ | Pressure loss due to sudden contraction |
| $p_i$ | Partial pressure of species $i$ |
| $R$ | Ideal gas constant |
| $r$ | Center-to-center radius between protein species |
| $R_h$ | Hollow fiber resistance to water flow |
| $R_m$ | Hydratable material resistance to water flow |
| $S$ | Entropy |
| $\mathrm{SASA}_{\mathrm{monomer}}$ | Solvent accessible surface area of a monomer |
| $\mathrm{SASA}_{\mathrm{dimer}}$ | Solvent accessible surface area of a homo-dimer |
| $T$ | Temperature |
| $V$ | Volume |
| $V_i$ | Specific volume of pure species $i$ |
| $v$ | Velocity |
| $\overline{V}_i$ | Specific volume of species $i$ |
| $W_i$ | Potential mean force between species $i$ |
| $W_{22}$ | Potential mean force for a two-body interaction for protein 2 |
| $w_i$ | Percent weight of species $i$ |
| $w_{\mathrm{dry}}$ | Dehydrated tissue weight |
| $w_{\mathrm{wet}}$ | Hydrated tissue weight |
| $x_i$ | Mole fraction of species $i$ |
| $x_i^K$ | Mole fraction of species $i$ in compartment $K$ |
| $Z$ | Size of the homo-multimer (*i.e.* $Z = \mathrm{ii}$ for homo-dimer, $Z = \mathrm{iii}$ for a homo-trimer, etc) |
| $\overline{Z}$ | Charge of protein |

*Greek*

| | |
|---|---|
| $\alpha$ | Monolayer ionic strength, ratio of ion binding to hydration |
| $\alpha_{j,Z}$ | Fractional amount of protein $j$ forming the homo-multimer of $Z$ units |
| $\beta_{ja,A:B}$ | Fractional amount of protein $j$ forming a hetero-multimer with protein $a$ containing $A$ units of protein $j$ and $B$ units of protein $a$ |
| $\beta_{jab,A:B:C}$ | Fractional amount of protein $j$ forming a hetero-multimer with proteins $a$ and $b$ containing $A$ units of protein $j$, $B$ units of protein $a$, and $C$ units of protein $b$ |
| $\Phi\big\vert_{j,Z}$ | Monomer to homo-multimer $Z$ molar ratio for protein $j$ |
| $\phi$ | Osmotic Coefficient |
| $\Gamma\big\vert_{ja,A:B}$ | Monomer to hetero-multimer $ja$ molar ratio with $A$ units of $j$ and $B$ units of $a$ |
| $\Gamma\big\vert_{jab,A:B:C}$ | Monomer to hetero-multimer $jab$ molar ratio with $A$ units of $j$, $B$ units of $a$, and $C$ units of $b$ |
| $\gamma_i$ | Activity coefficient of species $i$ |
| $\gamma_i^K$ | Activity coefficient of species $i$ in compartment $K$ |
| $\eta_h$ | Size of the $h$ multimer (i.e. $\eta_2 = 2$ for a two protein species interactions, $\eta_3 = 3$ for a three protein species interactions, etc.) |
| $\mu$ | Viscosity |
| $\mu_i$ | Chemical potential of species $i$ |
| $\nu_{ij}$ | Net number of moles of solvent component $i$ interacting with protein $j$ |
| $\nu_{ij,Z}$ | Moles of solvent species $i$ bound to the protein $j$ homo-multimer with $Z$ units |
| $\nu_{ija,A:B}$ | Moles of solvent species $i$ bound to the hetero-multimer between proteins $j$ and $a$ with $A$ units of protein $j$, and $B$ units of protein $a$ |
| $\nu_{ijab,A:B:C}$ | Moles of solvent species $i$ bound to the hetero-multimer between proteins $j$, $a$, and $b$ with $A$ units of protein $j$, $B$ units of protein $a$, and $C$ units of protein $b$ |
| $\nu_{jj,Z}$ | Moles of protein $j$ forming a homo-multimer with $Z$ units |
| $\nu_{ja,A:B}$ | Moles of protein $j$ interacting with protein $a$ to form the hetero-multimer between proteins $j$ and $a$ with $A$ units of protein $j$, and $B$ units of protein $a$ |

| | |
|---|---|
| $\nu_{jab,A:B:C}$ | Moles of protein $j$ interacting with proteins $a$ and $b$ to form the hetero-multimer between proteins $j$, $a$, and $b$ with $A$ units of protein $j$, $B$ units of protein $a$, and $C$ units of protein $b$ |
| $\nu N^{\mathrm{II}}_{\mathrm{homo-multimers}}$ | Moles of diffusible species bound to the homo-multimers |
| $\nu N^{\mathrm{II}}_{\mathrm{hetero-multimers}}$ | Moles of diffusible species bound to the hetero-multimers |
| $\nu N^{\mathrm{II}}_{\mathrm{monomers}}$ | Moles of diffusible species bound to the free monomers |
| $\nu_{\mathrm{monomer-ion}}$ | Ion binding of a monomer |
| $\nu_{\mathrm{dimer-ion}}$ | Ion binding of a dimer |
| $\nu_{\mathrm{solvent/homo-multimer}}$ | Moles of solvent bound to the homo-multimers |
| $\nu_{\mathrm{solvent/hetero-multimer}}$ | Moles of solvent bound to the hetero-multimers |
| $\nu_{\mathrm{solvent/monomer}}$ | Moles of solvent bound to the free monomers |
| $\pi$ | Osmotic pressure |
| $\pi_p$ | Protein contribution to the osmotic pressure |
| $\pi_D$ | Donnan contribution to the osmotic pressure |
| $\pi'$ | Number pi |
| $\theta_i$ | Composition variable of species $i$ |
| $\rho_i$ | Density concentration variable of species $i$ |
| $\sigma$ | Reflection coefficient |
| $\Omega$ | Resistance coefficient due to sudden contraction |

*Superscripts*:

| | |
|---|---|
| I | Compartment I (solvent) |
| II | Compartment II (solution) |
| $o$ | Reference state |
| $K$ | Compartment of a two-chamber osmometer |
| $\theta$ | Composition variable |
| $\psi_1, \psi_2$ | Phase of the system |

*Subscripts:*

| | |
|---|---|
| 1 | Solvent |
| 2 | Protein or macromolecule for a single macromolecule in solution |
| 3 | Salt for a single macromolecule in solution |
| FW | Free water |
| W | Total water |
| $2 \rightarrow (p+1)$ | Proteins or macromolecules for $p$ impermeable solutes |
| $(p+2) \rightarrow n$ | Salts for $p$ impermeable solutes |

| | |
|---|---|
| $h$ | Type of multimer (*i.e.* $h = 2$ for a two protein species interactions, $h = 3$ for a two protein species interactions, etc.) |
| $i$ | Individual species |
| $j$ | Individual monomeric protein species |
| $n$ | Number of individual species |
| $p$ | Number of individual monomeric proteins |
| $q$ | All other components in solution except $i$ |

# PART 1.

# FURTHER DEVELOPMENTS OF OSMOTIC PRESSURE MODELS

# CHAPTER 1.

# INTRODUCTION

## 1.1. Macromolecular Crowding

In nature, macromolecules, such as proteins, are usually found in crowded environments. These environments are typically solutions of mixed proteins with total concentrations between 50 - 400 g/L (Ellis 2001; Minton 2001). Many cells contain macromolecular crowded environments, and therefore, the crowded environment is an essential component of cells. One feature of macromolecular crowding is the deviation of the osmotic pressure from ideality; this is called crowed protein osmotic pressure.

Although crowded protein environments are abundant and naturally occurring, many studies focus on single protein solutions for studying and understanding the effect(s) of crowded environments. These concentrated solutions, in which a single macromolecule is examined at high concentrations, are more convenient than crowded solutions; they can yield information about the effects of excluded volume (volume which is occupied by the macromolecule) on various phenomenon, such as reaction kinetics and thermodynamics (Minton 1983).

Here, the effects of concentrated and crowded macromolecule solutions on osmotic pressure are studied. Macromolecular crowded systems, as well as concentrated solutions in general, exhibit highly non-ideal osmotic pressure at concentrations near-saturation. The osmotic pressure of concentrated protein solutions has been experimentally studied for several globular proteins such as hen egg lysozyme (HEL) (Yousef *et al.* 2002), bovine β-lactoglobulin (BLG) (Parker *et al*. 2005), ovalbumin (OVA) (Yousef *et al.* 2000), bovine serum albumin (BSA) (Yousef *et al.* 1998b), sheep hemoglobin (Hb) (Dick 1967), immune-gamma globulin (IgG) (Yousef *et al.* 1998a), and calf lens α-crystallin (Vérétout *et al.* 1989). However, limited data

exists for crowded protein osmotic pressure; a single dataset exists for near-saturation concentrations: equimolar OVA:BSA in 0.15 M NaCl at pH 7.0 (Yousef *et al.* 2001).

## 1.2. Osmotic Pressure

When a semi-permeable membrane separates solvent, such as water, and a solution containing an impermeable solute, a net flow of the solvent occurs from the solvent to the solution attempting to dilute the solution. The net flow is a phenomenon called osmosis.

For two solutions, separated by a semi-permeable membrane, solvent will flow across the membrane, and the chemical potential of the diffusible species will change, due to osmosis, until the chemical potential of each diffusible species is equal to its chemical potential in the other solution. It is experimentally convenient to fix the volume of both solutions so that the pressure in one of the solutions increases until the flow is prevented. The equilibrium pressure is known as the osmotic pressure and is directly related to the chemical potential of each species.

## 1.3. Thermodynamic Basis of Osmotic Pressure

The chemical potential of a component is defined as the change in the free energy with respect to the change in the mole number of each species. While the chemical potential can be written in terms of any free energy, typically Gibbs free energy (constant temperature and pressure) is used.

The chemical potential of component $i$, $\mu_i$, defined as the change in Gibbs free energy, $G$, for a change in the moles of component $i$ changes, $N_i$, at fixed temperature, $T$, pressure, $P$, and moles of all other components, $N_q$, or

$$\mu_i = \left( \frac{\partial G}{\partial N_i} \right)_{T,P,N_q} . \tag{1.1}$$

The change in Gibbs free energy is

$$dG = -SdT + VdP + \sum_i \mu_i dN_i \,, \tag{1.2}$$

and assuming that the process is at constant temperature and pressure, Eqn. 1.2 reduces to

$$dG = \sum_i \mu_i dN_i \,. \tag{1.3}$$

For a system of several phases, $\psi_i$,

$$dG = dG^{\psi_1} + dG^{\psi_1} + \ldots, \tag{1.4}$$

and at equilibrium, the change in Gibbs free energy is zero, or

$$dG = dG^{\psi_1} + dG^{\psi_1} + \ldots = 0 \,. \tag{1.5}$$

When the system consists of two phases, Eqn. 1.5, combined with Eqn. 1.3 for each phase, becomes

$$dG = \sum_i \mu_i^{\psi_1} dN_i^{\psi_1} + \sum_i \mu_i^{\psi_2} dN_i^{\psi_2} = 0 \,, \tag{1.6}$$

and, for each component, it follows that

$$\mu_i^{\mathrm{I}} dN_i^{\mathrm{I}} + \mu_i^{\mathrm{II}} dN_i^{\mathrm{II}} = 0 \,. \tag{1.7}$$

The conservation of mass requires that, for each component which transports from one phase to the other,

$$N_i^{\mathrm{I}} = -N_i^{\mathrm{II}} \,. \tag{1.8}$$

Thus, at equilibrium, the chemical potential of each component must be equal in the two phases,

$$\mu_i^{\mathrm{I}} = \mu_i^{\mathrm{II}} \,. \tag{1.9}$$

If a systems consisting of two solutions separated by a semi-permeable membrane, for which one solution (chamber II) contains an impermeable solute, at equilibrium, the chemical potential of the diffusible species, $i$, must be equal. Let the chemical potential of species $i$ in

chamber II, at pressure $P$, be $\left(\mu_i^{\mathrm{II}}\right)_P$ and the chemical potential of species $i$ in the solute-free chamber (chamber I), at pressure $P$, be $\left(\mu_i^{\mathrm{I}}\right)_P$, such that

$$\left(\mu_i^{\mathrm{II}}\right)_P < \left(\mu_i^{\mathrm{I}}\right)_P . \tag{1.10}$$

At equilibrium, assuming that the chemical potential of species $i$ in chamber I is the same as its initial value, that the temperature and pressure are constant, and that the number of all other diffusible species moving across the membrane is constant, then

$$\left(\mu_i^{\mathrm{II}}\right)_{P+\pi} = \left(\mu_i^{\mathrm{I}}\right)_P , \tag{1.11}$$

where $\pi$ is the increase in the pressure required to satisfy chemical potential equivalence of species $i$ in the two chambers (Eqn. 1.11).

The chemical potential of species $i$ at equilibrium is given as

$$\left(\mu_i^{\mathrm{II}}\right)_{P+\pi} = \left(\mu_i^{\mathrm{II}}\right)_P + \int_P^{P+\pi} \left(\frac{\partial \mu_i}{\partial P}\right)_T dP \tag{1.12}$$

where $\left(\mu_i^{\mathrm{II}}\right)_P$ is the chemical potential of species $i$ at the initial pressure $P$. Letting the specific (or partial molar) volume, $\overline{V}_i$, be defined as

$$\overline{V}_i = \left(\frac{\partial \mu_i}{\partial P}\right)_{T,n_k} , \tag{1.13}$$

Eqn. 1.12 becomes

$$\left(\mu_i^{\mathrm{II}}\right)_{P+\pi} = \left(\mu_i^{\mathrm{II}}\right)_P + \int_P^{P+\pi} \overline{V}_i dP , \tag{1.14}$$

and upon integration and reduction yields

$$\left(\mu_i^{\mathrm{II}}\right)_{P+\pi} = \left(\mu_i^{\mathrm{II}}\right)_P + \overline{V}_i \pi . \tag{1.15}$$

Now combining Eqn. 1.15 with Eqn. 1.11

$$\left(\mu_i^{\mathrm{II}}\right)_P + \overline{V}_i \pi = \left(\mu_i^{\mathrm{I}}\right)_P , \tag{1.16}$$

and rearranging, the osmotic pressure is defined as the difference in the chemical potential of species $i$ in the two chambers, or

$$\pi = \frac{\left(\mu_i^{\mathrm{I}}\right)_P - \left(\mu_i^{\mathrm{II}}\right)_P}{\bar{V}_i}. \tag{1.17}$$

1.3.1. Osmotic Pressure of Dilute Solutions

The chemical potential of any component is related to its activity, $a_i$, by

$$\mu_i^{\theta}\left(T,P,\theta_i\right) = \mu_i^{o\theta}\left(T,P^o,\theta_i^o\right) + RT\ln a_i^{\theta}\left(T,P,\theta_i\right), \tag{1.18}$$

where $\mu_i^o$ is the chemical potential of the component at a reference state, and the chemical potential and activity are both a function of the temperature, pressure, and composition variable, $\theta$.

For an arbitrary $\theta$, replacing the chemical potential in each chamber (Eqn. 1.17) with this relationship yields

$$\pi = \frac{RT}{\bar{V}_i}\left(\mu_i^{o\theta} + \ln a_i^{\mathrm{I}} - \mu_i^{o\theta} + \ln a_i^{\mathrm{II}}\right), \tag{1.19}$$

or

$$\pi = -\frac{RT}{\bar{V}_i}\ln\left(\frac{a_i^{\mathrm{II}}\left(T,P,\theta_i\right)}{a_i^{\mathrm{I}}\left(T,P,\theta_i\right)}\right). \tag{1.20}$$

The activity is typically rewritten in terms of a more convenient composition variable (such as $x_i$, $c_i$, $m_i$, $\rho_i$, etc.) and the corresponding activity coefficient, $\gamma_i^{\theta}$, or

$$a_i^{\theta}\left(T,P,\theta_i\right) = \gamma_i^{\theta}\theta_i. \tag{1.21}$$

While there exist many choices for the composition variable, van Laar chose to use the mole fraction, $x_i$ (van Laar 1894).

For a single protein, , in a monovalent salt aqueous solution, taking the solvent, solute, and salt species to be subscripts 1, 2, and 3, respectively, the osmotic pressure (Eqn. 1.20) becomes

$$\pi = -\frac{RT}{\bar{V}_1}\ln\left(\frac{\gamma_1^{\mathrm{II}} x_1^{\mathrm{II}}}{\gamma_1^{\mathrm{I}} x_1^{\mathrm{I}}}\right). \tag{1.22}$$

For an ideal system, in which no interactions between species occurs, the activity coefficients are unity, thus Eqn. 1.22 reduces to the van Laar equation,

$$\pi = -\frac{RT}{\bar{V}_1}\ln\left(\frac{x_1^{\mathrm{II}}}{x_1^{\mathrm{I}}}\right). \tag{1.23}$$

When a binary ideal solution, consisting of a protein and solvent, in which the protein is limited to chamber II and is rejected by the membrane, the mole fraction of solvent can be rewritten in terms of the protein mole fraction. In the binary model, the mole fraction of solvent in chamber I is unity, and Eqn. 1.23 becomes

$$\pi = -\frac{RT}{\bar{V}_1}\ln\left(1 - x_2\right). \tag{1.24}$$

At this point, the superscript II is dropped since chamber I contains no protein.

If the protein solution is dilute, the natural logarithm term can be expanded into a powers series and truncated after the first term to yield

$$\pi \approx \frac{RT}{\bar{V}_1} x_2^{\mathrm{II}}. \tag{1.25}$$

Often, the mole fraction of protein is replaced with protein mass concentration, $c_2$, because, in dilute solutions, the mole fraction per specific volume is approximately the mass concentration. This yields the van't Hoff equation

$$\pi \approx \frac{RT}{M_2} c_2, \tag{1.26}$$

where $c_2$ is the grams of protein per liter solution and $M_2$ is the protein molecular weight.

1.3.2. Osmotic Pressure of Concentrated and Crowded Solutions

While the van't Hoff equation (Eqn. 1.26) works well in dilute solutions, as the concentration of protein increases, the osmotic pressure rapidly deviates from ideality. As early as the late 19th century, the osmotic pressure of non-dilute solutions and its deviations from ideality were being studied by Ewan for concentrated sucrose solutions (Ewan 1899). Originally, it was thought that the solute was responsible for the observed deviations, thus the majority of models developed for understanding these solutions were centered on correcting for the effects of the solute. These models focus particularly on protein-protein interactions as the predominant contributor to the anomalous behavior. More recently, other models including the Scaled Particle Theory (Gibbons 1969, 1970; Chatlier and Minton 1987), mean spherical approximation (MSA) (Groot 1991; Sassi *et al.* 1996), mean-field theory (Miklavic and Woodward 1990), and Yukawa model (Lin *et al.* 2001; Xue *et al.* 2008) have been developed in an effort to explain the deviation from ideality. Nearly all of these models use a variant of the virial expansion paradigm that is based on the McMillan-Mayer theory (McMillan and Mayer 1945). However, primarily because these models are directly coupled to dilute solution theory, their application to further understanding of concentrated solution behavior has been elusive. More importantly, because these models are not focused on capturing all interactions between the available species, they are not usually effective in capturing behavioral variations in the physical phenomena due to subtle solution property changes such as pH. In addition, a number of these models lack physically significant parameters to represent the biological system.

While the modeling of osmotic pressure was dominated by solute effects, there exist some models which consider contribution due to solute-solvent interactions. In 1894, van Laar

(and later Lewis and Randall (Lewis and Randall 1961)) suggested that the appropriate concentration variable was the mole fraction of water and the free-solvent should be considered (van Laar 1984). Frazer and Myrick utilized this approach to provide excellent predictions of the osmotic pressure of concentrated sucrose solutions (Frazer and Myrick 1916). The free-solvent model was later revised by Yousef *et al.* with the addition of a solute-ion interaction parameter (Yousef *et al.* 1998a).

1.3.2.1. The Activity Coefficient Model

One of the most widely used methods for correcting the osmotic pressure for concentrated solutions was to attribute the deviations to be due to concentration dependent activity coefficients (Eqn. 1.22). While numerous models are developed assuming the activity coefficients are unity, the activity coefficient model relaxes this assumption and allows for the activity coefficient in the solution chamber (compartment II) to be a variable (while the activity coefficient in the solvent chamber is typically assumed to be unity for solute-free solution in compartment I).

Using the activity coefficient as a variable to correct for the deviations from ideality, the most prominent form of the activity coefficient model chooses the activity coefficient of the solute, $\gamma_2$, as the variable. For this derivation, beginning with Eqn. 1.22, the model follows the same assumptions to obtain Eqn. 1.25, at which point, the activity coefficient is placed into the equation, or

$$\pi = \frac{RT}{\overline{V}_1}\gamma_2 x_2, \tag{1.27}$$

and it is assumed that the activity coefficient is that of the solute since $\gamma_2 \to \infty$ as $x_2$ increases. The mole fraction of the solute and the activity coefficient of the solute are constrained to the solution chamber (compartment II), hence the compartment superscripts are dropped.

In terms of the solute mass concentration, Eqn. 1.27 is

$$\pi = \frac{RT}{M_2}\gamma_2 c_2 . \tag{1.28}$$

Various methods have been used to correlate the activity coefficient to the solute concentration including, the virial expansion of the Wilson Equation (Smith and Van Ness 1975), the Redlich-Kister expansion which yield the Margules equations (Smith and Van Ness 1975), and others (Lewis and Randall 1961; Tester and Modell 1997; Smith and Van Ness 1975; Prausnitz *et al.* 1999). However, all of the activity coefficients in these models are empirical parameters and do not have any physical basis.

1.3.2.1.1. The Osmotic Coefficient

Another model for correcting the non-ideal osmotic pressure is developed with the addition of an osmotic coefficient, $\phi_i$. The osmotic coefficient is incorporated into the van Laar equation (Eqn. 1.23) by

$$\pi = -\frac{\phi_1 RT}{\overline{V}_1}\ln\left(\frac{x_1^{\mathrm{II}}}{x_1^{\mathrm{I}}}\right), \tag{1.29}$$

or into the van't Hoff equation (Eqn. 1.26) by

$$\pi = \frac{\phi_2 RT}{M_2}c_2 , \tag{1.30}$$

where the osmotic coefficient is defined as the natural logarithm of the activity coefficient (in Eqn. 1.29), assuming the activity coefficient in the solvent chamber is unity. The osmotic

coefficient has been used as the osmotic coefficient of water (Eqn. 1.29) or as the osmotic coefficient of the protein (Eqn. 1.30).

Similar to the activity coefficient, the osmotic coefficient has a functional dependence on the concentration of the species and therefore must be calculated at each concentration. The osmotic coefficient is also an empirical parameter which does not provide physically realizable insight into the concentration dependency of the solute.

1.3.2.2. The Virial Expansion Model

Historically, the van't Hoff equation (Eqn. 1.26) has provided accurate estimations of the protein molecular weights, but only for dilute solutions. Assuming the non-ideality is coupled to solute-solute interaction, a correction of the ideal model using a power law series, similar to that as proposed by Onnes (Onnes 1901a, 1901b), with respect to the concentration variable, correct for these interactions.

A virial expansion on the van't Hoff equation which is truncated at the third term is

$$\pi = RT\left[B_1 c_2 + B_2 c_2^2 + B_3 c_2^3 + \ldots\right] \tag{1.31}$$

where $B_1$ is the first virial coefficient which is related to the protein molecular weight by

$$B_1 = \frac{1}{M_2}, \tag{1.32}$$

and $B_2$ and $B_3$ are the second and third virial coefficients which represent two-body and three-body solute-solute interactions.

Typically, the virial expansion model for the osmotic pressure of a crowded protein solution is truncated after three terms (Vilker *et al.* 1981; Wang and Bloomfield 1990; Haynes *et al.* 1992; Yousef 2000), although models have been reported which contain up to the seventh term (Ross and Minton 1977; Minton 1995). While there are various methods used for

determining the virial coefficients, there has been no functional relationship between the virial coefficients and physical parameters reported that accurately predicts the non-ideal osmotic pressure.

It is conventionally assumed that positive $B_2$ values are the result of a net negative interaction (repulsive interaction) between solute molecules, while negative $B_2$ values are observed for a net attractive interaction (George and Wilson 1994).

1.3.2.2.1. Regression

Traditionally, the virial coefficients were fit to the osmotic pressure data for dilute solutions. Given a dilute solution, the virial expansion model becomes

$$\pi = RT\left[\frac{1}{M_2}c_2 + B_2 c_2^2\right] \tag{1.33}$$

and, through linear regression, the second virial coefficient can be determined. For concentrated solutions, nonlinear regression is performed to determine the second and higher order virial coefficients.

While this method, with the appropriate number of virial coefficients, allows for a good fit to the experimental data, the values of the virial coefficients are not directly related to any physiological parameters, save for the first virial coefficient.

1.3.2.2.3. McMillan-Mayer Theory

A statistical mechanical model which attempts to understand the virial coefficients with respect to physiological phenomena is the McMillan-Mayer Theory. The McMillan-Mayer Dilute Solution Theory calculates the virial coefficients based on the potential mean force between the

protein molecules, $W_i$ (McMillan and Mayer 1945; Vilker 1976; Ross and Minton 1977). The virial coefficients are related to the potential mean force by

$$B_{\mathrm{i}} = \frac{B_i'}{M_2^i}, \tag{1.34}$$

where $B_{\mathrm{i}}$ is the i$^{\mathrm{th}}$ virial coefficient and $B_i'$ is related to the potential mean force of species $i$ via the McMillan-Mayer Theory. For a two body interaction between proteins (intra-protein species interactions), the relationship to the McMillan-Mayer Theory for the second virial coefficient, $B_{22}'$, is

$$B_{22}' = -2\pi' \int_0^\infty \left[ e^{-W_{22}/kT} - 1 \right] r^2 dr, \tag{1.35}$$

where $r$ is the center-to-center distance between two protein molecules.

In order to compare the McMillan-Mayer Dilute Solution Theory virial coefficients to those obtained from regression, Vilker *et al.* utilized a third order virial expansion model to study three bovine serum albumin (BSA) solutions. For the second and third virial coefficients, Vilker *et al.* accounted for various interactions, including electrostatic, induction, and dispersion forces. While the osmotic pressure, predicted from the McMillan-Mayer Theory virial coefficients, was the correct magnitude for all three solutions examined, the model did not fit well (Vilker 1976; Vilker *et al.* 1981). Vilker *et al.* extensively analyzed the McMillan-Mayer Theory, but speculated that the deviation might be due to additional interaction energy of a system due to the interactions of overlapping double layers between the solute macromolecules (Vilker 1976, 1981).

While recent developments for predicting the virial coefficients based on the McMillan-Mayer Theory have been pursued, none have been experimentally validated using osmotic pressure data (Mollerup and Breil 2009a, 2009b). Until now, there have been no further

explanations on the causes of the deviations between the fitted virial coefficients and those predicted by the McMillan-Mayer Dilute Solution Theory.

1.3.2.3. The Donnan Contribution to the Osmotic Pressure

To account for the movement of salt ions between the two chambers the Donnan contribution to the osmotic pressure was developed and the effect of the redistribution of the salts on the osmotic pressure, called the Donnan effect, is expressed as

$$\pi_D = RT\left[2\sqrt{\left(\frac{\overline{Z}c_2}{2M_2}\right)^2 + m_3^2} - 2m_3\right] \tag{1.36}$$

where $\overline{Z}$ is the protein charge and $m_3$ is the salt concentration in molal. At salt concentrations greater than 0.1 M, the Donnan effects is known to be negligible (Vilker *et al.* 1981).

1.3.2.3.1. The Virial Expansion Model Combined With the Donnan Contribution

The use of the virial coefficient model (truncated after the third term) or the Donnan contribution alone have limited success for varied solution properties, so in an attempt to recover some uniqueness (due to changes in the solution properties), the virial expansion model is typically coupled with the Donnan contribution to the osmotic pressure. The overall osmotic pressure is expressed as a combination of the van't Hoff equation with a virial expansion (Eqn. 1.31), $\pi_p$, and the Donnan contribution (Eqn. 1.36), $\pi_D$,

$$\pi \approx \pi_p + \pi_D \tag{1.37}$$

The sum of the protein, $\pi_p$, and salt contributions, $\pi_D$, yield the total osmotic pressure of the system, and when the virial expansion is truncated to three terms, the total osmotic pressure is

$$\pi = RT\left[\frac{1}{M_2}c_2 + B_2c_2^2 + B_3c_2^3 + 2\sqrt{\left(\frac{\overline{Z}c_2}{2M_2}\right)^2 + m_3^2} - 2m_3\right]. \quad (1.39)$$

Eqn. 1.39 allows for the osmotic pressure to be predicted if the virial coefficients are known. If the virial coefficients are unknown, the osmotic pressure data can be fit using Eqn. 1.39 to obtain the values of the virial coefficients.

1.3.2.3.2. Charge Dependency

In 1981, since the McMillan-Mayer theory was unable to completely explain the osmotic pressure of BSA with respect to varied pH of the solution (*i.e.* the charge of BSA varied), Vilker *et al.* decided to correlate the virial coefficients with the charge of the solute (Vilker *et al.* 1981). Three concentrated BSA solutions were used to develop the charge-based virial expansion model combined with the Donnan contribution,

$$\pi = \frac{RT}{M_2}\left[c_2 + B_2c_2^2 + B_3c_2^3\right] + RT\left[2\sqrt{\left(\frac{\overline{Z}c_2}{2M_2}\right)^2 + m_3^2} - 2m_3\right], \quad (1.40)$$

where the virial coefficients, $B_2$ and $B_3$, are taken to be quadratically dependent on charge, or

$$B_2 = \mathrm{A}_2 + \mathrm{B}_2\overline{Z} + \mathrm{C}_2\overline{Z}^2 \quad (1.41)$$

and

$$B_3 = \mathrm{A}_3 + \mathrm{B}_3\overline{Z} + \mathrm{C}_3\overline{Z}^2. \quad (1.42)$$

Vilker *et al.* performed non-linear regression of the osmotic pressure data in order to obtain the charge coefficients, $\mathrm{A}_i$, $\mathrm{B}_i$, and $\mathrm{C}_i$, for the i$^{th}$ virial coefficient term. This method yields numerical values for the virial coefficients, yet, similar to the nonlinear fitting of Eqn. 1.33, they lack realistic parameters and physical meaning since the charge coefficients are not given a fundamental basis.

1.3.2.3. The Free-Solvent Osmotic Pressure Model

Recently, a free-solvent model was developed that accurately describes the osmotic pressure of several globular proteins and binary solutions of proteins to near-saturation (Yousef *et al.* 1998a, 1998b, 2001, 2002a, 2002b). Unique to this modeling approach is that the associated model parameters used for predicting the osmotic pressure are physically significant and can be determined by independent methods.

A free-solvent model was originally developed by van Laar (van Laar 1894). He proposed (and later Lewis and Randall (Lewis and Randall 1961)), that the osmotic pressure was due to 'unbound' solvent in the two chambers and that the appropriate concentration variable to describe osmotic pressure is the mole fraction.

The free-solvent model relaxes the limitations of other osmotic pressure models and readdresses the potential contributions of the diffusible species to observed non-ideal behavior. As early as 1916, Frazer and Myrick analyzed the non-idealities in aqueous sucrose solutions using a free-solvent model (Frazer and Myrick 1916). Later, other researchers, in a similar approach, based their models on the van't Hoff equation but only had limited success for protein solutions up to moderate concentrations (Ling *et al.* 1980; Ling 1984; Cameron and Fullerton 1990; Fullerton *et al.* 1992). Essentially, the free-solvent model treats the hydrated protein as a separate macromolecule, and all associated water and salt ions are absorbed in its definition. In effect, this approach renders the solution ideal with respect to the remaining solvent species that have no attractive interactions. The modified mole fraction of the free-solvent is based on the hydrated macromolecule.

The free-solvent model was more recently revised by Yousef *et al.* to consider both the hydration and the ions that are influenced by the solute in describing the mole fraction of the hydrated macromolecule (Yousef *et al*. 1998a, 1998b, 2001, 2002a, 2002b). This free-solvent

model has been shown to provide excellent correlation between the observed osmotic pressure data and describe the underlying mechanisms for the observed behavior of concentrated protein environments, for both single and binary protein solutions, without any fitted parameters (Yousef *et al.* 1998a, 1998b, 2001, 2002a, 2002b). Furthermore, the osmotic pressure predicted by the free-solvent model is unique for the variation in solutions properties (such as ionic strength and pH).

For a two-chamber osmometer, with a semi-permeable membrane, letting the chamber containing the proteins denoted as compartment II and the chamber containing only the solvent and diffusible ions denoted as compartment I, the free-solvent model (Yousef *et al.* 1998a), with the mole fraction as the composition variable, is

$$\pi = -\frac{RT}{\bar{V}_1}\ln\left(\frac{x_1^{\mathrm{II}}}{x_1^{\mathrm{I}}}\right). \tag{1.43}$$

where the free-solvent mole fraction is the remaining moles of solvent that are not bound to the protein. Assuming the solution is made up of $n$ distinct species, $p$ proteins/macromolecules, and letting species 1 be the solvent, species 2 through $(p+1)$ be the proteins, and species $(p+2)$ through $n$ be the remaining diffusible species, the initial total moles of the solution in compartment II is $N^{\mathrm{II}} = \sum_{i=1}^{n} N_i^{\mathrm{II}}$, where $i$ denotes each species. The final total moles of free-solvent in chamber II, after solute-solvent interactions, is

$$N_*^{\mathrm{II}} = N^{\mathrm{II}} - \sum_{\substack{i=1 \\ i\neq 2\to p+1}}^{n} \sum_{j=2}^{p+1} \nu_{ij} N_j^{\mathrm{II}} - \sum_{j=2}^{p+1} N_j^{\mathrm{II}}\ , \tag{1.44}$$

where $N_i^K$ is the number of moles of species $i$ in compartment $K$ and $\nu_{ij}$ is the number of moles of species $i$ interacting with protein $j$ to make the hydrated macromolecule. Then, the mole fraction of free-solvent in chamber II is

$$x_1^{\mathrm{II}} = \frac{N_1^{\mathrm{II}} - \sum_{j=2}^{p+1} \nu_{1j} N_j^{\mathrm{II}}}{N_*^{\mathrm{II}} + \sum_{j=2}^{p+1} N_j^{\mathrm{II}}}, \tag{1.45}$$

while the mole fraction of free-solvent in chamber I is

$$x_1^{\mathrm{II}} = \frac{N_1^{\mathrm{I}}}{\sum_{\substack{i=1 \\ i \neq 2 \to p+1}}^{n} N_i^{\mathrm{I}}}. \tag{1.46}$$

The free-solvent model in terms of only physically relevant and measureable parameters is

$$\pi \approx \frac{RT}{\overline{V}_1} \ln\left\{ \frac{N_1^{\mathrm{I}} \left( \sum_{i=1}^{n} N_i^{\mathrm{II}} - \sum_{\substack{i=1 \\ i \neq 2 \to p+1}}^{n} \sum_{j=2}^{p+1} \nu_{ij} N_j^{\mathrm{II}} \right)}{N^{\mathrm{I}} \left( N_1^{\mathrm{II}} - \sum_{j=2}^{p+1} \nu_{1j} N_j^{\mathrm{II}} \right)} \right\}. \tag{1.47}$$

The free-solvent model for a single protein $(p = 1)$ in an aqueous solution with a single monovalent salt $(n = 3)$ is described as

$$\pi \approx \frac{RT}{\overline{V}_1} \ln\left( \frac{\left( N_1^{\mathrm{II}} + (1 - \nu_{12} - \nu_{32}) N_2^{\mathrm{II}} + N_3^{\mathrm{II}} \right) N_1^{\mathrm{I}}}{\left( N_1^{\mathrm{II}} - \nu_{12} N_2^{\mathrm{II}} \right) N^{\mathrm{I}}} \right). \tag{1.48}$$

Subscripts 1, 2, and 3 refer to the solvent, protein, and salt, respectively. The compartment containing the protein solution is denoted as superscript II, while the non-protein compartment is denoted as superscript I.

The two critical parameters in the free-solvent model for non-interacting proteins are the hydration and ion binding numbers. The hydration of macromolecules has been well documented for many proteins. Various methods have been used for determining water interaction with proteins, however it is difficult to determine exact hydration values (Rupley and Careri 1991). In addition, the value of hydration varies depending on the method used, yet the consensus from $^{17}$O NMR (nuclear magnetic resonance) and mathematical modeling is that globular proteins

contain about 1 g $H_2O$/g protein (Rupley and Careri 1991). Using the free-solvent model, the hydration regressed from concentrated osmotic pressure data is in good agreement with that from experimental methods (Yousef *et al.* 1998a, 1998b, 2001, 2002a, 2002b). More specifically, Yousef *et al.* showed that the hydration of a globular protein is 15.2 ± 0.5 molecules of water per $nm^2$ of surface area which corresponds to a single monolayer of water (Yousef *et al.* 2002b).

The interaction of ions with a protein is typically focused on specific (or tight) binding, such as calcium binding to calmodulin. However, a few studies have examined non-specific ion binding (Scatchard *et al.* 1950, 1957; Carr 1952, 1953, 1955; Tanford 1961; Curtis *et al.* 1998; Kuehner *et al.* 1999). A major limitation of the experimental methods used for non-specific ion binding, distribution method and electromotive force, is the large error associated with them, up to 40%. Alternatively, using the free-solvent model, the error associated with the ion binding value determined from regression is approximately 6%.

The parameters of the free-solvent model have been shown to be remarkably robust and well-within independently determined values when regressed relative to measured osmotic pressure for highly concentrated protein solutions (Yousef *et al.* 1998a, 1998b, 2001, 2002a, 2002b). As an example, the regressed hydration number, $\nu_{12}$, for all globular proteins measured was found to be well within the $^{17}O$ NMR approximation of 1 g $H_2O$/g globular protein (Sedykh and Sedykh 1967) but more precisely determines the value to be a monolayer of water within 2.1% when compared to each protein's SASA (Yousef *et al.* 2002b).

The robustness of the ion binding is more difficult to determine due to the larger error in experimental values. However, the ion binding value is obtained from the free-solvent model seems to be robust. For example, for BSA in 0.15 M NaCl, pH 7.4, using the value of hydration of 1.177 g $H_2O$/g BSA (Yousef *et al.* 1998b), if the value of ion binding is changed by a single ion (from 8.81 mol NaCl/mol BSA (Yousef *et al.* 1998b) to 9.81 mol NaCl/mol BSA), the

osmotic pressure predicted via the free-solvent model changes from 73 psi to 57 psi (for a protein concentration of 450 g BSA/L solution).

## 1.4. Scope of This Work

The focus of this work is on the osmotic pressure of crowded and concentrated macromolecule solutions and further understanding the free-solvent osmotic pressure model and its applications.

Herein, it is also shown that the free-solvent model can also provide an accurate estimation of the solvent accessible surface area (SASA) of several globular macromolecules, including proteins and sugar. The SASA is in agreement with that obtain from the molecular structures of the proteins when available. The free-solvent model physical parameters are also in agreement with those determined from experimental and/or computational methods, adding further validity to the free-solvent model. The method developed in this dissertation allows for an experimental alternative to obtaining the SASA of globular macromolecules.

The free-solvent model is also used to provide new insight into the activity coefficient and the second virial coefficient. These empirical parameters are given a new physical meaning based on solute-solvent interactions; the activity coefficient was previously not based on fundamental physical parameters. Here, the activity coefficient was shown to be dependent on only independently measureable and physically realistic parameters.

The second virial coefficient was previously thought to be dependent on the interactions between solute molecules (in the form of either repulsive or attractive solute-solute interactions). Here, the second virial coefficient was correlated to the ratio between the ionic strength of the protein influenced solvent and that of the bulk solution. Furthermore, the second virial coefficient is analyzed to determine the conditions and solution properties required for obtaining positive,

negative, and zero values. Using the ratio between the ionic strength of the protein influenced solvent and that of the bulk solution, when the ratio is less than 1 (*i.e.* the ionic strength of the protein influenced solvent is lower than the ionic strength of the bulk), the second virial coefficient is a positive value; when the ratio is greater than 1, the second virial coefficient is a negative value. This suggests that protein salts out before salt precipitates because the ionic strength when the protein influenced solvent is greater than the ionic strength in the bulk. When the hydration of the bound salt ions is considered, the second virial coefficient is zero when the ratio of the ionic strengths is 1. This work suggests that the free-solvent model can be used to understand the physical phenomena of salting-out, and possibly explain the observations of the Hofmeister series.

The free-solvent osmotic pressure model is revised to provide a generalized free-solvent model with accounts for protein-protein interactions in the form of homo- and hetero-multimers; new physically realistic parameters are incorporated into the closed-form solution of the developed free-solvent model which captures the interactions for protein multimers. The generalized model developed can be used to understand the osmotic pressure of crowded protein solutions for any number of solvent species (salts and water) and any number of macromolecules. Several case scenarios are developed to understand the free-solvent model for protein-protein interactions which are often observed in solution. The effects of the physical parameters on the osmotic pressure is also presented.

A novel osmometer is developed which allows for the solution studied to be concentrated. This concentrating osmometer allows for a single solution to be used to obtain an entire osmotic pressure-concentration profile while using approximately an order of magnitude less grams of protein. The concentrating osmometer was tested using two initial BSA solutions and the resulting osmotic pressures were compared to those available in literature. The practical

considerations of the concentrating osmometer and its possible applications within chemistry, biochemistry, and biology are discussed.

# CHAPTER 2.

# DETERMINING THE SOLVENT ACCESSIBLE SURFACE AREA OF PROTEINS WHEN STRUCTURAL DATA IS UNAVAILABLE USING OSMOTIC PRESSURE

## 2.1. Abstract.

Here, an algorithm that predicts solvent accessible surface area (SASA) using concentrated solution osmotic pressure data is developed. Six proteins are used for verification and two macromolecules are predicted using this method. The free-solvent model regressed physical parameters agree with those from literature, when available. The results illustrate that this novel method can provide an important experimental alternative in estimating the SASA for proteins, and possibly, their complexes in solution.

## 2.2. Solvent Accessible Surface Area

Computational estimations of the SASA, first introduced by Lee and Richards (Lee and Richards 1971), has tremendous applicability in terms of understanding free energies of solvent-protein interaction, protein-protein interactions, protein folding, and many other thermodynamic properties of the protein solution (Lee and Richards 1971; Greer and Bush 1978). Although a number of methods exist to estimate this important parameter, nearly all of them critically rely on the availability of the 3D structure of the protein of interest.

## 2.3. Methods for Determining the Structure of a Protein

Currently, two methods for determining the 3D structure of a protein are x-ray crystallography and nuclear magnetic resonance (NMR). For most proteins, only one of these two

methods is available to determine the structure due to the limitations of each method. In addition, the preparation of the sample for structural determination is unknown and is typically very difficult; each protein which is to be studied for structure determination needs to have the solution properties adjusted until a viable one is found.

Furthermore, the study of SASA is exacerbated by the vast number of proteins (approximately 1 million (Liu *et al.* 2004)) and limited number of protein structures deposited into the Protein Data Bank (approximately 94,000[*]). Of the 94,000 protein structures deposited into the Protein Data Bank, some proteins have their structures deposited multiple times based on the interaction of various ligands.

### 2.3.1. X-Ray Crystallography

X-ray crystallography has been used for decades to determine the structure of proteins. An x-ray beam is diffracted by the atoms in the crystallized protein, and, by measuring the diffracted beam (angle and intensity), the structure can be determined.

This method requires the protein to be crystallized, and thus can only get a single structure of the protein. The determined conformation may not occur often (or at all) in solution; however, x-ray crystallography can be used to obtain a structure of the protein given that it can be crystallized.

The limitations of this method for structure determination are the difficulty of determining the crystallization conditions, that the determined structure represents a crystal/rigid structure and/or non-realistic solution structure, and that the number of proteins which can have their structure solved via crystallography is limited since the proteins are unable to be crystallized (such as membrane proteins). In addition, crystal structures often suffer from crystal packing

[*] As of May 2013.

effects which may alter association interfaces or introduce non-specific and non-physiological interactions.

### 2.3.2. Nuclear Magnetic Resonance

The use of NMR for structure determination has become increasingly popular since many of the solution constraints of crystallography are relaxed. This method can obtain the structure in various solutions, and since the structure is that of the protein in solution, the structure is physiologically realistic. Often numerous structures can be obtained for a given sample which can provide information about the dynamics of a protein in solution.

For NMR, the nuclear spins of some atoms within the protein (such as $^{1}H$, $^{13}C$, and $^{15}N$) orient themselves when an external magnetic field is applied and by applying a second field, these atoms resonate, and the interactions between the different atomic spins can be used to determine their position with respect to other atoms. Using the atom distance relationships, the 3D structure can be obtained.

Since the distance relationship is not available for all atoms, the structural information is incomplete, but can normally be inferred. This method is constrained by the molecular mass since proteins larger than 15 kDa are often difficult to determine structure due to the overlapping distance relationships.

## 2.4. Methods

Using available concentrated osmotic pressure data, the SASA is predicted for various macromolecules. The free-solvent model (Eqn. 2.1) is used to model the osmotic pressure data, and using nonlinear regression (TableCurve 2D (Systat Software, San Jose, CA, USA) and Datafit (Oakdale Engineering, Oakdale, PA, USA)), the values of protein hydration and

protein-ion binding are determined. The resulting values for hydration and ion binding are compared to literature values, when available.

$$\pi \approx \frac{RT}{\overline{V}_1} \ln\left( \frac{\left(N_1^{II} + (1 - \nu_{12} - \nu_{32})N_2^{II} + N_3^{II}\right)N_1^{I}}{\left(N_1^{II} - \nu_{12}N_2^{II}\right)N^{I}} \right) \tag{2.1}$$

The predicted SASA (osmotic pressure-based SASA) for each protein is compared to the SASA calculated using molecular modeling software with the molecular structure(s).

### 2.4.1. Macromolecules

The osmotic pressure of hen egg lysozyme (HEL), bovine β-lactoglobulin (BLG), ovalbumin (OVA), bovine serum albumin (BSA), sheep hemoglobin (Hb), bovine immune-gamma globulin (IgG), calf lens α-crystallin, and sucrose are available in the literature and the SASA of each is predicted from the free-solvent model.

#### 2.4.1.1. Hen Egg Lysozyme

The osmotic pressure of HEL (molecular weight, 14.5 kDa) in 0.15 M KCl, pH 7.0, 25°C and 0.15 M NaCl, pH 7.0, 25°C (Yousef 2000; Yousef *et al.* 2002b) were previously modeled using the free-solvent model, and the values of hydration and ion binding are available (Yousef 2000; Yousef *et al.* 2002b).

The molecular structure of HEL, determined by crystallography, is available in the Protein Data Bank (PDB: 4LYZ (Diamond 1974)).

#### 2.4.1.2. Bovine β-Lactoglobulin

The osmotic pressure data, by Parker *et al.* (Parker *et al.* 2005), for aqueous solutions of BLG (molecular weight, 18.4 kDa) in 0.1 M NaCl at room temperature and three pH (5.1, 6.0,

and 8.0) have been modeled using the free-solvent model and the regressed hydration, ion binding, and SASA were determined (McBride and Rodgers 2012).

BLG has three crystallographic structures available in the Protein Data Bank (PDB: 2Q2M (Vijayalakshmi *et al.* 2008), 3NPO (Loch *et al.* 2011), and 3BLG (Qin *et al.* 1998)).

2.4.1.3. Ovalbumin

The osmotic pressure data for OVA (molecular weight, 45 kDa), by Yousef *et al.*, in 0.15 M NaCl and 0.50 M NaCl solutions at pH 7.0 and 25ºC were previously modeled using the free-solvent model and the hydration and ion binding values are available (Yousef *et al.* 2001).

The x-ray diffraction structure is available for OVA (PDB: 1OVA (Stein *et al.* 1991) and 1UHG (S-OVA) (Yamasaki *et al.* 2003)).

2.4.1.4. Bovine Serum Albumin

The osmotic pressure data for BSA (molecular weight, 66 kDa), by Vilker *et al.* (Vilker *et al.* 1981), in 0.15 M NaCl solutions at 25ºC and pH 4.5, 5.4, and 7.4 were previously modeled using the free-solvent model and the hydration and ion binding are available (Yousef *et al.* 1998b).

Until recently, the structure of BSA was unavailable, so a homology model of BSA was created using human serum albumin (Appendix A). The homology model is used to compute the SASA with the molecular modeling software. In addition, the available crystal structures of BSA are also be used to compute the SASA (PDB: 3V03 (Majork *et al.* 2012) and 4F5S (Bujacz 2012)).

2.4.1.5. Sheep Hemoglobin

Hb (molecular weight, 69 kDa) has been extensively studied to understand its structure and function, and was one of the first proteins for which a molecular structure was determined (Perutz *et al.* 1968). The osmotic pressure data of Hb, by Adair and published by Dick (Dick 1967), was used to predict the SASA. The osmotic pressure experiments were conducted for Hb in 0.10 M KCl solutions at pH 7.43 and 0ºC. The free-solvent model and its regressed values for hydration and ion binding have been previously reported (M$^{c}$Bride and Rodgers 2012).

The x-ray diffraction structure is available for sheep methemoglobin (PDB: 2QU0 (Neelagandan *et al.* 2007)).

2.4.1.6. Bovine Immuno-gamma Globulin

The osmotic pressure data for IgG (molecular weight, 155 kDa), by Yousef *et al.*, for 0.13 M salts solution at pH 7.4 and room temperature was previously modeled using the free-solvent model and the values of hydration and ion binding are available (Yousef *et al.* 1998a).

IgG has an x-ray diffraction structure available (PDB: 1IGT (Harris *et al.* 1997)).

2.4.1.7. Calf Lens α-Crystallin

The protein α-crystallin is the major component of mammalian lens. It is found as a dimer of two different subunits, αA-crystallin (αA) and αB-crystallin (αB). The αA and αB subunits have molecular weights of approximately 20 kDa each (Doss *et al.* 1997; Babizhayev *et al.* 2002, 2003; Regini *et al.* 2007). However, *in-vivo*, bovine and calf lens α-crystallin form aggregates of 30 - 50 subunits which have an average molecular weight of 800 kDa (Thomson and Augusteyn 1988; Bassi *et al.* 1995; Doss *et al.* 1997; Regini *et al.* 2007).

These aggregates have a ratio of 3αA:1αB for bovine lens α-crystallin (Singh *et al.* 1996; Doss *et al.* 1997; Horwitz *et al.* 1999) and Regini *et al.* determined that 39 subunits form the bovine lens α-crystallin aggregate (Regini *et al.* 2007). Here it will be assumed that calf lens α-crystallin forms a 39 subunit aggregate for predicting the SASA of the monomer. The molecular structure for calf lens α-crystallin (or its subunits) has not yet been determined.

The osmotic pressure data of calf lens α-crystallin (molecular weight, 800 kDa), by Vérétout *et al*. (Vérétout *et al*. 1989), in 0.15 M KCl, pH 6.8, room temperature has been modeled using the free-solvent model (M$^{c}$Bride and Rodgers 2012). The regressed values for hydration and ion binding are compared to literature values. In addition, the osmotic pressure data of calf lens α-crystallin in 0.017 M KCl, pH 6.8, room temperature (Vérétout *et al*. 1989) is fit using the free-solvent model to obtain the regressed values of the hydration and ion binding.

Since the molecular structure for α-crystallin is unavailable, the SASA of the aggregate and monomer will be predicted based on the hydration and assuming a 39 monomer aggregate, respectively.

2.4.1.8 Sucrose

The osmotic pressure of sucrose is available for concentrated solutions in water at 30$^{o}$C (Frazer and Myrick 1916). The free-solvent model is fit to the osmotic pressure data (assuming only hydration since no salt was present in the solution) and the regressed hydration value is used to predict the SASA. The regressed hydration value is compared to the hydration of sucrose available in literature.

The crystal structure is unavailable for sucrose; however various studies have been reported on the size of sucrose. These studies are used as a comparison for the predicted SASA.

### 2.4.2. Computational Methods for Computing Solvent Accessible Surface Area

Five molecular modeling software are used to calculate SASA: Swiss-Pdb Viewer (Guex and Peitsch 1997), MOLMOL (Koradi *et al.* 1996), UCSF Chimera (Pettersen *et al.* 2004), VegaZZ (Pedretti *et al.* 2002), and GETAREA (Fraczkiewicz and Braun 1998). Prior to computing the SASA, hydrogens are added to each molecular structure using Swiss-Pdb Viewer (Guex and Peitsch 1997).

Swiss-Pdb Viewer (Guex and Peitsch 1997) and MOLMOL (Koradi *et al.* 1996) allow for the accuracy of the SASA calculation to be adjusted. These quantities (quality for Swiss-Pdb Viewer (Guex and Peitsch 1997) and precisions for MOLMOL (Koradi *et al.* 1996)) are adjusted from 1 - 6 to determine the effect on SASA. UCSF Chimera (Pettersen *et al.* 2004), VegaZZ (Pedretti *et al.* 2002), and GETAREA (Fraczkiewicz and Braun 1998) do not allow for the calculation to be adjusted.

### 2.4.3. Effect of the Experimental Method Used for Protein Structure Determination on the Solvent Accessible Surface Area

While the range of SASA calculated can be determined using multiple molecular modeling software, it is important to: (1) determine the variation of the SASA for solution-based (NMR) structures and (2) compare the SASA for the crystallographic and NMR structures. These will be studied for human β-defensin-2. The crystallographic structure of human β-defensin-2 (PDB: 1FD3 (Hoover *et al.* 2000)) contains four monomers. The SASA of each monomer is computed separately. The NMR structure (1FQQ (Sawai *et al.* 2001)) has twenty structures of a single monomer, and all twenty structures are used to compute the SASA.

### 2.4.4. Predicting the Solvent Accessible Surface Area From Osmotic Pressure

Here the highly robust free-solvent model, that uses osmotic pressure data from proteins at near-saturation concentration, is used to extract the SASA with an accuracy equivalent to computational methods that require the molecular structure of the protein.

Unique to this modeling approach is that the associated free-solvent model parameters used for predicting the osmotic pressure are physically significant and can often be verified by independent methods. Recently, the free-solvent model regressed hydrations were found to correlate to a monolayer of water for several globular proteins (Yousef *et al.* 2002b).

The purpose of this study is to relate the measured osmotic pressure of aqueous protein solutions to their SASA via the free-solvent model. This method for predicting the SASA via osmotic pressure can offer understanding of the protein surface area for soluble, globular proteins for which the molecular structures have not yet been solved.

## 2.5. Results and Discussion

### 2.5.1. Effect of the Experimental Method Used for Protein Structure Determination on the Solvent Accessible Surface Area

The SASA was computed for human β-defensin-2 using its crystallographic and NMR structures. The crystallographic structure file contained a 4-mer and each monomer subunit within the structure was used to compute the SASA range. The NMR structure file contained 20 monomer structures and each structure was used to determine the SASA range of solution-based structures.

The SASA range computed for the x-ray crystal structure of human β-defensin-2 (PDB: 1FD3 (Hoover *et al.* 2000)) is 2,177 - 3,113 $Å^2$. This is a significantly large range for the SASA

of a small protein (41 amino acids). The SASA range for the NMR structures of human β-defensin-2 is similarly large, 2,169 - 3,387 $Å^2$.

While NMR structures are thought to be more accurate representations of the "true" SASA, both methods for structure determination yield large variations in the SASA, thus advocating for an alternative, more accurate, method for SASA determination.

### 2.5.2. Free-Solvent Model Regression of Osmotic Pressure Data

The free-solvent model best fit for the osmotic pressure of each macromolecule is shown in Figures 2.1 - 2.6. As can be seen, the free-solvent model, using the regressed parameters (solid curve), provides an excellent fit to all of the experimental data over the entire concentration range for each case. The regressed hydration, $\nu_{12}$, and ion binding, $\nu_{32}$, values for each macromolecule are shown in Tables 2.1 and 2.2.

#### 2.5.2.1. Hen Egg Lysozyme

Due to the lack of concentrated osmotic pressure data, regression on both parameters gave non-physiologically realistic values. Thus, only the regressed hydration was able to be determined using experimental ion binding values of HEL.

Using the experimental values of ion binding, Yousef *et al.* found the regressed hydration for HEL to be 0.724 ± 0.008 g $H_2O$/g HEL and 0.734 ± 0.003 g $H_2O$/g HEL (for an ion binding of 2 mol salt/mol HEL (Curtis *et al.* 1998)) and 1.614 ± 0.010 g $H_2O$/g HEL and 1.595 ± 0.007 g $H_2O$/g HEL (for an ion binding value of 4 mol salt/mol protein (Kuehner *et al.* 1999)) for HEL in 0.15 M NaCl and 0.15 M KCl, respectively (Yousef 2000; Yousef *et al.* 2002b). However, the large error associated with ion binding methods (20 - 40%) may have an effect on the regressed hydration and ultimately on the predicted SASA for HEL.

The free-solvent model regressed hydration values of HEL are consistent with that which was calculated by molecular dynamics (0.93 g $H_2O$/g HEL) (Hamaneh and Buck 2007) and (0.98 g $H_2O$/g HEL) (Panuszko *et al.* 2012) when an ion binding of 2 mol salt/mol HEL is used. The hydration values of HEL, for an ion binding of 4 mol salt/mol HEL, are similar to that of the two hydration layers.

2.5.2.2. Bovine β-Lactoglobulin

The regressed hydration values of BLG are 0.809 ± 0.0574 g $H_2O$/g BLG, 0.942 ± 0.0138 g $H_2O$/g BLG, and 1.313 ± 0.0206 g $H_2O$/g BLG in 0.1 M NaCl, pH 5.1, 6.0, and 8.0, respectively. These values are consistent with the hydration determined for BLG using $^{17}O$ NMR measurements (0.72 g $H_2O$/g BLG) (Mattea *et al.* 2008).

The regressed values of ion binding are 1.76 ± 0.068 mol NaCl/mol BLG, 1.17 ± 0.285 mol NaCl/mol BLG, and 1.57 ± 0.102 mol NaCl/mol BLG for BLG in 0.1 M NaCl, pH 5.1, 6.0, and 8.0, respectively. No ion binding studies, experimental or computational, were found for BLG for comparison.

The covariances resulting from the BLG results were $3.9 \times 10^{-8}$, $1.1 \times 10^{-5}$, and $2.1 \times 10^{-7}$, for pH 5.1, 6.0, and 8.0, respectively. Thus, the values for hydration and ion binding are unique and independent of each other.

Using the literature value of BLG hydration (0.72 g $H_2O$/g BLG (Mattea *et al.* 2008)), the regressed ion binding values for BLG in 0.1 M NaCl, pH 5.1, 6.0, and 8.0 which were 0.52 ± 0.150 mol NaCl/mol BLG, -0.72 ± 0.230 mol NaCl/mol BLG, and -1.71 ± 0.412 mol NaCl/mol BLG, respectively. The latter two values are non-physiological which suggests that the hydration of BLG is larger than the literature value.

2.5.2.3. Ovalbumin

Yousef *et al.* used the free-solvent model to determine the regressed hydration values for OVA in 0.01 M, 0.15 M, and 0.5 M NaCl at pH 7.0 (Yousef *et al.* 2001). These regressed hydrations are similar to those determined by vapor binding (0.54 - 0.82 g $H_2O$/g OVA (Bull and Breese 1968)) and to that which was modeled by Clark *et al.* (0.78 g $H_2O$/g OVA (Clark *et al.* 1982)). No ion binding studies have been published for OVA with NaCl for comparison.

Yousef *et al.* concluded that the ion binding value for OVA in 0.01 M NaCl is incorrect due to the low ionic strength causing a large Debye length (30 Å), reducing the ionic screening (Yousef *et al.* 2001). Thus, only the hydration values of OVA in 0.15 M and 0.5 M NaCl are used in predicting the SASA.

2.5.2.4. Bovine Serum Albumin

Yousef *et al.* determined the values of hydration for BSA by regression of the osmotic pressure data by Vilker *et al*. (using literature values of ion binding for BSA (Yousef 1998b)). The regressed values of hydration for BSA are similar to the hydration values determined from the frictional coefficient (1.07 g $H_2O$/g BSA (Tanford 1961)).

2.5.2.5. Sheep Hemoglobin

The free-solvent model regressed hydration value of sheep hemoglobin ($0.869 \pm 0.0118$ g $H_2O$/g Hb) is consistent with the hydration of bovine and human hemoglobin (0.51 g $H_2O$/g Hb) that was determined using static and dynamic light scattering (Arosio *et al.* 1999, 2002).

The free-solvent model regressed ion binding value of sheep hemoglobin ($5.20 \pm 0.135$ mol KCl/mol Hb) is in excellent agreement with chloride ion binding values

(6 mol $Cl^-$/mol Hb bound at pH 7.4) determined for bear, horse, and bovine hemoglobin using molecular dynamic simulations (De Rosa *et al.* 2004). The covariance value is $4.2x10^{-8}$ for the free-solvent model parameters.

The free-solvent model was also used to regress on the ion binding of Hb in 0.1 M KCl using the literature value of hydration. When the free-solvent model is plotted using the literature hydration (0.51 g $H_2O$/g Hb (Arosio *et al.* 1999, 2002)) and its corresponding, regressed ion binding (1.77 ± 0.101 mol KCl/mol Hb), the fit does not agree with the osmotic pressure data.

2.5.2.6. Bovine Immuno-gamma Globulin

For IgG, Yousef *et al.* determined the value of hydration to be 1.11 ± 0.041 g $H_2O$/g IgG (Yousef *et al.* 1998a). Limited hydration data of IgG exists in the literature. Goryunov and Käiväräinen studied the interaction of $H_2O$ and $D_2O$ with IgG at low temperatures (-35°C to -10°C) using $^1H$ NMR (Goryunov and Käiväräinen). The authors found that the hydration of IgG increased as the temperature increased, and at -10°C, the hydration of IgG was approximately 0.55 g $H_2O$/g IgG (Goryunov and Käiväräinen). The regressed value of hydration determined by Yousef *et al.* follows the trend observed by Goryunov and Käiväräinen and also agrees with the $^{17}O$ NMR approximation of 1 g $H_2O$/g globular protein (Sedykh and Sedykh 1967). No ion binding studies exist for IgG for comparison.

2.5.2.7. Calf Lens α-Crystallin

The free-solvent model regressed hydration of α-crystallin in 0.017 M KCl, pH 6.8, room temperature (1.465 ± 0.1275 g $H_2O$/g α-crystallin) and 0.15 M KCl, pH 6.8, room temperature (1.433 ± 0.0409 g $H_2O$/g α-crystallin) (McBride and Rodgers 2012) are in very good agreement

with the experimentally determined hydration of young adult bovine lens α-crystallin (1.9 g $H_2O$/g α-crystallin) using the NMR spin-echo technique (Babizhayev *et al.* 2002, 2003).

The regressed ion binding values for α-crystallin in 0.017 M KCl, pH 6.8, room temperature (10.40 ± 2.92 mol KCl/mol α-crystallin) and 0.15 M KCl, pH 6.8, room temperature (169 ± 5.27 mol KCl/mol α-crystallin) (M$^c$Bride and Rodgers 2012) were unable to be compared since no ion binding studies, experimental or computational, are available in literature.

α-crystallin has a large number of charges exposed on the surface near its isoelectric point, 7.0 (Xia *et al.* 1994). Furthermore, since the osmotic pressure was studied at a pH close to its isoelectric point, it is reasonable to assume that α-crystallin will bind a large number of ions at pH 6.8 and have a similar ionic strength in the monolayer as the bulk ionic strength.

The ionic strength of the monolayer is 0.009 ± 0.0016 for α-crystallin in 0.017 M KCl, pH 6.8, room temperature and 0.147 ± 0.0004 for α-crystallin in 0.15 M KCl, pH 6.8, room temperature. The deviation of the monolayer ionic strength for the 0.017 M KCl solution may be due to the charge repulsion between the protein molecules due to the low ionic strength (*i.e.* large Debye length, 23 Å). The covariance value is $2.0 \times 10^{-3}$ and $1.6 \times 10^{-5}$ for the calf α-crystallin free-solvent model regressed parameters in 0.017 M KCl and 0.15 M KCl, respectively.

If the literature value of hydration, 1.9 g $H_2O$/g α-crystallin (Babizhayev *et al.* 2002, 2003), is used to regress on the ion binding for α-crystallin in 0.017 M KCl, the value of the regressed ion binding is 20.59 ± 0.444 mol KCl/mol α-crystallin; However, the literature value cannot be used for α-crystallin in 0.15 M KCl since the saturation limit of α-crystallin, given a hydration of 1.9 g $H_2O$/g α-crystallin (Babizhayev *et al.* 2002, 2003), is 379 g/L solution and the osmotic pressure data is measured for concentrations up to 387 g/L solution.

2.5.2.8. Sucrose

The interaction of sucrose and water is well known, however, no interaction between sucrose and salt is possible in the solution studied by Adair (Dick 1967); the osmotic pressure was measured for up to near-saturation concentrations of sucrose in water. Thus, the free-solvent model is revised to only incorporate a hydration term, or

$$\pi \approx \frac{RT}{\overline{V}_1} \ln\left( \frac{\left(N_1^{\mathrm{II}} + (1-\nu_{12})N_2^{\mathrm{II}}\right)N_1^{\mathrm{I}}}{\left(N_1^{\mathrm{II}} - \nu_{12}N_2^{\mathrm{II}}\right)N^{\mathrm{I}}} \right), \tag{2.2}$$

where $N_1^{\mathrm{I}} = N^{\mathrm{I}}$ since no salt is present in either solution.

Using this model (Eqn. 2.2), the regressed hydration for sucrose in water at 30°C is 0.220 ± 0.0019 g $H_2O$/g sucrose (or 4.18 ± 0.036 mol $H_2O$/mol sucrose). This regressed value of hydration agrees well with the hydration of sucrose reported by Scatchard (3.5 - 6.0 mol $H_2O$/mol sucrose) (Scatchard 1921). Recently, Engelsen and Pérez used molecular dynamics and various models to calculate the hydration of sucrose to be between 5 and 13 molecules of water per sucrose molecule (Engelsen and Pérez 1996). Although the reported hydration values by both of these groups came after the initial study of the osmotic pressure of sucrose reported by Frazer and Myrick, the value of hydration for sucrose was determined, from osmotic pressure using the free-solvent model, to be 4 - 6 mol $H_2O$/mol sucrose (Frazer and Myrick 1916). Einstein (Einstein 1956) also observed a hydration of sucrose within the range of Frazer and Myrick (Frazer and Myrick 1916) and Scatchard (Scatchard 1921).

2.5.3. Solvent Accessible Surface Area Determined Computationally

The SASA determined by the computational software for the proteins which had available molecular structures are shown in Table 2.3.

The effect of quality and precision were determined for Swiss-Pdb Viewer (Guex and Peitsch 1997) and MOLMOL (Koradi *et al.* 1996). Changing the quality for Swiss-Pdb Viewer (Guex and Peitsch 1997) and the precision for MOLMOL (Koradi *et al.* 1996) had no observable trend for the computed SASA. For all calculations, a precision of 6 and quality of 6 were used for MOLMOL (Koradi *et al.* 1996) and Swiss-Pdb Viewer (Guex and Peitsch 1997), respectively.

Using the molecular structure of HEL (PDB: 4LYZ (Diamond 1974)), the SASA range was computed to be 5,732 - 7,927 $Å^2$. Using the available molecular structures, the SASA of BLG was computed to be 7,724 - 8,628 $Å^2$ (PDB: 2Q2M (Vijayalakshmi *et al.* 2008)), 7,666 - 8,644 $Å^2$ (PDB: 3NPO (Loch *et al.* 2011)), and 7,500 - 8,304 $Å^2$ (PDB: 3BLG (Qin *et al.* 1998)). The computational SASA computed for OVA was 13,556 - 16,434 $Å^2$ (PDB: 1OVA (Stein *et al.* 1991)) and 14,058 - 16,375 $Å^2$ (PDB: 1UHG (S-OVA) (Yamasaki *et al.* 2003)). Using the homology model and the two molecular structures of BSA, the SASA range was computed to be 27,746 - 28,188 $Å^2$ (1BM0 homology model), 27,495 - 34,563 $Å^2$ (PDB: 3V03 (Majork *et al.* 2012)), and 28,646 - 35,194 $Å^2$ (PDB: 4F5S (Bujacz 2012)). The SASA computed for Hb was 23,499 - 26,100 $Å^2$ (PDB: 2QU0 (Neelagandan *et al.* 2007)). The SASA range for IgG (PDB: 1IGT (Harris *et al.* 1997)) was 61,809 - 65,916 $Å^2$.

Although no molecular structure exist for α-crystallin or sucrose, the SASA can be approximated by using the dimensions of the molecules. However, for α-crystallin, it is described as a fenestrated sphere, but no information on the size of the fenestrations has been reported. The α-crystallin aggregate is approximately 169 Å in diameter and has a wall thickness of 10 Å (Regini *et al.* 2007). These yield a minimum SASA of approximately 160,000 $Å^2$.

Using the radius of sucrose determined by the Stokes-Einstein equation (4.6 Å (Walstra 2002)), the SASA is estimated to be 265 $Å^2$.

2.5.4. Predicting the Solvent Accessible Surface Area From Osmotic Pressure

The fact that the hydration and ion binding values are physically relevant and strongly independent in the regression analysis provides a strong indication of the validity of the free-solvent model for predicting the SASA.

The SASA was predicted for each protein using the regressed hydration and assuming that the 15.2 molecules of water per $nm^2$ of surface area (Yousef *et al.* 2002b). The predicted SASA calculated based on hydration are shown in Table 2.3. The SASA predicted for BLG in 0.1 M NaCl, pH 8.0, both OVA solutions, all three BSA solutions, Hb, and IgG are all in good agreement with those calculated by the computational software.

The SASA predicted from the regressed hydrations of HEL in 0.15 M NaCl, pH 7.0 are 3,783 ± 42 Å$^2$ ($\nu_{12} = 0.724$ g $H_2O$/g HEL) and 8,433 ± 52 Å$^2$ ($\nu_{12} = 1.614$ g $H_2O$/g HEL). For HEL in 0.15 M KCl, pH 7.0, the predicted SASA are 3,835 ± 16 Å$^2$ ($\nu_{12} = 0.734$ g $H_2O$/g HEL) and 8,333 ± 366 Å$^2$ ($\nu_{12} = 1.595$ g $H_2O$/g HEL). The deviation of the predicted and computational SASA for both HEL solutions may be due to the choice of the ion binding value or the lack of near-saturation osmotic pressure data.

The predicted SASA for BLG in 0.1 M NaCl, pH 5.1, 6.0, and 8.0 are 5,436 ± 93 Å$^2$, 6,330 ± 386 Å$^2$, and 8,823 ± 138 Å$^2$, respectively. The deviation of the SASA for BLG in 0.1 M NaCl at pH 5.1 and 6.0 from the molecular structure may be due to the lack of near-saturation osmotic pressure data.

For OVA in 0.15 M NaCl and 0.5 M NaCl, the predicted SASA are 14,133 ± 657 Å$^2$ and 14,625 ± 657 Å$^2$, respectively. For BSA in 0.15 M NaCl, pH 4.5, 5.4, and 7.4, the predicted SASA are 27,000 ± 146 Å$^2$, 27,583 ± 146 Å$^2$, and 28,533 ± 121 Å$^2$, respectively. The predicted SASA for Hb and IgG are 21,897 ± 302 Å$^2$ and 62,660 ± 2,343 Å$^2$, respectively.

The SASA predicted for α-crystallin in 0.017 M KCl and 0.15 M KCl are 427,999 ± 37,249 $Å^2$ and 418,651 ± 11,949 $Å^2$, respectively. These values differ from the SASA estimated using the diameter of α-crystallin which may be due to error in one or both of these methods. However, using the SASA from the osmotic pressure and assuming calf lens α-crystallin contains aggregates of 39 subunits and no loss in surface area during aggregation, the SASA per subunit (20 kDa) is 10,974 ± 955 $Å^2$ (0.017 M KCl) and 10,735 ± 306 $Å^2$ (0.15 M KCl), respectively. The SASA predicted for α-crystallin, while unable to computationally verified, falls on the expected monolayer of water for the 39-mer, as well as the predicted monolayer (Figure 2.7).

The SASA predicted by the hydration of sucrose is 27.5 ± 0.24 $Å^2$. This predicted SASA of sucrose does not agree well with the expected SASA calculated based on a sphere (using the hydrodynamic radius of sucrose). This may be due to the error in determining the hydrodynamic radius (Stokes-Einstein equation) or because the hydrodynamic radius may not correspond to a monolayer of water. However, the hydration of sucrose determined from the free-solvent model regression of the osmotic pressure data yields a value similar to that of other studies (Frazer and Myrick 1916; Scatchard 1921; Einstein 1956; Engelsen and Pérez 1996). If the hydrodynamic radius is assumed to be correct, the SASA, estimated to be 265 $Å^2$, yields a hydration value of 40.28 mol $H_2O$/mol sucrose. This value of hydration is unrealistic and thus this SASA is unlikely to occur in solution.

### 2.5.5. Osmotic Pressure Sensitivity With Respect to the Free-Solvent Model Protein Hydration

Previously, Yousef *et al.* showed that the osmotic pressure is sensitive to both of the free-solvent model parameters in the near-saturation concentration region. Assuming a single

macromolecule in a monovalent salt solution, the sensitivity of the free-solvent model with respect to the hydration parameter is

$$\frac{\partial \pi}{\partial \nu_{12}} = \frac{RT}{\overline{V}_1}\left( \frac{x_2^{\mathrm{II}} - x_2^{\mathrm{II}} x_1^{\mathrm{II}}}{x_1^{\mathrm{II}}} \right), \tag{2.3}$$

where $x_i^{\mathrm{II}}$ is the mole fraction of water ($i=1$) and macromolecule ($i=2$) in the solution chamber. It can be seen that for concentrated solutions, as $x_1^{\mathrm{II}} \to 0$, the result is a dramatic increase in the sensitivity of the osmotic pressure with respect to the hydration parameter, or $\frac{\partial \pi}{\partial \nu_{12}} \to \infty$. While in a dilute solution, as $x_2^{\mathrm{II}} \to 0$, the sensitivity of the osmotic pressure with respect to hydration is removed, or $\frac{\partial \pi}{\partial \nu_{12}} \to 0$.

2.5.6. Osmotic Pressure Sensitivity With Respect to the Free-Solvent Based Protein Solvent Accessible Surface Area

The sensitivity of the osmotic pressure with respect to the SASA for a macromolecule is

$$\frac{\partial \pi}{\partial (\mathrm{SASA})} = \frac{\partial \pi}{\partial \nu_{12}} \cdot \frac{\partial \nu_{12}}{\partial (\mathrm{SASA})} = \frac{RT}{\overline{V}_1}\left( \frac{x_2^{\mathrm{II}} - x_2^{\mathrm{II}} x_1^{\mathrm{II}}}{x_1^{\mathrm{II}}} \right)(0.152). \tag{2.3}$$

For dilute solutions, $x_1^{\mathrm{II}} \to 0$, $\frac{\partial \pi}{\partial \nu_{12}} \to 0$ and for concentrated solutions, $x_2^{\mathrm{II}} \to 0$, $\frac{\partial \pi}{\partial \nu_{12}} \to \infty$. Similar to the sensitivity of osmotic pressure to hydration, a large range of hydration and SASA can be used to fit the osmotic pressure of a dilute solution.

Since the hydration and SASA cause the osmotic pressure to become increasingly sensitive to these parameters, in order to obtain more accurate estimates of protein hydration, and

ultimately the SASA, a greater number of measured osmotic pressures in the near-saturation are required.

## 2.6. Conclusion

The free-solvent model is an appropriate representation of protein osmotic pressure in solution (albeit with moderate ionic strength (Yousef *et al.* 2001)) and the free-solvent model analysis of concentrated protein solutions can be used as a tool to predict hydration and ion binding, and, most importantly, the SASA of the protein. The fact that the regressed hydration value for all macromolecules examined to date results in values corresponding to a monolayer, that the ion binding data is consistent with independently determined methods (Scatchard *et al.* 1950, 1957; De Rosa *et al.* 2004), and that the resulting covariance for the regression of hydration and ion binding is extremely low, are compelling reasons in establishing the credibility of the corresponding SASA predictions from the free-solvent model. These observations collectively indicate that the free-solvent model regressed parameters, when considering osmotic pressure data up to saturation, can be use to predict the SASA, hydration, and ion binding for soluble globular macromolecules.

The SASA, hydration, and ion binding for HEL, BLG, OVA, BSA, Hb, IgG, α-crystallin, and sucrose (no ion binding) were determined by regression of the free-solvent model for their respective osmotic pressure data found in the literature. The predicted SASA for HEL, BLG, OVA, BSA, Hb, and IgG were in excellent agreement with the values computed from the molecular structures. The predicted SASA for α-crystallin, which has no available protein structure, is reasonable in comparison to similar globular protein estimates. Finally, the predicted SASA of sucrose seems to be a more reasonable estimate than that calculated using the available hydrodynamic radius since the regressed hydration values agree with the experimental values

This method of determining the SASA of a macromolecule has several critical applications in that it provides an experimental alternative to estimating SASA, as well as changes in SASA upon formation of protein complexes. Currently, crystallographic or NMR structures of protein complexes are needed to perform this task. Solution structure determination of protein complexes by NMR is constrained by the molecular mass limitation of NMR spectroscopy. Further, structure determination of protein complexes by crystallography is limited by the difficulty of determining the crystallization conditions. In addition, crystal structures often suffer from crystal packing effects which may alter association interfaces or introduce non-specific and non-physiological interactions. The study of SASA is further exacerbated by the vast number of proteins (approximately 1 million (Liu *et al.* 2004)) and limited number of protein structures deposited into the Protein Data Bank (approximately 94,000 as of May 2013). Extracting the SASA directly from experimental data of osmotic pressure may prove to be the more appropriate choice for these applications. In addition, this method may prove to be advantageous in predicting the binding location of a drug or an inhibitor by determining the SASA which is at the binding interface by examining the hydration value. Obtaining information on the SASA at the binding interface may provide a more direct way of determining possible binding locations compared to computational docking studies.

**Table 2.1.** The Values of Hydration for Various Macromolecules. The regressed hydration values obtained from free-solvent model regression to the osmotic pressure data are compared to literature values of hydration determined by experimental and computational methods.

| Macromolecule (MW, kDa) | Solution Properties Salt Conc., pH, Temp. | Regressed Hydration, $\nu_{12}$ $\left(\frac{\text{g } H_2O}{\text{g Protein}}\right)$ | Literature Value of Hydration $\left(\frac{\text{g } H_2O}{\text{g Protein}}\right)$ |
|---|---|---|---|
| Sucrose (0.342) | $H_2O$, 30°C | 0.220 ± 0.0019 | 0.184 - 0.316[a] |
| Hen Egg Lysozyme (HEL) (14.5) | 0.15 M NaCl, 7.0, 25°C | 0.724 ± 0.008[b] | 0.93,[c] 0.98[d] |
| | 0.15 M NaCl, 7.0, 25°C | 1.614 ± 0.01[b] | |
| | 0.15 M KCl, 7.0, 25°C | 0.734 ± 0.003[b] | |
| | 0.15 M KCl, 7.0, 25°C | 1.595 ± 0.007[b] | |
| Bovine β-Lactoglobulin (BLG) (18.4) | 0.1 M NaCl 5.1, 25°C | 0.809 ± 0.0138[e] | 0.72[f] |
| | 0.1 M NaCl, 6.0, 25°C | 0.942 ± 0.0574[e] | |
| | 0.1 M NaCl, 8.0, 25°C | 1.313 ± 0.0206[e] | |
| Ovalbumin (OVA) (45) | 0.15 M NaCl, 7.0, 25°C | 0.86 ± 0.04[g] | 0.54 - 0.82[h] |
| | 0.5 M NaCl, 7.0, 25°C | 0.89 ± 0.04[g] | |
| Bovine Serum Albumin (BSA) (66.4) | 0.15 M NaCl, 4.5, 25°C | 1.113 ± 0.006[i] | 1.07[j] |
| | 0.15 M NaCl, 5.4, 25°C | 1.137 ± 0.006[i] | |
| | 0.15 M NaCl, 7.4, 25°C | 1.177 ± 0.005[i] | |
| Sheep Hemoglobin (Hb) (69.7) | 0.1 M KCl, 7.43, 0°C | 0.869 ± 0.0118[e] | 0.51[k] |
| Bovine Immuno-gamma Globulin (IgG) (155) | 0.13 M Ph. Buff., 7.4, 25°C | 1.107 ± 0.0414[l] | N/A |
| Calf Lens α-Crystallin (800) | 0.017 M KCl, 6.8, 25°C | 1.465 ± 0.1275 | 1.9[m] |
| | 0.15 M KCl, 6.8, 25°C | 1.433 ± 0.0409[e] | |

[a] (Frazer and Myrick 1916; Scatchard 1921)
[b] (Yousef *et al.* 2002b)
[c] (Hamaneh and Buck 2007)
[d] (Panuszko *et al.* 2012)
[e] (M$^c$Bride and Rodgers 2012)
[f] (Mattea *et al.* 2008)
[g] (Yousef *et al.* 2001)
[h] (Bull and Breese 1968; Clark *et al.* 1982)
[i] (Yousef *et al.* 1998b)
[j] (Tanford 1961)
[k] (Arosio *et al.* 1999, 2002)
[l] (Yousef *et al.* 1998a)
[m] (Babizhayev *et al.* 2002, 2003)

**Table 2.2.** The Ion Binding Values for Various Macromolecules. The regressed ion binding values obtained from free-solvent model regression to the osmotic pressure data are compared to literature ion binding values determined experimentally and computationally.

| Macromolecule (MW, kDa) | Solution Properties Salt Conc., pH, Temp. | Regressed Protein-Ion Binding, $\nu_{32}$ $\left(\frac{\text{mol Salt}}{\text{mol Protein}}\right)$ | Literature Value of Protein-Ion Binding $\left(\frac{\text{mol Salt}}{\text{mol Protein}}\right)$ |
|---|---|---|---|
| Sucrose (0.342) | $H_2O$, 30°C | N/A | N/A |
| Hen Egg Lysozyme (HEL) (14.5) | 0.15 M NaCl, 7.0, 25°C<br>0.15 M NaCl, 7.0, 25°C | N/A | 2[a]<br>4[b] |
| Bovine β-Lactoglobulin (BLG) (18.4) | 0.1 M NaCl 5.1, 25°C<br>0.1 M NaCl, 6.0, 25°C<br>0.1 M NaCl, 8.0, 25°C | 1.76 ± 0.068[c]<br>1.17 ± 0.285[c]<br>1.57 ± 0.102[c] | N/A |
| Ovalbumin (OVA) (45) | 0.15 M NaCl, 7.0, 25°C<br>0.5 M NaCl, 7.0, 25°C | 4.08 ± 0.43[d]<br>18.87 ± 1.03[d] | N/A |
| Bovine Serum Albumin (BSA) (66.4) | 0.15 M NaCl, 4.5, 25°C<br>0.15 M NaCl, 5.4, 25°C<br>0.15 M NaCl, 7.4, 25°C | N/A | 11.59[e]<br>10.62[e]<br>8.81[e] |
| Sheep Hemoglobin (Hb) (69.7) | 0.1 M KCl, 7.43, 0°C | 5.20 ± 0.135[c] | 6 (pH 7.4)[f] |
| Bovine Immuno-gamma Globulin (IgG) (155) | 0.13 M Ph. Buff., 7.4, 25°C | 24.3 ± 0.97[g] | N/A |
| Calf Lens α-Crystallin (800) | 0.017 M KCl, 6.8, 25°C<br>0.15 M KCl, 6.8, 25°C | 10.40 ± 2.92<br>169 ± 5.27[c] | N/A |

[a] (Curtis *et al.* 1998)
[b] (Kuehner *et al.* 1999)
[c] (McBride and Rodgers 2012)
[d] (Yousef *et al.* 2001)
[e] (Yousef *et al.* 1998b)
[f] (De Rosa *et al.* 2004)
[g] (Yousef *et al.* 1998a)

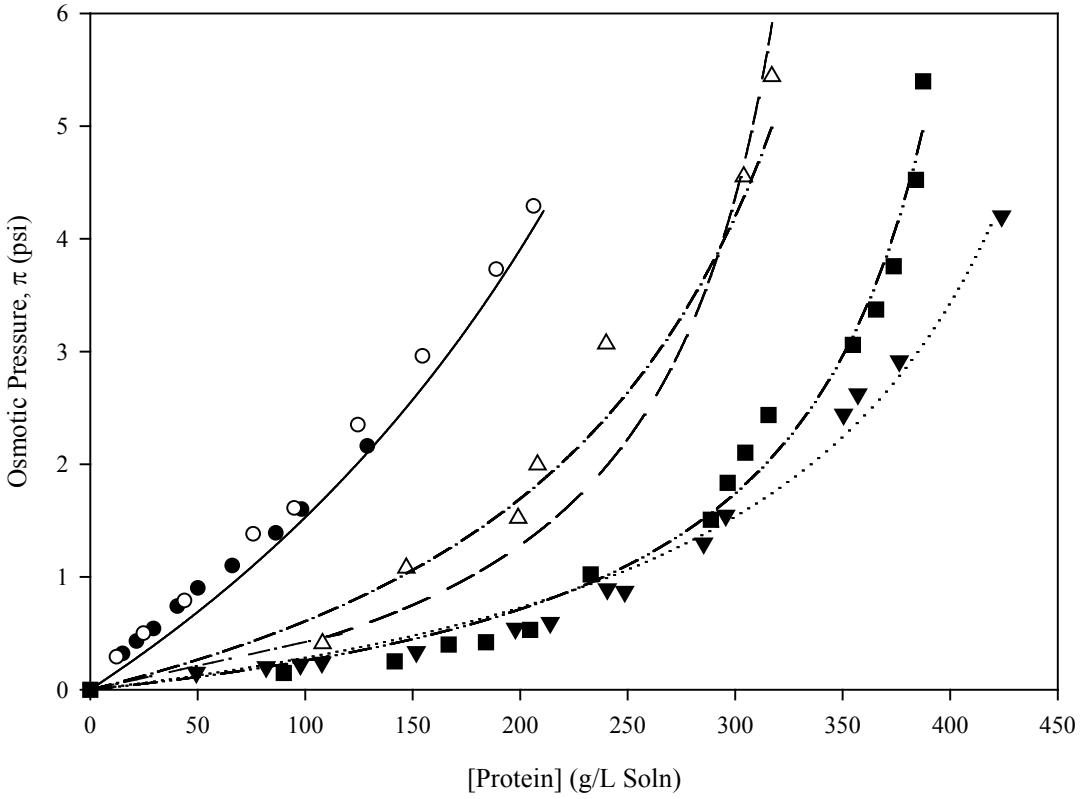


**Figure 2.1.** Osmotic Pressure vs. Concentration for HEL, IgG, and α-Crystallin. The experimental osmotic pressure of HEL in 0.15 M NaCl, pH 7.0 (closed circles) (Yousef *et al.* 2002b), HEL in 0.15 M KCl, pH 7.0 (open circles) (Yousef *et al.* 2002b), IgG (closed triangles) (Yousef *et al.* 1998a), and α-crystallin in 0.017 M KCl, pH 6.8 (open triangles) and 0.15 M KCl, pH 6.8 (closed squares) (Vérétout *et al.* 1989) are plotted. The free-solvent model is plotted using the regressed hydration and ion binding values for each protein: HEL (solid curve), IgG (dotted curve), and α-crystallin in 0.017 M KCl (dash-dot curve) and 0.15 M KCl (dash-dot-dot curve). The literature value of hydration for α-crystallin, $\nu_{12} = 1.9$ g $H_2O$/g α-crystallin (Babizhayev *et al.* 2002, 2003), is plotted with its corresponding ion binding value for 0.017 M KCl, pH 6.8 (dashed curve).

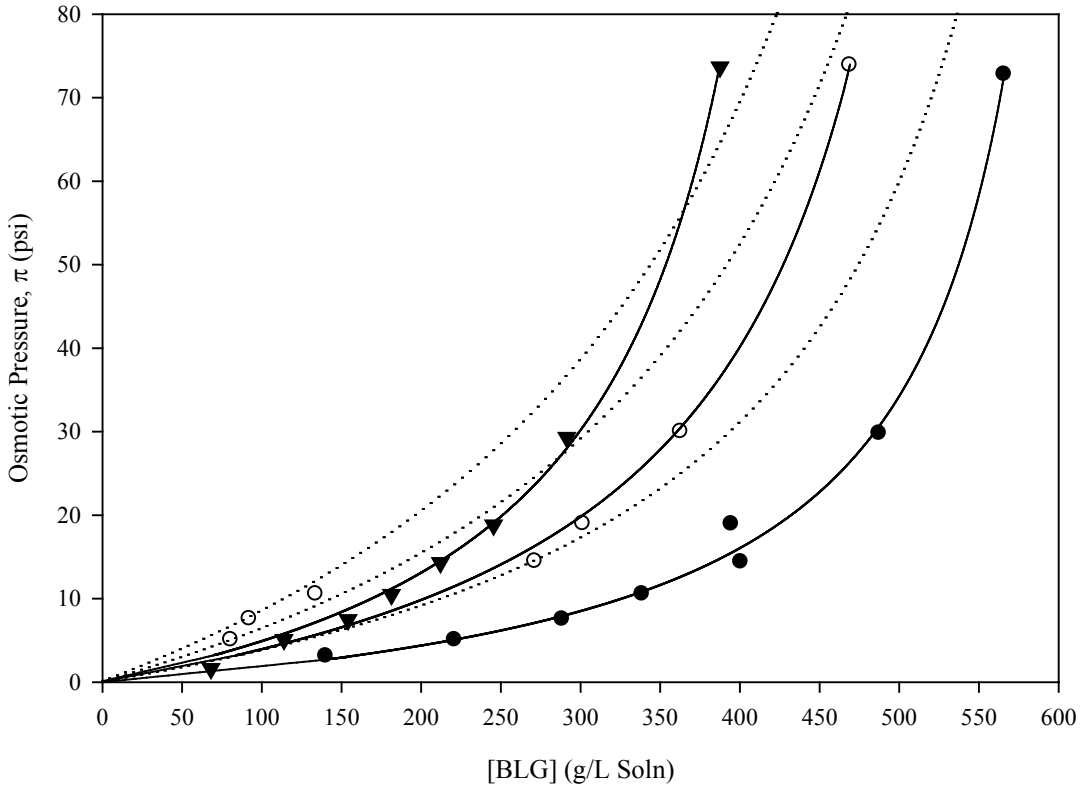


**Figure 2.2.** Osmotic Pressure vs. Concentration for BLG. The experimental osmotic pressure of BLG in 0.1 M NaCl, pH 5.1 (closed circles), pH 6.0 (open circles), and pH 8.0 (closed triangles) are that of Parker *et al.* (Parker *et al.* 2005). The free-solvent model is plotted using the regressed hydration and regressed ion binding values (solid curves) and using $\nu_{12} = 0.72$ g $H_2O$/g BLG (Mattea *et al.* 2008) with the corresponding regressed ion binding values (dotted curves).

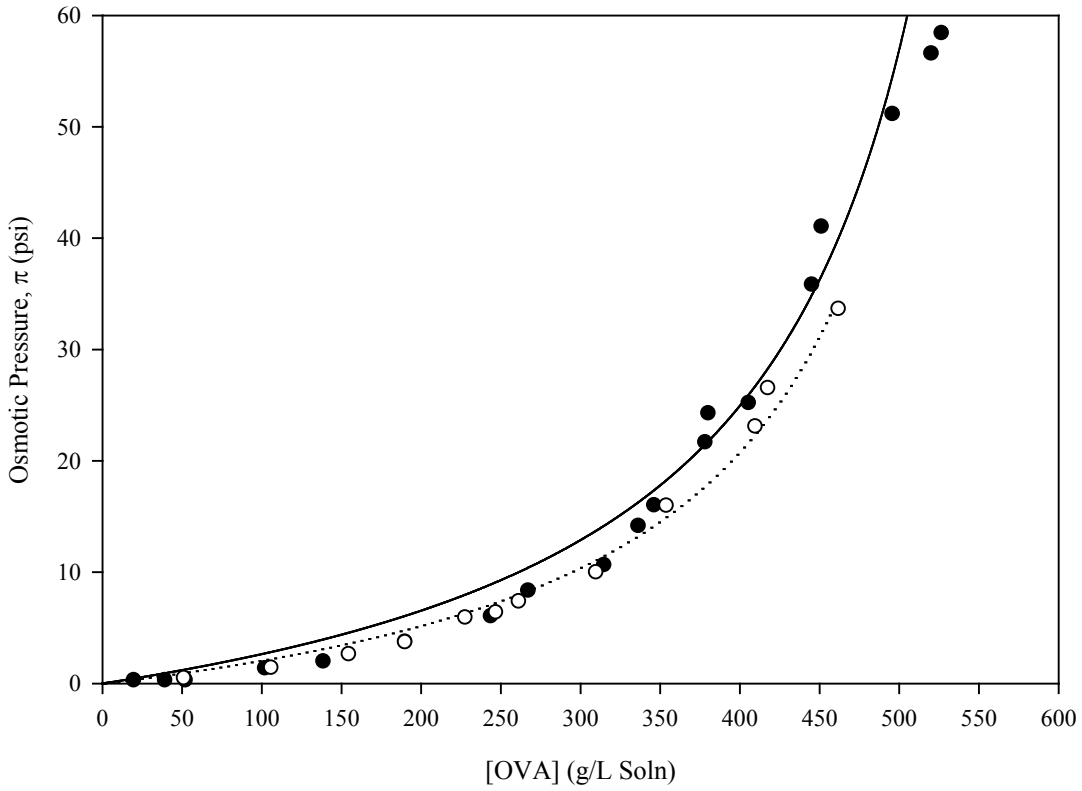


**Figure 2.3.** Osmotic Pressure vs. Concentration for OVA. The experimental osmotic pressure of OVA in 0.15 M NaCl, pH 7.0 (closed circles) and 0.5 M NaCl, pH 7.0 (open circles) are that of Yousef *et al.* (Yousef *et al.* 2001). The free-solvent model is plotted using the regressed hydration and ion binding values for OVA in 0.15 M NaCl, pH 7.0 (solid curve) and 0.5 M NaCl, pH 7.0 (dotted curve).

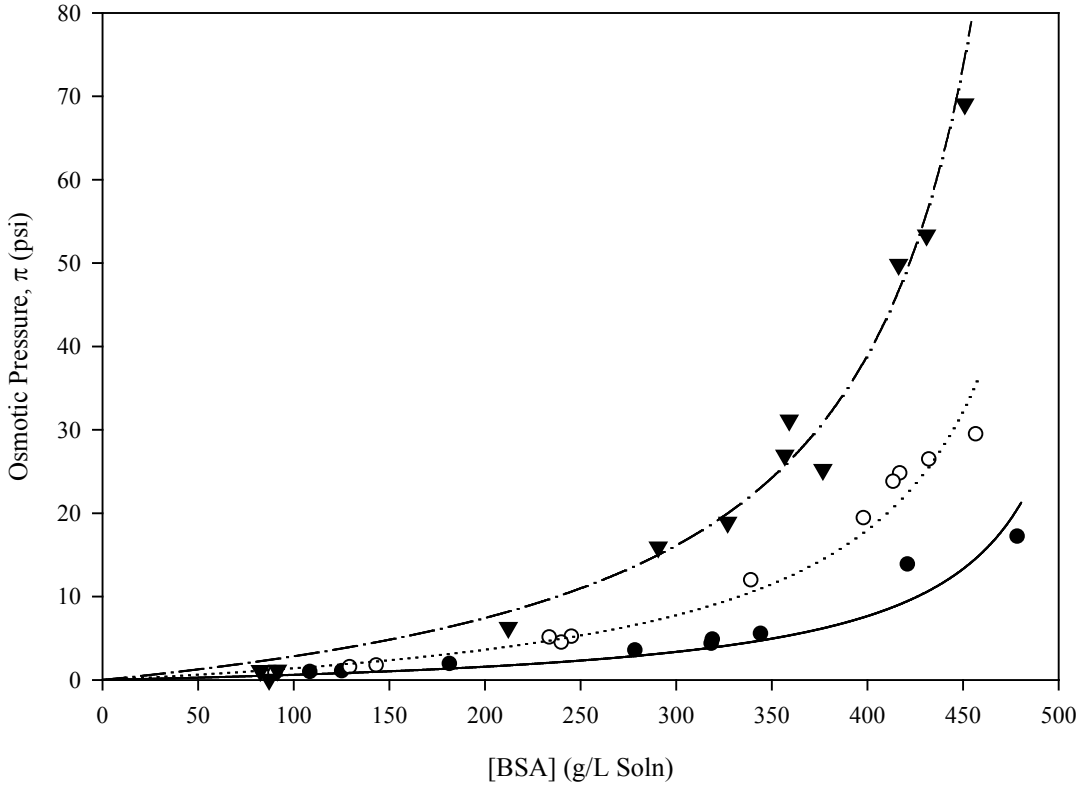


**Figure 2.4.** Osmotic Pressure vs. Concentration for BSA. The experimental osmotic pressure of BSA in 0.15 M NaCl at pH 4.5 (closed circles), 5.4 (open circles), and 7.4 (closed triangles) are that of Vilker *et al.* (Vilker *et al.* 1981). The free-solvent model is plotted using the regressed hydration and calculated ion binding values for BSA in 0.15 M NaCl, pH 4.5 (solid curve), 5.4 (dotted curve), and 7.4 (dash-dot curve).

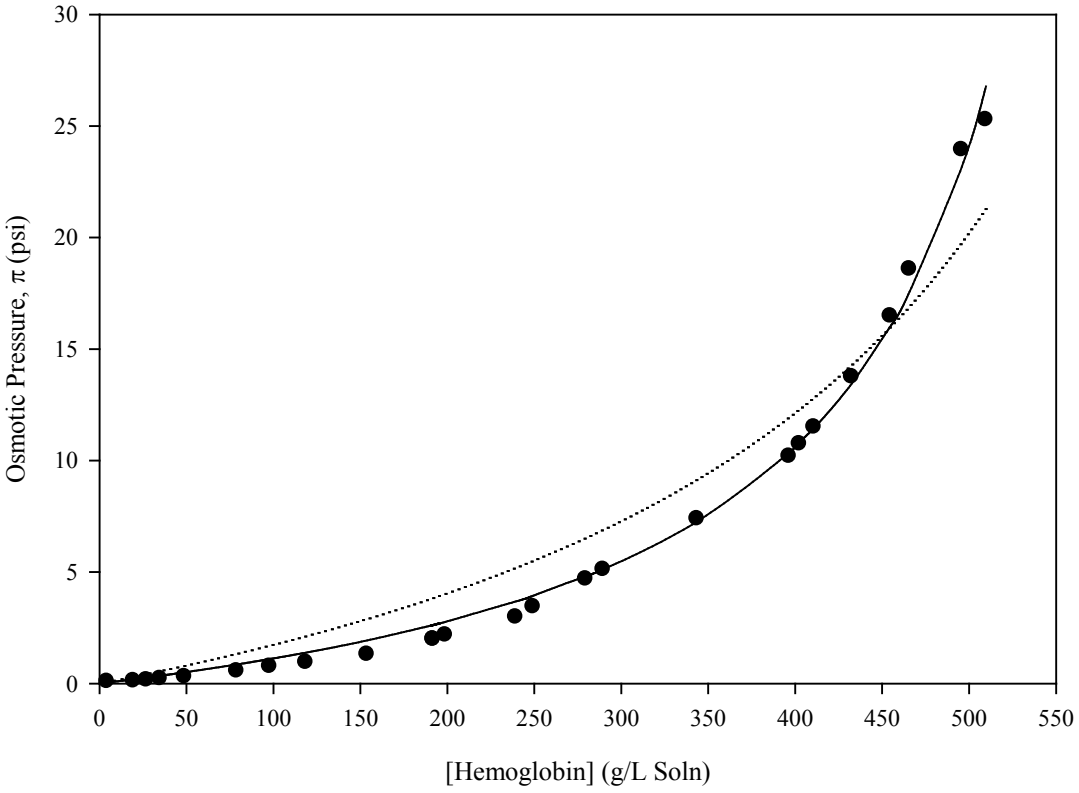


**Figure 2.5.** Osmotic Pressure vs. Concentration for Hb. The experimental osmotic pressure of Hb in 0.1 M KCl, pH 7.43, 0°C (closed circles) is that of Adair and published by Dick (Dick 1967). The free-solvent model is plotted using the regressed hydration and regressed ion binding (solid curve). The literature value of hydration is also plotted for comparison: $\nu_{12} = 0.51$ g $H_2O$/g Hb (Arosio *et al.* 1999, 2002) with a regressed ion binding of $\nu_{12} = 1.77$ mol KCl/mol Hb (dotted curve).

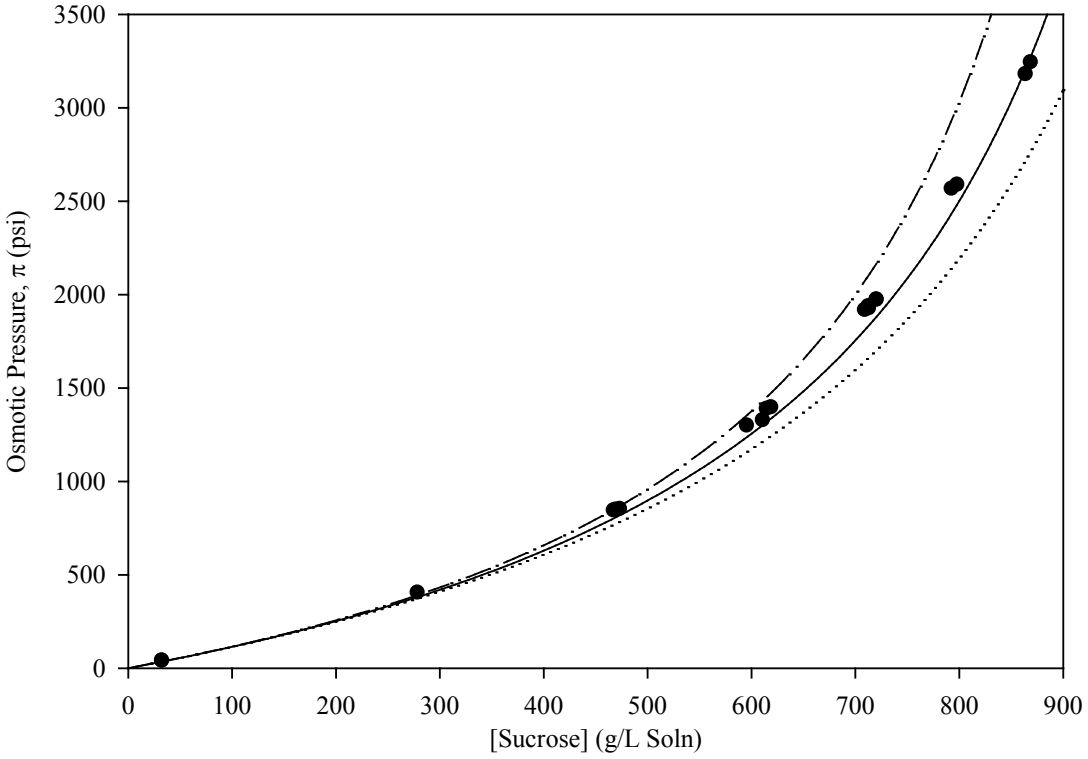


**Figure 2.6.** Osmotic Pressure vs. Concentration for Sucrose. The experimental osmotic pressure of sucrose in water at 30°C (closed circles) is that of Frazer and Myrick (Frazer and Myrick 1916). The free-solvent model is plotted using the regressed hydration, $\nu_{12} = 4.18$ mol $H_2O$/mol sucrose (solid curve). The literature values of hydration are also plotted for comparison: $\nu_{12} = 3.5$ mol $H_2O$/mol sucrose (dotted curve), and $\nu_{12} = 6$ mol $H_2O$/mol sucrose (dash-dot curve) (Frazer and Myrick 1916; Scatchard 1921).

**Table 2.3.** Comparison of the Predicted and Computational SASA. The free-solvent based (predicted) SASA are calculated using the regressed hydration values. The structure based SASA is the range calculated by five molecular modeling software. See Table 2.1 for references.

| Macromolecule (kDa) | Solution Properties Salt Conc., pH, Temp. | Regressed Hydration, $\nu_{12}$ $\left(\frac{\text{g } H_2O}{\text{g Protein}}\right)$ | Free-Solvent Based SASA (Å$^2$) | Structure Based SASA (Å$^2$) (PDB Code) |
|---|---|---|---|---|
| Sucrose (0.342) | $H_2O$, 30°C | 0.220 ± 0.0019 | 27.5 ± 0.24 | N/A |
| Hen Egg Lysozyme (HEL) (14.5) | 0.15 M NaCl, 7.0, 25°C | 0.724 ± 0.008[b] | 3,783 ± 42 | 5,732 - 6,763 (4LYZ) |
| | 0.15 M NaCl, 7.0, 25°C | 1.614 ± 0.01[b] | 8,433 ± 52 | |
| | 0.15 M KCl, 7.0, 25°C | 0.734 ± 0.003[b] | 3,835 ± 16 | |
| | 0.15 M KCl, 7.0, 25°C | 1.595 ± 0.007[b] | 8,333 ± 366 | |
| Bovine β-Lactoglobulin (BLG) (18.4) | 0.1 M NaCl 5.1, 25°C | 0.809 ± 0.0138[e] | 5,436 ± 93 | 7,724 - 8,628 (2Q2M) |
| | 0.1 M NaCl, 6.0, 25°C | 0.942 ± 0.0574[e] | 6,330 ± 386 | 7,666 - 8,644 (3NPO) |
| | 0.1 M NaCl, 8.0, 25°C | 1.313 ± 0.0206[e] | 8,823 ± 138 | 7,500 - 8,304 (3BLG) |
| Ovalbumin (OVA) (45) | 0.15 M NaCl, 7.0, 25°C | 0.86 ± 0.04[g] | 14,133 ± 657 | 13,556 - 16,434 (1OVA) |
| | 0.5 M NaCl, 7.0, 25°C | 0.89 ± 0.04[g] | 14,625 ± 657 | 14,058 - 16,375 (1UHG) |
| Bovine Serum Albumin (BSA) (66.4) | 0.15 M NaCl, 4.5, 25°C | 1.113 ± 0.006[i] | 27,000 ± 146 | 27,746 - 28,188 (1BM0*) |
| | 0.15 M NaCl, 5.4, 25°C | 1.137 ± 0.006[i] | 27,583 ± 146 | 27,495 - 34,563 (3V03) |
| | 0.15 M NaCl, 7.4, 25°C | 1.177 ± 0.005[i] | 28,533 ± 121 | 28,646 - 35,491 (4F5S) |
| Sheep Hemoglobin (Hb) (69.7) | 0.1 M KCl, 7.43, 0°C | 0.869 ± 0.012[e] | 21,897 ± 302 | 23,499 - 26,100 (2QU0) |
| Bovine Immuno-gamma Globulin (IgG) (155) | 0.13 M Ph. Buff., 7.4, 25°C | 1.107 ± 0.0414[l] | 62,660 ± 2,343 | 61,809 - 65,916 (1IGT) |
| Calf Lens α-Crystallin (800) | 0.017 M KCl, 6.8, 25°C | 1.465 ± 0.1275 | 427,999 ± 37,249 | N/A |
| | 0.15 M KCl, 6.8, 25°C | 1.433 ± 0.0409[e] | 418,651 ± 11,949 | |

* Based on the homology model of HSA with PDB Code 1BM0 (Appendix A).

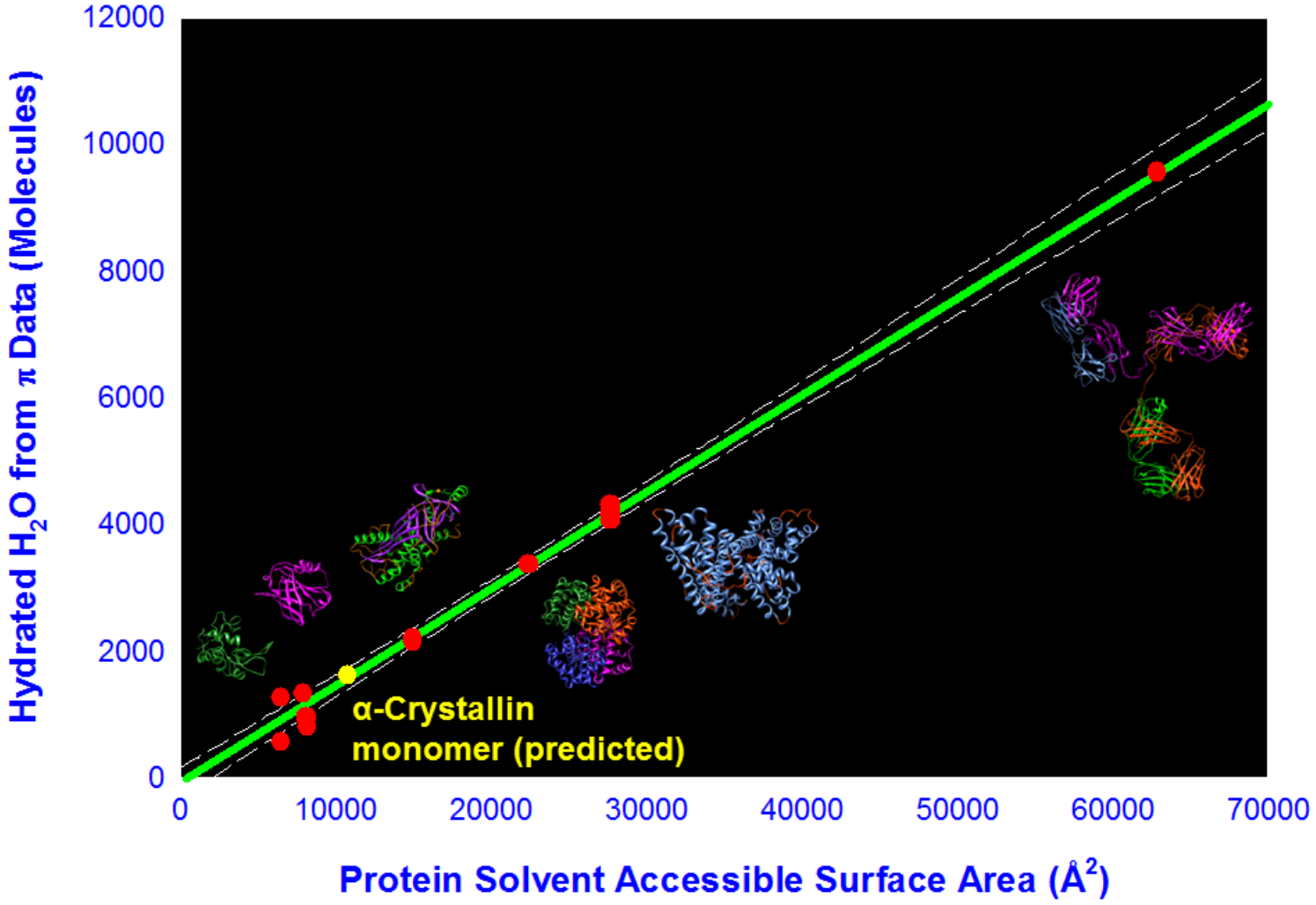


**Figure 2.7.** SASA vs. Macromolecule Hydration. The hydrations and SASA of HEL, BLG, α-crystallin, OVA, Hb, BSA, and IgG are plotted as the data points. The green line is that of a monolayer of water surrounding a macromolecule. The 95% confidence interval is shown as the dashed white line. The molecular images are those of PDB codes: 4LYZ (HEL), 2Q2M (BLG), 1OVA (OVA), Hb (2QU0), BSA homology model, and 1IGT (IgG).

# CHAPTER 3.

# DIRECT DETERMINATION OF THE ACTIVITY COEFFICIENT FROM INDEPENDENTLY MEASUREABLE PARAMETERS

## 3.1. Abstract

The activity coefficient of water is related to physically realistic parameters and a mathematical expression is developed to directly predict the activity coefficients of water, for aqueous protein solutions up to near-saturation concentrations, that uses only the independently determined quantities mole fraction, solvent accessible surface area, and ion binding. The model is based on the free-solvent model, which has previously been shown to provide excellent prediction of the osmotic pressure of concentrated and crowded globular proteins in aqueous solutions up to near-saturation concentrations. Predictions of the activity coefficients of water for near-saturated solutions of several macromolecules are compared to the calculated activity coefficients of water based on osmotic pressure data. It is observed that the predicted activity coefficients are increasingly dependent on the solute-solvent parameters as the protein concentration increases to near-saturation concentrations.

## 3.2. The Activity Coefficient Model

Historically, the activity coefficient model for relating concentrations to chemical potential was developed to correct for non-idealities observed in many equilibrium systems. Recall, that the chemical potential for species $i$ can be related to the species relative activity, $a_i$, as,

$$\mu_i^{\theta}(T,P,\theta_i) - \mu_i^{o\theta}(T,P^o,\theta_i) = RT\ln a_i^{\theta}(T,P,\theta_i)\,. \tag{3.1}$$

For an ideal system (with no attractive interactions), the relative activity is proportional to a composition variable, $\theta_i$ (such as $x_i$, $c_i$, $m_i$, $\rho_i$, etc.). For observed non-ideal behavior, an activity coefficient, $\gamma_i$, is introduced to 'correct' for the deviation, or

$$a_i^{\theta}\left(T,P,\theta_i\right) \equiv \gamma_i^{\theta}\left(T,P,\theta_i\right)\theta_i . \tag{3.2}$$

When a two-chamber osmometer, containing diffusible species on one side and diffusible and non-diffusible species on the other side, is separated by a semi-permeable membrane, an osmotic pressure develops which directly corresponds to the chemical potential of the diffusible species across the membrane. With the chamber containing proteins denoted as compartment II, and the chamber containing only solvent and diffusible ions denoted as compartment I, the osmotic pressure, in terms of the solvent activity, is

$$\pi = \frac{\mu_1^{\mathrm{I}} - \mu_1^{\mathrm{II}}}{\bar{V}_1} = -\frac{RT}{\bar{V}_1}\ln\left(\frac{a_1^{\mathrm{II}}}{a_1^{\mathrm{I}}}\right). \tag{3.2}$$

In an ideal system, the activity coefficient is unity, thus the activity is linearly related to the composition variable, and therefore the osmotic pressure is expressed as

$$\pi = -\frac{RT}{\bar{V}_1}\ln\left(\frac{\theta_1^{\mathrm{II}}}{\theta_1^{\mathrm{I}}}\right). \tag{3.3}$$

However, for a non-ideal system, such as observed in a concentrated or crowded protein environment, using the mole fraction of the solvent, $x_1$, as the composition variable, the osmotic pressure is related to mole fraction as

$$\pi = -\frac{RT}{\bar{V}_1}\ln\left(\frac{\gamma_1^{\mathrm{II}} x_1^{\mathrm{II}}}{\gamma_1^{\mathrm{I}} x_1^{\mathrm{I}}}\right). \tag{3.4}$$

Assuming that the activity coefficient of water in compartment I (non-protein solution) is unity, $\gamma_1^{\mathrm{I}} = 1$, Eqn. 3.4 can be used to fit the experimental osmotic pressure data to determine the value of the activity coefficient of water at each protein concentration.

Until now, there has been no rigorous assessment of how the activity coefficient of water is related to the solute and solution properties. Considering the protein as the solute in an aqueous environment, this work uses the free-solvent model, introduced by van Laar (van Laar 1894) and developed by Yousef *et al.* (Yousef *et al.* 1998a, 1998b, 2001, 2002a, 2002b), to directly couple the activity coefficient of water to physically realistic and independently determinable parameters.

## 3.3. The Free-Solvent Model

As early as 1916, Frazer and Myrick (Frazer and Myrick 1916) analyzed the non-idealities in concentrated, aqueous solutions of sucrose using a free-solvent model understanding that the mole fraction of water is affected by the hydration of sucrose. When the water that interacts with sucrose was removed from the total water available in the system, the free-solvent model provided an excellent prediction of the osmotic pressure data.

More recently, the free-solvent model was revised for aqueous protein solutions in which ion binding occurs, in addition to hydration (Yousef *et al.* 1998a). Essentially, the free-solvent model treats the protein with all associated water and salt ions as a unique species, the hydrated macromolecule. In effect, this approach renders the solution ideal with respect to the remaining, diffusible solvent species that have no attractive interactions. The modified mole fraction of the free water, $(x_1)_{\mathrm{FW}}$, considers the hydrated macromolecule as the impermeable solute. The free-solvent model with the mole fraction of the free water, $(x_1)_{\mathrm{FW}}$, as the composition variable is

$$\pi = -\frac{RT}{\overline{V}_1}\ln\left(\frac{\left(x_1^{\mathrm{II}}\right)_{\mathrm{FW}}}{\left(x_1^{\mathrm{I}}\right)_{\mathrm{FW}}}\right), \tag{3.5}$$

where the mole fraction of free water is the remaining moles of solvent that are not bound to the protein. Assuming the solutions is made up of $n$ distinct species and $p$ proteins, and letting

species 1 be the solvent, species 2 through $(p+1)$ be the proteins, and species $(p+2)$ through $n$ be the remaining diffusible species, the initial total moles of the solution in compartment II is $N^{\mathrm{II}} = \sum_{i=1}^{n} N_i^{\mathrm{II}}$, where $i$ denotes each species. The final total moles of free-solvent in chamber II, after protein-solvent interactions, is

$$N_*^{\mathrm{II}} = N^{\mathrm{II}} - \sum_{\substack{i=1,\\ i\neq 2\to p+1}}^{n} \sum_{j=2}^{p+1} \nu_{ij} N_j^{\mathrm{II}} - \sum_{j=2}^{p+1} N_j^{\mathrm{II}} \,, \tag{3.6}$$

where $N_j^{\mathrm{II}}$ denotes the moles of protein $j$ in solution and $\nu_{ij}$ is the number of moles of species $i$ interacting with protein $j$ to make the hydrated protein.

Then, the mole fraction of free-solvent in chamber II is

$$\left(x_1^{\mathrm{II}}\right)_{\mathrm{FW}} = \frac{N_1^{\mathrm{II}} - \sum_{j=2}^{p+1} \nu_{1j} N_j^{\mathrm{II}}}{N_*^{\mathrm{II}} + \sum_{j=2}^{p+1} N_j^{\mathrm{II}}} \tag{3.7}$$

while in chamber I, the mole fraction of free-solvent is

$$\left(x_1^{\mathrm{I}}\right)_{\mathrm{FW}} = \frac{N_1^{\mathrm{I}}}{\sum_{\substack{i=1,\\ i\neq 2\to p+1}}^{n} N_i^{\mathrm{I}}} \,. \tag{3.8}$$

For a single protein species in a monovalent salt aqueous solution, the free-solvent model reduces to

$$\pi \approx \frac{RT}{\overline{V}_1} \ln\left( \frac{\left(N_1^{\mathrm{II}} + (1-\nu_{12}-\nu_{32})N_2^{\mathrm{II}} + N_3^{\mathrm{II}}\right)N_1^{\mathrm{I}}}{\left(N_1^{\mathrm{II}} - \nu_{12} N_2^{\mathrm{II}}\right)N^{\mathrm{I}}} \right). \tag{3.9}$$

### 3.3.1. Robustness of the Physical Parameters in the Free-Solvent Osmotic Pressure Model

The parameters of the free-solvent model have been shown to be remarkably robust and well-within independently determined values when regressed relative to measured osmotic pressure for highly concentrated protein solutions (Yousef *et al.* 1998a, 1998b, 2001, 2002a,

2002b; M$^{c}$Bride and Rodgers 2012). As an example, the regressed hydration number, $\nu_{12}$, for all globular proteins measured was found to be well within the $^{17}$O NMR approximation of 1 g $H_2O$/g globular protein (Sedykh and Sedykh 1967) but more precisely determines the value to be a monolayer of water with $\pm 0.6\%$ when compared to the solvent accessible surface area (SASA) of each protein. Thus, the free-solvent model is likely to provide an excellent prediction of the activity coefficient of water that is predicted from only independently determined physical parameters.

3.4. Coupling the Free-Solvent Model and the Activity Coefficient Model

Using the free-solvent model (Eqn. 3.5), the activity coefficient of water can be determined based on the ratio of the mole fractions of total water, $\left(x_1\right)_{\mathrm{W}}$, and the ratio of the mole fractions of free water, $\left(x_1\right)_{\mathrm{FW}}$. Using $\left(x_1^{\mathrm{II}}\right)_{\mathrm{W}}$ and $\left(x_1^{\mathrm{I}}\right)_{\mathrm{W}}$ as the mole fractions of total water, and $\left(x_1^{\mathrm{II}}\right)_{\mathrm{FW}}$ and $\left(x_1^{\mathrm{I}}\right)_{\mathrm{FW}}$ as the mole fractions of free water, setting Eqns. 3.5 and 3.4 (with $\gamma_1^{\mathrm{I}}=1$) equal

$$-\frac{RT}{\bar{V}_1}\ln\left(\frac{\gamma_1^{\mathrm{II}}\left(x_1^{\mathrm{II}}\right)_{\mathrm{W}}}{\left(x_1^{\mathrm{I}}\right)_{\mathrm{W}}}\right)=-\frac{RT}{\bar{V}_1}\ln\left(\frac{\left(x_1^{\mathrm{II}}\right)_{\mathrm{FW}}}{\left(x_1^{\mathrm{I}}\right)_{\mathrm{FW}}}\right) \tag{3.10}$$

where

$$\left(x_1^{\mathrm{II}}\right)_{\mathrm{W}}=\frac{N_1^{\mathrm{II}}}{\sum_{i=1}^{n}N_i^{\mathrm{II}}} \tag{3.11}$$

and

$$\left(x_1^{\mathrm{I}}\right)_{\mathrm{W}}=\frac{N_1^{\mathrm{I}}}{\sum_{\substack{i=1,\\ i\neq 2\rightarrow \mathrm{p}}}^{n}N_i^{\mathrm{I}}}. \tag{3.12}$$

Substituting Eqns. 3.7 and 3.8 into Eqn. 3.10, and solving for the activity coefficient of water, results in

$$\gamma_1^{\mathrm{II}} = \left( \frac{N_1^{\mathrm{I}} \left( \sum_{i=1}^{n} N_i^{\mathrm{I}} \right)}{N_1^{\mathrm{II}} \left( \sum_{\substack{i=1, \\ i \neq 2 \rightarrow p+1}}^{n} N_i^{\mathrm{I}} \right)} \right) \left( \frac{\left( \sum_{\substack{i=1, \\ i \neq 2 \rightarrow p+1}}^{n} N_i^{\mathrm{I}} \right) \left( N_1^{\mathrm{II}} - \sum_{j=2}^{p+1} \nu_{1j} N_j^{\mathrm{II}} \right)}{N_1^{\mathrm{I}} \left( \sum_{i=1}^{n} N_i^{\mathrm{II}} - \sum_{\substack{i=1 \\ i \neq 2 \rightarrow p+1}}^{n} \sum_{j=2}^{p+1} \nu_{ij} N_j^{\mathrm{II}} \right)} \right). \tag{3.13}$$

For a single protein in an aqueous solution with a single monovalent salt, the activity coefficient of water becomes

$$\gamma_1^{\mathrm{II}} = \frac{\left( N_1^{\mathrm{II}} + N_2^{\mathrm{II}} + N_3^{\mathrm{II}} \right) \left( N_1^{\mathrm{II}} - \nu_{12} N_2^{\mathrm{II}} \right)}{N_1^{\mathrm{II}} \left( N_1^{\mathrm{II}} + \left( 1 - \nu_{12} - \nu_{32} \right) N_2^{\mathrm{II}} + N_3^{\mathrm{II}} \right)}. \tag{3.14}$$

Eqn. 3.14 gives the relationship of the activity coefficient of water to the protein-solvent interactions and moles of species in solution. Note that, again, only measurable physical properties are necessary to determine the activity coefficient and there are no arbitrary parameters.

## 3.5. Methods

Here, the activity coefficient of water is predicted based on solute-solvent interactions (Eqn. 3.14) using literature values for the physical parameters of the free-solvent model for three macromolecules. The predicted activity coefficients are compared to the calculated activity coefficients determined from the experimental osmotic pressure data (Eqn. 3.4).

The activity coefficients are also predicted when the regressed free-solvent model physical parameters, from osmotic pressure data, are used. These are compared to the calculated activity coefficients of water determined from the osmotic pressure data. The regressed physical parameters are compared to literature values, when available, to validate the use of the values. Six macromolecules are used for this method.

### 3.5.1. Macromolecules

The activity coefficient of water is predicted using only literature values of the physical parameters for bovine serum albumin (BSA), sheep hemoglobin (Hb), and sucrose.

The activity coefficient of water predicted using osmotic pressure regressed values of the physical parameters for hen egg lysozyme (HEL), bovine β-lactoglobulin (BLG), ovalbumin (OVA), BSA, Hb, bovine immune-gamma globulin (IgG), calf lens α-crystallin, and sucrose.

### 3.5.2. Predicting the Activity Coefficient of Water Based on Physical Parameters

#### 3.5.2.1. Using Only Literature Values

The activity coefficients of water are predicted based on protein-solvent interactions (Eqn. 3.14) and compared to the activity coefficients of water calculated from osmotic pressure data (Eqn. 3.4) for three macromolecules: BSA in 0.15 M NaCl, 25°C at pH 4.5, 5.4, and 7.4, Hb in 0.1 M KCl, 0°C, pH 7.43, and sucrose in water at 30°C. The calculated (osmotic pressure-based) activity coefficients of water are computed at each macromolecule concentration by fitting Eqn. 3.4, with $\gamma_1^{\mathrm{I}} = 1$, to the osmotic pressure data by Vilker *et al.* (Vilker *et al.* 1981) for the concentrated BSA solutions (0.15 M NaCl at 25°C, pH 4.5, 5.4, and 7.4), to the osmotic pressure data by Adair, published by Dick (Dick 1967), for concentrated Hb in 0.1 M KCl, 0°C, pH 7.43, and to the osmotic pressure data for sucrose in water by Frazer and Myrick (Frazer and Myrick 1916).

The activity coefficients of water based on solute-solvent interactions are predicted using available literature values for hydration and ion binding. Although the hydration can vary depending on the experimental method used, here the SASA was used to determine the value of hydration (Yousef *et al.* 2002b). The SASA, computed using five molecular modeling software as previously described (McBride and Rodgers 2012), was used to determine the values of hydration

assuming 15.2 molecules per $nm^2$ of surface area (Yousef *et al.* 2002b). The five molecular modeling software used are Swiss-Pdb Viewer (Guex and Peitsch 1997), MOLMOL (Koradi *et al.* 1996), UCSF Chimera (Pettersen *et al.* 2004), VegaZZ (Pedretti *et al.* 2002), and GETAREA (Fraczkiewicz and Braun 1998). For Swiss-Pdb Viewer and MOLMOL a quality and precision of 6 were used, respectively, for calculating the SASA.

For BSA, three molecular structures are available (two in the Protein Data Bank (PDB: 3V03 (Majorek *et al.* 2012) and 4F5S (Bujacz 2012)) and one homology model (1BM0 homology model)). Here, the hydration values used are determined from the SASA using the molecular structure obtained from homology modeling. The ion binding of BSA were those based on the two-site model by Scatchard *et al.* (Scatchard *et al.* 1957; Yousef *et al.* 1998b).

Similarly, for Hb the hydration value used is that of the hydration computed from the SASA of the molecular structure (PDB: 2QU0 (Neelagandan *et al.* 2007)) and the ion binding value was determined by De Rosa *et al.* (De Rosa *et al.* 2004).

For sucrose, the hydration values used are those of Frazer and Myrick (Frazer and Myrick 1916), Scatchard (Scatchard 1921), and Einstein (Einstein 1956).

3.5.2.2. Using Regressed Values

In addition to the literature value of physical parameters for predicting the activity coefficients of water, the values of the physical parameters determined by osmotic pressure regression using the free-solvent model are also used. The regressed physical parameters are used in order to compare the accuracy of the literature and the regressed physical parameters in predicting the activity coefficients of water.

The macromolecules studied for this method are ovalbumin (OVA) (in 0.15 M NaCl, pH 7.0 and 0.5 M NaCl, pH 7.0 (Yousef *et al.* 2001)), BSA (in 0.15 M NaCl, pH 4.5, 5.4, and 7.4

(Yousef *et al.* 1998b)), Hb (in 0.1 M KCl, pH 7.43 (Dick 1967)), bovine immuno-gamma globulin (IgG) (in 0.13 M sodium phosphate buffer, pH 7.4 (Yousef *et al.* 1998a)), calf lens α-crystallin (in 0.017 M KCl, pH 6.8 and 0.15 M KCl, pH 6.8 (Vérétout *et al.* 1989)), and sucrose (in water (Frazer and Myrick 1916)).

## 3.6. Results

### 3.6.1. The Activity Coefficients of Water Predicted Using Independently Determined Physical Parameters

Eqn. 3.14 was used to estimate the activity coefficients of water for three separate macromolecules in aqueous solutions up to near-saturation concentrations. Figures 3.1 - 3.5 show the calculated activity coefficients of water (Eqn. 3.4), based on the osmotic pressure data, and the activity coefficients of water based on solute-solvent interactions (Eqn. 3.14) applied to three BSA solutions, one Hb solution, and one sucrose solution using only the physical parameters available in literature (Table 3.1).

For all solutions, as the solute concentration increases, the activity coefficient of water decreases from unity as expected; the activity coefficient of water for a pure water solution should be unity. The calculated activity coefficients of water follow this trend for most of the solutions studied; however there is some deviation, which is most likely due to experimental error. The predicted activity coefficients of water based on protein-solvent interactions decrease from unity as the protein concentration increases for all five solutions studied.

The activity coefficients of water predicted based on protein-solvent interactions are compared to the calculated activity coefficients of water for BSA in 0.15 M NaCl, pH 4.5, 5.4, and 7.4 (Figures 3.1 - 3.3). The ion binding values are 11.59 mol NaCl/mol BSA, 10.62 mol NaCl/mol BSA, and 8.81 mol NaCl/mol BSA for BSA in 0.15 M NaCl, pH 4.5, 5.4,

and 7.4, respectively (Yousef *et al.* 1998b). The homology model SASA was computed using four molecular modeling software. The SASA are 27,746 $Å^2$ (GETAREA (Fraczkiewicz and Braun 1998)), 28,065 $Å^2$ (Swiss-Pdb Viewer (Guex and Peitsch 1997)), 28,188 $Å^2$ (MOLMOL (Koradi *et al.* 1996)), and 27,985 $Å^2$ (VegaZZ (Pedretti *et al.* 2002)) and the corresponding hydration values are 1.144 g $H_2O$/g BSA (GETAREA (Fraczkiewicz and Braun 1998)), 1.157 g $H_2O$/g BSA (Swiss-Pdb Viewer (Guex and Peitsch 1997)), 1.162 g $H_2O$/g BSA (MOLMOL (Koradi *et al.* 1996)), and 1.154 g $H_2O$/g BSA (VegaZZ (Pedretti *et al.* 2002)). The activity coefficient of water is predicted using the minimum and maximum hydration values (1.144 g $H_2O$/g BSA and 1.162 g $H_2O$/g BSA) and the corresponding ion binding values for each BSA solution. The predicted activity coefficients of water for all three BSA solutions follows the same trend as the calculated activity coefficients of water; the predicted activity coefficients are in excellent agreement with the calculated activity coefficients for BSA in 0.15 M NaCl, pH 5.4 and 7.4, and in good agreement for BSA in 0.15 M NaCl, pH 4.5.

The SASA from the molecular structure of Hb (PDB: 2QU0) for four of the molecular modeling software are 24,759 $Å^2$ (GETAREA (Fraczkiewicz and Braun 1998)), 24,304 $Å^2$ (Swiss-Pdb Viewer (Guex and Peitsch 1997)), 24,981 $Å^2$ (MOLMOL (Koradi *et al.* 1996)), and 26,100 $Å^2$ (UCSF Chimera (Pettersen *et al.* 2004)) and the corresponding hydration values are 0.973 g $H_2O$/g BSA (GETAREA (Fraczkiewicz and Braun 1998)), 0.955 g $H_2O$/g BSA (Swiss-Pdb Viewer (Guex and Peitsch 1997)), 0.981 g $H_2O$/g BSA (MOLMOL (Koradi *et al.* 1996)), and 1.025 g $H_2O$/g BSA (UCSF Chimera (Pettersen *et al.* 2004)). The activity coefficients of water was predicted for all four values of hydration using the literature value for ion binding, 6 mol KCl/mol Hb (De Rosa *et al.* 2004). The predicted activity coefficients of water using the SASA from three of the molecular modeling software are in excellent agreement with the

calculated activity coefficients, and the activity coefficients of water predicted using the SASA from UCSF Chimera (Pettersen *et al.* 2004) is in good agreement with the calculated values.

The predicted activity coefficients of water for sucrose are compared to the calculated activity coefficients of water from experimental osmotic pressure data (Figure 3.5). Many studies have determined the hydration of sucrose, with the most notable being those by Frazer and Myrick (Frazer and Myrick 1916), Scatchard (Scatchard 1921), and Einstein (Einstein 1956). The range of sucrose hydration values is 3.5 - 6 mol $H_2O$/mol sucrose (Frazer and Myrick 1916; Scatchard 1921; Einstein 1956). The activity coefficients of water was predicted using the minimum and maximum values (within the range) of sucrose hydration: 0.184 g $H_2O$/g sucrose (3.5 mol $H_2O$/mol sucrose) and 0.316 g $H_2O$/g sucrose (6 mol $H_2O$/mol sucrose) (Frazer and Myrick 1916; Scatchard 1921; Einstein 1956).

### 3.6.2. The Activity Coefficients of Water Based on Physical Parameters Determined From Osmotic Pressure Regression

When the regressed parameters (Table 3.2) are used to predict the activity coefficients of water, the predicted activity coefficients of water are in a much better agreement with the calculated activity coefficients of water compared to those based on the literature values (Figures 3.5 - 3.8). This is expected as the regressed values are obtained from the osmotic pressure data and the calculated activity coefficients are also obtained from the osmotic pressure data.

## 3.7. Discussion

The activity coefficient of water has now been given a physiological basis. Here, the activity coefficients of water are predicted for two macromolecules based on hydration and ion

binding. As expected, the activity coefficients of water for all solutions decrease from unity as the protein concentration increases. Using the Gibbs-Duhem relationships, the activity coefficients of water can be used to determine the activity coefficients of the protein or the salt based on physically realistic parameters.

### 3.7.1. Crystallization Solution Properties of Bovine Serum Albumin

Herein, the BSA molecular structure, based on the homology model, was used for calculating the SASA due to the experimental conditions used for the crystallization of the molecular structures available in the Protein Data Bank for BSA (PDB: 3V03 and 4F5S). Both of the structures were crystallized at pH 6.5 in polyethylene glycol (PEG) solutions: 20% (w/v) PEG 3350 (PDB: 3V03) and 20 - 24% (w/v) PEG monomethyl ether (MME) 5000 (PDB: 4F5S). In addition, 200 mM Ca acetate and 100 mM Tris-HCl were used in the crystallization of BSA by Majorek *et al.* (Majorek *et al.* 2012); 150 - 300 mM $NH_4Cl$ and 100 mM 2-(N-morpholino)ehanesulfonic acid (MES) were used in the crystallization of BSA by Bujacz (Bujacz 2012). In the former case, the authors mention that monoclinic crystals were observed (Majorek *et al.* 2012); however, in the latter case, the authors state that the crystals were not ideal (Bujacz 2012).

The effect of these solutions on the SASA compared to the SASA obtained from osmotic pressure for 0.15 M NaCl solutions is unknown. To investigate this, the osmotic pressure-based SASA can be determined for BSA in the crystallization solution properties.

Furthermore, the crystallization process, dehydrating the molecules, may have effects on the molecular structure due to charge repulsion. This is a very likely problem with the crystallization of BSA since it is a very negatively charged molecule in both of the crystallization solutions.

### 3.7.2. Limitations of the Activity Coefficients of Water Based on Protein-Solvent Interactions

Herein, the activity coefficient of water was only developed for protein solutions in which only solute-solvent interactions occur. However, for solutions in which protein-protein interactions occur, while Eqn. 3.14 is correct, the mole fraction of free-solvent in each compartment needs to be revised to include protein-protein interactions in order to determine the closed-form solution of the activity coefficient of water. The free-solvent model which accounts for protein-protein interactions, in addition to the protein-solvent interactions, has been recently developed (Chapter 7).

## 3.8. Conclusion

A model for the activity coefficient of water was developed based on solute-solvent interactions. Unique about this approach is that this model uses no adjustable parameters and is based only on the independently determined physical parameters associated with protein hydration and ion binding. The closed-form solution for the single macromolecule, monovalent salt system activity coefficient of water is provided, and the predicted activity coefficient of water based on physical parameters from literature for three single macromolecule solutions, up to near-saturation concentrations, is provided.

**Table 3.1.** Literature Values of the Physical Parameters for Various Macromolecules. The physical parameters are used in predicting the activity coefficient of water (Eqn. 3.14).

| Macromolecule (MW, kDa) | Solution Properties Salt Conc., pH, Temp. | Hydration, $\nu_{12}$ $\left(\frac{\text{g } H_2O}{\text{g Macromolecule}}\right)$ | Ion Binding, $\nu_{32}$ $\left(\frac{\text{mol Salt}}{\text{mol Protein}}\right)$ |
|---|---|---|---|
| Sucrose (0.342) | $H_2O$, 30°C | 0.184 - 0.316[a] | N/A |
| Bovine Serum Albumin (BSA) (66.4) | 0.15 M NaCl, 4.5, 25°C | 1.144 and 1.162ǂ | 11.59[b] |
| | 0.15 M NaCl, 5.4, 25°C | | 10.62[b] |
| | 0.15 M NaCl, 7.4, 25°C | | 8.81[b] |
| Sheep Hemoglobin (Hb) (69.7) | 0.1 M KCl, 7.43, 0°C | 0.973, 0.955, 0.981, and 1.025‡ | 6 (pH 7.4)[c] |

ǂ Based on the SASA from the homology model using GETAREA and MOLMOL, respectively

‡ Based on the SASA from the available PDB using GETAREA, Swiss-Pdb Viewer (Quality 6), MOLMOL (Precision 6), and UCSF Chimera, respectively

[a] (Frazer and Myrick 1916; Scatchard 1921; Einstein 1956)

[b] (Yousef *et al.* 1998b)

[c] (De Rosa *et al.* 2004)

**Table 3.2.** Regressed Values of the Physical Parameters for Various Macromolecules. The physical parameters are used in predicting the activity coefficient of water (Eqn. 3.14).

| Macromolecule (MW, kDa) | Solution Properties Salt Conc., pH, Temp. | Regressed Hydration, $\nu_{12}$ $\left(\frac{\text{g } H_2O}{\text{g Protein}}\right)$ | Ion Binding, $\nu_{32}$ $\left(\frac{\text{mol Salt}}{\text{mol Protein}}\right)$ |
|---|---|---|---|
| Sucrose (0.342) | $H_2O$, 30°C | 0.220 ± 0.0019 | N/A |
| Ovalbumin (OVA) (45) | 0.15 M NaCl, 7.0, 25°C | 0.86 ± 0.04[a] | 4.08 ± 0.43[a] |
| | 0.5 M NaCl, 7.0, 25°C | 0.89 ± 0.04[a] | 18.87 ± 1.03[a] |
| Bovine Serum Albumin (BSA) (66.4) | 0.15 M NaCl, 4.5, 25°C | 1.113 ± 0.006[b] | 11.59[b] |
| | 0.15 M NaCl, 5.4, 25°C | 1.137 ± 0.006[b] | 10.62[b] |
| | 0.15 M NaCl, 7.4, 25°C | 1.177 ± 0.005[b] | 8.81[b] |
| Sheep Hemoglobin (Hb) (69.7) | 0.1 M KCl, 7.43, 0°C | 0.869 ± 0.0118[c] | 5.20 ± 0.135[c] |
| Bovine Immuno-gamma Globulin (IgG) (155) | 0.13 M Ph. Buff., 7.4, 25°C | 1.107 ± 0.0414[d] | 24.3 ± 0.97[d] |
| Calf Lens α-Crystallin (800) | 0.017 M KCl, 6.8, 25°C | 1.465 ± 0.1275 | 10.4 ± 2.92 |
| | 0.15 M KCl, 6.8, 25°C | 1.433 ± 0.0409[c] | 169 ± 5.27[c] |

[a] (Yousef *et al.* 2001)
[b] (Yousef *et al.* 1998b)
[c] (McBride and Rodgers 2012)
[d] (Yousef *et al.* 1998a)

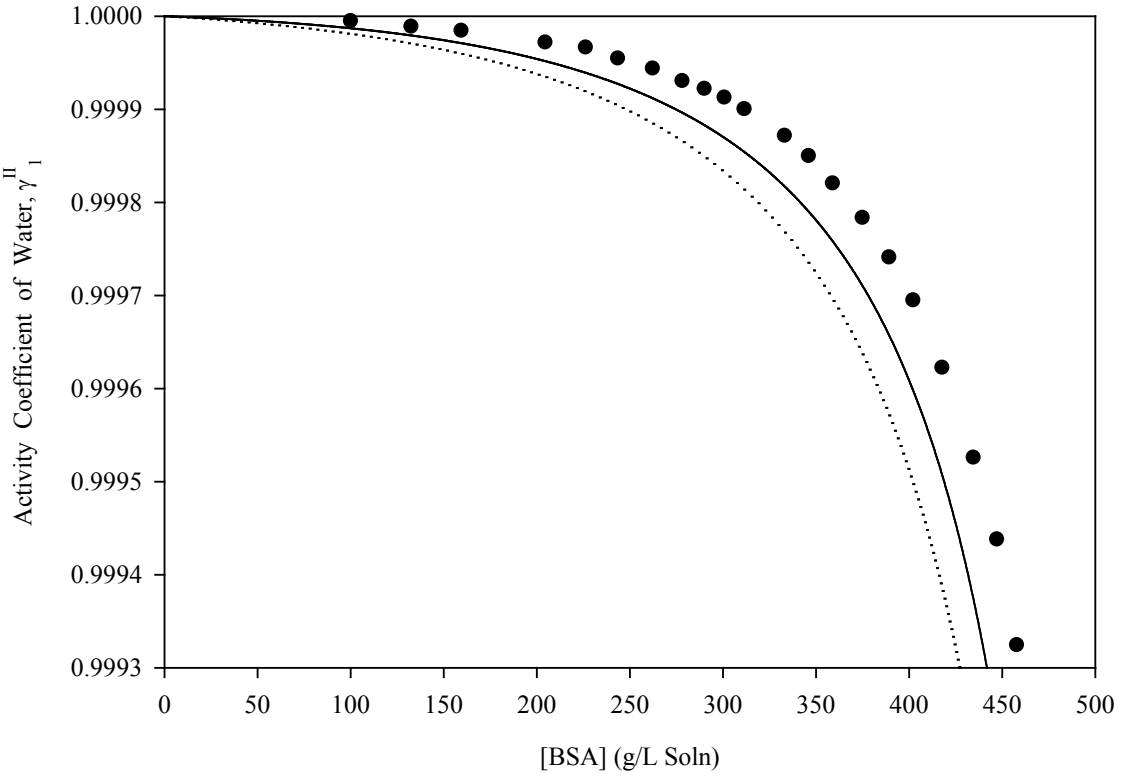


**Figure 3.1.** Activity Coefficient of Water Using Literature Values of the Physical Parameters vs. Concentration for BSA in 0.15 M NaCl, pH 4.5. The calculated activity coefficients of BSA in 0.15 M NaCl, pH 4.5 (closed circles) are shown. The predicted activity coefficients (Eqn. 3.14) are plotted using the physical parameters available in literature for BSA in 0.15 M NaCl, pH 4.5 ($\nu_{32} = 11.59$ mol NaCl/mol BSA (Yousef *et al.* 1998b)): $\nu_{12} = 1.144$ g $H_2O$/g BSA (solid curve) and $\nu_{12} = 1.162$ g $H_2O$/g BSA (dotted curve).

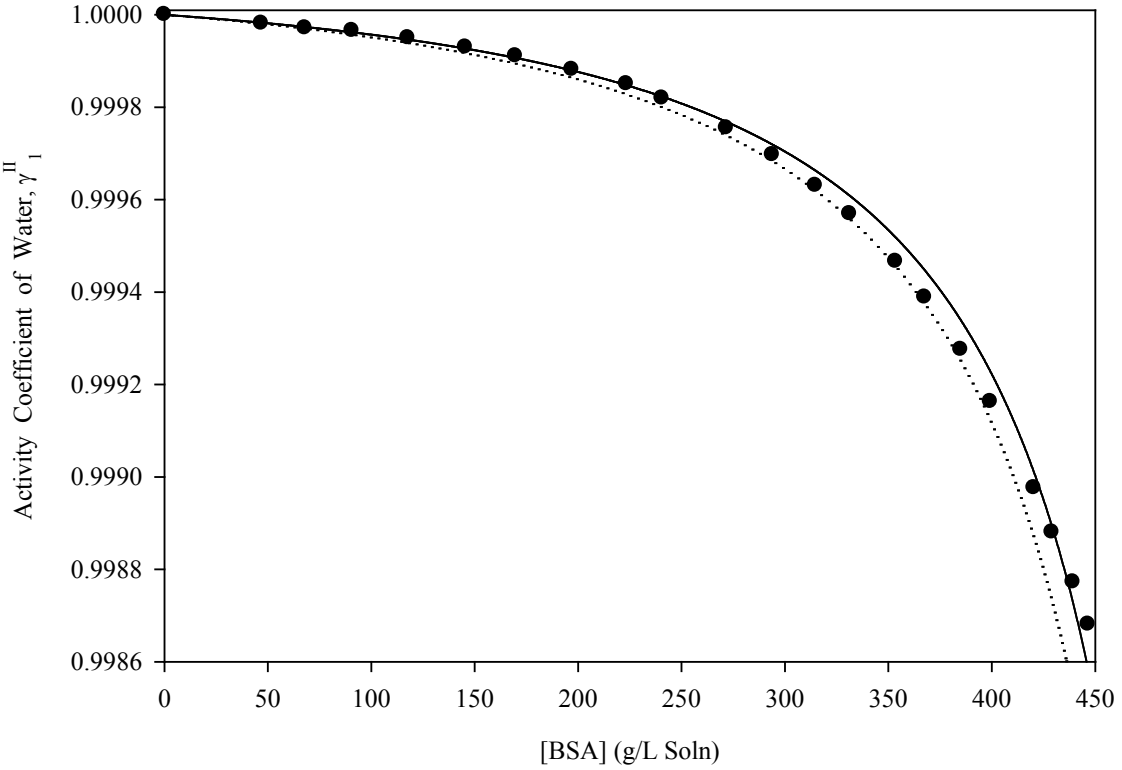


**Figure 3.2.** Activity Coefficient of Water Using Literature Values of the Physical Parameters vs. Concentration for BSA in 0.15 M NaCl, pH 5.4. The calculated activity coefficients of BSA in 0.15 M NaCl, pH 4.5 (closed circles) are shown. The predicted activity coefficients (Eqn. 3.14) are plotted using the physical parameters available in literature for BSA in 0.15 M NaCl, pH 5.4 ($\nu_{32} = 10.62$ mol NaCl/mol BSA (Yousef *et al.* 1998b)): $\nu_{12} = 1.144$ g $H_2O$/g BSA (solid curve) and $\nu_{12} = 1.162$ g $H_2O$/g BSA (dotted curve).

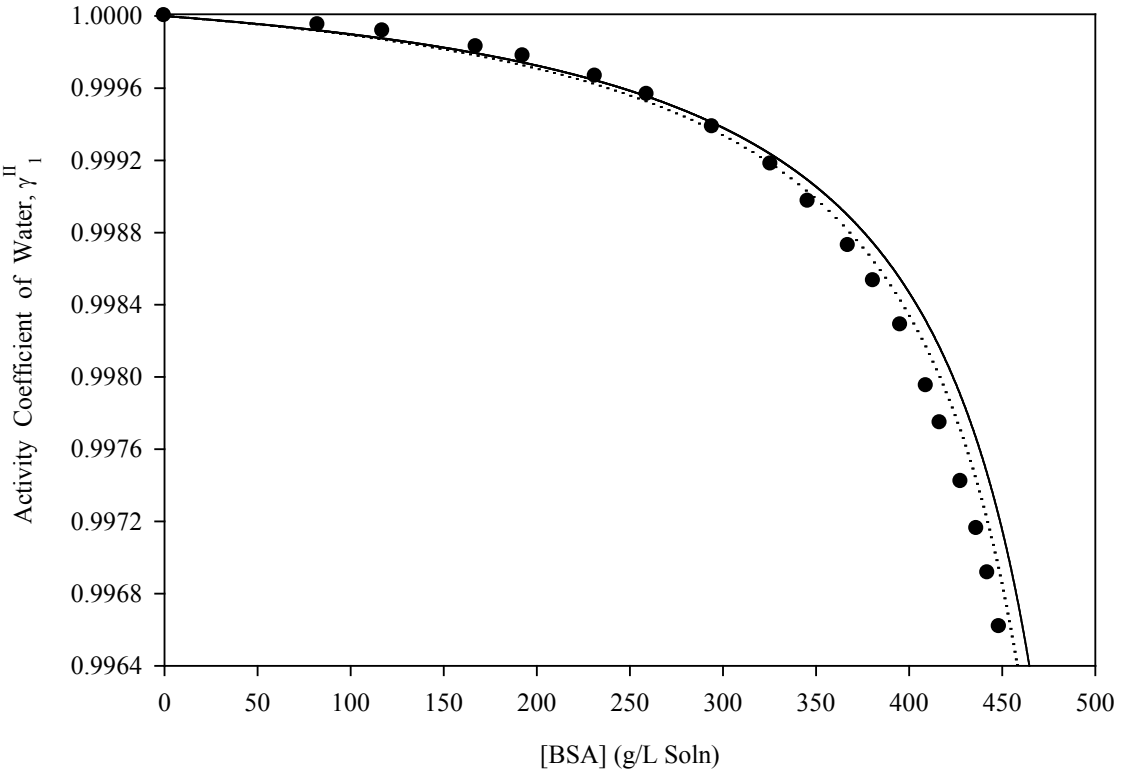


**Figure 3.3.** Activity Coefficient of Water Using Literature Values of the Physical Parameters vs. Concentration for BSA in 0.15 M NaCl, pH 7.4. The calculated activity coefficients of BSA in 0.15 M NaCl, pH 4.5 (closed circles) are shown. The predicted activity coefficients (Eqn. 3.14) are plotted using the physical parameters available in literature for BSA in 0.15 M NaCl, pH 4.5 ($\nu_{32} = 8.81$ mol NaCl/mol BSA (Yousef *et al.* 1998b)): $\nu_{12} = 1.144$ g $H_2O$/g BSA (solid curve) and $\nu_{12} = 1.162$ g $H_2O$/g BSA (dotted curve).

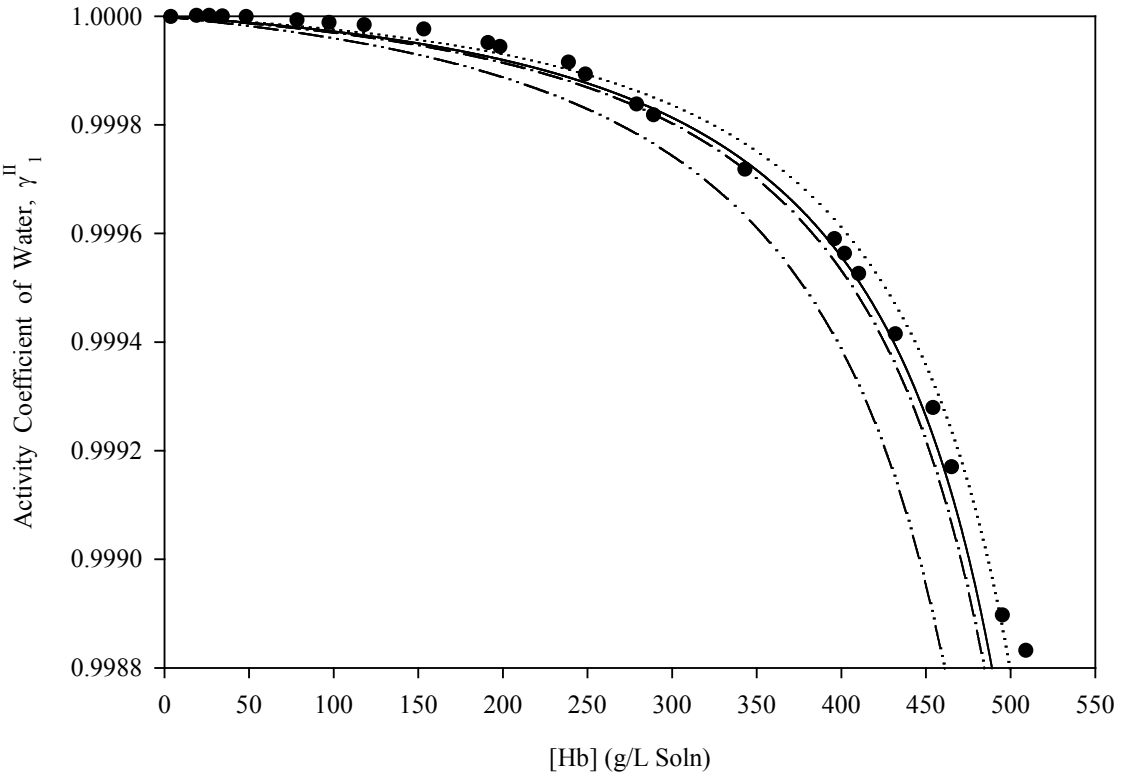


**Figure 3.4.** Activity Coefficient of Water Using Literature Values of the Physical Parameters vs. Concentration for Hb. The calculated activity coefficients of Hb in 0.1 M KCl, pH 7.43 (closed circles) are shown. The predicted activity coefficients (Eqn. 3.14) are plotted using the physical parameters available in literature for Hb ($\nu_{32} = 6$ mol KCl/mol Hb (De Rosa *et al.* 2004)). The hydration values, determined from the SASA, are: $\nu_{12} = 0.973$ g $H_2O$/g Hb (solid curve), $\nu_{12} = 0.955$ g $H_2O$/g Hb (dotted curve), $\nu_{12} = 0.981$ g $H_2O$/g Hb (dash-dot curve), and $\nu_{12} = 1.025$ g $H_2O$/g Hb (dash-dot-dot curve).

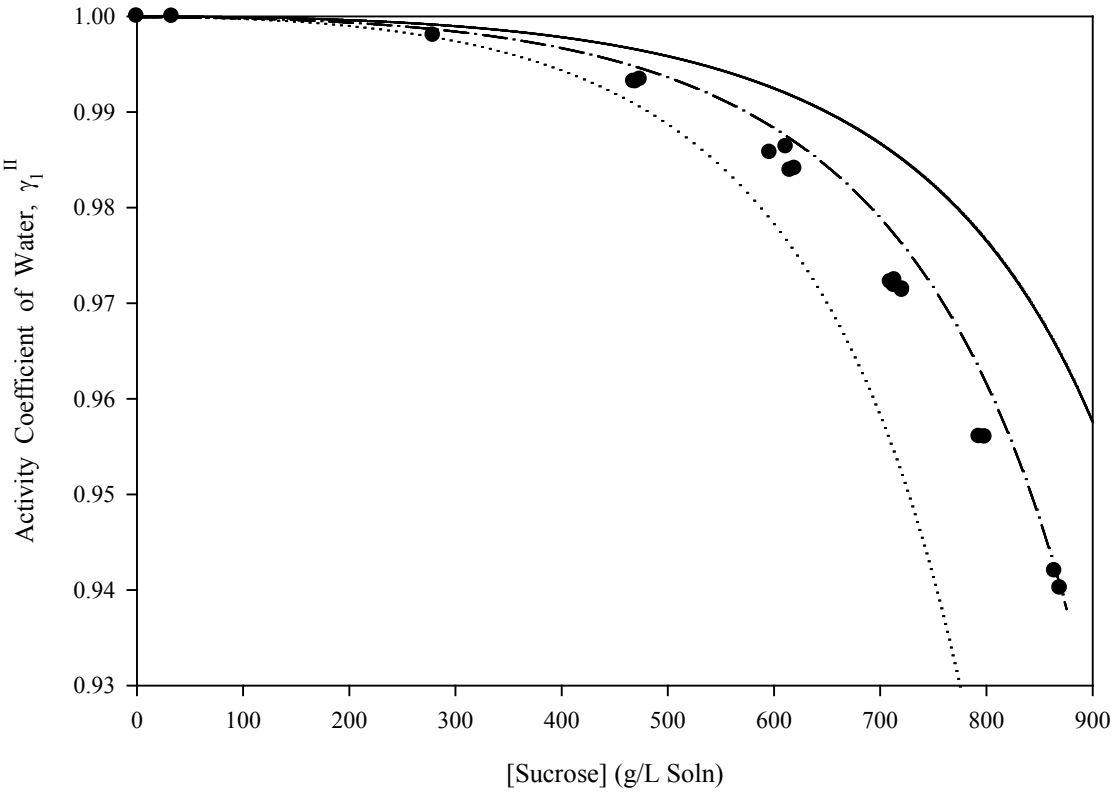


**Figure 3.5.** Activity Coefficient of Water vs. Concentration for Sucrose. The calculated activity coefficients of sucrose in water (closed circles) are shown. The predicted activity coefficient (Eqn. 3.14) is plotted using the literature values of hydration ($\nu_{12} = 0.184$ g $H_2O$/g sucrose (solid curve) and $\nu_{12} = 0.316$ g $H_2O$/g sucrose, (dotted curve)) and the regressed hydration ($\nu_{12} = 0.220$ g $H_2O$/g sucrose, dash-dot curve).

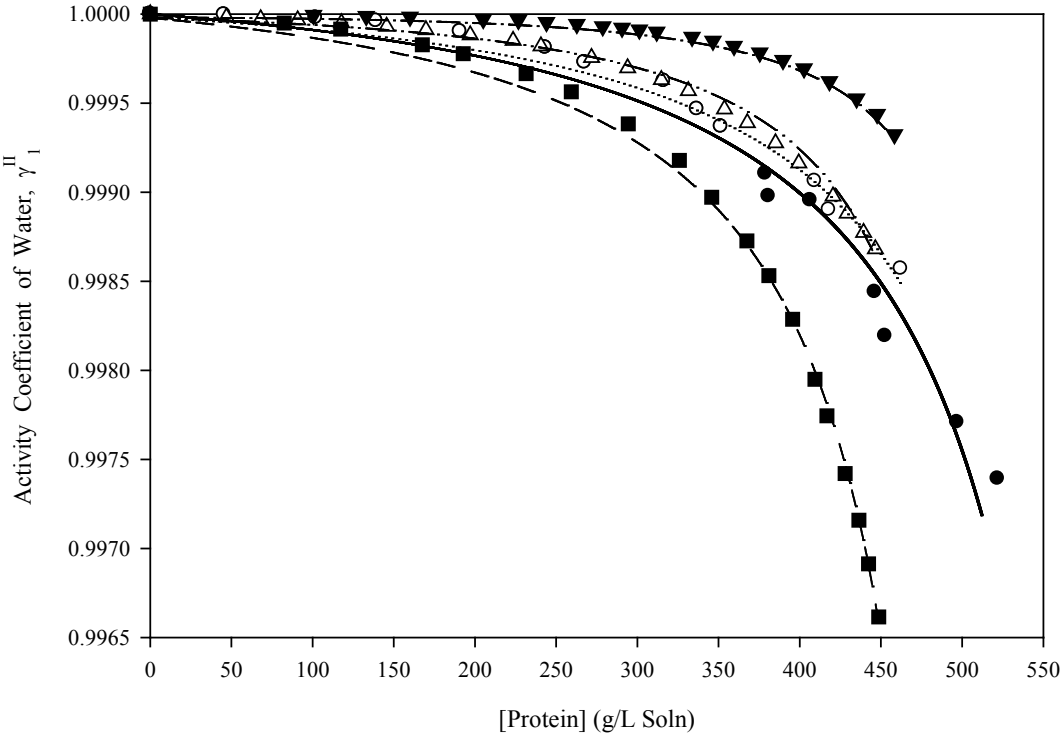


**Figure 3.6.** Activity Coefficient of Water vs. Concentration for OVA and BSA Solutions. The physical parameters used correspond to the best fit, regressed values. The calculated activity coefficients of OVA in 0.15 M NaCl, pH 7.0 (closed circles) and 0.5 M NaCl, pH 7.0 (open circles) and BSA in 0.15 M NaCl, pH 4.5, 5.4, and 7.4 (closed triangles, open triangles, and closed squares, respectively) are shown. The predicted activity coefficients (Eqn. 3.14) are plotted using the physical parameters for OVA in 0.15 M NaCl, pH 7.0 (solid curve) OVA in 0.5 M NaCl, pH 7.0 (dotted curve) and BSA in 0.15 M NaCl, pH 4.5, 5.4, and 7.4 (dash-dot curve, dash-dot-dot curve, and dashed curve, respectively).

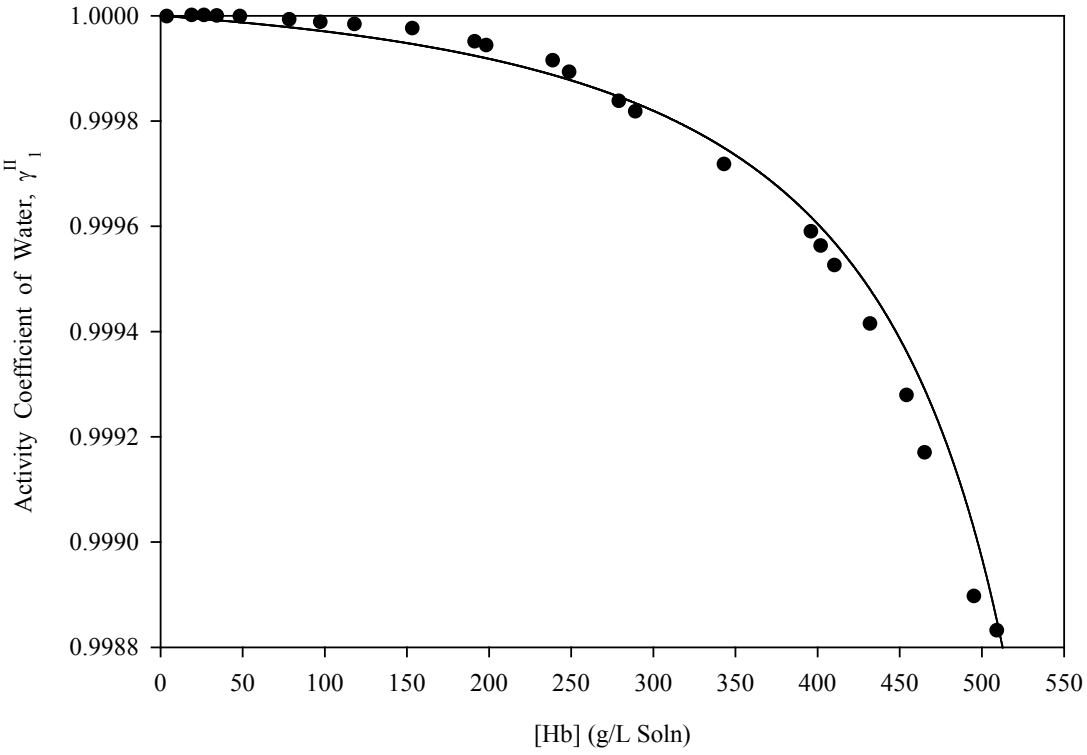


**Figure 3.7.** Activity Coefficient of Water vs. Concentration for Hb. The calculated activity coefficients of Hb in 0.1 M KCl, pH 7.43 (closed circles) are shown. The predicted activity coefficients (Eqn. 3.14) are plotted using the regressed values for physical parameters ( $\nu_{12} = 0.869$ g $H_2O$/g Hb and $\nu_{32} = 5.20$ mol KCl/mol Hb (M$^c$Bride and Rodgers 2012)) (solid curve).

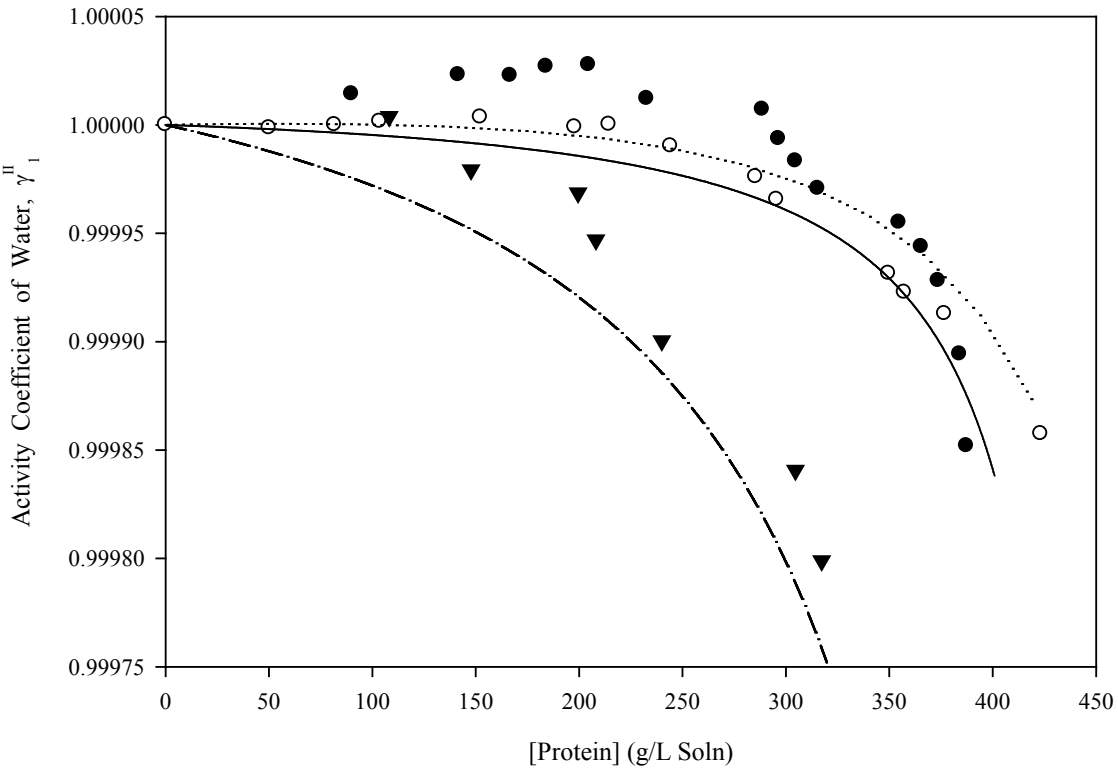


**Figure 3.8.** Activity Coefficient of Water vs. Concentration for α-Crystallin and IgG Solutions. The physical parameters used correspond to the best fit, regressed values. The calculated activity coefficients of α-crystallin in 0.017 M KCl, pH 6.8 (closed circles) and 0.15 M KCL, pH 6.8 (open circles) and IgG (closed triangles) are shown. The predicted activity coefficients (Eqn. 3.14) are plotted using the physical parameters for α-crystallin in 0.017 M KCl (solid curve) and 0.15 M KCl (dotted curve), and IgG (dash-dot curve).

# CHAPTER 4.

# UNDERSTANDING THE VIRIAL COEFFICIENT USING THE FREE-SOLVENT MODEL: AN ALTERNATE PERSPECTIVE BASED ON SOLUTE-SOLVENT INTERACTIONS

## 4.1. Abstract

The virial coefficients have long been thought to account for solute-solute interactions. One model for determining the values of the virial coefficients based on solute-solute interactions is the McMillan-Mayer Dilute Solution Theory; however, the reported virial coefficients predicted via the McMillan-Mayer Theory are unable to capture the significant variations in osmotic pressure for varied solution properties. Here, a model is developed for predicting the second virial coefficient based on solute-solvent interactions using the free-solvent model. The second virial coefficients calculated based on solute-solvent interactions are compared to the values of the traditional second virial coefficients. Herein, the dependency of the second virial coefficient on solute concentration is observed for the traditional method (virial expansion model) and the model based on solute-solvent interactions. It follows that the second virial coefficient can be fully explained, for non-aggregating protein solutions, by solute-solvent interactions.

## 4.2. Introduction

Many models have been developed in an attempt to correct for and understand the non-ideal behavior of the osmotic pressure for concentrated solutions. Some such models are based on the Scaled Particle Theory (Gibbons 1969, 1970; Chatelier and Minton 1987), mean spherical approximation (MSA) (Groot 1991; Sassi *et al.* 1996), mean-field theory (Miklavic and Woodward 1990), and Yukawa model (Lin *et al.* 2001; Xue *et al.* 2008).

The most widely used osmotic pressure model which corrects for the deviation of the osmotic pressure from ideality is the virial expansion of the van't Hoff equation, $\pi_p$, coupled with the Donnan contribution, $\pi_D$.

$$\pi \approx \pi_p + \pi_D \tag{4.1}$$

A virial expansion on the van't Hoff equation is

$$\pi_p = RT\left[B_1 c_2 + B_2 c_2^2 + B_3 c_2^3 + ...\right] \tag{4.2}$$

where $c_2$ is the concentration in grams per liter solution, $B_1$ is the first virial coefficient, which is related to the protein molecular weight by

$$B_1 = \frac{1}{M_2}, \tag{4.3}$$

and $B_2$ and $B_3$ are the second and third virial coefficients, which represent two-body and three-body solute-solute interactions. Typically, the virial expansion model is truncated after three terms (Vilker *et al.* 1981; Wang and Bloomfield 1990; Haynes *et al.* 1992), although models have been reported which contain up to the seventh term (Ross and Minton 1977).

It is conventionally assumed that a positive $B_2$ value is the result of a net negative interaction (repulsive interaction) between solute molecules, while a negative $B_2$ is the result of a net attractive interaction (George and Wilson 1994).

The contribution of the ion redistribution to the osmotic pressure, via the Donnan effect, is expressed as

$$\pi_D = RT\left[2\sqrt{\left(\frac{\overline{Z}c_2}{2M_2}\right)^2 + m_3^2} - 2m_3\right] \tag{4.4}$$

where $\overline{Z}$ is the protein charge and $m_3$ is the salt concentration in molal. At salt concentrations greater than 0.1 M, the Donnan effect is known to be negligible (Vilker *et al.* 1981). The Donnan contribution is an effect on the osmotic pressure caused by the redistribution of the salt ions.

The sum of the protein, $\pi_p$, and salt contributions, $\pi_D$, yield the total osmotic pressure of the system. When the virial expansion is truncated to three terms, the total osmotic pressure is

$$\pi = RT\left[\frac{1}{M_2}c_2 + B_2c_2^2 + B_3c_2^3 + 2\sqrt{\left(\frac{\overline{Z}c_2}{2M_2}\right)^2 + m_3^2} - 2m_3\right]. \quad (4.5)$$

Eqn. 4.5 allows for the osmotic pressure to be predicted if the virial coefficients are known. If the virial coefficients are unknown, the osmotic pressure data can be fit using Eqn. 4.5 to obtain the values of the virial coefficients.

## 4.3. Virial Coefficients

Virial coefficients are extensively used for understanding solutions and have been reported to be related to protein crystallization (George and Wilson 1994; Rosenbaum and Zukoski 1996; Neal *et al.* 1998, 1999; Guo *et al.* 1999; Tessier and Lenhoff 2003; Tessier *et al.* 2004; Dumetz *et al.* 2007), aggregation (Schaink and Smit 2000; Zhang and Liu 2003; Alford *et al*. 2008; Li *et al.* 2009; Weiss *et al.* 2009; Shain *et al.* 2010), protein stability (Krishnan *et al.* 2002; Chi *et al.* 2003; Ho *et al.* 2003) and solubility (George and Wilson 1994; Rosenbaum and Zukoski 1996; George *et al.* 1997; Guo *et al.* 1999; Haas *et al.* 1999; Ruppert *et al.* 2001), protein diffusion (Zhang and Liu 2003), and protein purification (Dickinson *et al.* 2001; Loll *et al.* 2001; Ruppert *et al.* 2001).

There are a variety of techniques which have been used to obtain second virial coefficients, such as osmotic pressure, sedimentation equilibrium, and static light scattering

(Kirkwood and Goldberg 1950; Stockmayer 1950; Hill 1959; Wills and Winzor 1992; Wills *et al.* 1993, 2000). While these methods all yield second virial coefficients, the values obtained from each method can vary due to the interactions accounted for by each method. However, all of these techniques are purported to yield the second virial coefficient based on protein-protein interactions.

### 4.3.1. A Function of Solute-Solute Interactions

Historically, virial coefficients are thought to account for solute-solute interactions in the form of attraction and repulsion between molecules. More specifically, the second virial coefficient accounts for interactions between two solute molecules, while the third virial coefficient accounts for the interactions between three solute molecules. Furthermore, since the virial coefficients account for solute-solute interactions, it is assumed that there is dependency of the virial coefficients on the solute concentration (McMillan and Mayer 1945; Alford *et al.* 2008). As the protein in solution nears saturation, higher order virial coefficients are required to account for larger, aggregate formations. Various models have been used for determining the virial coefficients, with the majority assuming solute-solute interactions are the dominant contributors.

#### 4.3.1.1. McMillan-Mayer Dilute Solution Theory

The McMillan-Mayer Dilute Solution Theory attempts to predict the virial coefficients based on the potential mean force between the protein molecules, $W_i$, is given as (McMillan and Mayer 1945; Vilker 1976; Ross and Minton 1977)

$$B_{\mathrm{i}} = \frac{B_i'}{M_2^i}, \tag{4.6}$$

where $B_i$ is the i[th] virial coefficient and $B_i'$ is related to the potential mean force of species $i$ via the McMillan-Mayer Theory (McMillan and Mayer 1945). For a two-body interaction between proteins (intra-protein interactions), the relationship to the McMillan-Mayer Theory for the second virial coefficient, $B_{22}'$, is

$$B_{22}' = -2\pi' \int_0^\infty \left[ e^{-W_{22}/kT} - 1 \right] r^2 dr \,, \tag{4.7}$$

where $r$ is the center-to-center distance between two protein molecules.

In order to compare the McMillan-Mayer Dilute Solution Theory virial coefficients to those obtained from regression, Vilker *et al.* utilized a third order virial expansion model for three bovine serum albumin (BSA) solutions. For the second and third virial coefficients, Vilker *et al.* accounted for various interactions, including electrostatic, induction, and dispersion forces. While the osmotic pressure for all three solutions examined, predicted from the McMillan-Mayer Theory virial coefficients, was the correct magnitude, the model did not fit well (Vilker 1976; Vilker *et al.* 1981). Vilker *et al.* extensively analyzed the McMillan-Mayer Theory, but could not conclude what the cause of deviation between the model and the data might be (Vilker 1976; Vilker *et al.* 1981).

While recent developments for predicting the virial coefficients based on the McMillan-Mayer Theory have been pursued, none have been experimentally validated for osmotic pressure data (Mollerup and Breil 2009a, 2009b). Until now, there have been no further explanations on the causes of the deviations between the fitted virial coefficients and those predicted by the McMillan-Mayer Dilute Solution Theory.

4.3.1.2. Traditional Virial Coefficient Model

Traditionally, the virial coefficients were fit to the osmotic pressure data for dilute solutions. Given the dilute solution, the virial expansion model becomes

$$\pi = RT\left[\frac{1}{M_2}c_2 + B_2 c_2^2\right] \tag{4.8}$$

and, through linear regression, the second virial coefficient can be determined. For concentrated solutions, non-linear regression is performed to determine the second and higher order virial coefficients.

While this method allows for a better prediction and fit of the experimental data compared with the virial expansion model based on the McMillan-Mayer Dilute Solution Theory, the values of the virial coefficients are not directly related to any physiological parameters.

4.3.1.3. Charge Dependency of the Virial Coefficients

In 1981, Vilker *et al.*, correlated the virial coefficients with the charge of the solute (Vilker *et al.* 1981). Using concentrated BSA solutions, the authors develop the charge-based virial expansion model.

$$\pi = \frac{RT}{M_2}\left[c_2 + B_2 c_2^2 + B_3 c_2^3\right] + RT\left[2\sqrt{\left(\frac{\overline{Z}c_2}{2M_2}\right)^2 + m_3^2} - 2m_3\right] \tag{4.9}$$

where the virial coefficients, $B_2$ and $B_3$, are taken to be quadratically dependent on charge, or

$$B_2 = \mathrm{A}_2 + \mathrm{B}_2\overline{Z} + \mathrm{C}_2\overline{Z}^2 \tag{4.10}$$

and

$$B_3 = \mathrm{A}_3 + \mathrm{B}_3\overline{Z} + \mathrm{C}_3\overline{Z}^2. \tag{4.11}$$

Vilker *et al.* performed non-linear regression of the osmotic pressure data in order to determine the charge coefficients, $A_i$, $B_i$, and $C_i$, for the $i^{th}$ virial coefficient term. While this method provides values of the virial coefficients, similar to the non-linear fitting of Eqn. 4.8, they lack realistic parameters and physical meaning.

4.3.2. Considering Solute-Solvent Interactions

Despite the overwhelming focus on the relationship between protein-protein interaction and the second virial coefficient, some research has considered solute-solvent interactions. Scatchard and Pigliacampi suggested that the second virial coefficient is dependent on the interaction of ions and the solute among other interactions (*i.e.* protein-protein interactions, and the Donnan effect). Their model fails to take water-solute interaction and thus requires the use of another term (assumed to be based on protein-protein interaction) in order to provide a good fit of the osmotic pressure data (Scatchard and Pigliacampi 1962).

More recently, the general contributions of solute-solvent interactions (protein-ion as well as protein hydration) have been viewed as significant factors in the solution of virial coefficients. Yousef *et al*. suggested that the free-solvent model may be expanded in a virial expansion-like way, eluding to the coupling between the virial coefficient and solute-solvent interactions (Yousef *et al.* 1998a, 1998b). Winzor *et al.* (Winzor *et al.* 2007) and Blanco *et al.* (Blanco *et al*. 2011) discuss the deviations observed for the second virial coefficient determined from sedimentation and that of static light scattering. Winzor *et al.* speculate that the deviation occurs because the second virial coefficient determined by sedimentation, similar to the value obtained from osmotic pressure, accounts for only solute-solute (or self) interactions, while the second virial coefficient determined by static light scattering yields a more true value since it accounts for solute-solvent interaction, as well as solute-solute interactions. Winzor *et al.*

(Winzor *et al.* 2007) and Blanco *et al.* (Blanco *et al*. 2011) argue that correcting the second virial coefficient to include solute-solvent interactions can provide a more accurate estimation of the parameter.

Until now, no functional relationship for the virial coefficients with respect to solute-solvent (specifically including hydration) interactions or concentration has been offered. Here, the second virial coefficient is reexamined in terms of the free-solvent model for protein osmotic pressure. Thus the second virial coefficient is developed considering solute-solvent interactions. The developed model is analyzed to determine the physical parameter conditions and solution properties for which positive, negative, and zero values of the second virial coefficient are obtained.

## 4.4. The Free-Solvent Model

The free-solvent model addresses protein-solvent interactions in determining non-idealities in concentrated protein solutions. Essentially, the model treats the hydrated protein as a separate macromolecule, and all associated water and salt ions are absorbed in its definition. In effect, this approach renders the solution ideal with respect to the remaining solvent species that have no attractive interactions. The modified mole fraction of the free-solvent is based on the hydrated macromolecules.

As early as 1916, Frazer and Myrick analyzed the non-idealities in aqueous sucrose solutions using a free-solvent model (Frazer and Myrick 1916). More recently, other researchers, in a similar approach, based their models on the van't Hoff equation but only had limited success for protein solutions up to moderate concentrations (Ling *et al*. 1980; Ling 1984; Cameron and Fullerton 1990; Fullerton *et al.* 1992).

For a two-chamber osmometer, with the chamber containing the proteins denoted as compartment II and the chamber containing only the solvent and diffusible ions denoted as compartment I (Yousef *et al.* 1998a), the free-solvent model with the mole fraction of the free-solvent as the composition variable follows the van Laar equation,

$$\pi = -\frac{RT}{\bar{V}_1}\ln\left(\frac{x_1^{\mathrm{II}}}{x_1^{\mathrm{I}}}\right). \tag{4.12}$$

Assuming the solutions is made up of $n$ distinct species, and letting species 1 be the solvent, species 2 through $(p+1)$ be the proteins (for $p$ protein species), and species $(p+2)$ through $n$ be the remaining diffusible species, the initial total moles of the solution in compartment II is $N^{\mathrm{II}} = \sum_{i=1}^{n} N_i^{\mathrm{II}}$, where $i$ denotes each species. The final total moles of free-solvent in chamber II is

$$N_*^{\mathrm{II}} = N^{\mathrm{II}} - \sum_{\substack{i=1 \\ i\neq 2\rightarrow p+1}}^{n}\sum_{j=2}^{p+1}\nu_{ij}N_j^{\mathrm{II}} - \sum_{j=2}^{p+1}N_j^{\mathrm{II}}\ , \tag{4.13}$$

where $N_j^{\mathrm{II}}$ denotes the moles of protein $j$ in solution and $\nu_{ij}$ is the number of moles of species $i$ interacting with protein $j$ to make the hydrated protein. Then, the mole fraction of free-solvent in chamber II is

$$x_1^{\mathrm{II}} = \frac{N_1^{\mathrm{II}} - \sum_{j=2}^{p+1}\nu_{1j}N_j^{\mathrm{II}}}{N_*^{\mathrm{II}} + \sum_{j=2}^{p+1}N_j^{\mathrm{II}}}\ , \tag{4.14}$$

while in chamber I, the mole fraction of free-solvent is

$$x_1^{\mathrm{I}} = \frac{N_1^{\mathrm{I}}}{N_1^{\mathrm{I}} + N_3^{\mathrm{I}}}\ . \tag{4.15}$$

For a two-chamber osmometer with a single protein species and one monovalent salt in aqueous solution, the free-solvent model reduces to

$$\pi \approx -\frac{RT}{\bar{V}_1}\ln\left(\frac{\left(N_1^{\mathrm{II}}-\nu_{12}N_2^{\mathrm{II}}\right)\left(N_1^{\mathrm{I}}+N_3^{\mathrm{I}}\right)}{\left(N_1^{\mathrm{II}}+\left(1-\nu_{12}-\nu_{32}\right)N_2^{\mathrm{II}}+N_3^{\mathrm{II}}\right)N_1^{\mathrm{I}}}\right). \tag{4.16}$$

4.5. The Dependency of Virial Coefficients on Solute-Solvent Interactions

Since the second virial coefficient, $B_2$, is predicted within the dilute region, the virial expansion model is typically reduced to a linear model as a function of concentration (in grams per liter), $c_2$, with the slope being the second virial coefficient.

By considering only the dilute region, the free-solvent model can similarly be reduced to a linear model. The linearized free-solvent model, valid only for dilute solution osmotic pressure, will be a function of solute hydration and solute-ion binding.

In order to determine the relationship of the second virial coefficient and solute-solvent interactions, the virial expansion model and free-solvent models need to be linearized about a similar concentration variable. The concentration variable of the virial expansion model is typically the concentration of the protein (in grams per liter), whereas the free-solvent model is the mole fraction of free water (after considering solute-solvent interactions).

Changing the virial expansion (Eqn. 4.8) concentration variable, $c_2$, to the mole fraction of protein in compartment II yields,

$$\pi = RT\left[\frac{1}{\bar{V}_1}x_2^{\mathrm{II}} + B_2\left(\frac{M_2}{\bar{V}_1}\right)^2\left(x_2^{\mathrm{II}}\right)^2\right], \tag{4.17}$$

where the mole fraction of protein in Eqn. 4.16 does not take into consideration the solute-solvent interactions, but rather is the conventional mole fraction of protein (using total water). For a single protein and monovalent salt in water, the mole fraction of protein is

$$x_2^{\mathrm{II}} = \frac{N_2^{\mathrm{II}}}{N_1^{\mathrm{II}}+N_2^{\mathrm{II}}+N_3^{\mathrm{II}}}. \tag{4.18}$$

Combining Eqn. 4.17 and 4.18 to obtain the virial expansion model in terms of mole numbers gives

$$\pi = RT\left[\frac{1}{\overline{V}_1}\left(\frac{N_2^{\mathrm{II}}}{N_1^{\mathrm{II}}+N_2^{\mathrm{II}}+N_3^{\mathrm{II}}}\right)+B_2\left(\frac{M_2}{\overline{V}_1}\right)^2\left(\frac{N_2^{\mathrm{II}}}{N_1^{\mathrm{II}}+N_2^{\mathrm{II}}+N_3^{\mathrm{II}}}\right)^2\right], \tag{4.19}$$

where $N_1^{\mathrm{II}}$, $N_2^{\mathrm{II}}$, and $N_3^{\mathrm{II}}$ are the number of moles of water (species $1$), protein (species $2$), and salt (species $3$) in the solution chamber (compartment $\mathrm{II}$), respectively.

The free-solvent model, for a single protein and a monovalent salt in water, in terms of the mole numbers is given by Eqn. 4.16.

Now that both models are in terms of the same concentration variable, $N_2^{\mathrm{II}}$, taking the derivative of the virial expansion model with respect to the mole number of protein yields

$$\frac{\partial\pi}{\partial N_2^{\mathrm{II}}} = RT\left[\frac{1}{\overline{V}_1}\left(\frac{N_1^{\mathrm{II}}+N_3^{\mathrm{II}}}{\left(N_1^{\mathrm{II}}+N_2^{\mathrm{II}}+N_3^{\mathrm{II}}\right)^2}\right)+2B_2\left(\frac{M_2}{\overline{V}_1}\right)^2\left(\frac{N_2^{\mathrm{II}}\left(N_1^{\mathrm{II}}+N_3^{\mathrm{II}}\right)}{\left(N_1^{\mathrm{II}}+N_2^{\mathrm{II}}+N_3^{\mathrm{II}}\right)^3}\right)\right], \tag{4.20}$$

while the derivative, with respect to the mole number of protein, of the free-solvent model is

$$\frac{\partial\pi}{\partial N_2^{\mathrm{II}}} = \frac{RT}{\overline{V}_1}\left(\frac{\nu_{12}\left(N_1^{\mathrm{II}}+\left(1-\nu_{12}-\nu_{32}\right)N_2^{\mathrm{II}}+N_3^{\mathrm{II}}\right)+\left(N_1^{\mathrm{II}}-\nu_{12}N_2^{\mathrm{II}}\right)\left(1-\nu_{12}-\nu_{32}\right)}{\left(N_1^{\mathrm{II}}-\nu_{12}N_2^{\mathrm{II}}\right)\left(N_1^{\mathrm{II}}+\left(1-\nu_{12}-\nu_{32}\right)N_2^{\mathrm{II}}+N_3^{\mathrm{II}}\right)}\right). \tag{4.21}$$

In the dilute region the derivatives can be equated to solve for the second virial coefficient, or

$$\begin{aligned} &RT\left[\frac{1}{\overline{V}_1}\left(\frac{N_1^{\mathrm{II}}+N_3^{\mathrm{II}}}{\left(N_1^{\mathrm{II}}+N_2^{\mathrm{II}}+N_3^{\mathrm{II}}\right)^2}\right)+2B_2\left(\frac{M_2}{\overline{V}_1}\right)^2\left(\frac{N_2^{\mathrm{II}}\left(N_1^{\mathrm{II}}+N_3^{\mathrm{II}}\right)}{\left(N_1^{\mathrm{II}}+N_2^{\mathrm{II}}+N_3^{\mathrm{II}}\right)^3}\right)\right]= \\ &=\frac{RT}{\overline{V}_1}\left(\frac{\nu_{12}\left(N_1^{\mathrm{II}}+\left(1-\nu_{12}-\nu_{32}\right)N_2^{\mathrm{II}}+N_3^{\mathrm{II}}\right)+\left(N_1^{\mathrm{II}}-\nu_{12}N_2^{\mathrm{II}}\right)\left(1-\nu_{12}-\nu_{32}\right)}{\left(N_1^{\mathrm{II}}-\nu_{12}N_2^{\mathrm{II}}\right)\left(N_1^{\mathrm{II}}+\left(1-\nu_{12}-\nu_{32}\right)N_2^{\mathrm{II}}+N_3^{\mathrm{II}}\right)}\right) \end{aligned}. \tag{4.22}$$

The second virial coefficient can now be solved for in terms of solute-solvent interactions and as a function of the concentrations of the species in the solution, or

$$B_2 = \frac{\overline{V}_1}{2(M_2)^2}\left[\left(\frac{\nu_{12}\left(N_1^{II}+(1-\nu_{12}-\nu_{32})N_2^{II}+N_3^{II}\right)+\left(N_1^{II}-\nu_{12}N_2^{II}\right)(1-\nu_{12}-\nu_{32})}{\frac{N_2^{II}\left(N_1^{II}+N_3^{II}\right)\left(N_1^{II}-\nu_{12}N_2^{II}\right)\left(N_1^{II}+(1-\nu_{12}-\nu_{32})N_2^{II}+N_3^{II}\right)}{\left(N_1^{II}+N_2^{II}+N_3^{II}\right)^3}}\right)-N_2^{II}\right]. \quad (4.23)$$

Using Eqn. 4.23, the second virial coefficient is directly calculated from physical parameters for BSA in 0.15 M NaCl solutions at pH 4.5, 5.4, 7.0, and 7.4, and Hen Egg Lysozyme (HEL) in 0.15 M NaCl, pH 7.0 and 0.15 M KCl, pH 7.0.

## 4.6. Methods

Concentrated osmotic pressure data of BSA in various solutions and HEL in various solutions were used to predict the second virial coefficient based on the solute-solvent interactions of each solution (Eqn. 4.23). The second virial coefficient based on solute-solvent interactions are compared to those solved by the traditional method.

### 4.6.1. Solution Properties Studied

The second virial coefficient was predicted for BSA (in 0.15 M NaCl at pH 4.5, 5.4, 7.0, and 7.4) and HEL (in 0.15 M NaCl, pH 7.0 and 0.15 M KCl, pH 7.0).

### 4.6.2. Osmotic Pressure Measurements

The osmotic pressure data for three of the BSA solutions (pH 4.5, 5.4 and 7.4) and both of the HEL solutions are available in the literature. The dilute osmotic pressure data for these three BSA solutions were measured by (Scatchard *et al.* 1946). Vilker *et al.* measured the concentrated osmotic pressure data for the three BSA solutions (Vilker *et al.* 1981). The osmotic pressure data for both HEL solutions is that of Yousef *et al.* (Yousef *et al.* 2002b).

The osmotic pressure data for BSA in 0.15 M NaCl at pH 7.0 was measured to provide an additional dataset for analysis of the second virial coefficient. Scatchard *et al.* measured the osmotic pressure of BSA in 0.15 M NaCl, pH 7.0 for dilute concentrations only (Scatchard *et al.* 1946).

The osmotic pressure of BSA in 0.15 M NaCl, 25°C, pH 7.0 was measured using the method and osmometer described by Yousef *et al.* (Yousef *et al.* 1998a). Briefly, the protein solution was prepared by dissolving a known amount of BSA in 0.15 M NaCl. The pH was adjusted using 1.0 M NaOH and 1.0 M HCl to a final pH of 7.0. The solvent solution was prepared by dissolving a known amount of NaCl in nanopure water. The pH was adjusted in a similar manner to the BSA solution.

The protein and solvent chambers were separated using a semi-permeable membrane (5000 MWCO, cellulose ester, Molecular/Por, Type C, Spectrum, Laguna Hills, CA). The pressure in the protein chamber was measured using one of two pressure transducers (PX-726 (range: 0 - 25 psi), PX-102 (range: 0 - 100 psi), Omega Engineering, Stamford, CN) connected to a National Instruments DAQ setup and collected by LabVIEW (National Instruments Corporation, Austin, TX).

### 4.6.3. Physical Parameters

The physical parameters of BSA in 0.15 M NaCl at pH 4.5, 5.4, and 7.4 (Yousef *et al.* 1998b) are available in literature and were used in this work. For BSA in 0.15 M NaCl at pH 7.0, the hydration and ion binding of BSA in 0.15 M NaCl at pH 7.0 was obtained by nonlinear regression of Eqn. 4.16 (TableCurve 2D (Systat Software, San Jose, CA, USA)).

The physical parameters for HEL in 0.15 M NaCl, pH 7.0, and 0.15 M KCl, pH 7.0, available in literature (Curtis *et al.* 1998; Kuehner *et al.* 1999; Yousef *et al.* 2002b). In addition to

using the literature values for the HEL physical parameters, a regressed ion binding was also used, and was obtained for a hydration value from the solvent accessible surface area (SASA) (Yousef *et al.* 2002b; M$^{c}$Bride and Rodgers 2012) of HEL (PDB Code: 4LYZ (Diamond 1974)) since the literature values of ion binding were 2 mol Cl/mol HEL or 4 mol Cl/mol HEL. Five molecular modeling software, Swiss-Pdb Viewer (Guex and Peitsch 1997), MOLMOL (Koradi *et al.* 1996), UCSF Chimera (Pettersen *et al.* 2004), VEGA ZZ (Pedretti *et al.* 2002), and GETAREA (Fraczkiewicz and Braun 1998), were used to determine the range of the SASA. The average value of SASA was used to determine the hydration of HEL, assuming 15.2 molecules of water per nm$^2$ of surface area (Yousef *et al.* 2002b). All sets of physical parameters were used to determine the second virial coefficient based on solute-solvent interactions for each solution.

### 4.6.4. Second Virial Coefficients Based on Solute-Solvent Interactions

The values of the second virial coefficient were predicted based on solute-solvent interactions, using Eqn. 4.23, for each of the protein solutions. The solute-solvent interaction parameters are assumed to be independent of solute concentration. However, since the predicted virial coefficient is dependent on the concentration, it is necessary to determine the appropriate concentration at which to predict its value. Then, using a mean-value approach, these second virial coefficients will then be examined to find the value which agrees with the traditional value. Propagation of error was used throughout this analysis to determine the range of error.

### 4.6.5. Traditional Second Virial Coefficient

Typically the first (reciprocal molecular weight) and second virial coefficients are regressed on. However, for the molecular weight to be accurately regressed, osmotic pressure data below 20 g/L is required. Here, osmotic pressure data for the protein solutions studied is

limited or does not exist below 20 g/L, so the molecular weight was taken to be the literature value. The traditional second virial coefficients are solved using the entire osmotic pressure range.

## 4.7. Results and Discussion

### 4.7.1. Physical Parameters

The near-saturation osmotic pressure data for BSA in 0.15 M NaCl, 25°C, pH 7.0 was used for regressing on the hydration and ion binding of BSA (Figure 4.1, solid curve). Nonlinear regression of the concentrated osmotic pressure data using the free-solvent model yielded a regressed BSA hydration value of 1.121 ± 0.0234 g $H_2O$/g BSA and a regressed ion binding value of 9.80 ± 0.356 mol NaCl/mol BSA (Table 4.1). The regressed value of hydration agrees with those of BSA in 0.15 M NaCl at pH 4.5, 5.4, and 7.4, as well as corresponding to a monolayer of water (Yousef *et al.* 2002b). The value of ion binding is similar to the value for ion binding to BSA at pH 5.4 and 7.4 (Yousef *et al.* 1998b).

The SASA of HEL was determined from the molecular structure to be between 5,732 - 7,927 $Å^2$. The monolayer hydration value of HEL is 0.872 - 1.206 g $H_2O$/g HEL (average hydration is 1.039 g $H_2O$/g HEL) (Table 4.1).

Using the osmotic pressure data of Yousef *et al.* for HEL in 0.15 M NaCl, pH 7.0 and 0.15 M KCl, pH 7.0 (Yousef 2000; Yousef *et al.* 2002b), the ion binding was regressed on using a hydration value of 1.039 g $H_2O$/g HEL (Figure 4.2). The regressed ion binding values for HEL in 0.15 M NaCl, pH 7.0 and 0.15 M KCl, pH 7.0 were 2.74 ± 0.015 mol NaCl/mol HEL and 2.74 ± 0.009 mol KCl/mol HEL, respectively (Table 4.1).

4.7.2. Is the Second Virial Coefficient Really Concentration Independent?

The mathematical development of the virial coefficients (*i.e.* performing a Taylor series expansion of the van't Hoff equation with respect to $c_2$) requires the virial coefficients to be constant. However, the value of the virial coefficient is largely dependent on the concentration range used to determine the value.

For BSA in 0.15 M NaCl, pH 7.4, if the virial expansion model is used to regress on the osmotic pressure data, the traditional second virial coefficients are $17.98 \times 10^{-8} \pm 0.978 \times 10^{-8}$ L·mol/g$^2$, $32.19 \times 10^{-8} \pm 3.802 \times 10^{-8}$ L·mol/g$^2$, and $38.84 \times 10^{-8} \pm 2.784 \times 10^{-8}$ L·mol/g$^2$.

The concentration dependence of the second virial coefficient has been purported by various studies (Vilker 1976; Alford *et al.* 2008), however, no explanation as to why this is observed for a constant. This anomaly suggests that the virial expansion of the van't Hoff equation is not the correct model due to the assumptions of expansion.

While the virial expansion model can be used to determine the concentration dependent virial coefficients, the model developed here, based on solute-solvent interactions, allows for the concentration dependency to be defined using physical parameters.

4.7.3. The Second Virial Coefficients

Recognizing that the traditional second virial coefficient is concentration dependent, the entire range of protein concentrations for the osmotic pressure data was used to predict the second virial coefficient based on solute-solvent interactions (Eqn. 21). The range of second virial coefficient values based on solute-solvent interactions is presented as the range of values (Table 4.2). Using the mean-value approach, the second virial coefficient based on solute-solvent interactions are compared to the traditional values. The concentration at which the predicted

second virial coefficient compares to the traditional value is also reported (Table 4.2). The error was propagated for the predicted second virial coefficient at the mean-value concentration.

In addition, the second virial coefficients are predicted using the concentration which deviates from the ideal model for the virial expansion model virial coefficients (Eqn. 4.8) and the virial coefficient based on solute-solvent interactions (Eqn. 4.23) can be found in Table 4.2.

4.7.3.1. Predicted Based on Solute-Solvent Interactions

The virial coefficients predicted based on solute-solvent interactions (Eqn. 4.23) for the protein concentration range is $-4.8 \times 10^{-8}$ L·mol/g$^2$ (for 56 g/L) to $20.8 \times 10^{-8}$ L·mol/g$^2$ (for 478 g/L) for BSA in 0.15 M NaCl, pH 4.5. For BSA in 0.15 M NaCl, pH 5.4, the virial coefficients ranged from $7.7 \times 10^{-8}$ L·mol/g$^2$ (for 8.9 g/L) to $41.3 \times 10^{-8}$ L·mol/g$^2$ (for 454 g/L). The virial coefficient range for BSA in 0.15 M NaCl, pH 7.0 is $12.8 \times 10^{-8}$ L·mol/g$^2$ (for 16.5 g/L) to $44.9 \times 10^{-8}$ L·mol/g$^2$ (for 450 g/L). For BSA in 0.15 M NaCl, pH 7.4, the virial coefficient range is $23.4 \times 10^{-8}$ L·mol/g$^2$ (for 8.6 g/L) to $101 \times 10^{-8}$ L·mol/g$^2$ (for 450 g/L). The mean-value second virial coefficients are $13.2 \times 10^{-8} \pm 2.38 \times 10^{-8}$ L·mol/g$^2$ (at 468 g/L), $30.8 \times 10^{-8} \pm 2.11 \times 10^{-8}$ L·mol/g$^2$ (at 442 g/L), $33.6 \times 10^{-8} \pm 13.38 \times 10^{-8}$ L·mol/g$^2$ (at 432 g/L), and $63.5 \times 10^{-8} \pm 2.32 \times 10^{-8}$ L·mol/g$^2$ (at 423 g/L), for BSA in 0.15 M NaCl, pH 4.5, 5.4, 7.0, and 7.4, respectively.

The virial coefficient ranges for HEL in 0.15 M NaCl and 0.15 M KCl using an ion binding of 2 mol salt/mol HEL (the corresponding hydration values are found in Table 4.1) are $-94.2 \times 10^{-8}$ L·mol/g$^2$ (for 15.6 g/L), to $-7.4 \times 10^{-8}$ L·mol/g$^2$ (for 129.5 g/L) and $-109.4 \times 10^{-8}$ L·mol/g$^2$ (for 12.8 g/L), to $-1.9 \times 10^{-8}$ L·mol/g$^2$ (for 207 g/L), respectively. For an ion binding of 4 mol salt/mol HEL and corresponding hydration, the virial coefficient ranges are $-109.6 \times 10^{-8}$ L·mol/g$^2$ (for 15.6 g/L), to $-4.6 \times 10^{-8}$ L·mol/g$^2$ (for 129.5 g/L) and $-146.3 \times 10^{-8}$ L·mol/g$^2$ (for 12.8 g/L), to $2.5 \times 10^{-8}$ L·mol/g$^2$ for HEL in 0.15 M NaCl and

0.15 M KCl, respectively. If the SASA is used for determining the hydration (1.039 g $H_2O$/g HEL) and corresponding ion binding, the virial coefficient ranges for HEL in 0.15 M NaCl and 0.15 M KCl are -83.6x10$^{-8}$ L·mol/g$^2$ (for 15.6 g/L), to -7.6x10$^{-8}$ L·mol/g$^2$ (for 129.5 g/L), and -130.9x10$^{-8}$ L·mol/g$^2$ (for 12.8 g/L), to -1.5x10$^{-8}$ L·mol/g$^2$ (for 207 g/L), respectively. In all cases, the mean-value second virial coefficients, -25.5x10$^{-8}$ L·mol/g$^2$ (at 57 g/L) for HEL in 0.15 M NaCl and -10.6x10$^{-8}$ L·mol/g$^2$ (at 105 g/L) for HEL in 0.15 M KCl, are within the ranges.

The mean-values of the second virial coefficient predicted based on solute-solvent interactions for all solutions are used to model the osmotic pressure using the virial expansion model (Figures 4.3 - 4.8).

4.7.3.2. Using the Traditional Method

The best fit virial coefficients (traditional method) within the ranges for BSA in 0.15 M NaCl at pH 4.5, 5.4, 7.0, and 7.4 are 13.2x10$^{-8}$ ± 1.57x10$^{-8}$ L·mol/g$^2$, 41.3x10$^{-8}$ ± 1.41x10$^{-8}$ L·mol/g$^2$, 44.9x10$^{-8}$ ± 2.04x10$^{-8}$ L·mol/g$^2$, and 63.5x10$^{-8}$ ± 4.84x10$^{-8}$ L·mol/g$^2$, respectively.

The best fit virial coefficients (traditional method) within these ranges for HEL in 0.15 M NaCl and HEL in 0.15 M KCl are -25.5x10$^{-8}$ ± 2.64x10$^{-8}$ L·mol/g$^2$ and -10.6x10$^{-8}$ ± 1.54x10$^{-8}$ L·mol/g$^2$, respectively.

The traditional second virial coefficient determined from the experimental data for all solutions are used to model the osmotic pressure using the virial expansion model (Figures 4.3 - 4.8).

4.7.4. Comparison of the Second Virial Coefficients Based on Solute-Solvent Interactions to Literature Values

4.7.4.1. Bovine Serum Albumin

The comprehensive study of Vilker *et al.* for the virial expansion coefficients of BSA solutions at pH 4.5, 5.4, and 7.4 in 0.15 M NaCl solutions at 25°C based on the McMillan-Mayer Dilute Solution Theory found the values of the second virial coefficient to be $10.63 \times 10^{-8}$ L·mol/g$^2$, $11.14 \times 10^{-8}$ L·mol/g$^2$, and $13.38 \times 10^{-8}$ L·mol/g$^2$ for BSA solutions at pH 4.5, 5.4, and 7.4, respectively (Vilker *et al.* 1981). While the second virial coefficient changes with the solution properties, they do not have a large enough change, and therefore have limited predictability of the virial expansion model using the McMillan-Mayer based second virial coefficient. Vilker *et al.* (Vilker 1976; Vilker *et al.* 1981) discussed the lack of the virial coefficients, based on McMillan-Mayer Theory, to be able to capture/predict the changes in osmotic pressure with respect to pH changes of the solutions; while these are not captured in the potential mean force used, no conclusions were made as to why were made.

The second virial coefficient has been predicted by Scatchard *et al.* for BSA in various solutions (Scatchard *et al.* 1946; Scatchard and Pigliacampi 1962). The authors' model, similar to the model developed here, is dependent on the concentrations of the solute, and similarly, Scatchard *et al.* values were for individual protein concentrations. The authors reported second virial coefficient values of $1.46 \times 10^{-9}$ L·mol/g$^2$ (BSA in 0.15 M NaCl, isoionic) (Scatchard and Pigliacampi 1962), 1.04 to $1.42 \times 10^{-9}$ L·mol/g$^2$ (BSA in 0.15 M NaCl, pH 5.4) (Scatchard *et al.* 1946), 1.95 to $2.11 \times 10^{-9}$ L·mol/g$^2$ (BSA in 0.15 M NaCl, pH 7.1 ± 0.1) (Scatchard *et al.* 1946).

4.7.4.2. Hen Egg Lysozyme

The best fit value for the virial coefficient predicted based on solute-solvent interactions is more negative for the NaCl solution than the KCl solution. This is expected since the virial coefficient is a predictor of the salting out and, according to the Hofmeister series; NaCl should cause protein to precipitate at a lower concentration than KCl.

No second virial coefficients are available in literature for HEL in either 0.15 M NaCl or 0.15 M KCl, pH 7.0. However, Curtis *et al.* reported an experimental second virial coefficient value of $-25 \times 10^{-8} \pm 4.9 \times 10^{-8}$ L·mol/g$^2$ for HEL in 0.1 M KCl, pH 6.0 using low-angle laser-light scattering (LALLS) (Curtis *et al.* 1998). This value is greater than that predicted based on solute-solute interactions (Eqn. 4.23, Table 4.2), but this may be due to the variation in solution properties or the differences between the two methods. The model developed here does not include solute-solute interactions which may take place in solution, while the LALLS virial coefficient is purported to be based on solute-solute, as well as solute-solvent, interactions (Winzor *et al.* 2007; Blanco *et al.* 2011).

4.7.5. Meaning of the Second Virial Coefficient

Since the second virial coefficients for HEL are negative, which are assumed to be due to protein-protein interactions, HPLC analysis of HEL in 0.15 M NaCl, pH 7.0 and HEL in 0.15 M KCl, pH 7.0 was obtained for HEL concentrations of 6, 12, 25, 50, 100, and 200 g/L (200 g/L was only measured for 0.15 M KCl, pH 7.0). For all concentrations of both solutions, only monomers were observed, thus no protein-protein interactions occurred. If no protein-protein interactions occur, then the thought that negative second virial coefficients are due to protein-protein interaction is false.

Based on the solution properties, it has been reported that for salt solutions which follow the Hofmeister series, the virial coefficients become more negative. For example, salt solutions of NaCl have been found to be better at salting-out than KCl solutions. This observation was also observed by Yousef *et al.* for HEL (Yousef *et al.* 2002b). However, no trend of the virial coefficients based on solute-solvent interactions for the NaCl and KCl solutions were observed. This anomaly may be explained by the lack of robust physical parameters; the hydration value of HEL used does not correspond with a monolayer of water.

### 4.7.6. Predicting Higher Order Virial Coefficients

While the second virial coefficient was the focus of this work, higher order virial coefficients can be predicted by taking higher order derivatives of both functions with respect to the moles of solutes. Although higher order virial coefficients are thought to be due to aggregation, thus not dependent on other virial coefficients, this method will provide an estimate of the higher order virial coefficients based on solute-solvent interactions. This method will also provide a functional relationship of lower order virial coefficients on the higher order ones. For example, the second virial coefficient will be dependent on solute-solvent interactions and the third virial coefficient.

While this may seem counter intuitive if the virial coefficients are considered to be solute-solute interactions (aggregate formation), if the polynomial function which is the basis of the virial expansion model is considered, it can be seen that the coefficients, which are various powers of the concentration, are required to be dependent on each other. Furthermore, this is proven also by the consensus that the virial coefficients are all modeled as functions of the molecular weight of the solute (Eqn. 4.6).

### 4.7.7. Limitations of Predicting the Virial Coefficients Based on Solute-Solvent Interactions

The model that was developed (Eqn. 4.23) only considers two types of solute-solvent interactions, solute hydration and solute-ion binding. However, other interactions occur between solutes and solvent, such as solute-proton binding and solute-hydroxide binding. Furthermore, for complex solutions, such as those containing higher valency salts or carbohydrate solutions, more solute-solvent interaction parameters may need to be considered.

In addition, since this model was developed for proteins which do not have attractive solute-solute interactions (*i.e.* aggregate formation), the model will need to be revisited and these interactions will need to be included for solutions in which these interactions occur. These limitations and the development of higher order virial expansion coefficients will be the focus of future work.

## 4.8. Conclusion

Previously no functional relationship was given for the second virial coefficient on the concentration or solute-solvent interactions. Herein, the second virial coefficient has now been coupled to solute-solvent interactions, as well as the concentrations of the solution species.

While the dependence of the second virial coefficient on solution concentration has now been given a mathematical representation, this alone will not allow for the prediction of the virial coefficient changes with respect to various solution properties, such as ionic strength and pH.

The dependence on solution properties of the virial coefficients are related to solute-solvent interactions just as Scatchard and Pigliacampi (Scatchard and Pigliacampi 1962), Yousef *et al.* (Yousef *et al.* 1998a, 1998b), Winzor *et al.* (Winzor *et al.* 2007), and Blanco *et al.* (Blanco *et al.* 2011) argued. This dependence on solute-solvent interactions has also been given a

functional relationship when considering solute hydration and solute-ion binding; however other solute-solvent and solute-solute interaction parameters may be included as necessary.

The predicted second virial coefficients, based on hydration, ion binding, and solution concentration, are in good agreement the traditional values of the second virial coefficients.

**Table 4.1.** Physical Parameters for BSA and HEL. Summary of the physical, solute-solvent parameters utilized in the prediction of the second virial coefficients based on solute-solvent interactions (Eqn. 4.23).

| Protein (kDa) | Soln. Properties: Salt, pH | Hydration, $\nu_{12}$ $\left(\frac{\text{g H}_2\text{O}}{\text{g Protein}}\right)$ | Ion Binding, $\nu_{32}$ $\left(\frac{\text{mol Salt}}{\text{mol Protein}}\right)$ |
|---|---|---|---|
| BSA (66.4) | 0.15 M NaCl, 4.5 | 1.113 ± 0.0063[a] | 11.59[a] |
| | 0.15 M NaCl, 5.4 | 1.137 ± 0.0059[a] | 10.62[a] |
| | 0.15 M NaCl, 7.0 | 1.121 ± 0.0234 | 9.80 ± 0.356 |
| | 0.15 M NaCl, 7.4 | 1.177 ± 0.0050[a] | 8.81[a] |
| HEL (14.3) | 0.15 M NaCl, 7.0 | 0.724 ± 0.008[b] | 2[c] |
| | | 1.614 ± 0.010[b] | 4[d] |
| | | 1.039* | 2.74 ± 0.015 |
| | 0.15 M KCl, 7.0 | 0.734 ± 0.003[b] | 2[c] |
| | | 1.595 ± 0.007[b] | 4[d] |
| | | 1.039* | 2.74 ± 0.009 |

* Calculated from the SASA of HEL

[a] (Yousef *et al.* 1998b)

[b] (Yousef *et al.* 2002b)

[c] (Curtis *et al.* 1998)

[d] (Kuehner *et al.* 1999)

**Table 4.2.** The Second Virial Coefficient Values. Summary of the virial coefficients for BSA solutions and HEL solutions computed from the experimental osmotic pressure data using the virial expansion model (Eqn. 4.8) and predicted using solute-solvent interactions (Eqn. 4.23).

| Protein (kDa) | Soln. Properties: Salt, pH | Traditional Virial Coefficients, $B_2 \times 10^8$ Mean Value $\left(\frac{\text{L}\cdot\text{mole}}{\text{g}^2}\right)$ | Predicted Based on Solute-Solvent Interactions, $B_2 \times 10^8$ Range (Mean Value, [Protein]) $\left(\frac{\text{L}\cdot\text{mole}}{\text{g}^2}\right)$ |
|---|---|---|---|
| BSA (66.4) | 0.15 M NaCl, 4.5 | 13.2 ± 1.57 | -4.77 to 20.8 (13.18 ± 2.375, 468 g/L) |
| | 0.15 M NaCl, 5.4 | 30.8 ± 1.41 | 7.66 to 41.3 (30.75 ± 2.107, 442 g/L) |
| | 0.15 M NaCl, 7.0 | 33.6 ± 2.04 | 12.79 to 44.9 (33.63 ± 13.378, 432 g/L) |
| | 0.15 M NaCl, 7.4 | 63.5 ± 4.84 | 23.38 to 101 (63.54 ± 4.319, 423 g/L) |
| HEL (14.3) | 0.15 M NaCl, 7.0 | -25.54 ± 2.640 | -94.21 to -7.37 (-25.54 ± 1.248, 54 g/L)ǂ<br>-109.63 to -4.64 (-25.54 ± 1.642, 57 g/L)‡<br>-83.64 to -7.55 (-25.54 ± 1.004, 59 g/L)† |
| | 0.15 M KCl, 7.0 | -10.55 ± 1.535 | -109.37 to -1.93 (-10.55 ± 2.685, 105 g/L)ǂ<br>-146.25 to 2.54 (-10.55 ± 0.731, 114 g/L)‡<br>-130.94 to -1.46 (-10.55 ± 0.349, 117 g/L)† |

ǂ Based on $\nu_{32} = 2$ mol salt/mol HEL and the corresponding hydration

‡ Based on $\nu_{32} = 4$ mol salt/mol HEL and the corresponding hydration

† Based on SASA and regressed ion binding

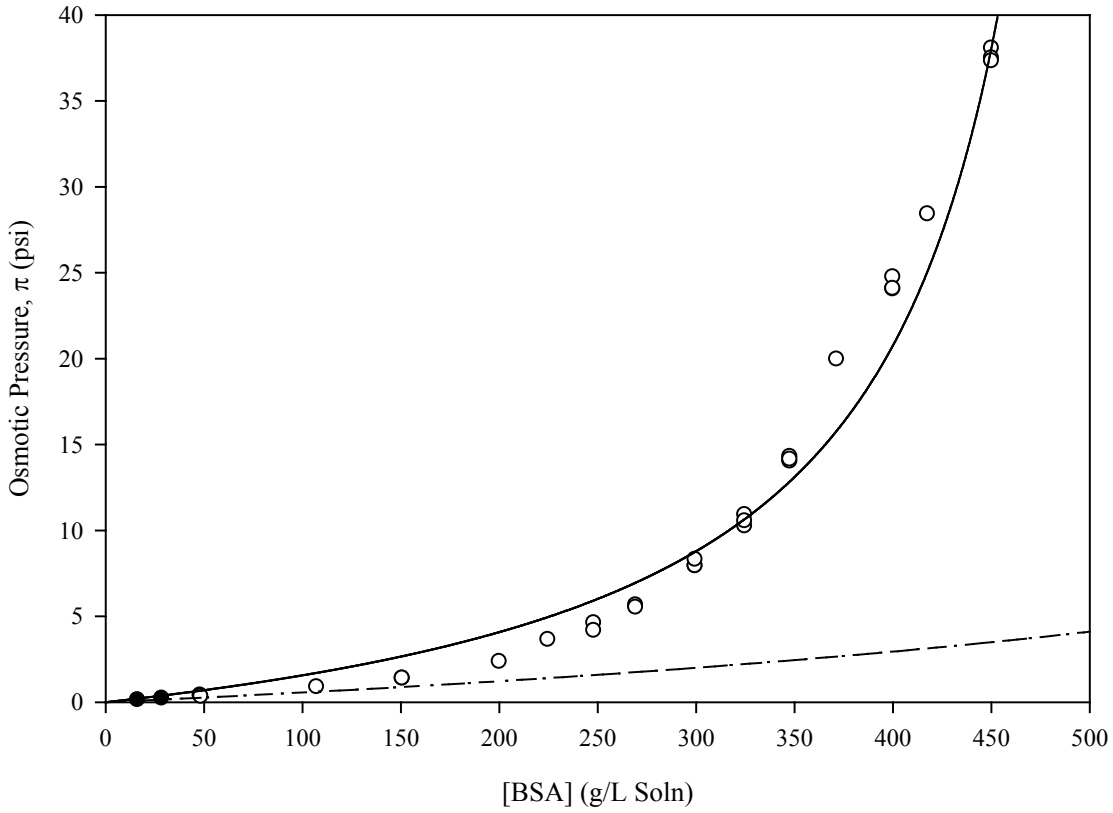


**Figure 4.1.** Osmotic Pressure vs. BSA Concentration. Measured osmotic pressure vs. concentration for BSA in 0.15 M NaCl, pH 7.0, 25ºC (closed circles are the data by Scatchard *et al.* (Scatchard *et al.* 1946), open circles are the data from this work). The free-solvent model (Eqn. 4.16) best fit (solid curve) for the experimental data is plotted using a regressed hydration value of 1.121 ± 0.0234 g $H_2O$/g BSA and a regressed ion binding value of 9.80 ± 0.356 mol NaCl/mol BSA (Table 4.1). The ideal osmotic pressure from the van't Hoff equation is plotted using the molecular of 66,430 kDa (dashed curve).

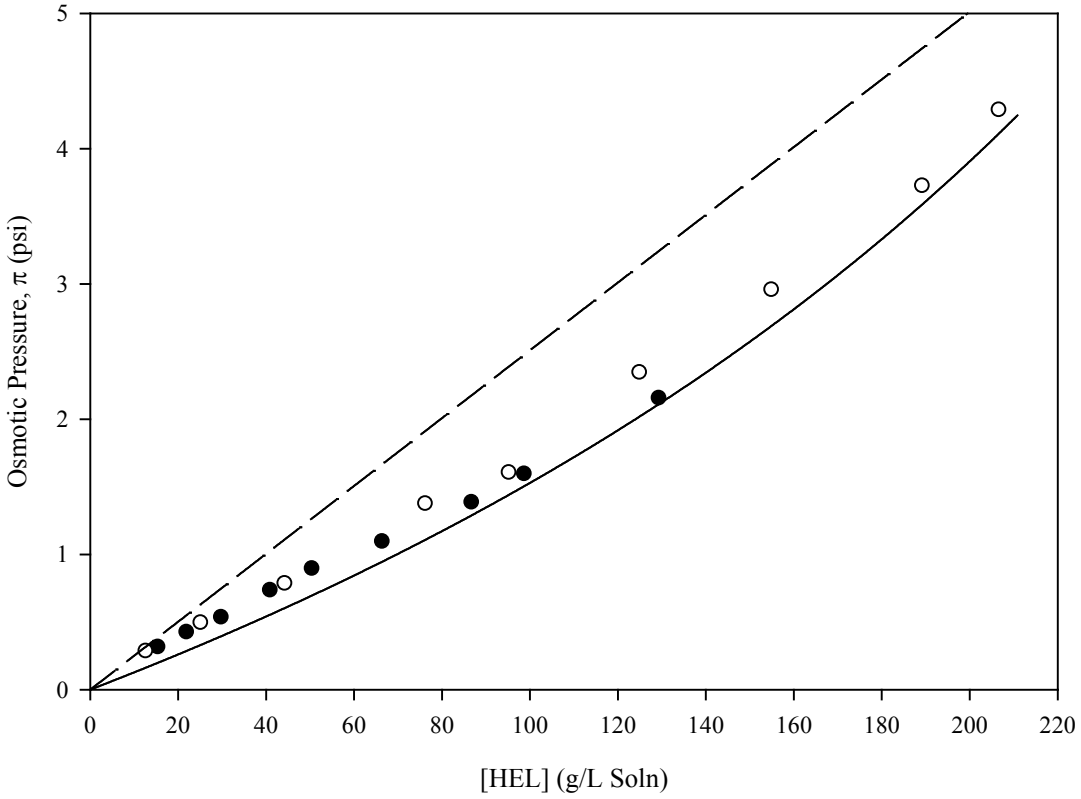


**Figure 4.2.** Osmotic Pressure vs. HEL Concentration. Measured osmotic pressure vs. concentration for HEL in 0.15 M NaCl, pH 7.0, 25°C (closed circles) and HEL in 0.15 M KCl, pH 7.0, 25°C (open circles) (Yousef *et al.* 2002b). The free-solvent model (Eqn. 4.16) best fit for both solutions are plotted using a hydration value of 1.039 g $H_2O$/g HEL and a regressed ion binding value of 2.74 mol NaCl/mol HEL (solid curve) (Table 4.1). The ideal osmotic pressure from the van't Hoff equation is plotted using the molecular of 14,307 kDa (dashed curve).

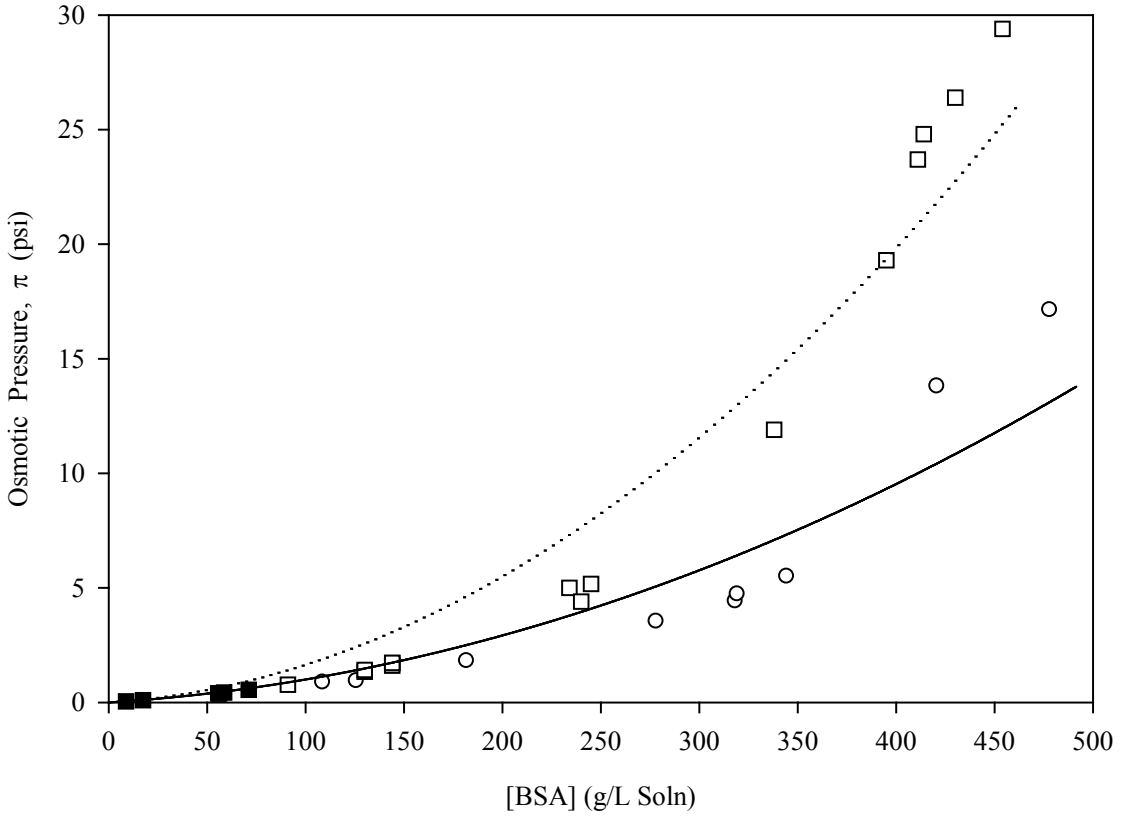


**Figure 4.3.** Osmotic Pressure Predicted by the Virial Expansion Model for BSA in 0.15 M NaCl, pH 4.5 and 5.4. Dilute osmotic pressure vs. concentration for BSA in 0.15 M NaCl, pH 4.5, 25ºC (closed circles are the data by Scatchard *et al.* (Scatchard *et al.* 1946), open circles are the data by Vilker *et al.* (Vilker *et al.* 1981) and BSA in 0.15 M NaCl, pH 5.4, 25ºC (closed squares are the data by Scatchard *et al.* (Scatchard *et al.* 1946), open squares are the data by Vilker *et al.* (Vilker *et al.* 1981). The second order virial expansion model is plotted for the best fit values (BSA at pH 4.5: solid curve, BSA at pH 5.4: dotted curve).

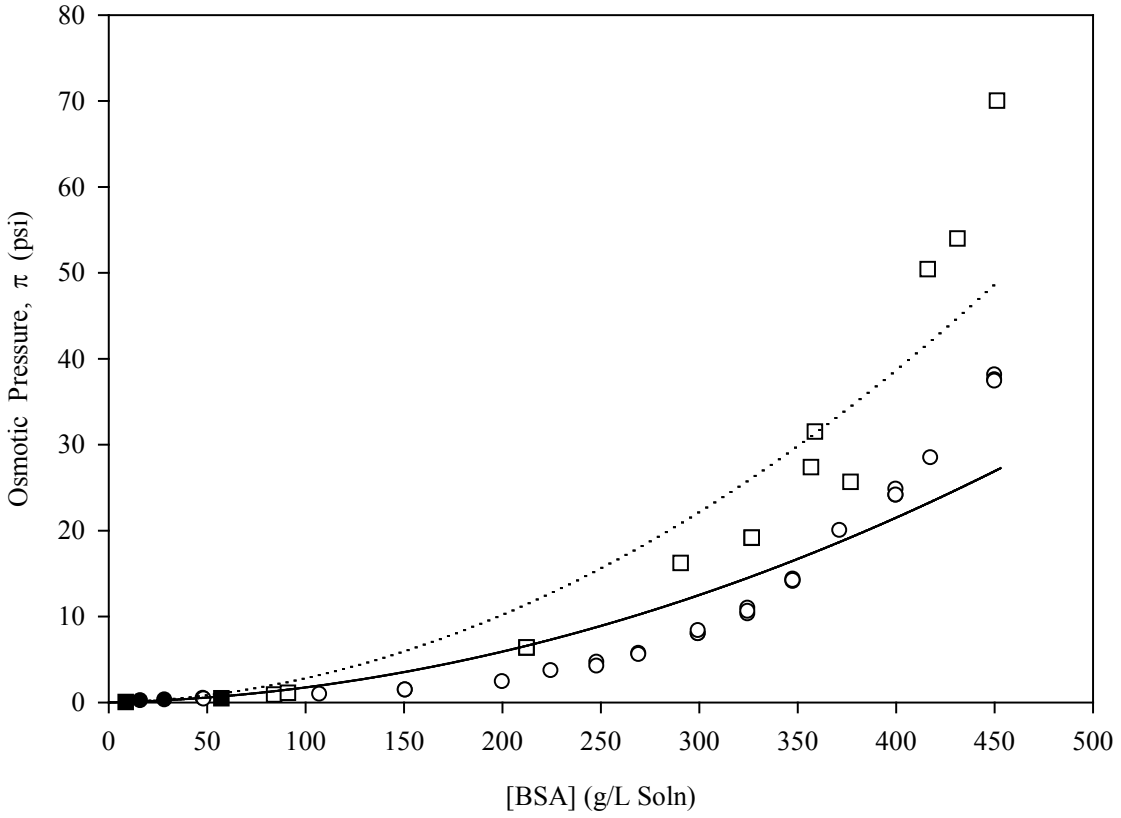


**Figure 4.4.** Osmotic Pressure Predicted by the Virial Expansion Model for BSA in 0.15 M NaCl, pH 7.0 and 7.4. Dilute osmotic pressure vs. for BSA in 0.15 M NaCl, pH 7.0, 25°C (closed circles are the data by Scatchard *et al.* (Scatchard *et al.* 1946), open circles are the data from this work) and BSA in 0.15 M NaCl, pH 7.4, 25°C (closed squares are the data by are the data by Scatchard *et al.* (Scatchard *et al.* 1946), open squares are the data by Vilker *et al.* (Vilker *et al.* 1981). The second order virial expansion model is plotted for the best fit values (BSA at pH 7.0: solid curve, BSA at pH 7.4: dotted curve). The second virial coefficient values for each curve are found in Table 4.2.

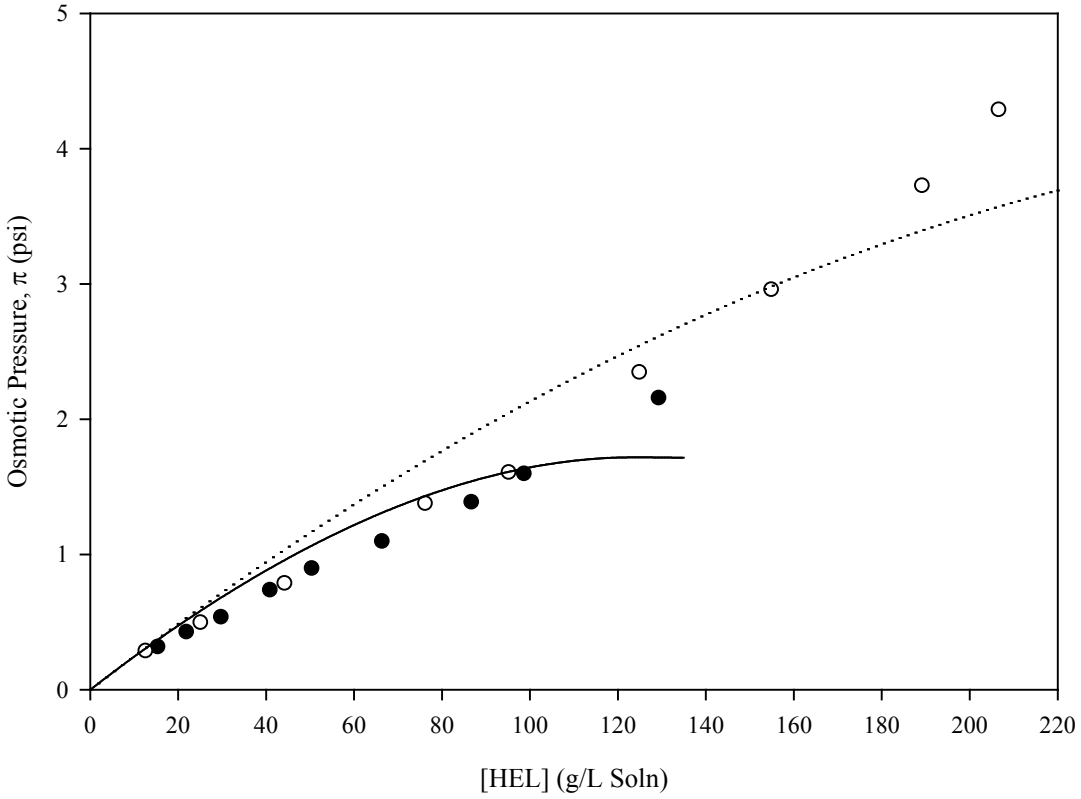


**Figure 4.5.** Osmotic Pressure Predicted by the Virial Expansion Model for HEL. Measured osmotic pressure vs. concentration for HEL in 0.15 M NaCl, pH 7.0, 25ºC (closed circles) and HEL in 0.15 M KCl, pH 7.0, 25ºC (open circles) (Yousef *et al.* 2002b). The second order virial expansion model is plotted for the best fit values (HEL in NaCl: solid curve, HEL in KCl: dotted curve). The second virial coefficient values for each curve are found in Table 4.2.

# CHAPTER 5.

# UNDERSTANDING THE EFFECT OF SOLUTION PROPERTIES ON THE SEVOND VIRIAL COEFFICIENT

## 5.1. Abstract

For some time, the molecular mechanism of salting-out has been discussed. Some theories focus on protein-protein interactions, while others focus on protein-solvent interactions. Of the latter group of theories, Timasheff and co-workers have argued that there is a balance between the surface tension and the interaction of salt with the proteins, and have developed a preferential interaction parameter for understanding salting-out. Separately, studies have observed negative virial coefficients are associated with salting-out. The focus of this work is to determine the cause of the negative virial coefficients by examining the effect of the ratio of the protein influenced solvent ionic strength to that of the bulk on the second virial coefficient. The conditions for obtaining negative, positive, and zero values of the second virial coefficient are explained when the ratio of the protein influenced solvent ionic strength to the bulk ionic strength is considered; a ratio greater than one yields a negative second virial coefficient, a ratio less than one yields positive second virial coefficients, and a ratio equal to one gives a second virial coefficient of zero.

## 5.2. Introduction

Salting-out is the observation of protein precipitation associated with increasing the concentration of salt in solution. The process of salting-out has long been used for the isolation and purification of proteins. Many times, ammonium sulfate is used as the salt of choice for

salting-out as it tends to aid in precipitation of most proteins. However, other salts have demonstrated successful salting-out.

The Hofmeister series provides an observed relationship of increasing effectiveness in salting-out for anions with a fixed cation ($SO_4^{2-} > HPO_4^{2-} > Cl^- > NO_3^-$) and cations with a fixed anion ($Li^+ > Na^+ > K^+ > NH_4^+$) (Hofmeister 1888; Green 1931, 1932). The critical concentration of salt required for salting-out of a protein decreases for the greater Hofmeister ions. For example, fixing the cation as ammonium, the concentration needed for salting-out using ammonium sulfate is lower than if ammonium chloride is used since $SO_4^{2-} > Cl^-$.

While many models have been developed for predicting the salting-out of a protein (Cohn and Edsall 1943; Melander and Horvath 1977; Coen *et al.* 1995), the molecular interactions responsible for the phenomenon remain unknown. Von Hippel *et al.* suggested that the interaction between ions and a protein's hydrophobic groups are related to salting-out (Hamabata and von Hippel 1973; Hamabata *et al.* 1973; von Hippel *et al.* 1973), while others have suggested that salting-out is dependent on electrostatic repulsion (Melander and Horvath 1977; Zhou 2005).

Timasheff and co-workers offered an alternative explanation to the observations of salting-out (Timasheff *et al.* 1976; Pittz and Timasheff 1978; Gekko and Timasheff 1981; Na and Timasheff 1981; Arakawa and Timasheff 1982a, 1982b, 1983, 1984a, 1984b, 1984c, 1985; Aune and Timasheff 1987; Timasheff and Arakawa 1988); they argued that the interaction of proteins and salt can be expressed using a preferential interaction parameter, $\zeta$. The preferential interaction parameter measures the amount of excess salt, which is present near the protein surface, compared to its concentration in the bulk. High-precision densimetry or differential refractometry have been used in determining this parameter (Pittz and Timasheff 1978; Arakawa and Timasheff 1982a, 1984a, 1985). The authors have shown that a positive preferential interaction parameter

corresponds to an excess of salt near the protein while a negative value is due to a deficiency of ions near the protein surface (Na and Timasheff 1981; Timasheff 1981). The latter can also be thought of as an excess of water interacting with the protein.

Timasheff and co-workers provided substantial amounts of work with respect to the preferential interaction parameter, yet experimental data is required for determining the water surface tension and the protein-ion interaction.

Another experimental parameter which has been used to estimate salting-out has been the second virial coefficient. The second virial coefficient can be determined by various methods, osmotic pressure, sedimentation equilibrium, and static light scattering, all which require experimental data. Furthermore, the molecular mechanisms which the virial coefficient is based on were only speculated: solute-solute interactions (Vilker 1976; Alford *et al.* 2008) or solute-solvent interactions (Yousef *et al.* 1998a, 1998b; Winzor *et al.* 2007; Blanco *et al.* 2011).

Although the molecular mechanisms of the virial coefficients remain elusive, the second virial coefficient is used as a predictor of salting-out. The second virial coefficient, with a value equal to or greater than zero, is considered to account for repulsive solute-solute interactions, while a negative second virial coefficient is thought to account for attractive solute-solute interactions (Tombs and Peacocke 1974) and ultimately salting-out (George and Wilson 1994; George *et al.* 1997; Dumetz *et al.* 2007).

More specifically, second virial coefficients between $-1x10^{-7}$ $L \cdot mol/g^2$ and $-8x10^{-7}$ $L \cdot mol/g^2$ are thought to provide the best crystallization solution properties as this range is the so-called crystallization slot (George and Wilson 1994; George *et al.* 1997). This range was experimentally observed by George and Wilson: for virial coefficients greater than $-1x10^{-7}$ $L \cdot mol/g^2$ no crystallization was observed and for virial coefficients less than $-8x10^{-7}$ $L \cdot mol/g^2$, the crystallization was too rapid, resulting in amorphous crystals (George and

Wilson 1994). The authors speculated that the former observation was caused by the protein-protein interactions being too weak, and the latter was caused by the protein-protein interactions being too strong (George and Wilson 1994).

Recently, a new model for predicting the virial coefficient was developed based on solute-solvent interactions (Chapter 4). This model requires only physical parameters, namely solute hydration, solute-ion binding, and species concentrations. The second virial coefficient based on solute-solvent interactions is

$$B_2 = \frac{\overline{V}_1}{2(M_2)^2}\left[\left(\frac{\nu_{12}\left(N_1^{II}+(1-\nu_{12}-\nu_{32})N_2^{II}+N_3^{II}\right)+\left(N_1^{II}-\nu_{12}N_2^{II}\right)(1-\nu_{12}-\nu_{32})}{\frac{N_2^{II}\left(N_1^{II}+N_3^{II}\right)\left(N_1^{II}-\nu_{12}N_2^{II}\right)\left(N_1^{II}+(1-\nu_{12}-\nu_{32})N_2^{II}+N_3^{II}\right)}{\left(N_1^{II}+N_2^{II}+N_3^{II}\right)^3}}\right)-N_2^{II}\right]. \quad (5.1)$$

Using this model (Eqn. 5.1), the effect of solute-solvent interactions on the ratio of the protein influenced solvent ionic strength to that of the bulk is examined for three model proteins: ovalbumin (OVA), bovine serum albumin (BSA), and hen egg lysozyme (HEL).

## 5.3. Methods

The solution properties examined for OVA were 0.15 M NaCl, pH 7.0 and 0.5 M NaCl, pH 7.0. BSA was examined for 0.15 M NaCl at pH 4.5, 5.4, 7.0, and 7.4. The solution properties studied for HEL in 0.15 M NaCl, pH 7.0 and 0.15 M KCl, pH 7.0.

Two of the model protein systems were used to understand the effect of interaction of protein with solvent for which the physical parameters (Curtis *et al.* 1998; Yousef *et al.* 1998b, 2001, 2002b; Kuehner *et al.* 1999) and second virial coefficients based on solute-solvent interactions are available in literature. For OVA, the second virial coefficients was determined as previously described (Chapter 4).

In order to understand the solution properties which cause the second virial coefficient to be positive and negative, the ionic strength of the solvent surrounding the protein, or protein influenced solvent ionic strength, was calculated, for each OVA solution, each BSA solution, and both HEL solutions, by taking the ratio of the ion binding to the hydration and comparing it to the bulk.

The protein influenced ionic strength and the second virial coefficient were examined for any correlation. Here, the ratio of the protein influenced solvent ionic strength to the bulk ionic strength, $\alpha$, was obtained by

$$\alpha = \frac{\nu_{32}/\nu_{12}}{M}, \tag{5.2}$$

where $M$ is the ionic strength of the bulk.

## 5.4. Results and Discussion

### 5.4.1. Physical Parameters

The physical parameters used in determining the virial coefficient based on solute-solvent interactions and the ratio of the ionic strength of the protein influenced solvent to the bulk ionic strength are given in Table 5.1.

### 5.4.2. The Second Virial Coefficients

The second virial coefficients for the OVA solutions are based on the best fit value to the experimental osmotic pressure data of Yousef *et al.* (Yousef *et al.* 2001). The range of the second virial coefficients for OVA in 0.15 M NaCl, pH 7.0 and 0.5 M NaCl, pH 7.0 are 14.96 - 55.99x$10^{-8}$ L·mol/$g^2$ (mean value is 43.12x$10^{-8}$ L·mol/$g^2$) and 13.13 - 30.90 x$10^{-8}$ L·mol/$g^2$ (mean value is 30.59x$10^{-8}$ L·mol/$g^2$), respectively. These values are

similar to those extrapolated by fitting the virial expansion model to osmotic pressure data (Yousef 2000).

The ionic strength of the solutions for OVA had a minimal effect on the virial coefficient based on solute-solvent interactions due to the similarity in the osmotic pressure profiles. For the BSA and HEL solutions, the virial coefficients based on solute-solvent interactions follow the expected trends for pH and salt changes.

### 5.4.3. The Effects of the Solute-Solvent Interactions on the Second Virial Coefficient

The second virial coefficient has long been thought of as being related to the solute-solute interactions; positive virial coefficients are due to repulsive interactions, negative virial coefficients are due to attractive interactions, and a virial coefficient of zero is observed for an ideal solution (*i.e.* the van't Hoff equation).

In this work, the basis of the second virial coefficient has been challenged by the fact that negative second virial coefficients for HEL in two different salt solutions were obtained considering only solute-solvent interactions. The negative virial coefficients obtained for the HEL solutions is expected since HEL reaches a concentration in solution at which it precipitates (approximately 130 g/L in 0.15 M NaCl, pH 7.0 and approximately 210 g/L in 0.15 M KCl, pH 7.0). Although the second virial coefficient was negative using only solute-solvent interactions, solute-solute interactions may still be present in solution. To verify the presence or absence of attractive protein-protein interactions (*i.e.* aggregates), HPLC analysis of both HEL solutions for HEL concentrations from 1 g/L to 120 g/L (for 0.15 M NaCl, pH 7.0) and 200 g/L (for 0.15 M KCl, pH 7.0). In all solutions, only monomers were observed, thus the determined negative virial coefficients are likely due to another phenomenon. This alternative phenomenon, previously proposed (Yousef *et al.* 1998a, 1998b; Winzor *et al.* 2007; Blanco *et al.* 2011) and

recently given a mathematical functional dependency (Chapter 4), is based on the interactions between the solute and the solvent. This can be extended to understand the relationship of the ionic strength of the protein influenced solvent.

The basis of the conditions yielding negative second virial coefficients is similar to the basis for salting-out by Timasheff and co-workers (Timasheff *et al.* 1976; Pittz and Timasheff 1978; Gekko and Timasheff 1981; Na and Timasheff 1981; Arakawa and Timasheff 1982a, 1982b, 1983, 1984a, 1984b, 1984c, 1985; Aune and Timasheff 1987; Timasheff and Arakawa 1988). Both of these independent formulations yield information about the interaction between the salt and the protein. Timasheff and co-workers have shown that their formulation can predict salting-out (Timasheff *et al.* 1976; Pittz and Timasheff 1978; Gekko and Timasheff 1981; Na and Timasheff 1981; Arakawa and Timasheff 1982a, 1982b, 1983, 1984a, 1984b, 1984c, 1985; Aune and Timasheff 1987; Timasheff and Arakawa 1988), while the formulation developed for predicting the second virial coefficient using the relationship of the solute-solvent interactions to obtained positive and negative values is shown herein.

### 5.4.4. Protein Influenced Solvent Ionic Strength

The interaction between a protein and water molecules is typically independent of the solution properties (*i.e.* ionic strength and pH) since a monolayer forms around the protein. Even if the solution properties cause structural changes to a protein, such as conformational changes or denaturing, although the number of water molecules will change, a monolayer will still be formed.

However, the interactions between a protein and ions are highly dependent on the solution properties. The protein charge, charged residues on the surface and their localization, pH, salt type, and ionic strength all effect the interaction of ions with the protein.

By understanding that the solution properties play a major role in these interactions, a correlation may be made between the second virial coefficient, a bulk solution parameter, and the molecular interactions of the protein. Here, the ratio of the ionic strength within the protein influenced solvent to that of the bulk is determined for three macromolecules in various solution properties (Table 5.1).

5.4.4.1. Second Virial Coefficient Dependency

From the OVA, BSA, and HEL solutions, a correlation between the sign of the second virial coefficient and the ionic strength of the protein influenced solvent is observed.

When the ionic strength of the protein influenced solvent is less than the bulk ionic strength, as is the case for the OVA and BSA solutions, the second virial coefficient is positive. As the protein influenced solvent ionic strength becomes closer to the bulk ionic strength, the second virial coefficient gets closer to zero. A positive virial coefficient is obtained for OVA in 0.5 M NaCl and BSA at pH 4.5 despite the observation that the protein influenced solvent ionic strength is slightly greater than the bulk. The large error in the ion binding value (for OVA in 0.5 M NaCl) and the deviation of the hydration value from the expected monolayer hydration (for BSA at pH 4.5) are possible explanations for these observations.

The protein influenced solvent ionic strength for the HEL solutions are greater than that of the bulk solution and negative values for the second virial coefficient are obtained. Regardless of which set of physical parameters is used for the HEL solutions, the ionic strength of the protein influenced solvent is greater than the bulk ionic strength and the virial coefficient is negative.

Using this correlation, the second virial coefficient was plotted as a function of the ratio of the protein influenced solvent ionic strength to the bulk ionic strength, $\alpha$ (Figure 5.1). The ionic strength ratio (protein influenced solvent ionic strength to the bulk ionic strength) for an

ideal solution (*i.e.* $B_2 = 0$) is 1.025. An ionic strength ratio less than 1.025 yields positive virial coefficients; an ionic strength ratio greater than 1.025 yields negative virial coefficients.

This is unexpected; intuitively, the ideal solution would be observed for an ionic strength ratio of 1 (*i.e.* the protein influenced solvent ionic strength is equal to the bulk ionic strength). This observation may be explained by considering the hydration of the protein bound ions.

5.4.4.2. Considering the Hydration of the Ions Bound to the Protein

It is well known that a protein in solution will interact with the solvent species, such as ion binding and hydration, which were utilized during the development of the free-solvent osmotic pressure model (Yousef *et al.* 1998a). Yousef *et al.* stated that, in order to better understand the dependence of the protein concentration on osmotic pressure, a new species, termed the hydrated macromolecule, should be considered (Yousef *et al.* 1998a, 1998b, 2001, 2002b). The hydrated macromolecule is the protein species containing a monolayer of water with the bound ions. The system then consists of only unbound, non-interacting solvent (water and salt) and hydrated macromolecules. However, some of the remaining, unbound water will have a chemical potential difference from the chemical potential of the bulk water. This is due to the hydration of the bound ions. A modified description of the hydrated macromolecule is the protein surrounded by the influenced solvent, via protein hydration and salt hydration (Figure 5.2). The protein influenced water is greater than the monolayer of water since the size of the bound ions extends further than the monolayer (2.8 Å).

If one considers the hydration of ions in the prediction of the virial coefficient, the number of water molecules which are part of the hydrated macromolecule will be altered. The hydration of ions is well documented in literature, so the protein influenced solvent ionic strengths were adjusted to include the hydration of the ions. For monovalent ions, depending on

the ion, the hydration is between 3 mol $H_2O$/mol ion and 8 mol $H_2O$/mol ion (Conway 1981; Varma and Rempre 2006) and for monovalent salts the hydration is between 8 and 15 mol $H_2O$/mol salt (Conway 1981).

Since the number of water molecules the ions bring to the hydrated molecule is unknown, the second virial coefficient has been plotted for different ion hydrations (Figure 5.2). If each bound ion pair brings all of its water, assuming 15.0 mol $H_2O$/mol salt (for NaCl (Conway 1981)), the number of water will increase and thus the protein influenced solvent ionic strength will decrease. With the decrease in the protein influenced solvent ionic strength, a zero second virial coefficient is obtained when the ratio of the protein influenced ionic strength to the bulk ionic strength, $\alpha$, is 0.984.

However, it is unlikely that the salt will bring all of its water to the protein since some water may be displaced by the ion-protein interaction in addition to some of the water being considered as part of the monolayer of water surrounding the protein (*i.e.* some water will be shared between the salt and the protein) and within 2.8 Å of the protein surface. For the majority of salt ions, the sizes of the ions are not the same size as a water molecule, thus if an ion, that is larger than water, is the predominantly bound ion (*i.e.* chloride predominantly binds to albumins compared with sodium or potassium and chloride has a radius of 1.81 Å), the water brought to the hydrated macromolecule by the ion pair will be greater than 50% since the counter ion is completely outside of the 2.8 Å thick monolayer in addition to the predominantly bound ion being partially outside of the monolayer. The value of hydration which yields a zero virial coefficient of $\alpha = 1$ is 8.9 mol $H_2O$/mol salt. This value corresponds with 60% of the bound salt being hydrated.

## 5.5. Conclusion

While it has been observed that the virial coefficients were dependent on the solution properties, specifically with respect to salting-in and salting-out, these observations can now be related to the ionic strength within the influence solvent surrounding the solute. If the protein influenced solvent ionic strength is less than the bulk solution, the second virial coefficient is positive and if the protein influenced solvent ionic strength is greater than the bulk, the second virial coefficient is negative. When the protein influenced solvent ionic strength is equal to the bulk, the second virial coefficient is zero which yields an ideal model.

**Table 5.1.** Protein Influenced Solvent Ionic Strength Ratio and the Corresponding Second Virial Coefficient for Various Macromolecules. Summary of the physical parameters, and the corresponding second virial coefficient based on solute-solvent interactions and ratio of the ionic strength in the solvent surrounding the protein (protein influenced solvent ionic strength).

| Protein (kDa) | Solution Properties Salt, pH | Hydration, $\nu_{12}$ $\left(\frac{\text{g H}_2\text{O}}{\text{g Protein}}\right)$ | Ion Binding, $\nu_{32}$ $\left(\frac{\text{mol Salt}}{\text{mol Protein}}\right)$ | Second Virial Coefficient, $B_2$ x$10^8$ $\left(\frac{\text{L}\cdot\text{mole}}{\text{g}^2}\right)$ | Ionic Strength Ratio $(\alpha)$ |
|---|---|---|---|---|---|
| OVA (45) | 0.15 M NaCl, 7.0 | 0.86 ± 0.04[a] | 4.08 ± 0.43[a] | 43.12 ± 26.25 | 0.81 ± 0.112 |
| | 0.5 M NaCl, 7.0 | 0.89 ± 0.04[a] | 18.87 ± 1.03[a] | 30.59 ± 37.33 | 1.04 ± 0.098 |
| BSA (66.4) | 0.15 M NaCl, 4.5 | 1.113 ± 0.0063[b] | 11.59[b] | 13.2 ± 2.38[c] | 1.05 ± 0.005 |
| | 0.15 M NaCl, 5.4 | 1.137 ± 0.0059[b] | 10.62[b] | 30.8 ± 2.11[c] | 0.94 ± 0.005 |
| | 0.15 M NaCl, 7.0 | 1.121 ± 0.0234[c] | 9.80 ± 0.356[c] | 33.6 ± 13.38[c] | 0.92 ± 0.051 |
| | 0.15 M NaCl, 7.4 | 1.177 ± 0.0050[b] | 8.81[b] | 63.5 ± 2.32[c] | 0.75 ± 0.003 |
| HEL (14.3) | 0.15 M NaCl, 7.0 | 0.724 ± 0.008[d] | 2[e] | -25.5 ± 1.25[c] | 1.30 ± 0.014 |
| | | 1.614 ± 0.010[d] | 4[f] | -25.5 ± 1.64[c] | 1.16 ± 0.007 |
| | | 1.039[c] | 2.74 ± 0.015[c] | -25.5 ± 1.00[c] | 1.24 ± 0.007 |
| | 0.15 M KCl, 7.0 | 0.734 ± 0.003[d] | 2[e] | -10.6 ± 2.69[c] | 1.27 ± 0.005 |
| | | 1.595 ± 0.007[d] | 4[f] | -10.6 ± 0.73[c] | 1.17 ± 0.005 |
| | | 1.039[c] | 2.74 ± 0.009[c] | -10.6 ± 0.35[c] | 1.23 ± 0.004 |

[a] (Yousef *et al.* 2001)
[b] (Yousef *et al.* 1998b)
[c] (Chapter 4)
[d] (Yousef *et al.* 2002b)
[e] (Curtis *et al.* 1998)
[f] (Kuehner *et al.* 1999)

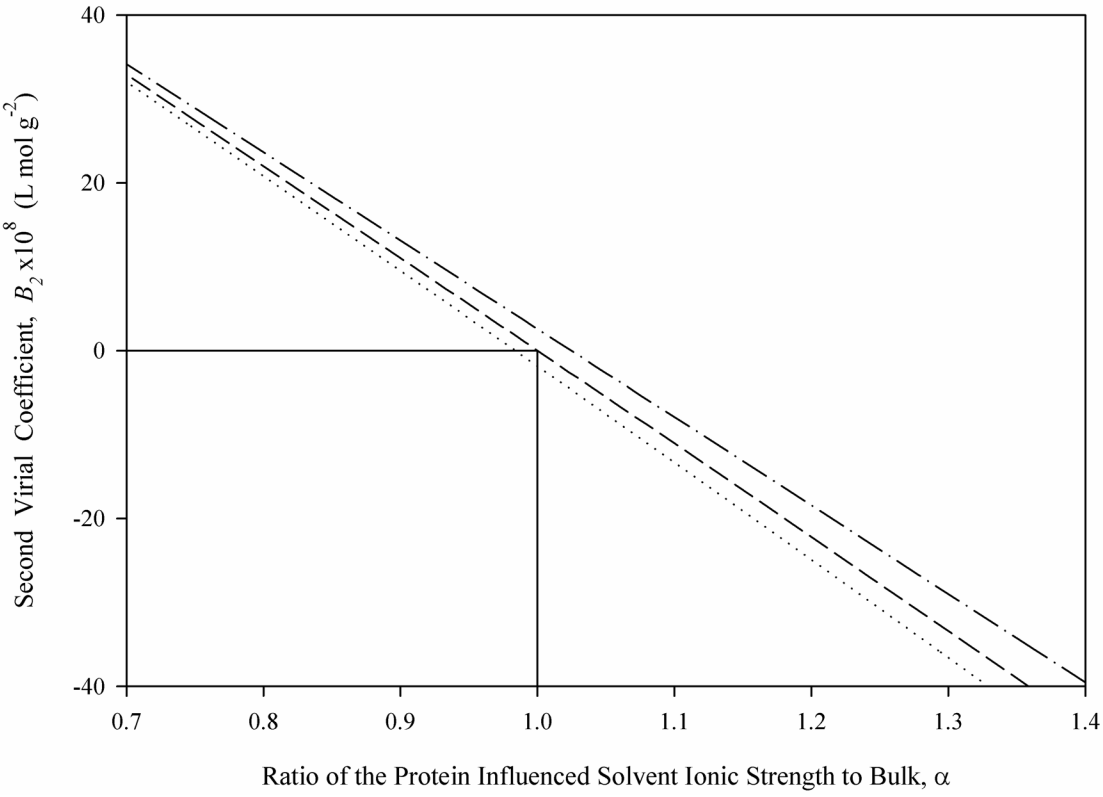


**Figure 5.1.** Second Virial Coefficient vs. Ionic Strength Ratio (ionic strength of the protein influenced solvent to bulk ionic strength), $\alpha$. The dependence of the second virial coefficient on the ionic strength ratio is shown assuming: no ion hydration (dash-dot curve), ion hydration of 8.9 mol $H_2O$/mol Salt (dashed curve), and 15 mol $H_2O$/mol Salt (dotted curve).

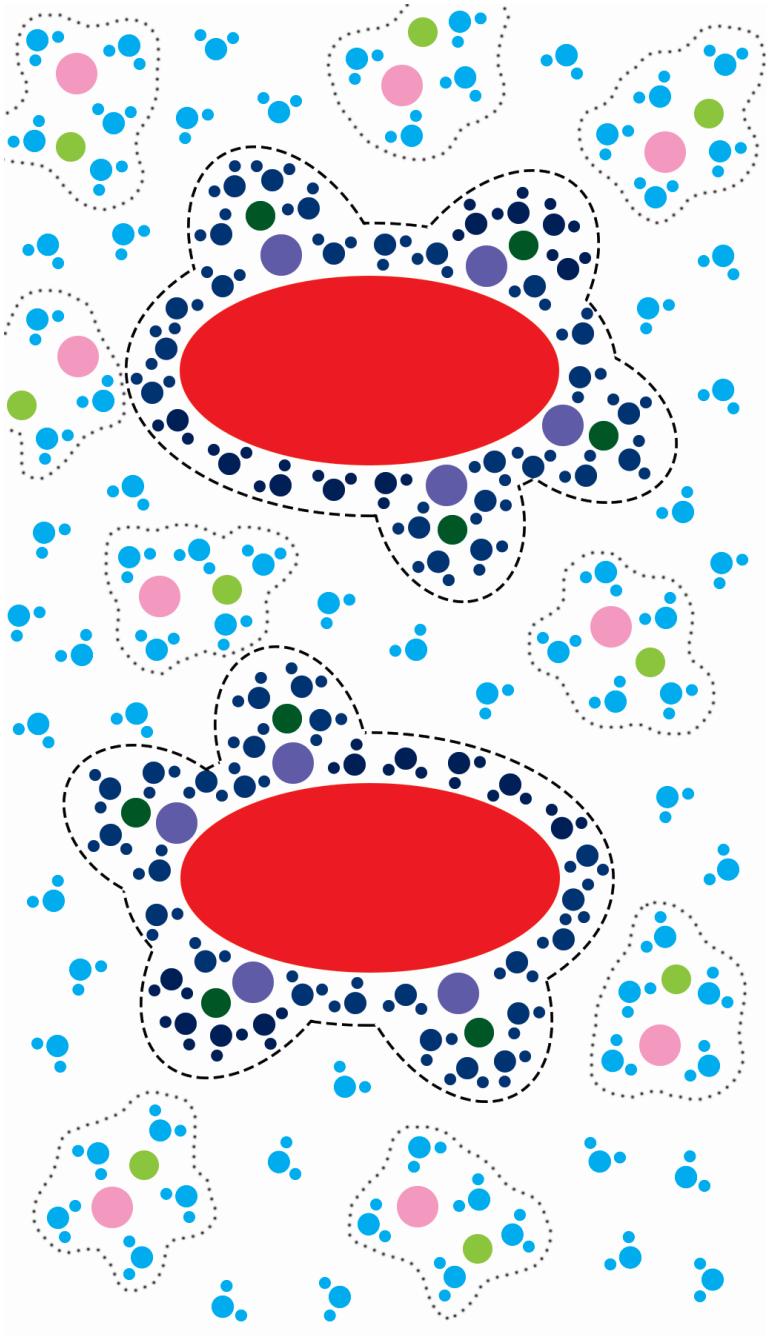

**Figure 5.2.** Schematic of Two Hydrated Macromolecules in Bulk Solution. The interaction between the solutes (pink ellipses) and the water (blue) (hydration), solutes and the salts (positive ion is green, negative ion is orange) (ion binding), and bound salts and water (hydration of the bound ions) are shown by the dashed lines. The dashed lines represent the revised hydrated macromolecule which includes bound water and hydrated ions. The hydrated ions which are not interacting with the solutes are shown by dotted lines.

# CHAPTER 6.

# ASSESSMENT OF THE SENSITIVITY OF THE OSMOTIC PRESSURE WITH RESPECT TO THE FREE-SOLVENT MODEL PHYSICAL PARAMETERS

## 6.1. Abstract

The robustness of the free-solvent model has been previously reported with respect to the experimental methods used for determining the physical parameters. However, no assessment of the robustness of the physical parameters with respect to macromolecules which have similar osmotic pressure-concentration profiles has been reported. Here the sensitivity of the physical parameters is addressed for the osmotic pressure of OVA and BSA in 0.15 M NaCl, pH 7.0 which, when plotted as osmotic pressure vs. protein concentration in grams per liter, overlap.

## 6.2. Robustness of the Free-Solvent Model

### 6.2.2. Protein Hydration

In order to determine whether a hydration is valid, the definition must first be explained. With the large number of studies which have been focused on understanding the interaction between water and proteins, two definitions for protein hydration have emerged. The first, in a more general sense of the word, is the total interaction of water with a solute (Timasheff 2002a, 2002b; Halle 2004). This definition allows for the hydration of water to be thought of in multiple layers around a solute (Jacobson 1953; Jacobson *et al.* 1954; Klotz 1958). The first layer is typically made up of the water which falls into the second category of bound water.

The second definition of protein hydration is the water which is perturbed by the interaction with a solute. In this sense, the water near the solute has a structure and dynamics

different from those of bulk water (Halle 2004). This is typically observed for the water which has large residence times in the vicinity of the solute (Timasheff 2002b).

The hydration, considered by the free-solvent model, is that of the former case; the protein hydration is the water which surrounds the protein until there is no available surface area for water to reside in, forming a monolayer of water. The water within the monolayer surrounding the solute can be made up of water with different residence times; however, it is assumed that whenever a water leaves the solute, it is immediately replaced by another water (Halle 2004). Furthermore, the water surrounding the protein is assumed to have a chemical potential different than that of the bulk water.

The free-solvent model provides a more accurate representation of the monolayer of hydration compared to $^{17}O$ NMR (Sedykh and Sedykh 1967), x-ray solution scattering (Svergun *et al.* 1998), and small angle neutron scattering (Svergun *et al.* 1998). These experimental methods yield hydration values which typically correspond with water molecules of the second type (high residence times).

### 6.2.2. Solvent Accessible Surface Area

The most reliable current methods for calculating the solvent accessible surface area (SASA) of proteins require the molecular structure, yet when the structure is unavailable, only the free-solvent model has been shown to provide an accurate measurement of the SASA for various globular macromolecules (M$^{c}$Bride and Rodgers 2012).

### 6.2.3. Protein-Ion Binding

Finally, the free-solvent model seemly provides a better estimate of the protein-ion binding compared to experimental methods due to the large error associated with them. The

free-solvent model predicts the ion binding for proteins, provided that an adequate amount of near-saturation osmotic pressure data exists, with an error of approximately 6% (Yousef *et al.* 1998a, 1998b, 2001, 2002a, 2002b; M$^{c}$Bride and Rodgers 2012).

## 6.3. Methods

The osmotic pressures of OVA in 0.15 M NaCl at pH 7.0 and BSA in 0.15 M NaCl at pH 7.0 are nearly identical (Figure 6.1). Thus, the osmotic pressure of these two proteins are used to determine the robustness of the free-solvent model with respect to the hydration and ion binding of each protein.

Using the osmotic pressure of OVA in 0.15 M NaCl, pH 7.0 (Yousef *et al.* 2001) and BSA in 0.15 M NaCl, pH 7.0, the free-solvent model is used to regress (nonlinear regression using TableCurve 2D (Systat Software, San Jose, CA, USA)) on the hydration and ion binding of both proteins. The regressed parameters are compared to those available in literature. In addition, the SASA computed for the regressed hydration (assuming a monolayer of water) (M$^{c}$Bride and Rodgers 2012) are compared to the expected SASA determined from the molecular structures of OVA (PDB: 1UHG (Yamasaki *et al.* 2003) and 1OVA (Stein *et al.* 1991)) and BSA (1BM0 homology model (Sugio *et al.* 1999) (Appendix A) and PDB: 3V03 (Majorek *et al.* 2012) and 4F5S (Bujacz 2012)).

## 6.4. Results and Discussion

The osmotic pressure of OVA in 0.15 M NaCl, pH 7.0 and BSA in 0.15 M NaCl, pH 7.0 and the best fit free-solvent models are shown in Figure 6.1. The free-solvent model has a unique curve for both protein solutions which provides a great deal of confidence in the regressed

parameters. The regressed physical parameters, and the corresponding SASA, are compared to the literature values (Table 6.1).

6.4.1. Assessing the Sensitivity of the Osmotic Pressure With Respect to Protein Hydration

When regression of both parameters is obtained, the regressed hydration values are $0.86 \pm 0.04$ g $H_2O$/g OVA for OVA in 0.15 M NaCl, pH 7.0 (Yousef *et al.* 2001) and $1.121 \pm 0.0235$ g $H_2O$/g BSA for BSA in 0.15 M NaCl, pH 7.0.

While the hydration for globular proteins is approximately 1 g $H_2O$/g protein (Rupley and Careri 1991), the hydration values obtained here, which agree with this this approximation, are unique for each protein. Although it is difficult to validate that the regressed values for hydration correspond to the actual physiological values, the experimental methods for determining protein hydration are also open to interpretation. For example, the value of hydration for BSA ranges from 0.32 g $H_2O$/g BSA (Bull and Breese 1968) to 1.07 g $H_2O$/g BSA (Tanford 1961).

In addition to determining the monolayer of water surrounding a protein, the free-solvent model may also capture the water which is interacting with the bound ions. Given sufficient data at near-saturation concentrations, the water bound to the protein forming a monolayer and the water molecules interacting with the bound ions (*i.e.* the water which is farther than 2.8 Å away from the protein surface and which are still influenced by the protein through hydration of the bound ions) may be uncoupled.

When the sensitivity of the osmotic pressure to the hydration parameter is assessed (Eqn. 6.1), it becomes apparent why the observed sensitivity for even overlapping osmotic pressure data (when plotted against the concentration variable, $c_2$).

$$\frac{\partial \pi}{\partial \nu_{12}} = \frac{RT}{\overline{V}_1}\left( \frac{x_2^{\mathrm{II}} - x_2^{\mathrm{II}} x_1^{\mathrm{II}}}{x_1^{\mathrm{II}}} \right) \tag{6.1}$$

6.4.2. Assessing the Sensitivity of the Osmotic Pressure With Respect to Solvent Accessible Surface Area

The SASA determined from the regressed values of hydration are 14,133 ± 657 $Å^2$ for OVA and 27,195 ± 568 $Å^2$ for BSA. Both of these SASA are in excellent agreement with the SASA determined from computational methods (Chapter 2). Depending on the choice of computational software, as well as the accuracy of the algorithm used to compute the actual SASA of a protein in solution, the SASA based on the regressed hydration value may have a smaller error than the SASA computed from computational software.

While many computational software have a fixed method and accuracy for calculating the SASA, two software which allow the SASA to be refined are Swiss-Pdb Viewer (Guex and Peitsch 1997) and MOLMOL (Koradi *et al.* 1996). The quality for Swiss-Pdb Viewer (Guex and Peitsch 1997), when adjusted from 1 - 6, computes the average SASA to be 14,934 ± 790 $Å^2$ (PDB: 1UHG (Yamasaki *et al.* 2003)) and 14,662 ± 830 $Å^2$ (PDB: 1OVA (Stein *et al.* 1991)) for OVA and 26,719 ± 1,468 $Å^2$ (1BM0 homology model), 26,384 ± 1,362 $Å^2$ (PDB: 3V03 (Majorek *et al.* 2012)), and 28,698 ± 94 $Å^2$ (PDB: 4F5S (Bujacz 2012)) for BSA. When the precision for MOLMOL (Koradi *et al.* 1996) is adjusted from 1 - 6, the average SASA are 16,408 ± 86 $Å^2$ (PDB: 1UHG (Yamasaki *et al.* 2003) and 16,332 ± 23 $Å^2$ (PDB: 1OVA (Stein *et al.* 1991)) for OVA and 28,199 ± 25 $Å^2$ (1BM0 homology model), 28,698 ± 94 $Å^2$ (PDB: 3V03 (Majorek *et al.* 2012), and 29,472 ± 40 $Å^2$ (PDB: 4F5S (Bujacz 2012)) for BSA.

The uniqueness of the SASA for each protein is captured by the free-solvent model regression of the osmotic pressure data despite the overlap of the osmotic pressure data. This can be explained by the uniqueness of the osmotic pressure with respect to the mole fraction concentration variables. Identical to the sensitivity of the osmotic pressure with respect to the hydration, the osmotic pressure is also sensitive with respect to the SASA (Eqn. 6.2).

$$\frac{\partial \pi}{\partial(\text{SASA})} = \frac{RT}{\overline{V}_1}\left(\frac{x_2^{\text{II}} - x_2^{\text{II}} x_1^{\text{II}}}{x_1^{\text{II}}}\right)(0.152) \tag{6.2}$$

6.4.3. Assessing the Sensitivity of the Osmotic Pressure With Respect to Protein-Ion Binding

The regressed ion binding values are 4.08 ± 0.43 mol NaCl/mol OVA (Yousef *et al.* 2001) and 9.80 ± 0.356 mol NaCl/mol BSA for OVA and BSA, respectively. Both of these ion binding values are unique.

The regressed ion binding value for BSA agrees with experimental ion binding (Scatchard *et al.* 1950; Reboiras *et al.* 1978). However, no ion binding studies have been published for OVA, yet, the regressed ion binding value yields an ionic strength within the protein influenced solvent similar to that of the bulk ( $\alpha = 0.703 \pm 0.074$ ).

Similarly, the ion binding is also sensitive and dependent on the mole fraction of protein (Eqn. 6.3).

$$\frac{\partial \pi}{\partial \nu_{32}} = -\frac{RT}{\overline{V}_1} x_2^{\text{II}} \tag{6.3}$$

6.5. Conclusion

Herein, the robustness of the free-solvent model's physical parameters were examined for nearly identical osmotic pressure data of two proteins. It was found that all three physical parameters, protein hydration, protein solvent accessible surface area, and protein-ion binding were unique for both proteins; no overlap in the values of any of the parameters was observed. The hydration values, which both agree with the observed 1 g $H_2O$/g protein, are different and both correlate to the SASA of each protein.

For macromolecule solutions which have unique mole fractions in the concentrated region, the free-solvent model will allow for unique values of hydration, ion binding, and SASA to be determined.

Furthermore, with the use of enough osmotic pressure data at near-saturation concentrations, other parameters may be able to be obtained, such as the hydration of the bound ions.

**Table 6.1.** Uniqueness of the Free-Solvent Model Physical Parameters for Overlapping Osmotic Pressure Data. The physical parameters obtained from osmotic pressure regression using the free-solvent model are compared to literature values. The computational SASA were determined using five computational software as previously described (M$^{c}$Bride and Rodgers 2012) (Chapter 2).

| Macromolecule (kDa) | Solution Properties Salt Conc., pH, Temp. | Regressed Hydration, $\nu_{12}$ $\left(\frac{\text{g H}_2\text{O}}{\text{g Protein}}\right)$ | Regressed Ion Binding, $\nu_{32}$ $\left(\frac{\text{mol Salt}}{\text{mol Protein}}\right)$ | Free-Solvent Based SASA (Å$^2$) | Structure Based SASA (Å$^2$) (PDB Code) |
|---|---|---|---|---|---|
| Ovalbumin (OVA) (45) | 0.15 M NaCl, 7.0, 25$^{o}$C | 0.86 ± 0.04[a] | 4.08 ± 0.43[a] | 14,133 ± 657 | 14,058 - 16,375 (1UHG)<br>13,556 - 16,434 (1OVA) |
| Bovine Serum Albumin (BSA) (66.4) | 0.15 M NaCl, 7.0, 25$^{o}$C | 1.121 ± 0.0234[b] | 9.80 ± 0.356[b] | 27,195 ± 568 | 27,746 - 28,188 (1BM0*)<br>27,495 - 34,563 (3V03)<br>28,646-35,491 (4F5S) |

[a] (Yousef *et al.* 2001)
[b] (Chapter 4)
* Homology model (Appendix A)

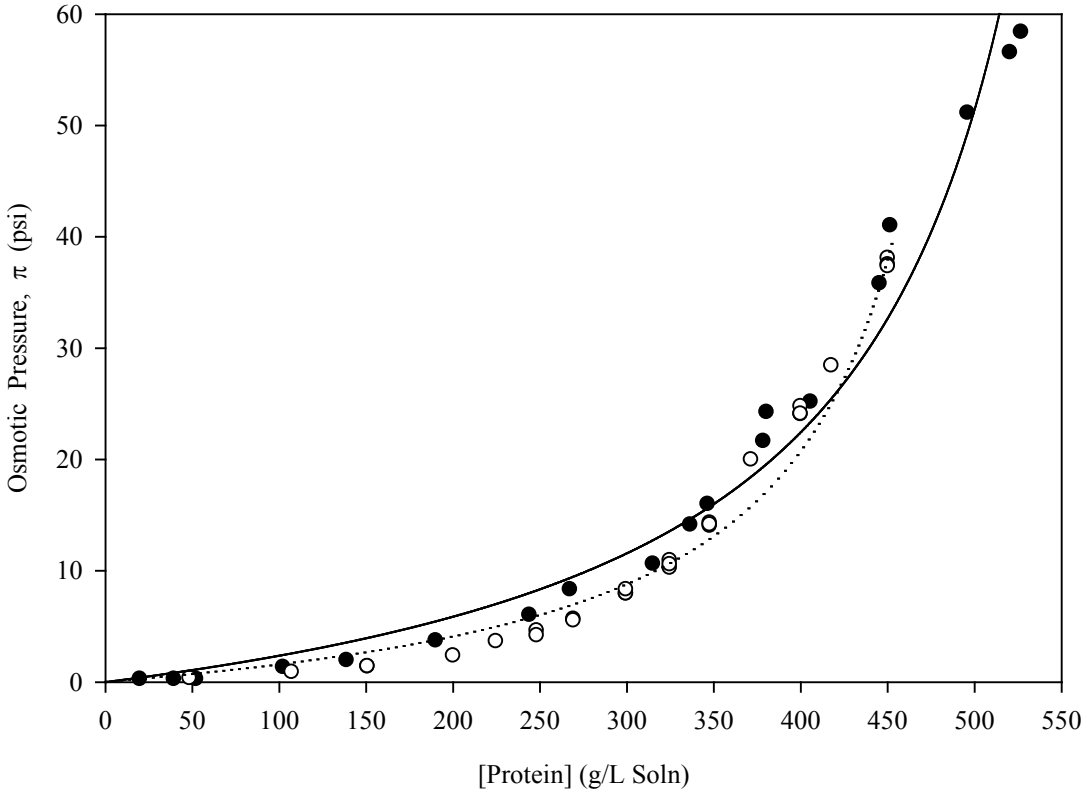


**Figure 6.1.** Osmotic Pressure vs. Protein Concentration for OVA and BSA in 0.15 M NaCl, pH 7.0. The osmotic pressure of OVA in 0.15 M NaCl, pH 7.0 (closed circles) (Yousef *et al.* 2001) and BSA in 0.15 M NaCl, pH 7.0 (open circles) are plotted. The corresponding free-solvent models (OVA: solid line, BSA: dotted line) are also shown.

# CHAPTER 7.

# DEVELOPMENT OF THE FREE-SOLVENT MODEL FOR THE OSMOTIC PRESSURE OF MULTI-COMPONENT SOLUTIONS CONTAINING PROTEIN-PROTEIN INTERACTIONS

## 7.1. Abstract

Here, the free-solvent osmotic pressure model is developed for multi-component protein solutions in which protein-protein interactions occur. The free-solvent model is extended to include the contributions of protein-protein interactions to the osmotic pressure of a solution in the form of homo- and hetero-multimers. The solute-solvent interactions are unique for each homo- and hetero-multimer in solution. Several case scenarios are presented and the free-solvent model is developed for each. The effect of the various free-solvent model parameters on the osmotic pressure are examined for a single protein solution with a homo-dimer, a binary protein solution with no protein-protein interactions, and a binary protein solution with a hetero-dimer. The limitations associated with the developed free-solvent model are discussed.

## 7.2. Introduction

The contribution of individual proteins to the osmotic pressure of the concentration polarization layer during multi-component protein ultrafiltration has received relatively little focus. However, the build-up of proteins, on the membrane, exhibit a unique osmotic pressure profile; increasing the protein concentration by small increments, near-saturation, have

exponentially high effects on the osmotic pressure (Vilker *et al.* 1981; Yousef *et al.* 1998a, 2002b).

While many models exist that attempt to understand and predict the non-ideal effects of crowded protein solutions on osmotic pressure, the majority of the models have had limited success because protein-protein interactions were thought to be the predominant contributor. Most of these models use a virial expansion model which is based on the McMillan-Mayer Dilute Solution Theory (McMillan and Mayer 1945). Yet these models lack physically realistic parameters and are unable to confidently predict the osmotic pressure of concentrations near-saturation.

Use of a free-solvent model circumvents the limitations of other osmotic pressure models because it is based on physical parameters, namely protein hydration and protein-ion binding, and thus is an accurate predictor of the osmotic pressure for concentrated and crowded protein solutions (Yousef *et al.* 1998a, 1998b, 2001, 2002a, 2002b; M$^{c}$Bride and Rodgers 2012). The fact that physical parameters are utilized in the free-solvent model allows for them to be determined independently.

The original free-solvent model was developed by van Laar (van Laar 1894) and further by Lewis and Randall (Lewis and Randall 1961). van Laar (van Laar 1894) proposed that solvent-solute interactions are coupled to the observed non-ideal behavior of the osmotic pressure and he argued that the mole fraction is the appropriate concentration variable to describe osmotic pressure. Recently, Yousef *et al.* revised the free-solvent model to include ion binding (Yousef *et al.* 1998a, 1998b). Furthermore, the revised free-solvent model describes the solute as a hydrated macromolecule, which contains a monolayer of water and bound ions, and, upon correcting the mole fraction for these interactions, provides excellent predictions for the observed

osmotic pressure (Yousef *et al.* 1998a, 1998b). In addition, the underlying mechanisms, for the observed osmotic pressure behavior, are well understood.

## 7.3. The Free-Solvent Model Revised to Account for Protein-Protein Interactions

The free-solvent model has been previously developed to understand the osmotic pressure for the single protein solutions (Yousef *et al.* 1998a, 1998b, 2001, 2002b) and binary protein solutions (Yousef *et al.* 2002a). While previous developments of the free-solvent model have fully described the solutions modeled (*i.e.* pH and salt(s)), a general free-solvent model in which intra- and inter-protein interactions occur does not exist. Here, the general free-solvent model is developed for multi-component solutions which protein-protein interactions can occur in the form of homo-multimers (intra-protein species interactions) and hetero-multimers (inter-protein species interactions).

For a two-chamber osmometer, with the chamber containing the proteins in aqueous solution denoted as compartment II and the chamber containing only the solvent and diffusible ions (*i.e.* proteins are absent) denoted as compartment I, the free-solvent model, with the mole fraction chosen as the appropriate composition variable, describes the osmotic pressure, $\pi$, as (Yousef *et al.* 1998a)

$$\pi = -\frac{RT}{\bar{V}_1} \ln \frac{x_1^{\mathrm{II}}}{x_1^{\mathrm{I}}}, \tag{7.1}$$

where the free-solvent mole fraction, $x_1$, is the remaining moles of solvent that are not bound to the protein.

For a solution containing $n$ distinct species with $p$ proteins, where species 1 is the solvent, species 2 through $(p+1)$ are the proteins, and species $(p+2)$ through $n$ are the

remaining diffusible solvent components, the initial total moles of the solution in compartment II is $\sum_{i=1}^{n} N_i^{\mathrm{II}}$, where $i$ denotes each individual species.

The final total moles of solution in compartment II, after solute-solvent and solute-solute interactions occur, is

$$\begin{aligned}&\sum_{\substack{i=1\\ i\neq 2\rightarrow p+1}}^{n} N_i^{\mathrm{II}} + \sum N_{\text{homo-multimers}}^{\mathrm{II}} + \sum N_{\text{hetero-multimers}}^{\mathrm{II}} + \dots \\ &\dots + \sum N_{\text{monomers}}^{\mathrm{II}} - \sum \nu N_{\text{homo-multimers}}^{\mathrm{II}} - \sum \nu N_{\text{hetero-multimers}}^{\mathrm{II}} - \sum \nu N_{\text{monomers}}^{\mathrm{II}}\end{aligned} \tag{7.2}$$

where the first term is the moles of solvent and salt species, the second term is the moles of protein forming homo-multimers (intra-protein species interactions), the third term is the moles of protein forming hetero-multimers (inter-protein species interactions), the fourth term is the moles of protein remaining as free (unbound, non-interacting) monomers, and the fifth, sixth, and seventh terms are the moles of diffusible species (water and salt) bound to the homo-multimers, hetero-multimers, and free monomers, respectively.

The moles of monomeric proteins forming homo-multimers are

$$\sum N_{\text{homo-multimers}}^{\mathrm{II}} = \sum_{j=2}^{p+1} \sum_{Z=\text{ii}} \alpha_{j,Z} N_j^{\mathrm{II}}\ , \tag{7.3}$$

where $N_j^{\mathrm{II}}$ is the moles of protein species $j$ in solution initially and $\alpha_{j,Z}$ is the fractional amount of protein $j$ forming the homo-multimer of $Z$ units.

The moles of solvent bound to the homo-multimers are

$$\sum \nu N_{\text{homo-multimers}}^{\mathrm{II}} = \sum_{\substack{i=1\\ i\neq 2\rightarrow p+1}}^{n} \sum_{j=2}^{p+1} \sum_{Z=\text{ii}} \nu_{ij,Z} \alpha_{j,Z} N_j^{\mathrm{II}}\ , \tag{7.4}$$

where $\nu_{ij,Z}$ is the moles of solvent species $i$ bound to the protein $j$ homo-multimer with $Z$ units.

The moles of monomeric proteins forming hetero-multimers is given as

$$\sum N^{\mathrm{II}}_{\text{hetero-multimers}} = \begin{bmatrix} \sum_{j=2}^{p} \sum_{a=j+1}^{p+1} \sum_{A=\mathrm{i}} \sum_{B=\mathrm{i}} \beta_{ja,A:B} N_j^{\mathrm{II}} + \ldots \\ \ldots + \sum_{j=2}^{p-1} \sum_{a=j+1}^{p} \sum_{\substack{b=j+2 \\ b\neq a}}^{p+1} \sum_{A=\mathrm{i}} \sum_{B=\mathrm{i}} \sum_{C=\mathrm{i}} \beta_{jab,A:B:C} N_j^{\mathrm{II}} + \ldots \end{bmatrix}, \quad (7.5)$$

where $N_j^{\mathrm{II}}$ is the moles of protein species $j$ in solution initially, $\beta_{ja,A:B}$ is the fractional amount of protein $j$ forming a hetero-dimer with protein $a$ containing $A$ units of protein $j$ and $B$ units of protein $a$, and $\beta_{jab,A:B:C}$ is the fractional amount of protein $j$ forming a hetero-trimer with proteins $a$ and $b$ containing $A$ units of protein $j$, $B$ units of protein $a$, and $C$ units of protein $b$.

Here, Eqn. 7.5 only accounts for the protein hetero-multimers in which two and three unique protein species form hetero-multimers. The first term is the moles of the hetero-multimers formed from two unique protein species. The second term is the moles of the hetero-multimers formed from three unique protein species. Each term includes the hetero-multimers in which multiple molecules of protein $j$ can bind to multiple molecules of another protein(s) to form hetero-multimers of various homo-multimers (*i.e.* $jjaaab$ is a three protein species hetero-multimer formed by a homo-dimer ($jj$), a homo-trimer ($aaa$), and a monomer ($b$)). Additional terms can be included in Eqn. 7.5 to account for hetero-multimers of any number of unique proteins. For all hetero-multimers, solute-solvent interactions need to be included (Eqn. 7.6) and the moles of these hetero-multimers need to be removed from the available monomers (Eqns. 7.7 and 7.8).

The moles of solvent bound to the hetero-multimers are

$$\sum \nu N^{\mathrm{II}}_{\text{hetero-multimers}} = \\ = \left[ \begin{array}{l} \sum_{\substack{i=1 \\ i\neq 2\rightarrow p+1}}^{n} \sum_{j=2}^{p} \sum_{a=j+1}^{p+1} \sum_{A=\mathrm{i}} \sum_{B=\mathrm{i}} \nu_{ija,A:B} \beta_{ja,A:B} N_j^{\mathrm{II}} + \ldots \\ \ldots + \sum_{\substack{i=1 \\ i\neq 2\rightarrow p+1}}^{n} \sum_{j=2}^{p-1} \sum_{a=j+1}^{p} \sum_{\substack{b=j+2 \\ b\neq a}}^{p+1} \sum_{A=\mathrm{i}} \sum_{B=\mathrm{i}} \sum_{C=\mathrm{i}} \nu_{ijab,A:B:C} \beta_{jab,A:B:C} N_j^{\mathrm{II}} + \ldots \end{array} \right], \quad (7.6)$$

where $\nu_{ija,A:B}$ is the moles of solvent species $i$ bound to the hetero-multimer between proteins $j$ and $a$ with $A$ units of protein $j$, and $B$ units of protein $a$, and $\nu_{ijab,A:B:C}$ is the moles of solvent species $i$ bound to the hetero-multimer between proteins $j$, $a$, and $b$ with $A$ units of protein $j$, $B$ units of protein $a$, and $C$ units of protein $b$.

The moles of monomeric proteins which remain in solution as free monomers (not forming homo- or hetero-multimers) are

$$\sum N^{\mathrm{II}}_{\text{monomers}} = \\ = \sum_{j=2}^{p+1} \left( \begin{array}{l} 1 - \sum_{Z=\mathrm{ii}} \nu_{jj,Z} \alpha_{j,Z} + \ldots \\ \ldots - \sum_{\substack{a=2 \\ a\neq j}}^{p+1} \sum_{A=\mathrm{i}} \sum_{B=\mathrm{i}} \nu_{ja,A:B} \beta_{ja,A:B} + \ldots \\ \ldots - \sum_{\substack{a=2 \\ a\neq j}}^{p+1} \sum_{\substack{b=2 \\ b\neq j \\ b\neq a}}^{p+1} \sum_{A=\mathrm{i}} \sum_{B=\mathrm{i}} \sum_{C=\mathrm{i}} \nu_{jab,A:B:C} \beta_{jab,A:B:C} + \ldots \end{array} \right) N_j^{\mathrm{II}} . \quad (7.7)$$

where $\nu_{jj,Z}$ is the moles of protein $j$ forming homo-multimers of $Z$ units, $\nu_{ja,A:B}$ is the moles of protein $j$ interacting with protein $a$ with $A$ units of protein $j$ and $B$ units of protein $a$, and $\nu_{jab,A:B:C}$ is the moles of protein $j$ interacting with proteins $a$ and $b$ with $A$ units of protein $j$, $B$ units of protein $a$, and $C$ units of protein $b$.

The remaining moles of monomeric protein $j$ is calculated by subtracting the moles of protein $j$ forming homo-multimers (second term in Eqn. 7.2) and hetero-multimers (third and fourth terms in Eqn. 7.2) from the initial total moles of protein $j$ monomers added, $N_j^{\mathrm{II}}$.

The moles of solvent bound to the free monomers are

$$\sum \nu N^{\mathrm{II}}_{\text{monomers}} = \\ = \sum_{\substack{i=1 \\ i\neq 2\rightarrow p+1}}^{n} \sum_{j=2}^{p+1} \nu_{ij} \left( \begin{array}{l} 1 - \sum_{Z=\mathrm{ii}} \nu_{jj,Z} \alpha_{j,Z} + \ldots \\ \ldots - \sum_{\substack{a=2 \\ a\neq j}}^{p+1} \sum_{A=\mathrm{i}} \sum_{B=\mathrm{i}} \nu_{ja,A:B} \beta_{ja,A:B} + \ldots \\ \ldots - \sum_{\substack{a=2 \\ a\neq j}}^{p+1} \sum_{\substack{b=2 \\ b\neq j \\ b\neq a}}^{p+1} \sum_{A=\mathrm{i}} \sum_{B=\mathrm{i}} \sum_{C=\mathrm{i}} \nu_{jab,A:B:C} \beta_{jab,A:B:C} + \ldots \end{array} \right) N_j^{\mathrm{II}}, \tag{7.8}$$

where $\nu_{ij}$ is the moles of solvent species $i$ bound to protein $j$.

The final moles of free-solvent in compartment II are

$$\begin{array}{l} N_1^{\mathrm{II}} - \sum \nu_{\text{solvent / homo-multimer}} N^{\mathrm{II}}_{\text{homo-multimers}} + \ldots \\ \ldots - \sum \nu_{\text{solvent / hetero-multimer}} N^{\mathrm{II}}_{\text{hetero-multimers}} + \ldots \\ \ldots - \sum \nu_{\text{solvent / monomer}} N^{\mathrm{II}}_{\text{monomers}} \end{array}, \tag{7.9}$$

where $N_1^{\mathrm{II}}$ is the initial moles of solvent. The second, third, and fourth terms (in Eqn. 7.9) are the moles of water bound to the homo-multimers, hetero-multimers, and free monomers, respectively, and are given by Eqns. 7.10 - 7.12

$$\sum \nu_{\text{solvent/homo-multimer}} N^{\mathrm{II}}_{\text{homo-multimers}} = \sum_{j=2}^{p+1} \sum_{Z=\mathrm{ii}} \nu_{1j,Z} \alpha_{j,Z} N_j^{\mathrm{II}} \tag{7.10}$$

$$\sum \nu_{\text{solvent/hetero-multimer}} N^{\mathrm{II}}_{\text{hetero-multimers}} = \\ = \left[ \begin{array}{l} \sum_{j=2}^{p} \sum_{a=j+1}^{p+1} \sum_{A=\mathrm{i}} \sum_{B=\mathrm{i}} \nu_{1ja,A:B} \beta_{ja,A:B} N_j^{\mathrm{II}} + \ldots \\ \ldots + \sum_{j=2}^{p-1} \sum_{a=j+1}^{p} \sum_{\substack{b=j+2 \\ b\neq a}}^{p+1} \sum_{A=\mathrm{i}} \sum_{B=\mathrm{i}} \sum_{C=\mathrm{i}} \nu_{1jab,A:B:C} \beta_{jab,A:B:C} N_j^{\mathrm{II}} + \ldots \end{array} \right] \tag{7.11}$$

$$\sum \nu_{\text{solvent/monomer}} N^{\text{II}}_{\text{monomers}} =$$

$$= \sum_{j=2}^{p+1} \nu_{1j} \left( \begin{array}{l} 1 - \sum_{Z=\text{ii}} \nu_{jj,Z} \alpha_{j,Z} + \ldots \\ \ldots - \sum_{\substack{a=2 \\ a \neq j}}^{p+1} \sum_{A=\text{i}} \sum_{B=\text{i}} \nu_{ja,A:B} \beta_{ja,A:B} + \ldots \\ \ldots - \sum_{\substack{a=2 \\ a \neq j}}^{p+1} \sum_{\substack{b=2 \\ b \neq j \\ b \neq a}}^{p+1} \sum_{A=\text{i}} \sum_{B=\text{i}} \sum_{C=\text{i}} \nu_{jab,A:B:C} \beta_{jab,A:B:C} + \ldots \end{array} \right) N_j^{\text{II}}, \tag{7.12}$$

where $\nu_{1j}$ is the moles of water bound to monomeric protein species $j$.

The mole fraction of free-solvent in compartment II is

$$x_1^{\text{II}} = \frac{\left[ \begin{array}{l} N_1^{\text{II}} - \sum \nu_{\text{solvent/homo-multimer}} N^{\text{II}}_{\text{homo-multimers}} + \ldots \\ \ldots - \sum \nu_{\text{solvent/hetero-multimer}} N^{\text{II}}_{\text{hetero-multimers}} - \sum \nu_{\text{solvent/monomer}} N^{\text{II}}_{\text{monomers}} \end{array} \right]}{\left[ \begin{array}{l} \sum_{\substack{i=1 \\ i \neq 2 \rightarrow p+1}}^{n} N_i^{\text{II}} + \sum N^{\text{II}}_{\text{homo-multimers}} + \sum N^{\text{II}}_{\text{hetero-multimers}} + \sum N^{\text{II}}_{\text{monomers}} + \ldots \\ \ldots - \sum \nu N^{\text{II}}_{\text{homo-multimers}} - \sum \nu N^{\text{II}}_{\text{hetero-multimers}} - \sum \nu N^{\text{II}}_{\text{monomers}} \end{array} \right]}. \tag{7.13}$$

In compartment I, the total moles of solvent is $\sum_{\substack{i=1 \\ i \neq 2 \rightarrow p+1}}^{n} N_i^{\text{I}}$, thus the mole fraction of free-solvent in compartment I is

$$x_1^{\text{I}} = \frac{N_1^{\text{I}}}{\sum_{\substack{i=1 \\ i \neq 2 \rightarrow p+1}}^{n} N_i^{\text{I}}}. \tag{7.14}$$

Inserting Eqns. 7.13 and 7.14 into Eqn. 7.1 yields the general free-solvent model for any number of proteins which have solute-solvent interactions and may participate in solute-solute interactions in the form of homo-multimers and hetero-multimers. It is important to note that this development of the free-solvent model does not consider protein homo-multimers and protein hetero-multimers as unique and individual protein species (*i.e.* a dimer is not considered as one of the protein species $j$, but rather $\left(\alpha_{j,\text{ii}} N_j^{\text{II}}\right)$ is the dimer species and is a unique and individual

species); since the homo-multimers and hetero-multimers have unique hydration and ion binding values, they are unique hydrated macromolecules.

7.4. Determining the Physical Parameters of the Free-Solvent Model

The number of physical parameters (*i.e.* hydration, ion binding, protein-protein interactions, and fractional amounts of the homo- and hetero-multimer forms) which are required in the free-solvent model are a minimum of $2p$ for $p$ proteins if only monomers are considered (*i.e.* no homo-multimers or hetero-multimers are formed).

For protein solutions containing protein-protein interactions in the form of homo- and/or hetero-multimers, the number of physical parameters required to describe the crowded protein osmotic pressure via the free-solvent model is given by

$$2\left(p + l_{\text{homo-multimer}} + l_{\text{hetero-multimer}}\right) + 2\left(l_{\text{homo-multimer}} + \sum_{h=2}\left(l_{\text{hetero-multimer},h}\right)\left(\eta_h\right)\right), \quad (7.15)$$

where $p$ is the number of protein species, $l_{\text{homo-multimer}}$ is the number of homo-multimers formed, $l_{\text{hetero-multimer}}$ is the number of hetero-multimers formed, $l_{\text{hetero-multimer},h}$ is the number of hetero-multimers forming the $h$ multimer (*i.e.* $h = 2$ for a two protein species interactions, $h = 3$ for a three protein species interactions, etc.), and $\eta_h$ is the size of the $h$ multimer (i.e. $\eta_2 = 2$ for a two protein species interactions, $\eta_3 = 3$ for a three protein species interactions, etc.).

The total number of hydration and ion binding parameters are each given by the first term of Eqn. 7.15, or

$$\left(p + l_{\text{homo-multimer}} + l_{\text{hetero-multimer}}\right) \quad (7.16)$$

and the total number of protein-protein interactions and fractional amounts are each given by

$$l_{\text{homo-multimer}} + \sum_{h=2} l_{\text{hetero-multimer},h}\eta_h \ . \quad (7.17)$$

Thus in order to utilize the free-solvent model for predicting the osmotic pressure of crowded protein solutions, methods, independent of the crowded protein osmotic pressure, need to be used to determine the hydration and ion binding of the unique species, as well as the protein-protein interactions and fractional amount of proteins forming homo- and hetero-multimers.

### 7.4.1. Protein Hydration

Many methods are available to determine protein hydration, such as $^{17}O$ NMR, yet it is often difficult to determine the exact values due to the variety of methods, the associated errors, and the type of hydration (*i.e.* total interaction of water or perturbed water) (Kuntz and Kauzmann 1974; Halle *et al.* 1981; Otting *et al.* 1991; Rupley and Careri 1991). Nevertheless, the consensus is that a globular protein contains about 1 g $H_2O$/g Protein (Rupley and Careri 1991). If this value of hydration is utilized in the free-solvent model, the prediction of the osmotic pressure at near-saturation concentrations will result in a deviation of the predicted and experimental values since this value of hydration is not accurate enough. Thus, a more exact value for protein hydration is required to ensure that the predicted osmotic pressure is nearly-identical to the experimental measurements.

An alternative method of calculating the hydration of a protein which yields a more accurate value, is to utilize the solvent accessible surface area (SASA) of the protein. This method requires that the molecular structure has been deposited into the Protein Data Bank or that the molecular structure can be determined using either NMR or x-ray crystallography. It has been previously shown that the hydration of a globular protein directly correlates to a monolayer of water, specifically $15.2 \pm 0.5$ molecules of water per $nm^2$ of SASA (Yousef *et al.* 2002b), and

thus, if the SASA is known, the protein hydration can be determined (M$^{c}$Bride and Rodgers 2012).

### 7.4.2. Protein-Ion Binding

Various methods exist for determining the ion binding to proteins, such as the electromotive force (EMF), distribution method, and isopiestic method (Scatchard *et al.* 1950, 1957; Carr 1952, 1953, 1955; Bull and Breese 1968; Reboiras *et al.* 1978, 1986). These methods have been used to quantify the number of ions interacting with proteins in various solution properties including salt types, salt concentration, pH, and protein concentration. A limitation of experimental methods for determining protein-ion binding is the large error (up to 40%).

An alternative method of determining ion binding is to utilize a predictive model, such as the two-site model developed by Scatchard *et al.* (Scatchard *et al.* 1950). Yousef *et al.* used this approach to calculate the ion binding for bovine serum albumin (BSA) in three different solutions and found that the predicted values of ion binding were in agreement with those obtained from experimental methods.

### 7.4.3. Protein-Protein Interactions and the Fractional Amounts of Homo- and Hetero-multimers

To determine the presence and mole number of proteins interacting to form homo- and hetero-multimers in a given multi-component solution, methods such as HPLC and light scattering can be used.

For the fractional amounts of homo-multimers, it is important to note that the fractional amount of each homo-multimer is restricted to $0 \le \alpha_{j,Z} \le 0.5$. The maximum is 0.5 since if a homo-dimer is the only homo-multimer and the entire solution is homo-dimers (*i.e.* no monomers exist in solution), when the fractional amount is 50% of the monomeric protein, every mole of the

monomeric protein is consumed. The sum of all fractional amounts of each protein $j$ forming homo-multimers is also restricted to 0.5 (or $0 \le \sum_{Z=\mathrm{ii}} \alpha_{j,Z} \le 0.5$).

Following a similar approach, the fractional amount of each hetero-multimer is restricted to $0 \le \beta \le 1$ since if a single hetero-multimer is formed, and the entire solution is hetero-multimers (*i.e.* 100% fractional amount), every mole of the monomeric protein is consumed. The sum of all fractional amounts of each protein $j$ forming homo-multimers is also restricted to 1 (or $0 \le \sum_{A=\mathrm{i}} \sum_{B=\mathrm{i}} \beta_{ja,A:B} + \sum_{A=\mathrm{i}} \sum_{B=\mathrm{i}} \sum_{C=\mathrm{i}} \beta_{jab,A:B:C} + \ldots \le 1$).

For a given protein $j$ with a known molar ratio of monomer:homo-multimer, the fractional amount of protein $j$ forming a homo-multimer of $Z$ units $\alpha_{j,Z}$ is calculated for each homo-multimer by

$$\frac{\left(\begin{array}{l} 1 - \sum_{Z=\mathrm{ii}} \nu_{jj,Z} \alpha_{j,Z} + \ldots \\ \ldots - \sum_{\substack{a=2 \\ a \neq j}}^{p+1} \sum_{A=\mathrm{i}} \sum_{B=\mathrm{i}} \nu_{ja,A:B} \beta_{ja,A:B} + \ldots \\ \ldots - \sum_{\substack{a=2 \\ a \neq j}}^{p+1} \sum_{\substack{b=2 \\ b \neq j \\ b \neq a}}^{p+1} \sum_{A=\mathrm{i}} \sum_{B=\mathrm{i}} \sum_{C=\mathrm{i}} \nu_{jab,A:B:C} \beta_{jab,A:B:C} + \ldots \end{array}\right)}{\alpha_{j,Z}\big|_{j,Z}} = \Phi\big|_{j,Z} \qquad (7.18)$$

where $\alpha_{j,Z}\big|_{j,Z}$ is the fractional amount of a specific homo-multimer, $Z$, for protein $j$ and $\Phi\big|_{j,Z}$ is the molar ratio of the monomer to homo-multimer $Z$ for protein $j$ for a specific homo-multimer. The hetero-multimer terms (terms 3 and 4 in the numerator of Eqn. 7.18) are evaluated for protein $j$ only.

The fractional amounts of hetero-multimers are given by

$$\frac{\left(\begin{array}{l} 1-\sum_{Z=\mathrm{ii}}\nu_{jj,Z}\alpha_{j,Z}+\ldots \\ \ldots-\sum_{\substack{a=2\\a\neq j}}^{p+1}\sum_{A=\mathrm{i}}\sum_{B=\mathrm{i}}\nu_{ja,A:B}\beta_{ja,A:B}+\ldots \\ \ldots-\sum_{\substack{a=2\\a\neq j}}^{p+1}\sum_{\substack{b=2\\b\neq j\\b\neq a}}^{p+1}\sum_{A=\mathrm{i}}\sum_{B=\mathrm{i}}\sum_{C=\mathrm{i}}\nu_{jab,A:B:C}\beta_{jab,A:B:C}+\ldots \end{array}\right)}{\beta_{ja,A:B}\Big|_{ja,A:B}}=\Gamma\Big|_{ja,A:B} \qquad (7.19)$$

for hetero-multimers formed from two unique proteins, and, for hetero-multimers formed from three unique proteins,

$$\frac{\left(\begin{array}{l} 1-\sum_{Z=\mathrm{ii}}\nu_{jj,Z}\alpha_{j,Z}+\ldots \\ \ldots-\sum_{\substack{a=2\\a\neq j}}^{p+1}\sum_{A=\mathrm{i}}\sum_{B=\mathrm{i}}\nu_{ja,A:B}\beta_{ja,A:B}+\ldots \\ \ldots-\sum_{\substack{a=2\\a\neq j}}^{p+1}\sum_{\substack{b=2\\b\neq j\\b\neq a}}^{p+1}\sum_{A=\mathrm{i}}\sum_{B=\mathrm{i}}\sum_{C=\mathrm{i}}\nu_{jab,A:B:C}\beta_{jab,A:B:C}+\ldots \end{array}\right)}{\beta_{jab,A:B:C}\Big|_{jab,A:B:C}}=\Gamma\Big|_{jab,A:B:C} \qquad (7.20)$$

where $\beta_{ja,A:B}\Big|_{ja,A:B}$ is the fractional amount of the two protein hetero-multimer at a specific hetero-multimer, $ja$, $\beta_{jab,A:B:C}\Big|_{jab,A:B:C}$ is the fractional amount of the three protein hetero-multimer at a specific hetero-multimer, $jab$, $\Gamma\Big|_{ja,A:B}$ is the molar ratio of the monomer to hetero-multimer $ja$ with $A$ units of $j$ and $B$ units of $a$, and $\Gamma\Big|_{jab,A:B:C}$ is the molar ratio of the monomer to hetero-multimer $jab$ with $A$ units of $j$, $B$ units of $a$, and $C$ units of $b$.

Eqns. 7.18 - 7.20 need to be solved for each protein, $j$, in solution. If more than 1 multimer forms, the system of equations must be solved to obtain all $\alpha_{j,Z}$, $\beta_{ja,A:B}$, $\beta_{jab,A:B:C}$, etc.

For example, if a single protein solution forms a homo-dimer ($\nu_{22,\mathrm{ii}} = 2$ mol Monomer/mol Dimer) and homo-trimer ($\nu_{22,\mathrm{iii}} = 3$ mol Monomer/mol Trimer), and if the molar ratio is 3:1:2 for the monomer:dimer:trimer (*i.e.* $\Phi\big|_{2,\mathrm{ii}} = 3/1$ and $\Phi\big|_{2,\mathrm{ii}} = 3/2$), Eqn. 7.18 yields two equations

$$\frac{1-2\alpha_{2,\mathrm{ii}}-3\alpha_{2,\mathrm{iii}}}{\alpha_{2,\mathrm{ii}}} = \frac{3}{1} \tag{7.21}$$

and

$$\frac{1-2\alpha_{2,\mathrm{ii}}-3\alpha_{2,\mathrm{iii}}}{\alpha_{2,\mathrm{iii}}} = \frac{3}{2}. \tag{7.22}$$

Solving the system of equations yields fractional amounts of $\alpha_{2,\mathrm{ii}} = 0.091$ and $\alpha_{2,\mathrm{iii}} = 0.182$.

## 7.5. Case Scenarios: The Free-Solvent Model Development and the Required Physical Parameters

Here, the free-solvent model (Eqn. 7.1 with Eqns. 7.13 and 7.14) is reduced for the following cases. All cases consider only a single monovalent salt species.

### 7.5.1. Case 1: Single Protein Forming a Homo-Dimer

Given a solution with a single protein ($p = 1,\ n = 3$), $A$, that only forms a homo-dimer (*i.e.* $AA$), Eqns. 7.13 and 7.14 become

$$x_1^{\mathrm{II}} = \frac{N_1^{\mathrm{II}} - \sum \nu_{\mathrm{solvent/homo\text{-}multimer}} N_{\mathrm{homo\text{-}multimers}}^{\mathrm{II}} - \sum \nu_{\mathrm{solvent/monomer}} N_{\mathrm{monomers}}^{\mathrm{II}}}{\sum_{\substack{i=1 \\ i\neq 2}}^{3} N_i^{\mathrm{II}} + \sum N_{\mathrm{homo\text{-}multimers}}^{\mathrm{II}} + \sum N_{\mathrm{monomers}}^{\mathrm{II}} - \sum \nu N_{\mathrm{homo\text{-}multimers}}^{\mathrm{II}} - \sum \nu N_{\mathrm{monomers}}^{\mathrm{II}}} \tag{7.23}$$

and

$$x_1^{\mathrm{I}} = \frac{N_1^{\mathrm{I}}}{\sum_{\substack{i=1 \\ i\neq 2}}^{3} N_i^{\mathrm{I}}} = \frac{N_1^{\mathrm{I}}}{N_1^{\mathrm{I}} + N_3^{\mathrm{I}}}. \tag{7.24}$$

The terms in Eqn. 7.18 are

$$\sum N_{\text{homo-multimers}}^{\mathrm{II}} = \sum_{j=2}^{3} \sum_{Z=\mathrm{ii}} \alpha_{j,Z} N_j^{\mathrm{II}} = \alpha_{2,\mathrm{ii}} N_2^{\mathrm{II}}, \tag{7.25}$$

$$\sum \nu N_{\text{homo-multimers}}^{\mathrm{II}} = \sum_{\substack{i=1 \\ i\neq 2}}^{3} \sum_{j=2}^{2} \sum_{Z=\mathrm{ii}} \nu_{\mathrm{ij},Z} \alpha_{j,Z} N_j^{\mathrm{II}}$$

$$\Rightarrow \sum \nu N_{\text{homo-multimers}}^{\mathrm{II}} = \nu_{12,\mathrm{ii}} \alpha_{2,\mathrm{ii}} N_2^{\mathrm{II}} + \nu_{32,\mathrm{ii}} \alpha_{2,\mathrm{ii}} N_2^{\mathrm{II}}, \tag{7.26}$$

$$\sum \nu_{\text{solvent/homo-multimer}} N_{\text{homo-multimers}}^{\mathrm{II}} = \sum_{j=2}^{2} \sum_{Z=\mathrm{ii}} \nu_{1j,Z} \alpha_{j,Z} N_j^{\mathrm{II}}$$

$$\Rightarrow \sum \nu_{\text{solvent/homo-multimer}} N_{\text{homo-multimers}}^{\mathrm{II}} = \nu_{12,\mathrm{ii}} \alpha_{2,\mathrm{ii}} N_2^{\mathrm{II}}, \tag{7.27}$$

$$\sum N_{\text{monomers}}^{\mathrm{II}} = \sum_{j=2}^{2} \left(1 - \sum_{Z=\mathrm{ii}} \nu_{jj,Z} \alpha_{j,Z}\right) N_j^{\mathrm{II}} = \left(1 - \nu_{22,\mathrm{ii}} \alpha_{2,\mathrm{ii}}\right) N_2^{\mathrm{II}}, \tag{7.28}$$

$$\sum \nu N_{\text{monomers}}^{\mathrm{II}} = \sum_{\substack{i=1 \\ i\neq 2}}^{3} \sum_{j=2}^{2} \nu_{ij} \left(1 - \sum_{Z=\mathrm{ii}} \nu_{jj,Z} \alpha_{j,Z}\right) N_j^{\mathrm{II}}$$

$$\Rightarrow \sum \nu N_{\text{monomers}}^{\mathrm{II}} = \nu_{12} \left(1 - \nu_{22,\mathrm{ii}} \alpha_{2,\mathrm{ii}}\right) N_2^{\mathrm{II}} + \nu_{32} \left(1 - \nu_{22,\mathrm{ii}} \alpha_{2,\mathrm{ii}}\right) N_2^{\mathrm{II}}, \tag{7.29}$$

and

$$\sum \nu_{\text{solvent/monomer}} N_{\text{monomers}}^{\mathrm{II}} = \sum_{j=2}^{2} \nu_{1j} \left(1 - \sum_{Z=\mathrm{ii}} \nu_{jj,Z} \alpha_{j,Z}\right) N_j^{\mathrm{II}}$$

$$\Rightarrow \sum \nu_{\text{solvent/monomer}} N_{\text{monomers}}^{\mathrm{II}} = \nu_{12} \left(1 - \nu_{22,\mathrm{ii}} \alpha_{2,\mathrm{ii}}\right) N_2^{\mathrm{II}}. \tag{7.30}$$

Substituting Eqns. 7.25 - 7.30 into Eqn. 7.23 and reducing yields

$$x_1^{\mathrm{II}} = \frac{N_1^{\mathrm{II}} - \left(\nu_{12,\mathrm{ii}} \alpha_{2,\mathrm{ii}} + \nu_{12}\left(1 - \nu_{22,\mathrm{ii}} \alpha_{2,\mathrm{ii}}\right)\right) N_2^{\mathrm{II}}}{N_1^{\mathrm{II}} + N_3^{\mathrm{II}} + \left(\alpha_{2,\mathrm{ii}} + \left(1 - \nu_{22,\mathrm{ii}} \alpha_{2,\mathrm{ii}}\right) - \left(\nu_{12,\mathrm{ii}} + \nu_{32,\mathrm{ii}}\right) \alpha_{2,\mathrm{ii}} - \left(\nu_{12} + \nu_{32}\right)\left(1 - \nu_{22,\mathrm{ii}} \alpha_{2,\mathrm{ii}}\right)\right) N_2^{\mathrm{II}}}. \tag{7.31}$$

For this case, $p=1$ and $l_{\text{homo-multimer}}=1$, thus there are a total of 6 parameters (solved using Eqn. 7.15) required in order to predict the osmotic pressure for this solution: 2 hydration ($\nu_{12}$ and $\nu_{12,\text{ii}}$), 2 ion binding ($\nu_{32}$ and $\nu_{32,\text{ii}}$), 1 protein-protein interaction ($\nu_{22,\text{ii}}$), and 1 fractional amount of protein ($\alpha_{2,\text{ii}}$).

7.5.2. Case 2: Single Protein Forming a Homo-Trimer

Given a solution with a single protein ($p=1,\ n=3$), $A$, that only forms homo-trimers, the free-solvent model mole fractions (Eqns. 7.13 and 7.14) can be solved in a similar manner to that of Case 1. After substitution and reduction, the mole fractions of the free-solvent are

$$x_1^{\text{II}}=\frac{N_1^{\text{II}}-\left(\nu_{12,\text{iii}}\alpha_{2,\text{iii}}+\nu_{12}\left(1-\nu_{22,\text{iii}}\alpha_{2,\text{iii}}\right)\right)N_2^{\text{II}}}{N_1^{\text{II}}+N_3^{\text{II}}+\left(\alpha_{2,\text{iii}}+\left(1-\nu_{22,\text{iii}}\alpha_{2,\text{iii}}\right)-\left(\nu_{12,\text{iii}}+\nu_{32,\text{iii}}\right)\alpha_{2,\text{iii}}-\left(\nu_{12}+\nu_{32}\right)\left(1-\nu_{22,\text{iii}}\alpha_{2,\text{iii}}\right)\right)N_2^{\text{II}}}, \tag{7.32}$$

and

$$x_1^{\text{I}}=\frac{N_1^{\text{I}}}{N_1^{\text{I}}+N_3^{\text{I}}}. \tag{7.33}$$

Identical to the free-solvent model solution for the homo-dimer case, $p=1$ and $l_{\text{homo-multimer}}=1$, thus there are a total of 6 parameters with 2 hydration ($\nu_{12}$ and $\nu_{12,\text{iii}}$), 2 ion binding ($\nu_{32}$ and $\nu_{32,\text{iii}}$), 1 protein-protein interaction ($\nu_{22,\text{iii}}$), and 1 fractional amount of protein ($\alpha_{2,\text{iii}}$).

7.5.3. Case 3: Single Protein Forming a Homo-Dimer and Homo-Trimer

For a solution containing a single protein ($p=1,\ n=3$), $A$, that form a homo-dimer and a homo-trimer, the free-solvent model mole fractions (Eqns. 7.13 and 7.14) are

$$x_1^{\mathrm{II}} = \frac{N_1^{\mathrm{II}} - \left(\nu_{12,\mathrm{ii}}\alpha_{2,\mathrm{ii}} + \nu_{12,\mathrm{iii}}\alpha_{2,\mathrm{iii}} + \nu_{12}\left(1 - \nu_{22,\mathrm{ii}}\alpha_{2,\mathrm{i}} - \nu_{22,\mathrm{iii}}\alpha_{2,\mathrm{iii}}\right)\right)N_2^{\mathrm{II}}}{\left[N_1^{\mathrm{II}} + N_3^{\mathrm{II}} + N_2^{\mathrm{II}}\begin{pmatrix}\alpha_{2,\mathrm{ii}} + \alpha_{2,\mathrm{iii}} + \left(1 - \nu_{22,\mathrm{ii}}\alpha_{2,\mathrm{ii}} - \nu_{22,\mathrm{iii}}\alpha_{2,\mathrm{iii}}\right) - \left(\nu_{12,\mathrm{ii}} + \nu_{32,\mathrm{ii}}\right)\alpha_{2,\mathrm{ii}} + \ldots \\ \ldots - \left(\nu_{12,\mathrm{iii}} + \nu_{32,\mathrm{iii}}\right)\alpha_{2,\mathrm{iii}} - \left(\nu_{12} + \nu_{32}\right)\left(1 - \nu_{22,\mathrm{ii}}\alpha_{2,\mathrm{ii}} - \nu_{22,\mathrm{iii}}\alpha_{2,\mathrm{iii}}\right)\end{pmatrix}\right]}, \quad (7.34)$$

and

$$x_1^{\mathrm{I}} = \frac{N_1^{\mathrm{I}}}{N_1^{\mathrm{I}} + N_3^{\mathrm{I}}}. \quad (7.35)$$

Here, $p = 1$ and $l_{\text{homo-multimer}} = 2$, giving a total of 10 parameters where 3 are hydration ($\nu_{12}$, $\nu_{12,\mathrm{ii}}$, and $\nu_{12,\mathrm{iii}}$), 3 are ion binding ($\nu_{32}$, $\nu_{32,\mathrm{ii}}$, and $\nu_{32,\mathrm{iii}}$), 2 are protein-protein interactions ($\nu_{22,\mathrm{ii}}$ and $\nu_{22,\mathrm{iii}}$), and 2 are fractional amounts of protein ($\alpha_{2,\mathrm{ii}}$ and $\alpha_{2,\mathrm{iii}}$).

7.5.4. Case 4: Two Proteins Forming a Hetero-Dimer

For a solution containing two proteins ($p = 2$, $n = 4$), $A$ and $B$, that form a hetero-dimer, $AB$, the free-solvent mole fractions (Eqns. 7.13 and 7.14) are

$$x_1^{\mathrm{II}} = \frac{N_1^{\mathrm{II}} - \sum \nu_{\text{solvent / hetero-multimer}} N_{\text{hetero-multimers}}^{\mathrm{II}} - \sum \nu_{\text{solvent / monomer}} N_{\text{monomers}}^{\mathrm{II}}}{\sum_{\substack{i=1 \\ i \neq 2 \rightarrow p+1}}^{n} N_i^{\mathrm{II}} + \sum N_{\text{hetero-multimers}}^{\mathrm{II}} + \sum N_{\text{monomers}}^{\mathrm{II}} - \sum \nu N_{\text{hetero-multimers}}^{\mathrm{II}} - \sum \nu N_{\text{monomers}}^{\mathrm{II}}} \quad (7.36)$$

and

$$x_1^{\mathrm{I}} = \frac{N_1^{\mathrm{I}}}{\sum_{\substack{i=1 \\ i \neq 2 \rightarrow 3}}^{4} N_i^{\mathrm{I}}} = \frac{N_1^{\mathrm{I}}}{N_1^{\mathrm{I}} + N_4^{\mathrm{I}}}. \quad (7.37)$$

The terms in Eqn. 7.36 are

$$\sum N_{\text{hetero-multimers}}^{\mathrm{II}} = \sum_{j=2}^{2} \sum_{a=j+1}^{3} \sum_{A=\mathrm{i}} \sum_{B=\mathrm{i}} \beta_{ja,A:B} N_j^{\mathrm{II}}$$

$$\Rightarrow \sum N_{\text{hetero-multimers}}^{\mathrm{II}} = \beta_{23,\mathrm{i:i}} N_2^{\mathrm{II}}, \quad (7.38)$$

$$\sum \nu N_{\text{hetero-multimers}}^{\mathrm{II}} = \sum_{\substack{i=1 \\ i \neq 2 \rightarrow 3}}^{4} \sum_{j=2}^{2} \sum_{a=j+1}^{3} \sum_{A=\mathrm{i}} \sum_{B=\mathrm{i}} \nu_{ija,A:B} \beta_{ja,A:B} N_j^{\mathrm{II}}$$

$$\Rightarrow \sum \nu N^{\mathrm{II}}_{\text{hetero-multimers}} = \nu_{123,\mathrm{i:i}}\beta_{23,\mathrm{i:i}}N_2^{\mathrm{II}} + \nu_{423,\mathrm{i:i}}\beta_{23,\mathrm{i:i}}N_2^{\mathrm{II}}, \tag{7.39}$$

$$\sum \nu_{\text{solvent/hetero-multimer}} N^{\mathrm{II}}_{\text{hetero-multimers}} = \sum_{j=2}^{2}\sum_{a=j+1}^{3}\sum_{A=\mathrm{i}}\sum_{B=\mathrm{i}}\nu_{1ja,A:B}\beta_{ja,A:B}N_j^{\mathrm{II}}$$

$$\Rightarrow \sum \nu_{\text{solvent/hetero-multimer}} N^{\mathrm{II}}_{\text{hetero-multimers}} = \nu_{123,\mathrm{i:i}}\beta_{23,\mathrm{i:i}}N_2^{\mathrm{II}}, \tag{7.40}$$

$$\sum N^{\mathrm{II}}_{\text{monomers}} = \sum_{j=2}^{3}\left(1 - \sum_{\substack{a=2\\a\neq j}}^{3}\sum_{A=\mathrm{i}}\sum_{B=\mathrm{i}}\nu_{ja,A:B}\beta_{ja,A:B}\right)N_j^{\mathrm{II}}$$

$$\Rightarrow \sum N^{\mathrm{II}}_{\text{monomers}} = \left(1-\nu_{23,\mathrm{i:i}}\beta_{23,\mathrm{i:i}}\right)N_2^{\mathrm{II}} + \left(1-\nu_{32,\mathrm{i:i}}\beta_{32,\mathrm{i:i}}\right)N_3^{\mathrm{II}} \tag{7.41}$$

$$\sum \nu N^{\mathrm{II}}_{\text{monomers}} = \sum_{\substack{i=1\\i\neq 2\rightarrow 3}}^{4}\sum_{j=2}^{3}\nu_{ij}\left(1 - \sum_{\substack{a=2\\a\neq j}}^{3}\sum_{A=\mathrm{i}}\sum_{B=\mathrm{i}}\nu_{ja,A:B}\beta_{ja,A:B}\right)N_j^{\mathrm{II}}$$

$$\Rightarrow \sum \nu N^{\mathrm{II}}_{\text{monomers}} = \left(\nu_{12}+\nu_{42}\right)\left(1-\nu_{23,\mathrm{i:i}}\beta_{23,\mathrm{i:i}}\right)N_2^{\mathrm{II}} + \left(\nu_{13}+\nu_{43}\right)\left(1-\nu_{32,\mathrm{i:i}}\beta_{32,\mathrm{i:i}}\right)N_3^{\mathrm{II}} \tag{7.42}$$

and

$$\sum \nu_{\text{solvent/monomer}} N^{\mathrm{II}}_{\text{monomers}} = \sum_{j=2}^{3}\nu_{1j}\left(1 - \sum_{\substack{a=2\\a\neq j}}^{3}\sum_{A=\mathrm{i}}\sum_{B=\mathrm{i}}\nu_{ja,A:B}\beta_{ja,A:B}\right)N_j^{\mathrm{II}}$$

$$\Rightarrow \sum \nu_{\text{solvent/monomer}} N^{\mathrm{II}}_{\text{monomers}} = \nu_{12}\left(1-\nu_{23,\mathrm{i:i}}\beta_{23,\mathrm{i:i}}\right)N_2^{\mathrm{II}} + \nu_{13}\left(1-\nu_{32,\mathrm{i:i}}\beta_{32,\mathrm{i:i}}\right)N_3^{\mathrm{II}}. \tag{7.43}$$

Substituting Eqns. 7.38 - 7.43 into Eqn. 7.36 and reducing yields

$$x_1^{\mathrm{II}} = \frac{N_1^{\mathrm{II}} - \nu_{123,\mathrm{i:i}}\beta_{23,\mathrm{i:i}}N_2^{\mathrm{II}} - \nu_{12}\left(1-\nu_{23,\mathrm{i:i}}\beta_{23,\mathrm{i:i}}\right)N_2^{\mathrm{II}} - \nu_{13}\left(1-\nu_{32,\mathrm{i:i}}\beta_{32,\mathrm{i:i}}\right)N_3^{\mathrm{II}}}{\left[\begin{array}{l} N_1^{\mathrm{II}} + N_4^{\mathrm{II}} + \left(\beta_{23,\mathrm{i:i}} + \left(1-\nu_{23,\mathrm{i:i}}\beta_{23,\mathrm{i:i}}\right)\right)N_2^{\mathrm{II}} + \left(1-\nu_{32,\mathrm{i:i}}\beta_{32,\mathrm{i:i}}\right)N_3^{\mathrm{II}} + \ldots \\ \ldots - \left(\left(\nu_{123,\mathrm{i:i}}+\nu_{423,\mathrm{i:i}}\right)\beta_{23,\mathrm{i:i}} + \left(\nu_{12}+\nu_{42}\right)\left(1-\nu_{23,\mathrm{i:i}}\beta_{23,\mathrm{i:i}}\right)\right)N_2^{\mathrm{II}} + .. \\ \ldots - \left(\nu_{13}+\nu_{43}\right)\left(1-\nu_{32,\mathrm{i:i}}\beta_{32,\mathrm{i:i}}\right)N_3^{\mathrm{II}} \end{array}\right]}. \tag{7.44}$$

Here, $p = 2$, $l_{\text{hetero-multimer}} = 1$, $l_{\text{hetero-multimer,2}} = 1$, and $\eta_2 = 2$, thus there are a total of 10 parameters (Eqn. 7.15) where 3 are hydration ($\nu_{12}$, $\nu_{13}$, and $\nu_{123,\mathrm{i:i}}$), 3 are ion binding ($\nu_{42}$, $\nu_{43}$, and $\nu_{423,\mathrm{i:i}}$), 2 are protein-protein interactions ($\nu_{23,\mathrm{i:i}}$ and $\nu_{32,\mathrm{i:i}}$), and 2 are fractional amounts of protein ($\beta_{23,\mathrm{i:i}}$ and $\beta_{32,\mathrm{i:i}}$).

7.5.5. Case 5: Three Proteins Forming a Hetero-Trimer

For a solution containing three proteins ( $p=3$, $n=5$ ), $A$, $B$, and $C$, that form a hetero-trimer, $ABC$, the free-solvent mole fractions (Eqns. 7.13 and 7.14) can be solved in a manner similar to that of Case 4. The free-solvent mole fractions, after substitution and reduction, are

$$x_1^{\mathrm{II}} = \frac{\begin{bmatrix} N_1^{\mathrm{II}} - \nu_{1234,\mathrm{i:i:i}}\beta_{234,\mathrm{i:i:i}}N_2^{\mathrm{II}} - \nu_{12}\left(1-\nu_{234,\mathrm{i:i:i}}\beta_{234,\mathrm{i:i:i}}\right)N_2^{\mathrm{II}} + \ldots \\ \ldots - \nu_{13}\left(1-\nu_{324,\mathrm{i:i:i}}\beta_{324,\mathrm{i:i:i}}\right)N_3^{\mathrm{II}} - \nu_{14}\left(1-\nu_{423,\mathrm{i:i:i}}\beta_{423,\mathrm{i:i:i}}\right)N_4^{\mathrm{II}} \end{bmatrix}}{\begin{bmatrix} N_1^{\mathrm{II}} + N_5^{\mathrm{II}} + \left(\beta_{234,\mathrm{i:i:i}} + \left(1-\nu_{234,\mathrm{i:i:i}}\beta_{234,\mathrm{i:i:i}}\right)\right)N_2^{\mathrm{II}} + \left(1-\nu_{324,\mathrm{i:i:i}}\beta_{324,\mathrm{i:i:i}}\right)N_3^{\mathrm{II}} + \ldots \\ + \ldots\left(1-\nu_{423,\mathrm{i:i:i}}\beta_{423,\mathrm{i:i:i}}\right)N_4^{\mathrm{II}} + \ldots \\ \ldots - \left(\left(\nu_{1234,\mathrm{i:i:i}} + \nu_{5234,\mathrm{i:i:i}}\right)\beta_{234,\mathrm{i:i}} + \left(\nu_{12}+\nu_{52}\right)\left(1-\nu_{234,\mathrm{i:i:i}}\beta_{234,\mathrm{i:i:i}}\right)\right)N_2^{\mathrm{II}} + \ldots \\ \ldots - \left(\nu_{13}+\nu_{53}\right)\left(1-\nu_{324,\mathrm{i:i:i}}\beta_{324,\mathrm{i:i:i}}\right)N_3^{\mathrm{II}} - \left(\nu_{14}+\nu_{54}\right)\left(1-\nu_{423,\mathrm{i:i:i}}\beta_{423,\mathrm{i:i:i}}\right)N_4^{\mathrm{II}} \end{bmatrix}}, \qquad (7.46)$$

and

$$x_1^{\mathrm{I}} = \frac{N_1^{\mathrm{I}}}{\sum_{\substack{i=1 \\ i\neq 2\rightarrow 4}}^{5} N_i^{\mathrm{I}}} = \frac{N_1^{\mathrm{I}}}{N_1^{\mathrm{I}} + N_5^{\mathrm{I}}}, \qquad (7.45)$$

where $p=3$, $l_{\text{hetero-multimer}}=1$, $l_{\text{hetero-multimer,3}}=1$, and $\eta_3=3$, which yields a total of 14 parameters: 4 hydration ( $\nu_{12}$, $\nu_{13}$, $\nu_{14}$, and $\nu_{1234,\mathrm{i:i:i}}$ ), 4 ion binding ( $\nu_{52}$, $\nu_{53}$, $\nu_{54}$, and $\nu_{5243,\mathrm{i:i:i}}$ ), 3 protein-protein interactions ( $\nu_{234,\mathrm{i:i:i}}$, $\nu_{324,\mathrm{i:i:i}}$, and $\nu_{423,\mathrm{i:i:i}}$ ), and 3 fractional amounts of protein ( $\beta_{234,\mathrm{i:i:i}}$, $\beta_{324,\mathrm{i:i:i}}$, and $\beta_{423,\mathrm{i:i:i}}$ ).

7.5.6. Case 6: Two Proteins Forming a Hetero-Dimer of Homo-Dimers

For a solution containing two proteins ( $p=2$, $n=4$ ), $A$ and $B$, that form a hetero-dimer, $AABB$, of homo-dimers, $AA$ and $BB$, the free-solvent mole fractions (Eqns. 7.13 and 7.14), after substitution and reduction, are

$$x_1^{\mathrm{II}} = \frac{N_1^{\mathrm{II}} - \nu_{123,\mathrm{ii:ii}}\beta_{23,\mathrm{ii:ii}}N_2^{\mathrm{II}} - \nu_{12}\left(1-\nu_{23,\mathrm{ii:ii}}\beta_{23,\mathrm{ii:ii}}\right)N_2^{\mathrm{II}} - \nu_{13}\left(1-\nu_{32,\mathrm{ii:ii}}\beta_{32,\mathrm{ii:ii}}\right)N_3^{\mathrm{II}}}{\left[\begin{array}{l} N_1^{\mathrm{II}} + N_4^{\mathrm{II}} + \left(\beta_{23,\mathrm{ii:ii}} + \left(1-\nu_{23,\mathrm{ii:ii}}\beta_{23,\mathrm{ii:ii}}\right)\right)N_2^{\mathrm{II}} + \left(1-\nu_{32,\mathrm{ii:ii}}\beta_{32,\mathrm{ii:ii}}\right)N_3^{\mathrm{II}} + \ldots \\ \ldots - \left(\left(\nu_{123,\mathrm{ii:ii}} + \nu_{423,\mathrm{ii:ii}}\right)\beta_{23,\mathrm{ii:ii}} + \left(\nu_{12}+\nu_{42}\right)\left(1-\nu_{23,\mathrm{ii:ii}}\beta_{23,\mathrm{ii:ii}}\right)\right)N_2^{\mathrm{II}} + \ldots \\ \ldots - \left(\nu_{13}+\nu_{43}\right)\left(1-\nu_{32,\mathrm{ii:ii}}\beta_{32,\mathrm{ii:ii}}\right)N_3^{\mathrm{II}} \end{array}\right]}, \tag{7.47}$$

and

$$x_1^{\mathrm{I}} = \frac{N_1^{\mathrm{I}}}{N_1^{\mathrm{I}} + N_4^{\mathrm{I}}}. \tag{7.48}$$

Here, $p = 2$, $l_{\text{hetero-multimer}} = 1$, $l_{\text{hetero-multimer,2}} = 1$, and $\eta_2 = 2$, thus, there is a total of 10 parameters: 3 hydration ($\nu_{12}$, $\nu_{13}$, and $\nu_{123,\mathrm{ii:ii}}$), 3 ion binding ($\nu_{42}$, $\nu_{43}$, and $\nu_{423,\mathrm{ii:ii}}$), 2 protein-protein interactions ($\nu_{23,\mathrm{ii:ii}}$ and $\nu_{32,\mathrm{ii:ii}}$), and 2 fractional amounts of protein parameters ($\beta_{23,\mathrm{ii:ii}}$ and $\beta_{32,\mathrm{ii:ii}}$).

### 7.5.7. Case 7: Two Proteins Forming a Hetero-Dimer of a Homo-Dimer and Monomer

For a solution containing two proteins ($p = 2$, $n = 4$), $A$ and $B$, that form a hetero-dimer, $AAB$, of a homo-dimer, $AA$, and a monomer, $B$, the free-solvent mole fractions (Eqns. 7.13 and 7.14), after substitution and reduction, are

$$x_1^{\mathrm{II}} = \frac{N_1^{\mathrm{II}} - \nu_{123,\mathrm{ii:i}}\beta_{23,\mathrm{ii:i}}N_2^{\mathrm{II}} - \nu_{12}\left(1-\nu_{23,\mathrm{ii:i}}\beta_{23,\mathrm{ii:i}}\right)N_2^{\mathrm{II}} - \nu_{13}\left(1-\nu_{32,\mathrm{i:ii}}\beta_{32,\mathrm{i:ii}}\right)N_3^{\mathrm{II}}}{\left[\begin{array}{l} N_1^{\mathrm{II}} + N_4^{\mathrm{II}} + \left(\beta_{23,\mathrm{ii:i}} + \left(1-\nu_{23,\mathrm{ii:i}}\beta_{23,\mathrm{ii:i}}\right)\right)N_2^{\mathrm{II}} + \left(1-\nu_{32,\mathrm{i:ii}}\beta_{32,\mathrm{i:ii}}\right)N_3^{\mathrm{II}} + \ldots \\ \ldots - \left(\left(\nu_{123,\mathrm{ii:i}} + \nu_{423,\mathrm{ii:i}}\right)\beta_{23,\mathrm{ii:i}} + \left(\nu_{12}+\nu_{42}\right)\left(1-\nu_{23,\mathrm{ii:i}}\beta_{23,\mathrm{ii:i}}\right)\right)N_2^{\mathrm{II}} + \ldots \\ \ldots - \left(\nu_{13}+\nu_{43}\right)\left(1-\nu_{32,\mathrm{i:ii}}\beta_{32,\mathrm{i:ii}}\right)N_3^{\mathrm{II}} \end{array}\right]}, \tag{7.49}$$

and

$$x_1^{\mathrm{I}} = \frac{N_1^{\mathrm{I}}}{N_1^{\mathrm{I}} + N_4^{\mathrm{I}}}. \tag{7.50}$$

There is a total of 10 parameters ($p = 2$, $l_{\text{hetero-multimer}} = 1$, $l_{\text{hetero-multimer,2}} = 1$, and $\eta_2 = 2$): 3 hydration ($\nu_{12}$, $\nu_{13}$, and $\nu_{123,\mathrm{ii:i}}$), 3 ion binding ($\nu_{42}$, $\nu_{43}$, and $\nu_{423,\mathrm{ii:i}}$), 2 protein-

protein interactions ($\nu_{23,ii:i}$ and $\nu_{32,i:ii}$), and 2 fractional amounts of protein parameters ($\beta_{23,ii:i}$ and $\beta_{32,i:ii}$).

7.5.8. Case 8: Three Proteins Forming a Hetero-Trimer and Two Hetero-Dimers

For a solution containing three proteins ($p=3$, $n=5$), $A$, $B$, and $C$, that form a hetero-trimer, $ABC$, and two hetero-dimers, $AB$ and $AC$, the free-solvent mole fractions (Eqns. 7.13 and 7.14) are

$$x_1^{\mathrm{II}} = \frac{\begin{bmatrix} N_1^{\mathrm{II}} - \left(\nu_{123,i:i}\beta_{23,i:i} + \nu_{124,i:i}\beta_{24,i:i} + \nu_{1234,i:i:i}\beta_{234,i:i:i}\right)N_2^{\mathrm{II}} + \ldots \\ \ldots - \nu_{12}\left(1 - \nu_{23,i:i}\beta_{23,i:i} - \nu_{24,i:i}\beta_{24,i:i} - \nu_{234,i:i:i}\beta_{234,i:i:i}\right)N_2^{\mathrm{II}} + \ldots \\ \ldots - \nu_{13}\left(1 - \nu_{32,i:i}\beta_{32,i:i} - \nu_{324,i:i:i}\beta_{324,i:i:i}\right)N_3^{\mathrm{II}} - \nu_{14}\left(1 - \nu_{42,i:i}\beta_{42,i:i} - \nu_{423,i:i:i}\beta_{423,i:i:i}\right)N_4^{\mathrm{II}} \end{bmatrix}}{\begin{bmatrix} N_1^{\mathrm{II}} + N_5^{\mathrm{II}} + \left(\beta_{23,i:i} + \beta_{24,i:i} + \beta_{234,i:i:i} + \left(1 - \nu_{23,i:i}\beta_{23,i:i} - \nu_{24,i:i}\beta_{24,i:i} - \nu_{234,i:i:i}\beta_{234,i:i:i}\right)\right)N_2^{\mathrm{II}} + \ldots \\ \ldots + \left(1 - \nu_{32,i:i}\beta_{32,i:i} - \nu_{324,i:i:i}\beta_{324,i:i:i}\right)N_3^{\mathrm{II}} + \left(1 - \nu_{42,i:i}\beta_{42,i:i} - \nu_{423,i:i:i}\beta_{423,i:i:i}\right)N_4^{\mathrm{II}} + \ldots \\ \ldots - \left(\left(\nu_{123,i:i} + \nu_{423,i:i}\right)\beta_{23,i:i} + \left(\nu_{12} + \nu_{52}\right)\left(1 - \nu_{23,i:i}\beta_{23,i:i} - \nu_{24,i:i}\beta_{24,i:i} - \nu_{234,i:i:i}\beta_{234,i:i:i}\right)\right)N_2^{\mathrm{II}} + \ldots \\ \ldots - \left(\nu_{13} + \nu_{53}\right)\left(1 - \nu_{32,i:i}\beta_{32,i:i} - \nu_{324,i:i:i}\beta_{324,i:i:i}\right)N_3^{\mathrm{II}} + \ldots \\ \ldots - \left(\nu_{13} + \nu_{53}\right)\left(1 - \nu_{42,i:i}\beta_{42,i:i} - \nu_{423,i:i:i}\beta_{423,i:i:i}\right)N_4^{\mathrm{II}} \end{bmatrix}}, \quad (7.51)$$

and

$$x_1^{\mathrm{I}} = \frac{N_1^{\mathrm{I}}}{N_1^{\mathrm{I}} + N_5^{\mathrm{I}}}. \quad (7.52)$$

where $p=3$, $l_{\text{hetero-multimer}}=3$ ($l_{\text{hetero-multimer},2}=2$ and $l_{\text{hetero-multimer},3}=1$), $\eta_2=2$, and $\eta_3=3$, which yields a total of 26 parameters: 6 hydration ($\nu_{12}$, $\nu_{13}$, $\nu_{14}$, $\nu_{1234,i:i:i}$, $\nu_{123,i:i}$, and $\nu_{124,i:i}$), 6 ion binding ($\nu_{52}$, $\nu_{53}$, $\nu_{54}$, $\nu_{5234,i:i:i}$, $\nu_{523,i:i}$, and $\nu_{524,i:i}$), 7 protein-protein interactions ($\nu_{234,i:i:i}$, $\nu_{324,i:i:i}$, $\nu_{423,i:i:i}$, $\nu_{23,i:i}$, $\nu_{24,i:i}$, $\nu_{32,i:i}$, and $\nu_{42,i:i}$), and 7 fractional amounts of protein ($\beta_{234,i:i:i}$, $\beta_{324,i:i:i}$, $\beta_{423,i:i:i}$, $\beta_{23,i:i}$, $\beta_{24,i:i}$, $\beta_{32,i:i}$, and $\beta_{42,i:i}$).

## 7.6. Understanding the Effects of the Free-Solvent Model Physical Parameters on the Osmotic Pressure of Crowded Protein Solutions

### 7.6.1. The Free-Solvent Model for a Single Protein Solution With a Homo-Dimer

The free-solvent model for a single protein solution, and a monovalent salt, in which a homo-dimer forms (Eqns. 7.24 and 7.31 substituted into Eqn. 7.1) is plotted for various homo-dimer SASA and the corresponding homo-dimer hydration value (Figure 7.1), various dimer-ion binding values (Figure 7.2), and various dimerization fractions (Figure 7.3). For all three cases, $\nu_{22,\mathrm{ii}} = 2$ mol Monomer/mol Dimer. The first two cases have a constant molar ratio of 3:1 monomer:homo-dimer (dimerization fractional amount is $\alpha_{2,\mathrm{ii}} = 0.2$).

Figure 7.1 shows the effect changing the SASA, upon homo-dimerization of a protein, has on osmotic pressure. If there is no change to the SASA upon dimerization (*i.e.* the SASA of the dimer, $\mathrm{SASA}_{\mathrm{dimer}}$, is two times the value of the monomer SASA, $\mathrm{SASA}_{\mathrm{monomer}}$, or $\mathrm{SASA}_{\mathrm{dimer}} = 2\left(\mathrm{SASA}_{\mathrm{monomer}}\right)$), and if the ion binding is twice that of the monomer, such as occurs if dimerization has no effect on the net charge, the osmotic pressure is nearly identical to the osmotic pressure of a purely monomer solution. The lack of a SASA change for the dimer is typically observed for weak protein-protein interactions.

If there is a reduction in the SASA of the dimer (*i.e.* $\mathrm{SASA}_{\mathrm{dimer}} < 2\left(\mathrm{SASA}_{\mathrm{monomer}}\right)$), the osmotic pressure of the solution decreases, while if the SASA of the dimer increases (*i.e.* $\mathrm{SASA}_{\mathrm{dimer}} > 2\left(\mathrm{SASA}_{\mathrm{monomer}}\right)$), the osmotic pressure of the solution increases (Figure 7.1). The former case occurs in the majority of strong protein-protein interactions since the solvent is displaced and replaced by electrostatic or van der Waals interactions. The latter case can occur if the protein-protein interaction causes a conformational change in one or more of the proteins.

Figure 7.2 shows the effect changing the ion binding, upon homo-dimerization of a protein, has on osmotic pressure. If the hydration values are keep constant for the dimer (or there is no change to the SASA upon dimerization, $\mathrm{SASA}_{\mathrm{dimer}} = 2(\mathrm{SASA}_{\mathrm{monomer}})$), the loss of ions (reduction in ion binding, $\nu_{\mathrm{dimer\text{-}ion}}$, compared to twice that of the monomer, $\nu_{\mathrm{monomer\text{-}ion}}$, or $\nu_{\mathrm{dimer\text{-}ion}} > 2(\nu_{\mathrm{monomer\text{-}ion}})$) upon dimerization results in an increase in the osmotic pressure, while an increase in the ion binding of the dimer (*i.e.* $\nu_{\mathrm{dimer\text{-}ion}} > 2(\nu_{\mathrm{monomer\text{-}ion}})$) yields a decrease in the osmotic pressure. When a protein-protein interaction occurs, there is typically an effect on the overall electrostatics (possibly affecting the net charge) of the dimer which causes a shift in the amount of ions bound. However this may occur (at the isoelectric point of the protein) if the ion binding value of the homo-dimer is be unaffected (*i.e.* $\nu_{\mathrm{dimer\text{-}ion}} = 2(\nu_{\mathrm{monomer\text{-}ion}})$); therefore, the osmotic pressure is nearly identical to the osmotic pressure of the pure monomer solution.

Figure 7.3 shows the effect increasing the amount of dimers in solution (*i.e.* $\alpha_{2,\mathrm{ii}}$ increases) has on osmotic pressure. The osmotic pressure, as the fractional amounts of dimers increase, reduces the osmotic pressure, assuming that the hydration is the same ($\mathrm{SASA}_{\mathrm{dimer}} > 2(\mathrm{SASA}_{\mathrm{monomer}})$) and the ion binding value is twice that of the monomer ($\nu_{\mathrm{dimer\text{-}ion}} = 2(\nu_{\mathrm{monomer\text{-}ion}})$). This effect is due to the mole fraction of water for homo-multimers being closer to unity compared to the mole fraction of water for the pure monomer solution. As the total protein concentration, in grams per liter solution, increases, the moles of monomer increase more rapidly than the moles of homo-multimers.

### 7.6.2. The Free-Solvent Model for a Binary Protein Solution

#### 7.6.2.1. When Only Monomers are Present

The free-solvent model for a binary protein solution, and a monovalent salt, in which only monomers are present is modeled (Figure 7.4). The free-solvent model for a binary protein solution of pure monomers was developed previously by Yousef *et al*. (Yousef *et al.* 2002a). As the molar ratio of protein A to protein B is changed, the osmotic pressure is affected such that the greater the molar ratio is in favor of protein A (*i.e.* the moles of A is greater than the moles of B, $(A/B)>1$), the osmotic pressure closes in on the osmotic pressure of the protein A monomer solution as $B \to 0$. Conversely, when the moles of protein B are greater than the moles of protein A ($(A/B)<1$), the osmotic pressure closes in on the protein B monomer solution osmotic pressure as $A \to 0$.

#### 7.6.2.2. With the Formation of Hetero-Dimers

The free-solvent model for a binary protein solution in which hetero-dimers occur, given by substituting Eqns. 7.37 and 7.44 into Eqn. 7.1, is modeled (Figure 7.5). As the fractional amount of dimerization, $\beta_{23,\text{i:i}}$, increases, the osmotic pressure decreases when all other parameters are held constant.

## 7.7. Discussion

### 7.7.1. Weak Protein-Protein Interactions

Weak protein-protein interactions are considered to be those for which no (or minimal) solvent is displaced from the proteins' surfaces (negligible loss in the SASA) by the interaction. An example of this is albumin (Atmeh *et al.* 2007; Wang 2008).

For the scenario when weak protein-protein interactions occur, the free-solvent model can be developed with the assumption that only monomers exist in solution (given that $\nu_{\text{dimer-ion}} = 2(\nu_{\text{monomer-ion}})$). While this assumption is not physiologically true, the displacement of no, or minimal, solvent allows for the hydration value of monomers and homo-multimers to be nearly-identical (if considering the units grams of water per gram of protein). This effect on osmotic pressure is shown in Figure 7.1 by comparing the solid curve (which is the pure monomer solution) and the dotted curve (homo-dimer solution with $\text{SASA}_{\text{dimer}} = 2(\text{SASA}_{\text{monomer}})$ and $\nu_{\text{dimer-ion}} = 2(\nu_{\text{monomer-ion}})$).

### 7.7.2. Strong Protein-Protein Interactions

Strong protein-protein interactions are considered as all interactions which displace solvent from the surface of each protein, resulting in a change in the SASA for the multimer (*i.e.* the multimer has a binding interface that does not contain solvent). The binding interface between the proteins forming a multimer can be driven by electrostatic and/or van der Waals interactions.

For any solution in which strong protein-protein interactions occur, the free-solvent model, developed herein, can be used after making the appropriate reduction in terms (similar to the case scenarios presented). Each of these interactions will have unique hydrations, ion binding values, and/or fractional amounts of protein which need to be considered.

### 7.7.3. Robustness and Limitations of the Multi-Component Free-Solvent Model

#### 7.7.3.1. Osmotic Pressure Prediction

Given that the values of hydration and ion binding are available for all proteins in solution, and that the amounts of proteins participating in protein-protein interactions are known,

the free-solvent model can provide excellent predictions of the crowded protein osmotic pressure (Yousef *et al.* 1998a, 1998b, 2001, 2002a, 2002b; McBride and Rodgers 2012).

While a solution with $n$ species and $p$ proteins can be modeled, there is a limit to the predictive power of the free-solvent model; there will be a point at which including additional parameters for more proteins will have a negligible effect on the predicted osmotic pressure due to the sensitivity of each parameter being reduced. This is especially apparent when two or more proteins and/or multimers have similar values of hydration. This effect was modeled by the solid and dotted curves in Figures 7.1 and 7.2.

7.7.3.2. Osmotic Pressure Regression

In addition to being used for osmotic pressure prediction, the free-solvent model has also been shown to provide information about the protein, such as hydration, ion binding, and SASA, when the free-solvent model is used for regression of concentrated osmotic pressure data (Yousef *et al.* 1998a, 1998b, 2001, 2002a, 2002b; McBride and Rodgers 2012). However, with the development of the multi-component free-solvent model which considers protein-protein interactions comes some limitations to the ability of the free-solvent model for regression of the osmotic pressure. The free-solvent model may have reduced success when it is used for regression of multi-component protein solutions due to the large number of parameters; the more parameters which are regressed on may cause the regressed parameters to have a high covariance and thus remove physiological significance from the values of the parameters. However, if the values of most of the physical parameters are known, the regression power of the free-solvent model, on the remaining parameters, will increase and may yield physiologically meaningful values for the regressed parameters.

#### 7.7.3.3. Truncating the Free-Solvent Model

In order to recover some of the robustness of the free-solvent model for predicting the osmotic pressure or for osmotic pressure regression to determine the values of the physical parameters, the free-solvent model may need to be truncated to remove some of the multimers. This should be done with caution; experimentally determining the values of the hydration and/or the fractional amounts of the homo- and/or hetero-multimers can be useful when determining the appropriate terms to remove in order to maintain the robustness of the free-solvent model. Alternatively, a sensitively analysis of the free-solvent model can provide insight into truncating the free-solvent model.

## 7.8. Conclusion

The free-solvent model is an excellent predictor of the osmotic pressure for concentrated single protein solutions. Here, a generalized free-solvent model for multi-component solutions in which protein-protein interactions occur has been developed. This generalized form of the free-solvent model considers both intra-protein species (homo-multimer) and inter-protein species (hetero-multimer) interactions. The model developed herein can be used for insight into crowded solutions for any number of solvent, salt, and protein species in which solute-solvent and solute-solute interactions are present. This model can be further revised to account for additional interaction parameters, such as proton and/or hydroxide interaction to the macromolecules.

Given that the physical parameters are available, experimental data for the osmotic pressure of crowded multi-component protein solutions no longer needs to be obtained because the free-solvent model allows for excellent predictability. This methodology can be extended to even predict the osmotic pressure within a biological system, such as a cell, given that the

hydration values, ion binding values, and the fractional amounts are known for each macromolecule in solution.

**Table 7.1.** The Physical Parameters Used in the Free-Solvent Model for a Single Protein Solution Forming a Homo-Dimer.

| Protein | Molecular Weight, $M_2$ (kDa) | Hydration $\left(\frac{\text{g } H_2O}{\text{g Protein}}\right)$ | Solvent Accessible Surface Area (Å$^2$) | Ion Binding $\left(\frac{\text{mol Salt}}{\text{mol Protein}}\right)$ | Fractional Amount of Homo-Dimer, $\alpha_{2,ii}$ | Protein-Protein Binding, $\nu_{22,ii}$ $\left(\frac{\text{mol Monomer}}{\text{mol Multimer}}\right)$ |
|---|---|---|---|---|---|---|
| Monomer (A) | 66.43 | 1.177 | 28,553 | 8.81 | N/A | N/A |
| Homo-Dimer (AA) | 132.86 | Varied:<br>1.177<br>0.942<br>1.295 | Varied:<br>57,106<br>45,705<br>62,832 | Varied:<br>17.62<br>13.22<br>8.81<br>26.43 | Varied:<br>0.20<br>0.33<br>0.43 | 2 |

**Table 7.2.** The Physical Parameters Used in the Free-Solvent Model for a Binary Protein Solution Forming a Hetero-Dimer.

| Protein | Molecular Weight, $M_2$ (kDa) | Hydration $\left(\frac{\text{g } H_2O}{\text{g Protein}}\right)$ | Solvent Accessible Surface Area (Å$^2$) | Ion Binding $\left(\frac{\text{mol Salt}}{\text{mol Protein}}\right)$ | Molar Ratio (A:B) | Fractional Amount of Hetero-Dimer, $\beta_{23,i:i}$ , $\beta_{32,i:i}$ | Protein-Protein Binding, $\nu_{23,i:i}$ , $\nu_{32,i:i}$ $\left(\frac{\text{mol Monomer}}{\text{mol Multimer}}\right)$ |
|---|---|---|---|---|---|---|---|
| Monomer (A) | 66.43 | 1.177 | 28,553 | 8.81 | Varied:<br>3:1 | N/A | N/A |
| Monomer (B) | 155 | 1.110 | 62,830 | 24.30 | 1:1<br>1:3 | N/A | N/A |
| Hetero-Dimer (AB) | 221.43 | 0.904 | 73,100 | 28.20 | N/A | Varied:<br>0.09<br>0.23<br>0.33<br>0.50 | 1 |

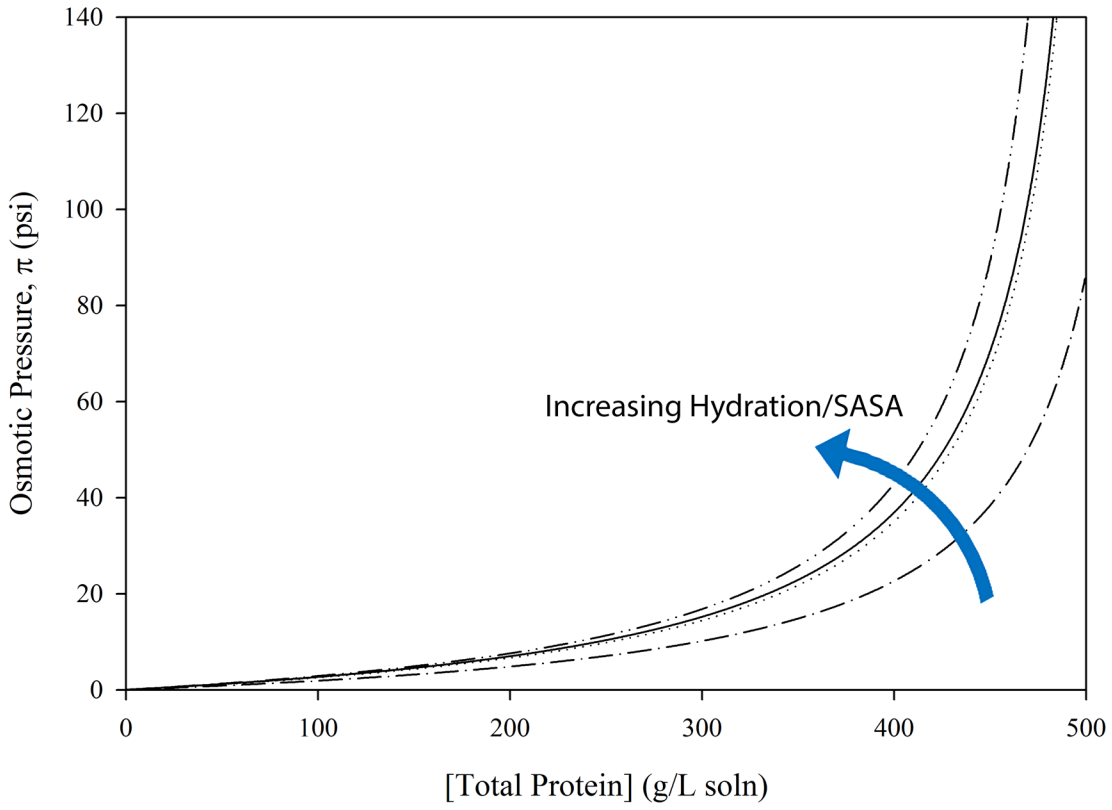


**Figure 7.1.** Osmotic Pressure vs. Concentration for a Theoretical Single Protein Solution in 0.15 M NaCl With the Formation of a Homo-Dimer: The Effect of Changing the Hydration and SASA. The free-solvent model is plotted when only the monomer is present with solute-solvent interaction parameters of $\nu_{12} = 1.177$ g $H_2O$/g protein A and $\nu_{32} = 8.81$ mol NaCl/mol protein A (solid curve). When a homo-dimer occurs and forms at a ratio of 3:1 protein A:dimer AA ($\alpha_{2,ii} = 0.2$ and $\nu_{22,ii} = 2$ mol protein A/mol dimer AA), with the monomer maintaining its hydration and ion binding, the free-solvent model is plotted for changes to the homo-dimer SASA which affects the homo-dimer hydration at a fixed ion binding (where $\nu_{\text{dimer-ion}} = 2(\nu_{\text{monomer-ion}})$ or $\nu_{32,ii} = 17.62$ mol NaCl/mol dimer AA): (1) the homo-dimer has no change to the hydration, $\nu_{12,ii} = 1.177$ g $H_2O$/g dimer AA (dotted curve); (2) the homo-dimer has a SASA that is 80% of 2 times the monomer SASA (thus $\nu_{12,ii} = 0.942$ g $H_2O$/g dimer AA) (dash-dot curve); and (3) the homo-dimer has a SASA that is 10% more than 2 times the monomer SASA (thus $\nu_{1,ii} = 1.295$ g $H_2O$/g dimer AA) (dash-dot-dot curve).

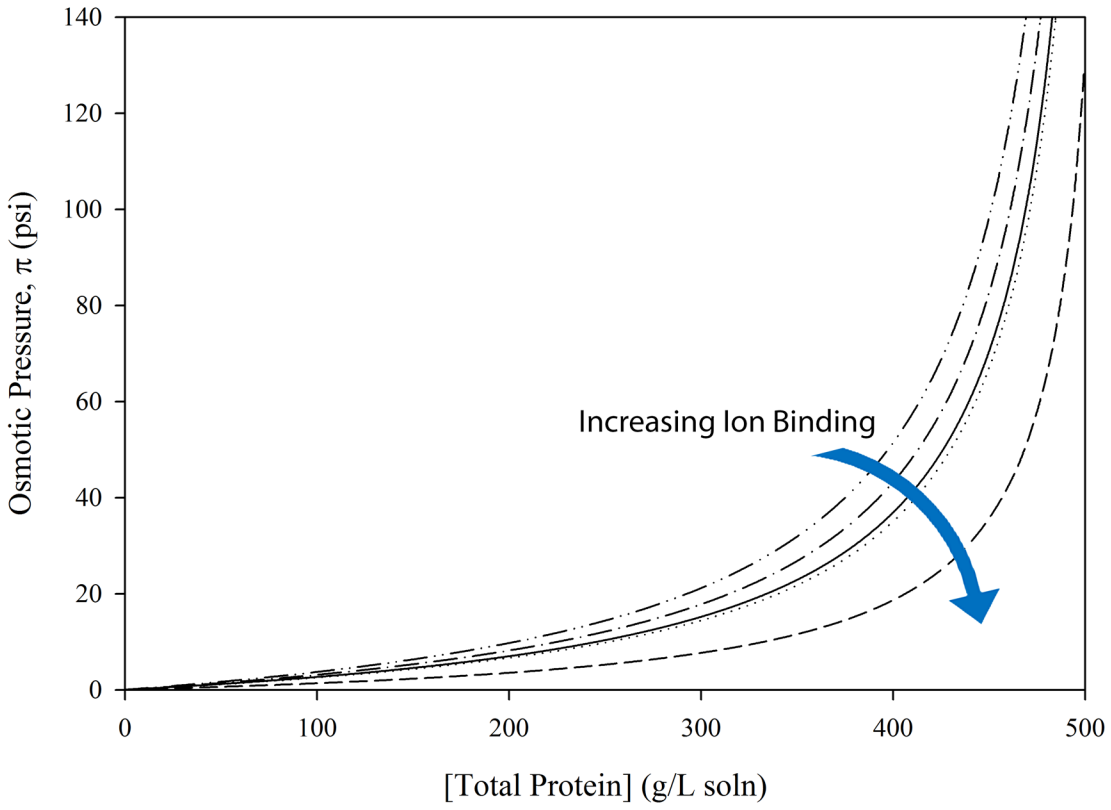


**Figure 7.2.** Osmotic Pressure vs. Concentration for a Theoretical Single Protein Solution in 0.15 M NaCl With the Formation of a Homo-Dimer: The Effect of Changing the Ion Binding. The free-solvent model is plotted when only the monomer is present with solute-solvent interaction parameters of $\nu_{12} = 1.177$ g $H_2O$/g protein A and $\nu_{32} = 8.81$ mol NaCl/mol protein A (solid curve).When a homo-dimer occurs and forms at a ratio of 3:1 protein A:dimer AA ($\alpha_{2,ii} = 0.2$ and $\nu_{22,ii} = 2$ mol protein A/mol dimer AA), with the monomer maintaining its hydration and ion binding, and the homo-dimer having no change to the SASA ($\text{SASA}_{\text{dimer}} = 2(\text{SASA}_{\text{monomer}})$ therefore $\nu_{12,ii} = 1.177$ g $H_2O$/g dimer AA), the free-solvent model is plotted when: (1) the ion binding of the homo-dimer is 2 times that of the monomer, $\nu_{32,ii} = 17.62$ mol NaCl/mol dimer AA (dotted curve); (2) the homo-dimer ion binding value is 1.5 times that of the monomer, $\nu_{32,ii} = 13.22$ mol NaCl/mol dimer AA (dash-dot curve); (3) the homo-dimer ion binding value is the same as the monomer, $\nu_{32,ii} = 8.81$ mol NaCl/mol dimer AA (dash-dot-dot curve); and (4) the ion binding of the homo-dimer is 3 times that of the monomer, $\nu_{32,ii} = 26.43$ mol NaCl/mol dimer AA (dashed curve).

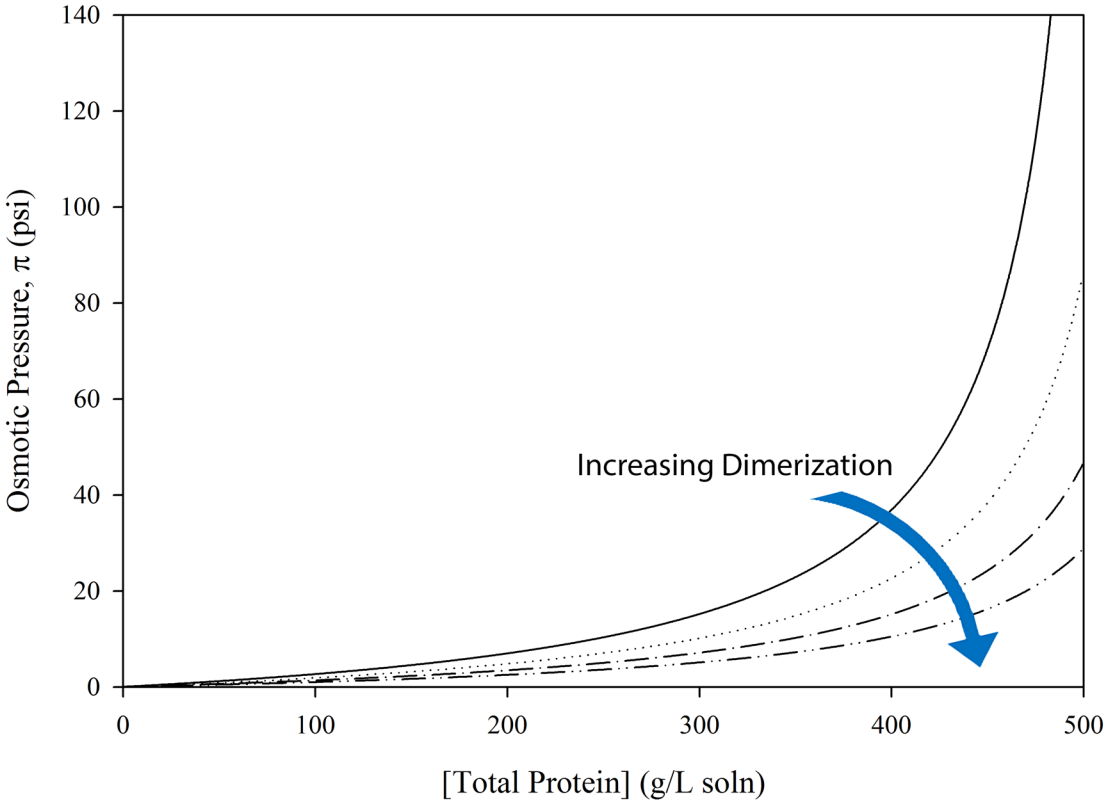


**Figure 7.3.** Osmotic Pressure vs. Concentration for a Theoretical Single Protein Solution in 0.15 M NaCl With the Formation of a Homo-Dimer: The Effect of Increased Dimerization. The free-solvent model is plotted when only the monomer is present with solute-solvent interaction parameters of $\nu_{12} = 1.177$ g $H_2O$/g protein A and $\nu_{32} = 8.81$ mol NaCl/mol protein A (solid curve). The homo-dimers ($\nu_{22,ii} = 2$ mol protein A/mol dimer AA) have solute-solvent interaction parameters of $\nu_{12,ii} = 0.942$ g $H_2O$/g dimer AA and $\nu_{32,ii} = 17.62$ mol NaCl/mol dimer AA in all cases. The free-solvent model is plotted for various fractional amounts of homo-dimerization: (1) 3:1 A:AA, $\alpha_{2,ii} = 0.2$ (dotted curve); (2) 1:1 A:AA, $\alpha_{2,ii} = 0.33$ (dash-dot curve); and (3) 1:3 A:AA, $\alpha_{2,ii} = 0.43$ (dash-dot-dot curve).

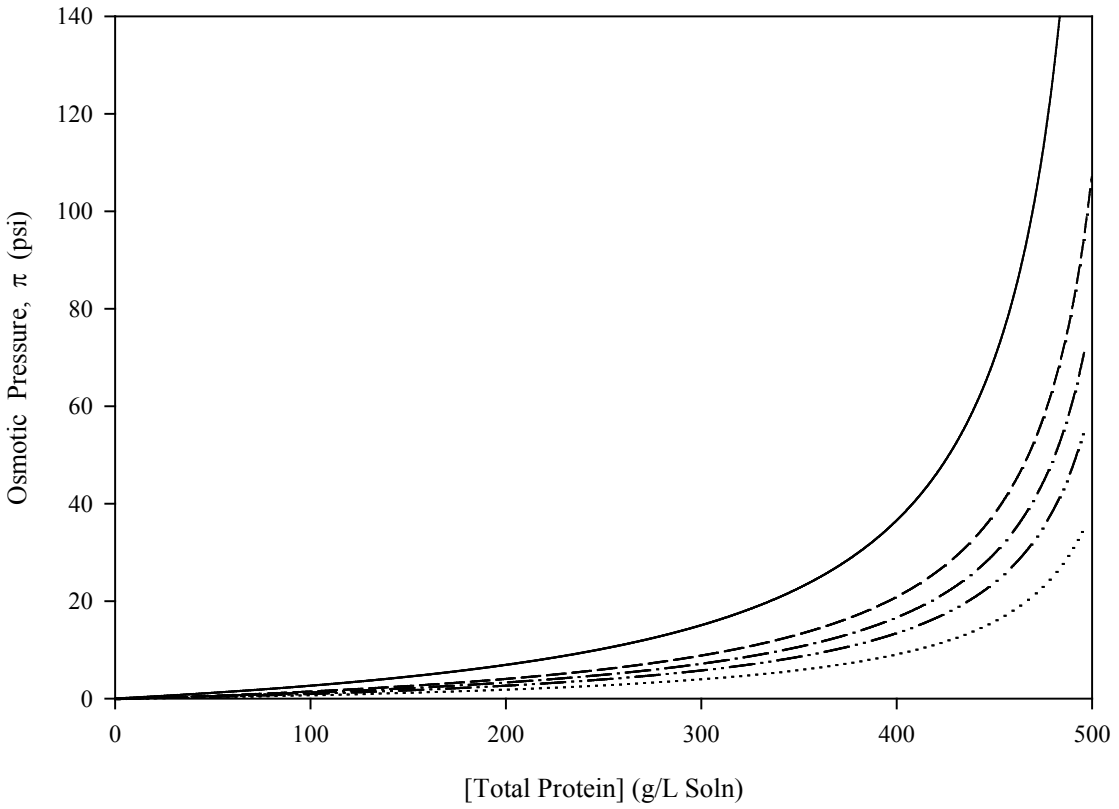


**Figure 7.4.** Osmotic Pressure vs. Concentration for a Theoretical Binary Protein Solution in 0.15 M NaCl: The Effect of Changing the Molar Ratio Between the Two Proteins. The free-solvent model for each single protein solution is plotted: protein A with $\nu_{12} = 1.177$ g $H_2O$/g protein A and $\nu_{32} = 8.81$ mol NaCl/mol protein A (solid curve) and protein B with $\nu_{12} = 1.110$ g $H_2O$/g protein B and $\nu_{32} = 24.30$ mol NaCl/mol protein B (dotted curve). The free-solvent model for various molar ratios between protein A and protein B is plotted: (1) 1:1 A:B (dash-dot curve); (2) 3:1 A:B (dash-dot-dot curve); and (3) 1:3 A:B (dashed curve).

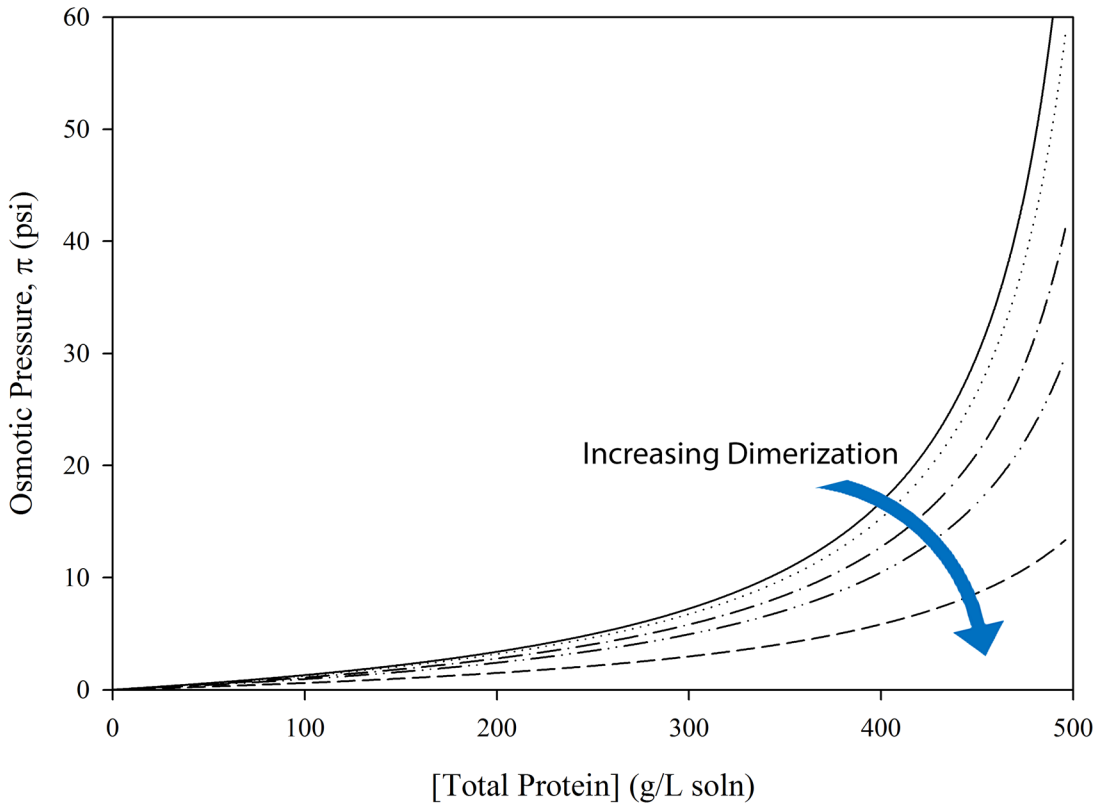


**Figure 7.5.** Osmotic Pressure vs. Concentration for a Theoretical Binary Protein Solution in 0.15 M NaCl With the Formation of a Hetero-Dimer: The Effect of Increased Dimerization. The free-solvent model for a 1:1 A:B binary protein solution is plotted when the solute-solvent parameters are $\nu_{12} = 1.177$ g $H_2O$/g protein A, $\nu_{32} = 8.81$ mol NaCl/mol protein A, $\nu_{12} = 1.110$ g $H_2O$/g protein B, and $\nu_{32} = 24.30$ mol NaCl/mol protein B (solid curve). When a hetero-dimer ($\nu_{23,i:i} = 1$ mol protein A/mol dimer AB and $\nu_{32,i:i} = 1$ mol protein B/mol dimer AB) occurs with solute-solvent parameters of $\nu_{123,i:i} = 0.904$ g $H_2O$/g dimer AB and $\nu_{423,i:i} = 28.02$ mol NaCl/mol dimer AB, the free-solvent model is plotted for various fractional amounts of hetero-dimerization: (1) 10% hetero-dimerization (A:AB = 9:1), $\beta_{23,i:i} = \beta_{32,i:i} = 0.1$ (dotted curve); (2) 30% hetero-dimerization (A:AB = 7:3), $\beta_{23,i:i} = \beta_{32,i:i} = 0.3$ (dash-dot curve); (3) 50% hetero-dimerization (A:AB = 1:1), $\beta_{23,i:i} = \beta_{32,i:i} = 0.5$ (dash-dot-dot curve); and (4) 100% hetero-dimerization (A:AB = 0:1), $\beta_{23,i:i} = \beta_{32,i:i} = 1.0$ (dashed curve).

# CHAPTER 8.

# DEVELOPMENT OF A CONCENTRATING OSMOMETER

## 8.1. Abstract

Here a concentrating osmometer is developed. The concentrating osmometer allows for the solution of interest to become concentrated in order to study the osmotic pressure at various solute concentrations. Herein, the design, development, and practical issues of a concentrating osmometer are described. The concentrating osmometer was tested using bovine serum albumin solutions and compared to the literature osmotic pressure. The concentrating osmometer decreases the amount of protein required for obtaining an entire osmotic pressure-concentration profile by an order of magnitude and it decreases the time for data collection from weeks to days. A few applications for which a concentrating osmometer is useful are obtaining the osmotic pressure-concentration profile, understanding the osmotic pressure of the cell cytosol, and detecting protein mutations.

## 8.2. Introduction

Concentrated osmotic pressure has fascinated scientists for over a hundred years because of the deviation from ideality which occurs as the solute concentration approaches saturation, and many studies have tried to determine the reasons and underlying mechanisms that are the basis of the observed non-idealities.

While studying near-saturation osmotic pressure can be used to understand the solutes and interactions in solution, concentrated osmotic pressure data in the literature is limited primarily because of the sheer quantity of protein required to study the complete the osmotic pressure-concentration profile. With current osmometers, such as those developed by Vilker *et al.*

(Vilker *et al.* 1981) and Yousef *et al.* (Yousef 2000), the volume of the protein solution required to measure a single osmotic pressure is approximately 7 mL. Thus, to obtain the entire osmotic pressure-concentration profile requires tens to hundreds of grams of the protein. Although many proteins are commercially available, by companies such as Sigma-Aldrich, the vast majority of proteins are not commercially available. Furthermore, the proteins which are commercially available can be extremely expensive, and thus it is unreasonable to purchase enough protein in order to get concentrated osmotic pressure data for the majority of proteins.

One way to circumvent the expense of purchasing enough mass of protein is to produce the protein via cell culturing. Yet this method of obtaining tens to hundreds of grams has its limitations, such as the time required to produce tens of grams of the desired protein and protein purification.

Here, we have designed and developed a concentrating osmometer which requires about an order of magnitude less protein. The use of a concentrating osmometer will allow for the study of the osmotic pressure of numerous other proteins and gain valuable information, such as the solvent accessible surface area (McBride and Rodgers 2012). The limitations of the concentrating osmometer are discussed.

## 8.3. Osmotic Pressure Theory

Osmotic pressure has long been used to obtain information about a solute, such as molecular weight, solute-solute interactions (Vilker *et al.* 1981), and solute-solvent interactions (Yousef *et al.* 1998a, 1998b, 2001, 2002a, 2002b). Many models have been developed for relating the osmotic pressure of a solution at a given concentration to physical parameters. For example, the van't Hoff equation is used to determine the molecular weight of the solute.

While many models only require dilute osmotic pressure data, it is the osmotic pressure of near-saturation concentrations which are the most notable due to the deviation from ideality. Various models have been developed to explain the phenomena which cause the observed non-idealities in the osmotic pressure as a function of increasing solute concentration, however, the vast majority of the models require fitted parameters since a variant of the virial expansion, based on the McMillan-Mayer Dilute Solution theory (McMillan and Mayer 1945), is used. One model which does not rely on fitted parameters, and furthermore requires only independently measureable and physically realistic parameters is the free-solvent model (Yousef *et al.* 1998a, 1998b, 2001, 2002a, 2002b).

8.3.1. Free-Solvent Model

The free-solvent model accounts for the hydration and ion binding (when applicable) of the solute. The free-solvent model has been previously examined for single protein solutions (Yousef *et al.* 1998a, 1998b, 2001, 2002b; M$^{c}$Bride and Rodgers 2012), a binary protein solution (Yousef *et al.* 2002a), and a sucrose solution.

Full mathematical development of the free-solvent model is described elsewhere (Yousef *et al.* 1998a, 1998b, 2001, 2002a, 2002b; M$^{c}$Bride and Rodgers 2012). Briefly, for a two chamber osmometer separated by a semi-permeable membrane in which there are $n$ distinct species, $p$ proteins (or other rejected solutes) are fully rejected and confined to chamber II and the remaining species, $(p+2)\rightarrow n$, are freely diffusible, the free-solvent model describes the osmotic pressure, $\pi$, as

$$\pi \approx \frac{RT}{\overline{V}_1}\ln\left(\frac{\left(\sum_{i=1}^{n} N_i^{\mathrm{II}} - \sum_{\substack{i=1,\\ i\neq 2\rightarrow p+1}}^{n}\sum_{j=2}^{p+1}\nu_{ij}N_j^{\mathrm{II}}\right)N_1^{\mathrm{I}}}{\left(N_1^{\mathrm{II}} - \sum_{j=2}^{p+1}\nu_{1j}N_j^{\mathrm{II}}\right)\sum_{\substack{i=1,\\ i\neq 2\rightarrow p+1}}^{n} N_i^{\mathrm{I}}}\right), \tag{8.1}$$

where $N_i^K$ is the number of moles of species $i$ in compartment $K$, and $\nu_{ij}$ is the net number of moles of solvent component $i$ interacting with protein $j$. The compartment containing the protein solution is denoted as superscript II, while the non-protein compartment is denoted as superscript I.

## 8.4. Why Use a Concentrating Osmometer?

Conventional osmometers are limited by the amount of protein which they require (even to measure the osmotic pressure of a single concentration). To study the osmotic pressure of a protein over the entire concentration range up to near-saturation only exacerbates this limitation. Furthermore, to obtain the osmotic pressure-concentration profile is time consuming and can take more than one week depending on the number of data points that are desired.

The concentrating osmometer which has been developed relaxes these limitations. To obtain the osmotic pressure-concentration profile using a conventional osmometer requires gram quantity of the protein (assuming nine data points from 50 - 450 g/L for BSA requires approximately 10 grams assuming a protein load volume of 5 mL (which is consistent for conventional osmometers). For the concentrating osmometer, if the solution begins at 50 g/L, then only 0.5 g of protein are required (assuming 10 mL of protein solution) to obtain the entire profile.

The concentrating osmometer also reduces the time required to obtain the osmotic pressure-concentration profile. This is possible because, for conventional osmometers, the protein solutions need to be made for each concentration desired, whereas for a concentrating osmometer only a single protein sample needs to be prepared. In addition, conventional osmometers need to have the solution removed and the osmometer cleaned between experiments.

8.5. Designing a Concentrating Osmometer

The concentrating osmometer consists of two chambers (a solution chamber and a solvent chamber) separated by a semi-permeable membrane (Figure 8.1). The membrane is supported by a plate containing holes to allow for the diffusible species to transport across the membrane. The solvent chamber that was designed is similar to that of Yousef *et al.* (Yousef 2000) except that the approximate volume is 4.5 mL (rather than 17 mL (Yousef 2000). This reduction in the solvent chamber is possible (*i.e.* able to maintain an infinite sink/source) since the solvent will be continuously feed into the chamber.

The designed protein solution chamber uses a plunger to concentrate the solution. The plunger concentrates the solution by turning into the solution chamber, reducing the internal volume. This motion increases the pressure in the solution chamber forcing solvent through the membrane and retaining the protein, thus increasing the concentration of the protein in the chamber. The protein solution chamber has a maximum volume of 5.2 mL and a minimum volume of 125 μL. This allows the solution of interest to be concentrated by a factor of 4.7; the concentrating factor is a function of the change in plunger tip height (Figure 8.2).

While the above concentrating osmometer design is used to validate the use of a concentrating osmometer, alterations may need be made to the design to: (1) further reduce the minimum and maximum volumes to a create micro- or nano-volume concentrating osmometer, (2) increase the concentrating factor by either increasing the amount of volume removed per turn of the plunger or by increasing the ratio between the maximum and minimum volumes, and (3) alter the device used for concentrating (one such option is to use a syringe rather than a plunger).

## 8.6. Methods

### 8.6.1. Concentrating Osmometer

A Cole Parmer pressure transducer (7356-51 30 psi, Vernon Hills, IL, USA) was used to measure the osmotic pressure. The osmotic pressure readings were recorded from the pressure transducer using a DAQ and the LabVIEW software (National Instruments). The pressure transducer was calibrated using nitrogen gas at known pressures. The calibration of the pressure transducer resulted in an error of less than ± 0.25 psi.

Upon completing the calibration of the pressure transducer, the concentrating osmometer was loaded with an initial BSA solution: either 100 or 200 g/L BSA in 0.15 M NaCl, pH 5.4. The sample was fed into the solution chamber until all of the air was removed (*i.e.* until no air was observed exiting). The concentrating osmometer was rotated as the solution was fed into it to aid in removing any trapped air. The protein chamber was closed and placed in contact with the solvent chamber.

The solvent chamber was filled and all the air was removed. Solvent, 100 mL, was continuously flowed, using a peristaltic pump, through the solvent chamber (with a residence time of approximately 1 minute) providing an infinite sink/source of solvent.

The osmotic pressure was allowed to reach steady state for the initial BSA solution. When the pressure reached steady state, the plunger was turned until the next concentration was achieved. The pressure was allowed to re-equilibrate to the new osmotic pressure. The volume within the solution chamber was calculated from the interior dimensions and the height of the plunger. Vernier calipers were used to measure the height of the plunger, which was subsequently used to calculate the solution volume.

The concentrations studied were 100 - 260 g/L BSA.

8.6.2. Osmotic Pressure of Protein Solutions

The osmotic pressure of BSA (A30075, RPI, Mount Prospect, IL) in 0.15 M NaCl, pH 5.4, 25ºC was measured using the concentrating osmometer. The BSA solution was created by dissolving a known amount of BSA in 0.15 M NaCl. The solution was adjusted to a final pH of 5.4 using either 1 M HCl or 1 M NaOH. The solvent solution was created by dissolving a known amount of NaCl in nanopure water ($DDH_2O$), and the pH was adjusted.

A 30 kDa molecular weight cut-off cellulose ester membrane was used (30 kDa MWCO, regenerated cellulose, NADIR UC030 T, MICRODYN-NADIR, Wiesbaden, Germany) to completely reject BSA while allowing unrestricted flow of the solvent.

The results of the concentrating osmometer osmotic pressure are compared to the available osmotic pressure for BSA in 0.15 M NaCl, pH 5.4 (Vilker *et al.* 1981).

8.7. Results

Two experiments were run for BSA in 0.15 M NaCl, pH 5.4, 25ºC. The first experiment had an initial BSA concentration of 100.99 g/L and the pressure during the experiment is plotted in Figure 8.3. The concentration was increased to 108.17 g/L, 122.71 g/L, 140.68 g/L, 164.81 g/L, and 177.63 g/L during the experiment.

The second experiment had an initial BSA concentration of 199.96 g/L and the pressure during the experiment is plotted in Figure 8.4. The concentration was increased to 207.10 g/L, 216.55 g/L, 229.91 g/L, and 257.09 g/L during the experiment.

## 8.8. Practical Considerations

### 8.8.1. High Pressure

Since a high pressure develops as the plunger is turned to concentrate the solution to a new concentration, the pressure within the concentrating osmometer must be monitored to ensure that the following do not occur: pressure overload for the transducer (*i.e.* that the pressure is within the measureable pressure range for the transducer used) and membrane rupture.

The selection of pressure transducer is critical in order to maximize the accuracy of the osmotic pressure measurements and minimize the time required to complete the osmotic pressure-concentration profile (by allowing a higher pressure drop upon concentration); a pressure transducer with a range to high for a given protein solution will introduce unnecessary error in the measurements, while a pressure transducer with a range too close to that of the protein solution will increase the time of the concentration process since the plunger cannot be turned as much (without risking pressure overload, or worse pressure transducer failure).

The membrane must be selected in order to completely reject the protein species of interest, while maximizing the solvent flux. In addition, the membrane must have a burst pressure much higher than the maximum pressure which the protein solution is going to experience during the concentrating process.

### 8.8.2. Flux Measurements

During the measurement of the osmotic pressure for each concentration, the solution will be concentrated by the removal of solvent via (Kedem and Katchalsky 1958)

$$J = L_p\left(\Delta P - \sigma\Delta\pi\right). \tag{8.2}$$

In Eqn. (8.2), $L_p$ is the membrane permeability, $\Delta P$ is the pressure drop across the membrane, $\Delta\pi$ is the osmotic pressure across the membrane, and $\sigma$ is the reflection coefficient.

In this study, the pressure within the osmometer is measured as the gage pressure, or $\Delta P = P$ and $\Delta\pi = \pi$ (since the solvent solution is solute-free), where $P$ and $\pi$ are the pressure and osmotic pressure within the solution chamber, respectively.

The increase in the pressure within the solution chamber, for the initial protein solution, follows a first order fit, or

$$P = \pi\left(1 - e^{-t/\tau}\right), \tag{8.3}$$

where $\tau$ is the time constant of the system.

Therefore, the flux of the solvent (at time $t$), for a fully rejected protein, is given as

$$J = L_p\left(\pi\left(1 - e^{-t/\tau}\right) - \pi\right). \tag{8.4}$$

As the plunger is turned, the pressure within the solution chamber increases (such that $\Delta P > \Delta\pi$) causing a flux of solvent out of the solution chamber. The solvent continues to leave the solution chamber and the pressure drops until the osmotic pressure (of the new concentration) is equal to the pressure within the solution chamber.

The pressure, within the solution chamber, for the solution after any concentrating turn of the plunger follows an exponential decay, or

$$P = P_o e^{-t/\tau} + \pi_c, \tag{8.5}$$

where $P_o$ is the initial pressure within the solution chamber immediately following the turning of the plunger and $\pi_c$ is the observed osmotic pressure (steady state pressure) within the chamber at protein concentration $c$. The observed osmotic pressure, $\pi_c$, may not be the actual osmotic pressure for the concentration of the bulk solution in the solution chamber, but rather it may reflect the osmotic pressure of the concentration polarization (or cake), $\pi_{\text{Wall}}$, which will develop at the membrane surface due to the flux of solvent leaving the solution chamber. The observed osmotic pressure is related to the actual osmotic pressure for the bulk solution by

$$\pi_c = \pi_{\text{Wall}} = \pi + \delta\pi \tag{8.6}$$

where $\delta\pi$ is the difference in the osmotic pressure of the bulk solution solute concentration and the observed osmotic pressure in chamber II. When no polarization layer is present, the observed osmotic pressure, $\pi_c$, is equal to the osmotic pressure of solute concentration in the bulk solution in chamber II.

The time-dependent flux from the solution chamber in response to the plunger being turned is

$$J = L_p\left(P_o e^{-t/\tau} + \pi + \delta\pi\right). \tag{8.7}$$

Alternatively, the flux of solvent through a membrane for a dead-end cell can be modeled using a mass transfer coefficient, $k$, and the ratio of the wall and bulk concentrations, $c_{\text{Wall}}$ and $c_{\text{Bulk}}$, or

$$J = k \ln\left(\frac{c_{\text{Wall}}}{c_{\text{Bulk}}}\right). \tag{8.8}$$

The ideal concentrating osmometer would have a mass transfer coefficient, for a given membrane and solute, that is independent of the solute concentration.

### 8.8.3. Osmotic Pressure of the Bulk Solution

When the osmotic pressure of the solution at a given concentration is known, the osmotic pressure of the cake layer can be determined. However, when the osmotic pressure is unknown, the osmotic pressure of protein concentration in the bulk needs to be determined using Eqn. 8.7. To achieve this, information needs to be known about the concentration of the protein in the cake layer and its osmotic pressure.

## 8.9. Conclusion

Here, a concentrating osmometer was developed and tested, and the practical issues were discussed. The concentrating osmometer was tested for concentrating a BSA solution for two initial concentrations.

The concentrating osmometer reduces the required quantity of protein to decrease by approximately one order of magnitude and reduces the time from weeks to days. Using such an osmometer will now allow for the osmotic pressure of solutions, which were previously unrealistic to be studied.

A concentrating osmometer has uses in chemical, physical, and biological research. A few applications for which a concentrating osmometer is useful are: obtaining the osmotic pressure-concentration profile, understanding the osmotic pressure of the cell cytosol, detecting protein mutations, and determining equilibrium constants (such as dissociation constants, $K_d$, and $IC_{50}$).

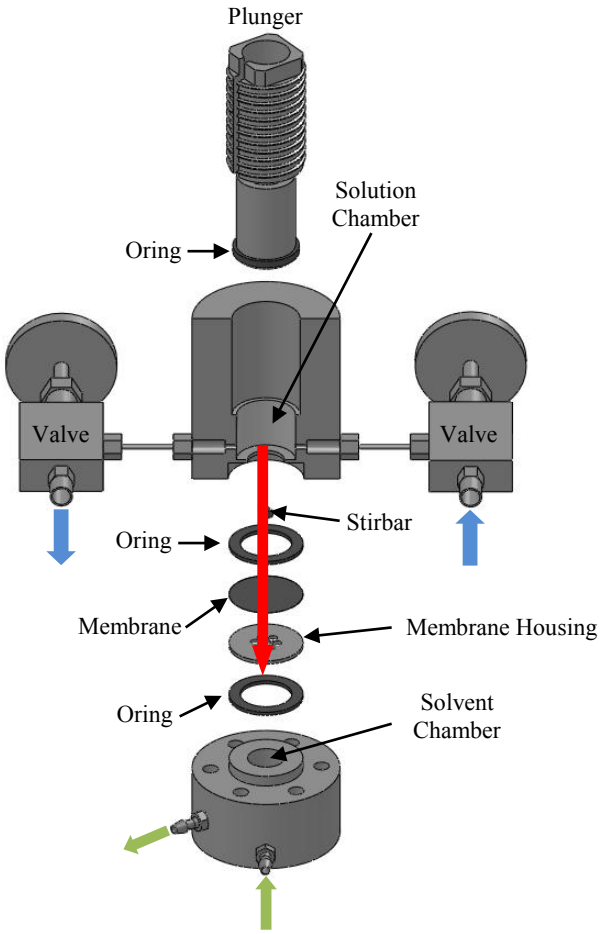


**Figure 8.1.** The Concentrating Osmometer. The plunger (top and bottom connected) threads into the solution chamber and forces solvent to flow across the membrane. The pressure transducer is sealed within the plunger such that the transducer sensor (face) is at the tip of the plunger and is in contact with the solution. The solution is put into the solution chamber through the valves (blue arrows). A stir bar is used to minimize the concentration polarization layer on the membrane, as the solvent (red arrow) is driven out of the solution chamber. Orings are used to seal the chambers. The solvent chamber has a continuous feed of solvent (green arrows) such that the residence time is much less than the time constant for the pressure within the solution chamber.

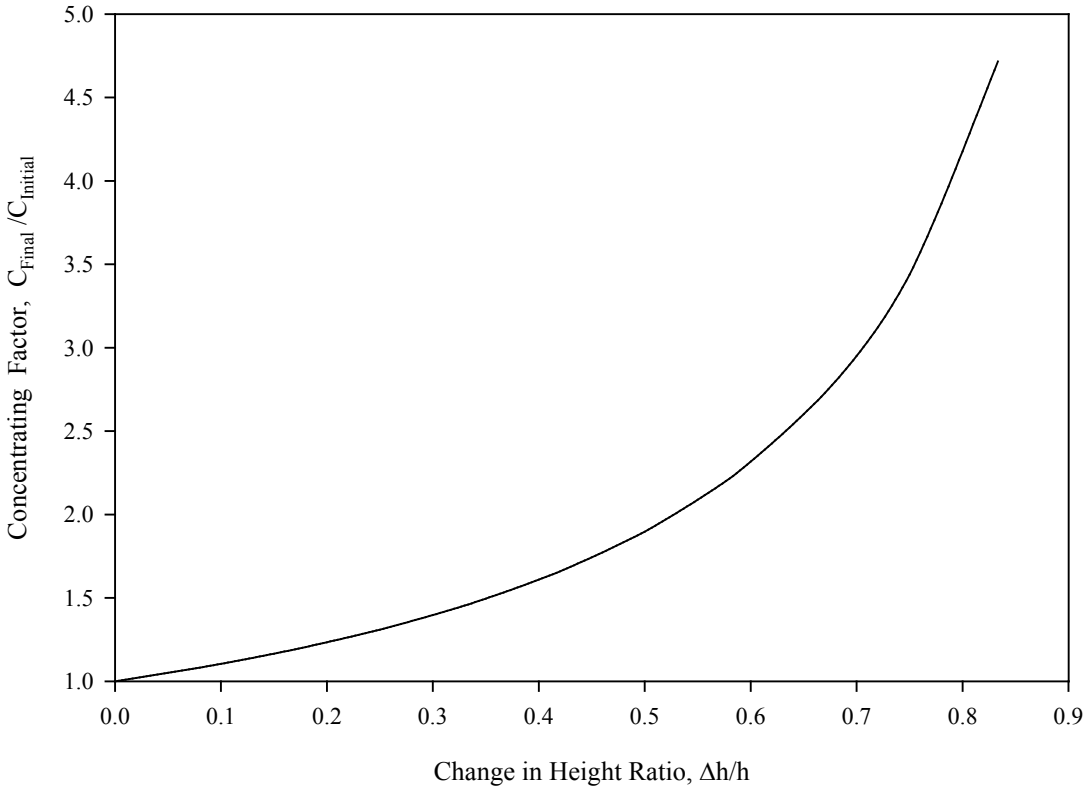


**Figure 8.2.** Concentrating Factor of the Initial Solution as the Solution Chamber Height Changes. The solution chamber height is reduced as the plunger is threaded into the concentrating osmometer.

**Table 8.1.** Measured Osmotic Pressure for the Concentrating Osmometer and the Time Constant of Each Plunger Turn. The time constants were calculated by fitting the pressure in the chamber to Eqn. 8.3 or Eqn. 8.5 for the experimental data set of each concentration. The mass transfer coefficients were calculated by equating Eqns. 8.7 and 8.8.

| $[BSA]_{Bulk}$ (g/L Soln) | Expected Osmotic Pressure (psi) | Measured Osmotic Pressure, $\pi_c$ (psi) | $[BSA]_{Wall}$ (g/L Soln) | Osmotic Pressure Difference, $\delta\pi$ (psi) | Time Constant, $\tau$ (min) | Mass Transfer Coefficient, $k$ $\left(\frac{cm^3}{cm^2 s}\right)$ |
|---|---|---|---|---|---|---|
| 100.99 | 0.9 | 0.9 ± 0.02 | 101 | 0 | 4 ± 1.1 | N/A |
| 107.00 | 1.0 | 1.1 ± 0.03 | 115 | 0.1 | 3 ± 0.0 | 0.003 ± 0.00008 |
| 118.79 | 1.1 | 1.4 ± 0.06 | 130 | 0.3 | 8 ± 0.5 | 0.003 ± 0.00013 |
| 132.68 | 1.4 | 1.6 ± 0.03 | 140 | 0.2 | 17 ± 1.7 | 0.006 ± 0.00011 |
| 150.25 | 1.8 | 2.1 ± 0.02 | 160 | 0.3 | 18 ± 0.4 | 0.006 ± 0.00006 |
| 159.12 | 2.1 | 3.6 ± 0.02 | 210 | 1.5 | 45 ± 2.6 | 0.003 ± 0.00001 |
| 199.96 | 3.0 | 3.2 ± 0.07 | 203 | 0.2 | 2 ± 1.0 | N/A |
| 207.10 | 3.3 | 4.3 ± 0.04 | 230 | 1.0 | 11 ± 0.2 | 0.008 ± 0.00007 |
| 216.55 | 3.6 | 6.3 ± 0.03 | 275 | 2.7 | 33 ± 0.5 | 0.005 ± 0.00002 |
| 229.91 | 4.4 | 8.7 ± 0.03 | 310 | 4.3 | 63 ± 1.3 | 0.006 ± 0.00002 |
| 257.09 | 5.4 | 30.2 ± 0.05 | 460 | 24.8 | 38 ± 4.3 | 0.010 ± 0.00002 |

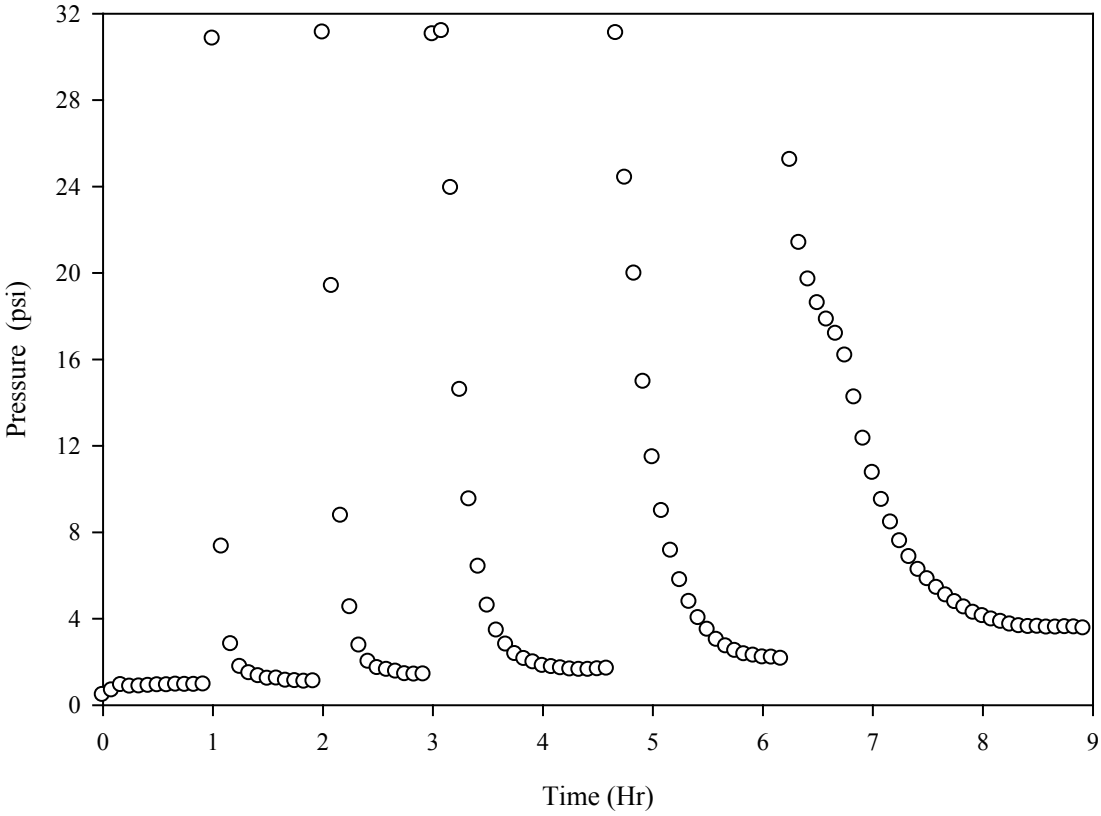


**Figure 8.3.** Pressure vs. Time for an Initial BSA Solution of 100.99 g/L BSA, 0.15 M NaCl, pH 5.4 using the Concentrating Osmometer. The data points are the experimental pressure values within the solution chamber. The turning of the plunger causes a large increase of the pressure within the chamber. This causes a flux of solvent out of the solution chamber until the pressure, within the solution chamber, is equal to the osmotic pressure of the solution in the chamber.

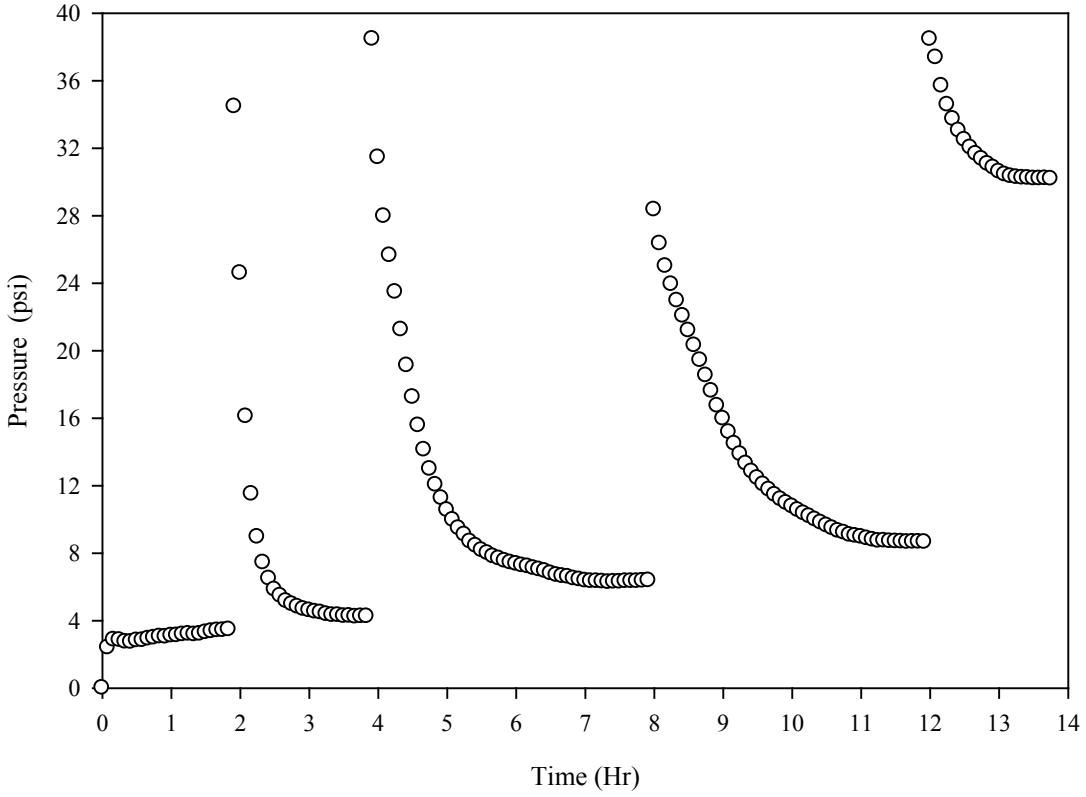


**Figure 8.4.** Pressure vs. Time for an Initial BSA Solution of 199.96 g/L BSA, 0.15 M NaCl, pH 5.4 using the Concentrating Osmometer. The data points are the experimental pressure values within the solution chamber. The turning of the plunger causes a large increase of the pressure within the chamber. This causes a flux of solvent out of the solution chamber until the pressure, within the solution chamber, is equal to the osmotic pressure of the solution in the chamber.

# CHAPTER 9.

# CONCLUSIONS

## 9.1. Findings of This Work

Herein, the free-solvent model was further developed to: (1) obtain another physical parameter (SASA) and (2) account for protein-protein interactions. The SASA was shown to have excellent agreement with the values calculated from the molecular structures for several globular proteins.

The SASA was equivalent, for a given protein, regardless of the solution properties studied; here only solution properties which did not affect protein structure were examined. Furthermore, the SASA was able to be predicted for sucrose and, in addition, the corresponding hydration was similar to literature values.

The free-solvent model was used to give physiological meaning to the parameters of two widely used osmotic pressure models. Both the activity coefficient and the virial coefficients were shown to be based on solute-solvent interactions rather than protein-protein interactions (for non-interacting proteins, which is true for all the protein solutions studied within this work). The coefficients based on solute-solvent interactions are in agreement with those obtained from fitting the experimental osmotic pressure data.

The second virial coefficient was examined for the conditions needed to obtain positive, negative, and zero values. The ratio of the ionic strength of the protein influenced solvent to that of the bulk was correlated to the sign of the second virial coefficient; when the ionic strength ratio of the protein influenced solvent to the bulk was less than 1, positive virial coefficients were obtained. For an ionic strength ratio, of the protein influenced solvent to the bulk, greater than 1, negative virial coefficients were obtained. If the hydration of the bound salt ions is considered, a

virial coefficient of zero was obtained for an ionic strength ratio of 1 (when 8.9 mol $H_2O$/mol bound salt was assumed).

The free-solvent model was revised to account for any number of species and proteins in which protein-protein interactions can occur in the form of intra-protein species interactions (homo-multimers) and/or inter-protein species interactions (hetero-multimers). Two additional parameters were added to the free-solvent model, protein-protein binding and a fractional amount of multimer formation. The revised free-solvent model was reduced for several cases and the effect of the various physical parameters on the osmotic pressure was examined.

A concentrating osmometer was developed and tested for known solution osmotic pressure using bovine serum albumin (BSA). The use of a concentrated osmometer can have applications in many areas, including disease diagnostics.

## 9.2. Future Directions

The activity and the second virial coefficient, developed in this dissertation, are valid for non-interacting protein solutions. These parameters can be revised, using the free-solvent model for protein-protein interactions (Chapter 7), to incorporate the new physical parameters, as necessary. A similar development to that of the activity coefficient (Chapter 3) and the virial coefficient (Chapter 4) can be used to determine the fitted parameters of other osmotic pressure models, such as the osmotic coefficient.

The second virial coefficient has been correlated to many observed phenomena, such as salting-out, and therefore, future work can be focused on understanding, explaining, and/or predicting these phenomena using the physical parameters of the free-solvent model.

The free-solvent model for accounting for protein-protein interactions remains to be experimentally verified. In order to verify the homo-multimer model, a homo-dimer protein

solution in which monomers are present would be ideal. For the hetero-multimer model, the use of proteins of similar size with a large binding interface area would be the ideal choice.

The use of a concentrated osmometer can be used for measuring the osmotic pressure of protein solutions which were previously unavailable, either due to mass quantity or cost. The concentrating osmometer can also be used to provide a large amount of data in the near-saturation range for better estimates of the free-solvent parameters, as well as saturation limits. Work remains to be completed in order to understand the irreversible thermodynamics of the concentrating osmometer.

# PART 2.

# DEVELOPMENT OF A TREATMENT FOR SEVERE CEREBRAL EDEMA

# CHAPTER 10.

# INTRODUCTION

## 10.1. Cerebral Edema

Cerebral (brain) edema, an increase in brain tissue water content, is responsible for significant morbidity and mortality in many different disease states, including traumatic brain injury (TBI), stroke, infection, tumor, spinal cord abscess, and a host of chemical and metabolic intoxications. The two types of cerebral edema are vasogenic edema and cytotoxic (cellular) edema.

### 10.1.1. Vasogenic Edema

Vasogenic edema is characterized by the disruption of the blood-brain barrier (BBB) and may be caused by direct injury or by breakdown of the BBB (*e.g.* by tumors). BBB disruption leads to the accumulation of blood components in the brain and an influx of water into the interstitial space between cells follows, causing swelling of the tissue.

### 10.1.2. Cytotoxic Edema

Cytotoxic edema is characterized by the flux of water into brain cells (predominantly brain glial cells) and is associated with trauma, ischemia, and toxins.

#### 10.1.2.1. The Roles of Glial Cells in Preventing Cerebral Edema

The roles of glial cells have only been recently discovered (Kettenmann and Ransom 2005) and include protecting and maintaining the homeostasis of the brain and maintaining the blood-brain barrier. A major role of glial cells (specifically astrocytes) is to maintain the delicate

balance of ions in the extracellular space to provide the necessary conditions for proper neuron function. As such, glial cells remove excess potassium which is greatly altered during many disease conditions. For example, normal extracellular potassium concentration is 2.5 mM, but during epileptic seizures, the extracellular potassium concentration can be 10 - 12 mM. The cytosol of glial cells contains about 30 - 160 nM $H^+$ and the pH is between 6.8 and 7.5 (Kettenmann and Ransom 2005). A results of the regulation of extracellular salt by uptake and release is that glia are subject to swelling.

Glial cells have compensatory mechanisms to restore water homeostasis across the cellular membrane, but following injury these mechanisms may be disrupted. Glial cells contain many membrane transporters to maintain the ion balance of the extracellular space. The common transporters on glial cells are: cation-chloride cotransporter, $Cl^-/HCO_3^-$ exchanger (AE), $Na^+Cl^-/HCO_3^-$ exchanger, and $Na^+/H^+$ exchanger (NHE). The cation-chloride cotransporter transports a $Na^+$, $K^+$, and 2 $Cl^-$ into the cell while pumping a $K^+$ and $Cl^-$ out. The AE transports a $Cl^-$ in and $HCO_3^-$ out. The $Na^+Cl^-/HCO_3^-$ exchanger transports a $Na^+$ and 2 $HCO_3^-$ in and a $H^+$ and $Cl^-$ out. The NHE transports a $Na^+$ into the cell and a $H^+$ out. The AE and NHE transporters are known to be responsible for regulating cell volume and cytosolic pH (Kettenmann and Ransom 2005).

In addition to these ion transporters, glial cells also have aquaporins. Aquaporins (AQPs) are membrane proteins (30 kDa), found in many cell types, which act as water channels (Amiry-Moghaddam *et al.* 2003; Verkman 2005). AQPs facilitate bidirectional water transport due to osmotic pressure (Verkman 2002). AQP4 is critically important to brain edema because it is expressed in the glial cells of the brain and spinal cord. AQP4 is localized mainly in the glial cell endfeet which are in contact with the blood vessels and neuronal synapses (Nielsen *et al.* 1997; Nagelhus *et al.* 2004).

Through the use of ion transporters and the AQP network, glial cells can rapidly respond to changes in extracellular ion imbalances and volume changes. The rapid response of glial cells to volume changes allows for them to regulate the extracellular environment, through the uptake and/or release of salts (Verkman and Mitra 2000).

10.1.2.2. Mechanisms of Glial Cell Swelling

Six mechanisms have been proposed for the swelling of glial cells (Figure 10.1). In each mechanism, the glial cells regulate the extracellular environment by transporting excess molecules, in response to physiological changes, in the extracellular space (ECS).

Mechanism A shows the transport of water into glial cells via AQPs and/or passive diffusion across the cell membrane. Both of these processes require no energy to transport the water across the cell membrane; therefore, this mechanism can also describe cell shrinking if the water is transported out of the cell. Glial cell swelling can be explained by the flow of water into the glial cell, down its chemical potential gradient, due to an increase in extracellular water or due to an increase in the concentration of the intracellular impermeable solutes. The increase in extracellular water and/or intracellular impermeable solutes accompanies many disease states.

The transport of ions into (or out of) the intracellular environment can shift the balance of ions within the cell (Mechanisms B and F). This can alter the interaction between the ions and the macromolecules within the cytosol, as well as the chemical potential of the intracellular water. All of these can cause water flux into the cell, inducing swelling.

The change in the cytosolic pH via the transport (by NHE activation) or generation of protons or acids, hydroxides or bases (such as ammonia), or buffering solutes (Mechanisms C and D) will tend to alter the chemical potential of intracellular water via altered proton binding by macromolecules (altered macromolecule charge), adjusted macromolecule-ion binding, and/or

adjusted macromolecule hydration (through structural changes). It has been observed that no swelling occurs at a pH lower than 6.0 in part because severe acidification inhibits potassium transport (Kettenmann and Ransom 2005).

Mechanism E has only been observed *in-vitro*; however, the concentrations of intracellular glutamate required to induce swelling via this mechanism is non-physiological. Typically, neurons uptake glutamate and release potassium, thereby increasing the extracellular potassium and increasing solutes within the cytosol and, consequently, inducing glial cell swelling (Kettenmann and Ransom 2005).

## 10.2. Traumatic Brain Injury

TBI is the foremost cause of morbidity and mortality in persons under 45 years of age worldwide, and accounts for a larger number of casualties in the combat in Iraq and Afghanistan than in any other recent U.S. war. After TBI, many patients experience a delayed rise in intracranial pressure (ICP) due to cerebral edema (Marmarou 2003; Castillo *et al.* 2009). Such increases in ICP can lead to reduced cerebral blood flow (cerebral ischemia), brain herniation, and death. TBI can be divided into two phases: primary and secondary injury.

### 10.2.1. Primary Injury

The primary injury of a TBI is caused by the direct external mechanical force. It results in immediate damage to the brain tissue. The tissue is typically not salvageable, thus few therapies are targeted at treating primary injuries for TBI.

### 10.2.2. Secondary Injury

Secondary injury refers to a cascade of delayed deleterious physiological events that may last hours to days. It plays a major role in the morbidity and mortality resulting from TBI, and is characterized by ischemia, BBB rupture, and cerebral edema (Kettenmann and Ransom 2005).

#### 10.2.2.1. Ischemia

Ischemia can occur due to a lack of metabolites and blood supply to a portion of the surviving tissue (*i.e.* the tissue not fatally injured by the primary injury). In ischemic-like environments, glial cells respond by pumping ions to minimize the effects on the neurons. This will alter the cytosolic conditions of the glial cell, which may lead to swelling or shrinking.

Since the delicate balance of ions is maintained by glial cells, any alterations in the intra- or extracellular ions, pH, and/or water can be detrimental. This is especially destructive when the ion imbalances become so great that it is toxic and damaging. In such conditions, in order to maintain the neuronal (extracellular) environment, the glial cells will regulate the extremely fine balance of ions in the extracellular space between neurons to keep the neurons from malfunctioning. As a consequence, the glial cells will adjust their internal, cytosolic environment, and induce swelling.

#### 10.2.2.2. Blood-Brain Barrier Rupture

The rupturing of the BBB is typically a result of the primary injury. Post-BBB rupture, the blood components (*i.e.* proteins, metabolites, waste, etc.) can flow into the parenchyma, and induce vasogenic and cytotoxic swelling.

Vasogenic swelling is induced first since the chemical potential of water gradient is shifted from the surrounding tissue to the local area of accumulated blood components (which is

often in the ECS). In response to the injury and the accumulation of blood components, glial cells will begin to uptake the debris. This causes another shift of the water chemical potential, now towards the glial cells, inducing cytotoxic swelling.

#### 10.2.2.3. Cerebral Edema Induced by Traumatic Brain Injury

Edema following a TBI is characterized by mixed cytotoxic and vasogenic edema mechanisms, both contributing to the overall cerebral edema. After a TBI, glial cells swell due to changes in the extracellular pH and concentrations of ions, including potassium, sodium, and chloride (Kettenmann and Ransom 2005). The resulting cytotoxic edema combines with the vasogenic edema caused by direct BBB injury. Furthermore, reduced blood flow to the affected brain area (cerebral ischemia) leads to additional ion shifts and cytotoxic edema. A vicious cycle involving components of both types of edema can proceed until the brain swells uncontrollably resulting in permanent brain damage or death.

### 10.3. Brain Trauma Foundation Guidelines for the Management of Severe Traumatic Brain Injury

In recent years, with the advances in diagnostic imaging, the Brain Trauma Foundation (BTF) guidelines for the treatment and surgical intervention of severe TBI have been refined (Bratton *et al.* 2007). In particular, these guidelines state that the management of severe TBI requires a combinatorial approach of surgical and therapeutic treatments including osmotherapy, barbiturates, ventriculostomy, and decompressive craniectomy. Osmotherapy includes the use of systemic circulation of either mannitol or hypertonic saline solutions to relieve cerebral edema. Barbiturates are thought to reduce ICP through metabolic suppression (Eisenberg *et al.* 1988). Ventriculostomy consists of cerebrospinal fluid (CSF) drainage via a ventricular catheter in an

attempt to cause water to fill the ventricles. In the most severe cases of TBI, a decompressive craniectomy is performed to relieve the increased ICP due to cerebral edema.

Although these treatments are suggested by the BTF guidelines, and they are often ineffective, and even combinations of these therapies may have limited success in treating severe TBI (Suarez *et al.* 1998; Park *et al.* 2008; Cooper *et al.* 2011). Recent studies suggest that alternative treatments/therapies are needed for managing severe TBI and improving outcome while preventing the limitations of the current therapies.

## 10.4. Current Treatments of Severe Cerebral Edema

The current treatments, therapies and surgical interventions, for cerebral edema all indirectly affect the cause of cerebral edema (water).

### 10.4.1. Craniectomy

A craniectomy is the most commonly used treatment for severe cerebral edema. During a craniectomy, a craniotomy is performed (when part of the skull is removed) to allow for the brain to swell out of the place where the skull was removed. This will relieve the ICP; however, there are a few major limitations. Although, the operation only lasts for a couple of hours, the treatment can take several months before the brain reduces to normal size. During this time, the brain is exposed which can lead to infections. Second, further damage can occur due to external brain herniation (the skull restricting the non-exposed half of the brain). Third, the cerebral veins at the margins of the craniectomy compress which may cause ischemia and further damage. Lastly, a second operation is needed to replace the skull after the swelling has reduced; therefore, the skull must be preserved during the treatment, so it is placed in the patient's intraperitoneal space.

### 10.4.2. Osmotherapy

Medical treatment of cerebral edema via osmotherapy uses intravenous mannitol or hypertonic saline solutions. These medications are aimed at osmotically removing water from edematous brain tissue via the bloodstream. While usually effective in acutely reducing ICP, they have significant disadvantages including clinical variability, temporary duration of effect, and potential deleterious systemic consequences on the cardiovascular and renal physiological systems (Keyrouz *et al.* 2008; Castillo *et al.* 2009). In addition, these medications are nonspecific in that they remove water from all tissues and can lead to significant volume and electrolyte imbalances. Even maximum concentrations of these medications are sometimes ineffective at treating severe cerebral edema. Furthermore, a rebound effect can occur following the initial ICP reduction.

### 10.4.3. Ventriculostomy

Treatment of cerebral edema by a ventriculostomy is not used as often as either a craniectomy or osmotherapy. A ventriculostomy is the removal of the CSF via a catheter placed into the cerebral ventricles. A craniotomy is performed, followed by removal of the CSF via suction. The skull is replaced, and the patient is allowed to heal. This procedure, while completed within a few hours, does not directly treat the injured tissue. One issue is that the total CSF volume (approximately 150 mL for adults) is a small portion of the brain volume. Thus, CSF drainage via a ventriculostomy is not very effective. A second issue is that since the water is allowed to "leak" into the space originally occupied by the CSF, potentially devastating ion imbalances can occur.

## 10.5. Scope of This Work

A method of directly removing water from brain tissue would circumvent the limitations of these current therapies, but only one such idea has ever been conceived and reduced to practice. This idea was to use a microcatheter to remove the water osmotically (a unique type of ventricular catheter). This method is quite invasive because the microcatheter is placed directly into the brain tissue. The very nature of this method is prone to damaging the brain.

Another method was developed and animal studies were performed, but no change to the clinical treatment protocol has occurred. This method was using membrane dialysis; a membrane was used to draw fluid out of the tissue via a gradient in the chemical potential of water (Shulyakov *et al.* 2008). In this method, a dextran solution osmotically removes water from the tissue. However, this method is limited by the batch-type solution chamber (Shulyakov *et al.* 2009). For this method of treatment, the water chemical potential gradient will eventually be reduced to zero as water is removed from the brain and "stored" in the membrane device.

The scope of this work was to design and develop a novel treatment for the direct removal of water from injured edematous tissue. The developed treatment uses the inevitable osmotic pressure of concentration solutions. The treatment (called direct osmotherapy, or DOT) seeks to remove water from the tissue by osmotically driven flow. An osmotic transport device (OTD) was designed and built to treat edema via DOT. The treatment is tested using two models of severe cerebral edema: water intoxication and traumatic brain injury. The water intoxication model, while it has limited clinical relevance, is a fatal model of edema, and thus the robustness of the developed therapy is tested; the traumatic brain injury model is clinically relevant, and the sensitivity of the treatment is determined.

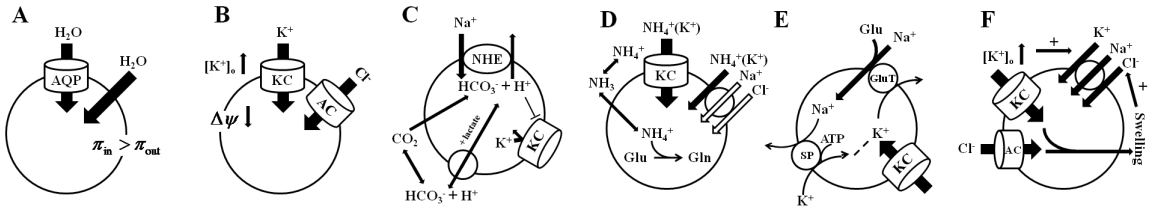


**Figure 10.1.** Proposed Mechanisms of Glial Cell Swelling. Glial cell swelling can be induced by water transport (Mechanism A), ion transport (Mechanisms B and F), pH change (Mechanisms C and D), and/or glutamate transport (Mechanism E) (Kettenmann and Ransom 2005).

# CHAPTER 11.

# DEVELOPMENT OF AN OSMOTIC TRANSPORT DEVICE

## 11.1 Abstract

Cerebral edema is a significant cause of morbidity and mortality in many disease states. The current therapies of cerebral edema are often ineffective in treating severe edema. Here, an osmotic transport device (OTD) is developed for direct surface contact-based treatment of severe cerebral edema by direct osmotherapy (DOT).

## 11.2. Introduction

A new method of directly removing water from brain tissue would potentially circumvent some limitations of the current therapies. For therapeutic benefit in treatment of cerebral edema, the ideal medical device would: (1) have the capacity to remove water from brain tissue in a controlled fashion, (2) have the flexibility for deployment on the surface of the brain, (3) not require brain tissue penetration, and (4) not do any harm to the underlying brain tissue.

Here, a direct surface-contact-based treatment using an osmotic transport device (OTD) which removes fluid osmotically was developed (Figures 11.1) (M$^{c}$Bride *et al.* 2012). In this work, three versions of the OTD were developed (Appendix F). The first consisted of modifying a commercial hollow fiber module (Baxter dialyzer, Baxter, IL). The second (hollow fiber-hydrogel device, HFHD) and third (OTD) generations were designed and developed at the University of California, Riverside. The second and third generations of the OTD were designed and developed using the protocol outlines in Appendix F.

## 11.3. Device Design

An OTD consists of a hollow fiber semi-permeable membrane system embedded in a moldable, soft hydratable material that is placed directly on the exposed injured tissue and will conform to the injured area to maximize the contact area (Figure 11.2). The hydratable material will ensure that the contact between the hollow fiber and tissue is maintained. An aqueous fluid containing concentrated, fully rejected species (such as proteins) is passed through the lumen of the fibers. The aqueous solution contact is continuous through the moldable hydratable material and the tissue, resulting in an inevitable osmotic pressure. This pressure gradient will gently remove fluid from the tissue through the hydratable material and ultimately through the fibers and away from the patient.

### 11.3.1. The Lumen Solution: Solute Selection

The lumen solution consists of an impermeable solute, which is responsible for the flux of water into the hollow fibers, and the solvent solution it is dissolved in. While there are a number of solutes which can be used, the selection of the solute can greatly affect to flux of water, and thus is essential to the success of an OTD. The optimal solute will provide a range of osmotic pressures.

The flux of water due to an osmotic pressure can be approximated by the Kedem-Katchalsky equation (Kedem and Katchalsky 1958),

$$J = \frac{\left(\Delta P - \sigma \Delta \pi\right)}{\mu\left(R_m + R_h\right)}, \tag{11.1}$$

where $\Delta P$ is the transmembrane pressure, $\Delta \pi$ is the osmotic pressure, $\sigma$ is the reflection coefficient which provides a measure of the membrane permselectivity, $\mu$ is the permeate

viscosity, $R_m$ is the membrane resistance to the flow of water, and $R_h$ is the hydratable material resistance to the flow of water.

The OTD should be operated such that the osmotic pressure is much larger than the transmembrane pressure ($\Delta\pi > \Delta P$). Osmotically driven water flux has the capability of controllability which can provide a therapeutic effect for any duration and/or magnitude of edema by altering the osmotic pressure of the lumen solution for instance.

Here, the OTD uses BSA as the impermeable solution because of its physical properties and because at high solution concentrations, its concentration-dependent osmotic pressure range is significantly larger than the proposed physiological application, while having manageable viscosity changes (Vilker *et al.* 1981; Yousef *et al.* 1998b; Buccola 2010).

### 11.3.2. The Lumen Solution: Solvent Selection

While selecting a solute requires little information about the injury, choosing the appropriate lumen solution solvent requires that the injury be known and well understood. While the most applicable solvent solution is one that allows easy uptake of water and other injury-associated components, which should not be present under normal conditions, it is difficult to have a wide variety of lumen solutions for different injuries. Yet, regardless of the injury, the transport rates should be tunable. For components which have non-physiological concentrations, if the concentration is greater during injury than normal, uptake of that component is beneficial; while if the concentration during injury is lower than normal, transport of the component into the tissue may be beneficial.

Generally, a solution which has the same ions at physiological concentrations as the normal tissue will be the best choice. In addition, for use in some injuries, the delivery of nutrients and/or therapeutics may provide added benefit given that they can pass through the

hollow fibers and that their gradient is in the direction of the tissue. This gradient must overcome the transport of water into the hollow fibers to allow delivery to the injured tissue. In this scenario, a Péclet number less than 1 is desired for the molecule(s) attempting to be transported into the tissue.

The solvent solution was initially chosen to be 0.15 M NaCl at pH 7.4. However, this was quickly changed to artificial cerebrospinal fluid (aCSF) (Csenkér *et al.* 1982) and was used in the majority of the studies in this dissertation.

### 11.3.3. Selection of the Hollow Fibers

The choice of hollow fibers requires flexibility and knowledge of the lumen solution properties. The hollow fiber outer diameter, as well as the hollow fiber material, will affect the flexibility and, more importantly, the range of surface area that can be treated. Flexible hollow fibers with a relatively small outer diameter (200 μm) will be able to mold to brain gyrations while the hydrogel ensures that fiber-tissue contact is maintained. However, the effect of the diameter on the transmembrane pressure must also be considered.

An additional concern is the choice of hollow fiber material. The hollow fibers need to be made from a material which is biocompatible and bio-inert; the membrane should not cause an immune response.

In this study, the OTD was developed using regenerated cellulose fibers with a molecular weight cutoff of 13 kDa (132294, Spectrum Laboratories, Inc.). The solution passing through the hollow fibers (lumen solution) operated at a flow rate with a Reynolds number *(Re)* less than 100.

### 11.3.4. Choice of the Hydratable Material

The selection of hydratable material can aid in successful treatment or cause the treatment to fail. It is beneficial to choose a material that can provide some water transport away from the tissue, however it should not deliver water into the tissue; a shift in the water gradient can potentially exacerbate the edema.

The optimal hydratable material would have a water content similar to that of native tissue, ensuring that no water can be delivered to the tissue while allowing for easy transport of ions and water through the material.

The majority of the studies in this work used an agar hydrogel (0.3% agar) in aCSF, but another hydratable material was tested for its material properties: Durepair (Durepair Dura Regeneration Matrix, Medtronic, Goleta, CA).

## 11.4. Device Challenges

Developing an OTD to treat severe cerebral edema presents several technical challenges. First, the lumen solution and solute concentration need to be selected carefully. Although there are many possibilities for the lumen solution, BSA in aCSF solution at physiological pH was chosen. Second, contact with the brain tissue and the liquid-liquid interface, if not maintained, could severely limit the removal of water and, ultimately, the success of the treatment. To better maintain the liquid-liquid interface and contact with the brain tissue, a hydratable material was used. One advantage of the hydratable material is that it allows for the OTD to conform to brain sulci and gyri. This was not specifically tested in this dissertation because mice are lissencephalic, but further testing in higher mammalian systems may show that the conformability of the hydratable material is a significant advantage. Third, another design parameter of importance is the flexibility of the hollow fibers. Very flexible hollow fibers were carefully chosen so as to

allow access through smaller openings in future applications (*i.e.* treatment via a burr hole); yet using hollow fibers with a small diameter may increase the transmembrane pressure.

## 11.5. Conclusion

A major advantage of using an OTD lies in its intrinsic nature. The water removal rate can be controlled and modified as treatment requires based on alterations in the properties of the lumen solution. A few of the possibilities are changes in the impermeable solute concentration to alter the osmotic pressure of the lumen solution, altering the flow properties (for example, flow rate or viscosity), and increasing the number of hollow fibers or treatment contact area.

Optimal OTD design includes minimization of the transmembrane pressure and resistances of the hollow fibers and hydratable material, maximization of the osmotic pressure within the lumen solution, and selection of the hollow fiber membrane MWCO such that the osmotic agent is completely rejected (preventing transport into the tissue) ($\sigma = 1$).

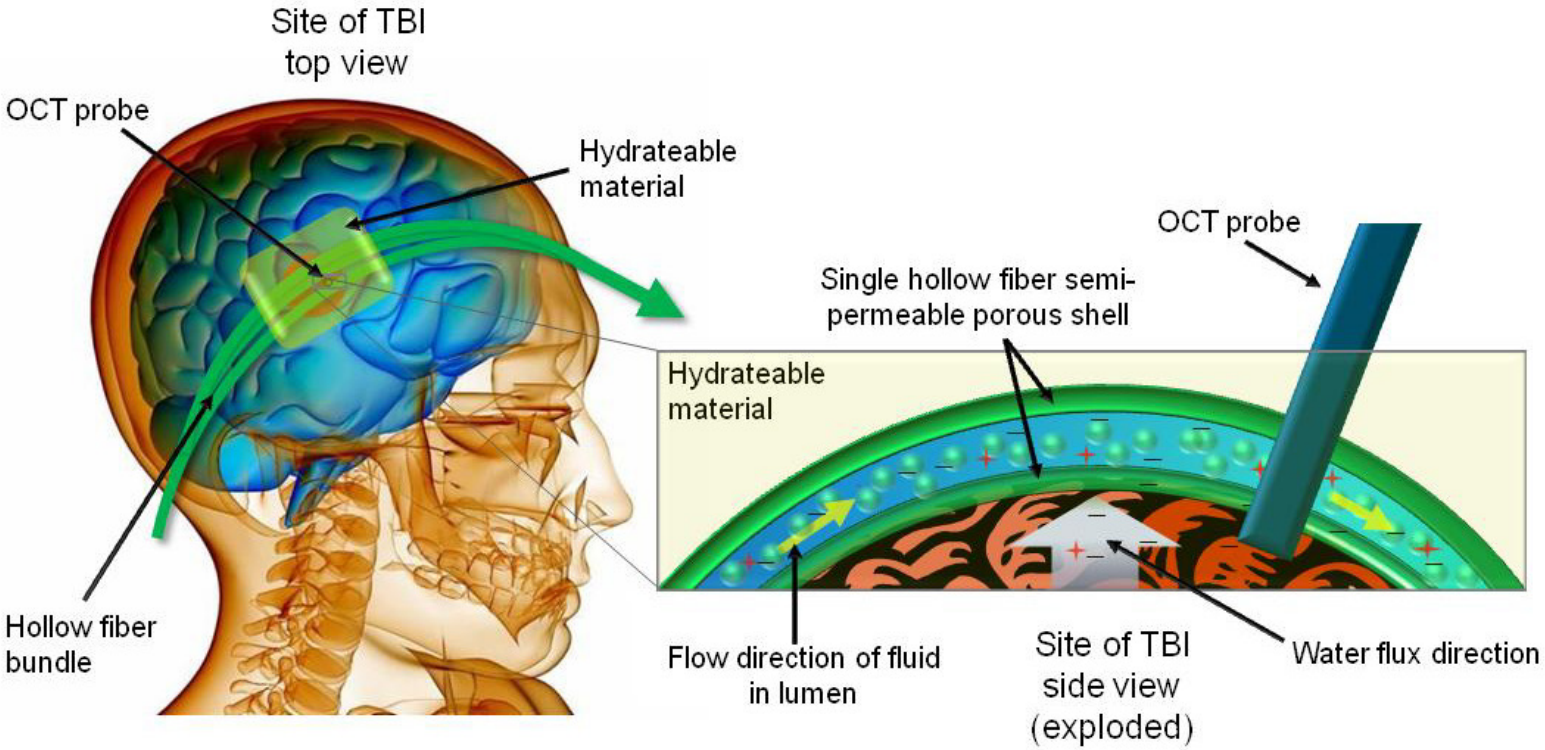


**Figure 11.1.** The Osmotic Transport Device for Treating Cerebral Edema. An aqueous protein solution is pumped across the injured tissue through the semi-permeable hollow fiber membrane lumen. The membrane is selected such that it completely rejects the solute but allows easy passage of water and ions. The protein is chosen so that it induces an osmotic pressure driving force for the transport of water into the OTD. The hydratable material has significant permeability to water and ions and maintains tissue-fiber contact (McBride *et al.* 2012).

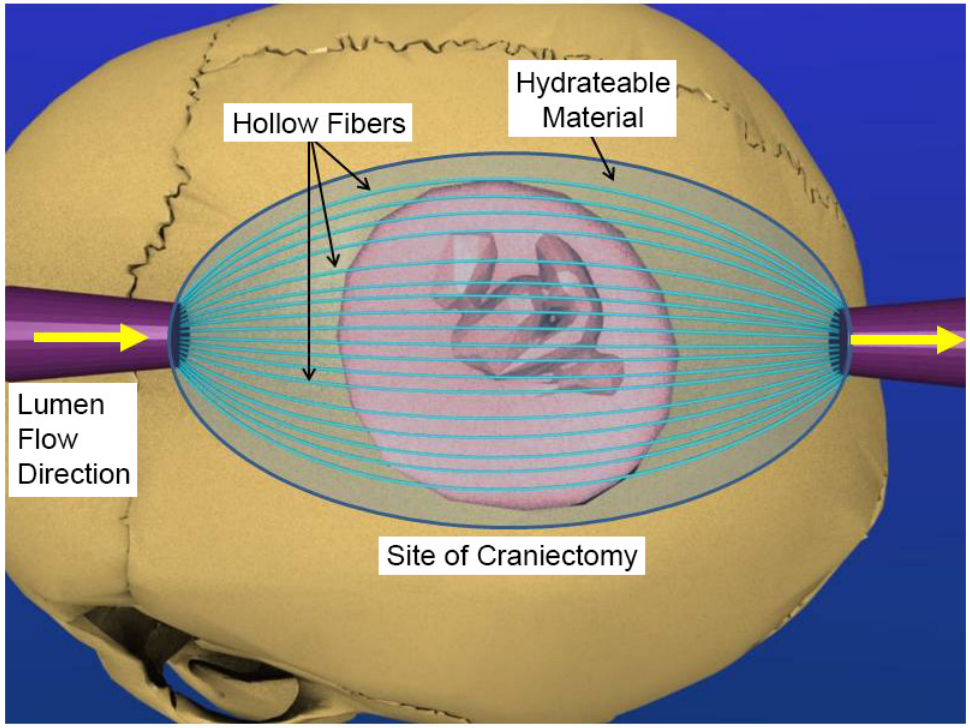


**Figure 11.2.** The Osmotic Transport Device Covering a Craniectomy. Following a craniectomy and opening of the dura, the osmotic transport device is placed with a hydratable material onto the exposed tissue. The hollow fibers are placed to maximize the surface area treated. An aqueous solution containing an impermeable osmotic agent is pumped across the injured surface area through the semi-permeable hollow fiber membrane lumen. The hollow fiber membrane is selected such that it rejects the osmotic agent but allows easy passage of ions and water. The lumen solution induces an osmotic pressure driving force for water removal. The rate of pumping is controlled to allow fluid from the tissue to flow up to the membrane device due to the chemical potential gradient of water. A hydratable material with significantly large permeability is used to maintain membrane-tissue contact and to cover the entirety of the exposed tissue.

# CHAPTER 12.

# WATER UPTAKE VIA AN OSMOTIC TRANSPORT DEVICE

## 12.1. Abstract

Following the development of an osmotic transport device (OTD), it was important to examine the water uptake for various solution properties and the properties of the hydratable materials. Herein, the water uptake by the OTD and the material properties of the hydratable materials were determined.

## 12.2. Methods

### 12.2.1 Water Uptake Via the Osmotic Transport Device

In order to determine the uptake of water using an OTD, two studies were performed. The first study was to understand the removal of water using an OTD without a hydratable material. These experiments were performed by placing the hollow fibers (with a lumen solution flowing through them) into a bath of saline solution (identical to the lumen saline solution). The water was removed by osmotically driven flow.

The second study was to determine the feasibility of water uptake through brain tissue. Four fixed, post-mortem brains were separated into two halves for testing. The groups studied (n = 2 each) were: no OTD (Control), gel only, fibers only, and fibers plus gel. For the fiber groups, a lumen solution of 80 g/L BSA in 3% NaCl, pH 7.4 was used. The gel (hydratable material) used was a 0.3 agar, 3% NaCl gel. For the fiber plus gel group, the fibers were placed on top of the gel which was in contact with the tissue. The gel was approximately 5 mm thick in all cases.

For all groups, the fixed tissue was placed in a water bath for 40 minutes to allow for rehydration. The rehydrated brains were removed from the water, weighed, and then placed in weigh boats for water removal. The tissue was placed such that the cortical surface was treated with one of the groups for 30 minutes.

### 12.2.2. Material Properties of the Hydratable Materials

The water content, swelling, and water uptake were determined for three hydratable materials: 0.3 % agar gel (either 3% NaCl or aCSF (Csenkér *et al.* 1982)), 0.4% agar, aCSF gel, and Durepair, a dura substitute matrix (Durepair Dura Regeneration Matrix, Medtronic, Goleta, CA).

The water content was determined by dehydrating the hydratable materials at 80°C until no change in the mass was observed. The swelling and water uptake were determined by placing the hydratable materials into a saline bath. The weights of the hydratable materials were measured after soaking for 1, 3, and 8 minutes, and compared to the initial weights.

## 12.3. Results and Discussion

### 12.3.1. Water Uptake Via the Osmotic Transport Device

The transport of water into the hollow fibers by osmotically driven flow was studied for various lumen solutions (Table 12.1). The Kedem-Katchalsky equation (Kedem and Katchalsky 1958) was used to determine the membrane resistance (Eqn. 12.1), $R_m$, and hydraulic permeability, $L_p$, (Eqn. 12.2).

$$J = \frac{\left(\Delta P - \sigma \Delta \pi\right)}{\mu\left(R_m + R_h\right)} \tag{12.1}$$

$$L_p = \frac{1}{\mu(R_m + R_h)} \tag{12.2}$$

where $\Delta P$ is the transmembrane pressure, $\Delta\pi$ is the osmotic pressure, $\sigma$ is the reflection coefficient which provides a measure of the membrane permselectivity, $\mu$ is the permeate viscosity, and $R_h$ is the hydratable material resistance to the flow of water.

In these studies, no hydratable material was present, so $R_h = 0$ $cm^2 \cdot cm^{-3}$. The flux was calculated, assuming $\sigma = 1$ and $\mu = 1$ mPa·s.

The transmembrane pressure,

$$\Delta P = \frac{P_1 + P_2}{2} - P_3 \tag{12.3}$$

where $P_1$ is the inlet pressure of the hollow fibers, $P_2$ is the outlet pressure, and $P_3$ is the permeate pressure, was calculated using $P_2 = 0$ psi and $P_3 = 0$ psi (which were experimentally verified using pressure sensors). The feed pressure, $P_{\text{feed}}$, (measured upstream of the sudden contraction fitting) was used to determine the inlet pressure of the hollow fibers by

$$P_1 = P_{\text{feed}} - P_L \tag{12.4}$$

where $P_L$ is the pressure loss (in feet of fluid) which can be estimated by

$$P_L = \Omega \frac{v^2}{2g} \tag{12.5}$$

and

$$\Omega = 0.5\left(1 - \frac{d_1^2}{d_2^2}\right) \tag{12.6}$$

where $\Omega$ is the resistance due to the sudden contraction, $v$ is the average velocity (ft·s), $g$ is the acceleration of gravity ($ft \cdot s^{-2}$), $d_1$ is the diameter (inches) of the hollow fibers and $d_2$ is the diameter (inches) of the tubing just before the sudden contraction (Crane Co 1981).

The transmembrane pressures for BSA in aCSF, pH 7.4 at room temperature were determined for concentrations of BSA from 50 - 450 g/L (Figure 12.1). The flux of water from a water bath into the hollow fibers using a 350 g BSA/L solution was measured by weighing the water loss from a water bath (after removing the amount of water that evaporated). Using the transmembrane pressure for a BSA solution of 350 g/L, the hydraulic permeability (Eqn. 12.1 with 12.2) and the hollow fiber membrane resistance (Eqn. 12.1) were calculated.

### 12.3.2. Water Removal From *ex-vivo* Brain Tissue

For all treated cases (fiber and gel, fiber only, and gel only), the water removed from the brain tissue was approximately 8% (mass/mass), while the control case removed 4% of the water (Figure 12.1). For the gel only case, a wicking effect was observed which could have enhanced the removal of water from the tissue. In the fiber groups (fibers and gel, and fibers only), part of the hollow fibers were exposed to the air which may have hindered the water removal from the tissue. In addition, the water transport through fixed tissue may also be further hindered by the fixation process. Regardless of the limitations of this preliminary study, the results suggest that the use of an OTD may be successful in removing water from edematous tissue for the treatment of cerebral edema.

### 12.3.3. Material Properties of the Hydratable Materials

The water content before and after water uptake, water uptake rate, and swelling were determined for three agar hydrogels and Durepair (Table 12.3).

The water content after water uptake for all four hydratable materials is larger than most injured tissue water contents; the three agar hydrogels have a water content that is much higher than that of injured tissue, while the Durepair has a water content slightly higher than that of

injured tissue. A higher water content for the hydratable materials (compared to that of injured tissue) will cause a water flux from the hydrogels into the tissue, which will need to be reversed with the lumen solution in the hollow fibers. The initial water content of the Durepair is much lower than that of normal tissue, but its steady-state water content is slightly higher than that of injured tissue. Since the initial water content of Durepair is much lower than that of tissue, the Durepair will need to be hydrated, partially or completely, before use with an OTD.

A larger water uptake rate by the hydratable materials is desirable to ensure that the hydratable material can absorb water faster. This will provide a more beneficial effect for the treatment of the injured tissue (compared to a lower water uptake rate). The rate of water uptake from a water bath is initially very small for all three hydrogels tested, but that of the Durepair is initially much larger. The water uptake rates, after 8 minutes of soaking in a water bath, are similar for all four hydratable materials since they are all reaching the maximum (steady-state) water content.

The material properties of the agar hydrogels were found to be undesirable for used as the hydratable material in an OTD. Only the material properties of Durepair seems promising for use with the OTD since its steady-state water content is only slightly higher than that of injured tissue and it has a larger water uptake rate (initially). The optimal hydratable material properties can provide a rapid initial amelioration of the edematous tissue.

## 12.4. Conclusion

The preliminary results of the experiments here can be used, with a more comprehensive material property assessment, for development of the optimal conditions for treatment using an OTD. While further work needs to be completed to optimize the OTD, the results of the *ex-vivo*

brain tissue experiments were promising and verified the use of an OTD as a potential treatment for cerebral edema.

**Table 12.1.** The Effect of Bovine Serum Albumin Concentration on the Lumen Solution Transport for the Osmotic Transport Device. The lumen solution was BSA in aCSF, pH 7.4. The outlet pressure and permeate pressure were assumed to be a constant 0 psi.

| [BSA] (g/L Soln) | Pressure Before Inlet (psi) | Flowrate, $\dot{F}$ $\left(\frac{\text{cm}^3}{\text{min}}\right)$ | Pressure Loss Due to Sudden Constriction, $P_L$ (psi) | Inlet Pressure, $P_1$ (psi) | Transmembrane Pressure, $\Delta P$ (psi) |
|---|---|---|---|---|---|
| 49.5 | 18.99 ± 1.993 | 8.25 ± 0.75 | 16.91 ± 1.804 | 2.08 ± 0.189 | 1.04 ± 0.094 |
| 98.6 | 23.97 ± 2.435 | 6.86 ± 0.86 | 21.95 ± 2.182 | 2.02 ± 0.253 | 1.01 ± 0.127 |
| 147.9 | 23.02 ± 1.296 | 4.73 ± 0.32 | 21.27 ± 1.178 | 1.75 ± 0.188 | 0.87 ± 0.059 |
| 197.3 | 31.74 ± 2.612 | 6.00 ± 0.60 | 28.77 ± 2.315 | 2.97 ± 0.297 | 1.48 ± 0.148 |
| 246.8 | 36.44 ± 3.303 | 4.60 ± 0.36 | 33.25 ± 3.053 | 3.19 ± 0.250 | 1.59 ± 0.125 |
| 300.3 | 36.93 ± 2.381 | 1.43 ± 0.07 | 35.46 ± 2.309 | 1.47 ± 0.072 | 0.74 ± 0.036 |
| 344.2 | 40.92 ± 2.772 | 1.25 ± 0.10 | 39.13 ± 2.629 | 1.79 ± 0.143 | 0.89 ± 0.072 |
| 393.4 | 38.49 ± 1.462 | 0.34 ± 0.019 | 37.79 ± 1.424 | 0.70 ± 0.038 | 0.35 ± 0.019 |
| 442.6 | 53.64 ± 2.148 | 0.25 ± 0.021 | 52.90 ± 2.086 | 0.74 ± 0.062 | 0.37 ± 0.031 |

**Table 12.2.** Flux and Membrane Permeability of the Osmotic Transport Device. The lumen solution, 350 g/L BSA in aCSF at pH 7.4, has an osmotic pressure of approximately 28 psi and the transmembrane pressure was assumed to be 0.8 psi. The viscosity of the permeate was assumed to be 1 mPa·s (1 cP).

| Trial | Flux Into the Fibers, $J$ x$10^6$ $\left(\frac{cm^3}{cm^2 \cdot s}\right)$ | Hydraulic Permeability, $L_p$ x$10^7$ $\left(\frac{cm^3}{cm^2 \cdot s \cdot Psi}\right)$ | Hollow Fiber Resistance, $R_m$ x$10^{-6}$ $\left(\frac{cm^2}{cm^3}\right)$ |
|---|---|---|---|
| 1 | 18.1 | 6.65 | 1.503 |
| 2 | 17.7 | 6.51 | 1.537 |
| 3 | 18.3 | 6.73 | 1.486 |
| 4 | 9.5 | 3.42 | 2.925 |
| 5 | 19.9 | 7.32 | 1.367 |
| 6 | 51.1 | 18.79 | 0.532 |
| 7 | 20.1 | 7.39 | 1.353 |
| 8 | 74.6 | 27.43 | 0.365 |
| **Average** | **29 ± 22.3** | **10.53 ± 8.19** | **1.383 ± 0.7734** |

**Table 12.3.** The Material Properties of the Hydratable Materials. The water contents were determined by wet-dry weights. The swelling was determined by comparing the volumes before and after water uptake.

| Hydratable Material | Initial Water Content (%) | Final Water Content After Absorbing Water (%) | Water Uptake | | | Swelling (%) |
|---|---|---|---|---|---|---|
| | | | Time (min) | (%) | Rate (%/min) | |
| 0.3% Agar, 3% NaCl (n = 2) | 95.41 ± 0.01 | N/A | Steady-State | 14.93 ± 1.89 | N/A | N/A |
| 0.3% Agar, aCSF (n = 4) | 97.86 ± 0.08 | 98.12 ± 0.15 | 1<br>3<br>8 | 7.94 ± 7.49<br>10.19 ± 3.85<br>18.93 ± 4.05 | 13.24 ± 12.23<br>5.67 ± 2.11<br>3.94 ± 0.80 | -10.21 ± 5.38 |
| 0.4% Agar, aCSF (n = 4) | 97.81 ± 0.12 | 97.80 ± 0.44 | 1<br>3<br>8 | 5.41 ± 1.55<br>11.89 ± 1.81<br>21.37 ± 8.91 | 13.47 ± 4.08<br>9.89 ± 1.84<br>6.66 ± 2.90 | 24.40 ± 4.77 |
| Durepair (n = 4) | 13.30 ± 0.81 | 84.75 ± 1.46 | 1<br>3<br>8 | 385.92 ± 74.65<br>382.81 ± 41.11<br>392.44 ± 70.86 | 43.38 ± 3.40<br>14.48 ± 1.05<br>5.56 ± 0.89 | 17.97 ± 13.77 |

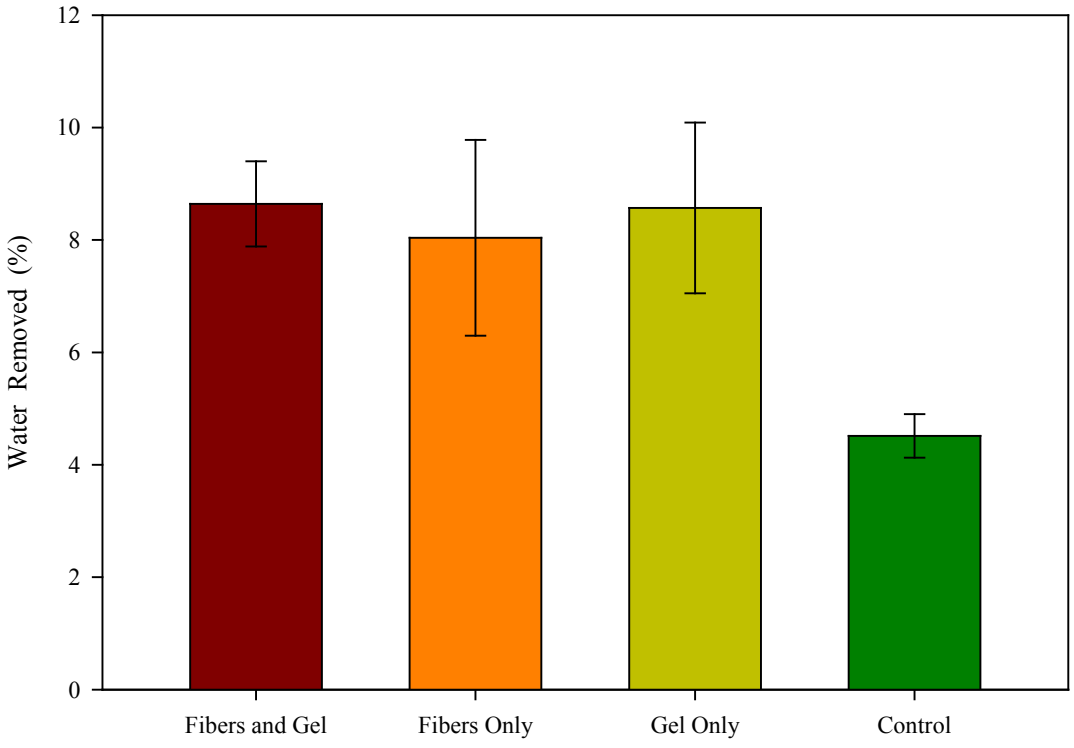


**Figure 12.1.** Water Removal From Fixed Brain Tissue. For the fiber groups, a lumen solution of 80 g/L BSA, 3% saline was used. The gel was 0.3% agar, 3% NaCl. For all cases, n = 2.

# CHAPTER 13.

# IMPROVED SURVIVAL FOLLOWING SEVERE CEREBRAL EDEMA USING AN OSMOTIC TRANSPORT DEVICE

## 13.1. Abstract

Cerebral edema is a significant cause of morbidity and mortality in many disease states, yet the current therapies of cerebral edema are often ineffective in treating severe edema. Here, the osmotic transport device (OTD) is used to treat water intoxicated animals, a model of severe edema. The water intoxication model used here is 100% fatal for untreated and craniectomy treated mice. Water intoxication is a model of pure cytotoxic edema. The survival of water intoxicated animals improved from 0% to 80% when treated using an OTD compared to those treated by a craniectomy.

## 13.2. Water Intoxication

The accumulation of water in the brain, called cerebral edema, inducing swelling as a result of consuming excess water is called water intoxication. The mechanism by which edema forms following water intoxication is cytotoxic edema; water flows into the brain, without disrupting the blood-brain barrier, as a result of the gradient of water being shifted. The water flows into the astrocytes through the aquaporin channels in the endfeet of the glia in contact with the blood vessels, inducing cell swelling.

The occurrence of water intoxication is generally limited in the clinical literature since it is typically unrecognized. In the mild to moderate cases of water intoxication, patients may experience confusion, disorientation, and nausea/vomiting, thus, they may not seek medical help. However, severe cases of water intoxication, if untreated, can lead to coma, seizures, and death (Farrell and Bower 2003).

The most severe cases of water intoxication, which lead to morbidity and mortally, are often unsuccessfully treated by current therapies since the rate of swelling, which is greater than that of most cases of edema, is greater than the water removal rates of current therapies. A treatment which can operate with water removal rates on the order of the rate of water transport into the brain tissue would be ideal for treating cerebral edema induced by water intoxication.

Here, an OTD was used to treat water intoxicated mice. The endpoints were survival (time and percent), brain water content, and histology.

## 13.3. Methods

### 13.3.1. Osmotic Transport Device

Treatment with the OTD consisted of the fibers being placed directly onto the mouse cerebral cortex after craniectomy, with a hydratable material covering the fibers and the exposed tissue (Figure 13.1). The contact area between the hollow fibers and the cerebral cortex was $17.8 \pm 2.2$ mm$^2$ (mean ± SEM).

### 13.3.2. Lumen Solution

The lumen solution consists of concentrated bovine serum albumin (BSA) in a saline solution at pH 7.4. BSA was chosen because the osmotic pressure of concentrated BSA solutions has been extensively studied for various solution properties (Vilker *et al.* 1981; Yousef *et al.*

1998b) and because it is completely rejected by the selected hollow fiber membrane. The lumen solution was made by dissolving BSA in the saline solution. The BSA was mixed using a stir-plate at room temperature, and the pH was adjusted using 1 M NaOH or 1 M HCl. In these experiments, a BSA concentration of 350 g/L in aCSF at pH 7.4 was used. This BSA concentration has an osmotic pressure of approximately 28 psi (Vilker *et al.* 1981). The effect of a 280 g/L BSA lumen solution was observed for a single animal.

Two saline solutions were used in this study: 3% NaCl, pH 7.4 and aCSF, pH 7.4. The saline solution was prepared by dissolving the salt(s) in nanopure (ddH2O) water. The aCSF was prepared following the protocol described for aCSF (Csenkér *et al.* 1982). The pH was adjusted using 1 M NaOH or 1 M HCl.

### 13.3.3. Hydratable Material

The hydratable material chosen here was an agar hydrogel. It was created by dissolving agar into the same solution properties as the lumen solution without the impermeable solute. Two hydrogels were used in this study: a 0.3% agar, 3% saline, pH 7.4 gel and a 0.3% agar, aCSF, pH 7.4 gel.

### 13.3.4. Animals and Surgical Technique

All experiments were conducted under protocols (A-20100018) approved by the University of California, Riverside IACUC. Adult female ten- to twelve-week-old CD1 mice were used in all experiments.

Prior to induction of water intoxication, the mice were anesthetized with a mixture of 80 mg/kg ketamine and 10 mg/kg xylazine. Surgical procedures began only after determining that an adequate plane of anesthesia had been reached with the loss of paw pinch reflex. Reflex

activity was continuously monitored throughout the procedure and supplemental doses of half of the initial dose were provided as needed.

After anesthesia, the animals were placed into a standard rodent stereotactic frame. A midline skin incision was made and reflected. A right-sided craniectomy was performed (anterior border, coronal suture; posterior border, lambdoid suture; medial border, midline; and lateral border, temporalis attachment). The dura was carefully and atraumatically opened with microdissection. In a subset of animals, the dura remained intact to determine the effect of dura removal.

13.3.5. Water Intoxication Model

Cytotoxic cerebral edema from water intoxication was induced as previously described (Gill *et al.* 2011); the mice were injected with distilled water intraperitoneally (at 30% body weight). Approximately 5 minutes post-injection, treatment began. The three experimental groups for water intoxicated animals were: no treatment (water intoxication only), craniectomy only, and direct osmotherapy (DOT) via an OTD. A subset of the water intoxicated animals were used to examine the effect of an intact dura; one animal in the craniectomy group and two animals in the DOT group. Another subset of the DOT group had varied lumen solutions: 280 g/L BSA, 3% NaCl, pH 7.4 (n=1), 350 g/L BSA, 3% NaCl, pH 7.4 (n = 5), and 350 g/L BSA, aCSF, pH 7.4 (n = 5).

13.3.6. Endpoints

End points included survival and brain water content analysis. The survival was assessed over the course of 360 minutes after water intoxication for all groups. The brain water content

was determined by wet-dry weight comparisons postmortem (Zweckerberger *et al.* 2006; Gill *et al.* 2011).

13.3.6.1. Survival

The survival of water intoxicated animals was determined by the time of survival and the percent of animals surviving during the monitoring period. The survival percent was plotted using a Kaplan-Meier survival curve.

13.3.6.2. Brain Water Content

In all animals, the brains were dissected out postmortem. Each brain was separated into four pieces (right-left hemispheres, cerebrum-cerebellum pieces), placed onto a piece of foil, and weighed for the wet weight, $w_{\text{wet}}$. The tissue was then dehydrated at 80°C for 2 days until no change in the weight was observed. The dehydrated tissue was weighed to determine the dry weight, $w_{\text{dry}}$. For each weight, the weight of the foil was subtracted in order to determine the wet and dry weights of the tissue. The brain water content was calculated by

$$\frac{w_{\text{wet}} - w_{\text{dry}}}{w_{\text{wet}}} \text{x}100 . \qquad (13.1)$$

Eqn. 13.1 was used for each section, right-left hemisphere, and total brain water content.

13.3.6.3. Histology After Directed Osmotherapy

To examine any histological changes following DOT, an OTD was applied directly to the cortex for 3 hours in a subset of mice (n = 3). The animals were deeply anesthetized, brains were dissected and frozen, and 50-μm coronal cryostat sections were prepared and subjected to Nissl staining.

13.3.7. Data Analysis

Intergroup comparisons of survival times and brain tissue water content were done using 1-way ANOVAs and post-hoc Bonferroni tests. Brain water content values are presented as the mean ± SEM.

13.4. Results

13.4.1. Survival of Water Intoxicated Animals

13.4.1.1. The Effect of an Intact Dura

The effect of dura removal was tested for three water intoxicated animals: one animal was treated with a craniectomy and two animals were treated with an OTD (lumen solution: 350 g/L BSA, 3% NaCl, pH 7.4). The survival times for the dura intact craniectomy treated animal (40 min) and the two dura intact OTD treated animals (44 min and 49 min) were slightly longer than the survival time of untreated water intoxication animals (31.0 ± 3.1 min, n = 5). The dura intact craniectomy treated animal's survival time was reduced compared to that of the dura removed craniectomy treated animals (48.4 ± 4.0 min, n = 5). The survival time of the animals treated with an OTD when the dura is intact is similar to the dura removed craniectomy treated animals, but greatly reduced compared to the case in which the dura is removed for the OTD treated animals (255.0 ± 64.2 min, n = 5). This is expected as the craniectomy allows the brain to swell outside of the skull, relieving intracranial pressure (ICP), and dura removal further reduces the ICP; an intact dura prevents the tissue from swelling unhindered. Therefore, in the remaining studies, the dura was removed for all treatment groups.

13.4.1.2. DOT Via an OTD: Concentration of BSA in the Lumen Solution

In the initial treatment studies, the lumen solution was chosen to be 350 g/L BSA in 3% NaCl, pH 7.4. The OTD, with this lumen solution, provided an enhanced survival time compared to untreated ($p < 0.001$, $n = 5$) and craniectomy treated animals ($p < 0.001$, $n = 5$). The survival time of untreated animals, craniectomy treated animals, and OTD treated animals were 31.0 ± 1.4 min (n = 5), 48.4 ± 1.8 min (n = 5), and 255.0 ± 28.7 min (n = 5), respectively.

A lumen solution of 280 g/L BSA, 3% NaCl, pH 7.4 was used on a single water intoxicated animal. This animal expired and its survival time decreased to 134 minutes compared to animals treated with a lumen solution of 350 g/L BSA, 3% saline, pH 7.4. This is most likely caused by the water flux for the 280 g/L BSA lumen solution being lower than water flux into the brain; the maximum flux of water into the hollow fibers for a 280 g/L BSA lumen solution is approximately $15 \times 10^{-6}$ $cm^3 \cdot cm^{-2} \cdot s$ while that of a 350 g/L BSA lumen solution is approximately $29 \times 10^{-6}$ $cm^3 \cdot cm^{-2} \cdot s$. Although the water intoxicated animals treated with a 280 g/L BSA lumen solution expired, it is important to note that the use of the 280 g/L BSA lumen solution still had a positive effect on the survival time compared to the craniectomy group; the survival time for this animal was more than two times as long as the craniectomy treated animals.

13.4.1.3. DOT Via an OTD: Choice of the Saline Lumen Solution

In our preliminary studies, the lumen solution containing the BSA was 3% NaCl, pH 7.4. While this choice of saline solution provided an enhanced survival (Figure 13.2), in about 20% of animals, minor seizures were observed, corresponding to a 2 on the Racine seizure scale. In the remaining studies, the lumen solution was an aCSF solution to mimic ion concentrations similar to those in normal brain tissue.

13.4.1.4. Survival Time of Water Intoxicated Animals

The mean survival times after water intoxication were determined for untreated, craniectomy treated, and DOT treated mice (Figure 13.2). The survival time for the untreated group was 31 ± 1.4 minutes (n = 5) and treatment with a craniectomy slightly increased survival time to 48 ± 1.8 minutes (n = 5). Treatment with the OTD markedly improved survival time to 255.0 ± 28.7 (350 g/L BSA, 3% NaCl lumen solution, n = 5) and 333.2 ± 12.7 minutes (350 g/L BSA, aCSF lumen solution, n = 5). Thus, animals treated with the OTD survived approximately 5 hours longer before termination than animals receiving no treatment or a craniectomy treatment (Figure 13.2). Significant differences in survival time were observed between the OTD treated groups and craniectomy-treated group ($p < 0.001$), and the OTD treated group and untreated group ($p < 0.001$).

13.4.1.5. Percent Survival of Water Intoxicated Animals

The untreated and the craniectomy treated water intoxicated animal groups both had a 0% survival after 33 minutes and 50 minutes, respectively (Figure 13.3). Although the craniectomy treatment improved the survival time (of water intoxicated animals), compared to untreated water intoxicated animals, the survival % was unaffected. Four of five (80%) of the DOT-treated animals for both of the lumen solutions (350 g/L BSA, 3% NaCl and 350 g/L BSA, aCSF) survived throughout the entire 360 minute observation period (and then were euthanized to obtain brain water content data).

13.4.2. Brain Water Content

The brain water contents for water-intoxicated animals (79.0% ± 0.09%; n = 5), water-intoxicated animals treated with a craniectomy (79.1% ± 0.21%; n = 4), and

water-intoxicated animals treated with an OTD (lumen solution: 350 g/L BSA, aCSF, pH 7.4) (80.1% ± 0.34%; n = 5) were significantly higher than brain water content for untreated control animals (77.0% ± 0.13%; n = 5) ($p < 0.001$ for all treatment groups compared to the Control group) (Figure 13.4). No significant difference in water content was observed among any of the treatment groups ($p > 0.05$).

While the brain water content of all treatment groups involving water intoxication was significantly higher than that of the untreated, injured control animals ($p < 0.001$), the brain water content of non-water intoxicated animals receiving either craniectomy (Control + C) or DOT treatment (Control + OTD) was not significantly different from untreated control animals ($p > 0.05$) (Table 13.1).

In addition, no significant differences were found in brain water content between hemispheres ipsilateral and contralateral to OTD application in any treatment group (Table 13.1).

### 13.4.3. Histology Following Direct Osmotherapy

To examine whether the use of the OTD was associated with any histological changes in tissue underneath the device, Nissl staining of the brain for non-water intoxicated animals treated with an OTD was performed. Nissl-stained histological sections (n = 3) demonstrated that there was minimal histological damage ipsilateral (Figure 13.5 Right) and contralateral (Figure 13.5 Left) to OTD application.

## 13.5. Discussion

The use of an OTD directly applied to the brain surface to enhance survival was validated in a cytotoxic model of cerebral edema. Conceivably, the OTD could be used flexibly to treat any anatomical location and severity of edema given that the appropriate device parameters (lumen

solution and concentration, flow rate, and contact surface area) are chosen to provide the therapeutically appropriate water removal rate.

### 13.5.1. Device Efficacy

In the present study, use of the OTD to treat induced cytotoxic edema resulted in markedly improved survival compared with no treatment or craniectomy only treatment. These results provide proof of principle for direct controlled water extraction as a novel form of treatment for cerebral edema. The device-brain surface contact is gentle, and simple application of the device is not associated with any histological damage. One important finding is that device application to a single small quadrant of the brain over the right hemisphere (based on atlas calculations we estimated contact of the device with approximately 17% of cortical surface area on the right hemisphere only) led to uniform water content throughout the brain and even in the contralateral hemisphere. These results suggest that even for large areas of hemispheric edema, the area of contact may not need to be extensive to attain adequate water extraction. This interesting result is likely due to rapid osmotic water equilibration via aquaporin-rich astrocyte networks (Verkman *et al.* 2006).

### 13.5.2. Implications for Treatment

One limitation of this study is that the results are confined to a model of "pure" cytotoxic edema (water intoxication). Post-stroke edema is thought to be largely cytotoxic in nature, whereas brain tumor edema and post-infectious edema are largely vasogenic, and posttraumatic edema is mixed cytotoxic and vasogenic (Marmarou 2003). Therefore, future studies will need to test the device for efficacy in models of vasogenic edema and more clinically relevant models of posttraumatic edema models.

## 13.6. Conclusion

A novel device to directly remove water from brain tissue in a controlled fashion was examined for its ability to treat severe cerebral edema induced by water intoxication. First, the use of the OTD, with the correct lumen solution properties, in conjunction with a craniectomy to apply the device to the brain *in vivo*, was validated. Second, in the water intoxication model, application of the OTD was demonstrated to be associated with significantly enhanced survival.

**Table 13.1.** Brain Water Content Analysis of Water Intoxicated Animals. The brain water content for the total tissue and left-right hemispheres for uninjured (Control) animals, untreated water intoxicated animals (W), water intoxicated animals treated with a craniectomy (W + C), water intoxicated animals treated with an OTD (lumen solution: 350 g/L BSA, aCSF, pH 7.4) (W + OTD), non-water intoxicated animals treated with a craniectomy (Control + C), and non-water intoxicated animals treated with a OTD (lumen solution: 350 g/L BSA, aCSF, pH 7.4) (Control + OTD) are presented as the mean ± SEM.

| | Treatment Time (min) | Brain Water Content (%) | | |
|---|---|---|---|---|
| | | Total | Left Hemisphere | Right Hemisphere |
| Control | N/A | 77.0 ± 0.13 | 77.0 ± 0.16 | 77.1 ± 0.11 |
| W | 31 ± 1.4 | 79.0 ± 0.09 | 79.0 ± 0.04 | 79.0 ± 0.15 |
| W + C | 48 ± 1.8 | 79.1 ± 0.21 | 79.1 ± 0.25 | 79.1 ± 0.17 |
| W + OTD | 333 ± 12.7 | 80.1 ± 0.34 | 80.0 ± 0.29 | 80.2 ± 0.41 |
| Control + C | 180 | 77.1 ± 0.08 | 77.0 ± 0.07 | 77.2 ± 0.11 |
| Control + OTD | 180 | 77.1 ± 0.03 | 77.0 ± 0.12 | 77.2 ± 0.06 |

Note that there were no ipsilateral vs. contralateral differences in the water content following OTD treatment and that the OTD itself did not dehydrate the tissue.

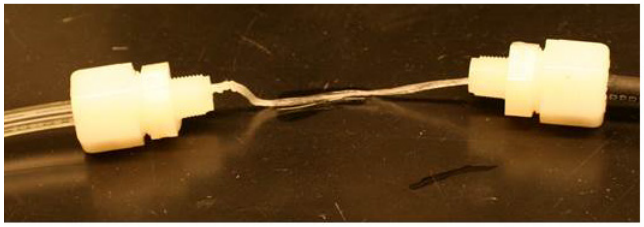

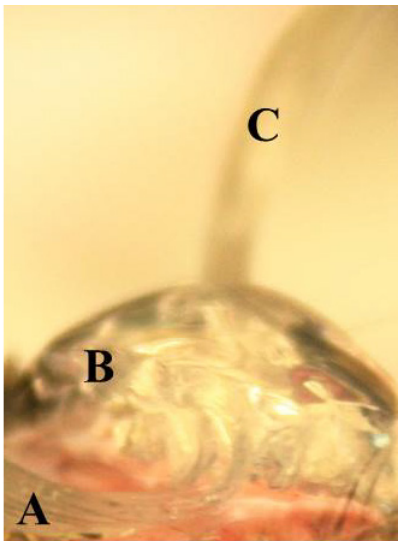


**Figure 13.1.** Application of the Osmotic Transport Device. **Left:** Picture of the OTD with the inlet and outlet ports. **Right:** The OTD applied to the tissue surface and embedded in a hydratable material. **A** is the inlet of the hollow fiber bundle. **B** is the hydratable material placed directly on the tissue surface on top of the hollow fiber bundle. **C** is the outlet of the hollow fiber bundle. Fluid passes through the hollow fibers at **A**, osmotically removes water from the tissue at **B**, and transports the water away from the injured tissue at **C**.

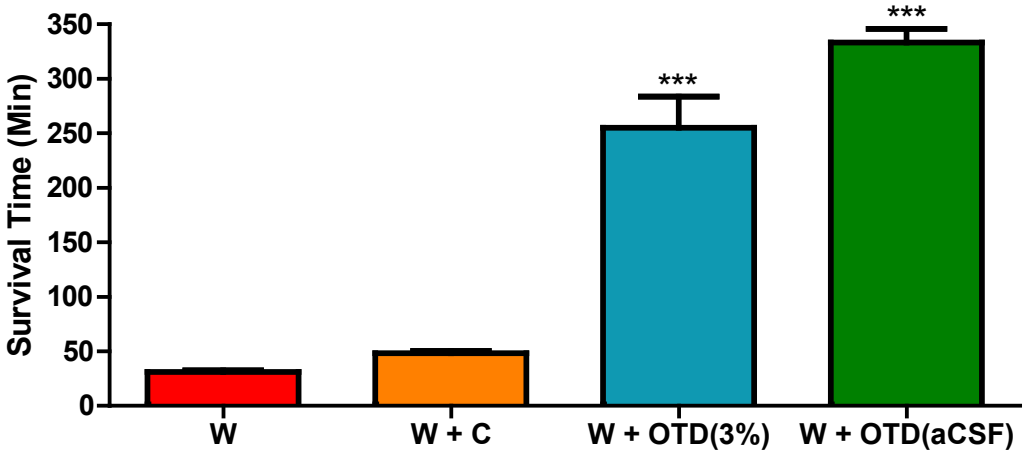


**Figure 13.2.** The Survival Time of Water Intoxicated Animals. The mean survival times of four groups are plotted for the time when animals expired. All animals in the untreated (W) and craniectomy treated (W + C) groups expired due to cerebral edema caused by the injury. One of the five animals in the OTD (lumen solution: 350 g/L BSA, 3% NaCl, pH 7.4) treated group (W + OTD(3%)) and one of the five animals in the OTD (lumen solution: 350 g/L BSA, aCSF, pH 7.4) treated group (W + OTD(aCSF)) expired due to injury. The remaining four animals in the latter two groups were sacrificed. *** $p < 0.001$ compared to untreated (W) and craniectomy treated (W + C) water intoxicated animals.

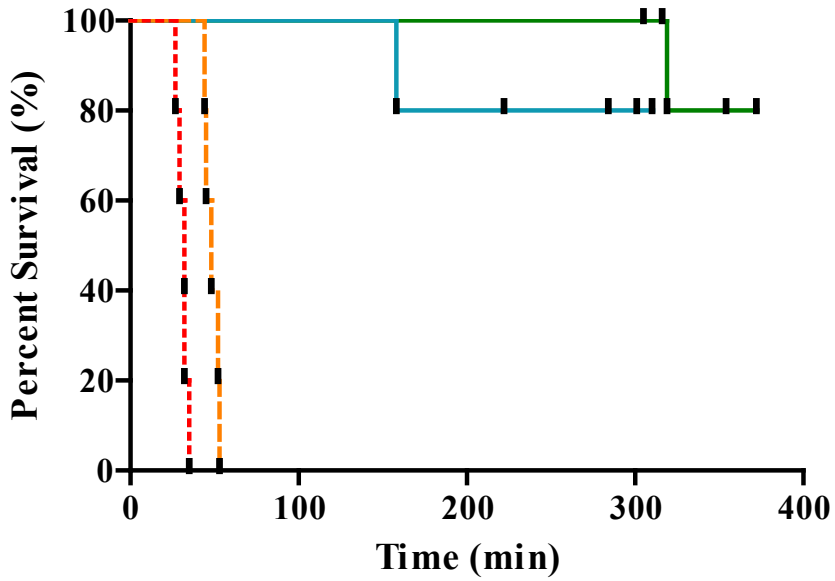


**Figure 13.3.** The Kaplan-Meier Survival Curve of Water Intoxicated Animals. Comparison of the survival curves for the untreated animals (red dotted curve), craniectomy treated animals (orange dashed curve), OTD (lumen solution: 350 g/L BSA, 3% NaCl, pH 7.4) treated animals (blue solid curve), and OTD (lumen solution: 350 g/L BSA, aCSF, pH 7.4) treated animals (green solid curve). Individual animals are depicted as closed ovals.

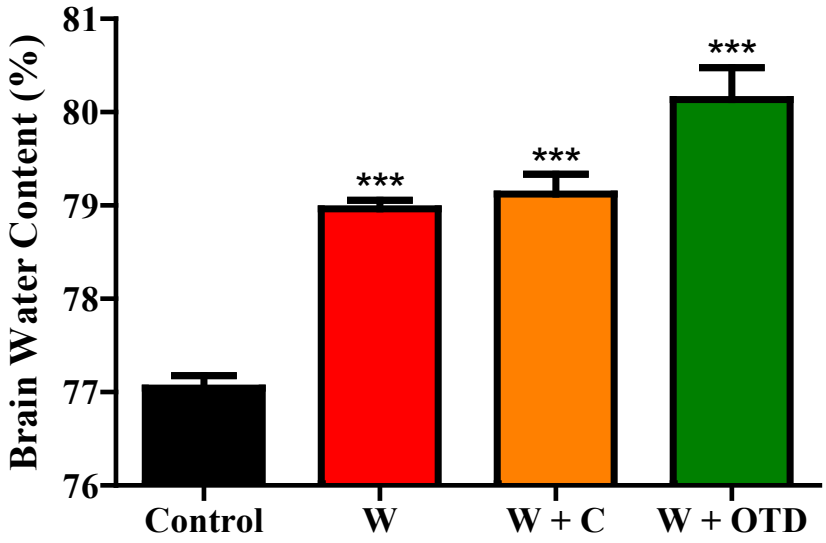


**Figure 13.4.** Brain Water Content Analysis of Water Intoxicated Animals. The brain water content (%) is compared for uninjured (Control) animals, untreated water intoxicated animals (W), water intoxicated animals treated with a craniectomy (W + C), and water intoxicated animals treated with an OTD (lumen solution: 350 g/L BSA, aCSF, pH 7.4) (W + OTD). *** $p < 0.001$ compared to non-water intoxicated animals (Control).

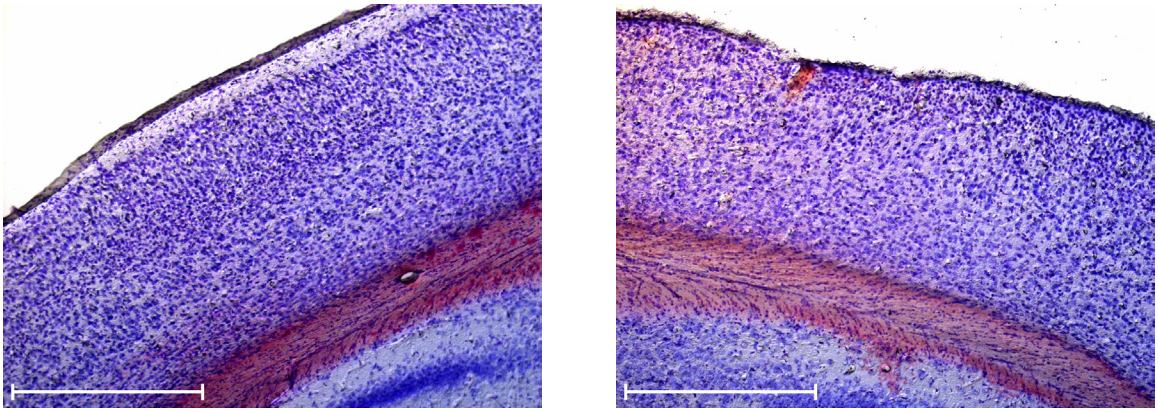

**Figure 13.5.** Photomicrographs Obtained After Direct Osmotherapy. Representative histological sections after three hours of OTD application in non-water intoxicated animals (n = 3). **Left:** Cortex contralateral to OTD application. **Right:** Cortex ipsilateral to OTD application. Scale bar = 500 μm.

# CHAPTER 14.

# AN OSMOTIC TRANSPORT DEVICE REDUCES CEREBRAL EDEMA FOLLOWING SEVERE TRAUMATIC BRAIN INJURY

## 14.1. Abstract

Cerebral edema is a significant cause of morbidity and mortality in many disease states, yet the current therapies of cerebral edema are often ineffective in treating severe edema. Here, the osmotic transport device (OTD) is used to treat animals with a traumatic brain injury (TBI). The brain water content of injured animals was successfully reduced back to normal levels following treatment with an OTD, while the brain water content of injured animals treated with a craniectomy was not reduced compared to that of untreated animals.

## 14.2. Traumatic Brain Injury

TBI is the foremost cause of morbidity and mortality in persons under 45 years of age worldwide, and accounts for a larger number of casualties in combat in Iraq and Afghanistan than in any other recent U.S. war (Marmarou 2003; Park *et al.* 2008). In the U.S., about 200,000 victims of TBI need hospitalization annually, and approximately 52,000 U.S. deaths per year result from TBI (Marmarou 2003). TBI can be divided into two phases: primary and secondary injury. Primary injury is caused by the direct external mechanical force, whereas secondary injury refers to a cascade of delayed deleterious physiological events that may last from hours to days. Secondary injury plays a major role in the morbidity and mortality resulting from TBI, and is characterized by ischemia, blood-brain barrier (BBB) rupture, and cerebral edema (Kettenmann and Ransom 2005).

14.2.1. Traumatic Brain Injury in the General Population

The 2010 report of the U.S. Department of Health and Human Services Centers for Disease Control and Prevention National Center for Injury Prevention and Control showed that the most prevalent causes of TBI are falls (35%), motor vehicle and traffic accidents (17%), struck by or against an object (16.5%), assault (10%), and unknown/other (21%).[*] Of these occurrences, approximately 60% of the hospitalized patients who suffer from severe TBI die or survive with major disabilities (Murray *et al*. 1999; Myburgh *et al.* 2008; Stocchetti *et al.* 2008).

14.2.2. Traumatic Brain Injury in the Military

In addition to being the leading cause of morbidity and mortality in the general population, TBI are becoming more increasingly common in combat due to the advances in medical care, as well as due to the use of cost-effective explosives (Warden 2006). It is estimated that between 12 - 20% of Iraq and Afghanistan veterans have received a TBI (Hoge *et al.* 2008; Schneiderman *et al.* 2008).

14.2.3. Impacts on the Healthcare System

The burden of traumatic brain injury placed on the U.S. healthcare system is more than $60 billion (Maas *et al.* 2010). Since the most affected age range by TBI are persons between 18 and 45 years old, it is imperative to develop treatments which can prevent functional damage to reduce the morbidity for these persons. The ideal treatment would allow them to regain full, or near-full, function to reduce the burden on the healthcare system.

[*] U.S. Department of Health and Human Services Centers for Disease Control and Prevention National Center for Injury Prevention and Control, 2010 (www.cdc.gov/TraumaticBrainInjury).

## 14.3. Methods

In the present study, the reduction of edema for severe TBI is compared for treatment via a craniectomy and direct osmotherapy (DOT) via an OTD. The mechanisms of water removal from brain tissue are explained for these two treatments and a discussion is provided on the components of the OTD.

### 14.3.1. Osmotic Transport Device

Briefly, the OTD consists of hollow fibers embedded in a moldable hydratable material, such as a hydrogel or dura substitute material. The hydratable material is in direct contact with and conforms to the exposed injured tissue, following a craniectomy, to maximize the treatment area.

A lumen solution is flowed through the hollow fibers at a flowrate so that the Reynolds number is less than 100. The lumen solution consists of an osmotic agent, such as proteins or polymers, in an aqueous salt solution. The osmotic agent is chosen for its ability to: (1) induce osmotic pressure greater than the transmembrane pressure across the hollow fiber, (2) allow for a range of osmotic pressures to be achieved by varying its concentration, and (3) be impermeable to the hollow fiber pores.

In this study, the lumen solution was 350 g/L bovine serum albumin (BSA) in artificial cerebrospinal fluid (aCSF), pH 7.4. BSA was the chosen osmotic agent because its concentration-dependent osmotic pressure range is well-known (Vilker *et al.* 1981; Yousef *et al.* 1998b) and its concentration-dependent viscosity is manageable (Buccola 2010). The BSA is also impermeable to the hollow fibers used (regenerated cellulose, 13 kDa molecular weight cut-off (MWCO), 132294, Spectra/Por, Inc.). aCSF, chosen in order to aid in ion balance, was prepared as previously described (Csenkér *et al.* 1982). The hydratable material used was an agar hydrogel

(0.3% agar in aCSF). The treatment area of the cerebral cortex was $13.7 \pm 0.4$ mm$^2$ (mean ± SEM).

14.3.2. Animals and Surgical Technique

All experiments were conducted under protocols (A-2010-0018) approved by the University of California, Riverside IACUC. Adult female eight- to seventeen-week-old CD-1 mice were used in all experiments.

The six experimental groups were: (1) no injury (Control), (2) no treatment (TBI only), (3) TBI treated with a craniectomy only, (4) TBI treated with a craniectomy and a hydratable material placed on the exposed tissue, (5) TBI treated using an OTD without BSA (only aCSF, no osmotic agent), and (6) TBI treated with DOT via an OTD with BSA.

Prior to induction of cerebral edema via controlled cortical impact (CCI), animals were anesthetized with an 80 mg/kg ketamine, 10 mg/kg xylazine mixture (0.09% of body weight). After determining an adequate plane of anesthesia via the loss of paw pinch reflex, surgical procedures began. The reflex activity was monitored continuously throughout the entire study and supplemental doses of half of the initial dose were administered as needed.

Anesthetized animals were placed into a standard rodent stereotactic frame. A midline skin incision was made and reflected. A right-sided craniectomy was performed (anterior border: coronal suture, posterior border: lambdoid suture, medial border: midline, lateral border: temporalis attachment).

14.3.3. Severe Traumatic Brain Injury Model

Severe TBI was induced via CCI. A 3 mm impactor tip was discharged at a 20$^o$ angle with a velocity of 5.0 m/s with a 200 ms dwell time and an impact depth of 1.0 mm. After TBI

was induced, the skull was replaced for three hours to allow for the formation of edema. For the TBI only group, the skull remained intact for a total of five hours.

After the formation of edema (three hours), treatment began and lasted for two hours. For all treatment groups, a second craniectomy was performed and the dura was carefully and atraumatically opened with microdissection. Post dura removal, treatment began and was either a craniectomy, a craniectomy with a hydratable material, an OTD without BSA, or an OTD with BSA.

### 14.3.4. Endpoint: Brain Water Content

Reduction of cerebral edema was determined by analyzing the brain water content. After the treatment procedure, brains were dissected out post-mortem, separated into four pieces (right-left hemispheres, cerebrum-cerebellum pieces), and subjected to wet-dry weight comparisons to determine tissue water content as previously described (Zweckerberger *et al.* 2006; Gill *et al.* 2011) (Eqn. 13.1).

### 14.3.5. Data Analysis

Intergroup comparisons of survival times and brain tissue water content were done using one-way ANOVA and post-hoc Bonferroni tests. Brain water content values are presented as the mean ± SEM.

## 14.4. Results

During the experiments, mortality was observed due to the severity of the TBI induced. Three of the eight (37.5%) untreated TBI animals, one of the seven (14.3%) TBI animals treated with a craniectomy, one of the six (16.7%) TBI animals treated using an OTD, zero of the three

animals treated with a craniectomy and hydrogel, and zero of the three animals treated with an OTD without BSA expired over the five hour monitoring period. Animals expiring over this time period were excluded from the 5-hour brain water content analysis. The remainder of the animals provided useful information about the effects of the various treatments on our outcome variable (brain water content).

### 14.4.1. Brain Water Content

The brain water content of all groups was analyzed for the rostral-right hemisphere (right cerebrum) (ipsilateral to the injury and OTD placement), rostral-left hemisphere (left cerebrum), and total tissue (Table 14.1). Statistical significance is observed for the rostral-right hemisphere brain water content between untreated, injured control animals (Control, 77.97 ± 0.094%, n = 7) and untreated TBI animals (TBI, 79.10 ± 0.096%, n = 5) ($p < 0.001$), TBI animals treated with a craniectomy only (TBI + C, 78.79 ± 0.142%, n = 6) ($p < 0.01$), TBI animals treated with a craniectomy and a hydrogel (TBI + C + G, 79.04 ± 0.292%, n = 3) ($p < 0.01$), and TBI animals treated using an OTD without BSA (TBI + OTD w/o BSA, 78.78 ± 0.037%, n = 3) ($p < 0.05$) **(**Figure 14.1**)**. No statistical significance was observed for the rostral-right hemisphere brain water content between the control animals and the TBI animals treated using an OTD (TBI + OTD, 78.42 ± 0.184%, n = 5) ($p > 0.05$).

No significant difference in rostral-right hemisphere brain water content was observed among the untreated TBI animals, TBI animals treated with a craniectomy, TBI animals treated with a craniectomy and a hydrogel, and TBI animals treated using an OTD without BSA ($p > 0.05$). The brain water content of TBI animals treated using an OTD was significant compared to that of the untreated TBI animals ($p < 0.05$).

For all treatments, no change was observed for the brain water content of the contralateral hemisphere (rostral-left hemisphere) compared to that of the control animals nor was there any difference in the total brain water content of any treated groups compared to that of the control animals ($p > 0.05$). The lack of an effect of the OTD on the brain water content of the entire brain tissue and the contralateral hemisphere suggests that the OTD at the chosen parameters and solution properties (350 g/L BSA, aCSF, pH 7.4) is not so aggressive as to dehydrate the uninjured brain tissue.

## 14.5. Discussion

Here an OTD was utilized to reduce posttraumatic cerebral edema following a TBI via DOT. This study provides several novel findings not observed in the water intoxication model. First, an OTD is capable of reducing cerebral edema in a mixed model of cerebral edema (TBI). Second, an OTD demonstrates enhanced water removal, and thus can treat edematous tissue more rapidly than a craniectomy alone. Third, an osmotic agent is required for successful treatment via an OTD. Fourth, an OTD can treat focal injuries while preventing the dehydration of the surrounding tissue.

### 14.5.1. Water Transport and Mechanisms of Water Removal From Brain Tissue

Any new treatment aimed at treating cerebral edema must be capable of removing water from the injured tissue in order to prevent further (secondary) damage. Here, the possible mechanisms for removal of water from the studied treatment groups are examined (Figure 14.2). The transport of water into the injured tissue (red) following a TBI is shown by the blue arrows (Figure 14.2.A). For the treatments described in this work, the transport of water into the brain tissue in response to the injury remains unaffected. In addition, despite the general flow of water

into the tissue, the regulatory mechanisms for removing water from the tissue via astrocytes may still be in effect, yet unable to cope with the magnitude of water transport into the tissue, thus requiring treatment to relieve the edema.

If the injury is treated via a craniectomy, the water is indirectly removed. While a craniectomy is primarily for reducing the ICP, water may be removed by evaporation from the surface of the brain (dashed curved green arrows) (Figure 14.2.B). This mechanism of water removal is driven by the amount of the water in the tissue and the partial pressure of the water in the air that the tissue is exposed to, and can be approximated by Henry's law (Truskey *et al.* 2004).

When a hydrogel (light blue) is applied to the exposed tissue following a craniectomy, water is transported into the tissue due to the water chemical potential in the hydrogel compared to its chemical potential in the brain tissue (Figure 14.2.C). The gradient of the chemical potential of water is towards the brain tissue and thus the diffusion of water proceeds into the tissue until equilibrium is established (*i.e.* the chemical potential of water in the hydrogel is equal to the chemical potential of water in the tissue). The green arrows display the diffusive water flux into the brain tissue from the hydrogel. The flux can be approximated by Fick's law assuming that the diffusion coefficient of the water is independent of its concentration (Truskey *et al.* 2004). Of course, the absolute mass of water transported can be quite small if the volume of the hydrogel and/or the hydrogel-tissue contact area is minimal.

However, when hollow fibers are placed within the hydrogel, and an aCSF lumen solutions (no osmotic agent) is passed through them (blue circles) (Figure 14.2.D), there is a flux of water from the tissue into the hydrogel, then into the hollow fibers, and is ultimately transported away from the injured tissue. The chemical potential of water in the aCSF solution is such that the gradient of water diffusion is shifted towards the hollow fibers. Similar to the case in

which only the hydrogel is present on the injured tissue, the flux can be approximated by Fick's law (Truskey *et al.* 2004). However, in this case, the flux of water, driven by the gradient of the chemical potential of water, is from the brain tissue to the hollow fibers containing aCSF (green arrows).

Finally, when an osmotic agent is used within the lumen solution, the OTD is capable of treating the tissue by DOT. With this treatment method, the flux of water, still with the chemical potential gradient of water in the direction of the hollow fibers (pink circles), is osmotically driven (Figure 14.2.E). The osmotically driven flux, $J$, can be approximated using the Kedem-Katchalsky equation (Eqn. 14.1) (Kedem and Katchalsky 1958).

$$J = \frac{\left(\Delta P - \sigma \Delta \pi\right)}{\mu\left(R_m + R_h\right)}, \tag{14.1}$$

where $\Delta P$ is the transmembrane pressure, $\Delta \pi$ is the osmotic pressure, $\sigma$ is the reflection coefficient which provides a measure of the membrane permselectivity, $\mu$ is the permeate viscosity, $R_m$ is the membrane resistance to the flow of water, and $R_h$ is the hydratable material resistance to the flow of water.

This design clearly allows for osmotic water extraction from edematous tissue, as indicted by the right-most bar in Figure 14.1, hence satisfying the requirement for an osmotic transport device. Optimized OTD design includes minimization of the transmembrane pressure and resistances of the hollow fibers and hydratable material, maximization of the osmotic pressure within the lumen solution, and selection of the hollow fiber membrane MWCO such that the osmotic agent is completely rejected (preventing transport into the tissue) ($\sigma = 1$).

With a sufficiently high osmotic pressure, such that the osmotic pressure is much larger than the transmembrane pressure ($\Delta \pi > \Delta P$), the osmotically driven flux is greater than the diffusive flux (shown by the increased magnitude of the green arrows) (Figure 14.2.E).

Osmotically driven water flux has the capability of controllability which can be altered to provide a therapeutic effect for any duration and/or magnitude of edema.

14.5.2. Device Design and Efficacy

Developing an OTD to treat severe cerebral edema presents several technical challenges. First, the lumen solution needs to be carefully selected such that it provides a chemical potential gradient of water capable of removing water from the injured tissue. The BSA was carried in aCSF to maintain ion similarities between the lumen solution and the tissue. In this study, the beneficial effect of an impermeable osmotic agent (BSA) was tested. As seen by analyzing the brain water content of the rostral-right hemisphere, the osmotic agent is required to have a reduction in the brain tissue water content following TBI.

Second, the selection of a hydratable material is paramount. The chosen hydratable material must offer structural support for the hollow fibers, provide minimal resistance to water transport, and prevent water flux from the hydratable material into the tissue (*i.e.* water flows only away from the injured tissue). Here, an agar hydrogel was utilized as the hydratable material. While the use of a 0.3% agar hydrogel is capable of structural support and allowing easy passage of water, it does not have negligible water transport in the direction of the tissue (specifically in the absence of an OTD). When a 0.3% agar hydrogel is used with a craniectomy, the brain water content has a mean higher than that of untreated TBI animals. This observation is explained by the larger water content of the hydrogel (approximately 99%) compared to that of the brain tissue (approximately 78%). The use of a 0.3% agar hydrogel can be replaced with alternative hydratable materials, such as other FDA approved materials (*i.e.* dural substitutes which are hydratable collagen matrices), to achieve optimal DOT via an OTD. An ideal hydratable material would have water content similar to, or lower than, that of uninjured brain tissue.

### 14.5.3. Implications for Treatment

One limitation of this study is that our results are confined to an acute treatment of TBI. Here, edema was allowed to form for three hours prior to treatment. However, edema is known to increase over 24 to 48 hours (Zweckberger *et al.* 2006). Therefore, future studies need to address the treatment of maximum edema formation to determine the effectiveness DOT via an OTD and length of treatment required to completely and irreversibly reduce edema following severe TBI.

Another limitation of this study is that these results show a reduction in brain water content but whether this translates to improved neurological outcome is unknown. Future studies also need to address the effects of DOT via an OTD on the neurological function of animals receiving a severe TBI.

A third limitation of the OTD used in this study is the choice of hydratable material. While many biocompatible materials may be selected, it is essential to use a material that is hydratable (allows for water to be absorbed and transported within/through) but also has a water content similar to, or slightly lower than, uninjured tissue (78% water content) to prevent water transport into the injured tissue and optimize DOT via an OTD. The effect of the chosen hydratable material and its water content on the efficacy of DOT via an OTD remains to be examined.

## 14.6. Conclusion

In summary, the use of an OTD to directly remove water and reduce cerebral edema was validated in a severe TBI model. This represents a novel concept in the treatment of severe TBI, and is the first direct surface contact-based treatment for TBI-associated edema. Future studies will need to validate the longer-term efficacy of an OTD to treat posttraumatic edema, understand the device's effectiveness for improving neurological function, and optimize the flux of DOT via

an OTD. Given the appropriate device parameters, an OTD may be used to treat and reduce moderate to severe cerebral edema and improve neurological outcome. Furthermore, such a device may be amenable to online feedback control to titrate levels of water removal to suit particular severities of cerebral edema. Ultimately, the BTF guidelines may be altered to include treatment by an OTD, or another DOT, for moderate to severe TBI.

**Table 14.1.** Brain Water Content Analysis of Animals With Traumatic Brain Injury. The water content of total brain tissue, rostral-left hemisphere tissue, and rostral-right hemisphere tissue are presented for uninjured, untreated animals (Control), TBI injured animals receiving no treatment (TBI), TBI injured animals treated with a craniectomy (TBI + C), TBI injured animals treated with a craniectomy and a hydrogel (TBI + C + G), TBI injured animals treated using an OTD without BSA in the lumen solution (TBI + OTD - BSA), and TBI injured animals treated using an OTD (TBI + OTD).

| | Brain Water Content (%) | | |
|---|---|---|---|
| | Total | Rostral-Left Hemisphere | Rostral-Right Hemisphere |
| Control | 77.15 ± 0.120 | 77.79 ± 0.130 | 77.97 ± 0.094 |
| TBI | 77.80 ± 0.193 | 78.04 ± 0.150 | 79.10 ± 0.096 |
| TBI + C | 77.86 ± 0.166 | 78.21 ± 0.159 | 78.79 ± 0.142 |
| TBI + C + G | 77.69 ± 0.150 | 77.78 ± 0.220 | 79.04 ± 0.292 |
| TBI + OTD - BSA | 77.55 ± 0.067 | 77.88 ± 0.060 | 78.78 ± 0.037 |
| TBI + OTD | 77.43 ± 0.100 | 77.80 ± 0.098 | 78.42 ± 0.184 |

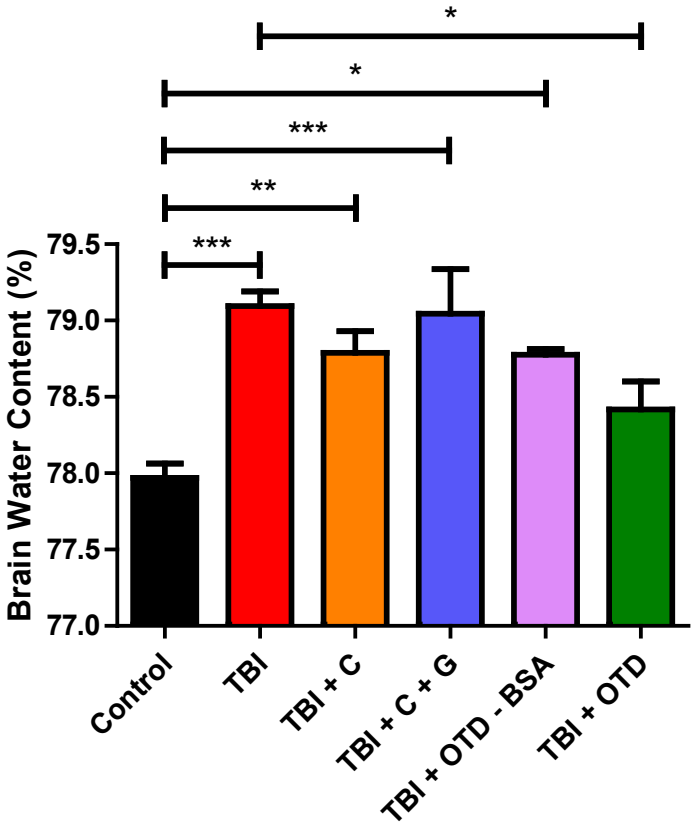


**Figure 14.1.** Brain Water Content Analysis of Animals With Traumatic Brain Injury. Brain water content (%) of rostral-right hemisphere is shown for untreated, uninjured control animals (Control), injured animals receiving no treatment (TBI), injured animals treated with craniectomy only (TBI + C), injured animals treated with a craniectomy and a hydrogel (TBI + C + G), injured animals treated using an OTD without BSA (TBI + OTD - BSA), and injured animals treated using an OTD (TBI + OTD). The brain water content of control animals was significantly different from that of untreated TBI animals (***, $p < 0.001$), animals treated with a craniectomy (**, $p < 0.01$), animals treated with a craniectomy and a hydrogel (**, $p < 0.01$), and animals treated using an OTD without BSA (*, $p < 0.05$). No significance is observed between the brain water content for control animals and that of animals treated using an OTD ($p > 0.05$). Statistical significance is also observed for brain water content between untreated TBI animals and animals treated using an OTD (*, $p < 0.05$). No significance was observed between any of the other treated TBI animal groups.

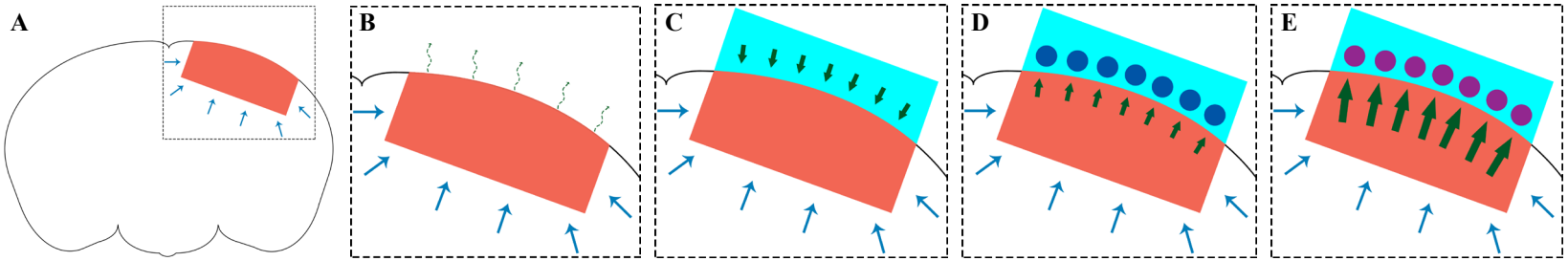


**Figure 14.2.** Transport of Water Through Brain Tissue for Four Treatments. **A.** Schematic of the mouse brain and the injury site following TBI (from CCI) is presented with the injury site and penetration into the tissue shown in red. The water transport into the injured tissue is shown by the blue arrows. **B.** Schematic of the injured mouse brain showing water transport and removal via a craniectomy. The possible mechanism of indirect water removal by a craniectomy is evaporation (dashed curved green arrows) which can be approximated by Henry's law (Truskey *et al.* 2004). **C.** Schematic of the injured mouse brain showing water transport with only the hydrogel (light blue) placed on the tissue following a craniectomy. Due to the chemical potential gradient of water, water flows (via diffusion) from the hydrogel into the brain tissue (green arrows). The water diffusion can be approximated by Fick's law (Truskey *et al.* 2004). **D.** Schematic of the injured mouse brain showing water transport and removal by an OTD with no osmotic agent in the lumen solution. The aCSF lumen solution allows for the water flux to be in the direction (green arrows) of the hollow fibers (blue circles). The water flux is approximated by Fick's law (Truskey *et al.* 2004). **E.** Schematic of the injured mouse brain showing water transport and removal by DOT via an OTD. The osmotic agent allows for the chemical potential gradient of water to be towards the OTD. Osmotically driven flow (Kedem and Katchalsky 1958) causes the water to be transported (green arrows) into the hollow fibers (pink circles) for removal from the injured tissue. DOT via an OTD has the capability for enhanced water removal compared to diffusive flux (increased magnitude of the green arrows compared to **D**).

# CHAPTER 15.

# CONCLUSIONS

## 15.1. Findings of This Work

The successful treatment of mice with cerebral edema by direct osmotherapy (DOT) via an osmotic transport device (OTD) has been shown in two models of severe cerebral edema: water intoxication and traumatic brain injury.

The first model of severe cerebral edema, water intoxication induced by a 30% bolus intraperitoneal injection, was previously fatal 100% of the time within 60 minutes for treated and untreated animals. The use of an OTD improved the percent survival of injured animals to 80%. This survival improvement was significant compared to the gold standard for severe cerebral edema, a craniectomy. The percent survival for animals treated with a craniectomy was 0%.

The second model of severe cerebral edema, traumatic brain injury induced by an open skull controlled cortical impact, caused an increase in the brain tissue water content of treated (non-OTD treated) and untreated animals. When the OTD was used to treat the injured animals, the brain water content was reduced compared to the untreated, injured animals. Furthermore, the brain water content for injured animals treated with an OTD was similar to that of the uninjured, untreated animals.

The OTD transport properties studied for various BSA lumen solutions to obtain the maximum flux of water for the chosen properties. The material properties of four hydratable materials (three agar hydrogels and one dura substitute matrix) was studied; the water content, water uptake rate, and swelling volumes were determined.

## 15.2. Future Directions

Herein, the OTD was used to treat a global brain tissue swelling, pure cytotoxic model and a focal (cortical), mixed edema injury model. There are various other models which can be used to study the efficacy of an OTD for treatment of cerebral edema (stoke and tumor models) and/or treatment of other types of edema, such as spinal cord swelling.

Future work also includes optimization of the OTD components, scale-up of the OTD for use in large animal models, and treatment of these animals. While preliminary investigations were presented in this dissertation, other hydratable materials need to be examined to improve the efficacy of the OTD. The OTD also needs to be scaled-up for use in a large animal model. The pig model offers many similarities to the human brain, and thus would be the most appropriate model to study TBI in prior to going to clinical trials.

Ultimately, it is expected that an OTD, or similar DOT, will be included in the BTF Guidelines for treatment of severe cerebral edema.

# PART 3.

# APPENDICES

# APPENDIX A.

# DEVELOPMENT OF THE MOLECULAR STRUCTURE OF BOVINE SERUM ALBUMIN

## A.1. Molecular Structure of Serum Albumin

In order to study bovine serum albumin (BSA) utilizing molecular modeling software, the molecular structure is required. However, the structure for BSA was not deposited in the Protein Data Bank until recently (Bujacz 2012; Majorek *et al.* 2012).

During the development of the free-solvent model for predicting the solvent accessible surface area of proteins (M$^{c}$Bride and Rodgers 2012), no structure had been deposited, so the structure of BSA was created using the molecular structure of human serum albumin (HSA) as the template for homology modeling.

### A.1.1. Structure of Human Serum Albumin

The structure of HSA based on x-ray diffraction, deposited in the Protein Data Bank (PDB: 1BM0 (Sugio *et al.* 1999)), contained the dimer. While the structure is for the HSA dimer, BSA can be found as a monomer (such as in water) or as a solution containing monomers, dimers, and trimmers (such as in salt solutions) (Appendix C). For the BSA homology model, only the monomer structure of HSA was used to create the structure of BSA.

## A.2. Validation of Human Serum Albumin as the Homology Model Template

Prior to using HSA as the template for the structure of BSA, the sequences of both proteins were aligned to determine the amount of identity. It is generally accepted that if two sequences have an identity (or similarity) of greater than 40%, the structure and function of both

proteins are very similar. This has been observed for approximately 95% of proteins with similar structure and function. When the sequence identity is greater than 20%, the proteins are likely to have a similar structure (Petsko and Ringe 2004). In the case of HSA and BSA, it is known that the functions are similar.

The sequence alignments require the primary structure (amino acid sequence) of each protein. For HSA, the PDB file (1BM0 (Sugio *et al.* 1999)) contained the amino acid sequence (in the FASTA sequence file) of the molecular structure which was 585 amino acids. The sequence of BSA (P02769) was obtained from UniProt (which contains the sequences of proteins (Jain *et al.* 2009)). The BSA sequence contained 607 amino acids which is significantly more than that of the HSA structure. Therefore, the sequence of HSA (P02768) was also obtained from UniProt for comparison with the sequence in the FASTA sequence file.

### A.2.1. Human Serum Albumin Sequence Alignment

The sequence of HSA from UniProt (P02768) was aligned to the sequence of HSA in the FASTA sequence file (PDB: 1BM0 (Sugio *et al.* 1999)). The UniProt sequence contained 609 residues for HSA, while the sequence in the PDB file contained 585 residues.

These two sequences were aligned using ClustalW2 (Larkin *et al.* 2007). All residues in the sequences were identical, save that the UniProt sequence contained 24 residues not included in the FASTA sequence file of the molecular structure. These additional 24 residues in the UniProt sequence were located at the N-terminus of the protein (Figure A.1).

For many secreted proteins, a signal peptide (or signal sequence) is included on the folded protein which codes for the protein's destination. When a folded protein still contains the signal peptide, it is considered to be the immature form (called the nascent protein). Following cleavage of the signal peptide, the protein is mature and fully functional.

The 24 residues present in the UniProt file which were absent from the FASTA sequence file were assumed to be cleaved during the maturation of HSA; the UniProt sequence is that of the nascent HSA protein (UniProt states that this sequence of HSA is further processed into a mature form), while the PDB file protein was assumed to be that of the mature protein. The latter assumption is valid because the PDB file sequence was obtained from the purified HSA protein (Sigma Cat. No. A-3782) and that all 24 residues were present at the N-terminus of HSA. Thus, in order to obtain the sequence of the mature HSA, these 24 residues were removed from the UniProt sequence.

### A.2.2. Sequence Alignment of Nascent Human Serum Albumin and Nascent Bovine Serum Albumin

To determine the similarity of the signal peptide between HSA and BSA, the UniProt sequences for nascent HSA (P02768) and nascent BSA (P02769) were compared using ClustalW2 (Figure A.2).

The nascent BSA has 607 residues, while the nascent HSA has 609 residues. One of the two residues that are not in BSA is the C-terminus, while the other residue is in the interior of the protein. The signal peptide sequence of BSA was identical to that of HSA except for a single residue which has similar properties. The assumption that the first 24 residues of the HSA sequence (at the N-terminus) are the signal peptide was confirmed by the identity of the two signal peptide sequences (Patterson and Geller 1977).

A.2.3. Sequence Alignment of Mature Human Serum Albumin and Mature Bovine Serum Albumin

Following "cleavage" of the signal peptide from the nascent BSA sequence creating the "mature" BSA sequence, ClustalW2 (Larkin *et al.* 2007) and T-COFFEE (Notredame *et al.* 2000) were used for sequence alignments (Figure A.3). The identity of the sequence alignment was found to be 99% and 75% for ClustalW2 and T-COFFEE, respectively. Thus the assumption of similar structure is valid, and therefore HSA can be used as the homology model for BSA.

A.3. Structure of Bovine Serum Albumin

After the sequence alignments, and validation of HSA as a homology model for BSA, the structure of BSA was created using the MODELLER software (Eswar *et al.* 2006). The software creates the 3-D structure of a protein using the sequence of that protein (BSA) and another protein's 3D structure (HSA) as a template.

Following the BSA structure creation, Swiss-Pdb Viewer (Guex and Peitsch 1997) was used to view the structure and to determine any structural clashes. There were 141 non-conserved residues of which 82 were very similar, 24 similar, and 35 not similar. All of the non-conserved residues were analyzed for possible changes to structure after the BSA structure was created; the 24 similar and 36 not similar residues were further analyzed for any disruptions to the interior of the protein and for electrostatic repulsion.

Energy minimization was applied to the structure of BSA to relax the structure and remove any van der Waals (vdw) clashes and electrostatic clashes. No vdw clashes were present in the original structure obtained from MODELLER, however, upon analysis of the residue changes from HSA to BSA (Figure A.4), there seemed to be some steric and electrostatic hindrances; after energy minimization, the torsion angles for these residues were minimally

altered. The structures of BSA (post-energy minimization) and HSA are nearly identical (Figure A.5).

```
sp|P02768|HSA      MKWVTFISLLFLFSSAYSRGVFRRDAHKSEVAHRFKDLGEENFKALVLIAFAQYLQQCPFEDHVKLVNEVTEFAKTC 77
HSA PDB: 1BM0      ----------------------DAHKSEVAHRFKDLGEENFKALVLIAFAQYLQQCPFEDHVKLVNEVTEFAKTC 53
                                         **************************************************

sp|P02768|HSA      VADESAENCDKSLHTLFGDKLCTVATLRETYGEMADCCAKQEPERNECFLQHKDDNPNLPRLVRPEVDVMCTAFHDN 154
HSA PDB: 1BM0      VADESAENCDKSLHTLFGDKLCTVATLRETYGEMADCCAKQEPERNECFLQHKDDNPNLPRLVRPEVDVMCTAFHDN 130
                   ********************************************************************************

sp|P02768|HSA      EETFLKKYLYEIARRHPYFYAPELLFFAKRYKAAFTECCQAADKAACLLPKLDELRDEGKASSAKQRLKCASLQKFG 231
HSA PDB: 1BM0      EETFLKKYLYEIARRHPYFYAPELLFFAKRYKAAFTECCQAADKAACLLPKLDELRDEGKASSAKQRLKCASLQKFG 207
                   ********************************************************************************

sp|P02768|HSA      ERAFKAWAVARLSQRFPKAEFAEVSKLVTDLTKVHTECCHGDLLECADDRADLAKYICENQDSISSKLKECCEKPLL 308
HSA PDB: 1BM0      ERAFKAWAVARLSQRFPKAEFAEVSKLVTDLTKVHTECCHGDLLECADDRADLAKYICENQDSISSKLKECCEKPLL 284
                   ********************************************************************************

sp|P02768|HSA      EKSHCIAEVENDEMPADLPSLAADFVESKDVCKNYAEAKDVFLGMFLYEYARRHPDYSVVLLLRLAKTYETTLEKCC 385
HSA PDB: 1BM0      EKSHCIAEVENDEMPADLPSLAADFVESKDVCKNYAEAKDVFLGMFLYEYARRHPDYSVVLLLRLAKTYETTLEKCC 361
                   ********************************************************************************

sp|P02768|HSA      AAADPHECYAKVFDEFKPLVEEPQNLIKQNCELFEQLGEYKFQNALLVRYTKKVPQVSTPTLVEVSRNLGKVGSKCC 462
HSA PDB: 1BM0      AAADPHECYAKVFDEFKPLVEEPQNLIKQNCELFEQLGEYKFQNALLVRYTKKVPQVSTPTLVEVSRNLGKVGSKCC 438
                   ********************************************************************************

sp|P02768|HSA      KHPEAKRMPCAEDYLSVVLNQLCVLHEKTPVSDRVTKCCTESLVNRRPCFSALEVDETYVPKEFNAETFTFHADICT 539
HSA PDB: 1BM0      KHPEAKRMPCAEDYLSVVLNQLCVLHEKTPVSDRVTKCCTESLVNRRPCFSALEVDETYVPKEFNAETFTFHADICT 515
                   ********************************************************************************

sp|P02768|HSA      LSEKERQIKKQTALVELVKHKPKATKEQLKAVMDDFAAFVEKCCKADDKETCFAEEGKKLVAASQAALGL         609
HSA PDB: 1BM0      LSEKERQIKKQTALVELVKHKPKATKEQLKAVMDDFAAFVEKCCKADDKETCFAEEGKKLVAASQAALGL         585
                   ***********************************************************************
```

**Figure A.1.** ClustalW2 Sequence Alignment for Nascent HSA and Mature HSA; nascent HSA: UniProt P02768, mature HSA: PDB Code 1BM0. Residues 1-24 are not present in the mature HSA sequence, and thus are cleaved during maturation. * represent identical residues, : represent very similar residues (similar properties), . represents similar residues, and blank represents no similarity.

```
sp|P02768|HSA      MKWVTFISLLFLFSSAYSRGVFRRDAHKSEVAHRFKDLGEENFKALVLIAFAQYLQQCPFEDHVKLVNEVTEFAKTC 77
sp|P02769|BSA      MKWVTFISLLLLFSSAYSRGVFRRDTHKSEIAHRFKDLGEEHFKGLVLIAFSQYLQQCPFDEHVKLVNETEFAKTCL 77
                   **********:**************:****:**********:**.******:********::*******:*******

sp|P02768|HSA      VADESAENCDKSLHTLFGDKLCTVATLRETYGEMADCCAKQEPERNECFLQHKDDNPNLPRLVRPEVDVMCTAFHDN 154
sp|P02769|BSA      VADESHAGCEKSLHTLFGDELCKVASLRETYGDMADCCEKQEPERNECFLSHKDDSPDLPKLK-PDPNTLCDEFKAD 153
                   *****  .*:**********:**.**:******:***** ***********.****.*:**:*  *: ::.:*  *: :

sp|P02768|HSA      EETFLKKYLYEIARRHPYFYAPELLFFAKRYKAAFTECCQAADKAACLLPKLDELRDEGKASSAKQRLKCASLQKFG 231
sp|P02769|BSA      EKKFWGKYLYEIARRHPYFYAPELLYYANKYNGVFQECCQAEDKGACLLPKIETMREKVLASSARQRLRCASIQKFG 230
                   *:.*  ********************::*::*:..* ***** **.******:: :*::  ****:***:***:****

sp|P02768|HSA      ERAFKAWAVARLSQRFPKAEFAEVSKLVTDLTKVHTECCHGDLLECADDRADLAKYICENQDSISSKLKECCEKPLL 308
sp|P02769|BSA      ERALKAWSVARLSQKFPKAEFVEVTKLVTDLTKVHKECCHGDLLECADDRADLAKYICDNQDTISSKLKECCDKPLL 307
                   ***:***:******:******.**:**********.**********************:***:**********:****

sp|P02768|HSA      EKSHCIAEVENDEMPADLPSLAADFVESKDVCKNYAEAKDVFLGMFLYEYARRHPDYSVVLLLRLAKTYETTLEKCC 385
sp|P02769|BSA      EKSHCIAEVEKDAIPENLPPLTADFAEDKDVCKNYQEAKDAFLGSFLYEYSRRHPEYAVSVLLRLAKEYEATLEECC 384
                   **********:* :* :**.*:***.*.******* ****.*** *****:****:*:* :****** **:***:**

sp|P02768|HSA      AAADPHECYAKVFDEFKPLVEEPQNLIKQNCELFEQLGEYKFQNALLVRYTKKVPQVSTPTLVEVSRNLGKVGSKCC 462
sp|P02769|BSA      AKDDPHACYSTVFDKLKHLVDEPQNLIKQNCDQFEKLGEYGFQNALIVRYTRKVPQVSTPTLVEVSRSLGKVGTRCC 461
                   *  *** **:.***::* **:**********: **:**** *****:****:**************.*****::**

sp|P02768|HSA      KHPEAKRMPCAEDYLSVVLNQLCVLHEKTPVSDRVTKCCTESLVNRRPCFSALEVDETYVPKEFNAETFTFHADICT 539
sp|P02769|BSA      TKPESERMPCTEDYLSLILNRLCVLHEKTPVSEKVTKCCTESLVNRRPCFSALTPDETYVPKAFDEKLFTFHADICT 538
                   .:**::****:*****::**:***********::******************  ******* *: : *********

sp|P02768|HSA      LSEKERQIKKQTALVELVKHKPKATKEQLKAVMDDFAAFVEKCCKADDKETCFAEEGKKLVAASQAALGL         609
sp|P02769|BSA      LPDTEKQIKKQTALVELLKHKPKATEEQLKTVMENFVAFVDKCCAADDKEACFAVEGPKLVVSTQTALA-         607
                   *.:.*:***********:*******:****:**::*.***:*** *****:*** ** ***.::*:**.
```

**Figure A.2.** ClustalW2 Sequence Alignment for Nascent HSA and Nascent BSA; nascent HSA: UniProt P02768, nascent BSA: UniProt P02769. Residues 141 and 609 are not present in BSA. * represent identical residues, : represent very similar residues (similar properties), . represents similar residues, and blank represents no similarity.

```
HSA PDB: 1BM0      DAHKSEVAHRFKDLGEENFKALVLIAFAQYLQQCPFEDHVKLVNEVTEFAKTCVADESAENCDKSLHTLFGDKLCTV 77
“Mature” BSA       DTHKSEIAHRFKDLGEEHFKGLVLIAFSQYLQQCPFDEHVKLVNELTEFAKTCVADESHAGCEKSLHTLFGDELCKV 77
                   *:****:**********:**.******:********::*******:***********  .*:**********:**.*

HSA PDB: 1BM0      ATLRETYGEMADCCAKQEPERNECFLQHKDDNPNLPRLVRPEVDVMCTAFHDNEETFLKKYLYEIARRHPYFYAPEL 154
“Mature” BSA       ASLRETYGDMADCCEKQEPERNECFLSHKDDSPDLPKLK-PDPNTLCDEFKADEKKFWGKYLYEIARRHPYFYAPEL 153
                   *:******:***** ***********.****.*:**:*  *: :.:*  *: :*:.*  ******************

HSA PDB: 1BM0      LFFAKRYKAAFTECCQAADKAACLLPKLDELRDEGKASSAKQRLKCASLQKFGERAFKAWAVARLSQRFPKAEFAEV 231
“Mature” BSA       LYYANKYNGVFQECCQAEDKGACLLPKIETMREKVLASSARQRLRCASIQKFGERALKAWSVARLSQKFPKAEFVEV 230
                   *::*::*:.* ***** **.******:: :*::  ****:***:***:*******:***:******:******.**

HSA PDB: 1BM0      SKLVTDLTKVHTECCHGDLLECADDRADLAKYICENQDSISSKLKECCEKPLLEKSHCIAEVENDEMPADLPSLAAD 308
“Mature” BSA       TKLVTDLTKVHKECCHGDLLECADDRADLAKYICDNQDTISSKLKECCDKPLLEKSHCIAEVEKDAIPENLPPLTAD 307
                   :**********.**********************:***:*********:**************:* :* :**.*:**

HSA PDB: 1BM0      FVESKDVCKNYAEAKDVFLGMFLYEYARRHPDYSVVLLLRLAKTYETTLEKCCAAADPHECYAKVFDEFKPLVEEPQ 385
“Mature” BSA       FAEDKDVCKNYQEAKDAFLGSFLYEYSRRHPEYAVSVLLRLAKEYEATLEECCAKDDPHACYSTVFDKLKHLVDEPQ 384
                   *.*.******* ****.*** *****:****:*:* :***** * **:***:***  *** **:.***::* **:**

HSA PDB: 1BM0      NLIKQNCELFEQLGEYKFQNALLVRYTKKVPQVSTPTLVEVSRNLGKVGSKCCKHPEAKRMPCAEDYLSVVLNQLCV 462
“Mature” BSA       NLIKQNCDQFEKLGEYGFQNALIVRYTRKVPQVSTPTLVEVSRSLGKVGTRCCTKPESERMPCTEDYLSLILNRLCV 461
                   *******: **:**** *****:****:***************.*****::**.:**::****:*****::**:***

HSA PDB: 1BM0      LHEKTPVSDRVTKCCTESLVNRRPCFSALEVDETYVPKEFNAETFTFHADICTLSEKERQIKKQTALVELVKHKPKA 539
“Mature” BSA       LHEKTPVSEKVTKCCTESLVNRRPCFSALTPDETYVPKAFDEKLFTFHADICTLPDTEKQIKKQTALVELLKHKPKA 538
                   ********::********************  ******* *: : **********.::*:***********:******

HSA PDB: 1BM0      TKEQLKAVMDDFAAFVEKCCKADDKETCFAEEGKKLVAASQAALGL                                 585
“Mature” BSA       TEEQLKTVMENFVAFVDKCCAADDKEACFAVEGPKLVVSTQTALA-                                 583
                   *:****:**::*.***:*** *****:*** ** ***.::*:**.
```

**Figure A.3.** ClustalW2 Sequence Alignment of Mature HSA and Mature BSA; mature HSA: PBB Code 1BM0, mature BSA: Uniprot P02769.
***** represent identical residues, **:** represent very similar residues (similar properties), **.** represents similar residues, and blank represents no similarity.

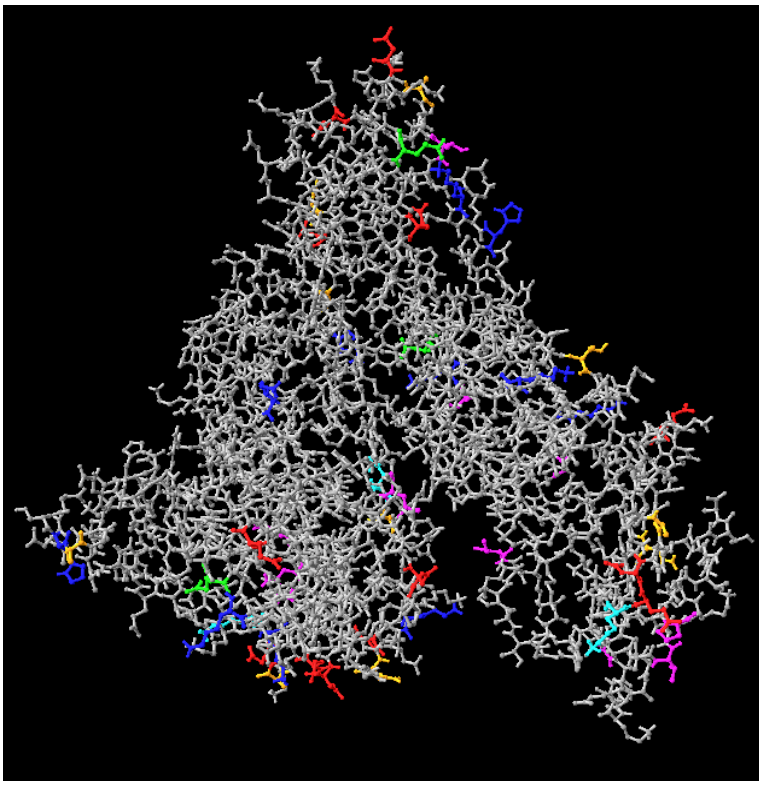

**Figure A.4.** Residue Changes Between HSA and BSA. The molecular structure is that of the BSA homology model. The residues of BSA which are different than those of HSA are shown in color. Blue residues represent those which are uncharged in HSA and positively charged in BSA. Red residues are those which are uncharged in HSA and negatively charged in BSA. Purple residues are those which are positively charged in HSA and uncharged in BSA. Orange residues are those which are negatively charged in HSA and uncharged in BSA. Green residues are those which are positively charged in HSA and negatively charged in BSA. Teal residues are those which are negatively charged in HSA and positively charged in BSA.

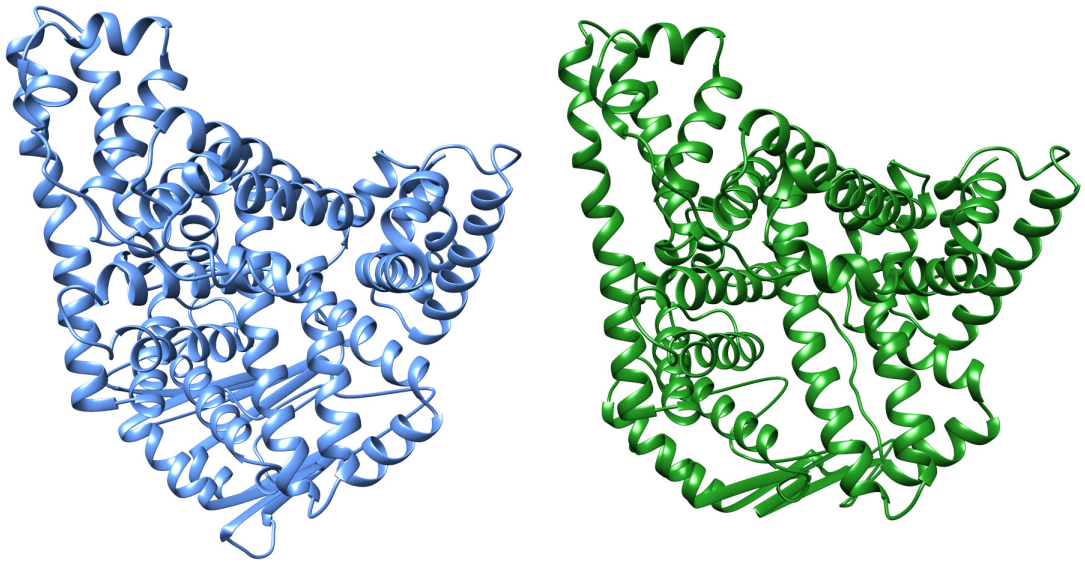

**Figure A.5.** Molecular Structures of HSA and BSA. The x-ray crystal structure of HSA (left) and the Homology-Modeled BSA (right) are both extensively α-helical. Only minor differences can be seen between the two serum albumins.

# APPENDIX B.

# OSMOTIC PRESSURE DATA

## B.1. Bovine Serum Albumin

**Table B.1.** Osmotic Pressure of Bovine Serum Albumin in 0.15 M NaCl, pH 7.0.

| [BSA] (g/L Soln) | [NaCl] (M) | pH | Osmotic Pressure (psi) |
|---|---|---|---|
| 48.75 | 0.15 | 7.0 | 0.3 ± 0.02 |
| 107.52 | 0.15 | 7.0 | 0.9 ± 0.02 |
| 151.07 | 0.15 | 7.0 | 1.4 ± 0.02 |
| 151.07 | 0.15 | 7.0 | 1.4 ± 0.02 |
| 200.39 | 0.15 | 7.0 | 2.3 ± 0.01 |
| 225.04 | 0.15 | 7.0 | 3.6 ± 0.02 |
| 248.39 | 0.15 | 7.0 | 4.6 ± 0.12 |
| 248.39 | 0.15 | 7.0 | 4.1 ± 0.02 |
| 269.61 | 0.15 | 7.0 | 5.6 ± 0.02 |
| 269.61 | 0.15 | 7.0 | 5.5 ± 0.02 |
| 299.85 | 0.15 | 7.0 | 7.9 ± 0.01 |
| 299.85 | 0.15 | 7.0 | 7.9 ± 0.01 |
| 299.85 | 0.15 | 7.0 | 8.3 ± 0.02 |
| 325.01 | 0.15 | 7.0 | 10.2 ± 0.02 |
| 325.01 | 0.15 | 7.0 | 10.9 ± 0.03 |
| 325.01 | 0.15 | 7.0 | 10.5 ± 0.01 |
| 347.98 | 0.15 | 7.0 | 14.3 ± 0.05 |
| 347.98 | 0.15 | 7.0 | 14.0 ± 0.01 |
| 347.98 | 0.15 | 7.0 | 14.1 ± 0.03 |
| 371.72 | 0.15 | 7.0 | 19.9 ± 0.02 |
| 400.28 | 0.15 | 7.0 | 24.0 ± 0.01 |
| 400.28 | 0.15 | 7.0 | 24.7 ± 0.07 |
| 400.28 | 0.15 | 7.0 | 24.0 ± 0.10 |
| 417.97 | 0.15 | 7.0 | 28.4 ± 0.02 |
| 450.44 | 0.15 | 7.0 | 38.0 ± 0.03 |
| 450.44 | 0.15 | 7.0 | 37.5 ± 0.01 |
| 450.44 | 0.15 | 7.0 | 37.3 ± 0.02 |

**Table B.2.** Osmotic Pressure of Bovine Serum Albumin in NaCl.

| [BSA] (g/L Soln) | [NaCl] (M) | pH | Osmotic Pressure (psi) |
|---|---|---|---|
| 213.30 | 0.15 | 4.5 | 2.95 ± 0.08 |
| 337.40 | 0.5 | 4.5 | 5.4 ± 0.29 |
| 347.00 | 0.5 | 4.5 | 7.5 ± 0.08 |
| 375.00 | 0.5 | 4.5 | 7.0 ± 0.27 |
| 313.10 | 0.5 | 7.4 | 12.2 ± 0.06 |
| 405.18 | 0.5 | 7.4 | 21.6 ± 0.20 |
| 474.42 | 0.5 | 7.4 | 29.3 ± 0.11 |

**Table B.3.** Osmotic Pressure of Bovine Serum Albumin in KCl.

| [BSA] (g/L Soln) | [KCl] (M) | pH | Osmotic Pressure (psi) |
|---|---|---|---|
| 310.10 | 0.05 | 7.4 | 14.0 ± 0.04 |
| 310.10 | 0.05 | 7.4 | 16.2 ± 0.02 |
| 310.10 | 0.05 | 7.4 | 17.9 ± 0.05 |
| 309.04 | 0.1 | 7.4 | 12.1 ± 0.09 |
| 309.04 | 0.1 | 7.4 | 15.0 ± 0.02 |
| 309.04 | 0.1 | 7.4 | 16.2 ± 0.12 |

**Table B.4.** Osmotic Pressure of Bovine Serum Albumin in $CaCl_2$.

| [BSA] (g/L Soln) | [$CaCl_2$] (M) | pH | Osmotic Pressure (psi) |
|---|---|---|---|
| 269.00 | 0.003 | 4.5 | 1.6 ± 0.08 |
| 270.00 | 0.003 | 4.5 | 1.8 ± 0.29 |
| 270.00 | 0.003 | 5.4 | 2.5 ± 0.09 |
| 242.84 | 0.003 | 7.4 | 13.8 ± 0.31 |
| 271.01 | 0.003 | 7.4 | 13.9 ± 0.12 |
| 242.90 | 0.075 | 7.4 | 1.1 ± 0.05 |
| 337.18 | 0.075 | 7.4 | 9.5 ± 0.07 |
| 443.15 | 0.10 | 7.4 | 18.3 ± 0.44 |
| 252.42 | 0.15 | 4.5 | 1.4 ± 0.01 |
| 412.11 | 0.15 | 4.5 | 8.9 ± 0.05 |
| 447.18 | 0.15 | 4.5 | 23.7 ± 0.27 |
| 251.50 | 0.15 | 7.4 | 3.0 ± 0.05 |
| 312.87 | 0.15 | 7.4 | 6.7 ± 0.18 |
| 315.02 | 0.15 | 7.4 | 6.1 ± 0.05 |
| 384.82 | 0.15 | 7.4 | 12.3 ± 0.31 |
| 402.00 | 0.15 | 7.4 | 12.8 ± 0.18 |
| 437.56 | 0.15 | 7.4 | 15.3 ± 0.29 |
| 447.00 | 0.15 | 7.4 | 18.9 ± 0.36 |
| 450.16 | 0.15 | 7.4 | 26.6 ± 0.06 |
| 466.33 | 0.15 | 7.4 | 25.4 ± 0.06 |
| 238.00 | 0.5 | 4.5 | 2.6 ± 0.25 |
| 269.03 | 0.5 | 4.5 | 2.9 ± 0.01 |
| 443.42 | 0.5 | 4.5 | 18.1 ± 0.12 |
| 472.00 | 0.5 | 4.5 | 15.9 ± 0.09 |
| 367.73 | 0.5 | 7.4 | 9.8 ± 0.08 |
| 446.34 | 0.5 | 7.4 | 18.3 ± 0.42 |
| 461.92 | 0.5 | 7.4 | 29.1 ± 0.32 |

**Table B.5.** Osmotic Pressure of Bovine Serum Albumin in $MgCl_2$.

| [BSA] (g/L Soln) | [$MgCl_2$] (M) | pH | Osmotic Pressure (psi) |
|---|---|---|---|
| 94.00 | 0.5 | 4.5 | 1.1 ± 0.5 |
| 350.00 | 0.5 | 4.5 | 3.7 ± 0.26 |
| 450.00 | 0.5 | 4.5 | 12.5 ± 0.14 |

## B.2. Ovalbumin

**Table B.6.** Osmotic Pressure of Ovalbumin in 0.15 M NaCl.

| [OVA] (g/L Soln) | [NaCl] (M) | pH | Osmotic Pressure (psi) |
|---|---|---|---|
| 149.11 | 0.15 | 4.5 | 0.5 ± 0.01 |
| 198.82 | 0.15 | 4.5 | 0.9 ± 0.02 |
| 198.82 | 0.15 | 4.5 | 1.0 ± 0.02 |
| 216.30 | 0.15 | 4.5 | 1.3 ±0.04 |
| 229.68 | 0.15 | 4.5 | 1.5 ± 0.02 |
| 279.30 | 0.15 | 4.5 | 1.7 ± 0.04 |
| 297.30 | 0.15 | 4.5 | 1.7 ± 0.02 |
| 362.67 | 0.15 | 4.5 | 2.4 ± 0.02 |
| 371.63 | 0.15 | 4.5 | 3.4 ± 0.02 |
| 400.00 | 0.15 | 4.5 | 5.5 ± 0.10 |
| 433.00 | 0.15 | 4.5 | 6.9 ± 0.05 |
| 495.49 | 0.15 | 4.5 | 7.7 ± 0.21 |
| 99.43 | 0.15 | 5.4 | 0.8 ± 0.01 |
| 200.13 | 0.15 | 5.4 | 2.1 ± 0.01 |
| 295.36 | 0.15 | 5.4 | 5.4 ± 0.20 |
| 347.86 | 0.15 | 5.4 | 8.0 ± 0.33 |
| 391.58 | 0.15 | 5.4 | 11.5 ± 0.47 |
| 497.31 | 0.15 | 5.4 | 19.5 ± 0.27 |
| 535.65 | 0.15 | 5.4 | 33.6 ± 0.90 |
| 138.40 | 0.15 | 7.4 | 1.7 ± 0.02 |
| 150.00 | 0.15 | 7.4 | 1.6 ± 0.03 |
| 193.80 | 0.15 | 7.4 | 2.5 ± 0.02 |
| 249.14 | 0.15 | 7.4 | 5.9 ± 0.05 |
| 298.00 | 0.15 | 7.4 | 6.1 ± 0.05 |
| 362.27 | 0.15 | 7.4 | 13.5 ± 0.08 |
| 362.27 | 0.15 | 7.4 | 14.8 ± 0.28 |
| 398.62 | 0.15 | 7.4 | 20.8 ± 0.05 |
| 405.95 | 0.15 | 7.4 | 21.8 ± 0.08 |
| 451.72 | 0.15 | 7.4 | 36.7 ± 0.11 |
| 476.38 | 0.15 | 7.4 | 38.4 ± 0.79 |
| 514.00 | 0.15 | 7.4 | 41.6 ± 0.56 |

## B.3. Ovalbumin-Bovine Serum Albumin Binary Solutions

**Table B.7.** Osmotic Pressure of 3:1 Ovalbumin:Bovine Serum Albumin in 0.15 M NaCl.

| [Protein] (g/L Soln) | Molar Ratio (OVA:BSA) | [NaCl] (M) | pH | Osmotic Pressure (psi) |
|---|---|---|---|---|
| 48.60 | 3:1 | 0.15 | 4.5 | 0.1 ± 0.01 |
| 185.09 | 3:1 | 0.15 | 4.5 | 1.1 ± 0.05 |
| 185.09 | 3:1 | 0.15 | 4.5 | 1.1 ± 0.07 |
| 185.09 | 3:1 | 0.15 | 4.5 | 1.0 ± 0.01 |
| 250.28 | 3:1 | 0.15 | 4.5 | 1.6 ± 0.02 |
| 354.50 | 3:1 | 0.15 | 4.5 | 4.1 ± 0.03 |
| 418.60 | 3:1 | 0.15 | 4.5 | 6.5 ± 0.08 |
| 444.76 | 3:1 | 0.15 | 4.5 | 6.7 ± 0.10 |
| 80.76 | 3:1 | 0.15 | 7.4 | 0.2 ± 0.02 |
| 197.40 | 3:1 | 0.15 | 7.4 | 3.1 ± 0.02 |
| 296.12 | 3:1 | 0.15 | 7.4 | 9.2 ± 0.03 |
| 351.77 | 3:1 | 0.15 | 7.4 | 15.4 ± 0.07 |
| 433.82 | 3:1 | 0.15 | 7.4 | 30.6 ± 0.12 |
| 509.50 | 3:1 | 0.15 | 7.4 | 53.7 ± 0.24 |

**Table B.8.** Osmotic Pressure of 1:1 Ovalbumin:Bovine Serum Albumin in 0.15 M NaCl, pH 7.0.

| [Protein] (g/L Soln) | Molar Ratio (OVA:BSA) | [NaCl] (M) | pH | Osmotic Pressure (psi) |
|---|---|---|---|---|
| 50.20 | 1:1 | 0.15 | 7.0 | 0.5 ± 0.01 |
| 119.30 | 1:1 | 0.15 | 7.0 | 1.6 ± 0.03 |
| 152.70 | 1:1 | 0.15 | 7.0 | 2.4 ± 0.01 |
| 206.52 | 1:1 | 0.15 | 7.0 | 3.9 ± 0.02 |
| 258.00 | 1:1 | 0.15 | 7.0 | 7.1 ± 0.04 |
| 296.71 | 1:1 | 0.15 | 7.0 | 8.9 ± 0.01 |
| 305.49 | 1:1 | 0.15 | 7.0 | 9.1 ± 0.02 |
| 310.00 | 1:1 | 0.15 | 7.0 | 11.7 ± 0.12 |
| 361.40 | 1:1 | 0.15 | 7.0 | 17.8 ± 0.08 |
| 406.00 | 1:1 | 0.15 | 7.0 | 26.9 ± 0.12 |

**Table B.9.** Osmotic Pressure of 1:3 Ovalbumin:Bovine Serum Albumin in 0.15 M NaCl, pH 7.0.

| [Protein] (g/L Soln) | Molar Ratio (OVA:BSA) | [NaCl] (M) | pH | Osmotic Pressure (psi) |
|---|---|---|---|---|
| 53.40 | 1:3 | 0.15 | 7.0 | 0.4 ± 0.01 |
| 100.11 | 1:3 | 0.15 | 7.0 | 0.9 ± 0.11 |
| 100.11 | 1:3 | 0.15 | 7.0 | 1.0 ± 0.03 |
| 100.20 | 1:3 | 0.15 | 7.0 | 0.9 ± 0.02 |
| 152.82 | 1:3 | 0.15 | 7.0 | 2.0 ± 0.03 |
| 198.82 | 1:3 | 0.15 | 7.0 | 3.7 ± 0.02 |
| 198.82 | 1:3 | 0.15 | 7.0 | 3.1 ± 0.01 |
| 223.99 | 1:3 | 0.15 | 7.0 | 4.0 ± 0.01 |
| 223.99 | 1:3 | 0.15 | 7.0 | 4.7 ± 0.03 |
| 224.26 | 1:3 | 0.15 | 7.0 | 4.2 ± 0.03 |
| 248.20 | 1:3 | 0.15 | 7.0 | 5.1 ± 0.01 |
| 248.20 | 1:3 | 0.15 | 7.0 | 4.5 ± 0.01 |
| 248.20 | 1:3 | 0.15 | 7.0 | 5.6 ± 0.03 |
| 248.69 | 1:3 | 0.15 | 7.0 | 5.2 ± 0.02 |
| 275.13 | 1:3 | 0.15 | 7.0 | 5.5 ± 0.01 |
| 275.13 | 1:3 | 0.15 | 7.0 | 5.5 ± 0.01 |
| 275.13 | 1:3 | 0.15 | 7.0 | 4.8 ± 0.01 |
| 292.09 | 1:3 | 0.15 | 7.0 | 6.4 ± 0.02 |
| 292.09 | 1:3 | 0.15 | 7.0 | 6.2 ± 0.01 |
| 292.09 | 1:3 | 0.15 | 7.0 | 7.5 ± 0.03 |
| 292.09 | 1:3 | 0.15 | 7.0 | 6.7 ± 0.02 |
| 331.30 | 1:3 | 0.15 | 7.0 | 11.0 ± 0.01 |
| 331.30 | 1:3 | 0.15 | 7.0 | 10.6 ± 0.02 |
| 339.60 | 1:3 | 0.15 | 7.0 | 18.7 ± 0.39 |
| 348.50 | 1:3 | 0.15 | 7.0 | 13.2 ± 0.01 |
| 348.50 | 1:3 | 0.15 | 7.0 | 14.2 ± 0.01 |
| 391.59 | 1:3 | 0.15 | 7.0 | 19.4 ± 0.02 |
| 391.59 | 1:3 | 0.15 | 7.0 | 18.8 ± 0.02 |
| 391.59 | 1:3 | 0.15 | 7.0 | 18.8 ± 0.01 |
| 521.57 | 1:3 | 0.15 | 7.0 | 54.4 ± 0.90 |

# APPENDIX C.

# EXAMPLE HPLC CHROMATOGRAPHS

For all of the following HPLC chromatographs, the carrier (solvent) solution is identical to the sample solution except for the protein(s). The running parameters for each sample are within the figure captions.

## C.1. Hen Egg Lysozyme

HEL in 0.15 M NaCl, pH 7.0 was analyzed for three concentrations (25g/L, 50 g/L, and 100 g/L) to determine if the formation of aggregates increased as the concentration got closer to the saturation limit (129 g/L) (Figures C.1 - C.3). Only a single peak was observed in all solutions which suggests that the species observed at low concentrations is the same molecular weight as those observed at near-saturation concentrations.

## C.2. Ovalbumin

OVA (2 g/L) in 0.15 M NaCl was analyzed at pH 4.5, 5.4, and 7.4 for aggregation (Figures C.4 - C.6). For all three pH, the OVA solution had monomers, dimers, trimers, and a higher molecular weight multimer.

## C.3. Bovine Serum Albumin

BSA (2 g/L) in 0.15 M NaCl was analyzed at pH 4.5, 5.4, and 7.4 for aggregation (Figures C.7 - C.9). For all three pH, the BSA solution had monomers, dimers, and trimers.

The chromatographs of BSA in $CaCl_2$ were analyzed for 0.003 M, 0.05 M, and 0.5 M at pH 4.5, 5.4, and 7.4 (Figures C.10 - C.19). For the 0.003 M and 0.05 M solutions, BSA

monomers were observed. An additional peak at approximately 16.3 minutes was observed. This peak is prominent at 278 nm (corresponding to the aromatic residues); however, at 218 nm (due to disulfide bonds), at which BSA typically has a large absorbance, this peak is greatly reduced (Figures C.11 and C.16) which is most likely caused by denaturation of BSA. This may also be due to fragmentation of BSA into identical molecular weight pieces, most likely three fragments of approximately 20 kDa each (corresponding to the three identical domains)

C.4. Ovalbumin-Bovine Serum Albumin Solutions

The chromatograph of a 1:1 OVA:BSA binary solution in 0.15 M NaCl, pH 5.4 is shown in Figure C.20. The chromatograph loses the multimers of OVA since they overlap with the peaks corresponding to the BSA multimers. However, no hetero-multimers are observed.

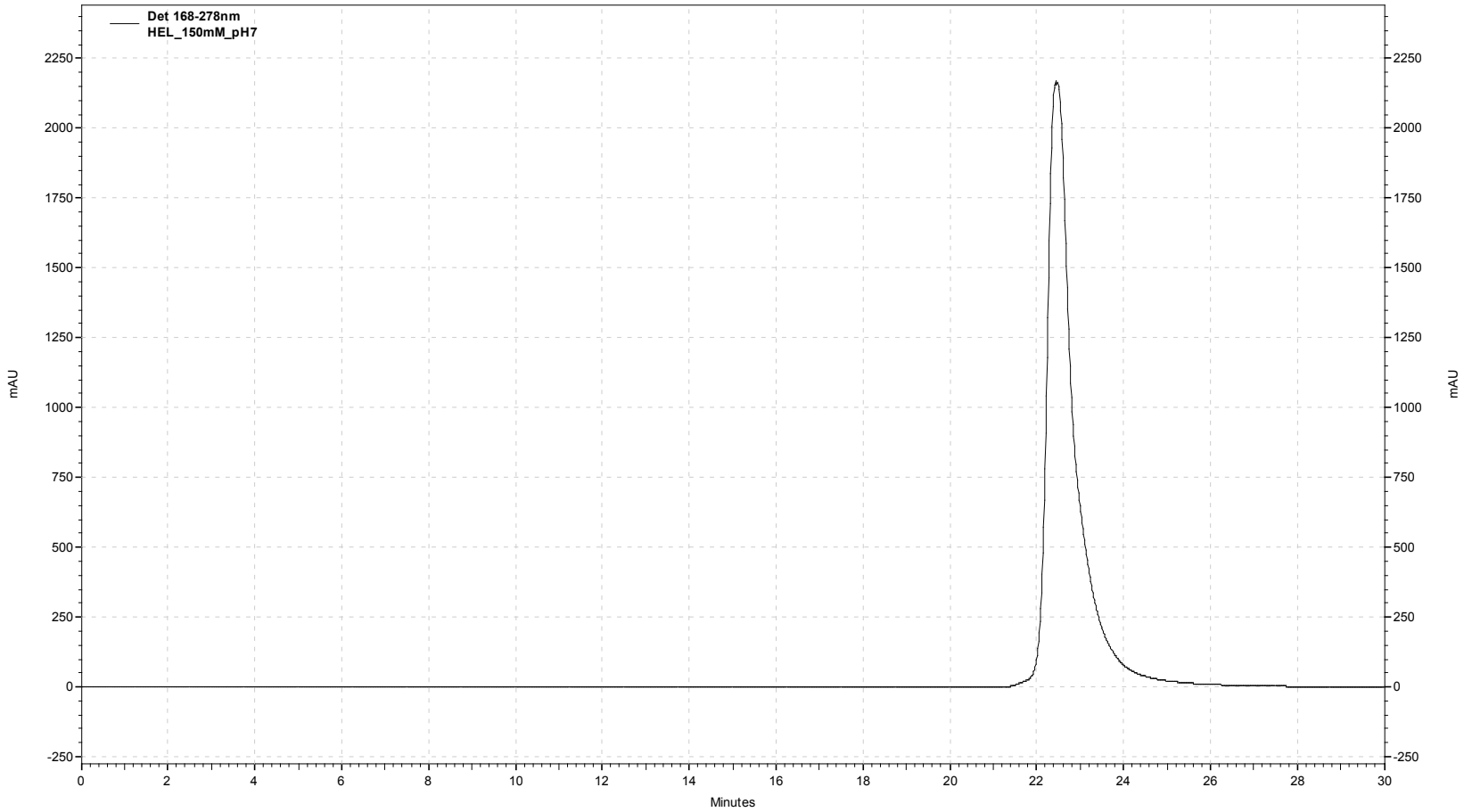


**Figure C.1.** Chromatograph of 25 g/L HEL in 0.15 M NaCl, pH 7.0. Flowrate: 1.0 mL/min. Wavelength: 278 nm. Retention Time (peak area): 22.450 min (960,207,474 mAu).

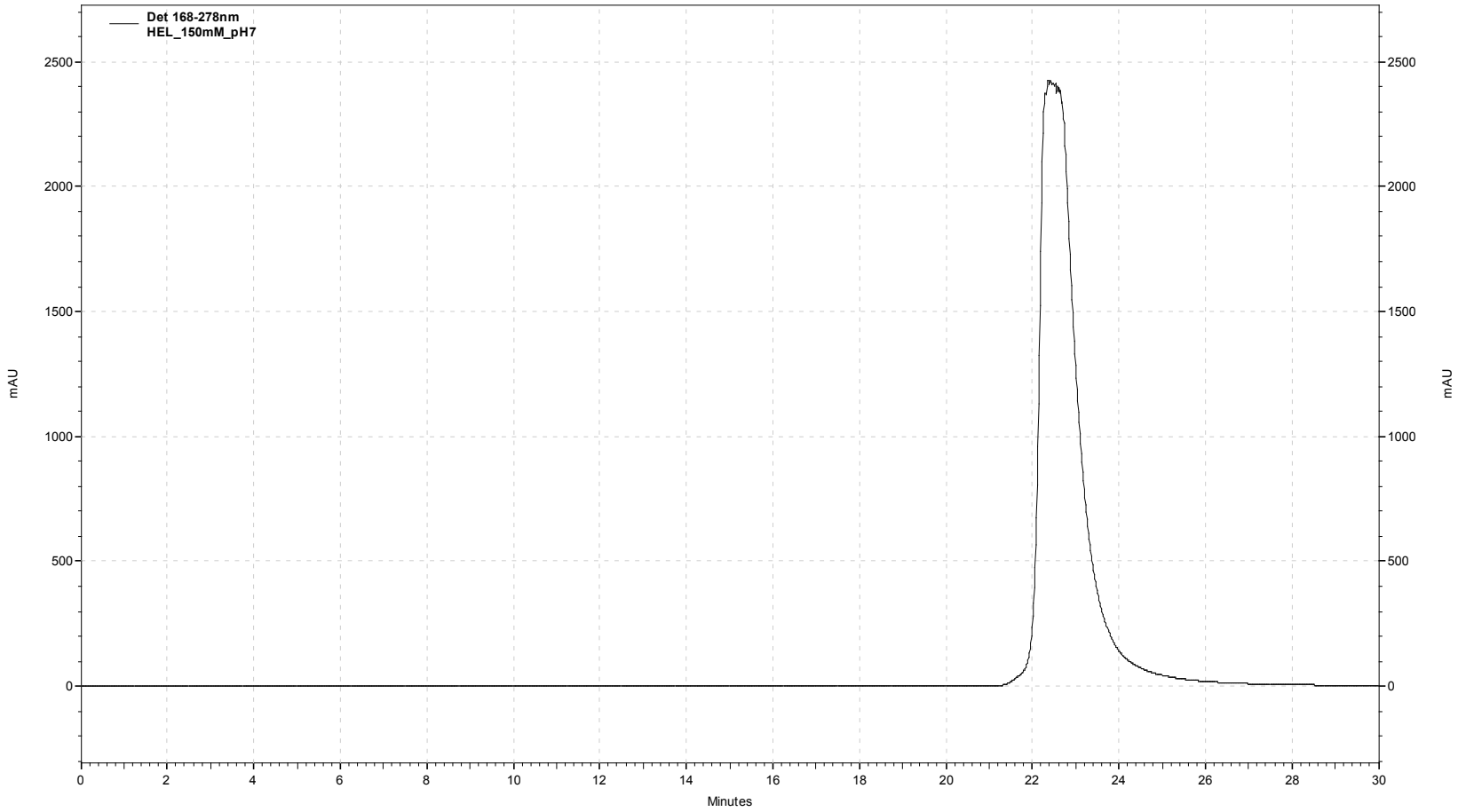


**Figure C.2.** Chromatograph of 50 g/L HEL in 0.15 M NaCl, pH 7.0. Flowrate: 1.0 mL/min. Wavelength: 278 nm. Retention Time (peak area): 22.433 min (151,494,622 mAu).

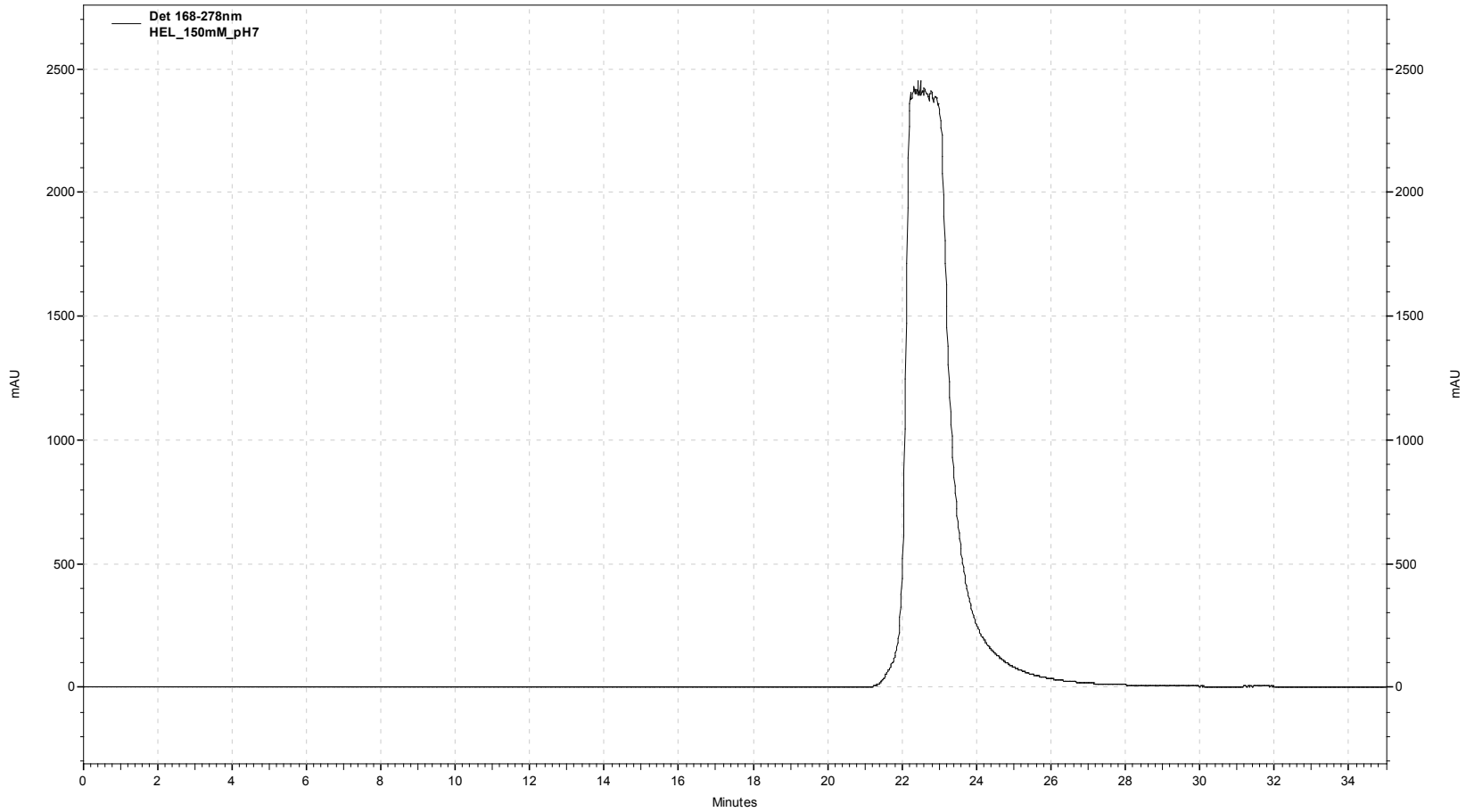


**Figure C.3.** Chromatograph of 100 g/L HEL in 0.15 M NaCl, pH 7.0. Flowrate: 1.0 mL/min. Wavelength: 278 nm. Retention Time (peak area): 22.600 min (205,218,170 mAu).

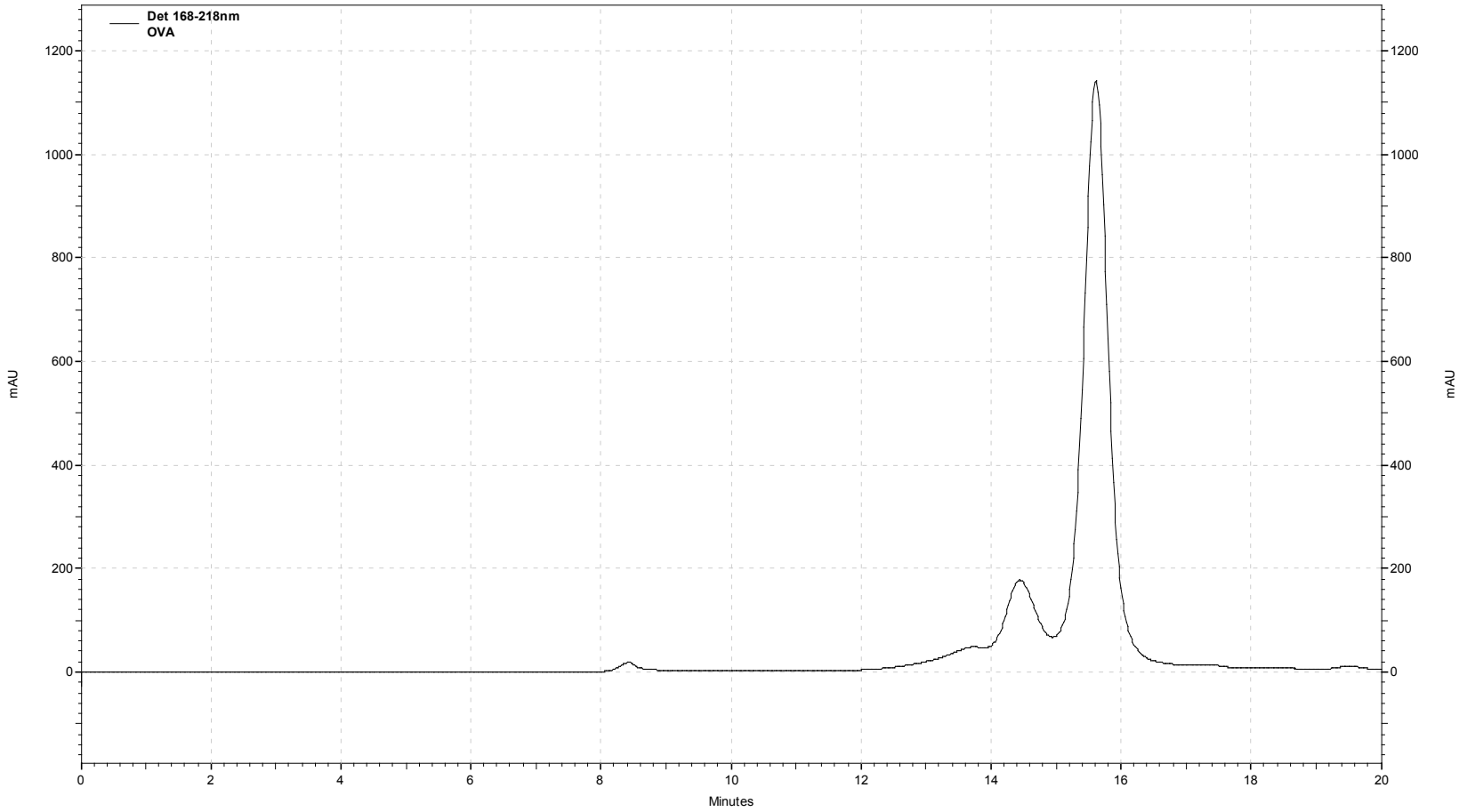


**Figure C.4.** Chromatograph of OVA in 0.15 M NaCl, pH 4.5. [OVA]: 2 g/L. Flowrate: 0.5 mL/min. Wavelength: 218 nm. Retention Time (peak area): 8.417 min (550,806 mAu), 13.750 min (2,365,861 mAu), 14.750 min (6,708,932 mAu), 15.617 min (33,359,003 mAu).

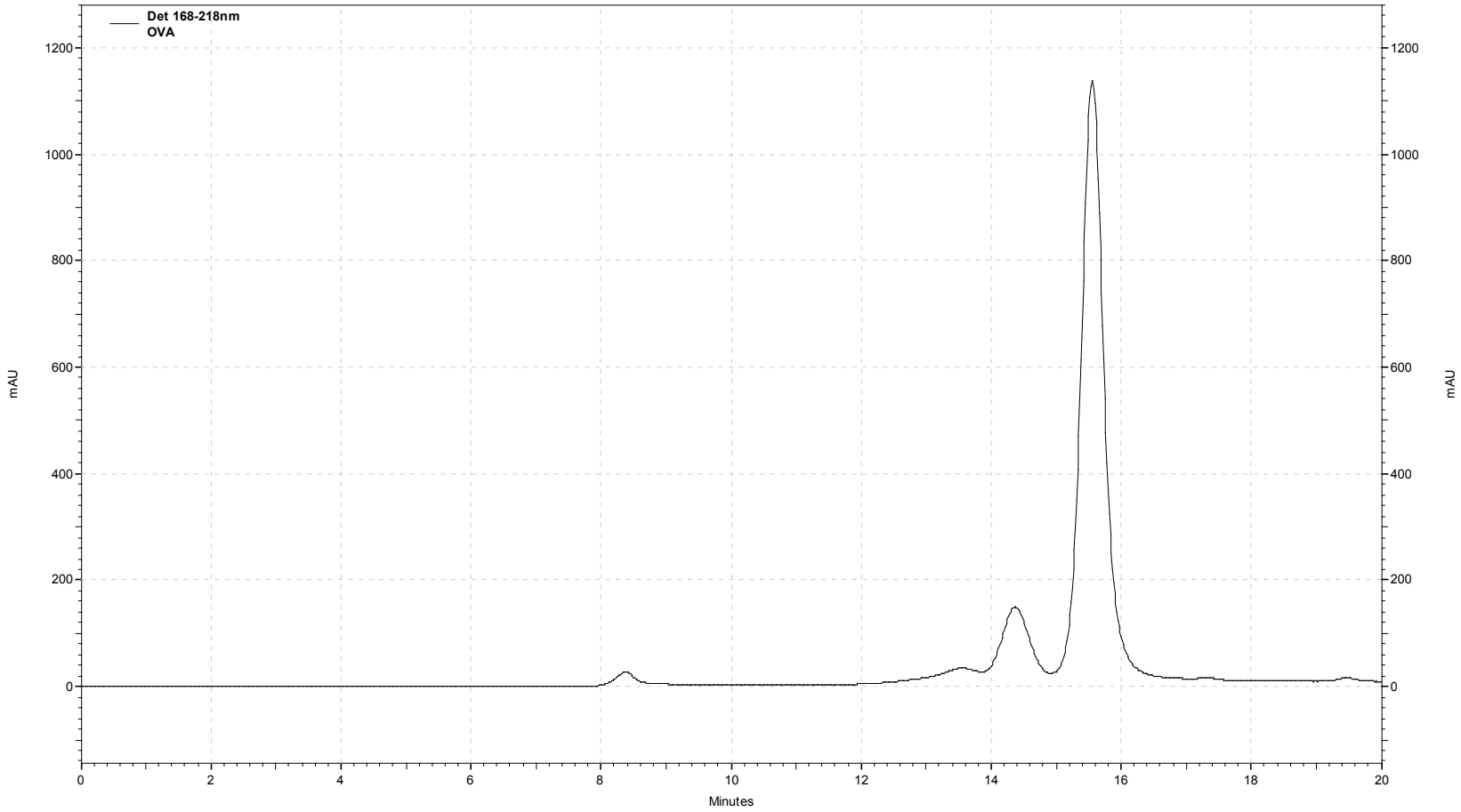


**Figure C.5.** Chromatograph of OVA in 0.15 M NaCl, pH 5.4. [OVA]: 2 g/L. Flowrate: 0.5 mL/min. Wavelength: 218 nm. Retention Time (peak area): 3.383 min(792,200 mAu), 13.567 min (1,593,578 mAu), 14.367 min (4,687,636 mAu), 15.550 min (29,170,900 mAu).

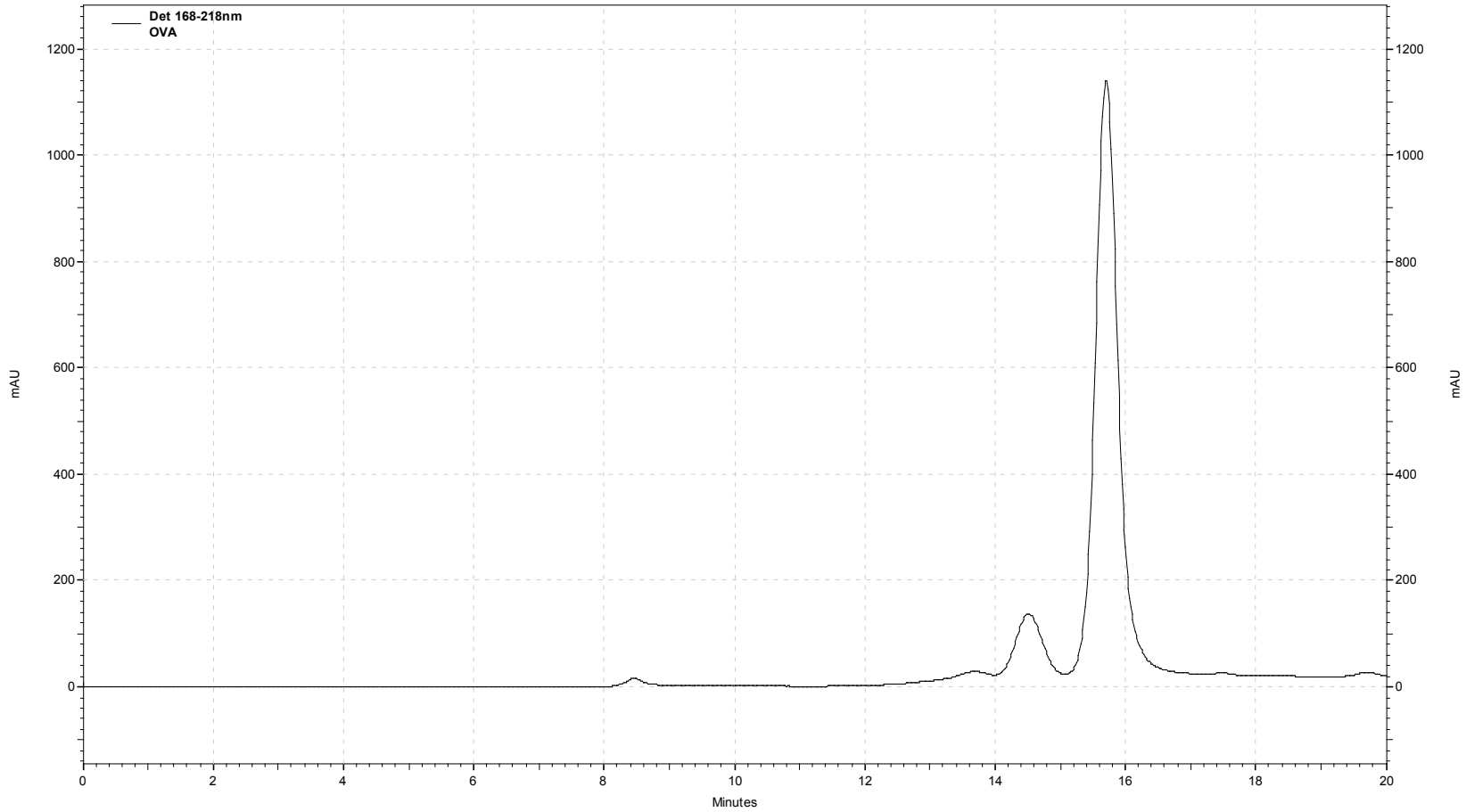


**Figure C.6.** Chromatograph of OVA in 0.15 M NaCl, pH 7.4. [OVA]: 2 g/L. Flowrate: 0.5 mL/min. Wavelength: 218 nm. Retention Time (peak area): 8.467 min (124,960 mAu), 13.683 min (1,076,164 mAu), 14.517 min (4,099,616 mAu), 15.700 min (29,197,677 mAu).

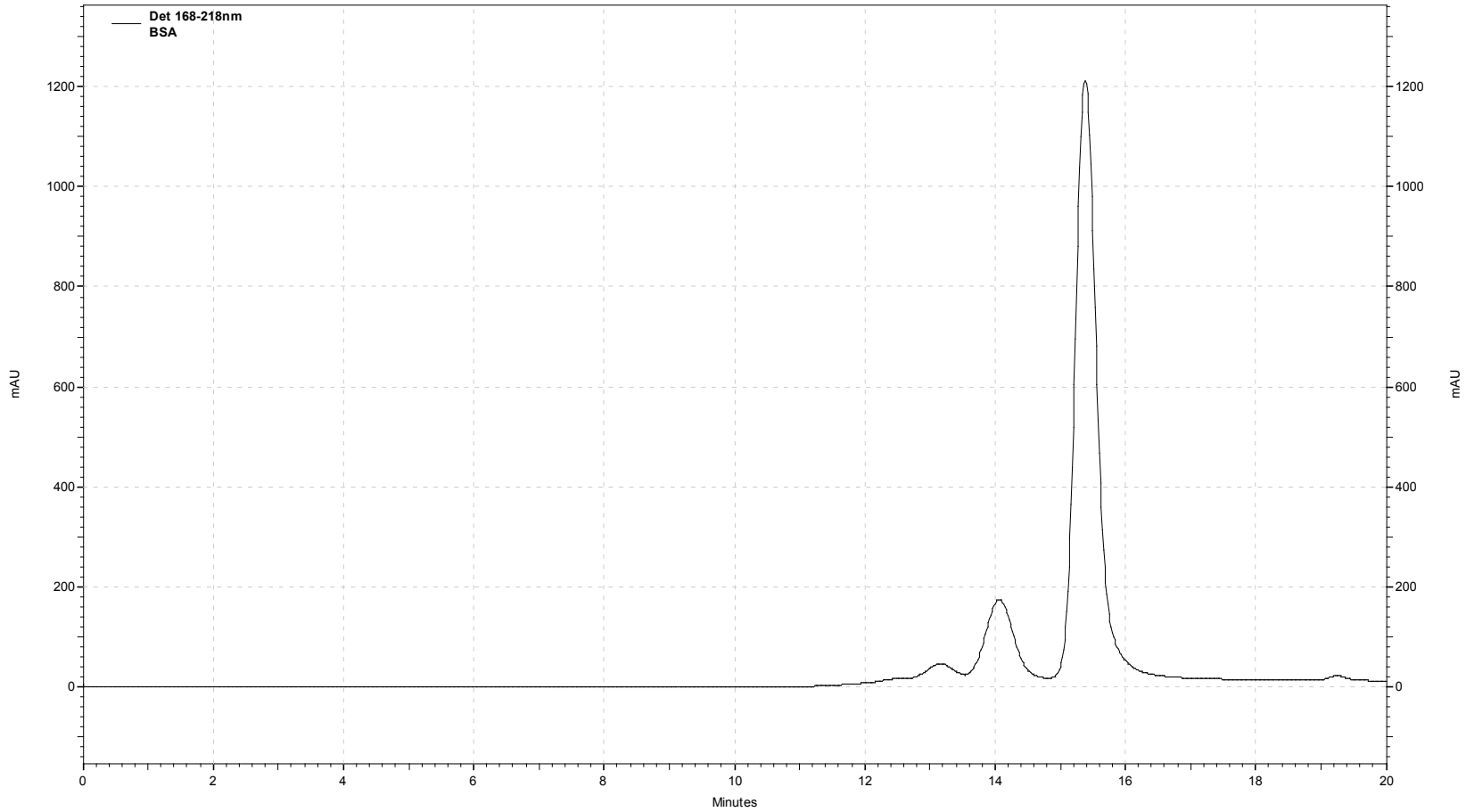


**Figure C.7.** Chromatograph of BSA in 0.15 M NaCl, pH 4.5. [BSA]: 2 g/L. Flowrate: 0.5 mL/min. Wavelength: 218 nm. Retention Time (peak area): 13.167 min (2,176,713 mAu), 14.067 min (5,699,036 mAu), 15.383 min (29,735,897 mAu).

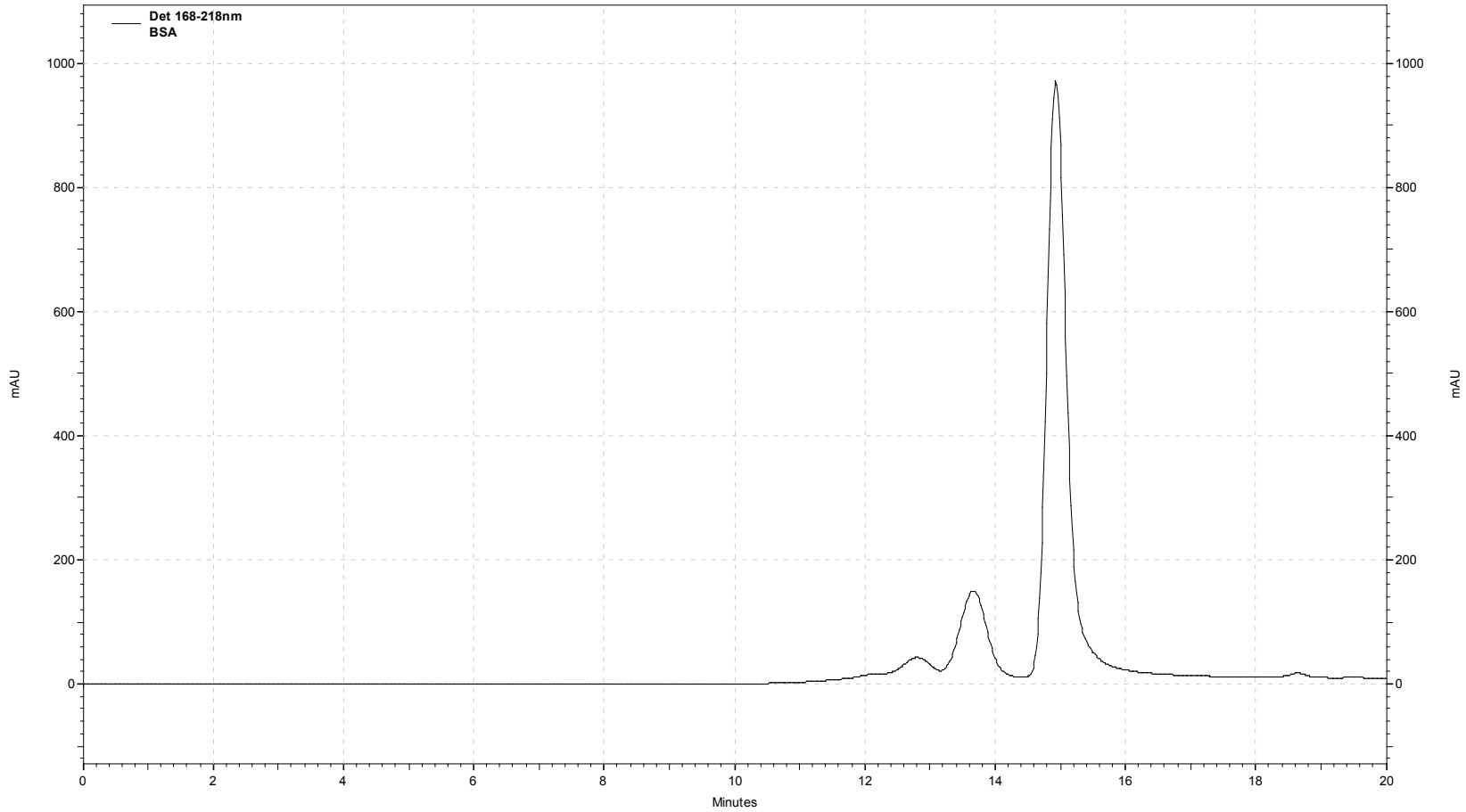


**Figure C.8.** Chromatograph of BSA in 0.15 M NaCl, pH 5.4. [BSA]: 2 g/L. Flowrate: 0.5 mL/min. Wavelength: 218 nm. Retention Time (peak area): 12.800 min (2,043,605 mAu), 13.667 min (4,628,336 mAu), 14.933 min (22,698,255 mAu).

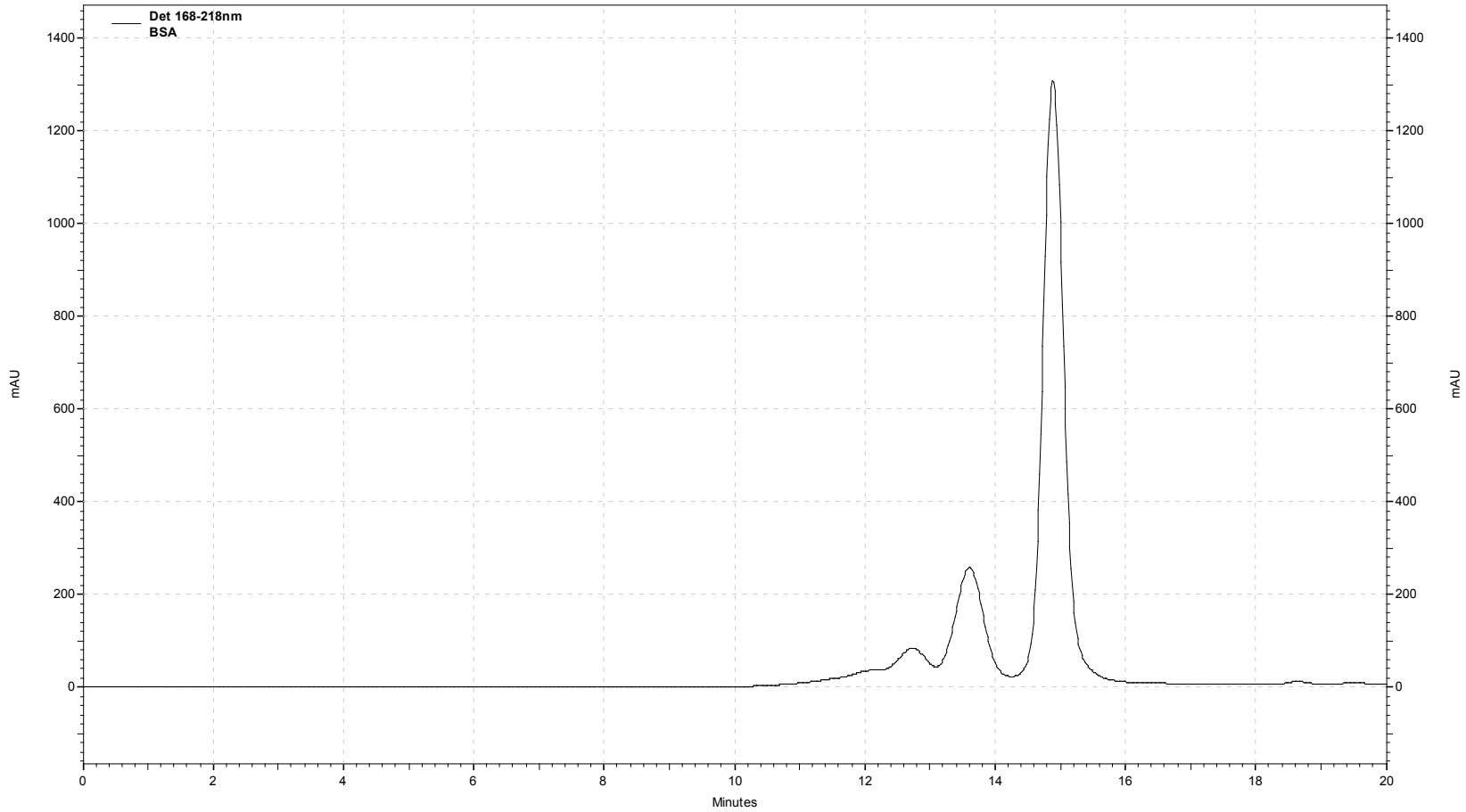


**Figure C.9.** Chromatograph of BSA in 0.15 M NaCl, pH 7.4. [BSA]: 2 g/L. Flowrate: 0.5 mL/min. Wavelength: 218 nm. Retention Time (peak area): 12.733 min (4,901,944 mAu), 13.600 min (8,680,141 mAu), 14.833 min (31,059,292 mAu).

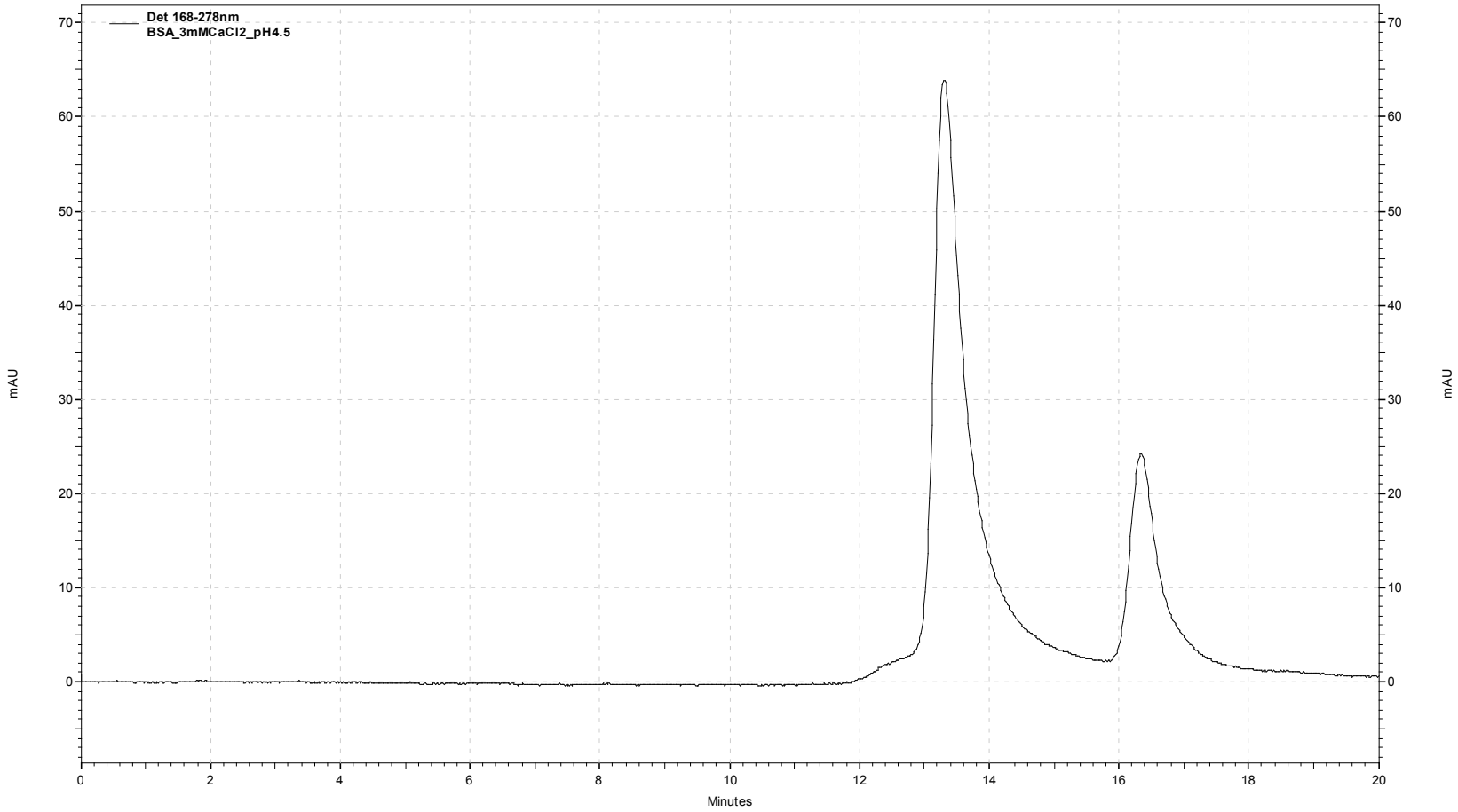


**Figure C.10.** Chromatograph of BSA in 0.003 M $CaCl_2$, pH 4.5, 278 nm. [BSA]: 12 g/L. Flowrate: 0.7 mL/min. Wavelength: 278 nm. Retention Time (peak area): 13.300 min (2,790,080 mAu), 16.350 min (939,899 mAu).

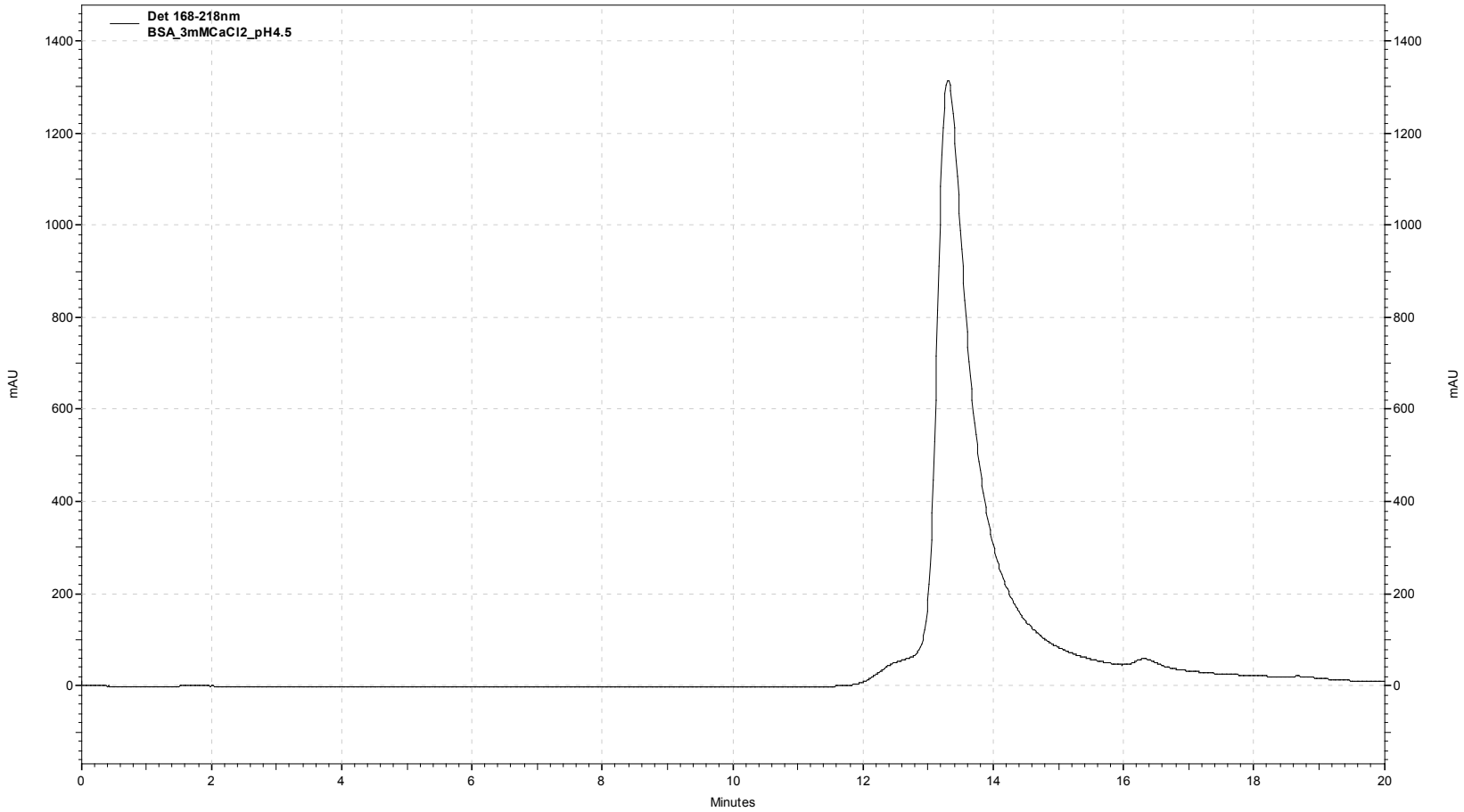


**Figure C.11.** Chromatograph of BSA in 0.003 M $CaCl_2$, pH 4.5, 218 nm. [BSA]: 12 g/L. Flowrate: 0.7 mL/min. Wavelength: 218 nm. This is the same sample as Figure C.12 but analyzed at 218 nm. The second peak at 16.350 min is almost non-existent.

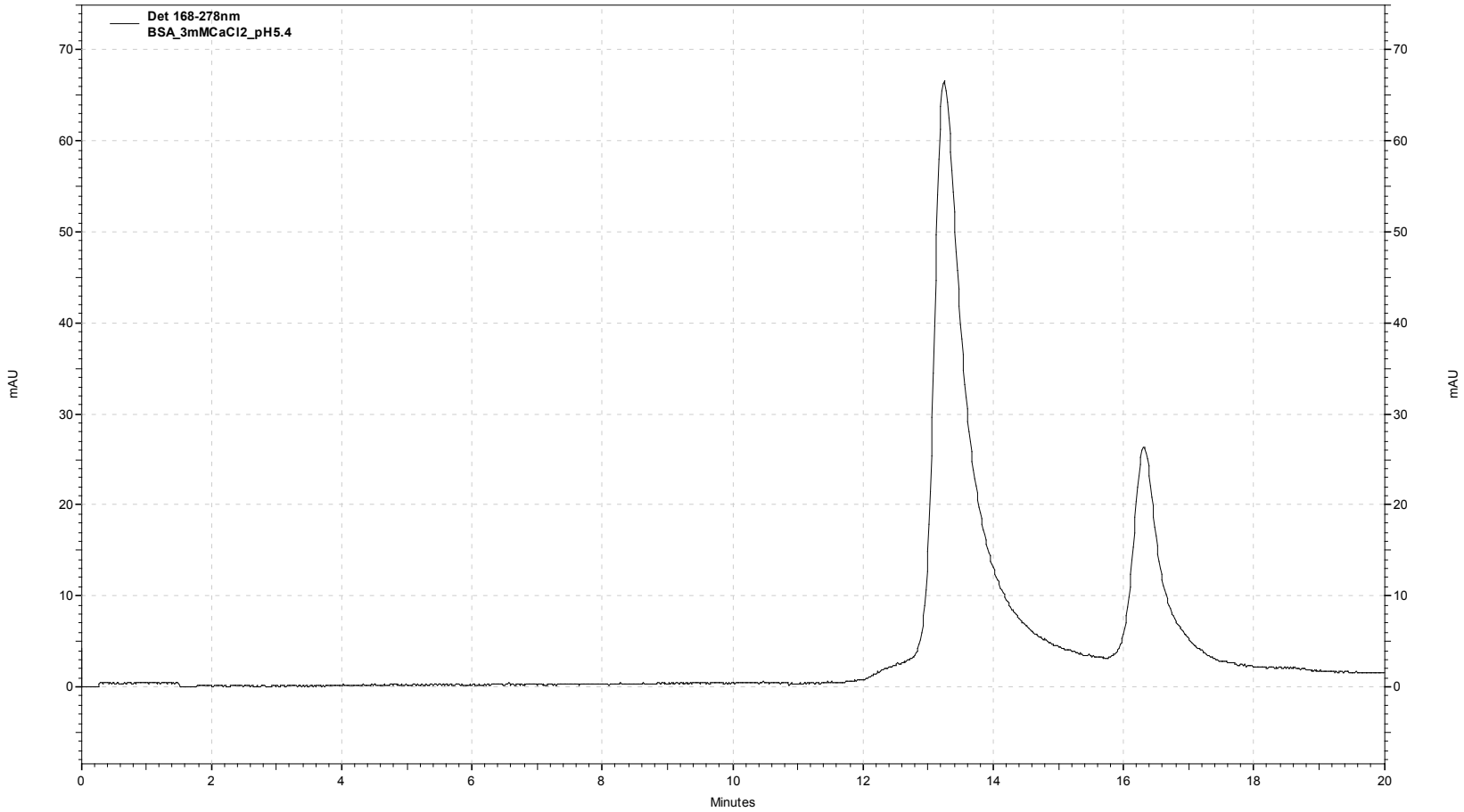


**Figure C.12.** Chromatograph of BSA in 0.003 M $CaCl_2$, pH 5.4. [BSA]: 12 g/L. Flowrate: 0.7 mL/min. Wavelength: 278 nm. Retention Time (peak area): 13.250 min (2,838,881 mAu), 16.317 min (913,255 mAu).

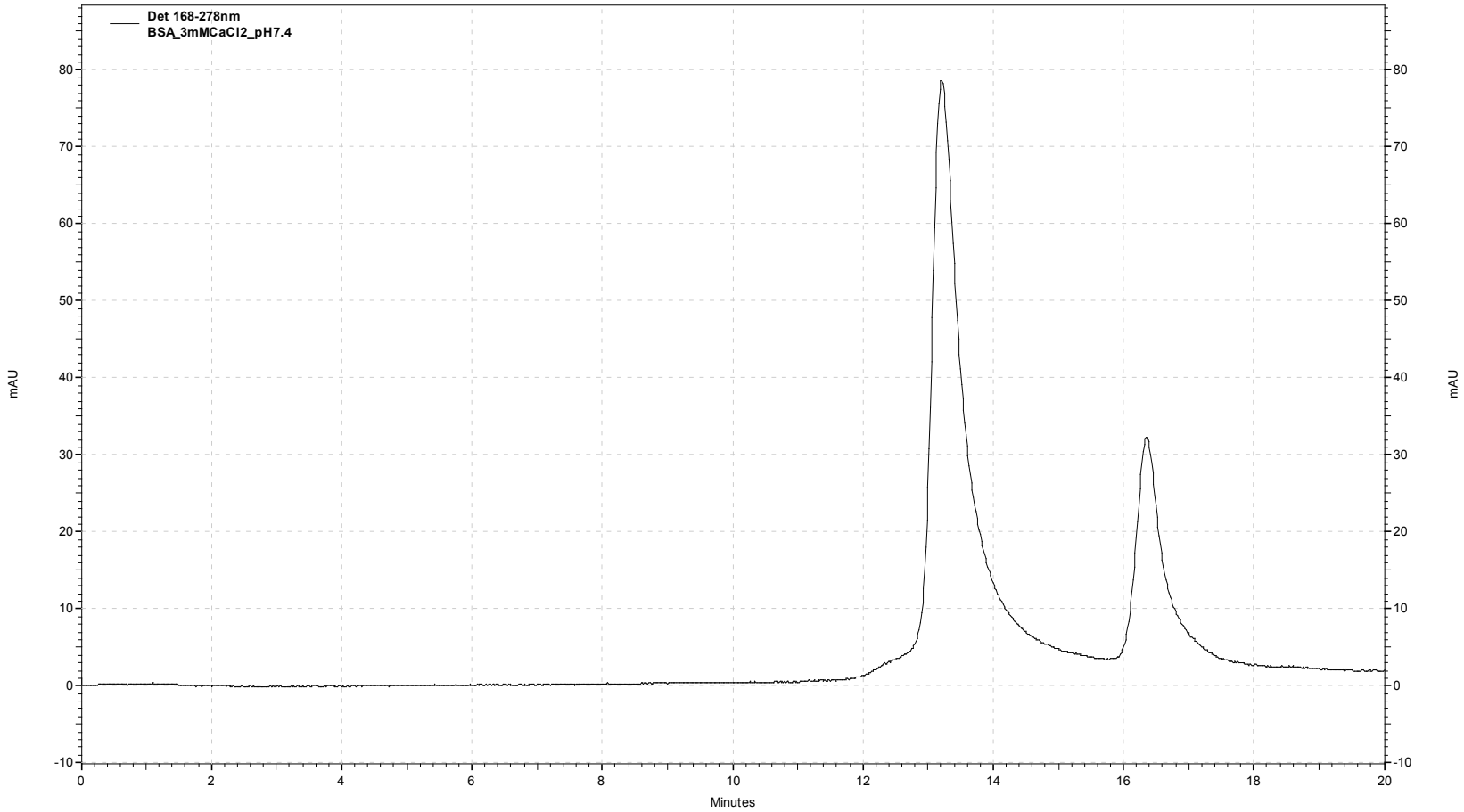


**Figure C.13.** Chromatograph of BSA in 0.003 M $CaCl_2$, pH 7.4. [BSA]: 12 g/L. Flowrate: 0.7 mL/min. Wavelength: 278 nm. Retention Time (peak area): 13.217 min (3,235,495 mAu), 16.350 min (1,116,361 mAu).

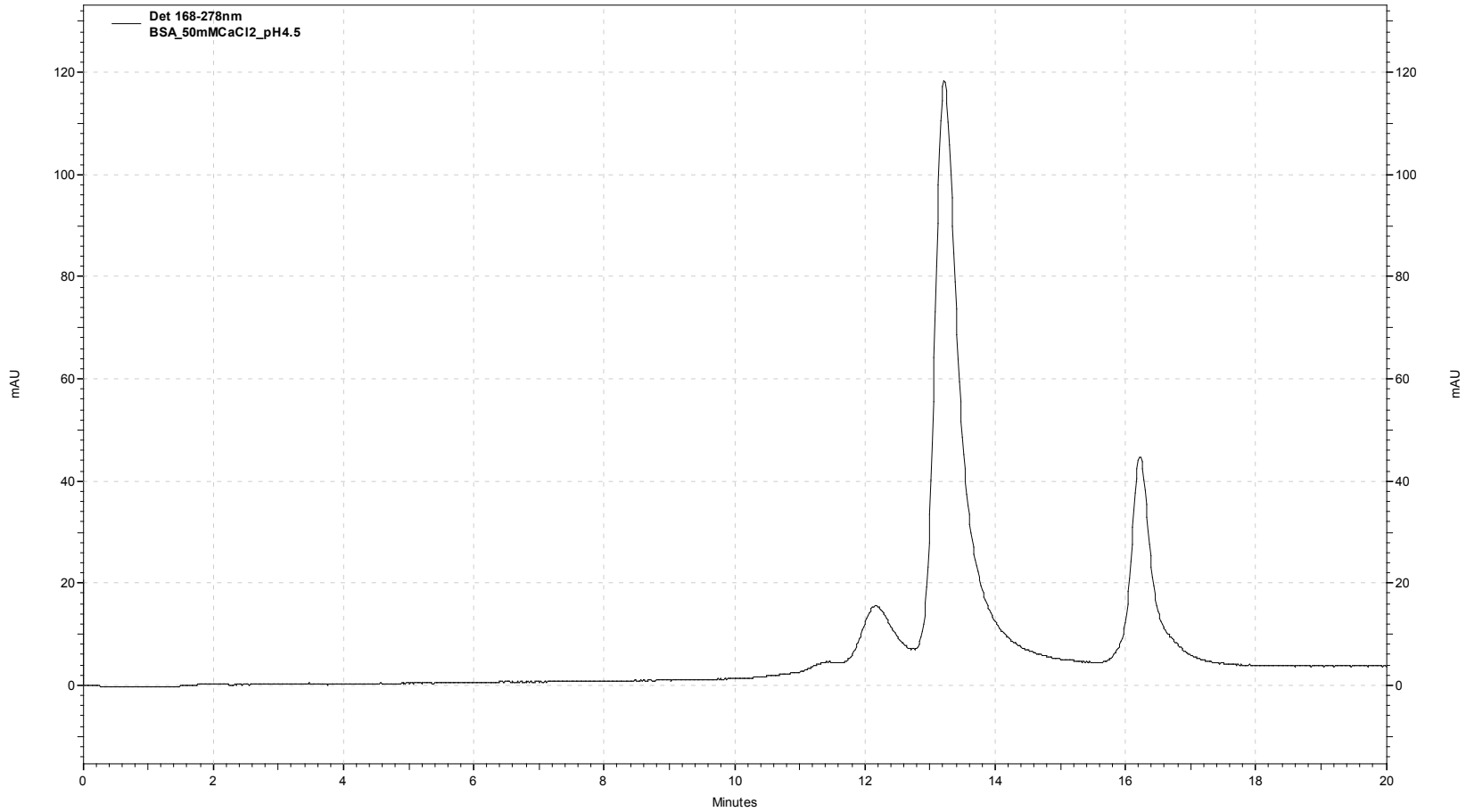


**Figure C.14.** Chromatograph of BSA in 0.05 M $CaCl_2$, pH 4.5. [BSA]: 12 g/L. Flowrate: 0.7 mL/min. Wavelength: 278 nm. Retention Time (peak area): 11.417 min (134,247 mAu), 12.167 min (546,095 mAu), 13.217 min (3,722,196 mAu), 16.217 min (1,166,748 mAu).

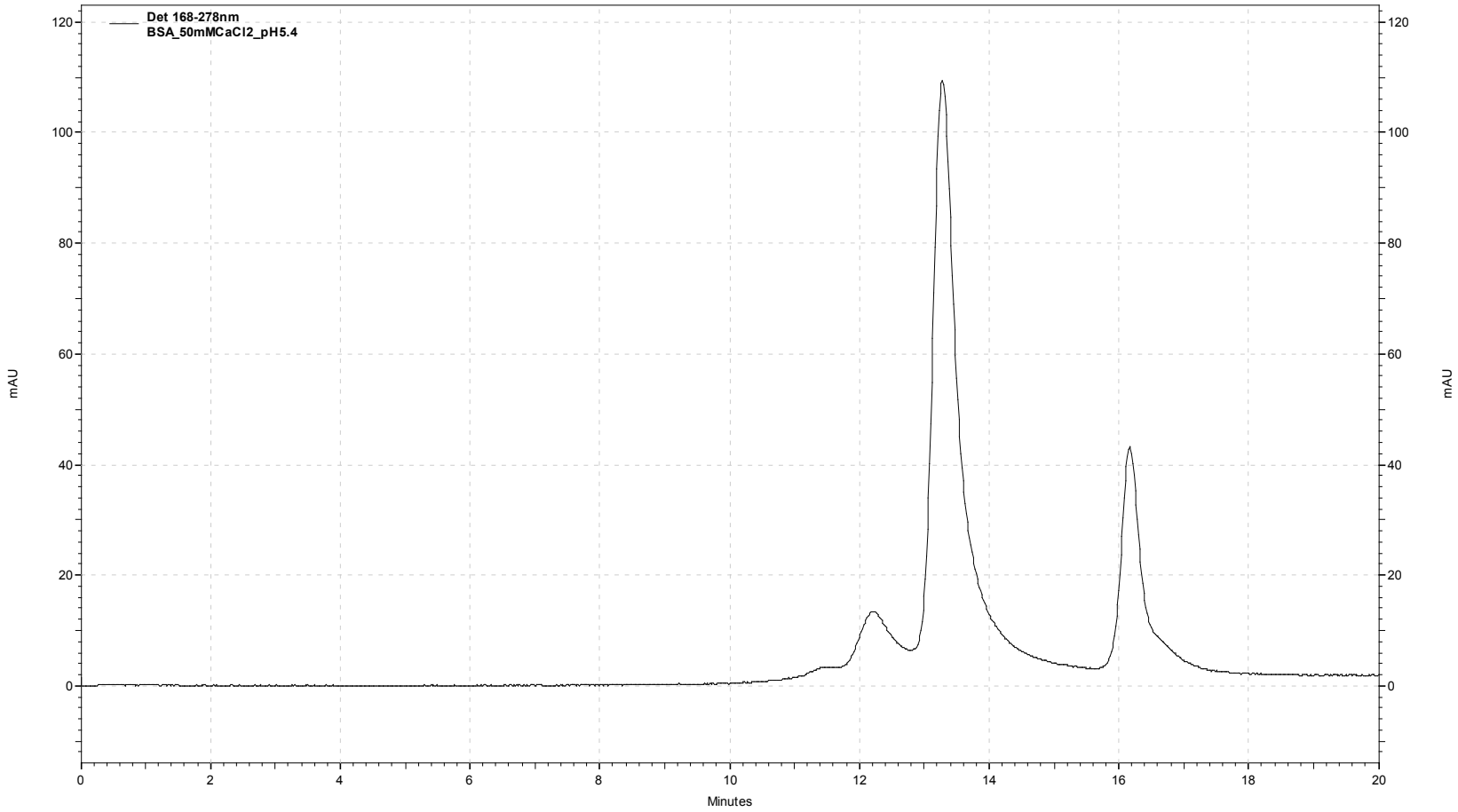


**Figure C.15.** Chromatograph of BSA in 0.05 M $CaCl_2$, pH 5.4, 278 nm. [BSA]: 12 g/L. Flowrate: 0.7 mL/min. Wavelength: 278 nm. Retention Time (peak area): 11.483 min (96,965 mAu), 12.217 min (535,311 mAu), 13.283 min (3,498,126 mAu), 16.167 min (1,089,452 mAu).

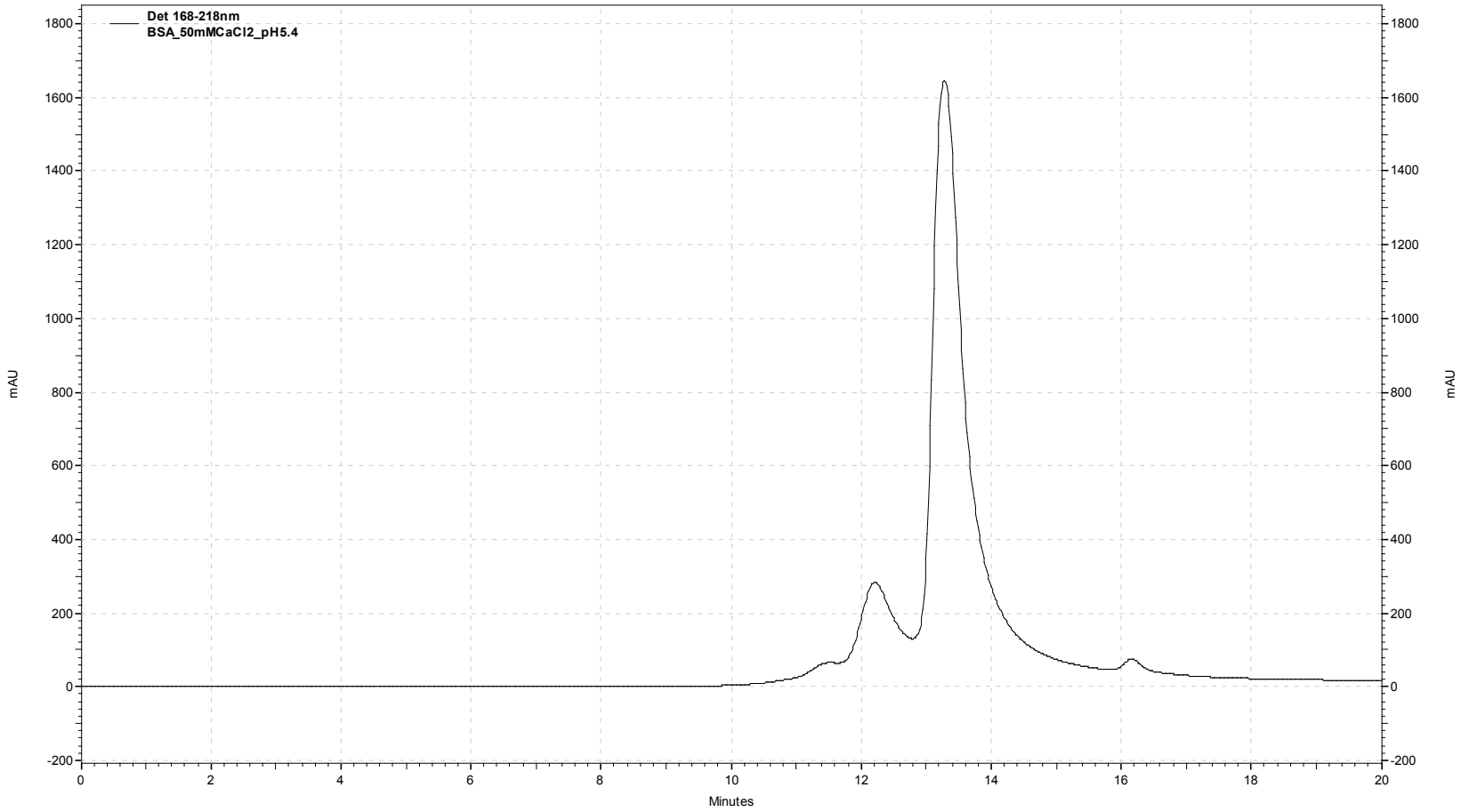


**Figure C.16.** Chromatograph of BSA in 0.05 M $CaCl_2$, pH 5.4, 218 nm. [BSA]: 12 g/L. Flowrate: 0.7 mL/min. Wavelength: 218 nm. This is the same sample as Figure C.15 but analyzed at 218 nm. The second peak at 16.167 min is almost non-existent.

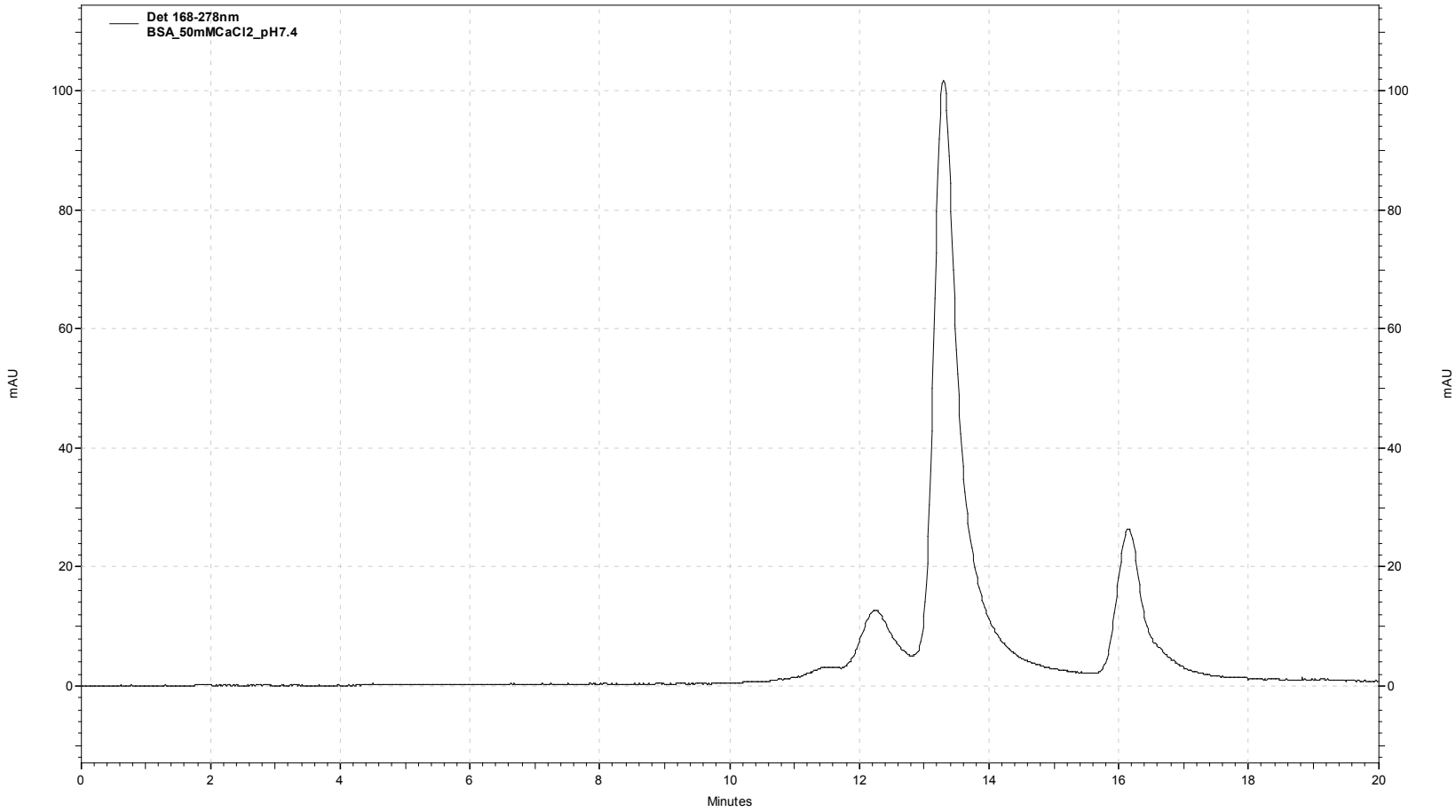


**Figure C.17.** Chromatograph of BSA in 0.05 M $CaCl_2$, pH 7.4. [BSA]: 12 g/L. Flowrate: 0.7 mL/min. Wavelength: 278 nm. Retention Time (peak area): 11.517 min (117,220 mAu), 12.233 min (503,617 mAu), 13.300 min (3,219,367 mAu), 16.167 min (900,194 mAu).

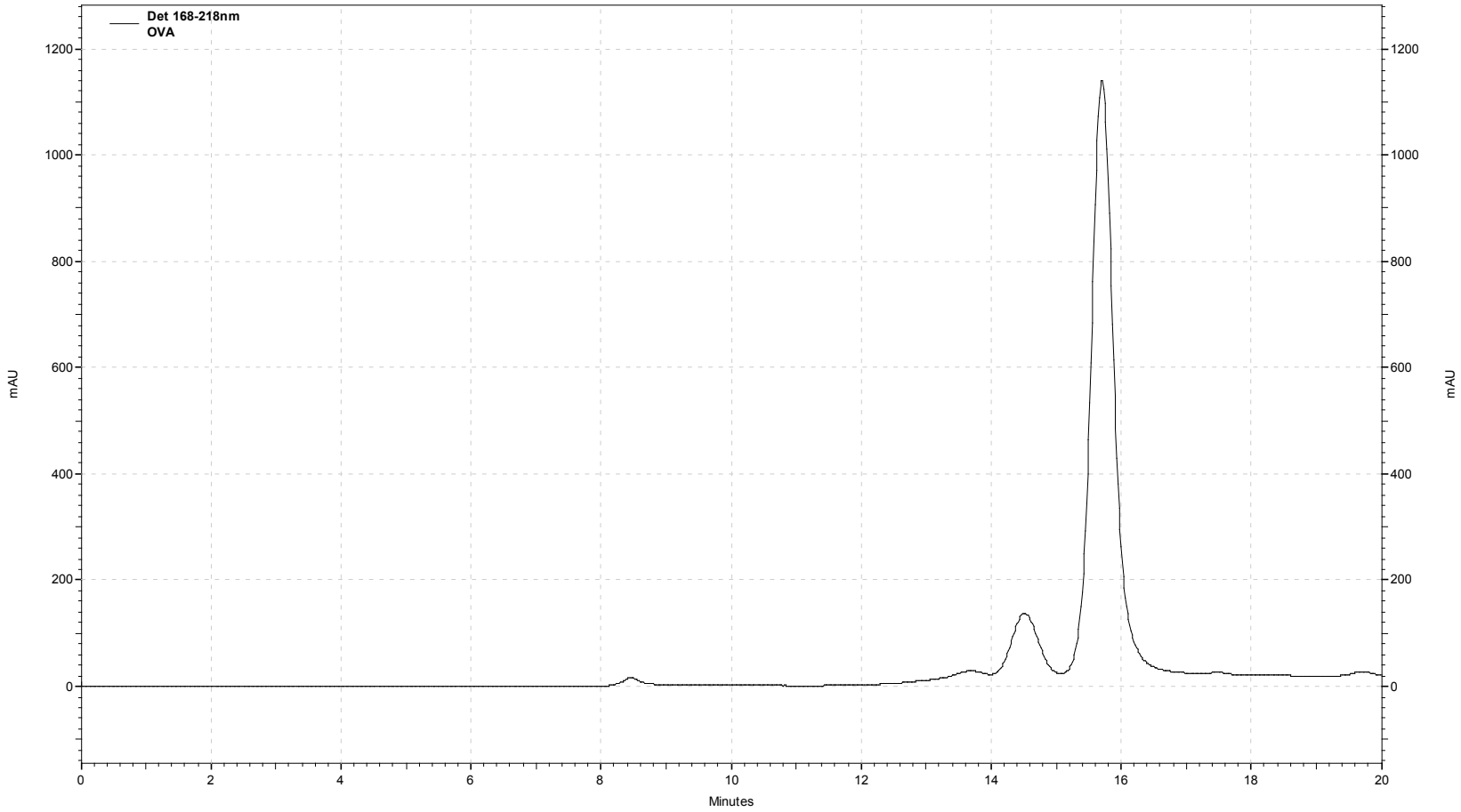


**Figure C.18.** Chromatograph of BSA in 0.5 M $CaCl_2$, pH 5.4. [BSA]: 25 g/L. Flowrate: 0.7 mL/min. Wavelength: 218 nm. Retention Time (peak area): 11.183 min (694,949 mAu), 11.950 min (1,351,101 mAu), 13.067 min (5,856,596 mAu).

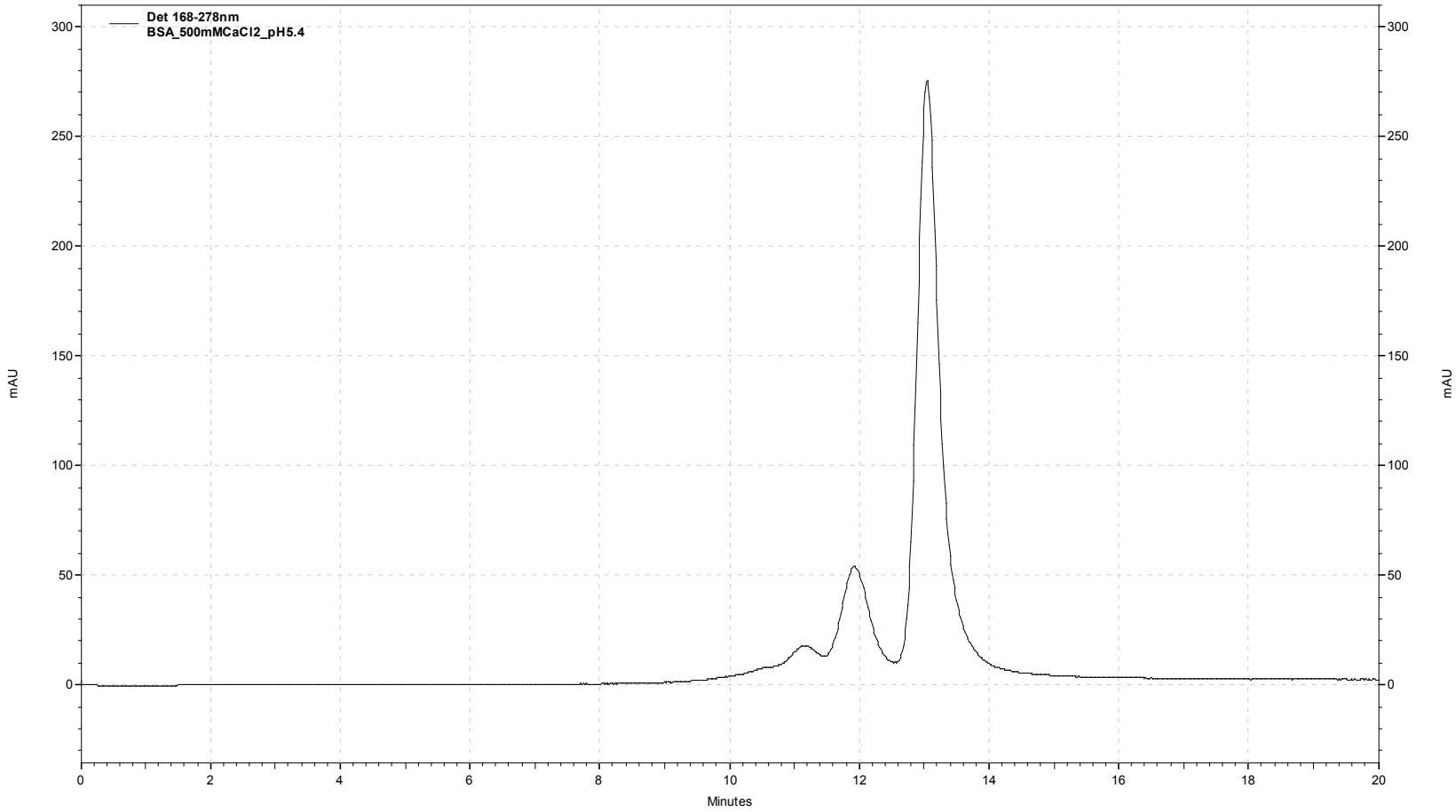


**Figure C.19.** Chromatograph of BSA in 0.5 M $CaCl_2$, pH 7.4. [BSA]: 12 g/L. Flowrate: 0.7 mL/min. Wavelength: 278 nm. Retention Time (peak area): 11.167 min (845,610 mAu), 11.933 min (1,824,267 mAu), 13.050 min (7,448,617 mAu).

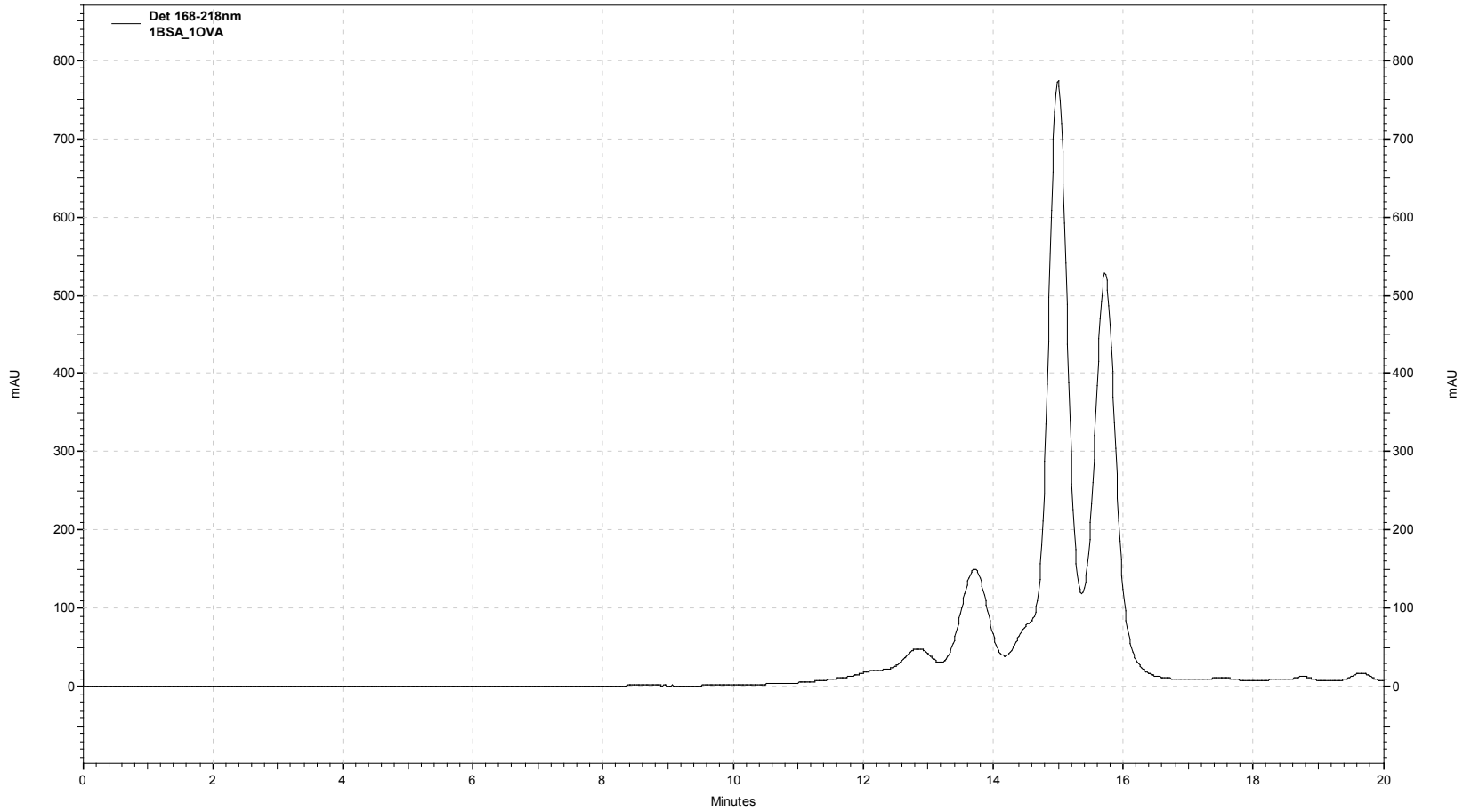


**Figure C.20.** Chromatograph of 1:1 OVA:BSA in 0.15 M NaCl, pH 5.4. Flowrate: 0.5 mL/min. Wavelength: 218 nm. Retention Time (peak area): 12.850 min (2,597,074 mAu), 13.717 min (4,938,472 mAu), 15.000 min (18,607,238 mAu), 5.717 min (13,227,851 mAu).

# APPENDIX D.

# THE MULTI-COMPONENT FREE-SOLVENT MODEL FOR A SOLUTION OF SEVEN PROTEINS FORMING HOMO- AND HETERO-MULTIMERS

## D.1. Monomeric Proteins in Solution Forming Homo- and Hetero-multimers

Consider a multi-component protein mixture, containing seven monomeric proteins, in an aqueous solution with a single monovalent salt in which homo-multimers and hetero-multimers are present. For illustration purposes, let the monomeric proteins be labeled proteins $A \to G$, and let the solution contain the formation of several homo-multimers ( $AA$, $BBB$, $EE$, and $FFFFF$ ) and hetero-multimers ( $BCC$, $CCDD$, $EF$, $ABE$, $BEFG$, and $ABCDEFG$ ).

### D.1.1. Free-Solvent in Compartment II

In this solution, the total number of monomeric proteins is seven $(p = 7)$ and the total number of species is nine $(n = 9)$. The solvent and salt are species 1 and 9, respectively, while the proteins are species 2 - 8 (where protein $A$ is species 2, protein $B$ is species 3, etc).

For the solution in compartment II, the solvent bound to the proteins and their interactions become

$$\sum \nu_{\text{solvent/homo-multimer}} N^{\text{II}}_{\text{homo-multimers}} = \sum_{j=2}^{8} \sum_{Z=\text{ii}} \nu_{1j,Z} \alpha_{j,Z} N^{\text{II}}_{j} ,$$

$$\sum \nu_{\text{solvent/hetero-multimers}} N^{\text{II}}_{\text{hetero-multimers}} =$$

$$\left[\begin{array}{l}
\\
\sum_{j=2}^{7}\sum_{a=3}^{8}\sum_{A=\text{i}}\sum_{B=\text{i}}\nu_{1\,ja,A:B}\beta_{ja,A:B}N_j^{\text{II}} + \sum_{j=2}^{6}\sum_{a=j+1}^{7}\sum_{\substack{b=j+2\\ b\neq a}}^{8}\sum_{A=\text{i}}\sum_{B=\text{i}}\sum_{C=\text{i}}\nu_{1\,jab,A:B:C}\beta_{jab,A:B:C}N_j^{\text{II}} + \ldots \\
\ldots + \sum_{j=2}^{5}\sum_{a=j+1}^{6}\sum_{\substack{b=j+2\\ b\neq a}}^{7}\sum_{\substack{c=j+3\\ c\neq a\\ c\neq b}}^{8}\sum_{A=\text{i}}\sum_{B=\text{i}}\sum_{C=\text{i}}\sum_{D=\text{i}}\nu_{1\,jabc,A:B:C:D}\beta_{jabc,A:B:C:D}N_j^{\text{II}} + \ldots \\
\ldots + \sum_{j=2}^{2}\sum_{a=j+1}^{3}\sum_{\substack{b=j+2\\ b\neq a}}^{4}\sum_{\substack{c=j+3\\ c\neq a\\ c\neq b}}^{5}\sum_{\substack{d=j+4\\ d\neq a\\ d\neq b\\ d\neq c}}^{6}\sum_{\substack{e=j+5\\ e\neq a\\ e\neq b\\ e\neq c\\ e\neq d}}^{7}\sum_{\substack{f=j+6\\ f\neq a\\ f\neq b\\ f\neq c\\ f\neq d\\ f\neq e}}^{8}\sum_{A=\text{i}}\sum_{B=\text{i}}\sum_{C=\text{i}}\sum_{D=\text{i}}\sum_{E=\text{i}}\sum_{F=\text{i}}\sum_{G=\text{i}}\nu_{1\,jabcdef,A:B:C:D:E:F:G}\beta_{jabcdef,A:B:C:D:E:F:G}N_j^{\text{II}} \\
\\
\end{array}\right],$$

and

$$\sum \nu_{\text{solvent/monomer}} N^{\text{II}}_{\text{monomers}} =$$

$$\sum_{j=2}^{8}\nu_{1j}\left(\begin{array}{l}
1 - \sum_{Z=\text{ii}}\nu_{jj,Z}\alpha_{j,Z} + \ldots \\
\ldots - \sum_{a=2}^{8}\sum_{A=\text{i}}\sum_{B=\text{i}}\nu_{ja,A:B}\beta_{ja,A:B} + \sum_{a=2}^{8}\sum_{\substack{b=2\\ b\neq a}}^{8}\sum_{A=\text{i}}\sum_{B=\text{i}}\sum_{C=\text{i}}\nu_{jab,A:B:C}\beta_{jab,A:B:C} + \ldots \\
+ \ldots \sum_{a=2}^{8}\sum_{\substack{b=2\\ b\neq a}}^{8}\sum_{\substack{c=2\\ c\neq a\\ c\neq b}}^{8}\sum_{A=\text{i}}\sum_{B=\text{i}}\sum_{C=\text{i}}\sum_{D=\text{i}}\nu_{jabc,A:B:C:D}\beta_{jabc,A:B:C:D} + \ldots \\
\ldots + \sum_{a=2}^{8}\sum_{\substack{b=2\\ b\neq a}}^{8}\sum_{\substack{c=2\\ c\neq a\\ c\neq b}}^{8}\sum_{\substack{d=2\\ d\neq a\\ d\neq b\\ d\neq c}}^{8}\sum_{\substack{e=2\\ e\neq a\\ e\neq b\\ e\neq c\\ e\neq d}}^{8}\sum_{\substack{f=2\\ f\neq a\\ f\neq b\\ f\neq c\\ f\neq d\\ f\neq e}}^{8}\sum_{A=\text{i}}\sum_{B=\text{i}}\sum_{C=\text{i}}\sum_{D=\text{i}}\sum_{E=\text{i}}\sum_{F=\text{i}}\sum_{G=\text{i}}\nu_{jabcdef,A:B:C:D:E:F:G}\beta_{jabcdef,A:B:C:D:E:F:G} \\
\\
\end{array}\right)N_j^{\text{II}}.$$

The above equations reduce to

$$\sum \nu_{\text{solvent/homo-multimer}} N^{\text{II}}_{\text{homo-multimers}} = \nu_{12,\text{ii}}\alpha_{2,\text{ii}}N_2^{\text{II}} + \nu_{13,\text{iii}}\alpha_{3,\text{iii}}N_3^{\text{II}} + \nu_{16,\text{ii}}\alpha_{6,\text{ii}}N_6^{\text{II}} + \nu_{17,\text{v}}\alpha_{7,\text{v}}N_7^{\text{II}},$$

$$\sum \nu_{\text{solvent/hetero-multimers}} N^{\text{II}}_{\text{hetero-multimers}} = \begin{bmatrix} \nu_{134,\text{i:ii}}\beta_{34,\text{i:ii}}N_3^{\text{II}} + \nu_{145,\text{ii:ii}}\beta_{45,\text{ii:ii}}N_4^{\text{II}} + \nu_{167,\text{i:i}}\beta_{67,\text{i:i}}N_6^{\text{II}} + \nu_{1236,\text{i:i:i}}\beta_{236,\text{i:i:i}}N_2^{\text{II}} + \ldots \\ \ldots + \nu_{13678,\text{i:i:i:i}}\beta_{3678,\text{i:i:i:i}}N_3^{\text{II}} + \nu_{12345678,\text{i:i:i:i:i:i:i}}\beta_{2345678,\text{i:i:i:i:i:i:i}}N_2^{\text{II}} \end{bmatrix},$$

and

$$\sum \nu_{\text{solvent/monomer}} N^{\text{II}}_{\text{monomers}} = \begin{bmatrix} \nu_{12}\left(1-\nu_{22,\text{ii}}\alpha_{2,\text{ii}} - \nu_{236,\text{i:i:i}}\beta_{236,\text{i:i:i}} - \nu_{2345678,\text{i:i:i:i:i:i:i}}\beta_{2345678,\text{i:i:i:i:i:i:i}}\right)N_2^{\text{II}} + \ldots \\ \ldots + \nu_{13}\left(1-\nu_{33,\text{iii}}\alpha_{3,\text{iii}} - \nu_{34,\text{i:ii}}\beta_{34,\text{i:ii}} - \nu_{326,\text{i:i:i}}\beta_{326,\text{i:i:i}} - \nu_{3678,\text{i:i:i:i}}\beta_{3678,\text{i:i:i:i}} - \nu_{3245678,\text{i:i:i:i:i:i:i}}\beta_{3245678,\text{i:i:i:i:i:i:i}}\right)N_3^{\text{II}} + \ldots \\ \ldots + \nu_{14}\left(1-\nu_{43,\text{iii}}\beta_{43,\text{iii}} - \nu_{45,\text{i:ii}}\beta_{45,\text{i:ii}} - \nu_{4235678,\text{i:i:i:i:i:i:i}}\beta_{4235678,\text{i:i:i:i:i:i:i}}\right)N_4^{\text{II}} + \ldots \\ \ldots + \nu_{15}\left(1-\nu_{54,\text{ii:ii}}\beta_{54,\text{ii:ii}} - \nu_{5234678,\text{i:i:i:i:i:i:i}}\beta_{5234678,\text{i:i:i:i:i:i:i}}\right)N_5^{\text{II}} + \ldots \\ \ldots + \nu_{16}\left(1-\nu_{66,\text{ii}}\alpha_{6,\text{ii}} - \nu_{67,\text{i:i}}\beta_{67,\text{i:i}} - \nu_{623,\text{i:i:i}}\beta_{623,\text{i:i:i}} - \nu_{6378,\text{i:i:i:i}}\beta_{6378,\text{i:i:i:i}} - \nu_{6234578,\text{i:i:i:i:i:i:i}}\beta_{6234578,\text{i:i:i:i:i:i:i}}\right)N_6^{\text{II}} + \ldots \\ \ldots + \nu_{17}\left(1-\nu_{77,\text{v}}\alpha_{7,\text{v}} - \nu_{76,\text{i:i}}\beta_{76,\text{i:i}} - \nu_{7368,\text{i:i:i:i}}\beta_{7368,\text{i:i:i:i}} - \nu_{7234568,\text{i:i:i:i:i:i:i}}\beta_{7234568,\text{i:i:i:i:i:i:i}}\right)N_7^{\text{II}} + \ldots \\ \ldots + \nu_{18}\left(1-\nu_{7368,\text{i:i:i:i}}\beta_{7368,\text{i:i:i:i}} - \nu_{7234568,\text{i:i:i:i:i:i:i}}\beta_{7234568,\text{i:i:i:i:i:i:i}}\right)N_8^{\text{II}} \end{bmatrix}.$$



Then moles of free-solvent becomes

$$\begin{aligned} & N_1^{\text{II}} - \left(\nu_{12,\text{ii}}\alpha_{2,\text{ii}}N_2^{\text{II}} + \nu_{13,\text{iii}}\alpha_{3,\text{iii}}N_3^{\text{II}} + \nu_{16,\text{ii}}\alpha_{6,\text{ii}}N_6^{\text{II}} + \nu_{17,\text{v}}\alpha_{7,\text{v}}N_7^{\text{II}}\right) + \ldots \\ & \ldots - \left(\nu_{134,\text{i:ii}}\beta_{34,\text{i:ii}}N_3^{\text{II}} + \nu_{145,\text{ii:ii}}\beta_{45,\text{ii:ii}}N_4^{\text{II}} + \nu_{167,\text{i:i}}\beta_{67,\text{i:i}}N_6^{\text{II}} + \nu_{1236,\text{i:i:i}}\beta_{236,\text{i:i:i}}N_2^{\text{II}}\right) + \ldots \\ & \ldots - \left(\nu_{13678,\text{i:i:i:i}}\beta_{3678,\text{i:i:i:i}}N_3^{\text{II}} + \nu_{12345678,\text{i:i:i:i:i:i:i}}\beta_{2345678,\text{i:i:i:i:i:i:i}}N_2^{\text{II}}\right) - \left(1-\nu_{22,\text{ii}}\alpha_{2,\text{ii}} - \nu_{236,\text{i:i:i}}\beta_{236,\text{i:i:i}} - \nu_{2345678,\text{i:i:i:i:i:i:i}}\beta_{2345678,\text{i:i:i:i:i:i:i}}\right)N_2^{\text{II}} + \ldots \\ & \ldots - \left(1-\nu_{33,\text{iii}}\alpha_{3,\text{iii}} - \nu_{34,\text{i:ii}}\beta_{34,\text{i:ii}} - \nu_{326,\text{i:i:i}}\beta_{326,\text{i:i:i}} - \nu_{3678,\text{i:i:i:i}}\beta_{3678,\text{i:i:i:i}} - \nu_{3245678,\text{i:i:i:i:i:i:i}}\beta_{3245678,\text{i:i:i:i:i:i:i}}\right)N_3^{\text{II}} + \ldots \\ & \ldots - \left(1-\nu_{43,\text{iii}}\beta_{43,\text{iii}} - \nu_{45,\text{i:ii}}\beta_{45,\text{i:ii}} - \nu_{4235678,\text{i:i:i:i:i:i:i}}\beta_{4235678,\text{i:i:i:i:i:i:i}}\right)N_4^{\text{II}} - \left(1-\nu_{54,\text{ii:ii}}\beta_{54,\text{ii:ii}} - \nu_{5234678,\text{i:i:i:i:i:i:i}}\beta_{5234678,\text{i:i:i:i:i:i:i}}\right)N_5^{\text{II}} + \ldots \\ & \ldots - \left(1-\nu_{66,\text{ii}}\alpha_{6,\text{ii}} - \nu_{67,\text{i:i}}\beta_{67,\text{i:i}} - \nu_{623,\text{i:i:i}}\beta_{623,\text{i:i:i}} - \nu_{6378,\text{i:i:i:i}}\beta_{6378,\text{i:i:i:i}} - \nu_{6234578,\text{i:i:i:i:i:i:i}}\beta_{6234578,\text{i:i:i:i:i:i:i}}\right)N_6^{\text{II}} + \ldots \\ & \ldots - \left(1-\nu_{77,\text{v}}\alpha_{7,\text{v}} - \nu_{76,\text{i:i}}\beta_{76,\text{i:i}} - \nu_{7368,\text{i:i:i:i}}\beta_{7368,\text{i:i:i:i}} - \nu_{7234568,\text{i:i:i:i:i:i:i}}\beta_{7234568,\text{i:i:i:i:i:i:i}}\right)N_7^{\text{II}} + \ldots \\ & \ldots - \left(1-\nu_{7368,\text{i:i:i:i}}\beta_{7368,\text{i:i:i:i}} - \nu_{7234568,\text{i:i:i:i:i:i:i}}\beta_{7234568,\text{i:i:i:i:i:i:i}}\right)N_8^{\text{II}} \end{aligned} \qquad \text{(D.1)}$$

D.1.2. Total Moles in Compartment II

The total moles of proteins and the bound solvent in compartment II are

$$\sum N^{\mathrm{II}}_{\text{homo-multimers}} = \sum_{j=2}^{8} \sum_{Z=\mathrm{ii}} \alpha_{j,Z} N_j^{\mathrm{II}} \ ,$$

$$\sum \nu N^{\mathrm{II}}_{\text{homo-multimers}} = \sum_{\substack{i=1 \\ i\neq 2\to 8}}^{9} \sum_{j=2}^{8} \sum_{Z=\mathrm{ii}} \nu_{ij,Z} \alpha_{j,Z} N_j^{\mathrm{II}} \ ,$$

$$\sum N^{\mathrm{II}}_{\text{hetero-multimers}} = \left[ \begin{array}{l} \sum_{j=2}^{7} \sum_{a=j+1}^{8} \sum_{A=\mathrm{i}} \sum_{B=\mathrm{i}} \beta_{ja,A:B} N_j^{\mathrm{II}} + \ldots \\ \ldots + \sum_{j=2}^{6} \sum_{a=j+1}^{7} \sum_{\substack{b=j+2 \\ b\neq a}}^{8} \sum_{A=\mathrm{i}} \sum_{B=\mathrm{i}} \sum_{C=\mathrm{i}} \beta_{jab,A:B:C} N_j^{\mathrm{II}} + \ldots \\ \ldots + \sum_{j=2}^{5} \sum_{\substack{a=j+1 \\ a\neq j}}^{6} \sum_{\substack{b=j+2 \\ b\neq j \\ b\neq a}}^{7} \sum_{\substack{c=j+3 \\ c\neq j \\ c\neq a}}^{8} \sum_{A=\mathrm{i}} \sum_{B=\mathrm{i}} \sum_{C=\mathrm{i}} \sum_{D=\mathrm{i}} \beta_{jabc,A:B:C:D} N_j^{\mathrm{II}} + \ldots \\ \ldots + \sum_{j=2}^{2} \sum_{\substack{a=j+1 \\ a\neq j}}^{3} \sum_{\substack{b=j+2 \\ b\neq j \\ b\neq a}}^{4} \sum_{\substack{c=j+3 \\ c\neq j \\ c\neq a \\ c\neq b}}^{5} \sum_{\substack{d=j+4 \\ d\neq j \\ d\neq a \\ d\neq b \\ d\neq c}}^{6} \sum_{\substack{e=j+5 \\ e\neq j \\ e\neq a \\ e\neq b \\ e\neq c \\ e\neq d}}^{7} \sum_{\substack{f=j+6 \\ f\neq j \\ f\neq a \\ f\neq b \\ f\neq c \\ f\neq d \\ f\neq e}}^{8} \sum_{A=\mathrm{i}} \sum_{B=\mathrm{i}} \sum_{C=\mathrm{i}} \sum_{D=\mathrm{i}} \sum_{E=\mathrm{i}} \sum_{F=\mathrm{i}} \sum_{G=\mathrm{i}} \beta_{jabcdef,A:B:C:D:E:F:G} N_j^{\mathrm{II}} \end{array} \right] ,$$

$$\sum \nu N^{\mathrm{II}}_{\text{hetero-multimers}} = \left[ \begin{array}{l} \sum_{\substack{i=1 \\ i\neq 2\to 8}}^{9} \sum_{j=2}^{7} \sum_{a=j+1}^{8} \sum_{A=\mathrm{i}} \sum_{B=\mathrm{i}} \nu_{ija,A:B} \beta_{ja,A:B} N_j^{\mathrm{II}} + \ldots \\ \ldots + \sum_{\substack{i=1 \\ i\neq 2\to 8}}^{9} \sum_{j=2}^{6} \sum_{a=j+1}^{7} \sum_{\substack{b=j+2 \\ b\neq a}}^{8} \sum_{A=\mathrm{i}} \sum_{B=\mathrm{i}} \sum_{C=\mathrm{i}} \nu_{ijab,A:B:C} \beta_{jab,A:B:C} N_j^{\mathrm{II}} + \ldots \\ \ldots + \sum_{\substack{i=1 \\ i\neq 2\to 8}}^{9} \sum_{j=2}^{5} \sum_{\substack{a=2 \\ a\neq j}}^{6} \sum_{\substack{b=2 \\ b\neq j \\ b\neq a}}^{7} \sum_{\substack{c=2 \\ c\neq j \\ c\neq a}}^{8} \sum_{A=\mathrm{i}} \sum_{B=\mathrm{i}} \sum_{C=\mathrm{i}} \sum_{D=\mathrm{i}} \nu_{ijabc,A:B:C:D} \beta_{jabc,A:B:C:D} N_j^{\mathrm{II}} + \ldots \\ \ldots + \sum_{\substack{i=1 \\ i\neq 2\to 8}}^{9} \sum_{j=2}^{2} \sum_{\substack{a=2 \\ a\neq j}}^{3} \sum_{\substack{b=2 \\ b\neq j \\ b\neq a}}^{4} \sum_{\substack{c=2 \\ c\neq j \\ c\neq a \\ c\neq b}}^{5} \sum_{\substack{d=2 \\ d\neq j \\ d\neq a \\ d\neq b \\ d\neq c}}^{6} \sum_{\substack{e=2 \\ e\neq j \\ e\neq a \\ e\neq b \\ e\neq c \\ e\neq d}}^{7} \sum_{\substack{f=2 \\ f\neq j \\ f\neq a \\ f\neq b \\ f\neq c \\ f\neq d \\ f\neq e}}^{8} \sum_{A=\mathrm{i}} \sum_{B=\mathrm{i}} \sum_{C=\mathrm{i}} \sum_{D=\mathrm{i}} \sum_{E=\mathrm{i}} \sum_{F=\mathrm{i}} \sum_{G=\mathrm{i}} \nu_{ijabcdef,A:B:C:D:E:F:G} \beta_{jabcdef,A:B:C:D:E:F:G} N_j^{\mathrm{II}} \end{array} \right] ,$$

$$\sum N^{\mathrm{II}}_{\mathrm{monomers}} = \sum_{j=2}^{8} \left( \begin{array}{l} 1 - \sum_{Z=\mathrm{ii}} \nu_{jj,Z} \alpha_{j,Z} + \ldots \\ \ldots - \sum_{\substack{a=2 \\ a\neq j}}^{8} \sum_{A=\mathrm{i}} \sum_{B=\mathrm{i}} \nu_{ja,A:B} \beta_{ja,A:B} - \sum_{\substack{a=2 \\ a\neq j}}^{8} \sum_{\substack{b=2 \\ b\neq j \\ b\neq a}}^{8} \sum_{A=\mathrm{i}} \sum_{B=\mathrm{i}} \sum_{C=\mathrm{i}} \nu_{jab,A:B:C} \beta_{jab,A:B:C} + \ldots \\ \ldots - \sum_{\substack{a=2 \\ a\neq j}}^{8} \sum_{\substack{b=2 \\ b\neq j \\ b\neq a}}^{8} \sum_{\substack{c=2 \\ c\neq j \\ c\neq a}}^{8} \sum_{A=\mathrm{i}} \sum_{B=\mathrm{i}} \sum_{C=\mathrm{i}} \sum_{D=\mathrm{i}} \nu_{jabc,A:B:C:D} \beta_{jabc,A:B:C:D} + \ldots \\ \ldots - \sum_{\substack{a=2 \\ a\neq j}}^{8} \sum_{\substack{b=2 \\ b\neq j \\ b\neq a}}^{8} \sum_{\substack{c=2 \\ c\neq j \\ c\neq a \\ c\neq b}}^{8} \sum_{\substack{d=2 \\ d\neq j \\ d\neq a \\ d\neq b \\ d\neq c}}^{8} \sum_{\substack{e=2 \\ e\neq j \\ e\neq a \\ e\neq b \\ e\neq c \\ e\neq d}}^{8} \sum_{\substack{f=2 \\ f\neq j \\ f\neq a \\ f\neq b \\ f\neq c \\ f\neq d \\ f\neq e}}^{8} \sum_{A=\mathrm{i}} \sum_{B=\mathrm{i}} \sum_{C=\mathrm{i}} \sum_{D=\mathrm{i}} \sum_{E=\mathrm{i}} \sum_{F=\mathrm{i}} \sum_{G=\mathrm{i}} \nu_{jabcdef,A:B:C:D:E:F:G} \beta_{jabcdef,A:B:C:D:E:F:G} \end{array} \right) N_j^{\mathrm{II}} ,$$

and

$$\sum \nu N^{\mathrm{II}}_{\mathrm{monomers}} = \sum_{\substack{i=1 \\ i\neq 2 \to 8}}^{9} \sum_{j=2}^{8} \nu_{ij} \left( \begin{array}{l} 1 - \sum_{Z=\mathrm{ii}} \nu_{jj,Z} \alpha_{j,Z} + \ldots \\ \ldots - \sum_{\substack{a=2 \\ a\neq j}}^{8} \sum_{A=\mathrm{i}} \sum_{B=\mathrm{i}} \nu_{ja,A:B} \beta_{ja,A:B} - \sum_{\substack{a=2 \\ a\neq j}}^{8} \sum_{\substack{b=2 \\ b\neq j \\ b\neq a}}^{8} \sum_{A=\mathrm{i}} \sum_{B=\mathrm{i}} \sum_{C=\mathrm{i}} \nu_{jab,A:B:C} \beta_{jab,A:B:C} + \ldots \\ \ldots - \sum_{\substack{a=2 \\ a\neq j}}^{8} \sum_{\substack{b=2 \\ b\neq j \\ b\neq a}}^{8} \sum_{\substack{c=2 \\ c\neq j \\ c\neq a}}^{8} \sum_{A=\mathrm{i}} \sum_{B=\mathrm{i}} \sum_{C=\mathrm{i}} \sum_{D=\mathrm{i}} \nu_{jabc,A:B:C:D} \beta_{jabc,A:B:C:D} + \ldots \\ \ldots - \sum_{\substack{a=2 \\ a\neq j}}^{8} \sum_{\substack{b=2 \\ b\neq j \\ b\neq a}}^{8} \sum_{\substack{c=2 \\ c\neq j \\ c\neq a \\ c\neq b}}^{8} \sum_{\substack{d=2 \\ d\neq j \\ d\neq a \\ d\neq b \\ d\neq c}}^{8} \sum_{\substack{e=2 \\ e\neq j \\ e\neq a \\ e\neq b \\ e\neq c \\ e\neq d}}^{8} \sum_{\substack{f=2 \\ f\neq j \\ f\neq a \\ f\neq b \\ f\neq c \\ f\neq d \\ f\neq e}}^{8} \sum_{A=\mathrm{i}} \sum_{B=\mathrm{i}} \sum_{C=\mathrm{i}} \sum_{D=\mathrm{i}} \sum_{E=\mathrm{i}} \sum_{F=\mathrm{i}} \sum_{G=\mathrm{i}} \nu_{jabcdef,A:B:C:D:E:F:G} \beta_{jabcdef,A:B:C:D:E:F:G} \end{array} \right) N_j^{\mathrm{II}}$$

which reduce to

$$\sum N^{\mathrm{II}}_{\text{homo-multimers}} = \alpha_{2,\mathrm{ii}} N_2^{\mathrm{II}} + \alpha_{3,\mathrm{iii}} N_3^{\mathrm{II}} + \alpha_{6,\mathrm{ii}} N_6^{\mathrm{II}} + \alpha_{7,\mathrm{v}} N_7^{\mathrm{II}} ,$$

$$\sum \nu N^{\mathrm{II}}_{\text{homo-multimers}} = \begin{bmatrix} \nu_{12,\mathrm{ii}}\alpha_{2,\mathrm{ii}}N_2^{\mathrm{II}} + \nu_{92,\mathrm{ii}}\alpha_{2,\mathrm{ii}}N_2^{\mathrm{II}} + \nu_{13,\mathrm{iii}}\alpha_{3,\mathrm{iii}}N_3^{\mathrm{II}} + \nu_{93,\mathrm{iii}}\alpha_{3,\mathrm{iii}}N_3^{\mathrm{II}} + \ldots \\ \ldots + \nu_{16,\mathrm{ii}}\alpha_{6,\mathrm{ii}}N_6^{\mathrm{II}} + \nu_{96,\mathrm{ii}}\alpha_{6,\mathrm{ii}}N_6^{\mathrm{II}} + \nu_{17,\mathrm{v}}\alpha_{7,\mathrm{v}}N_7^{\mathrm{II}} + \nu_{97,\mathrm{v}}\alpha_{7,\mathrm{v}}N_7^{\mathrm{II}} \end{bmatrix},$$

$$\sum N^{\mathrm{II}}_{\text{hetero-multimers}} = \begin{bmatrix} \beta_{34,\mathrm{i:ii}}N_3^{\mathrm{II}} + \beta_{45,\mathrm{ii:ii}}N_4^{\mathrm{II}} + \beta_{67,\mathrm{i:i}}N_6^{\mathrm{II}} + \beta_{236,\mathrm{i:i:i}}N_2^{\mathrm{II}} + \ldots \\ \ldots + \beta_{3678,\mathrm{i:i:i:i}}N_3^{\mathrm{II}} + \beta_{2345678,\mathrm{i:i:i:i:i:i:i}}N_2^{\mathrm{II}} \end{bmatrix},$$

$$\sum \nu N^{\mathrm{II}}_{\text{hetero-multimers}} = \begin{bmatrix} \nu_{134,\mathrm{i:ii}}\beta_{34,\mathrm{i:ii}}N_3^{\mathrm{II}} + \nu_{934,\mathrm{i:ii}}\beta_{34,\mathrm{i:ii}}N_3^{\mathrm{II}} + \nu_{145,\mathrm{ii:ii}}\beta_{45,\mathrm{ii:ii}}N_4^{\mathrm{II}} + \nu_{945,\mathrm{ii:ii}}\beta_{45,\mathrm{ii:ii}}N_4^{\mathrm{II}} + \ldots \\ \ldots + \nu_{167,\mathrm{i:i}}\beta_{67,\mathrm{i:i}}N_6^{\mathrm{II}} + \nu_{967,\mathrm{i:i}}\beta_{67,\mathrm{i:i}}N_6^{\mathrm{II}} + \nu_{1236,\mathrm{i:i:i}}\beta_{236,\mathrm{i:i:i}}N_2^{\mathrm{II}} + \nu_{9236,\mathrm{i:i:i}}\beta_{236,\mathrm{i:i:i}}N_2^{\mathrm{II}} + \ldots \\ \ldots + \nu_{13678,\mathrm{i:i:i:i}}\beta_{3678,\mathrm{i:i:i:i}}N_3^{\mathrm{II}} + \nu_{93678,\mathrm{i:i:i:i}}\beta_{3678,\mathrm{i:i:i:i}}N_3^{\mathrm{II}} + \ldots \\ \ldots + \nu_{12345678,\mathrm{i:i:i:i:i:i:i}}\beta_{2345678,\mathrm{i:i:i:i:i:i:i}}N_2^{\mathrm{II}} + \nu_{92345678,\mathrm{i:i:i:i:i:i:i}}\beta_{2345678,\mathrm{i:i:i:i:i:i:i}}N_2^{\mathrm{II}} \end{bmatrix},$$

$$\sum N^{\mathrm{II}}_{\text{monomers}} = \begin{bmatrix} \left(1 - \nu_{22,\mathrm{ii}}\alpha_{2,\mathrm{ii}} - \nu_{236,\mathrm{i:i:i}}\beta_{236,\mathrm{i:i:i}} - \nu_{2345678,\mathrm{i:i:i:i:i:i:i}}\beta_{2345678,\mathrm{i:i:i:i:i:i:i}}\right)N_2^{\mathrm{II}} + \ldots \\ \ldots + \left(1 - \nu_{33,\mathrm{iii}}\alpha_{3,\mathrm{iii}} - \nu_{34,\mathrm{i:ii}}\beta_{34,\mathrm{i:ii}} - \nu_{326,\mathrm{i:i:i}}\beta_{326,\mathrm{i:i:i}} - \nu_{3678,\mathrm{i:i:i:i}}\beta_{3678,\mathrm{i:i:i:i}} - \nu_{3245678,\mathrm{i:i:i:i:i:i:i}}\beta_{3245678,\mathrm{i:i:i:i:i:i:i}}\right)N_3^{\mathrm{II}} + \ldots \\ \ldots + \left(1 - \nu_{43,\mathrm{iii}}\beta_{43,\mathrm{iii}} - \nu_{45,\mathrm{i:ii:i}}\beta_{45,\mathrm{i:ii:i}} - \nu_{4235678,\mathrm{i:i:i:i:i:i:i}}\beta_{4235678,\mathrm{i:i:i:i:i:i:i}}\right)N_4^{\mathrm{II}} + \ldots \\ \ldots + \left(1 - \nu_{54,\mathrm{ii:ii}}\beta_{54,\mathrm{ii:ii}} - \nu_{5234678,\mathrm{i:i:i:i:i:i:i}}\beta_{5234678,\mathrm{i:i:i:i:i:i:i}}\right)N_5^{\mathrm{II}} + \ldots \\ \ldots + \left(1 - \nu_{66,\mathrm{ii}}\alpha_{6,\mathrm{ii}} - \nu_{67,\mathrm{i:i}}\beta_{67,\mathrm{i:i}} - \nu_{623,\mathrm{i:i:i}}\beta_{623,\mathrm{i:i:i}} - \nu_{6378,\mathrm{i:i:i:i}}\beta_{6378,\mathrm{i:i:i:i}} - \nu_{6234578,\mathrm{i:i:i:i:i:i:i}}\beta_{6234578,\mathrm{i:i:i:i:i:i:i}}\right)N_6^{\mathrm{II}} + \ldots \\ \ldots + \left(1 - \nu_{77,\mathrm{v}}\alpha_{7,\mathrm{v}} - \nu_{76,\mathrm{i:i}}\beta_{76,\mathrm{i:i}} - \nu_{7368,\mathrm{i:i:i:i}}\beta_{7368,\mathrm{i:i:i:i}} - \nu_{7234568,\mathrm{i:i:i:i:i:i:i}}\beta_{7234568,\mathrm{i:i:i:i:i:i:i}}\right)N_7^{\mathrm{II}} + \ldots \\ \ldots + \left(1 - \nu_{8367,\mathrm{i:i:i:i}}\beta_{8367,\mathrm{i:i:i:i}} - \nu_{8234567,\mathrm{i:i:i:i:i:i:i}}\beta_{8234567,\mathrm{i:i:i:i:i:i:i}}\right)N_8^{\mathrm{II}} \end{bmatrix},$$

and

$$\sum \nu N^{\mathrm{II}}_{\mathrm{monomers}} = \left[\begin{array}{l}
\nu_{12}\left(1-\nu_{22,\mathrm{ii}}\alpha_{2,\mathrm{ii}}-\nu_{236,\mathrm{i:i:i}}\beta_{236,\mathrm{i:i:i}}-\nu_{2345678,\mathrm{i:i:i:i:i:i:i}}\beta_{2345678,\mathrm{i:i:i:i:i:i:i}}\right)N_2^{\mathrm{II}}+\nu_{92}\left(1-\nu_{22,\mathrm{ii}}\alpha_{2,\mathrm{ii}}-\nu_{236,\mathrm{i:i:i}}\beta_{236,\mathrm{i:i:i}}-\nu_{2345678,\mathrm{i:i:i:i:i:i:i}}\beta_{2345678,\mathrm{i:i:i:i:i:i:i}}\right)N_2^{\mathrm{II}}+\ldots \\
\ldots+\nu_{13}\left(1-\nu_{33,\mathrm{iii}}\alpha_{3,\mathrm{iii}}-\nu_{34,\mathrm{i:ii}}\beta_{34,\mathrm{i:ii}}-\nu_{326,\mathrm{i:i:i}}\beta_{326,\mathrm{i:i:i}}-\nu_{3678,\mathrm{i:i:i:i}}\beta_{3678,\mathrm{i:i:i:i}}-\nu_{3245678,\mathrm{i:i:i:i:i:i:i}}\beta_{3245678,\mathrm{i:i:i:i:i:i:i}}\right)N_3^{\mathrm{II}}+\ldots \\
\ldots+\nu_{93}\left(1-\nu_{33,\mathrm{iii}}\alpha_{3,\mathrm{iii}}-\nu_{34,\mathrm{i:ii}}\beta_{34,\mathrm{i:ii}}-\nu_{326,\mathrm{i:i:i}}\beta_{326,\mathrm{i:i:i}}-\nu_{3678,\mathrm{i:i:i:i}}\beta_{3678,\mathrm{i:i:i:i}}-\nu_{3245678,\mathrm{i:i:i:i:i:i:i}}\beta_{3245678,\mathrm{i:i:i:i:i:i:i}}\right)N_3^{\mathrm{II}}+\ldots \\
\ldots+\nu_{14}\left(1-\nu_{43,\mathrm{iii}}\beta_{43,\mathrm{iii}}-\nu_{45,\mathrm{ii:ii}}\beta_{45,\mathrm{ii:ii}}-\nu_{4235678,\mathrm{i:i:i:i:i:i:i}}\beta_{4235678,\mathrm{i:i:i:i:i:i:i}}\right)N_4^{\mathrm{II}}+\nu_{94}\left(1-\nu_{43,\mathrm{iii}}\beta_{43,\mathrm{iii}}-\nu_{45,\mathrm{ii:ii}}\beta_{45,\mathrm{ii:ii}}-\nu_{4235678,\mathrm{i:i:i:i:i:i:i}}\beta_{4235678,\mathrm{i:i:i:i:i:i:i}}\right)N_4^{\mathrm{II}}+\ldots \\
\ldots+\nu_{15}\left(1-\nu_{54,\mathrm{ii:ii}}\beta_{54,\mathrm{ii:ii}}-\nu_{5234678,\mathrm{i:i:i:i:i:i:i}}\beta_{5234678,\mathrm{i:i:i:i:i:i:i}}\right)N_5^{\mathrm{II}}+\nu_{95}\left(1-\nu_{54,\mathrm{ii:ii}}\beta_{54,\mathrm{ii:ii}}-\nu_{5234678,\mathrm{i:i:i:i:i:i:i}}\beta_{5234678,\mathrm{i:i:i:i:i:i:i}}\right)N_5^{\mathrm{II}}+\ldots \\
\ldots+\nu_{16}\left(1-\nu_{66,\mathrm{ii}}\alpha_{6,\mathrm{ii}}-\nu_{67,\mathrm{i:i}}\beta_{67,\mathrm{i:i}}-\nu_{623,\mathrm{i:i:i}}\beta_{623,\mathrm{i:i:i}}-\nu_{6378,\mathrm{i:i:i:i}}\beta_{6378,\mathrm{i:i:i:i}}-\nu_{6234578,\mathrm{i:i:i:i:i:i:i}}\beta_{6234578,\mathrm{i:i:i:i:i:i:i}}\right)N_6^{\mathrm{II}}+\ldots \\
\ldots+\nu_{96}\left(1-\nu_{66,\mathrm{ii}}\alpha_{6,\mathrm{ii}}-\nu_{67,\mathrm{i:i}}\beta_{67,\mathrm{i:i}}-\nu_{623,\mathrm{i:i:i}}\beta_{623,\mathrm{i:i:i}}-\nu_{6378,\mathrm{i:i:i:i}}\beta_{6378,\mathrm{i:i:i:i}}-\nu_{6234578,\mathrm{i:i:i:i:i:i:i}}\beta_{6234578,\mathrm{i:i:i:i:i:i:i}}\right)N_6^{\mathrm{II}}+\ldots \\
\ldots+\nu_{17}\left(1-\nu_{77,\mathrm{v}}\alpha_{7,\mathrm{v}}-\nu_{76,\mathrm{i:i}}\beta_{76,\mathrm{i:i}}-\nu_{7368,\mathrm{i:i:i:i}}\beta_{7368,\mathrm{i:i:i:i}}-\nu_{7234568,\mathrm{i:i:i:i:i:i:i}}\beta_{7234568,\mathrm{i:i:i:i:i:i:i}}\right)N_7^{\mathrm{II}}+\ldots \\
\ldots+\nu_{97}\left(1-\nu_{77,\mathrm{v}}\alpha_{7,\mathrm{v}}-\nu_{76,\mathrm{i:i}}\beta_{76,\mathrm{i:i}}-\nu_{7368,\mathrm{i:i:i:i}}\beta_{7368,\mathrm{i:i:i:i}}-\nu_{7234568,\mathrm{i:i:i:i:i:i:i}}\beta_{7234568,\mathrm{i:i:i:i:i:i:i}}\right)N_7^{\mathrm{II}}+\ldots \\
\ldots+\nu_{18}\left(1-\nu_{8367,\mathrm{i:i:i:i}}\beta_{8367,\mathrm{i:i:i:i}}-\nu_{8234567,\mathrm{i:i:i:i:i:i:i}}\beta_{8234567,\mathrm{i:i:i:i:i:i:i}}\right)N_8^{\mathrm{II}}+\nu_{98}\left(1-\nu_{8367,\mathrm{i:i:i:i}}\beta_{7368,\mathrm{i:i:i:i}}-\nu_{8234567,\mathrm{i:i:i:i:i:i:i}}\beta_{8234567,\mathrm{i:i:i:i:i:i:i}}\right)N_8^{\mathrm{II}}
\end{array}\right].$$

Finally, the total moles in compartment II is

$$
\begin{aligned}
&N_{1}^{\mathrm{II}}+N_{9}^{\mathrm{II}}+\alpha_{2,\mathrm{ii}}N_{2}^{\mathrm{II}}+\alpha_{3,\mathrm{iii}}N_{3}^{\mathrm{II}}+\alpha_{6,\mathrm{ii}}N_{6}^{\mathrm{II}}+\alpha_{7,\mathrm{v}}N_{7}^{\mathrm{II}}+\beta_{34,\mathrm{i:ii}}N_{3}^{\mathrm{II}}+\beta_{45,\mathrm{ii:ii}}N_{4}^{\mathrm{II}}+\beta_{67,\mathrm{i:i}}N_{6}^{\mathrm{II}}+\beta_{236,\mathrm{i:i:i}}N_{2}^{\mathrm{II}}+\beta_{3678,\mathrm{i:i:i:i}}N_{3}^{\mathrm{II}}+\beta_{2345678,\mathrm{i:i:i:i:i:i:i}}N_{2}^{\mathrm{II}}+\ldots\\
&\ldots+\left(1-\nu_{22,\mathrm{ii}}\alpha_{2,\mathrm{ii}}-\nu_{236,\mathrm{i:i:i}}\beta_{236,\mathrm{i:i:i}}-\nu_{2345678,\mathrm{i:i:i:i:i:i:i}}\beta_{2345678,\mathrm{i:i:i:i:i:i:i}}\right)N_{2}^{\mathrm{II}}+\ldots\\
&\ldots+\left(1-\nu_{33,\mathrm{iii}}\alpha_{3,\mathrm{iii}}-\nu_{34,\mathrm{i:ii}}\beta_{34,\mathrm{i:ii}}-\nu_{326,\mathrm{i:i:i}}\beta_{326,\mathrm{i:i:i}}-\nu_{3678,\mathrm{i:i:i:i}}\beta_{3678,\mathrm{i:i:i:i}}-\nu_{3245678,\mathrm{i:i:i:i:i:i:i}}\beta_{3245678,\mathrm{i:i:i:i:i:i:i}}\right)N_{3}^{\mathrm{II}}+\ldots\\
&\ldots+\left(1-\nu_{43,\mathrm{i:i:i}}\beta_{43,\mathrm{i:i:i}}-\nu_{45,\mathrm{ii:ii}}\beta_{45,\mathrm{ii:ii}}-\nu_{4235678,\mathrm{i:i:i:i:i:i:i}}\beta_{4235678,\mathrm{i:i:i:i:i:i:i}}\right)N_{4}^{\mathrm{II}}+\left(1-\nu_{54,\mathrm{ii:ii}}\beta_{54,\mathrm{ii:ii}}-\nu_{5234678,\mathrm{i:i:i:i:i:i:i}}\beta_{5234678,\mathrm{i:i:i:i:i:i:i}}\right)N_{5}^{\mathrm{II}}+\ldots\\
&\ldots+\left(1-\nu_{66,\mathrm{ii}}\alpha_{6,\mathrm{ii}}-\nu_{67,\mathrm{i:i}}\beta_{67,\mathrm{i:i}}-\nu_{623,\mathrm{i:i:i}}\beta_{623,\mathrm{i:i:i}}-\nu_{6378,\mathrm{i:i:i:i}}\beta_{6378,\mathrm{i:i:i:i}}-\nu_{6234578,\mathrm{i:i:i:i:i:i:i}}\beta_{6234578,\mathrm{i:i:i:i:i:i:i}}\right)N_{6}^{\mathrm{II}}+\ldots\\
&\ldots+\left(1-\nu_{77,\mathrm{v}}\alpha_{7,\mathrm{v}}-\nu_{76,\mathrm{i:i}}\beta_{76,\mathrm{i:i}}-\nu_{7368,\mathrm{i:i:i:i}}\beta_{7368,\mathrm{i:i:i:i}}-\nu_{7234568,\mathrm{i:i:i:i:i:i:i}}\beta_{7234568,\mathrm{i:i:i:i:i:i:i}}\right)N_{7}^{\mathrm{II}}+\left(1-\nu_{7368,\mathrm{i:i:i:i}}\beta_{7368,\mathrm{i:i:i:i}}-\nu_{7234568,\mathrm{i:i:i:i:i:i:i}}\beta_{7234568,\mathrm{i:i:i:i:i:i:i}}\right)N_{8}^{\mathrm{II}}+\ldots\\
&\ldots-\left(\nu_{12,\mathrm{ii}}\alpha_{2,\mathrm{ii}}N_{2}^{\mathrm{II}}+\nu_{92,\mathrm{ii}}\alpha_{2,\mathrm{ii}}N_{2}^{\mathrm{II}}+\nu_{13,\mathrm{iii}}\alpha_{3,\mathrm{iii}}N_{3}^{\mathrm{II}}+\nu_{93,\mathrm{iii}}\alpha_{3,\mathrm{iii}}N_{3}^{\mathrm{II}}\right)-\left(\nu_{16,\mathrm{ii}}\alpha_{6,\mathrm{ii}}N_{6}^{\mathrm{II}}+\nu_{96,\mathrm{ii}}\alpha_{6,\mathrm{ii}}N_{6}^{\mathrm{II}}+\nu_{17,\mathrm{v}}\alpha_{7,\mathrm{v}}N_{7}^{\mathrm{II}}+\nu_{97,\mathrm{v}}\alpha_{7,\mathrm{v}}N_{7}^{\mathrm{II}}\right)+\ldots\\
&\ldots-\left(\nu_{134,\mathrm{i:ii}}\beta_{34,\mathrm{i:ii}}N_{3}^{\mathrm{II}}+\nu_{934,\mathrm{i:ii}}\beta_{34,\mathrm{i:ii}}N_{3}^{\mathrm{II}}+\nu_{145,\mathrm{ii:ii}}\beta_{45,\mathrm{ii:ii}}N_{4}^{\mathrm{II}}+\nu_{945,\mathrm{ii:ii}}\beta_{45,\mathrm{ii:ii}}N_{4}^{\mathrm{II}}+\nu_{167,\mathrm{i:i}}\beta_{67,\mathrm{i:i}}N_{6}^{\mathrm{II}}\right)+\ldots\\
&\ldots-\left(\nu_{967,\mathrm{i:i}}\beta_{67,\mathrm{i:i}}N_{6}^{\mathrm{II}}+\nu_{1236,\mathrm{i:i:i}}\beta_{236,\mathrm{i:i:i}}N_{2}^{\mathrm{II}}+\nu_{9236,\mathrm{i:i:i}}\beta_{236,\mathrm{i:i:i}}N_{2}^{\mathrm{II}}+\nu_{13678,\mathrm{i:i:i:i}}\beta_{3678,\mathrm{i:i:i:i}}N_{3}^{\mathrm{II}}\right)+\ldots\\
&\ldots-\left(\nu_{93678,\mathrm{i:i:i:i}}\beta_{3678,\mathrm{i:i:i:i}}N_{3}^{\mathrm{II}}+\nu_{12345678,\mathrm{i:i:i:i:i:i:i}}\beta_{2345678,\mathrm{i:i:i:i:i:i:i}}N_{2}^{\mathrm{II}}+\nu_{92345678,\mathrm{i:i:i:i:i:i:i}}\beta_{2345678,\mathrm{i:i:i:i:i:i:i}}N_{2}^{\mathrm{II}}\right)+\ldots\\
&\ldots-\nu_{12}\left(1-\nu_{22,\mathrm{ii}}\alpha_{2,\mathrm{ii}}-\nu_{236,\mathrm{i:i:i}}\beta_{236,\mathrm{i:i:i}}-\nu_{2345678,\mathrm{i:i:i:i:i:i:i}}\beta_{2345678,\mathrm{i:i:i:i:i:i:i}}\right)N_{2}^{\mathrm{II}}-\nu_{92}\left(1-\nu_{22,\mathrm{ii}}\alpha_{2,\mathrm{ii}}-\nu_{236,\mathrm{i:i:i}}\beta_{236,\mathrm{i:i:i}}-\nu_{2345678,\mathrm{i:i:i:i:i:i:i}}\beta_{2345678,\mathrm{i:i:i:i:i:i:i}}\right)N_{2}^{\mathrm{II}}+\ldots\\
&\ldots-\nu_{13}\left(1-\nu_{33,\mathrm{iii}}\alpha_{3,\mathrm{iii}}-\nu_{34,\mathrm{i:ii}}\beta_{34,\mathrm{i:ii}}-\nu_{326,\mathrm{i:i:i}}\beta_{326,\mathrm{i:i:i}}-\nu_{3678,\mathrm{i:i:i:i}}\beta_{3678,\mathrm{i:i:i:i}}-\nu_{3245678,\mathrm{i:i:i:i:i:i:i}}\beta_{3245678,\mathrm{i:i:i:i:i:i:i}}\right)N_{3}^{\mathrm{II}}+\ldots\\
&\ldots-\nu_{93}\left(1-\nu_{33,\mathrm{iii}}\alpha_{3,\mathrm{iii}}-\nu_{34,\mathrm{i:ii}}\beta_{34,\mathrm{i:ii}}-\nu_{326,\mathrm{i:i:i}}\beta_{326,\mathrm{i:i:i}}-\nu_{3678,\mathrm{i:i:i:i}}\beta_{3678,\mathrm{i:i:i:i}}-\nu_{3245678,\mathrm{i:i:i:i:i:i:i}}\beta_{3245678,\mathrm{i:i:i:i:i:i:i}}\right)N_{3}^{\mathrm{II}}+\ldots\\
&\ldots-\nu_{14}\left(1-\nu_{43,\mathrm{i:i:i}}\beta_{43,\mathrm{i:i:i}}-\nu_{45,\mathrm{ii:ii}}\beta_{45,\mathrm{ii:ii}}-\nu_{4235678,\mathrm{i:i:i:i:i:i:i}}\beta_{4235678,\mathrm{i:i:i:i:i:i:i}}\right)N_{4}^{\mathrm{II}}-\nu_{15}\left(1-\nu_{54,\mathrm{ii:ii}}\beta_{54,\mathrm{ii:ii}}-\nu_{5234678,\mathrm{i:i:i:i:i:i:i}}\beta_{5234678,\mathrm{i:i:i:i:i:i:i}}\right)N_{5}^{\mathrm{II}}+\ldots\\
&\ldots-\nu_{94}\left(1-\nu_{43,\mathrm{i:i:i}}\beta_{43,\mathrm{i:i:i}}-\nu_{45,\mathrm{ii:ii}}\beta_{45,\mathrm{ii:ii}}-\nu_{4235678,\mathrm{i:i:i:i:i:i:i}}\beta_{4235678,\mathrm{i:i:i:i:i:i:i}}\right)N_{4}^{\mathrm{II}}-\nu_{95}\left(1-\nu_{54,\mathrm{ii:ii}}\beta_{54,\mathrm{ii:ii}}-\nu_{5234678,\mathrm{i:i:i:i:i:i:i}}\beta_{5234678,\mathrm{i:i:i:i:i:i:i}}\right)N_{5}^{\mathrm{II}}+\ldots\\
&\ldots-\nu_{16}\left(1-\nu_{66,\mathrm{ii}}\alpha_{6,\mathrm{ii}}-\nu_{67,\mathrm{i:i}}\beta_{67,\mathrm{i:i}}-\nu_{623,\mathrm{i:i:i}}\beta_{623,\mathrm{i:i:i}}-\nu_{6378,\mathrm{i:i:i:i}}\beta_{6378,\mathrm{i:i:i:i}}-\nu_{6234578,\mathrm{i:i:i:i:i:i:i}}\beta_{6234578,\mathrm{i:i:i:i:i:i:i}}\right)N_{6}^{\mathrm{II}}+\ldots\\
&\ldots-\nu_{96}\left(1-\nu_{66,\mathrm{ii}}\alpha_{6,\mathrm{ii}}-\nu_{67,\mathrm{i:i}}\beta_{67,\mathrm{i:i}}-\nu_{623,\mathrm{i:i:i}}\beta_{623,\mathrm{i:i:i}}-\nu_{6378,\mathrm{i:i:i:i}}\beta_{6378,\mathrm{i:i:i:i}}-\nu_{6234578,\mathrm{i:i:i:i:i:i:i}}\beta_{6234578,\mathrm{i:i:i:i:i:i:i}}\right)N_{6}^{\mathrm{II}}+\ldots\\
&\ldots-\nu_{17}\left(1-\nu_{77,\mathrm{v}}\alpha_{7,\mathrm{v}}-\nu_{76,\mathrm{i:i}}\beta_{76,\mathrm{i:i}}-\nu_{7368,\mathrm{i:i:i:i}}\beta_{7368,\mathrm{i:i:i:i}}-\nu_{7234568,\mathrm{i:i:i:i:i:i:i}}\beta_{7234568,\mathrm{i:i:i:i:i:i:i}}\right)N_{7}^{\mathrm{II}}-\nu_{98}\left(1-\nu_{7368,\mathrm{i:i:i:i}}\beta_{7368,\mathrm{i:i:i:i}}-\nu_{7234568,\mathrm{i:i:i:i:i:i:i}}\beta_{7234568,\mathrm{i:i:i:i:i:i:i}}\right)N_{8}^{\mathrm{II}}+\ldots\\
&\ldots-\nu_{97}\left(1-\nu_{77,\mathrm{v}}\alpha_{7,\mathrm{v}}-\nu_{76,\mathrm{i:i}}\beta_{76,\mathrm{i:i}}-\nu_{7368,\mathrm{i:i:i:i}}\beta_{7368,\mathrm{i:i:i:i}}-\nu_{7234568,\mathrm{i:i:i:i:i:i:i}}\beta_{7234568,\mathrm{i:i:i:i:i:i:i}}\right)N_{7}^{\mathrm{II}}-\nu_{18}\left(1-\nu_{7368,\mathrm{i:i:i:i}}\beta_{7368,\mathrm{i:i:i:i}}-\nu_{7234568,\mathrm{i:i:i:i:i:i:i}}\beta_{7234568,\mathrm{i:i:i:i:i:i:i}}\right)N_{8}^{\mathrm{II}}
\end{aligned}
\tag{D.2}
$$

The free-solvent model mole fraction ratio for a solution which has seven proteins forming four homo-multimers and six hetero-multimers is given as Eqn. D.1 divided by Eqn. D.2.

Assuming that the number of moles of each monomeric protein species is known, there are 82 unknowns, all of which are physically realistic and independently measurable. Of these unknowns, 17 are hydration values, 17 are ion binding, 24 are protein-protein interactions, and 24 are the fractional amounts of the monomeric proteins.

# APPENDIX E.

# DETAILED DESIGNS OF A CONCENTRATING OSMOMETER AND A MICRO-VOLUME OSMOMETER

The designs of the concentrating osmometer components used in Chapter 8 is presented below. The final schematic of the concentrating osmometer is shown in Figure E.1. The SolidWorks designs are presented in Figures E.2 - E.6. The plunger is created by threading the plunger top (Figure E.4) and plunger bottom (Figure E.5) together; the pressure transducer is placed in the plunger bottom with an oring between the transducer and the plunger bottom material to create a seal. With the transducer in place, the plunger top and plunger bottom can be threaded together.

A small volume osmometer was also designed to reduce the amount of protein required for a single osmotic pressure measurement. The design of a micro-volume conventional (non-concentrating) osmometer is shown in Figures E.7 - E.9. The small volume osmometer uses the solvent chamber designed for the concentrating osmometer (Figure E.3) and the membrane housing (Figure E.6).

In addition, a valve was designed which has a greatly reduced volume (Figures E.10 and E.11). The current valves used in the osmotic pressure experiments (2-way angle valve, 02-0121, ChromTech, Inc., Apple Valley, MN) each have a solution volume of 190 μL between the valve seal and the solution chamber. While this can be reduced using a tube which has a smaller diameter, the pressure required to pump a solution into the solution chamber is greatly increased which will cause a larger pressure drop across the valve. A high pressure pump drive can be used to drive the solution into the solution chamber, but the use of the developed low volume valve

allows for the solution to be driven using a much lower pressure. The volume of the developed low volume valve is 8.4 μL.

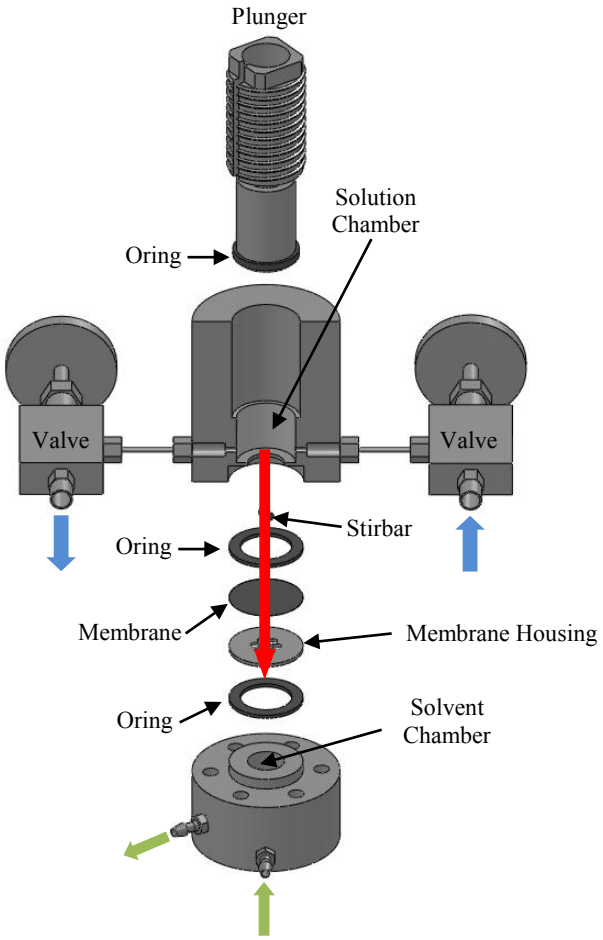


**Figure E.1.** SolidWorks Schematic of a Concentrating Osmometer. The plunger (top and bottom connected) threads into the solution chamber and forces solvent to flow across the membrane. The pressure transducer is sealed in the plunger such that the transducer sensor (face) is at the tip of the plunger. The solution is put into the solution chamber through the valves (blue arrows). A stir bar is use to disrupt the concentration polarization layer on the membrane, as the solvent (red arrow) is driven out of the solution chamber. Orings are used to prevent leaks. The solvent chamber has a continuous feed of solvent (green arrows) such that the residence time is much less than the time constant for the pressure in the solution chamber.

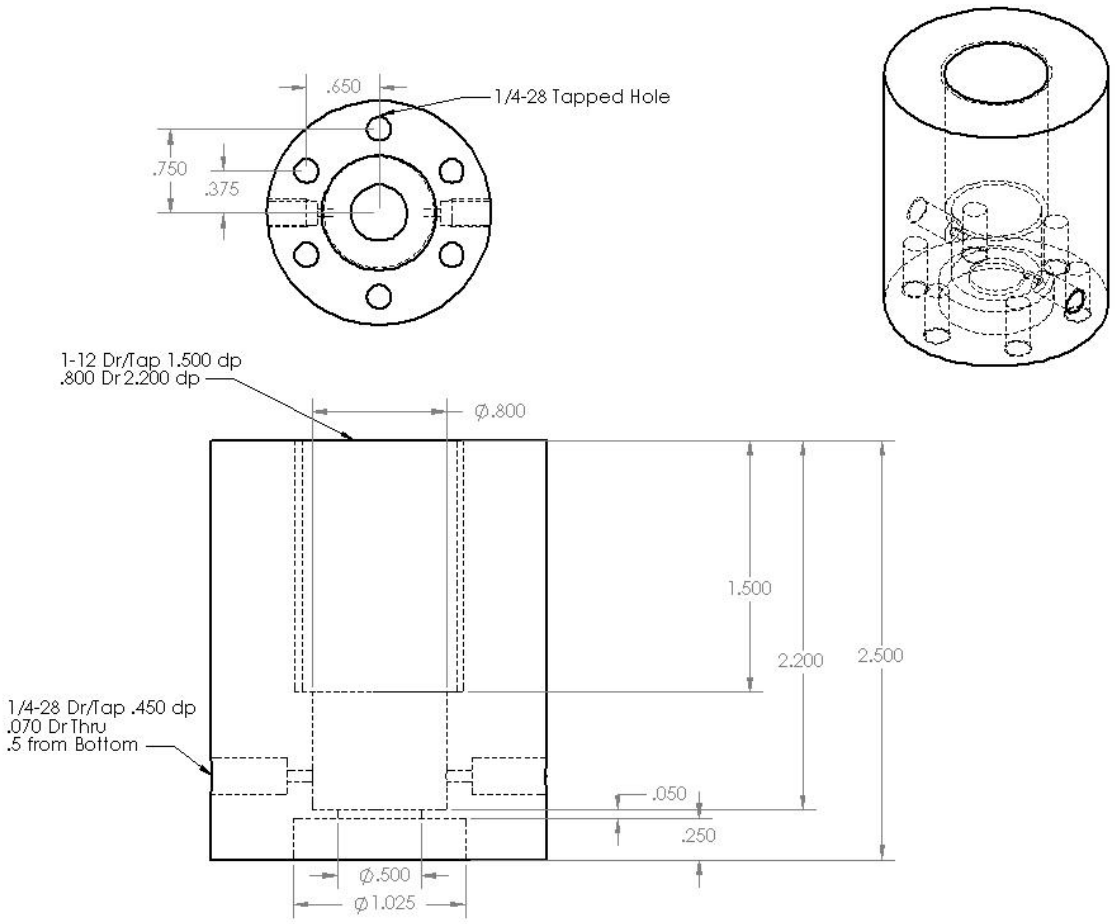


**Figure E.2.** SolidWorks Design of the Concentrating Osmometer Solution Chamber. All units are in inches.

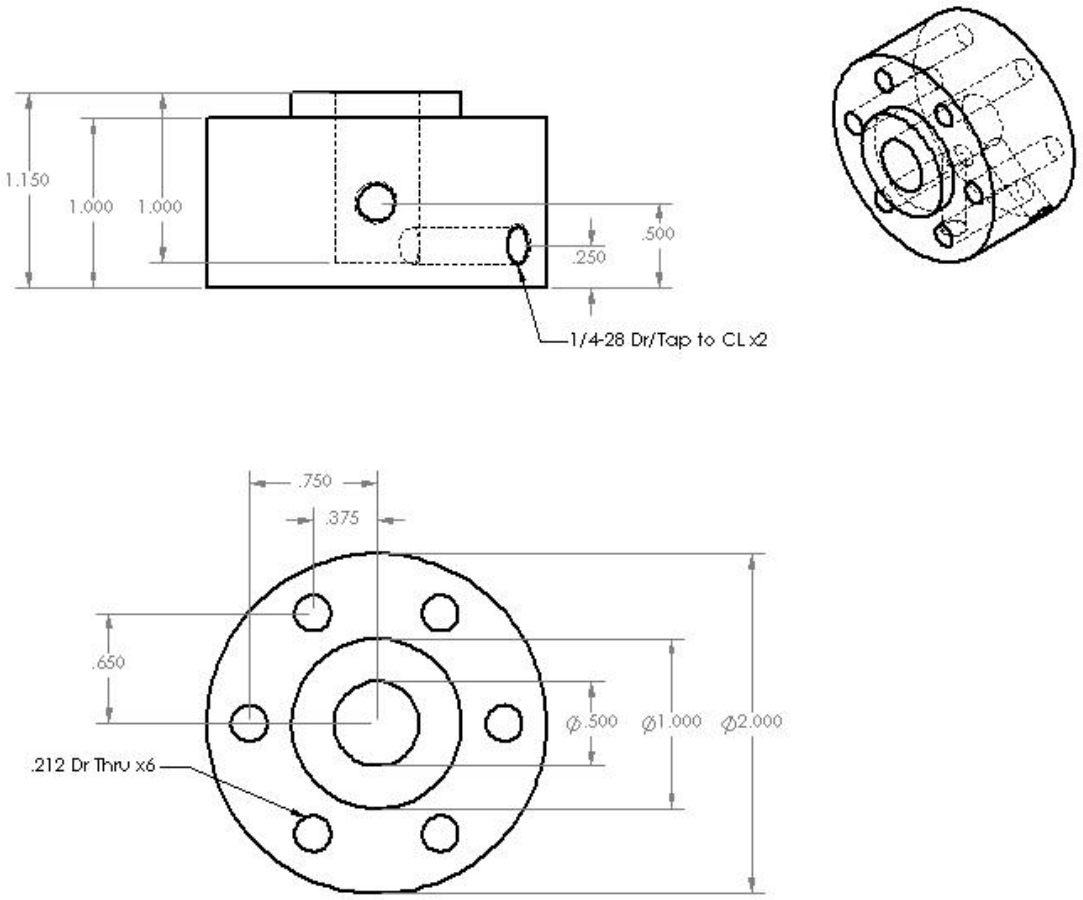


**Figure E.3.** SolidWorks Design of the Concentrating Osmometer Solvent Chamber. All units are in inches.

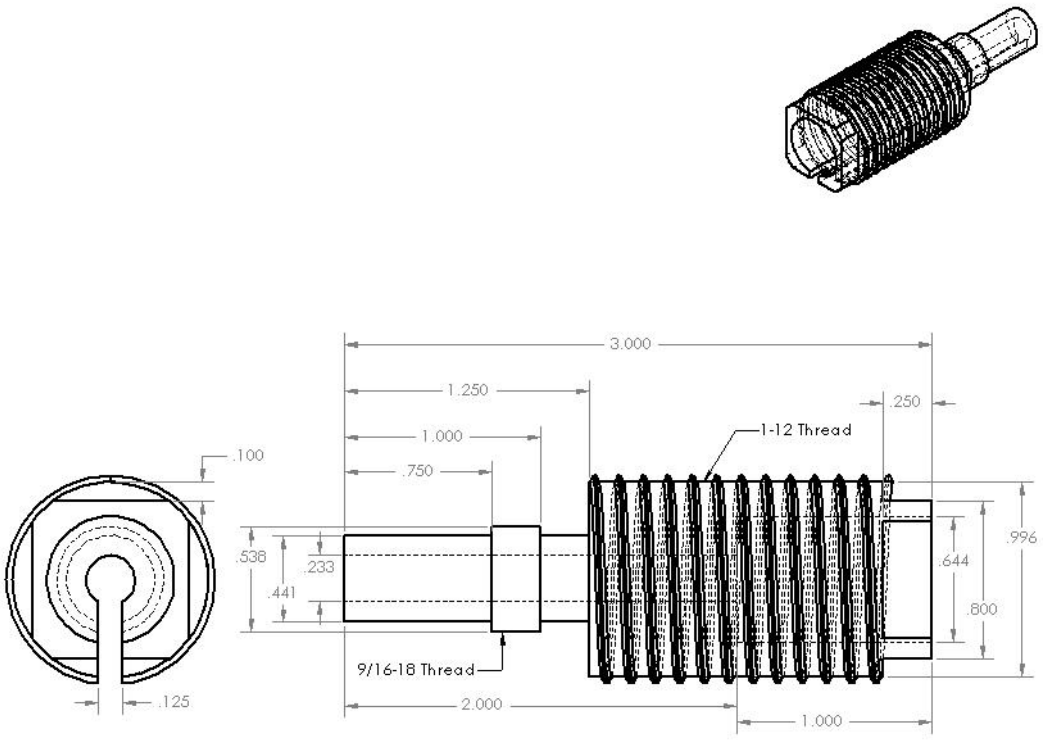


**Figure E.4.** SolidWorks Design of the Concentrating Osmometer Plunger Top. All units are in inches.

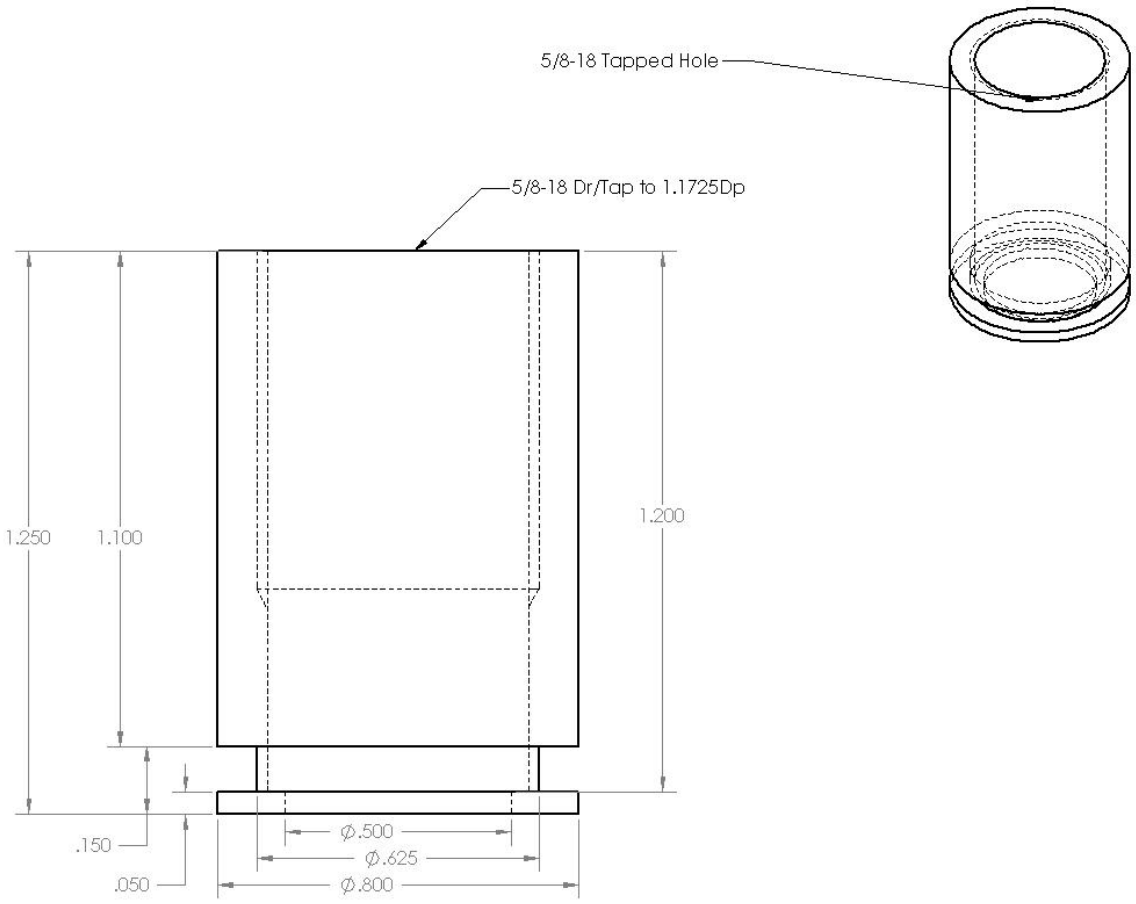


**Figure E.5.** SolidWorks Design of the Concentrating Osmometer Plunger Bottom. All units are in inches.

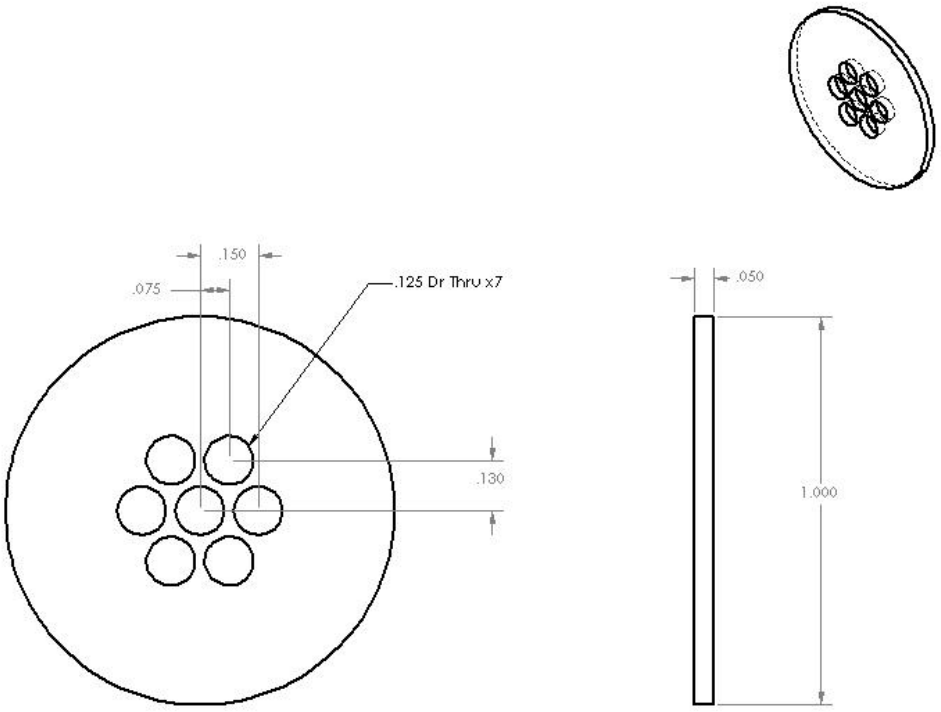


**Figure E.6.** SolidWorks Design of the Concentrating Osmometer Membrane Housing. All units are in inches.

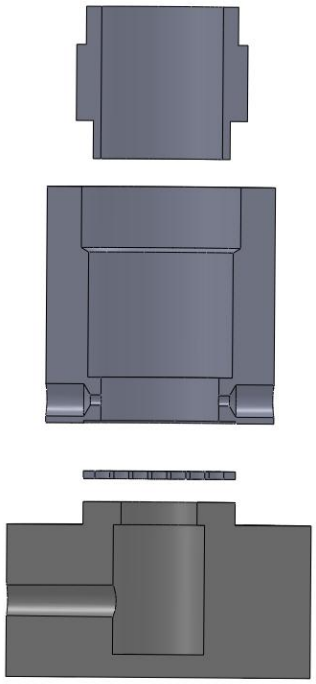

**Figure E.7.** SolidWorks Schematic of the Micro-Volume Osmometer.

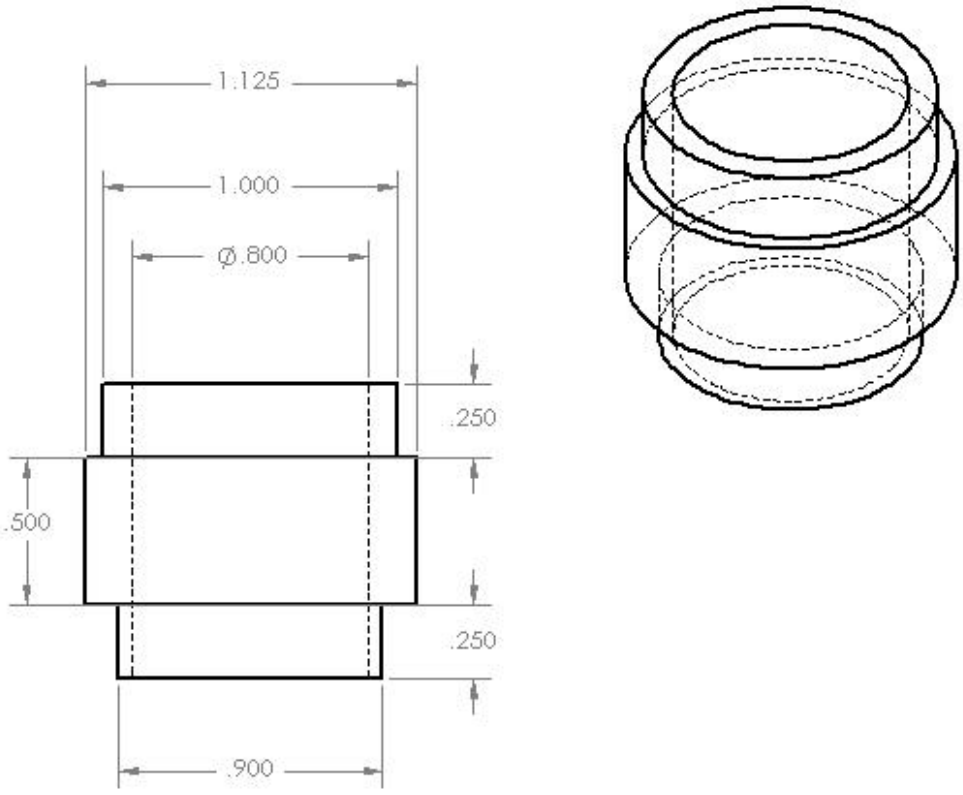


**Figure E.8.** SolidWorks Design of the Micro-Volume Osmometer Transducer Housing. All units are in inches.

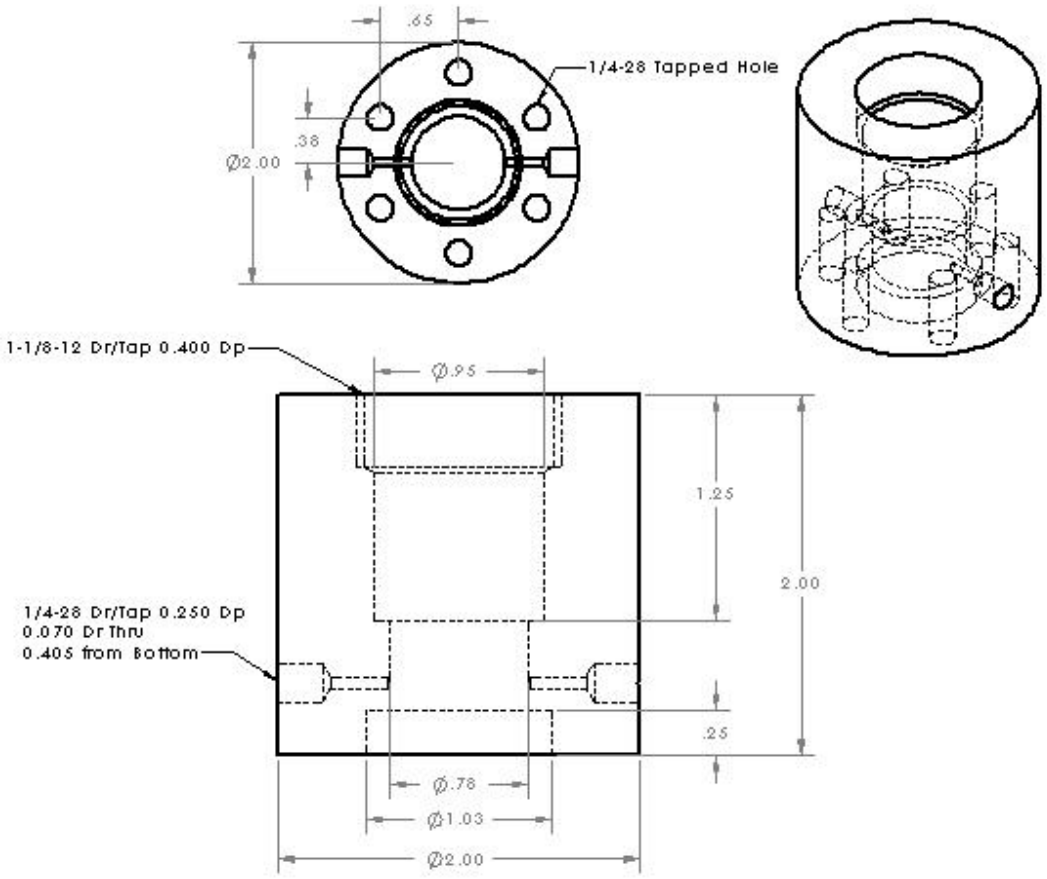


**Figure E.9.** SolidWorks Design of the Micro-Volume Osmometer Solution Chamber. All units are in inches.

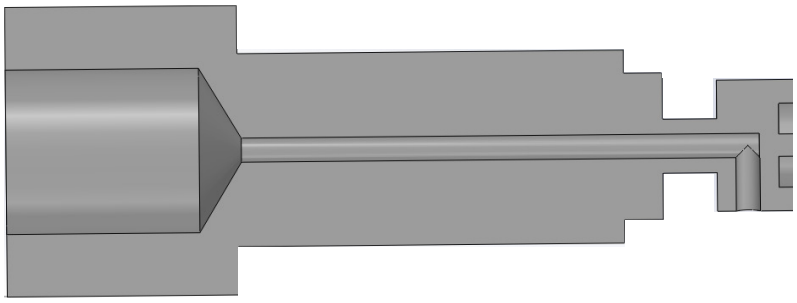

**Figure E.10.** SolidWorks Schematic of the Low Volume Valve.

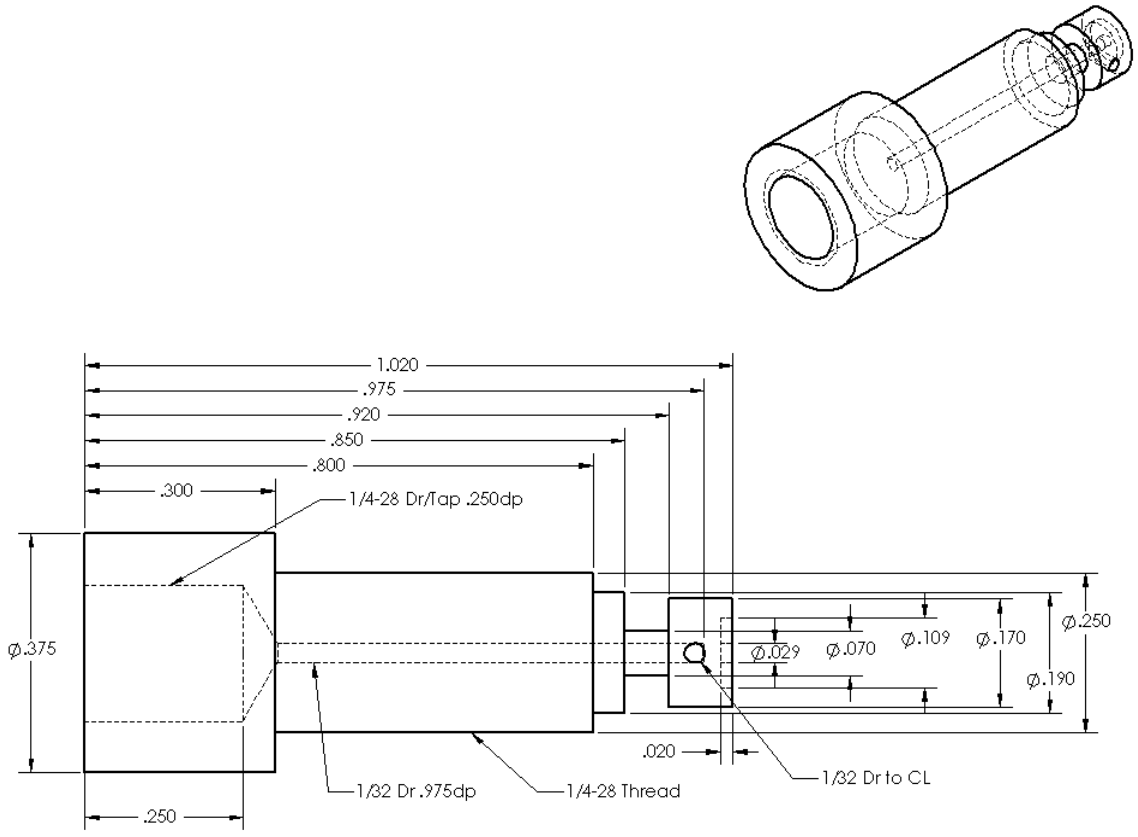


**Figure E.11.** SolidWorks Design of the Low Volume Valve. All units are in inches.

# APPENDIX F.
# DETAILED DESIGN OF AN OSMOTIC TRANSPORT DEVICE

## F.1. Potting Hollow Fiber Modules

The method for potting hollow fibers and the figures were graciously provided by Richard Hausman and Dr. Isabel Escobar at the University of Toledo. The protocol was for creating hollow fiber modules (Figures F.1 - F.6.). This protocol was altered for the development of the osmotic transport device.

### F.1.1. Epoxy Selection and Preparation

The selection of the appropriate epoxy is paramount to the creation of a hollow fiber module. For this, a hardener (slow non-bleaching epoxy hardener, 30-026, MAS Epoxies, NJ) and a resin (low viscosity epoxy resin, 30-002, MAS Epoxies, NJ) mixture are used in a 2 to 1 ratio. Upon mixing the resin and the hardener, wait approximately 30 minutes for the epoxy to become viscous. During this time, the epoxy will also degas.

### F.1.2. Selection and Preparation of the Hollow Fibers

This protocol can be used for any size hollow fiber. The choice of membrane material may affect the choice of the epoxy used. Here the membrane was regenerated cellulose.

Teflon tape is used to hold the hollow fibers together creating the hollow fiber bundle (Figure F.1). The Teflon tape allows for a small amount of space between the hollow fibers which can be filled by the epoxy to effectively seal the module.

Begin by wrapping a single fiber two times. Place another fiber next to the first and wrap the tape around it and the existing fiber(s) (already wrapped). Continue this procedure until all fibers are bundled together.

Next, feed the hollow fiber bundle through the tube being used to create the housing (Figure F.2). The Teflon tape helps to keep the fibers together during this process. Any tube can be used as long as it is rated for the desired pressure and the epoxy seals. Make sure the Teflon tape wrap is fully through the tube.

Wrap the hollow fiber bundle with cotton inside of the tube (Figure F.3). Use of the cotton keeps the epoxy from leaking out of the tube allowing for effectively hardening and sealing. Without the cotton, the epoxy can flow down the length of the fibers causing a length of the fibers to be sealed together rather than only the entrance region.

When placing the cotton around the fibers, hold the ends of the fibers so they don't slide through the tape while packing the cotton. Using forceps will help to pack the cotton around the fibers, but make sure to keep the forceps towards the tube wall (well away from the fibers) to prevent breaking the fibers. Fibers should be kept in the middle of the tube.

### F.1.3. Sealing the Fibers

When the epoxy has reached an appropriate viscosity, use a glass 1 mL pipet to fill in the epoxy around the fibers (Figure F.4). Keep adding epoxy to the tube until the epoxy stays level with the top edge of the tube. Gently spread the fibers to ensure that the epoxy gets between all fibers. The epoxy will cure over the next 24 hours.

The epoxy will soak into the cotton so it is important to continue to monitor the level of the epoxy. If the epoxy leaks through the cotton, either the epoxy was not viscous enough or the cotton was not packed tightly enough.

Repeat this procedure for the other side.

## F.2. Osmotic Transport Device

The osmotic transport device (OTD) consists of a hollow fiber membrane module embedded within (or placed under) a moldable and hydratable material. While there are many variations of such a device, in this work, three such devices have been developed. The first version of the osmotic transport device consisted of opening a hollow fiber dialysis module (Baxter dialyzer, Baxter, IL) to expose the hollow fiber bundle. An agar hydrogel was used as the hydratable material.

### F.2.1. Hollow Fiber-Hydrogel Device

The second generation device was designed and developed in this work. While many prototypes of this device were developed and various epoxies were tested. The final design (Figure F.5) uses a threaded adaptor (Barb adaptor, 5116K198, McMaster-Carr, GA) as the tubes holding the fibers.

An agar hydrogel was used for this device which led to the name hollow fiber-hydrogel device (HFHD). The use of threaded tubes adaptors offered a few challenges, including slow deployment (potential cross threading) and fluid leaks if the adaptors were threaded too much (oring would curl, thus not sealing) or not enough (oring wouldn't seal).

This device was also adapted for use in an MRI. This was completed by removing the metal sealing piece which is placed around the Teflon tubing. The epoxies used here contain no trace metals.

### F.2.2. Osmotic Transport Device Version 3

The third version of the OTD changed the tubes from threaded tube adaptors to quick disconnect tube couplings (Coupling insert pipe thread (48607246) and Barbed coupling body (48608657), MSC, NY) (Figure F.6). These allowed for rapid deployment and consistent sealing, preventing leaks. One potential limitation is that these have a maximum pressure of 125 psi.

For this version, two hydratable materials were tested: agar hydrogel (0.3 % and 0.4 %) and Durepair (Durepair Dura Regeneration Matrix, Medtronic, Goleta, CA).

## F.3. Field-Ready Osmotic Transport Device

These current designs of an OTD are not readily field-deployable. While the components of a field-ready OTD are present, the fibers should be packaged embedded within the hydratable material as a sterile roll (similar to gauze). The hydratable material will be packaged as a dehydrated layer, but can quickly be hydrated with an isotonic saline solution (0.9 % saline). The field-ready OTD can be unrolled and placed directly on the exposed injured tissue. Head pressure can be used to flow the lumen solution past the injured tissue. The field-ready OTD will be lightweight, robust, and small in size.

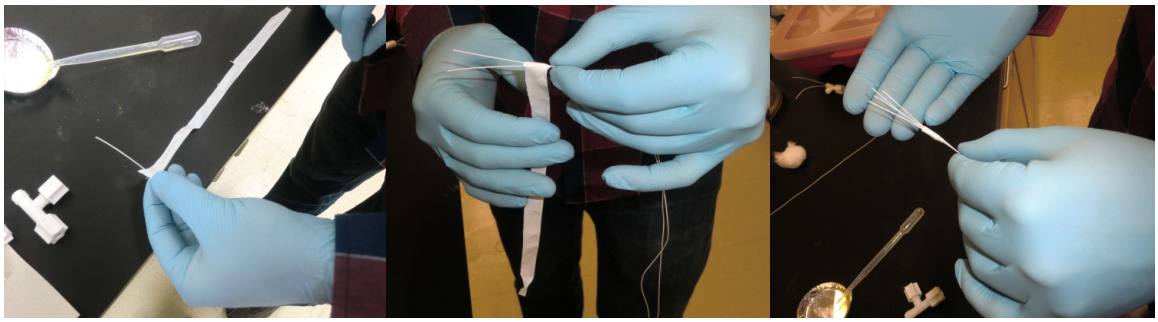

**Figure F.1.** Preparation of the Hollow Fiber Module. Beginning with a single fiber (**Left**), wrap Teflon tape around to hold all fibers together (**Middle**), until all fibers are taped creating the module (**Right**).

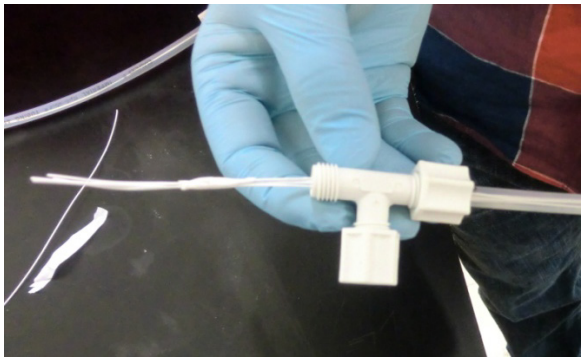

**Figure F.2.** Hollow Fiber Bundle Pulled Through the Tube.

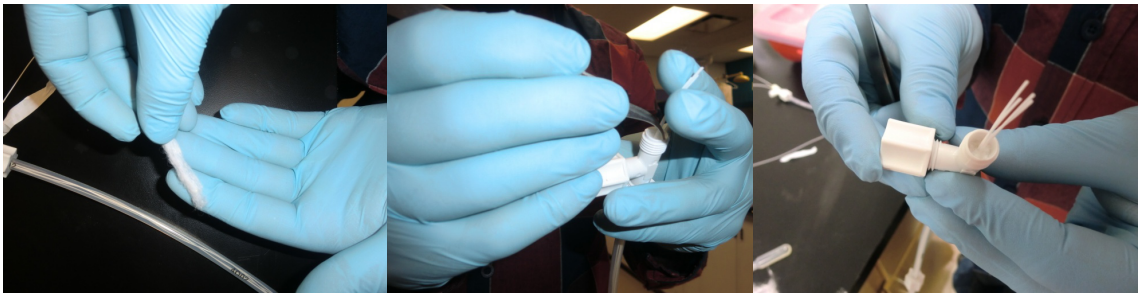

**Figure F.3.** Placing the Cotton in the Tube.

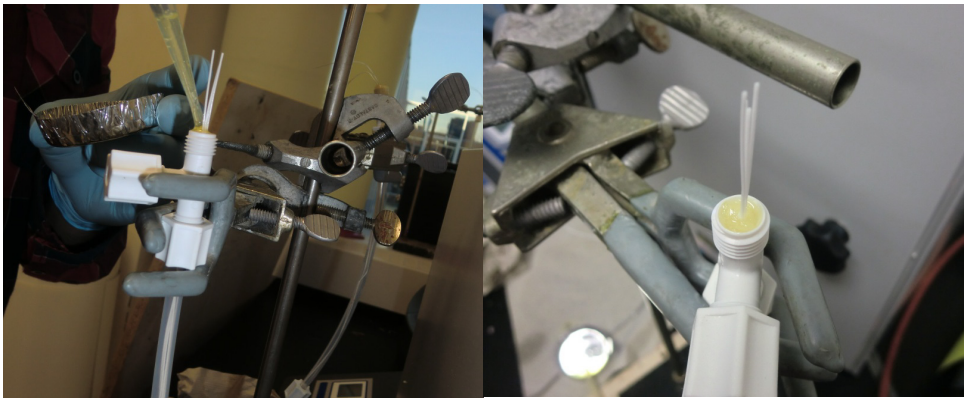

**Figure F.4.** Filling in the Epoxy Around the Hollow Fibers.

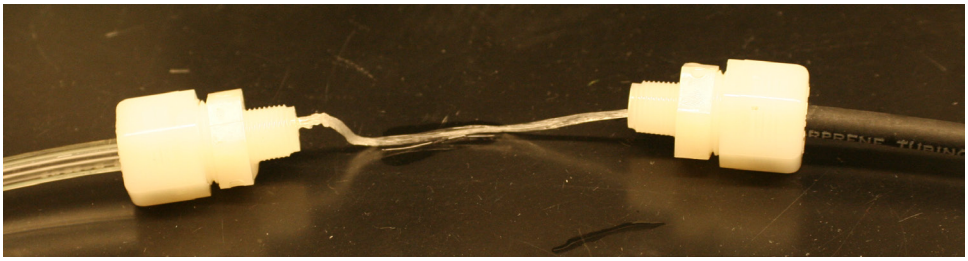

**Figure F.5.** Hollow Fiber-Hydrogel Device. Hydrogel not shown.

**Figure F.6.** Third Generation Osmotic Transport Device. Hydrogel not shown.

# APPENDIX G.

# OPTICAL COHERENCE TOMOGRAPHY OF THE OSMOTIC TRANSPORT DEVICE

Here the use of an optical coherence tomography (OCT) for imaging tissue underneath an osmotic transport device (OTD) was tested to determine if the OCT probe needed to be placed in-line with the OTD hollow fibers or if the OCT could image through the OTD hollow fibers. Each condition was imaged for 1 min at 10 Hz. Each image is 3 mm in height by 5 mm in width.

When a 0.3% agar, 3% saline hydrogel (Figures G.2, G.5, and G.8) or hollow fibers without a solution in them (Figures G.3 and G.6) are imaged through, a significant amount of intensity is lost. Similarly, when a solution is flowed through the fibers, intensity is reduced (Figures G.4, G.5, G.7, and G.8). When a gel and fibers are coupled together (Figures G.5 and G.8), a further reduction in intensity is observed.

To understand the effect of the OTD components on the OCT intensity, the extinction coefficient was calculated by fitting the intensity loss as a function of depth. The extinction coefficient for the finger in each image was determined by plotting the intensity vs. depth at a given section of the image. For Figures G.1 and G.2, the analyzed section was arbitrarily selected to be the middle of the figure. However, for Figures G.3 - G.5, the line was selected to be underneath a fiber. Three images in the dataset for each condition were used for calculating the extinction coefficients (Table G.1).

This preliminary study suggests that the use of an OCT probe with an OTD requires that the OCT probe is placed in-line with the hollow fibers. Alternatively, a portion of the tissue can remain uncovered by any OTD component for only imaging use (*i.e.* the uncovered tissue is only for imaging.

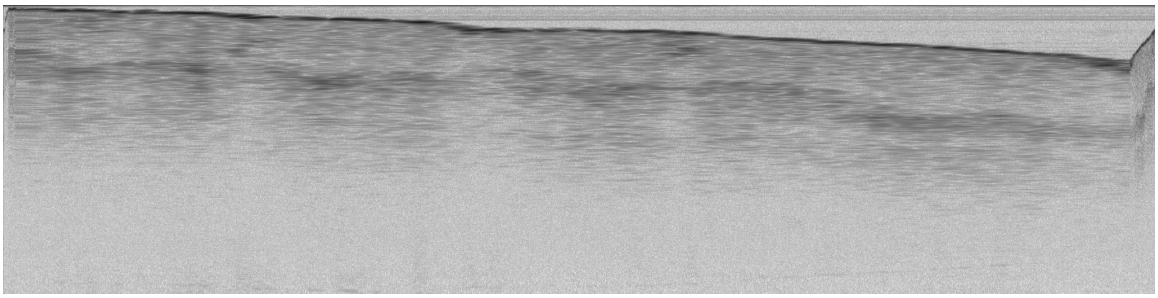

**Figure G.1.** OCT Image of a Finger. The underside of a finger is imaged. No OTD is present.

**Figure G.2.** OCT Image of a Finger With a Gel. The gel is placed on top of the tissue (between the tissue and the OCT probe).

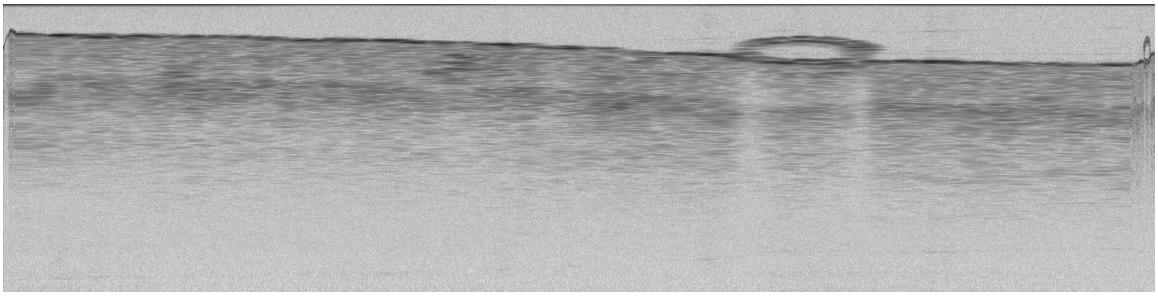

**Figure G.3.** OCT Image of a Finger With a Single Hollow Fiber. The fiber is placed on top of the tissue (between the tissue and the OCT probe).

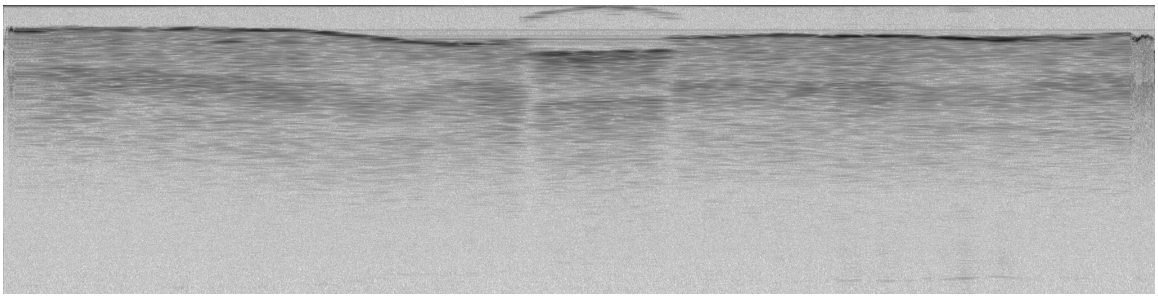

**Figure G.4.** OCT Image of a Finger With a Single Hollow Fiber Containing a Flowing BSA Solution. The gel is placed on top of the tissue with a fiber (between the tissue and the OCT probe). The fiber is in the center of the image.

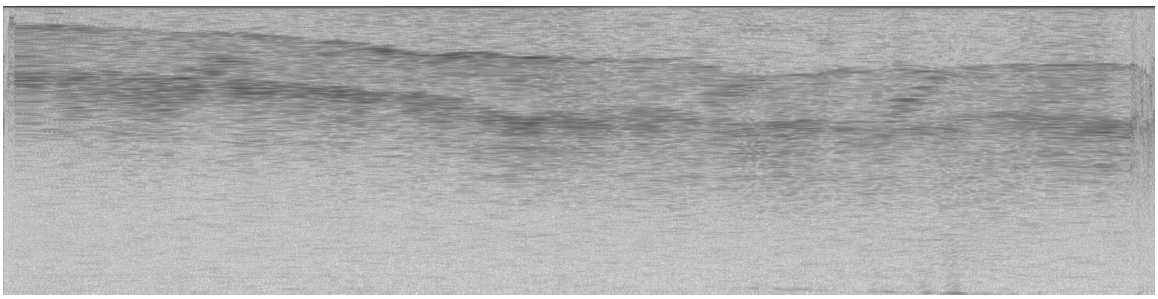

**Figure G.5.** OCT Image of a Finger With a Gel and a Single Hollow Fiber Containing a Flowing BSA Solution. The gel is placed on top of the tissue with a fiber (between the tissue and the OCT probe). The fiber is placed about two-thirds of the image from the left.

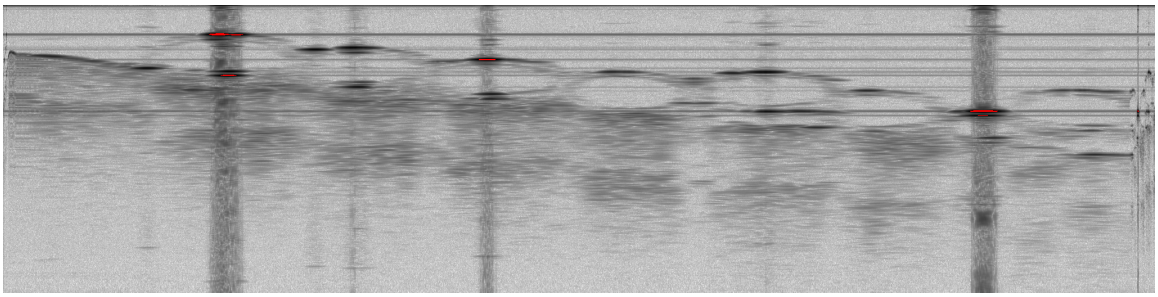

**Figure G.6.** OCT Image of a Finger With Multiple Hollow Fibers. The fibers are placed in a monolayer on top of the tissue (between the tissue and the OCT probe). There is no flow. The red specks are due to oversaturation.

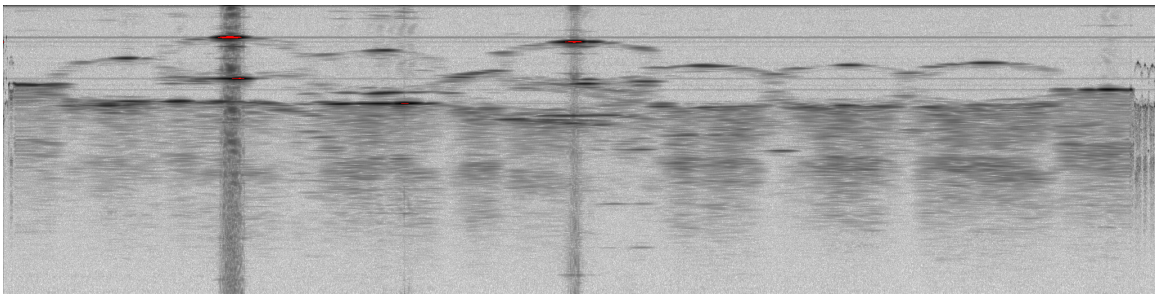

**Figure G.7.** OCT Image of a Finger With Multiple Hollow Fibers Containing a Flowing BSA Solution. The fibers are placed in a monolayer on top of the tissue (between the tissue and the OCT probe). The red specks are due to oversaturation.

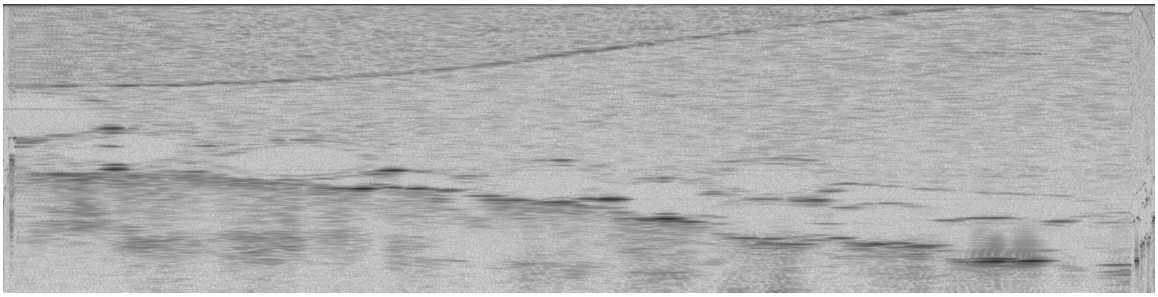

**Figure G.8.** OCT Image of a Finger With a Gel and Multiple Hollow Fibers Containing a Flowing BSA Solution. The gel is placed on top of the tissue with a monolayer of fibers (between the tissue and the OCT probe). There is some mirror image overlapping of the gel on the top left of the image.

**Table G.1.** OCT Tissue Extinction Coefficients for the Various OTD Conditions. For all cases, n = 3.

| Condition | Extinction Coefficient | $R^2$ |
|---|---|---|
| Finger (F) Only | -4.8 ± 0.62 | 0.60 ± 0.02 |
| F + Gel | -6.0 ± 0.70 | 0.62 ± 0.03 |
| F + Single Fiber (SF) | -4.9 ± 2.57 | 0.36 ± 0.15 |
| F + SF w/Flow | -14.1 ± 1.80 | 0.81 ± 0.03 |
| F + Gel + SF w/Flow | -2.7 ± 1.87 | 0.09 ± 0.07 |
| F + Multiple Fibers (MF) | -18.3 ± 5.98 | 0.72 ± 0.04 |
| F + MF w/Flow | -7.8 ± 2.74 | 0.39 ± 0.06 |
| F + Gel + MF w/Flow | -27.0 ± 9.90 | 0.53 ± 0.11 |

# APPENDIX H.

# A REAL-TIME ANALYSIS OF T2 MAGNETIC RESONANCE IMAGES USING A SYMMETRY-BASED ALGORITHM: DEVELOPMENT OF AN AUTOMATIC ALGORITHM

## H.1. Detecting the Damage Following a Traumatic Brain Injury

Traumatic brain injury (TBI) is the foremost cause of morbidity and mortality in persons between 15 and 45 years of age (Finkelstein *et al.* 2006; Tagliaferri *et al.* 2006). It is important from a public health standpoint since TBI places a burden of approximately $80 billion on the U.S. health care system (Finkelstein *et al.* 2006). Early TBI symptoms may appear mild, but they can lead to significant, life-long impairment in an individual's ability to function physically, cognitively, and psychologically (Reilly and Bullock 2005).

About 2 million incidents of TBI result in fatality or hospitalization in the U.S. annually. Among these incidents, approximately 7% are fatal (Finkelstein *et al.* 2006), and approximately 90% of these fatal TBIs occur within 48 hours of injury, thus successful treatment of TBI lies in early detection of brain damage after trauma (Park *et al.* 2008). Computed Tomography (CT) and Magnetic Resonance Imaging (MRI) are widely utilized, clinically, to noninvasively diagnose and evaluate moderate to severe TBI, as well as provide information to determine the appropriate treatment. The latter also provides tools to monitor the neuropathological evolution (Lee and Newberg 2005; Ashwal *et al.* 2006).

Conventional MRI imaging, such as T2 weighted imaging (T2WI) is sensitive to edema and large hemorrhagic contusions (Lee and Newberg 2005). Increased sensitivity has made T2WI a favored technique for lesion evaluation and therefore, it is used in detecting abnormalities in

brain tissue, as well as the severity of brain damage in human and animal studies (Gerber *et al.* 2004).

The diagnosis of TBI is typically based on the visual inspection of CT or MRI scans. Usually, the boundary or region of an injury is manually selected. Although an abnormality can be easily seen by the trained person, manual region drawing of an injury, to determine the exact lesion size, is arduous and time consuming. Furthermore, large deviations in lesion size can occur due to intra- and inter-operator performance. Therefore, a sensitive and reliable algorithm for assessing lesion size and classifying the injury is an essential part in providing rapid evaluation of patient status and allowing more effective and timely treatment.

H.2. Current Algorithms for Detecting Lesions

Various algorithms have been developed in an attempt to address this need. Most of the proposed methods are based on MRI image segmentation of anatomical brain structures (Akselrod-Ballin *et al.* 2009). For example, Rouaïnia *et al.* used an EM (Expectation-Maximization) algorithm to segment the anatomical brain structures and the outliers of the normal tissue models are classified as a lesion (Rouaïnia *et al.* 2006).

In another study, Schmidt *et al.* developed an automatic technique to detect white-matter lesions in multiple sclerosis (Schmidt e*t al.* 2012). They used a 3D gradient echo T1-weighted image and a FLAIR image. The authors used the belief map to detect normal tissue, and similar to Rouaïnia *et al.*, the outliers are classified as lesion. Finally, an iterative algorithm is used to grow the lesion area based on a voxel-based morphometric criterion.

Recently, Ghosh *et al.* introduced Hierarchical Region Splitting (HRS) for automatic ischemic lesion detection (Ghosh *et al.* 2011). The authors used normalized T2 values to recursively split the region. Each segment had a uniform T2 value associated with it and,

therefore, the region of interest could be detected based on T2 value of lesion. A complete review of the state of the art of computational techniques in lesion detection is presented by Lladó *et al.* (Lladó *et al.* 2012) and Ghosh *et al.* (Ghosh *et al.* 2012). The majority of these methods rely either on large amount of training data or a prior model. Therefore, the current automatic lesion detection methods are computationally intensive and not clinically useable due to the lack of real-time detection.

Herein an automatic algorithm for detection and classification of lesion in T2WI MRI is developed based on symmetry structure of the brain. The proposed algorithm is computationally inexpensive and allows for real-time detection with accuracy comparable to manual detection. The performance of the proposed algorithm is evaluated over several TBI, shame, and control cases and is compared to manual detection method ("gold standard").

## H.3. Methods

An experimental model of TBI in mice was used to obtain the MRI images utilized for development and validation an automatic lesion detection method.

### H.3.1. Experimental Data

Mice models of TBI induced by open-head controlled cortical impact were imaged at various time-points post injury. All animal experiments were approved by Loma Linda University IACUC.

H.3.1.1. Animals and Surgical Technique

A total of 18 male Sprague-Dawley rats (72 - 93 days old at the time of experiment) were randomized into three groups: 1) repetitive TBI (n = 10), 2) sham (n = 6), and 3) control animals (n = 2).

H.3.1.2. Inducing Traumatic Brain Injury

TBI was induced using controlled cortical impact (CCI). A 5 mm craniotomy was performed, 3 mm posterior and 3 mm lateral to bregma, to expose the right cortical surface. The CCI was delivered using an electromagnetic driven piston with a 4 mm tip diameter at a depth of 2 mm, speed of 6.0 m/s, and contact duration of 200 ms (Leica Biosystems Inc., Richmond, Il). TBI was induced on day 0 and repeated on day 2. The animals in the sham group went through the same surgical procedure with no TBI inductions.

H.3.1.3. Magnetic Resonance Imaging

Each animal was imaged on days 1 (24 hr-post first injury), 3 (72 hr-post first injury and 24 hr-post second injury), and 14 (14 days-post first injury).

MRI studies were performed using a 4.7 Tesla Bruker Advance MRI scanner (Bruker Biospin, Billerica, MA). T2-sequence data with 25 coronal slices were obtained. The scanner had a 30 cm bore and the imaging parameters were: TR/TE = 2850 ms/20 ms, number of echoes = 6, field of view = 3x3 cm with 2 averages.

H.3.2. Lesion Detection Methods

To detect lesions in the MRI images, both manual and the automatic methods were used. The manual method was used for establishing the location of the lesion(s).

H.3.2.1. Manual Lesion Detection

To circumvent the limitations of inter-observer manual lesion detection, a single operator was used for all analysis, including lesion area, and was considered the "gold-standard".

The T2 maps were analyzed using Cheshire (Parexel International Corp). Because T2 images reflect water content in edema and iron-content in blood, the regions of hyper/hypo intensity were used to delineate lesions (edema/blood) and the lesion boundaries were manually drawn. The operator drew the region of interest (ROI) blinded to the subject groups.

H.3.2.2. Automatic Lesion Detection

The proposed automatic algorithm was created using two algorithms combined together. The first algorithm removes the skull and all tissue not associated with the brain tissue (skull stripping) by comparing the T2 values. The second algorithm detects the lesion (if present) based on the brain symmetry for the T2 values (Figure H.1).

H.4. Results

H.4.1. T2 Values of Brain Tissue

Table H.1 shows the T2 values of the normal tissue components and lesion which is used as the belief map in the automatic detection method.

H.4.2. Automatic Algorithm

The proposed computational method is composed of two parts: skull stripping and lesion detection. Skull stripping is used for extracting the brain region by removing the surrounding muscle and skull. In the lesion detection, first the axis of symmetry of the brain structure is found

then, using the symmetry criteria with respect to this axis, any lesion which is present is detected. The lesions are defined by a difference in the T2 values across the axis of symmetry

H.4.2.1. Skull Stripping

Numerous studies which have been developed to extract human brain tissue from an MRI image using methods such as pulse coupled neural networks (Murugavel and Sullivan 2009) or geometrical and statistical 3D model of brain (Huang *et al.* 2009). However there is still no robust and fully automatic method for extracting mouse brain tissue which can be used in a real-time system. In this study, skull stripping is a preprocessing step, and its focus is mainly on the computational time rather than accuracy of extraction. The T2 map and the 2nd Echo of each brain slice are used to find the area associated with the brain tissue.

As shown in Figure H.2, the algorithm for skull stripping consists of three main steps: foreground separation, finding the brain bounding box, and checking the 3D connectivity.

Foreground separation is achieved by applying two separate thresholds, one on the T2 map and the other on the 2nd Echo.

Let $I_{i,j}$ denote each pixel value of the gray scaled image of the 2nd Echo and $T_{i,j}$ is its associated T2 value. The foreground extraction can be described by Eqn. H.1.

$$I'_{i,j} = \begin{cases} I_{i,j} & I_{i,j} > \varepsilon \text{ and } 36 < T_{i,j} < 450 \\ 0 & \text{other} \end{cases}, \quad \varepsilon = \min\left\{\sigma_I^2, 0.27\right\} \tag{H.1}$$

where $\sigma_I^2$ is an adaptive threshold calculated based on Otsu's method (Otsu 1979). Otso's method maps an arbitary image into a binary one by selecting a threshold value which minimizes the intra-class variance. The final threshold, $\varepsilon$, is the minimum value of $\sigma_I^2$ and a constatnt value of 0.27. Also, the threshold value for the T2 map is calculated based on the T2 belief map (Table H.1).

In Eqn. H.1, $I'_{i,j}$ is the result of foreground separation after morphological cleaning, which is shown in Figure H.2.A.

Removing the foreground from all the slides, the cumulative roundness index (CRI) is calculated for the 3D image. CRI is an estimate of the likelihood of $I'_{i,j}$ to be part of the brain tissue. It combines 2D geometrical constrains (roundness) and 3D connectivity.

Let's assume that after foreground separation, the $s^{\text{th}}$ slide has $M$ clusters in which $I'_{i,j}$ belongs to the $m^{\text{th}}$ cluster ($C_{m,s}$) with an area, $A_{m,s}$, and perimeter, $P_{m,s}$, associated with it. CRI can be represented by Eqns. H.2 and H.3.

$$ {}^{S}R_{i,j} = \begin{cases} 4\pi A_{m,s} \big/ P_{m,j}^2 & I'_{i,j} \in C_{m,s} \\ 0 & \text{other} \end{cases} \tag{I.2} $$

$$ \text{CRI}_{i,j} = \sum_{s=1}^{25} \left[ \left( {}^{S}R_{i,j} \right)^{1.5} \right] \tag{I.3} $$

${}^{s}R_{i,j}$ is the roundness index which is zero for a straight line, and one for a circle. The brain has almost a round geometry and therefore, the area with a higher roundness index has a higher probability that it is brain tissue. The power of 1.5 is used to increase the sensitivity of CRI to the roundness index. Since the clusters in $I'_{i,j}$ are calculated based on T2 value, CRI takes both the physical and the geometrical properties of the cluster into account. Hence, the CRI is a good measure for the probability of the area being in the brain tissue. After calculating CRI, a recursive adaptive thresholding (Otsu's algorithm) is implemented to select the most probable location of the brain. The termination criteria, is that the calculated threshold should remain under 0.9.

The result is a bounding box indicating the most probable location of brain tissue in each slice. This bounding box is used for morphological cleaning by only keeping the largest cluster of pixels in its region. The new calculated images, $I''_{i,j}$, are used to calculate the 3D connectivity and

to update the CRI value. The evolution of CRI can be seen in Figure H.2.B.

The final brain region is found by applying two adaptive thresholds ($\sigma^2_{\text{CON}}$ and $\sigma^2_{\text{CRI}}$) on 3D connectivity and CRI as described by Eqn. H.4.

$$I''_{i,j} = \begin{cases} I''_{i,j} & \text{CON}_{i,j} > \sigma^2_{\text{CON}} \text{ and } \text{CRI}_{i,j} > \sigma^2_{\text{CRI}} \\ 0 & \text{other} \end{cases} \quad \text{(H.4)}$$

For each brain slice, 3D connectivity $\left(\text{CON}_{i,j}\right)$ considers the previous three slices and next three slices, and is defined as the number of slices in which $I''_{i,j}$ is not zero.

H.4.2.2. Lesion Detection

The lesion detection method consists of two main parts: seed selection and region growing. The seed selection part indicates a set of pixels which have a higher probability of being a abnormal brain tissue rather than normal tissue. The growth of the lesion uses the initialized seed points to either expand or shrink the seeded region based on the statistics of the neighboring pixels. The seed selection, and therefore region growing, is done independently for the detection of the blood and edema. The final lesion is the combination of the two (as shown in Figure H.2).

Correct seed point selection is the basic requirement for region growing. The main criteria for selecting the seed points are the T2 value and T2 asymmetry in brain structure. The proposed lesion detection method has two parallel seed selection and lesion growing, one for edema and the other for blood. The seed selection algorithm is dependent on the symmetrical structure of the brain in T2 Map.

Although the pathological structure of the human brain is not perfectly symmetrical, there is a high degree of bilateral symmetry. The various types of brain tissue have different T2 values, such that a uniform region likely represents a single brain tissue type. This is due to the variation in water content of the tissue types. Therefore, the T2 map of normal brain should have a high

degree of bilateral symmetry with respect to its axis of symmetry. Seed point selection is based on the assumption that lesions are generally not symmetrically placed in both hemispheres, while the whole brain is approximately symmetrical. Therefore, the automatic detection of this slice in the brain images is the first step in detecting brain abnormalities (Figure H.3).

To find the axis of symmetry, the bounding box of the brain region is calculated for each slice. The averaged center point of all bounding boxes is selected as the point of origin. Finally, the projection of the brain along the vertical axis of the image is found. The local minimum within 20 pixels of the center is selected as the second point where the axis of symmetry is passed through (Figure H.3.A). A line of symmetry is drawn using these two points.

The fact that TBI is associated with blood and edema, a discrete label, $L_{ij}$, is used to separate pixels with T2 values close to blood ($BL$) and edema ($ED$) from that of the normal appearing brain tissue ($NABT$) using the criteria shown in Eqn. H.5.

$$L_{ij} = \begin{cases} BL & T_{i,j} < 60 \\ ED & 110 < T_{i,j} < 150 \\ NABT & \text{other} \end{cases} \tag{H.5}$$

where $T_{i,j}$ and $T'_{i,j}$ denote the T2 value of $(i,j)^{th}$ pixel and of its symmetric pixel respectively. Asymmetrical values are then equal to the absolute value of their difference, $\delta_{i,j} = \left| T_{i,j} - T'_{i,j} \right|$. The final sets of seed points for blood ($S_{BL}$) and edema ($S_{ED}$) are selected based on the following criteria (Eqns. H.6 and H.7):

$$S_{BL} = \left\{ I_{i,j} \middle| I_{i,j} \in BL, \quad \delta_{i,j} < 30 \right. \tag{H.6}$$

$$S_{ED} = \left\{ I_{i,j} \middle| I_{i,j} \in ED, \quad 60 < \delta_{i,j} < 135 \right. \tag{H.7}$$

The selected blood and edema seed points are shown in Figure H.3.B. In this figure, seeds are shown in gray scale, in which the brightness of the seeds corresponds to a higher difference in the T2 values.

Upon seed selection, a diffusion based region growing is then implemented to group the statistically similar pixels in the region. The main criterion used in the region growing is region homogeneity. Pixels, or groups of pixels, are included in a region only if their characteristics are sufficiently similar to the characteristics of the pixels already in the region.

Similar to seed selection, the characteristics of interest are the T2 value of the pixel and the abnormality in brain symmetry structure which result in a significant difference between the T2 value of a pixel and the mirrored pixel across the axis of symmetry.

It should be noted that depending on the local statistics of the characteristics of interest, the diffusion technique may act as region shrinking. In this case, the selected seeds are essentially the captured noise in T2 value and are not consistent with the neighboring pixels.

The difference between the T2 value of selected seeds and their mirrored pixels as the asymmetric value ($\delta_{i,j}$) and the selected seeds as the lesion sources. The region growing algorithm allows the asymmetric value to diffuse across the neighboring pixels. Wherever, there are neighboring seeds with a higher T2 value difference, $\delta$, (white seeds in Figure H.3.B), the concentration of lesion value will be relatively higher. However, if the T2 value difference of the seeds is relatively small (dark points in Figure H.3.B), or there are smaller seed points around them, the overall concentration of lesion value will be smaller than threshold. This in turn will result in growing or shrinking of the region around the seed points.

To implement the two-dimensional diffusion, an implicit method is used (Eqn. H.8),

$$\delta_{i,j}^{n+1} = (1-4\Delta t)\delta_{i,j}^{n} + \Delta t\left(\delta_{i,j+1}^{n} + \delta_{i,j-1}^{n} + \delta_{i+1,j}^{n} + \delta_{i-1,j}^{n}\right) \tag{H.8}$$

where $\delta_{i,j}^{n+1}$ is the asymmetric value evaluated at $(n+1)$ iteration and $\Delta t$ is the time step and is selected to be 0.2 sec (Eqn. H.8 is numerically stable for $\Delta t < 0.25$).

The diffusion was terminated based on the number of pixels set to diffuse. This region was set as a circle with a radius of 25 pixels. Since the radial diffusion rate for Eqn. H.8 is approximately 5 pixels/sec, the diffusion time is set to be 5 seconds.

The final lesion area is detected by comparing the final asymmetric value of blood and edema with their corresponding threshold (15 for edema and 0.6 for blood). Figure H.4 illustrates the lesion growing at different iterations.

H.4.3. Analyzing the Detection of Lesions

The T2 symmetry method is tested on three TBI data sets, two sham data sets, and two naïve data sets. Figure H.4 compares the asymmetry cloud and detected lesion in a representative TBI data set.

It can be seen that lesion area is correctly classified in the majority of cases before checking the 3D connectivity of lesion area. The 3D connectivity criterion has detected the circled area as the misclassified regions in this figure. The lesion area determined using manual detection is compared to that of the T2 symmetry-based method in Figure H.5.

Similarity, sensitivity, and specificity were used to determine the performance between the T2 symmetry-based algorithm and the manual method. Similarity measures the similarities between the lesion location and area for both methods. Sensitivity measures the degree to which the lesions overlap between the two methods. Specificity measures the overlap in the normal brain tissue between the two methods. The sensitivity determines the positive detection rate, while the specificity determines the negative detection rate.

These performance indices are defined as (Shen *et al.* 2008; Schmidt *et al.* 2012):

$$\text{Similarity} = \frac{2TP}{2TP + FP + FN} \tag{H.9}$$

$$\text{Sensitivity} = \frac{TP}{TP + FN} \tag{H.10}$$

$$\text{Specificity} = \frac{TN}{TN + FP} \tag{H.11}$$

$$\text{Accuracy} = \frac{TN + TP}{TN + TP + FP + FN} \tag{H.12}$$

where $TP$ and $TN$ are true positive and true negative, respectively. $FP$ and $FN$ stand for false positive and false negative, respectively. The similarity index is the same as the Dice Coefficient (Dice 1945). It measures location and volume similarities between lesions derived from both methods. Note that the similarity index actually measures the accuracy of automatic detection in comparison to the gold standard, in terms of location, size, and overlap of the detected lesion. All the measuring indexes range between [0 - 1] and higher values indicate better performance of the algorithm. The similarity and sensitivity indexes for TBI are 0.49 ± 0.32 and 0.52 ± 0.28, respectively. The similarity, sensitivity, and specificity indices are compared to the HRS algorithm (Table H.2).

The lesion T2 value is extremely different for the 24 hr- and 72 hr-post injury images. The 24 hr-post injury T2 value corresponds to the edema that develops immediately following TBI (within a day) (Zweckberger *et al*. 2006). The T2 values observed for the edema are similar to those for CSF. After a couple of days, the edema is replaced by blood in the tissue due to hemorrhagic progression. This is observed in the 72 hr-post injury images. Furthermore, the blood remains indefinitely, and is thus observed in the 14 day-post injury images. The T2 values drop below the T2 value of grey matter when the blood accumulates in the tissue due to the iron in the blood.

The use of the T2 symmetry method was determined to accurately identify a lesion in TBI animals, while no lesion was detected in the naïve animals. Furthermore, the T2 symmetry method is able to detect a lesion area similar to that of the manual detection method. This computational algorithm operates in real-time which will provide immediate analysis to clinicians of injury using only T2 MRI images.

## H.5. Conclusion

Herein a computationally inexpensive and yet effective method for automatic, real-time lesion detection in T2 weighted images was developed. This algorithm uses the T2 values of edema and blood, as well symmetrical structures of the brain, to detect all possible abnormalities. This method is evaluated on a series of TBI, sham, and naïve subjects. Comparison of the results with manual detection method shows a high level of similarity, sensitivity, and specificity between the two methods. Furthermore, no false positives were observed.

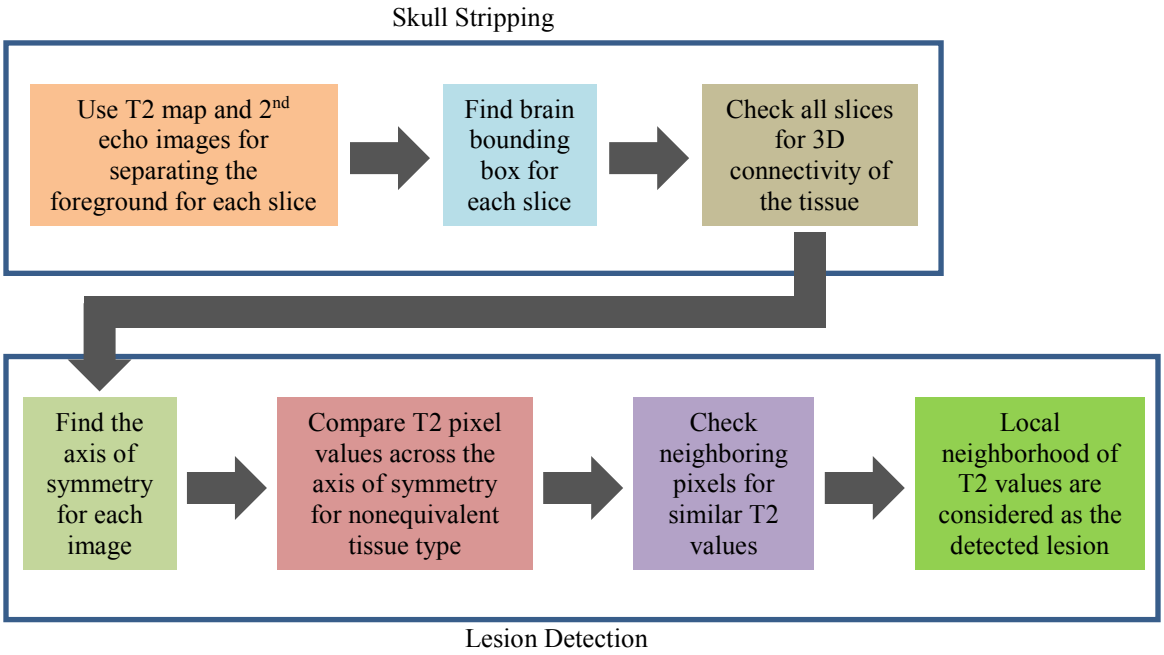


**Figure H.1.** Pseudo-Code for the Automatic Algorithm.

**Table H.1.** T2 Values Determined by Manual Detection.

| Tissue Type | T2 Value (ms) | | |
|---|---|---|---|
| | Mean ± STD | 95% Confidence | |
| Grey Matter | 73.8 ± 8.33 | 70.03 | 77.61 |
| CSF | 159.7 ± 29.14 | 132.8 | 186.7 |
| Skull | 34.1 ± 0.62 | 38.74 | 43.54 |
| Edema | 132.2 ± 12.09 | 117.2 | 129.2 |
| Blood | 58.4 ± 4.78 | 56.23 | 60.58 |

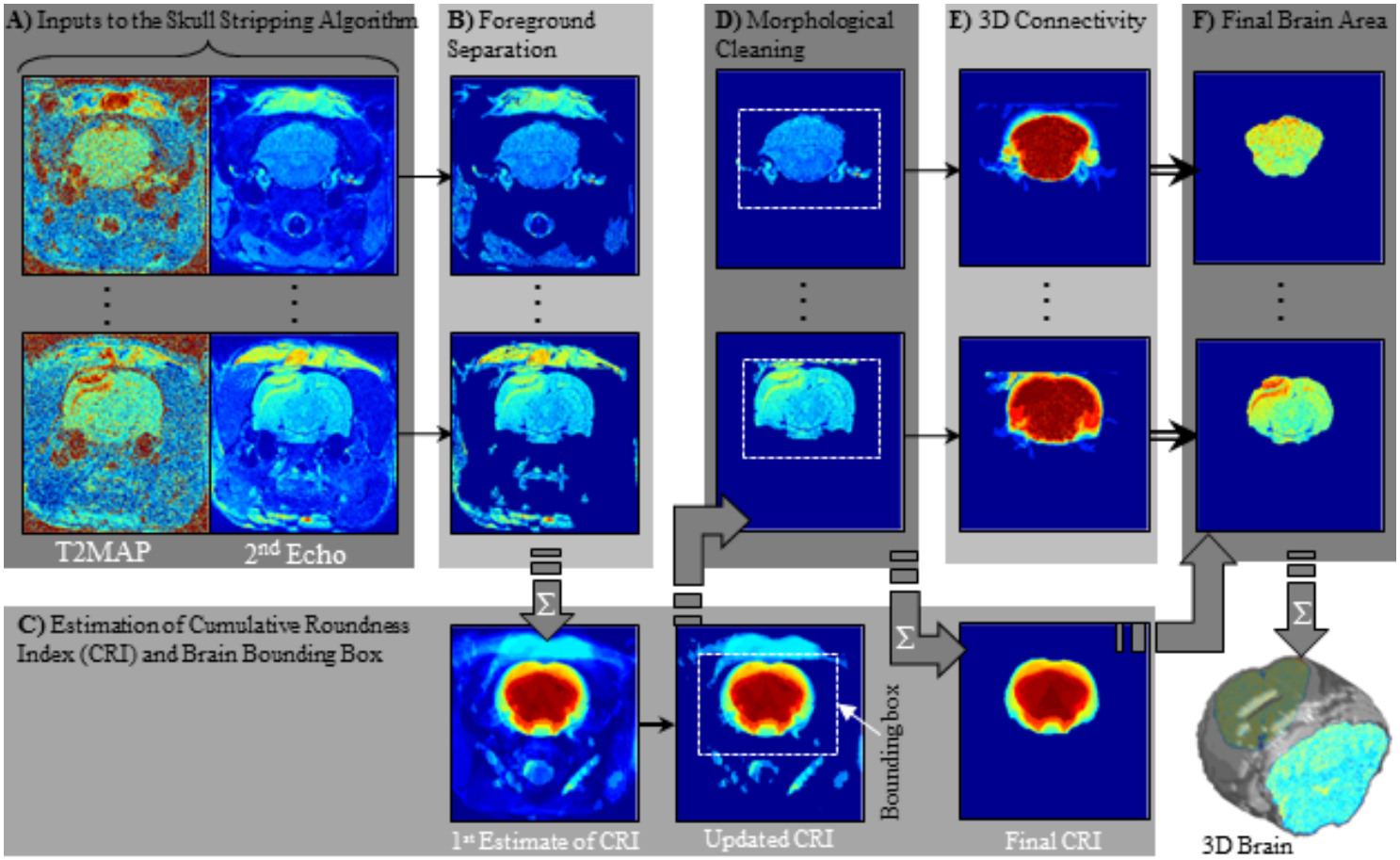


**Figure H.2.** Skull Stripping Main Steps.

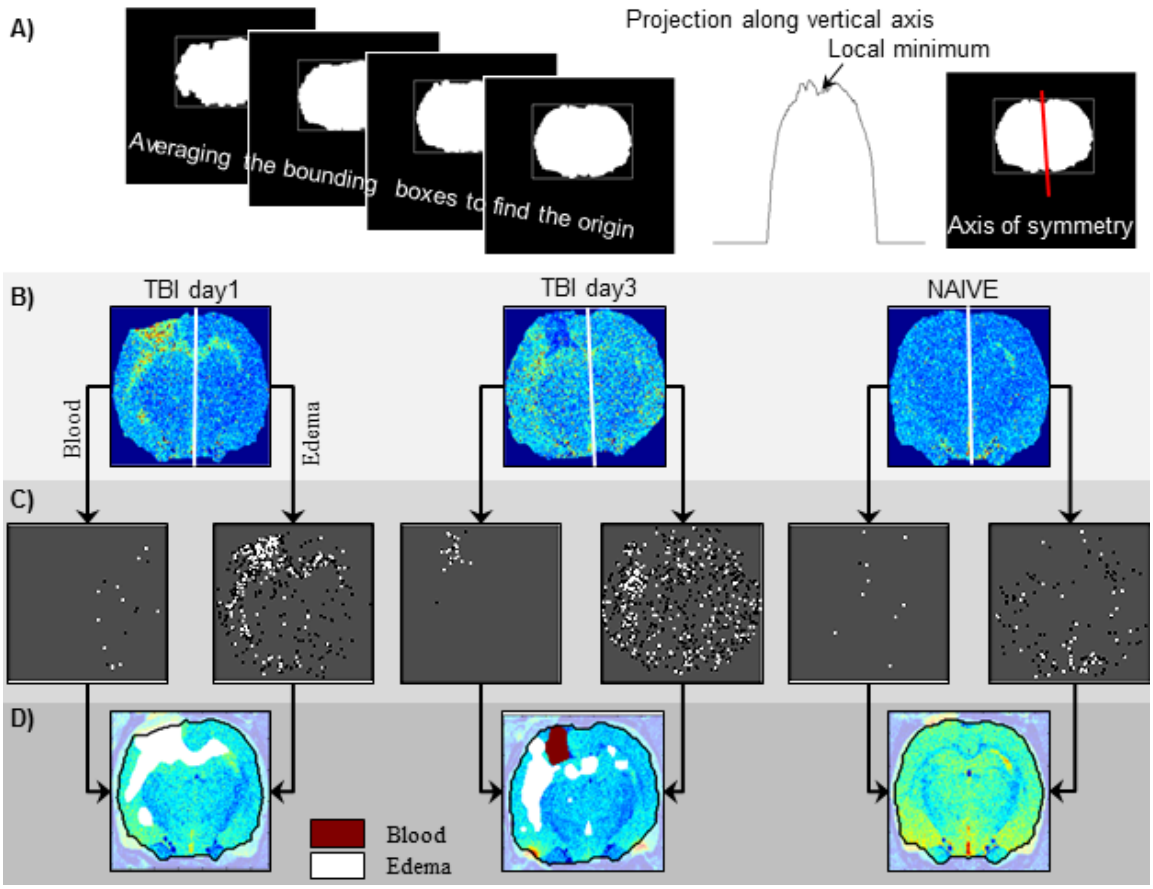


**Figure H.3.** Lesion Detection Main Steps. Three data sets are shown (1 day post-TBI, 3 days post-TBI, and naïve) **A.** Finding the axis of symmetry **B.** Seed point selection for edema and blood **C.** Region growing/shrinking. **D.** Final lesion area(s) of the tissue containing edema and blood.

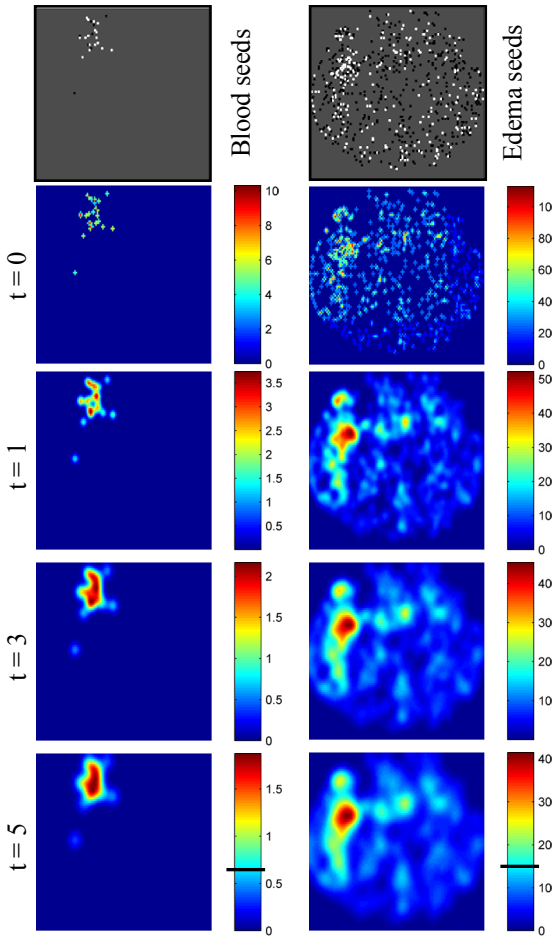


**Figure H.4.** Region Growing/Shrinking. The diffusion of T2 asymmetric values for region growing/shrinking for an animal receiving a TBI. The black bar on the color bar is the threshold.

**Table H.2.** Similarity, Sensitivity, Specificity, and Accuracy Indices. The automatic algorithm and HRS are compared.

| | Similarity | Sensitivity | Specificity | Accuracy |
|---|---|---|---|---|
| 1 Day Post-TBI | 0.60 ± 0.18 | 0.56 ± 0.23 | 0.99 ± 0.00 | 0.99 ± 0.01 |
| 3 Days Post-TBI | 0.40 ± 0.32 | 0.32 ± 0.30 | 0.99 ± 0.00 | 0.99 ± 0.00 |
| 14 Days Post-TBI | 0.43 ± 0.22 | 0.50 ± 0.32 | 0.99 ± 0.00 | 0.99 ± 0.00 |
| **Total** | **0.48 ± 0.24** | **0.46 ± 0.28** | **0.99 ± 0.00** | **0.99 ± 0.00** |
| **HRS[a]** | **0.40 ± 0.25** | **0.47 ± 0.12** | **0.87 ± 0.02** | **N/A** |

[a] (Ghosh *et al.* 2011)

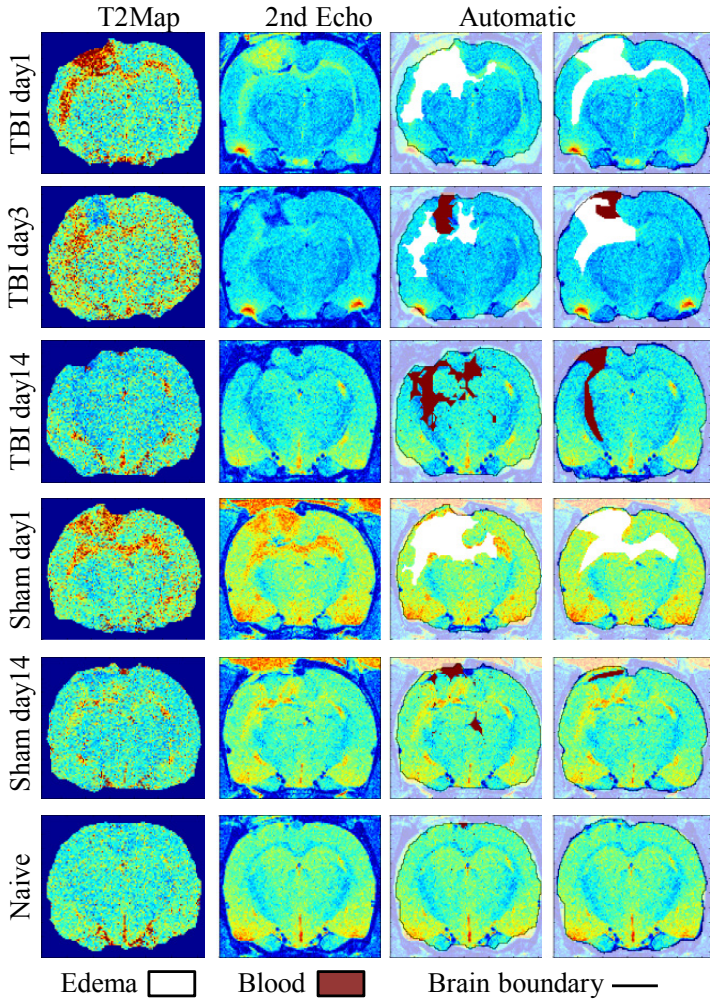


**Figure H.5.** Comparison of Lesion Visualization.

# APPENDIX I.

# A REAL-TIME ANALYSIS OF T2 MAGNETIC RESONANCE IMAGES USING A SYMMETRY-BASED ALGORITHM: PREDICTING WHEN A TRAUMATIC BRAIN INJURY OCCURRED

## I.1. Traumatic Brain Injury

The foremost cause of morbidity and mortality in persons under the age of 45 years worldwide is traumatic Brain injury (TBI). Annually, in the U.S., about 200,000 TBI victims require hospitalization, and 52,000 deaths result (Marmarou 2003). While the primary injury (impact causing the initial injury) may vary in severity and mechanism, it is the secondary injury which plays a significant role in the damage to the brain tissue. The secondary injury, such as cerebral edema, occurs within minutes of the primary injury and can last several weeks (Marmarou 2003; Kettenmann and Ransom 2005).

Cerebral edema is the increase in brain tissue water content. The two major types of cerebral edema are vasogenic edema and cytotoxic (cellular) edema. Vasogenic edema occurs with the disruption of the blood-brain barrier which can occur during the primary injury. Cytotoxic edema is the swelling of brain glial cells due to an influx of water. Cerebral edema following TBI is characterized by mixed vasogenic and cytotoxic edema.

## I.2. Detecting Traumatic Brain Injury

Current clinical methods of detecting cerebral edema are computed tomography (CT) and magnetic resonance imaging (MRI). While many TBI patents receive a CT scan when admitted to the hospital, an MRI scan provides higher resolution and contains quantitative measurements of

the cerebral edema. T2 MRI imaging allows for the relaxation time of the swollen tissue to be measured. This can potentially provide information about the time-course of the injury.

To utilize the quantitative information from T2 MRI scans, much research has been done to develop computer algorithms for analyzing, detecting, and predicting TBI.

Although there are many algorithms which can achieve these goals, the ideal algorithm would: 1) use a single modality scan (such as T2), 2) analyze and detect lesion(s), and 3) predict when a lesion occurred. Furthermore, this ideal algorithm would utilize the raw MRI images and operate in real-time to provide analysis and prediction bed-side for rapid prognosis.

An algorithm which has been developed for detecting and quantifying lesions in TBI as that of Bianchi *et al.* (Bianchi *et al.* 2012). The method of Bianchi *et al.* achieves a high level of accuracy in detecting the lesion. Furthermore, their method quantifies the T2 value of each pixel in the lesion. However, one down-fall to the method of Bianchi *et al.* is that the algorithm is unable to give real-time (bed-side) results and analysis.

The previously developed a symmetry-based algorithm which analyzes the T2 values in T2 MRI scans for differences across a line of symmetry utilizes only raw T2 scans, detects lesion(s), and, most importantly, operates in real-time for rapid analysis (Appendix H).

Currently, algorithms for predicting when an injury occurred are lacking. However, the need for such algorithms are apparent due to the benefits such algorithms can offer (Lee and Newberg 2005).

Here, the symmetry-based algorithm was extended to predict the time-course of a TBI. This is accomplished by quantifying the T2 values of the individual pixels in the lesion site and comparing the number of edematous, blood, and normal pixels.

I.3. Methods

Briefly, the algorithm developed for predicting the time that a TBI occurred computes the T2 value of each pixel within a detected lesion, determines the quantity of each pixel type (of which there are three), and utilizes the fraction of each of the three pixel types to predict when a TBI occurred.

I.3.1. Experimental Data

Nineteen repetitive TBI T2 MRI scans of male Sprague-Dawley rats (2 months old) were obtained from Dr. Andre Obenaus at Loma Linda University (Huang *et al.* 2013).

(TBI was induced using controlled cortical impact (CCI). A 5 mm craniotomy was performed, 3 mm posterior and 3 mm lateral to bregma, to expose the right cortical surface. The CCI was delivered using an electromagnetic driven piston with a 4 mm tip diameter at a depth of 2 mm, speed of 6.0 m/s, and contact duration of 200 ms (Leica Biosystems Inc., Richmond, Il).

TBI was induced on day 0 and repeated on day 2. Each animal was imaged on days 1 (24 hr-post first injury), 3 (72 hr-post first injury and 24 hr-post second injury), and 14 (14 days-post first injury).

MRI studies were performed using a 4.7 Tesla Bruker Advance MRI scanner (Bruker Biospin, Billerica, MA). T2-sequence data with 25 coronal slices were obtained. The scanner had a 30 cm bore and the imaging parameters were: TR/TE = 2850 ms/20 ms, number of echoes = 6, field of view = 3x3 cm with 2 averages. The image resolution was 256x256 (Huang *et al.* 2013).

All experiments were approved by Loma Linda University IACUC.

I.3.2. T2 Values Within a Lesion

Prior to development of the predictive algorithm, ten T2 MRI scans for day 1, day 3 and day 14 were used to obtain the T2 values typical of the tissue containing blood, edema, or nothing (normal tissue).

The T2 values of each tissue type (blood, edema, or normal) were determined by fitting three Gaussians to the T2 values in the detected lesion.

Using the T2 values of each pixel type (blood, normal, or edema), each pixel within the detected lesion is determined to be of one of these three types. The total number of each pixel type is determined for the entire data set (for all slices containing lesion). The fractional number of each pixel type within the lesion is calculated by:

$$\text{Fracion of Pixel Type } i = \frac{\text{Pixel Type } i}{\text{Total Pixels}} \tag{I.1}$$

I.3.3. Prediction Algorithm

The fractions of each pixel type are used for determining when a TBI occurred. In order to develop the predictive model, four day 1, three day 3, and four day 14 data sets were used to determine the fractions of each pixel type. Within the scan for each day, the fraction of pixels which are blood, normal, and edema are calculated. For each time point (1 day-post injury, 3 days-post injury, and 14 days-post injury), a Gaussian was fit to each pixel type to determine the average and variance for each pixel type's fraction.

Using the Gaussian fit for each pixel type fraction at each time point (day 1, day 3, or days 8 - 14), the predictive model was developed based on the relationships observed.

## I.4. Results

During the development of the algorithm, thirty T2 MRI scans (ten of each day 1, day 3, and days 8 - 14) were used to quantify the T2 values of the tissue containing blood, edema, or nothing (normal tissue). Table H.1 contains the T2 values of each tissue type (blood, edematous, or normal). Although the value of T2 changes for each pixel type during the course of TBI, the only T2 value which changes significantly is that of edema

### I.4.1. Histograms of T2 Values

The ranges of the T2 values were used to classify each pixel as one of the three pixel types (Figure I.1). The T2 range for the pixels classified as blood is 43 - 69 ms. The range of T2 values for normal tissue is 70 - 89 ms. The range of the edema T2 values is 90 - 200 ms.

A histogram of the frequency of each pixel type was obtained for the data sets to determine the total number of each type of pixel in the entire scan (Figure I.2). The frequency of each pixel type varies depending on the area of the lesion detected; however, the ratio of each pixel type remains fairly constant across each slice in the data set.

### I.4.2. Fractional Amount of Each Pixel Type

The frequency of each pixel type in the lesion was used to quantify the fraction of the total pixels in the lesion that each pixel type occurred.

The total count of each pixel type was determined for the entire data set. Then the fractional amount of each pixel type was determined using Eqn. I.1.

To develop the relationships between the fractions for each pixel type, a single Gaussian was fit to the data for each pixel type (blood, normal, and edema) at each time point (day 1, day 3,

and day 14). A total of eleven data sets were used to develop the relationships (four 1 day-post injury, three 3 days-post injury, and four 14 days-post injury).

Table I.2 contains the fraction amounts of each pixel type at each time point. The fractional amount of blood pixels in the lesion changes slightly for each time point. The fractional amount of normal pixels and edema pixels in the lesion for the images at 1 day-post injury is nearly identical. The same relation is observed for the 3 days-post injury images. However, the fractional amount of edema pixels is higher than that of the normal pixels for the 14 days-post injury images.

I.4.3. Predicting When an Injury Occurred

The fraction of blood pixels ($F_{blood}$), normal pixels ($F_{normal}$), and edema pixels ($F_{edema}$) were used to identify when an injury occurred (based on the available data at 1 day-post injury, 3 days-post injury, and 14 days-post injury). The relationship identified between the fractional amounts of each pixel type and the time points was:

1.) For lesions 1 day-post injury

$$\left(F_{blood} > 0.52\right) \text{ and } \left(\left|F_{normal} - F_{edema}\right| < 0.03\right)$$

or

$$\left(F_{blood} < 0.52\right) \text{ and } \left(F_{normal} > 0.245\right) \text{ and } \left(\left|F_{normal} - F_{edema}\right| < 0.028\right)$$

2.) For lesions 3 days-post injury

$$\left(F_{blood} < 0.52\right) \text{ and } \left(F_{normal} > 0.245\right) \text{ and } \left(\left|F_{normal} - F_{edema}\right| > 0.028\right)$$

3.) For lesions 14 days-post injury

$$\left(F_{blood} > 0.52\right) \text{ and } \left(\left|F_{normal} - F_{edema}\right| > 0.03\right)$$

or

$$\left(F_{blood} < 0.52\right) \text{ and } \left(F_{normal} < 0.245\right)$$

Utilizing the conditions of the predicting a TBI for the three time points, the eight remaining data sets were analyzed and the occurrence of a TBI was predicted. Of the eight remaining data sets, two data sets were 1 day-post injury, two data sets were 3 days-post injury, and four data sets were 14 days-post injury.

A confusion matrix was created for the prediction results (Table I.3). The prediction for the T2 MRI images at 1 day-post injury (two data sets) at 3 days-post injury (two data sets) were correctly predicted for all cases. The prediction for the T2 MRI images at 14 days-post injury were correctly identified 75% of the time (3 of 4).

## I.5. Conclusion

Here, an algorithm has been developed to predict when a TBI occurred. The algorithm was tested and successfully predicted when an injury occurred 87.5% (7 of 8) of the image sets. This algorithm was coupled with a symmetry-based method for detecting and analyzing T2 MRI images in real-time. This combined algorithm now satisfies the aspects which makes an ideal algorithm for this problem.

Future studies include applying this algorithm to additional T2 MRI scans which have been collected at time points other than 1 day-post injury, 3 days-post injury, and 14 days-post injury. In addition, the predictive model can be refined and have enhanced predictive power if the T2 value changes are utilized (specifically the T2 value changes of edematous tissue) rather than the range the T2 values over the time-course of injury.

**Table I.1.** T2 Values of Three Types of Brain Tissue. T2 values observed during TBI for three time points (Day 1: 1 day-post injury, Day 3: 3 days-post injury, Days 8 - 14: 8 - 14 days-post injury). T2 values are presented as mean ± SEM.

| | Day 1 | Day 3 | Days 8 - 14 |
|---|---|---|---|
| Blood | 66.4 ± 3.1 | 57.5 ± 4.2 | 56.8 ± 2.7 |
| Normal | 76.8 ± 4.4 | 76.5 ± 1.9 | 77.3 ± 5.9 |
| Edema | 139.2 ± 23.7 | 98.0 ± 6.2 | 91.1 ± 6.0 |

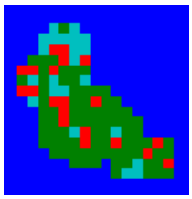

**Figure I.1.** A Representative Pixel Classification Image. The image displays the classification of each pixel type in a detected lesion (Day 3 chosen as the example). The pixel types are blood (green), normal (red), and edema (light blue). The blue background is classified as non-lesion.

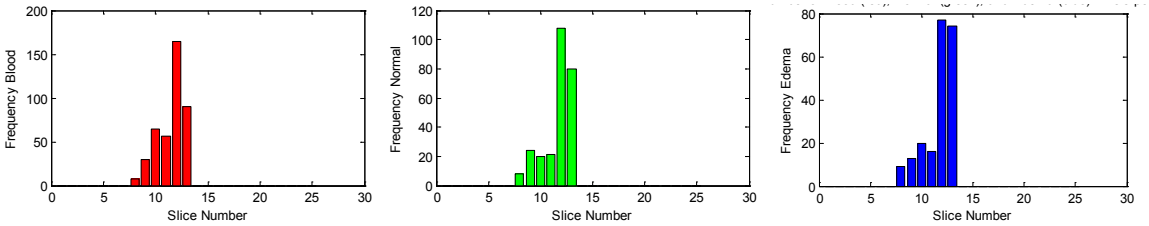


**Figure I.2.** Representative Histograms of Each Pixel Type. Pixels corresponding to blood (left), normal (middle), and edema (right) T2 values (Day 3). The frequency of each pixel type is shown for each image containing a lesion in the entire data set (25 slices).

**Table I.2.** Fractional Amount of Each Pixel Type. Pixel types (blood, normal, and edema) for each time point (Day 1, Day 3, and Day 14). The fractional amount is presented as mean ± STD.

| | Day 1 | Day 3 | Day 14 |
|---|---|---|---|
| Blood | 0.528 ± 0.050 | 0.511 ± 0.036 | 0.483 ± 0.027 |
| Normal | 0.236 ± 0.018 | 0.246 ± 0.008 | 0.240 ± 0.003 |
| Edema | 0.236 ± 0.033 | 0.245 ± 0.029 | 0.277 ± 0.025 |

**Table I.3.** Confusion Matrix of the Prediction Algorithm.

| | | Ground Truth | | |
|---|---|---|---|---|
| | | Day 1 | Day 3 | Day 14 |
| Predicted | Day 1 | 1.0 | 0.0 | 0.0 |
| | Day 3 | 0.0 | 1.0 | 0.0 |
| | Day 14 | 0.25 | 0.0 | 0.75 |

# APPENDIX J.

# ANIMAL STUDY PROTOCOLS AND SOLUTIONS

## J.1. aCSF Solution Components

The aCSF solution was prepared following Csenkér *et al.* (Csenkér *et al.* 1982):
130 mM NaCl
3 mM KCl
1.2 mM $KH_2PO_4$
20 mM $NaHCO_3$
2.4 mM $CaCl_2$
1.3 mM $MgSO_4$
10 mM glucose
pH 7.4

## J.2. Craniectomy Protocol

This protocol is courtesy of Dr. Devin Binder's Lab Group.

1. Always lift animal by the tail
2. Weigh animal
    a. Pour a little anesthesia on a paper towel and place lid back on to knockout the mouse
    b. Subtract 1.5 g from the weight because of the box on the balance
3. Give an injection of ketamine/xylazine (usually last for 1 hr, then half doses every 1 hr)
    a. Mix/shake well before using
    b. Flatten belly (after animal is on its back) to push organs out of the way
    c. Pinch skin, lift up, and inject at the base
4. Apply ointment to the eyes
5. Check for pinch-paw reflex (do this periodically)
6. Insert animal into the stereotactic frame
    a. Hook teeth
    b. Place 1 ear holder
    c. Place the other ear holder
    d. Adjust to make sure that:
        i. Head does not move
        ii. Head is flat
        iii. Both holders have same distance
    e. Secure snout
7. Once the animal is secured into the frame, cut the skin area
    a. Pinch the skin and lift with forceps
    b. Make a mid-line incision
    c. Cut semi-circles from mid-line (close to the eyes and back near the ears)
8. Make sure the head does not move
9. Make sure Bregma and Lambda are on the same plane (Figure J.1)

10. Insert the frame into the operating microscope
11. Use saline and swab to remove hair from skull
    a. Non-sterile swabs are okay to use on the skull
12. Choose a burr to use
    a. Usually a medium burr is best
13. Check for reflex and head movement
14. Use forceps to scrape off connective tissue
15. Craniectomy
    a. Use forceps to hold skull down on opposite side of drilling
        b. Always start at the mid-line
        c. Cut a groove around the area to be exposed (Figure J.1)
        d. Cut past the Bregma into frontal lobe
        e. Continue cutting until you pop through the skull (feel the skull give way)
        f. Periodically:
            i. Wipe off the burr with alcohol wipe
            ii. Use saline and swab to clean the skull of bone dust
            iii. Check reflexes
        g. When skull pops, bleeding may occur
        h. Once skull has popped everywhere along the groove:
            i. Stop any bleeding with saline and a swab
            ii. Use saline (2 - 4 drops) to lift skull up
            iii. Gently use forceps to grab the skull and lift off
        i. Use saline and sterile swab to stop bleeding after the brain is exposed
16. Use 2 - 4x anesthesia dose to expire mouse

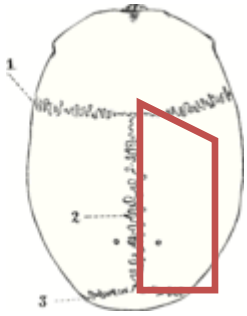


**Figure J.1.** Schematic of a Craniectomy. The red lines are the craniectomy. The numbers 1, 2, and 3 correspond to the Bregma suture, the Midline, and the Lambda suture.

J.3. Removing the Brain for Wet-Dry Weights

This protocol is courtesy of Dr. Devin Binder's Lab Group. After completing an experiment, if the animal is for weight-dry weight brain measurements:

1. Inject the animal with the correct amount of ketamine/xylazine (according to its weight) to sacrifice.
2. When the animal has stopped breathing, remove the animal's head as close to the skull as possible. Cut back the fur and remove the fascia to expose the skull.
3. Use scissors to clip the skull at the base near the spine. Use forceps to clip the skull off, exposing the brain. Be careful not to remove brain tissue.
4. Gently lift the meninges covering the brain and cut the membrane so it can be pulled off the brain.
5. Gently lift the brain out of the cranium by lifting from the underside. Sever the nerves between the brain and cranium.

J.4. Perfusion Methods - Tissue Preservation

This protocol is courtesy of Dr. Devin Binder's Lab Group. It is similar to the protocol used by Dr. Andre Obenaus' Lab Group (Loma Linda University). Detailed images of this Protocol can be found in Devin M$^{c}$Bride's Laboratory Notebook 4 pages 72 - 79. The images are from Dr. Andre Obenaus' Lab.

1. Set-up the perfusion equipment and allow the perfusate (4% paraformaldehyde (PFA)) to come to room temperature. Make sure that the PFA is free of bubbles.
2. Inject the animal with the correct amount of ketamine/xylazine (according to its weight) to sacrifice. Check for the level of anesthesia by paw pinch reflex.
3. When the animal is thoroughly under and breathing is slow, attach the animal to the perfusion dish belly-up. Make sure to secure the animals limbs.
4. Using toothed forceps, pull the skin just below the ribs and make a cut into the abdomen and continue down both sides
5. Reposition the forceps to make a small cut to expose the xyphoid process
6. Release the skin and pull up on the xyphoid process. Cut down both sides of the abdomen to expose the diaphragm, and then cut across the rib-cage towards the arm pits to expose the heart.
7. Make a small incision in the animal's right atria to allow for the blood to flow out of the system
8. Quickly insert the needle into the apex of the heart and pump the PFA through the animal's circulatory system. The animal may twitch due to the PFA flowing through the system. Blood, and eventually PFA, should be observed flowing from the right atria. Allow ~30 mL of PFA (for every 10 g of animal weight) to flow through the animal.
9. When finished flowing PFA, remove the needle, and take the animal out of the dish.
10. Remove the animal's head as close to the skull as possible. Cut back the fur and remove the fascia to expose the skull.
11. Use scissors to clip the skull at the base near the spine. Use forceps to clip the skull off, exposing the brain. Be careful not to remove brain tissue.

12. Gently lift the meninges covering the brain and cut the membrane so it can be pulled off the brain.
13. Gently lift the brain out of the cranium by lifting from the underside. Sever the nerves between the brain and cranium.
14. Lift the brain out and place it in 4% PFA overnight
15. Then transfer the brain in 30% sucrose overnight
16. When the brains are not floating, they are ready for freezing
17. Crush dry ice into a box and leave some in the pestle. Place 15 mL tubes into the dry ice to get cold.
18. Put the metal beaker into the pestle and dig it into the dry ice
19. Let the beaker get cold (condensation will form around the beaker)
20. Pour isopentane quickly into the beaker
21. Isopentane is cold when it is cloudy
22. Drop the brain into the isopentane and wait for 30 s
23. Grab the brain using forceps. Be gentle so you don't leave marks on the tissue.
24. Drop the brain into a new 15 mL tube (which is in the dry ice)
25. Store the brains in -80$^{o}$C until ready for staining

J.4. Cryostat Protocol

This protocol is courtesy of Dr. Devin Binder's Lab group. This protocol is used on samples which have already been preserved. When in the cryo-chamber, everything must be cold.

1. Crush dry ice for keeping the sample cold
2. Put 400 µL of 1x phosphate buffered saline (PBS) into well plates
3. Clean the cryostat blade with ethanol wipe and then Kimwipe
4. Slide the blade into place. Do not touch the blade. Tap the blade with a brush. Place a paper towel to catch the waste.
5. Clean the dental probe. The natural (sable) brush is better since they don't lose the hairs. Use size 0 and lower.
6. Place a sterilized razor blade in the cryostat to get it cold
7. Optical cutting temperature compound is used to mount the tissue
8. Put optical cutting temperature compound on the sample bed. Use enough to cover the surface.
9. Put the sample bed into the cryostat and let it cool. It will turn white when ready.
10. Trim the optical cutting temperature compound to create a flat surface for mounting. Use large slices. If the optical cutting temperature compound comes off, there were bubbles or bad contact with the sample bed.
11. Remove the sample bed. Make sure you know the orientation of slicing.
12. Add the sample to the cryostat to bring it to the same temperature. The brain tissue becomes tan.
13. Use the razor blade to slice a flat surface on your tissue. Make sure to cut on a side opposite from what you are interested in.
14. Place 1 drop of optical cutting temperature compound onto the sample bed. Immediately place your sample in the drop with the flat side down. Place an excess of optical cutting temperature compound around the tissue to set it completely. This will prevent the sample from moving or falling off during cutting.

15. Make sure you are cutting at the right size. Start the blade well away from your sample so that it can cut the right size. The first few slices are required to change the slice size from what is was to what you want it to be.
16. Make sure your sample is even.
17. Begin cutting your sample. We use the brush to prevent the tissue from rolling. This also prevents serrations in the tissue.
18. Cut a few tissue slices, and then use the dental tool to pick up the slices and place them into the PBS wells. The tissue will adhere to the dental tool metal. PBS removes optical cutting temperature compound.

J.5. Nissl Stain

Mix 50 mL of A, 300 mL of B, and 200 mL of C together to make the Nissl stain.

A: 0.3 g cresyl echt violet in 50 mL of $ddH_2O$
B: 2.32 mL glacial acetic acid in 300 mL of $ddH_2O$
C: 5.44 g sodium acetate in 200 mL $ddH_2O$

J.6. Histological Staining

This protocol is courtesy of Dr. Devin Binder's Lab Group. The purpose of this protocol is to prepare tissue slices for Nissl staining. Super frost slides are used to mount the tissues on. Here the tissue samples were brain tissue.

1. To remove the tissue samples from the wells
    a. Add 400 µL of 1x PBS into a well (or more if the well is low)
    b. Use a scooper to remove the sample
    c. Drop the sample into another container with the slide immersed in 1x PBS
2. Placing the sample onto the slide
    a. Move the sample over the slide with a brush
    b. Using the brush, pat the sample down on the slide surface
        i. If the sample doesn't stick, use the brush to rub the slide surface and try again
    c. When the sample is on the slide, evenly lift the slide out of the PBS
3. Dab the slide with a Kimwipe to remove excess PBS
4. Let the sample dry (~20 min)
5. When the sample is dry, a series of ethanol washes is used to loosen the fats/lipids to allow for better penetration of the stain. This also rehydrates the tissue post-opening pores which prevents the cells from lysing and loosening the tissue from the slide. The $ddH_2O$ is used to remove PBS crystals.
    a. Beginning with a 100% ethanol solution, immerse the slide (with sample on it) and let it soak for 1 min
    b. Then transfer the sample into a 95% ethanol solution and let it soak for 1 min
    c. Then transfer the slide into a 70% ethanol solution and let it soak for 1 min
    d. Finally, place the slide into $ddH_2O$ to rehydrate completely for 1 - 3 min. Be careful when placing the slide into the $ddH_2O$ since the sample can fall off as the sample will swell.
6. Remove the sample from the $ddH_2O$ and let it dry (~5 min)

7. Place the slide into the cresyl violet solution. The time varies, but you want to get a nice color to the tissue sample (10 - 30 min). Use tweezers to remove the slide when it has stained.
8. Pipet some 70% ethanol onto the slide to remove non-specifically bound and excess dye
9. The sample is now stained and prepared for visualization

## J.7. Loma Linda University Traumatic Brian Injury Animal Study

The schematic of the TBI protocol and outcomes studied is found in Figure J.2. Detailed images of the Loma Linda Protocols can be found in Devin McBride's Laboratory Notebook 4 pages 41 - 53.

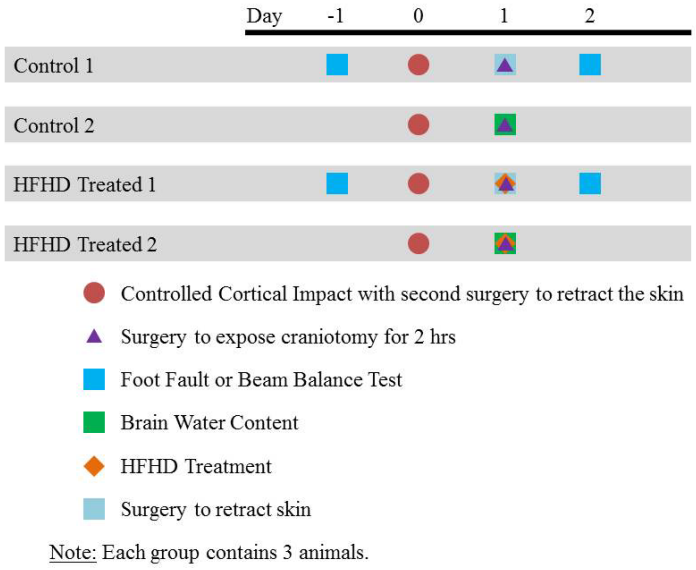


**Figure J.2.** Animal Protocol Diagram for the Traumatic Brain Injury Study at Loma Linda University.

## J.8. Neurological Tests

These protocols were provided by Dr. Andre Obenaus at Loma Linda University. Neurological testing was measured after CCI using beam balance, to evaluate proprioception and balance, and foot fault, to evaluate sensorimotor response and proprioception. All testing was carried out within a 3-hour morning time block (7 - 10AM).

Beam Balance: The beam balance task was elevated 62 cm using a Plexiglas beam 60 cm long and 0.5 cm wide. At the center, animals were placed perpendicular to the beam and allowed to walk unrestricted in either direction. The duration spent on the beam without falling and distance traveled was recorded. The average of 2 trials per day, each trail not exceeding 60 s, was used for statistical analysis.

Foot fault: Animals were given 60 s to explore a 50 cm by 155 cm platform (ClosetMaid, Ocala, FL) with parallel wires bars 1.5 cm apart. The apparatus was elevated 100 cm and the number of foot faults were recorded. A foot fault was defined as the misplacement of a fore- or hind-limb, such that the paw fell completely through the bars. The average of 2 trials per day was

used for statistical analysis. Beam balance and foot fault test were recorded for different sets of animals.

NOTES:
1. For any test, do not stimulate the subject in any way (even if it appears non-active). Also avoid excessive variability in the testing conditions - keep the background noise, lab coat, equipment set-up, etc. as consistent as possible.
2. Carry out all tests within the same time-block during the day

J.7.1. Foot Fault Test

1. Clean the top of the grid with Quatricide
2. Turn on the webcam. Set-up the webcam to visualize the grid. Make sure it is level with the grid so the foot faults can be viewed. Check resolution. Begin capturing the video.
3. Lifting the subject by the tail, gently place it in the middle of the grid, facing the wall
4. View the subject's limbs from eye-level. Allow the subject to move for 60 s. Use a tally clicker to record the number of food faults (times a limb misses the grid and falls through).
5. Return the subject to a cage.
6. Record the number of ticks (foot faults). Also record other behaviors (dragging of hind-limb).
7. Stop the video after the experiment is completed and save it
8. Clean the grid after each animal
9. Repeat for other animals. Then repeat the set of animals two more times.

Other measures can be tested, such as faults per active (moving) time or ipsilateral vs. contralateral faults or fore-limb vs. hind-limb faults.

J.7.2. Beam Balance Test

1. Clean the top of the beam with Quatricide ensuring that the "5 cm" marks are still visible. Redraw them if needed.
2. Turn on the webcam. Set-up the webcam to visualize the beam. Check resolution. Begin capturing the video.
3. Lifting the subject by the tail, gently place it perpendicular to the length of the beam (facing the wall) right in the midpoint of the beam (marked "0")
4. Have the stopwatch in one hand and begin the time right after the subject is placed on the beam. Stop the time if the subject falls off, or 60 s, whichever comes first.
5. After placing the subject on the beam and starting the time, pick up the tally clicker with your other hand, record each time the subject's nose crosses one of the marks. Each mark that is crossed becomes the reference point.
6. When the time has been reached, or the subject falls off, recover the subject and place it into another cage for recovery
7. Record the time spent on the beam and the number of ticks (distance traveled). Also record other behaviors (dragging of hind-limb).
8. Stop the video after the experiment is completed and save it
9. Clean the beam after each animal
10. Repeat for other animals. Then repeat the set of animals two more times.

Other measures can be tested, such as number of right/left turns.

# REFERENCES


Akselrod-Ballin A, Galun M, Gomori JM, Filippi M, Valsasina P, Basri R, and Brandt A (2009) "Automatic Segmentation and Classification of Multiple Sclerosis in Multichannel MRI," *IEEE Trans Biomed Eng*, **56**:2461-9.

Alford JR, Kendrick BS, Carpenter JF, and Randolph TW (2008) "Measurement of the Second Osmotic Virial Coefficient for Protein Solutions Exhibiting Monomer-Dimer Equilibrium," *Anal Biochem*, **377**:128-33.

Amiry-Moghaddam M and Ottersen OP (2003) "The Molecular Basis of Water Transport in the Brain," *Nature Rev Neurosci*, **4**:991-1001.

Arakawa T and Timasheff SN (1982a) "Stabilization of Protein Structure by Sugars," *Biochem*, **21**:6536-44.

Arakawa T and Timasheff SN (1982b) "Preferential Interactions of Proteins With Salts in Concentrated Solutions," *Biochem*, **21**:6545-52.

Arakawa T and Timasheff SN (1983) "Preferential Interactions of Proteins With Solvent Components in Aqueous Amino-Acid Solutions," *Arch Biochem Biophys*, **224**:169-77.

Arakawa T and Timasheff SN (1984a) "Mechanism of Protein Saliting-In and Salting-Out by Divalent Cation Salts: Balance Between Hydration and Salt Binding," *Biochem*, **23**:5912-23.

Arakawa T and Timasheff SN (1984b) "Protein Stabilization and Destabilization by Guanidinium Salts," *Biochem*, **23**:5924-9.

Arakawa T and Timasheff SN (1984c) "The Mechanism of Action of Na Glutamate, Lysine HCl, and Piperazine-*N*,*N*'-Bis(2-Ethanesulfonic Acid) in the Stabilization of Tubulin and Microtubule Formation," *J Biol Chem*, **259**:4979-86.

Arakawa T and Timasheff SN (1985) “Mechanism of Poly(Ethylene Glycol) Interaction With Proteins,” *Biochem*, **24**:6756-62.

Arosio D, Kwansa HE, and Bucci E (1999) “Preferential Hydration and Buoyancy of Hemoglobins Detected by Static and Dynamic Light Scattering,” *Biophys J*, **76**:A426.

Arosio D, Kwansa HE, Gering H, Piszczek G, and Bucci E (2002) “Static and Dynamic Light Scattering Approach to the Hydration of Hemoglobin and Its Supertetramers in the Presence of Osmolites,” *Biopolymers*, **63**:1-11.

Ashwal S, Holshouser BA, and Tong KA (2006) “Use of Advanced Neuroimaging Techniques in the Evaluation of Pediatric Traumatic Brain Injury,” *Developmental Neurosci*, **28**:309-26.

Atmeh RF, Arafa IM, and Al-Khateeb M (2007) “Albumin Aggregates: Hydrodynamic Shape and Physico-Chemical Properties,” *Jordan J Chem*, **2**:169-82.

Aune KC and Timasheff SN (1987) “Abnormal Solubility Behavior of β-Lactoglobulin: Salting-In by Glycine and NaCl,” *Biochem*, **26**:5147-53.

Babizhayev MA, Nikolayev GN, Goryachev SN, and Bours J (2002) “NMR Spin-Echo Studies of Hydration Properties of the Molecular Chaperone α-Crystallin in the Bovine Lens,” *Biochim Biophys Acta*, **1598**:46-54.

Babizhayev MA, Nikolayev GN, Goryachev SN, Bours J, and Martin R (2003) “Hydration Properties of the Molecular Chaperone α-Crystallin in the Bovine Lens,” *Biochem (Moscow)*, **68**:1145-55.

Bassi FA, Arcovito G, De Spirito M, Mordente A, and Martorana GE (1995) “Self-Similarity Properties of α-Crystallin Supramolecular Aggregates,” *Biophys J*, **69**:2720-7.

Bianchi A, Bhanu B, Donovan C, Obenaus A (2012) “Contextual and Visual Modeling for Detection of Mild Traumatic Brain Injury in MRI,” *ICIP 2012*, 1261-4.

Blanco MA, Sahin E, Li Y, and Roberts CJ (2011) "Reexamining Protein-Protein and protein-Solvent Interactions From Kirkwood-Buff Analysis of Light Scattering in Multi-Component Solutions," *J Chem Phys*, **134**:225103-12.

Bratton SL *et al.* (2007) "Guidelines for the Management of Severe Traumatic Brain Injury," *J Neurotrauma*, **24**:S1-S106.

Buccola JR (2010) "Significance of the Choice of a Concentration Variable on Viscosity Model Predictions for BSA in Aqueous Media," University of California, Riverside, Masters Thesis.

Bujacz A (2012) "Structures of Bovine, Equine and Leporine Serum Albumin," *Acta Crystallogr Sect D*, **68**:1278-89.

Bull HB and Breese K (1968) "Protein Hydration .I. Binding Sites," *Arch Biochem Biophys*, **128**:488-96.

Cameron IL and Fullerton GD (1990) "A Model to Explain the Osmotic Pressure Behavior of Hemoglobin and Serum Albumin," *Biochem Cell Biol*, **68**:894-8.

Carr CW (1952) "Studies on the Binding of Small Ions in Protein Solutions With the Use of Membrane Electrodes .I. The Binding of the Chloride Ion and Other Inorganic Anions in Solutions of Serum Albumin," *Arch Biochem Biophys*, **40**:286-94.

Carr CW (1953) "Studies on the Binding of Small Ions in Protein Solutions With the Use of Membrane Electrodes .II. The Binding of Calcium Ions in Solutions of Bovine Serum Albumin," *Arch Biochem Biophys*, **43**:147-56.

Carr CW (1955) "Competitive Binding of Calcium and Magnesium with Serum Albumin," *Proc Soc Exp Biol Med*, **89**:546-9.

Castillo LB, Bugedo GA, and Paranhos JL, (2009) "Mannitol or Hypertonic Saline for Intracranial Hypertension? A Point of View," *Crit Care Resusc*, **11**:151-4.

Chatelier RC and Minton AP (1987) "Sedimentation Equilibrium in Macromolecular Solutions of Arbitrary Concentration .II. Two Protein Components," *Biopolymers*, **26**:1097-113.

Chi EY, Krishnan S, Kendrick BS, Chang BS, Carpenter JF, and Randolph TW (2003) "Roles of Conformational Stability and Colloid Stability in the Aggregation of Recombinant Human Granulocyte Colony-Stimulating Factor," *Protein Sci*, **12**:903-13.

Coen CJ, Blanch HW, and Prausnitz JM (1995) "Salting-Out of Aqueous Proteins - Phase Equilibria and Intermolecular Potential," *AIChE J*, **41**:996-1004.

Cohn EJ and Edsall JT (1943) Proteins, Amino Acids and Peptides as Ionds and Dipolar Ions, Reinhold.

Clark ME, Burnell EE, Chapman NR, and Hinke JAM (1982) "Water in Barnacle Muscle .IV. Factors Contributing to Reduced Self-Diffusion," *Biophys J*, **39**:289-99.

Conway BE (1981) Ionic Hydration in Chemistry and Biophysics, Elsevier Scientific Pub. Co.

Cooper DJ *et al.* (2011) "Decompressive Craniectomy in Diffuse Traumatic Brain Injury," *New Eng J Med*, **364**:1493-1502.

Crane Co (1981) "Flow of Fluids Through Valves, Fittings, and Pipe."

Csenkér É, Dioszeghy P, Fekete I, and Mechler F (1982) "Ion Concentrations in Serum and Cerebrospinal Fluid of Patients With Neuromuscular Diseases," *Arch Fuer Psychiatrie Nervenkrankheiten*, **231**:251-8.

Curtis RA, Prausnitz JM, and Blanch HW (1998) "Protein-Protein and Protein-Salt Interactions in Aqueous Protein Solutions Containing Concentrated Electrolytes," *Biotechnol Bioeng*, **57**:11-21.

De Rosa MC, Castagnola M, Bertonati C, Galtieri A, and Giardina B (2004) "From the Arctic to Fetal Life: Physiological Importance and Structural Basis of an "Additional" Chloride-Binding Site in Haemoglobin," *Biochem J*, **380**:889-96.

Diamond R (1974) “Real-Space Refinement of the Structure of Hen Egg-White Lysozyme,” *J Mol Biol*, **82**:371-91.

Dice LR (1945) “Measures of the Amount of Ecologic Association Between Species,” *Ecology*, **26**:297-302.

Dick DAT (1967) “An Approach to the Molecular Structure of the Living Cell by Water Fluxes,” in Physical Bases of Circulatory Transport, Saunders Co.

Dickinson E, Semenova MG, Belyakova LE, Antipova AS, Il'in MM, Tsapkina EN, and Ritzoulis C (2001) “Analysis of light Scattering Data on the Calcium Ion Sensitivity of Caseinate Solution Thermodynamics: Relationship to Emulsion Flocculation,” *J Colloid Interface Sci*, **239:**87-97.

Doss EW, Ward KA, and Koretz JF (1997) “Preliminary Studies on the Aggregation Process of α-Crystallin,” *Exp Eye Res*, **65**:255-66.

Dumetz AC, Snellinger-O'Brien AM, Kaler EW, and Lenhoff AM (2007) “Patterns of Protein-Protein Interactions in Salt Solutions and Implications for Protein Crystallization,” *Protein Sci*, **16**:1867-77.

Einstein (1956) Investigations on the Theory of the Brownian Movement, Dover Publications.

Eisenberg HM, Frankowski RF, Contant CF, Marshall LF, and Walker MD (1988) “High-Dose Barbiturate Control of Elevated Intracranial Pressure in Patients With Severe Head Injury,” *J Neurosurg*, **69**:15-23.

Ellis RJ (2001) “Macromolecular Crowding: Obvious but Underappreciated,” *Trends Biochem Sci*, **26**:597-604.

Engelsen SB and Pérez S (1996) “The Hydration of Sucrose,” *Carbohydrate Res*, **292**:21-38.

Eswar N, Marti-Renom B, Webb B, Madhusudhan MS, Eramian D, Shen M, Pieper U, and Sali A (2006) "Comparative Protein Structure modeling with MODELLER" in Current Protocols in Bioinformatics, Wiley & Sons.

Ewan T (1899) "The Osmotic Pressure of Concentrated Solutions," *Zeit Fuer Physik Chem*, **31**:22-34.

Farrell DJ and Bower L (2003) "Fatal Water Intoxication," *J Clin Path*, **56**:803-4.

Finkelstein E, Corso P, and Miller T (2006) The Incidence and Economic Burden of Injuries in the United States, Oxford University Press.

Fraczkiewicz R and Braun W (1998) "Exact and Efficient Analytical Calculation of the Accessible Surface Areas and Their Gradients for Macromolecules," *J Comp Chem*, **19**:319-33.

Frazer JCW and Myrick RT (1916) "The Osmotic Pressure of Sucrose Solutions at 30 Degrees," *J Am Chem Soc*, **38**:1907-22.

Fullerton GD, Zimmerman RJ, Cantu C, and Cameron IL (1992) "New Expression to Describe Solution Nonideal Osmotic Pressure, Freezing Point Depression, and Vapor Pressure," *Biochem Cell Biol*, **70**:1325-31.

Gekko K and Timasheff SN (1981) "Mechanism of Protein Stabilization by Glycerol: Preferential Hydration in Glycerol-Water Mixtures," *Biochem*, **20**:4667-76.

George A and Wilson WW (1994) "Predicting Protein Crystallization from a Dilute-Solution Property," *Acta Crystallogr Sect D*, **50**:361-5.

George A, Chiang Y, Guo B, Arabshahi A, Cali Z, and Wilson WW (1997) "Second Virial Coefficient as Predictor in Protein Crystal Growth," *Macromol Crystallogr Pt A*, **276**:100-10.

Gerber DJ, Weintraub AH, Cusick CP, Ricci PE, and Whiteneck GG (2004) "Magnetic Resonance Imaging of Traumatic Brain Injury: Relationship of T2*SE and T2GE to Clinical Severity and Outcome," *Brain Injury*, **18**:1083-97.

Ghosh N, Recker R, Shah A, Bhanu B, Ashwal S, and Obenaus A, (2011) "Automated Ischemic Lesion Detection in a Neonatal Model of Hypoxic Ischemic Injury," *J MRI*, **33**:772-81.

Ghosh N, Sun Y, Turenius C, Bhanu B, Obenaus A, and Ashwal S (2012) "Computational Analysis: A Bridge to Translational Stroke Treatment" in Translational Stroke Research, Springer.

Gibbons RM (1969) "The Scaled Particle Theory for Particles of Arbitrary Shape," *Mol Physics*, **17**:81-6.

Gibbons RM (1970) "The Scaled Particle Theory for Mixtures of Hard Convex Particles," *Mol Physics*, **18**:809-16.

Gill AS, Rajneesh KF, Owen CM, Yeh J, Hsu M, and Binder DK (2011) "Early Optical Detection of Cerebral Edema *in vivo*," *J Neurosurg*, **116**:470-7.

Goryunov AS and Käiväräinen A "A Low-Temperature 1H NMR Study of $H_2O$ and $D_2O$ Associated Competitively With Immunoglobulin G in Solution."

Green AA (1931) "Studies in the Physical Chemistry of the Proteins .VIII. The Solubility of Hemoglobin in Concentrated Salt Solutions. A Study of the Salting Out of Proteins," *J Biol Chem*, **93**:495-516.

Green AA (1932) "Studies in the Physical Chemistry of the Proteins .X. The Solubility of Hemoglobin in Solutions of Chlorides and Sulfates of Varying Concentration," *J Biol Chem*, **95**:47-66.

Greer J and Bush BL (1978) "Macromolecular Shape and Surface Maps by Solvent Exclusion," *PNAS*, **75**:303-7.

Groot RD (1991) “On the Equation of State of Charged Colloidal Systems,” *J Chem Phys*, **94**:5083-9.

Guex N and Peitsch MC (1997) “SWISS-MODEL and the Swiss-Pdb Viewer: An Environment for Comparative Protein modeling,” *Electrophoresis*, **18**:2714-23.

Guo B, Kao S, McDonald H, Asanov A, Combs LL, and Wilson WW (1999) “Correlation of Second Virial Coefficients and Solubilities Useful in Protein Crystal Growth,” *J Cryst Growth*, **196**:424-33.

Halle B, Andersson T, Forsen S, and Lindman B (1981) "Protein Hydration from Water O-17 Magnetic-Relaxation," *J Am Chem Soc*, **103**:500-8.

Halle B (2004) “Protein Hydration Dynamics in Solution: A Critical Survey,” *Philosophical Trans: Biol Sci*, **359**:1207-24.

Hamabata A and von Hippel PH (1973) “Model Studies on Effects of Netural Salts on Conformational Stability of Biological Macromolecules .II. Effects of Vicinal Hydrophobic Groups on Specificity of Binding of Ions to Amide Groups,” *Biochem*, **12**:1264-71.

Hamabata A, Chang S, and von Hippel PH (1973) “Model Studies on Effects of Netural Salts on Conformational Stability of Biological Macromolecules .III. Solubility of Fatty-Acid Amides in Ionic Solutions,” *Biochem*, **12**:1271-8.

Hamaneh MB and Buck M (2007) “Acceptable Protein and Solvent Behavior in Primary Hydration Shell Simulations of Hen Lysozyme,” *Biophys J*, **92**:L49-51.

Harris LJ, Larson SB, Hasel KW, and McPherson A (1997) “Refined Structure of an Intact IgG2a Monoclonal Antibody,” *Biochem*, **36**:1581-97.

Haas C, Drenth J, and Wilson WW (1999) “Relation Between the Solubility of Proteins in Aqueous Solutions and the Second Virial Coefficient of the Solution,” *J Phys Chem B*, **103**:2808-11.

Haynes CA, Tamura K, Korfer HR, Blanch HW, and Prausnitz JM (1992) "Thermodynamic Properties of Aqueous α-Chymotrypsin Solutions from Membrane Osmometry Measurements," *J Phys Chem*, **96**:905-12.

Hill TL (1959) "Theory of Solutions .II. Osmotic Pressure Virial Expansion and Light Scattering in Two Component Solutions," *J Chem Phys*, **30**:93-7.

Ho JGS, Middelberg APJ, Ramage P, and Kocher HP (2003) "The Likelihood of Aggregation During Protein Renaturation can be Assessed Using the Second Virial Coefficient," *Protein Sci*, **12**:708-16.

Hofmeister F (1888) "Ueber Regelmässigkeiten in Deer Eiweissfällenden Wirkung der Salze und Ihre Beziehun zum Physiologischen Verhalten Derselben," *Arch Exp Pathol Pharmakol*, **24**:247-60.

Hoge CW, McGurk D, Thomas JL, Cox AI, Engel CC, and Castro CA (2008) "Mild Traumatic Brain Injury in U.S. Soldiers Returning From Iraq," *New Eng J Med*, **358**:453-63.

Hoover DM, Rajashankar KR, Blumenthal R, Puri A, Oppenheim JJ, Chertov O, and Lubkowski J (2000) "The Structure of Human β-Defensin-2 Shows Evidence of Higher Order Oligomerization," *J Biol Chem*, **275**:32911-8.

Horwitz J, Bova MP, Ding LL, Haley DA, and Stewart PL (1999) "Lens α-Crystallin: Function and Structure," *Eye*, **13**:403-8.

Huang A, Abugharbieh R, and Tam R (2009) "A Hybrid Geometric-Statistical Deformable Model for Automated 3D Segmentation in Brain MRI," *IEEE Trans Biomedical Eng*, **56**:1838-48.

Huang L *et al.* (2013) "Tissue Vulnerability is Increased Following Repetitive Mild traumatic Brain Injury in the Rat," *Brain Res*, **1499**:109-20.

Jacobson B (1953) "Hydration Structure of Deoxyribonucleic Acid and Its Physio-Chemical Properties," *Nature*, **172**:666-7.

Jacobson B, Anderson WA, and Arnold JT (1954) “A Proton Magnetic Resonance Study of the Hydration of Deoxyribonucleic Acid,” *Nature*, **173**:772-3.

Jain E, Bairoch A, Duvaud S, Phan I, Redaschi N, Suzek BE, Martin MJ, McGarvey P, and Gasteiger E (2009) “Infrastructure for the Life Sciences: Design and Implementation of the UniProt Website,” *BMC Bioinformatics*, **10**:136.

Kedem O and Katchalsky A (1958) “Thermodynamic Analysis of the Permeability of Biological Membranes to Non-Electrolytes,” *Biochim Biophys Acta*, **27**:229-46.

Kettenman H and Ransom BR (2005) Neuroglia (2nd Ed), Oxford University Press.

Keyrouz SG, Dhar R, and Diringer MN (2008) “Variation in Osmotic Response to Sustained Mannitol Administration,” *Neurocrit Care*, **9**:204-9.

Kirkwood JG and Goldberg RJ (1950) “Light Scattering Arising from Composition Fluctuations in Multi-Component Systems,” *J Chem Phys*, **18**:54-7.

Klotz IM (1958) “Protein Hydration and Behavior,” *Science*, **128**:815-22.

Koradi R, Billeter M, and Wüthrich K (1996) “MOLMOL: A Program for Display and Analysis of Macromolecular Structures,” *J Mol Graphics*, **14**:51-5.

Krishnan S, Chi EY, Webb JN, Chang BS, Shan DX, Goldenberg M, Manning MC, Randolph TW, and Carpenter JF (2002) “Aggregation of Granulocyte Colony Stimulating Factor Under Physiological Conditions: Charaterization and Thermodynamic Inhibition,” *Biochem*, **41**:6422-31.

Kuehner DE, Engmann J, Fergg F, Wernick M, Blanch HW, and Prausnitz JM (1999) “Lysozyme Net Charge and Ion Binding in Concentrated Aqueous Electrolyte Solutions,” *J Phys Chem B*, **103**:1368-74.

Kuntz ID and Kauzmann W (1974) "Hydration of Proteins and Polypeptides," *Adv Protein Chem*, **28**:239-345.

Larkin MA *et al.* (2007) "ClustalW and ClustalX Version 2," *Bioinformatics*, **23**:2947-8.

Lee B and Newberg A (2005) "Neuroimaging in Traumatic Brain Imaging", *NeuroRx: J Am Soc Exp Neurotherapeutics*, **2**:372-83.

Lee B and Richards FM (1971) "Interpretation of Protein Structures: Estimation of Static Accessibility," *J Mol Biol*, **55**:379-400.

Lewis GN and Randall M (1961) Thermodynamics (2nd Ed), McGraw-Hill.

Li Y, Weiss WF, and Roberts CJ (2009) "Characterization of High-Molecular-Weight Nonnative Aggregates and Aggregation Kinetics by Size Exclusion Chromatography With inline Multi-Angle Laser Light Scattering," *J Pharm Sci*, **98**:3997-4016.

Lin YZ, Li YG, and Lu JF (2001) "Correlation and Prediction of Osmotic Pressures for Aqueous Bovine Serum Albumin-NaCl Solutions Based on Two Yukawa Potentials," *J Colloid Interface Sci*, **239**:58-63.

Ling GN, Ochsenfeld MM, Walton C, and Bersinger TJ (1980) "Mechanism of Solute Exclusion from Cells – The Role of Protein-Water Interaction," *Physiol Chem Phys*, **12**:3-10.

Ling GN (1984) In Search of the Physical Basis of Life, Plenum Press.

Liu XS, Fan K, and Wang W (2004) "The Number of Protein Folds and Their Distribution Over Families in Nature," *Proteins: Structure Function Genetics*, **54**:491-9.

Lladó X, *et al.* (2012) "Segmentation of Multiple Sclerosis Lesions in Brain MRI: A Review of Automated Approaches" *Inform Sci*, **186**:164-85.

Loch J, Polt A, Górecki A, Bonarek P, Kurpiewska K, Dziedzicka-Wasylewska M, and Lewiński K (2011) "Two Modes of Fatty Acid Binding to Bovine β-Lactoglobulin – Crystallographic and Spectroscopic Studies," *J Mol Recog*, **24**:341-9.

Loll PJ, Allaman M, and Wiencek J (2001) "Assessing the Role of Detergent-Detergent Interactions in Membrane Protein Crystallization," *J Cryst Growth*, **232**:432-8.

Maas WI, Roozenbeek B, Manley GT (2010) "Clinical Trials in Traumatic Brain Injury: Past Experience and Current Developments," *Neurotherapeutics*, **7**:115-26.

Majorek KA, Porebski PJ, Dayal A, Zimmerman MD, Jablonska K, Stewart AJ, Chruszcz M, and Minoe W (2012) "Structural and Immunologic Characterization of Bovine, Horse, and Rabbit Serum Albumins," *Mol Immunol*, **52**:174-82.

Marmarou A, (2003) "Pathophysiology of Traumatic Brain Edema: Current Concepts," *Acta Neurochirurgica Supp*, **86**:7-10.

Mattea C, Qvist J, and Halle B (2008) "Dynamics at the Protein-Water Interface From $^{17}O$ Spin Relaxation in Deeply Supercooled Solutions," *Biophys J*, **95**:2951-63.

M$^{c}$Bride DW and Rodgers VGJ (2012) "Obtaining Protein Solvent Accessible Surface Area (SASA) When Structural Data is Unavailable Using Osmotic Pressure," *AIChE J*, **58**:1012-7.

M$^{c}$Bride DW, Hsu MS, Rodgers VGJ, and Binder DK (2012) "Improved Survival Following Cerebral Edema Using a novel Hollow Fiber-Hydrogel Device," *J Neurosurg*, **116**:1389-94.

McMillan WC and Mayer JE (1945) "The Statistical Thermodynamics of Multicomponent Systems," *J Chem Phys*, **13**:276-305.

Melander W and Horvath C (1977) "Salt Effects on Hydrophobic Interactions in Precipitation and Chromatography of Proteins - Interpretation of Lyotropic Series," *Arch Biochem Biophys*, **183**:200-15.

Miklavic SJ and Woodward CE (1990) "The Osmotic Pressure in Polyelectrolyte Solutions: Exact and Mean-Field Results," *J Chem Phys*, **93**:1369-75.

Minton AP (1983) "The Effect of Volume Occupancy Upon the Thermodynamic Activity of Proteins: Some Biochemical Consequences," *Mol Cell Biochem*, **55**:119-40.

Minton AP (1995) "A Molecular Model for the Dependence of the Osmotic Pressure of Bovine Serum Albumin Upon Concentration and pH," *Biophys Chem*, **57**:65-70.

Minton AP (2001) "The Influence of Macromolecular Crowding and Macromolecular Confinement on Biochemical Reactions in Physiological Media," *J Biol Chem*, **276**:10577-80.

Mollerup JM and Breil MP (2009a) "On the Thermodynamics of the McMillan-Mayer State Function," *Fluid Phase Equilibria*, **276**:18-23.

Mollerup JM and Breil MP (2009b) "The Osmotic Second Virial Coefficient and the Gibbs-McMillan-Mayer Framework," *Fluid Phase Equilibria*, **286**:88-94.

Murray GD *et al.* (1999) "The European Brain Injury Consortium Survey of Head Injuries," *Acta Neurochirurgica*, **141**:223-36.

Murugavel M and Sullivan JM (2009) "Automatic Cropping of MRI Rat Brain Volumes Using Pulse Coupled Neural Networks," *NeuroImage*, **45**:845-54.

Myburgh JA, Cooper DJ, Finfer SR, Venkatesh B, Jones D, Higgins A, Bishop N, and Higlet T (2008) "Epidemiology and 12-Month Outcomes From Traumatic Brain Injury in Australia and New Zealand," *J Trauma - Injury Infect Crit Care*, **64**:854-62.

Na GC and Timasheff SN (1981) "Interaction of Calf Brain Tubulin With Gycerol," *J Mol Biol*, **151**:165-78.

Nagelhus EA, Mathiisen TM, and Ottersen OP (2004) "Aquaporin-4 in the Central Nervous System: Cellular and Subcellular Distribution and Coexpression With Kir4.1," *Neurosci*, **129**:905-13.

Neal BL, Asthagiri D, and Lenhoff AM (1998) "Molecular Origins of Osmotic Second Virial Coefficients of Proteins," *Biophys J*, **75**:2469-77.

Neal BL, Asthagiri D, Velev OD, Lenhoff AM, and Kaler EW (1999) "Why is the Osmotic Second Virial Coefficient Related to Protein Crystallization?" *J Cryst Growth*, **196**:377-87.

Neelagandan K, Moorthy PS, Balasubramanian M, Sundaresan S, and Ponnuswamy MN (unpublished) “Crystal Structure Determination of Sheep (Ovis aries) Methemoglobin at 2.7 Angstrom Resolution.”

Nielsen S, Nagelhus EA, Amiry-Moghaddam M, Bourque C, Arge P, and Ottersen OP (1997) “Specialized Membrane Domains for Water Transport in Glial Cells: High-Resolution Immunogold Cytochemistry of Aquaporin-4 in Rat Brain,” *J Neurosci*, **17**:171-180.

Notredame C, Higgins DG, and Heringa J (2000) “T-Coffee: A Novel Methods for Fast and Accurate Multiple Sequence Alignment,” *J Mol Biol*, **302**:205-17.

Onnes HK (1901a) *Communications from the Physical Laboratory at the University of Leiden*, Number 71.

Onnes HK (1901b) *Communications from the Physical Laboratory at the University of Leiden*, Number 74.

Otsu N (1979) “A Threshold Selection Method from Gray-Level Histograms,” *IEEE Trans Sys Man Cybernetics*, **9**:62-6.

Otting G, Liepinsh E, and Wuthrich K (1991) "Protein Hydration in Aqueous Solution," *Science*, **254**:974-80.

Panuszko A, Wojciechowski M, Bruździak P, Rakowska PW, and Stangret J (2012) “Characteristics of Hydration Water Around Hen Egg Lysozyme as the Protein model in Aqueous Solution. FTIR Spectroscopy and Molecular Dynamics Simulation,” *Phys Chem Chem Phys*, **14**:15765-73.

Park E, Bell JD, and Baker AJ (2008) “Traumatic Brian Injury: Can the Consequences be Stopped?” *Canadian Med Ass J*, **178**:1163-70.

Parker R, Noel TR, Brownsey GJ, Laos K, and Ring SG (2005) “The Nonequilibrium Phase and Glass Transition Behavior of β-Lactoglobulin,” *Biophys J*, **89**:1227-36.

Patterson JE and Geller DM (1977) “Bovine Microsomal Albumin: Amino Terminal Sequence of Bovine Proalbumin,” *Biochem Biophys Res Commun*, **43**:1220-6.

Pedretti A, Villa L, and Vistoli G (2002) “VEGA: A Program to Convert, Handle and Visualize Molecular Structure on Windows-Based PCs,” *J Mol Graphics*, **21**:47-9.

Perutz MF, Muirhead H, Cox JM, and Goaman LCG (1968) “Three-Dimensional Fourier Synthesis of Horse Oxyghaemoglobin at 2.8 A Resolution: The Atomic Model,” *Nature*, **219**:131-9.

Petsko GA and Ringe D (2004) Protein Structure and Function, New Science Press.

Pettersen EF, Goddard TD, Huang CC, Couch GS, Greenblatt DM, Meng EC, and Ferrin TE (2004) “UCSF Chimera - A Visualization System for Exploratory Research and Analysis,” *J Comp Chem*, **25**:1605-12.

Pittz EP and Timasheff SN (1978) ”Interaction of Ribonuclease A With Aqueous 2-Methyl-2,4-Pentanediol at pH 5.8,” *Biochem*, **17**:615-23.

Prausnitz JM, Lichtenthaler RN, and Gomes de Azevedo E (1999) Molecular Thermodynamics of Fluid-Phase Equilibria (3rd Ed), Prentice Hall.

Qin BY, Bewley MC, Creamer LK, Baker HM, Baker EN, Jameson GB (1998) “Structural basis of the Tanford Transition of Bovine β-Lactoglobulin,” *Biochem*, **37**:14014-23.

Reboiras MD, Pfister H, and Pauly H (1978) “Activity Coefficients of Salts in Highly Concentrated Protein Solutions .I. Alkali Chlorides in Isoionic Bovine Serum Albumin Solutions,” *Biophys Chem*, **9**:37-46.

Reboiras MD, Pfister H, and Pauly H (1986) “Activity Coefficients of Salts in Highly Concentrated Protein Solutions .II. Potassium-Salts in Isoionic Bovine Serum Albumin Solutions,” *Biophys Chem*, **24**:249-57.

Regini JW, Grossmann JG, Timmins P, Harding JJ, Quantock AJ, Hodson SA, and Elliott GF (2007) "X-Ray- and Neutron-Scattering Studies of α-Crystallin and Evidence That the Target Protein Sits in the Fenestrations of the α-Crystallin Shell," *Invest Ophthal Vis Sci*, **48**:2695-2700.

Reilly P and Bullock R (2005) Head Injury, Pathophysiology and Management (2nd Ed), Hodder Arnold Pub.

Rosenbaum DF and Zukoski CF (1996) "Protein Interactions and Crystallization," *J Cryst Growth* **169**:752-8.

Ross PD and Minton AP (1977) "Analysis of Non-Ideal Behavior in Concentrated Hemoglobin Solutions," *J Mol Biol*, **112**:437-52.

Rouaïnia M, Medjram MS, and Doghmane N (2006) "Brain MRI Segmentation and Lesions Detection by EM Algorithm," *Preceed World Aca Sci, Eng Technol*, **24**:139-42.

Rupley JA and Careri G (1991) "Protein Hydration and Function," *Adv Protein Chem*, **41**:37-172.

Ruppert S, Sandler SI, and Lenhoff AM (2001) "Correlation Between the Osmotic Second Virial Coefficient and the Solubility of Proteins," *Biotechnol Prog*, **17**:182-7.

Sahin E, Grillo AO, Perkins MD, and Roberts CJ (2010) "Comparative Effects of pH and Ionic Strength on Protein-Protein Interactions, Unfolding, and Aggregation for IgG1 Antibodies," *J Pharm Sci*, **99**:4830-48.

Sandler SI (1999) Chemical Engineering Thermodynamics (3rd Ed), Wiley & Sons.

Sassi AP, Blanch HW, and Prausnitz JM (1996) "Phase Equilibria for Aqueous Protein/Polyelectrolyte Gel Systems," *AIChE J*, **42**:2335-53.

Sawai MV, Jia HP, Liu L, Aseyev V, Wiencek JM, McCray PB, Ganz WR, Kearney WR, and Tack BF (2001) "The NMR Structure of Human β-Defensin-2 Reveals a Novel α-Helical Segment," *Biochem*, **40**:3810-6.

Scatchard G (1921) “The Hydration of Sucrose in Water Solution as Calculated From Vapor Pressure Measurements,” *J Am Chem Soc*, **43**:2406-18.

Scatchard G, Batchelder AC, Brown A, and Zosa M (1946) “Preparation and Properties of Serum and Plasma Proteins .VII. Osmotic Equilibria in Concentrated Solutions of Serum Albumin,” *J Am Chem Soc*, **68**:2610-2.

Scatchard G, Scheinberg IH, and Armstrong SH (1950) “Physical Chemistry of Protein Solutions .IV. The Combination of Human Serum Albumin with Chloride Ion,” *J Am Chem Soc*, **72**:535-40.

Scatchard G, Coleman JS, and Shen AL (1957) “Physical Chemistry of Protein Solutions .VII. The Binding of Small Anions to Serum Albumin,” *J Am Chem Soc*, **79**:12-20.

Scatchard G and Pigliacampi J (1962) “Physical Chemistry of Protein Solutions .XI. Osmotic Pressures of Serum Albumin, Carbonylhemogloin and Their Mixtures in Aqueous Sodium Chloride at 25 Degrees,” *J Am Chem Soc*, **84**:127-34.

Schaink HM and Smit JAM (2000) “Determination of the Osmotic Second Virial Coefficient and the Dimerization of β-Lactoglobulin in Aqueous Solutions With Added Salt at the Isoelectric Point,” *Phys Chem Chem Phys*, **2**:1537-41.

Schmidt P *et al.* (2012) “An Automated Tool for Detection of FLAIR-Hyperintense White-Matter Lesions in Multiple Sclerosis” *NeuroImage*, **59**:3774-83.

Schneiderman AI, Braver ER, and Kang HK (2008) “Understanding Sequelae of Injury Mechanisms and Mild Traumatic Brain Injury Incurred During the Conflicts in Iraq and Afghanistan: Persistent Postconcussive Symptoms and Posttraumatic Stress Disorder,” *Am J Epidemiology*, **167**:1446-52.

Sedykh LG and Sedykh NV (1967) “Mathematical Model of Phenomenon of Hydration of Biopolymers in Solution,” *Biofizika*, **12**:936-8.

Shen S, Szameitat AJ, and Sterr A, (2008) "Detection of Infarct Lesions From Single MRI Modality Using Inconsistency Between Voxel Intensity and Spatial Location - A 3-D Automatic Approach," *IEEE Trans Inform Technol Biomed*, 12:532-40.

Shulyakov AV, Benour M, and Del Bigio MR (2008) "Surface Dialysis After Experimental Brain Injury: Modification of Edema Fluid Flow in the Rat Model," *J Neurosurg*, **109**:670-7.

Singh K, Groth-Vasselli B, and Farnsworth PN (1996) "Electrostatic Parameters of the Theoretical Quaternary Structure of Bovine α-Crystallin," *Int J Biol Macromol*, **18**:205-9.

Smith JM and Van Ness HC (1975) Introduction to Chemical Engineering Thermodynamics (3rd Ed), McGraw-Hill.

Stein PE, Leslie AG, Finch JT, and Carrell RW (1991) "Crystal Structure of Uncleaved Ovalbumin at 1.95 A Resolution," *J Mol Biol*, **221**:941-59.

Stocchetti N, Zanaboni C, Colombo A, Citerio G, Beretta L, Ghisoni L, Zanier ER, and Canavesi K (2008) "Refractory Intracranial Hypertension and "Second-Tier" Therapies in Traumatic Brain Injury," *Inten Care Med*, **34**:461-7.

Stockmayer WH (1950) "Light Scattering in Multicomponent Systems," *J Chem Phys*, **18**:58-61.

Suarez JI, Qureshi AI, Bhardwaj A, Williams MA, Schnitzer MS, Mirski M, Hanley DF, and Ulatowski JA (1998) "Treatment of Refractory Intracranial Hypertension With 23.4% Saline," *Crit Care Med*, **26**:1118-22.

Sugio S, Kashima A, Mochizuki S, Noda M, and Kobayashi K (1999) "Crystal Structure of Human Serum Albumin at 2.5 Angstrom Resolution," *Protein Eng*, **12**:439-46.

Svergun DI, Richard S, Koch MHJ, Sayers Z, Huprin S, and Zaccai G (1998) "Protein Hydration in Solution: Experimental Observation by X-Ray and Neutron Scattering," *PNAS*, **95**:2267-72.

Tagliaferri F, Compagnone C, Korsic M, Servadei F, and Kraus J (2006) "A Systematic Review of Brain Injury Epidemiology in Europe," *Acta Neurochirurgica*, **148**:255-68.

Tanford C (1961) Physical Chemistry of Macromolecules, Wiley & Sons.

Tessier PM and Lenhoff AM (2003) "Measurements of Protein Self-Aossciation as a Guide to Crystallization," *Curr Opin Biotechnol*, **14**:512-6.

Tessier PM. and Verruto, VJ, Sandler SI, and Lenhoff AM (2004) "Correlation of Diafiltration Sieving Behavior of Lysozyme-BSA Mixtures With Osmotic Second Virial Cross-Coefficients," *Biotechnol Bioeng*, **87**:303-10.

Tester JW and Modell M (1997) Thermodynamics and Its Applications (3rd Ed), Prentice Hall.

Thomson JA and Augusteyn RC (1988) "On the Structure of α-Crystallin: The Minimum Molecular Weight," *Curr Eye Res*, **7**:563-9.

Timasheff SN, Lee JC, Pittz EP, and Tweedy N (1976) "The Interaction of Tubuling and Other Proteins With Structure Stabilizing Solvents," *J Colloid Interface Sci*, **55**:658-63.

Timasheff SN and Arakawa T (1988) "Mechanism of Protein Precipitation and Stabilization by Co-Solvents," *J Cryst Growth*, **90**:39-46.

Timasheff SN (2002a) "Protein-Solvent Preferential Interactions, Protein Hydration, and the Modulation of Biochemical Reactions by Solvent Components," *PNAS*, **99**:9721-6.

Timasheff SN (2002b) "Protein Hydration, Thermodynamic Binding, and Preferential Hydration," *Biochem*, **41**:13473-82.

Tombs MP and Peacocke AR (1974) The Osmotic Pressure of Biological Macromolecules, Clarendon Press.

Truskey GA, Yuan F, and Katz DF (2004) Transport Phenomena in Biological Systems, Prentice Hall.

van Laar JJ (1894) "On the Exact Formulas for the Osmotic Pressure, for the Changes to the Solubility, for Freezing Point - and Boiling Point - Changes, and for the Solutions - and Dilutions - Warm with Bodies Dissociated in Solution," *Zeit Fuer Physik Chem*, **15**:457-97.

Varma S and Rempe SB (2006) "Coordination Numbers of Alkali Metal Ions in Aqueous Solutions," *Biophys Chem*, **124**:192-9.

Vérétout F, Delaye M, and Tardieu A (1989) "Molecular Basis of Eye Lens Transparency Osmotic Pressure and X-Ray - Analysis of α-Crystallin Solutions," *J Mol Biol*, **205**:713-28.

Verkman AS and Mitra AK (2000) "Structure and Function of Aquaporin Water Channels," *Am J Physiol - Renal Physiol*, **278**:F13-F28.

Verkman AS (2002) "Physiological Importance of Aquaporin Water Channels," *Annals Med*, **34**:192-200.

Verkman AS (2005) "More Than Just Water Channels: Unexpected Cellular Roles of Aquaporins," *J Cell Sci*, **188**:3225-32.

Verkman AS, Binder DK, Bloch O, Auguste K, and Papadopoulos MC (2006) "Three Distinct Roles of Aquaporin-4 in Brain Function Revealed by Knockout Mice," *Biochim Biophys Acta - Biomembranes*, **1758**:1085-93.

Vijayalakshmi L, Krishna R, Sankaranarayanan R, and Vijayan M (2008) "An Asymmetric Dimer of β-Lactoglobulin in a Low Humidity Crystal Form - Structural Changes That Accompany Partial Dehydration and Protein Action," *Proteins: Structure Function and Bioinformatics*, **71**:241-9.

Vilker VL (1976) "The Ultrafiltration of Biological Macromolecules," MIT. Ph.D. Thesis.

Vilker VL, Colton CK, and Smith KA (1981) "The Osmotic Pressure of Concentrated Protein Solutions: Effect of Concentration and pH in Saline Solutions of Bovine Serum Albumin," *J Colloid Interface Sci*, **79**:548-66.

von Hippel PH, Peticola V, Schack L, and Karlson L (1973) "Model Studies on Effects of Neutral Salts on Conformational Stability of Biological Macromolecles I.. Ion Binding to Polyacrylamide and Polystrene Columns," *Biochem*, **12**:1256-64.

Walstra P (2002) Physical Chemistry of Foods, CRC Press.

Warden D (2006) "Military TBI During the Iraq and Afghanistan Wars," *J Head Trauma Rehab*, **21**:398-402.

Wang Y (2008) "Electrostatic Contributions in Binary Protein Ultrafiltration," University of California, Riverside, Ph.D. Thesis.

Wang LX and Bloomfield VA (1990) "Osmotic Pressure of Semidilute Solutions of Flexible, Globular, and Stiff-Chain Polyelectrolytes With Added Salt," *Macromol*, **23**:194-9.

Weiss WF, Young TM and Roberts CJ (2009) "Principles, Approaches, and Challenges for Predicting Protein Aggregation Rates and Shelf Life," *J Pharm Sci*, **98**:1246-77.

Wills PR and Winzor DJ (1992) "Thermodynamic Nonideality and Sedimentation Equilibrium," in Analytical Ultracentrifugation in Biochemistry and Polymer Science, Royal Society of Chemistry.

Wills PR, Comper WD, and Winzor DJ (1993) "Thermodynamic Nonideality in Macromolecular Solutions: Interpretation of Virial Coefficients," *Arch Biochem Biophys*, **300**:206-12.

Wills PR, Hall DR, and Winzor DJ (2000) "Interpretation of Thermodynamic Nonideality in Sedimentation Equilibrium Experiments on Proteins," *Biophys Chem*, **84**:217-25.

Winzor DJ, Deszczynski M, Harding SE, and Wills PR (2007) "Nonequilivance of Second Virial Coefficients from Sedimentation Equilibrium and Static Light Scattering Studies of Protein Solutions," *Biophys Chem*, **128**:46-55.

Xia JZ, Aerts T, Donceel K, and Clauwaert J (1994) "Light-Scattering by Bovine α-Crystallin Proteins in Solution: Hydrodynamic Structure and Interparticle Interaction," *Biophys J*, **66**L861-72.

Xue XY, Sun JX, and Mo WJ (2008) "Correlation and Prediction of Osmotic Pressures for Three Aqueous Protein-Electrolyte Solutions Based on the Ross Perturbation Theory and Soft-Core Three-Yukawa Potential," *J Mol Liquids*, **139**:80-8.

Yamasaki M, Takahashi N, and Hirose M (2003) "Crystal Structure of S-Ovalbumin as a Non-Loop-Inserted Thermostabilitzed Serpin Form," *J Biol Chem*, **278**:35524-30.

Yousef MA, Datta R, and Rodgers VGJ (1998a) "Free-Solvent Model of Osmotic Pressure Revisited: Application to Concentrated IgG Solution Under Physiological Conditions," *J Colloid Interface Sci*, **197**:108-18.

Yousef MA, Datta R, and Rodgers VGJ (1998b) "Understanding the Nonidealities of the Osmotic Pressure of Concentrated Bovine Serum Albumin," *J Colloid Interface Sci*, **207**:273-82.

Yousef MA (2000) "The Effect of Molecular Interactions on the Osmotic Pressure and Diffusion Coefficients of Protein Solutions," University of Iowa. Ph.D. Thesis.

Yousef MA, Datta R, and Rodgers VGJ (2001) "Confirmation of Free Solvent Model Assumptions in Predicting the Osmotic Pressure of Concentrated Globular Proteins," *J Colloid Interface Sci*, **243**:321-5.

Yousef MA, Datta R, and Rodgers VGJ (2002a) "Model of Osmotic Pressure for High Concentrated Binary Protein Solutions," *AIChE J*, **48**:913-7.

Yousef MA, Datta R, and Rodgers VGJ (2002b) "Monolayer Hydration Governs Nonideality in Osmotic Pressure of Protein Solutions," *AIChE J*, **48**:1301-8.

Zhang J and Liu XY (2003) "Effect of Protein-Protein Interactions on Protein Aggregation Kinetics," *J Chem Phys*, **119**:10972-6.

Zhou HX (2005) “Interactions of Macromolecules With Salt Ions: An Electrostatic Theory for the Hofmeister Effect,” *Proteins - Structure Function and Bioinformatics*, **61**:69-78.

Zweckberger K, Eros C, Zimmerman R, Kim SW, Engel D, and Plesnila N (2006) “Effect of Early and Delayed Decompressive Craniectomy on Secondary Brain Damage After Controlled Cortical Impact in Mice,” *J Neurotrauma*, **23**:1083-93.